



UNIVERSITAT DE
BARCELONA

Passive air and water sampling in high-altitude lakes: occurrence and distribution of legacy and emerging organic pollutants

Raimon Martínez Prats



Aquesta tesi doctoral està subjecta a la llicència **Reconeixement- NoComercial – SenseObraDerivada 4.0. Espanya de Creative Commons.**

Esta tesis doctoral está sujeta a la licencia **Reconocimiento - NoComercial – SinObraDerivada 4.0. España de Creative Commons.**

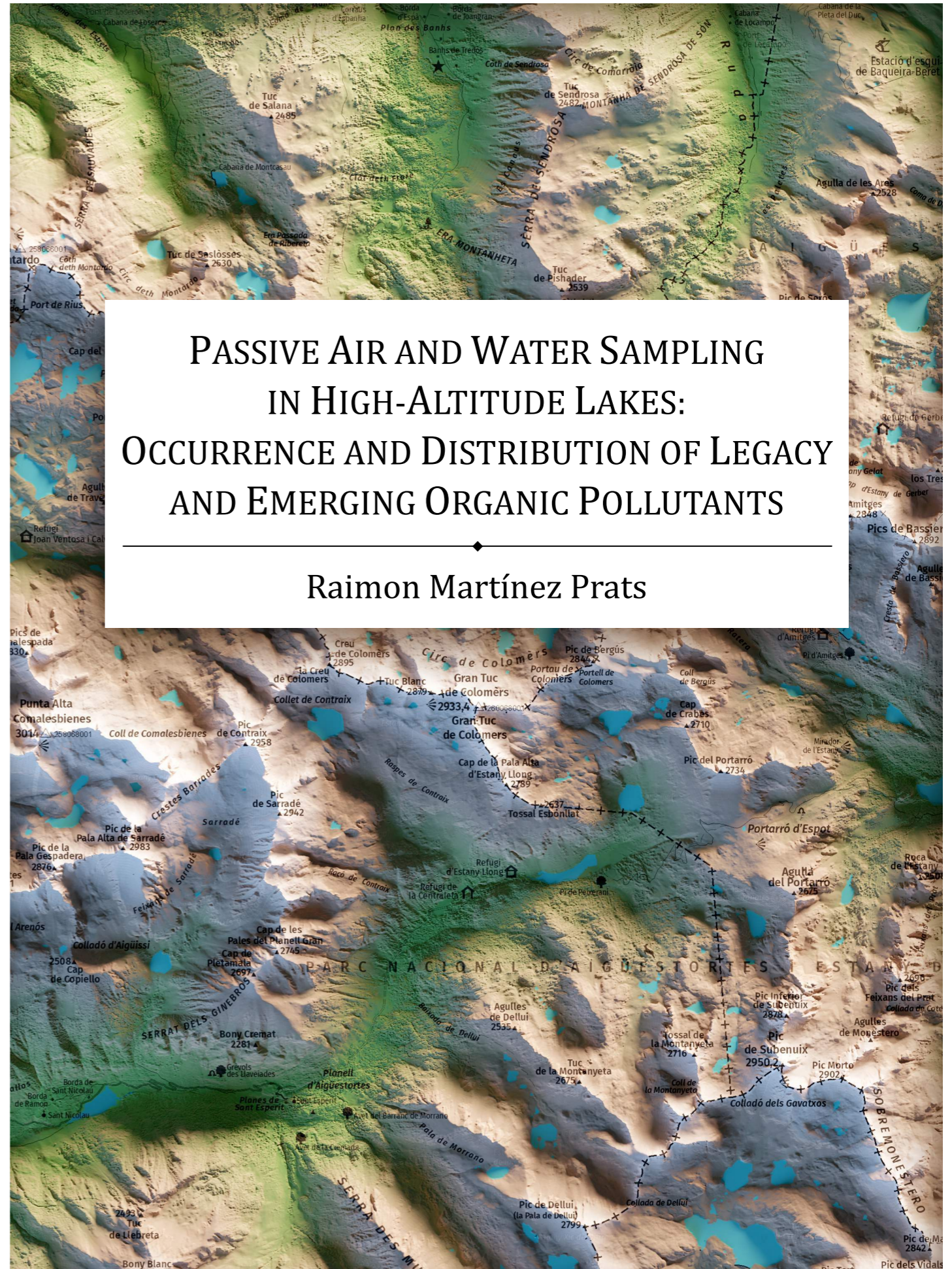
This doctoral thesis is licensed under the **Creative Commons Attribution-NonCommercial-NoDerivs 4.0. Spain License.**



Raimon Martínez Prats

PhD Thesis

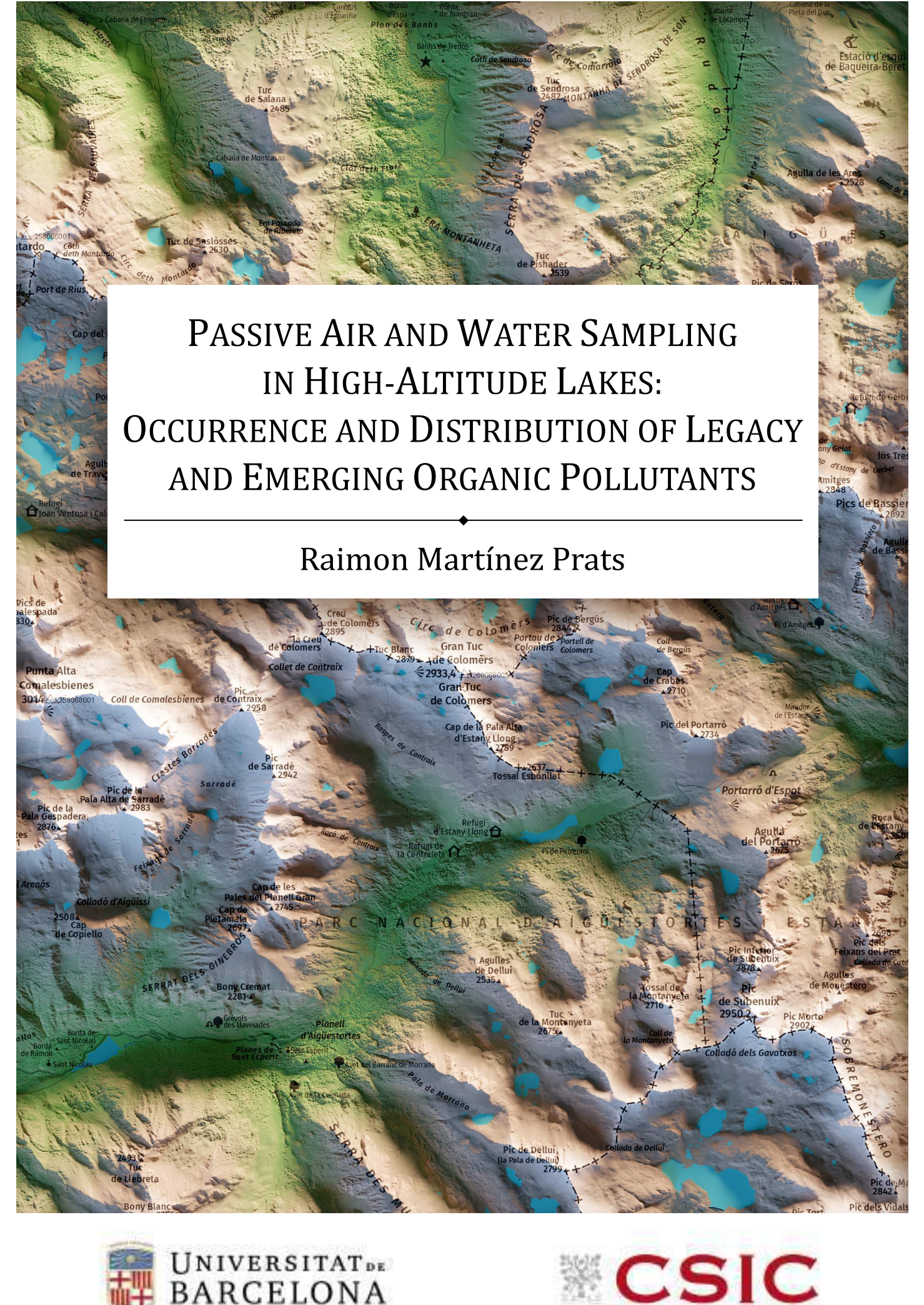
2022



PASSIVE AIR AND WATER SAMPLING
 IN HIGH-ALTITUDE LAKES:
 OCCURRENCE AND DISTRIBUTION OF LEGACY
 AND EMERGING ORGANIC POLLUTANTS

Raimon Martínez Prats





PASSIVE AIR AND WATER SAMPLING IN HIGH-ALTITUDE LAKES: OCCURRENCE AND DISTRIBUTION OF LEGACY AND EMERGING ORGANIC POLLUTANTS

Raimon Martínez Prats

Cover image: Trobart. Reproduced with permission.



UNIVERSITAT DE
BARCELONA



CSIC
CONSEJO SUPERIOR DE INVESTIGACIONES CIENTÍFICAS

Universitat de Barcelona

Programa de Doctorat
Química Analítica i Medi Ambient

**PASSIVE AIR AND WATER SAMPLING IN HIGH-ALTITUDE LAKES:
OCCURRENCE AND DISTRIBUTION OF LEGACY AND
EMERGING ORGANIC POLLUTANTS**

Memòria presentada per optar al
Grau de Doctor per la Universitat de Barcelona

Raimon Martínez Prats

Director

Dr. Joan Grimalt i Obrador
Professor d'Investigació

Directora

Dra. Pilar Fernández Ramón
Científic Titular

Tutor Acadèmic

Dr. Francisco Javier Santos Vicente
Professor Titular d'Universitat

Institut de Diagnosi Ambiental i Estudis de l'Aigua,
Consell Superior d'Investigacions Científiques

Departament d'Enginyeria Química
i Química Analítica,
Universitat de Barcelona

Barcelona, setembre de 2022

El Dr. Joan Grimalt i Obrador, Professor d'Investigació, i la Dra. Pilar Fernández Ramón, Científic Titular, de l'Institut de Diagnosi Ambiental i Estudis de l'Aigua (IDAEA) del Consell Superior d'Investigacions Científiques (CSIC),

FAN CONSTAR:

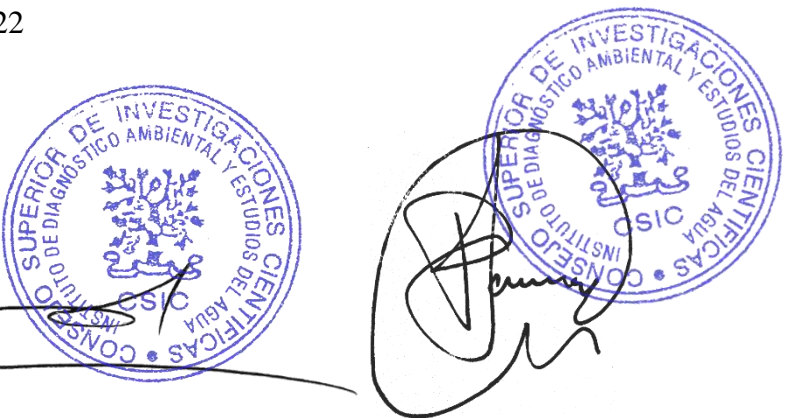
Que la present memòria, presentada per optar al Grau de Doctor de la Universitat de Barcelona, titulada

Passive Air and Water Sampling in High-Altitude Lakes: Occurrence and Distribution of Legacy and Emerging Organic Pollutants

ha estat realitzada sota la seva direcció pel Sr. Raimon Martínez Prats a l'Institut de Diagnosi Ambiental i Estudis de l'Aigua (IDAEA) del Consell Superior d'Investigacions Científiques (CSIC) i que tots els resultats presentats són fruit del treball experimental realitzat pel citat doctorand.

I, perquè consti així i tingui els efectes que corresponguin, signen aquest certificat.

Barcelona, 15 de setembre de 2022



Dr. Joan Grimalt i Obrador

Dra. Pilar Fernández Ramón

a l'adversitat

Agraïments

El meu més sincer agraïment va dedicat a Joan Grimalt i a Pilar Fernández per dirigir aquesta tesi. Per l'oportunitat, la confiança i per donar valor a tot allò que he fet. També a Xavier Santos, de la Universitat de Barcelona, per acceptar la tutorització d'aquesta tesi i per dur-la a bon port. Han estat uns anys increïbles.

No puc deixar passar més línies sense mostrar el meu més sentit agraïment a Barend van Drooge. No concebo l'existència d'aquesta tesi sense tu, de la mateixa manera que no imagino els últims anys sense el teu suport, consells i ajuda. Gràcies per deixar-me lloc per créixer i per ser-hi quan més perdut anava. Per les converses a peu de muntanya i per les sessions de rock a la *Navara*. Al laboratori com pujant als llacs més alts, la teva àgil silueta sempre m'ha ajudat a trobar forces per seguir endavant.

Moltes gràcies també als actuals i anteriors companys de doctorat, Natalia Bravo, Isabel Díez, Clara Jaén, Eva Junqué, Nupur Nagar i Marco Capodiferro. Per ser-hi, colze a colze, dia rere dia. Uns per oferir ajuda desinteressada, altres per la confiança que dipositeu en venir a buscar-la amb un tímid "*Rai, una pregunta...*". Feu que m'adoni del que he après i del que em queda per aprendre. També a la resta del grup de Geoquímica i Contaminació, Inma Fernández, Yolanda González, Marta Casado, Esther Marco, Jordi López, Àlex Caro, Mercè Garí, Belen Martrat i Aleix Cortina, i a l'equip d'Espectrometria de Masses, Roser Chaler, Àlex García i Dori Fanjul.

Te reservo un pequeño rincón a ti, Àlex González. Gracias por compartir la carga subiendo a los lagos, por los improperios lanzados al aire con quince kilos a la espalda, quinientos metros de desnivel por delante y dos metros de nieve bajo las raquetas, y por una buena *Desagradecido* en el Redon. Fue en realidad más breve de lo que recuerdo, lo cual atestigua su intensidad.

No puc oblidar tothom qui ha aportat, d'una manera o altra, el seu granet de sorra durant els últims anys: Lluís Camarero, Mireia Bartrons, Anna Canals, Carlos Escorza, Helena García, Roger Garatachea, Núria Penalva i Anna Zawrotniak. Menció especial per a la Margarita, de Casa Hortal a Barruera, per l'hospitalitat i l'interès. També per al personal de la Casa del Parc Nacional d'Aigüestortes i Estany de Sant Maurici a Boí, per a la gent del CRAM i per als nois de Sorelló.

Un record per a Unai Pérez i Gaspar Giner. També per a Roberto Sánchez. A vegades la muntanya troba la pitjor manera de guanyar-se el nostre respecte.

A heartfelt thank you to Foppe Smedes and Branislav Vrana for taking me in for a brief period of time at RECETOX in Brno and for teaching me in a disinterested way. Thank you too, Jaromír Sobotka and Jakub Martínk, for the much-needed assistance.

Sobren paraules per als amics, tots aquells que hi sou des de fa ja més temps del que hem assimilat. Especialment, Roger Oriol, Marina Pérez, Imma Carbó, Mar Mulero, Eva Ferrer, Guillem Martínez, Mònica Longares i Gerard Pastor, pels nombrosos vespres a una terrassa d'un bar i les converses fins tard adonant-nos que ens fem grans tot queixant-nos d'aquests últims anys. També Macarena Duran, per un cafè ben necessari de tant en tant, i Marc Marín, per mirar de desxifrar plegats aquest laberint acadèmic.

En últim lloc, però per a mi el més important, gràcies a la família pel suport i la paciència.

This work was supported by the Spanish Ministry of Science and Innovation through projects CTM2015-71832-P and PGC2018-102288-B-I00 and through fellowship BES-2016-076339. IDAEA-CSIC is a Severo Ochoa Centre of Research Excellence, grant CEX2018-000794-S funded by MCIN/AEI/10.13039/501100011033. Part of the work was carried out with the support of RECETOX Research Infrastructure (ID LM2018121, MEYS CR, 2020-2022).

Table of Contents

Summary	I
Resum	V
List of Tables	IX
List of Figures	IX
Abbreviations and variables.....	XV
CHAPTER 1. Introduction	1
1.1 Diffuse pollution	3
1.1.1 Global distillation effect and mountain cold-trapping	5
1.1.2 High mountains as sentinel ecosystems for the study of diffuse pollution.....	8
1.1.3 Alpine lakes, continental reservoirs of anthropogenic pollutants.....	10
1.2 Semi-volatile and hydrophobic organic pollutants	12
1.2.1 Polychlorinated biphenyls.....	15
1.2.2 Organochlorine compounds	16
1.2.3 Polycyclic aromatic hydrocarbons	18
1.2.4 Organophosphate esters	20
1.3 Passive sampling as a tool for the global monitoring of pollution	22
1.3.1 Passive air samplers	24
1.3.2 Passive water samplers	27
CHAPTER 2. Objectives and structure	31
2.1 Objectives	33
2.2 Structure.....	35
CHAPTER 3. Legacy and currently emitted organic pollutants in air and water from urban and high-altitude ecosystems	37
3.1 Introduction.....	39
3.1.1 Background: previous studies and circumstances of the present work	39
3.1.1.1 The study of diffuse pollution in the Pyrenean mountains	39
3.1.1.2 The strict lockdown of a country: an opportunity to assess pollution trends at their source.....	42
3.1.2 Pollutant sources and partitioning between environmental compartments ...	47
3.1.3 Passive sampling theory: diffusive uptake of pollutants	50
3.1.3.1 Calibration of passive samplers	53

3.2 Methodology	59
3.2.1 Area of study	59
3.2.2 Meteorology	65
3.2.3 Passive air sampler configuration and deployment.....	71
3.2.4 Passive water sampler configuration and deployment	74
3.2.5 Diffusive exchange of pollutants between air and water	77
3.3 Results	86
Article 1. FIELD COMPARISON OF PASSIVE POLYURETHANE FOAM AND ACTIVE AIR SAMPLING TECHNIQUES FOR ANALYSIS OF GAS-PHASE SEMI-VOLATILE ORGANIC COMPOUNDS AT A REMOTE HIGH-MOUNTAIN SITE	89
Article 2. CHANGES IN URBAN GAS-PHASE PERSISTENT ORGANIC POLLUTANTS DURING THE COVID-19 LOCKDOWN IN BARCELONA.....	113
Article 3. OCCURRENCE AND TEMPERATURE DEPENDENCE OF ATMOSPHERIC GAS-PHASE ORGANOPHOSPHATE ESTERS IN HIGH-MOUNTAIN AREAS (PYRENEES).....	133
Article 4. CHANGES AND DISTRIBUTION OF GAS-PHASE POLYCYCLIC AROMATIC HYDROCARBONS AND ORGANOCHLORINE COMPOUNDS IN A HIGH-MOUNTAIN GRADIENT OVER A THREE-YEAR PERIOD (PYRENEES, 2017–2020).....	151
Article 5. PASSIVE WATER SAMPLING AND AIR-WATER DIFFUSIVE EXCHANGE OF LONG-RANGE TRANSPORTED SEMI-VOLATILE ORGANIC POLLUTANTS IN HIGH-MOUNTAIN LAKES	179
3.4 Discussion	223
3.4.1 Performance and uncertainty of passive air and water sampling	223
3.4.2 Urban and alpine levels of atmospheric pollutants and perspectives for their reduction.....	233
3.4.3 The lingering threat of persistent organic pollutants.....	237
3.4.4 The growing issue of emerging organic pollutants	240
3.4.5 High mountains, sinks and secondary emitters of anthropogenic pollutants	243
3.4.6 Uncertainty in air–water exchange flux calculations	252
CHAPTER 4. Conclusions.....	261
References	269
Appendices	299
Appendix I: Lake catchments.....	301
Appendix II: Meteorology.....	305

Summary

Remote areas like high mountains offer the opportunity of studying the ultimate environmental fate of legacy and emerging anthropogenic chemicals that are part of a worldwide diffuse background layer of pollution. Compounds like polychlorinated biphenyls (PCBs), polycyclic aromatic hydrocarbons (PAHs), organophosphate esters (OPEs), and other organochlorine compounds like hexachlorobenzene (HCB) are semi-volatile species that have become ubiquitous by undergoing long-range atmospheric transport, penetrating other environmental compartments (e.g., water, soils, sediments, and biota), and often remaining unperturbed for decades due to their high resistance to degradation. Moreover, pollutant levels in these remote regions tend to be amplified because of cold-trapping, a series of physical and thermodynamical processes that occur at low temperatures and high altitudes. Toxic and deleterious effects to living organisms have been linked to the exposure to these chemicals, even in remote sites located away from any active emission sources. Thus, the accumulation of these substances constitutes a serious threat to wildlife and the health of some of the most fragile ecosystems of the world.

However, high mountains pose a set of unique challenges that complicate the assessment of pollutant levels, including their inaccessibility and the harsh environmental and meteorological conditions that they are subject to. This is why pollution studies in such locations are not abundant, especially for relatively novel compound groups like OPEs. In recent decades, the development and increase in popularity of passive samplers have allowed an alternative way of monitoring pollutants in a variety of environmental compartments, providing significant benefits for studies in remote sites. Passive samplers are inexpensive, easy to use, and do not require access to an energy supply. They can be deployed in environmental matrices like air or water for extended periods and allow the time-integrated assessment of average pollutant levels. Although data interpretation is not as straightforward as with traditional active sampling techniques, the versatility of passive samplers makes them invaluable tools for the study of global environmental pollution.

In the present work, passive samplers were used for the determination of semi-volatile and hydrophobic organic compounds in air and water from six alpine lacustrine

areas forming an altitudinal gradient in the Pyrenees, between 1619 and 2453 m above sea level. Polyurethane foam (PUF) was used for sampling the atmospheric gas-phase, and low-density polyethylene (LDPE) and silicone rubber (SR) were used for the dissolved phase of water. The performance of these samplers was assessed and the uncertainty in their measurements was determined. The deployment of these sampling devices has allowed to observe and study long-term changes in pollutant levels and their environmental fate and distribution between compartments at the studied sites. Additionally, passive air samplers were used for the study of pollutant levels in the city of Barcelona before and during the implementation of restrictive lockdown measures at the beginning of the COVID-19 global pandemic. The results of these measurements not only provided reference values for comparison between urban and alpine levels but also allowed the assessment of sudden changes in the composition of atmospheric organic pollution that were caused by an unprecedented halt in anthropogenic activities and emissions in an urban site.

The passive samplers showed adequate performance for the study of most considered compounds even in a remote environment with trace-level pollutant concentrations. In the air, the results agreed with those obtained from active sampling, and the performance of the passive sampler housings acting as effective wind and particle shields was validated. In water, two different sampler materials were tested, and their analysis was compared to independent measurements for testing the reliability of the results. Most chemicals showed adequate agreement between samplers and measurements, except for some OPEs which may have suffered from errors in the determination of their partitioning behaviour between sampler and water. Overall, the uncertainty in the results derived from passive sampling was sufficiently low for a confident assessment of average concentrations.

In Barcelona, most pollutants in the air presented concentrations up to more than two orders of magnitude higher than in the Pyrenees. As a result of lockdown restrictions, the concentrations of PAHs, PCBs, HCB, and other organochlorine compounds decreased by -60 to -91%. The levels of other air quality indicators like CO, PM₁₀, NO, and NO₂ also decreased by -28 to -76%. This shows the prominence of active sources in urban environments, even for already banned and restricted pollutants, and how an immediate halt in certain anthropogenic activities can lead to a substantial decrease in urban

pollution. On the other hand, OPE concentrations remained stable because their release is diffusive and does not depend directly on the type of activities that stopped with the restrictions.

Pollutant levels in air and water in the Pyrenees were generally low and comparable to or sometimes lower than those in other high mountains and remote sites. PCBs, HCB, and most compounds typically regarded as persistent were found at levels very similar to those reported over two decades ago in the same area. PAHs, less persistent than the rest, were detected at around half of their previously measured concentrations, agreeing with estimated reductions of their emissions. In the air, the concentrations of half of the studied pollutants significantly increased with temperature, showing the influence of re-volatilization from surfaces (e.g., soils, water, snow) on the atmospheric gas-phase concentrations of these compounds. These secondary emissions were especially prominent for OPEs and the heavier PCBs and PAHs, as their lower volatilities cause them to partition more prominently from the gas phase towards other environmental compartments. HCB and the lighter PAHs and PCBs did not present significant changes with temperature, as expected from their higher volatility and lower tendency for penetrating other compartments.

Diffusive exchange fluxes between air and water at the lakes revealed a general scenario of deposition of actively emitted pollutants like PAHs, slight deposition or near-equilibrium state for most PCBs, OPEs, and other chlorinated compounds, and slight volatilization of HCB and the diagenetically generated methylated PAH retene. Overall, it seems that this high-mountain region may be acting as a sink for several organic pollutants that accumulate in its soils, lakes, snow, and other surfaces. Some of these compounds may have reached equilibrium conditions between air and other compartments and may thus experience seasonal secondary emissions towards the atmosphere depending on the ambient temperature.

Resum

Les zones remotes com l'alta muntanya ofereixen l'oportunitat d'estudiar el destí ambiental final de substàncies químiques antropogèniques històriques i emergents que formen part d'una capa difusa de contaminació de fons a tot el món. Compostos com els policlorobifenils (PCBs), els hidrocarburs aromàtics policíclics (PAHs), els èsters organofosforats (OPEs) i altres compostos organoclorats com l'hexaclorobenzè (HCB) són espècies semi-volàtils que s'han convertit en ubiqües com a conseqüència del transport atmosfèric de llarg abast, penetrant altres compartiments ambientals (per exemple, aigua, sòls, sediments i biota) i sovint romanent impertorbables durant dècades a causa de la seva alta resistència a la degradació. A més, els nivells de contaminants en aquestes regions remotes tendeixen a amplificar-se a causa del “*cold-trapping*”, una sèrie de processos físics i termodinàmics que es produeixen a baixes temperatures i altituds elevades. L'exposició a aquestes substàncies químiques s'ha relacionat amb una sèrie d'efectes tòxics i nocius per a organismes vius, fins i tot en llocs remots situats lluny de fonts d'emissió actives. Així, la seva acumulació constitueix una greu amenaça per a la salut d'alguns dels ecosistemes més fràgils del món i dels organismes que els habiten.

Tanmateix, l'alta muntanya planteja un conjunt de reptes únics que dificulten l'avaluació dels nivells de contaminants, incloses la seva inaccessibilitat i les seves dures condicions ambientals i meteorològiques. Per això els estudis de contaminació en aquests llocs no són abundants, especialment per a grups de compostos relativament nous com els OPEs. En les darreres dècades, el desenvolupament i la popularització dels mostrejadors passius ha ofert una alternativa per al monitoratge de contaminants en una varietat de compartiments ambientals, proporcionant beneficis significatius per als estudis en zones remotes. Els mostrejadors passius són econòmics, fàcils d'utilitzar i no requereixen accés a fonts d'energia. Es poden desplegar en matrius ambientals com l'aire o l'aigua durant períodes de temps prolongats i permeten l'avaluació integrada en el temps dels nivells mitjans de contaminants. Tot i que la interpretació de dades no és tan senzilla com amb les tècniques tradicionals de mostreig actiu, la versatilitat dels mostrejadors passius els converteix en eines inestimables per a l'estudi de la contaminació ambiental global.

En aquest treball, s'han utilitzat mostrejadors passius per a la determinació de compostos orgànics semi-volàtils i hidròfobs en aire i aigua de sis zones lacustres alpines formant un gradient altitudinal als Pirineus, entre 1619 i 2453 m sobre el nivell del mar. S'ha utilitzat escuma de poliuretà (PUF) per a la presa de mostres de la fase gasosa de l'aire, i polietilè de baixa densitat (LDPE) i silicona (SR) per a la fase dissolta de l'aigua. S'ha avaluat el rendiment d'aquests mostrejadors i s'ha determinat la incertesa en les seves mesures. La implementació d'aquests sistemes de mostreig ha permès observar i estudiar els canvis en els nivells de contaminants a llarg termini, així com el seu destí ambiental i distribució entre compartiments a la zona d'estudi. A més, s'han utilitzat mostrejadors passius d'aire per a l'estudi dels nivells de contaminants a la ciutat de Barcelona abans i durant la implantació de mesures restrictives de confinament a l'inici de la pandèmia global de la COVID-19. Els resultats d'aquestes mesures no només han proporcionat valors de referència per a la comparació entre nivells urbans i alpins, sinó que també han permès avaluar els canvis sobtats en la composició de la contaminació orgànica atmosfèrica provocats per una aturada sense precedents de les activitats i emissions antropogèniques en una zona urbana.

El rendiment dels mostrejadors passius ha estat adequat per a l'estudi de la majoria de compostos considerats, fins i tot en un entorn remot amb concentracions a nivell de traça. A l'aire, els resultats coincideixen amb els obtinguts per mostreig actiu i s'ha validat el rendiment de les cobertes dels mostrejadors com a protecció efectiva del vent i de partícules. En aigua, s'han provat dos materials diferents i s'han comparat els resultats amb anàlisis independents per determinar-ne la fiabilitat. Les mesures de la majoria de compostos han mostrat un grau de concordança adequat entre mostrejadors i anàlisis, excepte per alguns OPEs que poden haver patit errors en la determinació del seu comportament de partició entre mostrejador i aigua. En general, la incertesa dels resultats derivats del mostreig passiu ha sigut prou baixa per a una avaluació segura de les concentracions.

A Barcelona, la majoria de contaminants a l'aire han presentat concentracions fins a més de dos ordres de magnitud superiors a les dels Pirineus. Com a resultat de les restriccions del confinament, les concentracions de PAHs, PCBs, HCB i altres compostos organoclorats van disminuir entre un -60 i un -91%. Els nivells d'altres indicadors de qualitat de l'aire com CO, PM₁₀, NO i NO₂ també van disminuir entre -28 i -76%. Això

demostra el protagonisme que tenen les fonts actives en entorns urbans, fins i tot per a contaminants ja prohibits i restringits, i com l'aturada total de determinades activitats antropogèniques pot provocar una disminució substancial de la contaminació urbana. D'altra banda, les concentracions d'OPEs es van mantenir estables degut probablement a que el seu alliberament és difusiu i no depèn directament del tipus d'activitats que es van aturar amb les restriccions.

Els nivells de contaminants trobats a l'aire i l'aigua dels Pirineus són generalment baixos i comparables o de vegades inferiors als d'altres muntanyes i llocs remots. Les concentracions de PCB, HCB i la majoria de compostos normalment considerats persistents són molt similars a les descrites fa més de dues dècades a la mateixa zona. Els PAHs, menys persistents que la resta, s'han detectat a concentracions al voltant de la meitat d'aquelles mesurades anteriorment, fet que coincideix amb les reduccions estimades de les seves emissions. A l'aire, les concentracions de la meitat dels contaminants estudiats van augmentar significativament amb la temperatura, tot posant de manifest la influència de la re-volatilització des de superfícies (per exemple, sòls, aigua o neu) sobre els seus nivells a la fase gas de l'aire. Aquestes emissions secundàries van ser especialment destacades per als OPEs i per als PCBs i PAHs més pesats, ja que les seves volatilitats baixes fan que la seva partició des de la fase gas cap a altres compartiments ambientals sigui més alta. Els nivells d'HCB i dels PAHs i PCBs més lleugers no van presentar canvis significatius amb la temperatura, tal i com s'esperava segons les seves volatilitats més elevades i la seva tendència menor a penetrar altres compartiments.

Els fluxos d'intercanvi difús entre aire i aigua als llacs revelen un escenari general de deposició de contaminants emesos activament com els PAHs, deposició lleu o gairebé equilibri per a la majoria de PCBs, OPEs i altres compostos clorats, i una lleugera volatilització de l'HCB i el PAH metilat retè. En general, sembla que aquesta regió d'alta muntanya pot estar actuant com a receptor de diversos contaminants orgànics que s'acumulen als seus sòls, llacs, neu i altres superfícies. Alguns d'aquests compostos poden haver assolit condicions d'equilibri entre l'aire i altres compartiments i, per tant, poden experimentar una emissió secundària estacional cap a l'atmosfera segons sigui la temperatura ambient.

List of Tables

Table 1. List of compounds and properties. M: molar mass (g mol^{-1}); V: molar volume ($\text{cm}^3 \text{mol}^{-1}$); H_{298} : Henry's Law constant at 25 °C ($\text{atm m}^3 \text{mol}^{-1}$); partition coefficients at 25 °C: $\log K_{\text{OA}}$ (octanol–air), $\log K_{\text{OW}}$ (octanol–water), $\log K_{\text{PUF-A}}$ (polyurethane foam–air), $K_{\text{LDPE-W}}$ (low-density polyethylene–water), $K_{\text{SR-W}}$ (silicone rubber–water).....	14
Table 2. Environmental half-lives of most SVOCs considered in the present work. All values from Howard et al. (1991), except for PCBs from Sinkkonen and Paasivirta (2000) and OPEs from Liagkouridis et al. (2015). Units in hours (h), days (d), and years (y).....	239

List of Figures

Figure 1. Global distribution of persistent organic pollutants. Reprinted with permission from Wania and Mackay (1996). Copyright 1996 American Chemical Society.	6
Figure 2. Mountain cold-trapping of persistent organic pollutants and daytime mountain wind cycles. Reprinted with permission from Daly and Wania (2005). Copyright 2005 American Chemical Society. ..	7
Figure 3. Polychlorinated biphenyls studied in the present work.	16
Figure 4. Organochlorine compounds studied in the present work.....	18
Figure 5. Polycyclic aromatic hydrocarbons studied in the present work.....	19
Figure 6. Organophosphate esters studied in the present work.....	21
Figure 7. Moving average (7 days) of the changes in population movement trends over time during and after the 2020 lockdown in Barcelona, Spain. Figure created using aggregated location data by Google LLC “Google COVID-19 Community Mobility Reports”.....	44
Figure 8. Uptake phases of passive sampling through first-order uptake kinetics, where C_{PSM} is the concentration of compound taken up by the passive sampler medium and t is the exposure time.	51
Figure 9. Dissipation profile of a PRC over time through first order release kinetics.	55
Figure 10. PRC retained fractions as a function of $\log(K'_{\text{PUF-A}})$	56
Figure 11. PRC retained fractions as a function of $\log(K_{\text{PWS-W}}/M^{-0.47})$ (left), where the curved black line is an NLS fit for a water boundary layer-controlled uptake sampling rate, and difference between experimental and calculated retained fractions (right).....	58
Figure 12. Pyrenean lakes studied in the present work. Base map: Produced Work by the OpenStreetMap Foundation using OpenStreetMap data under the Open Database License, © OpenStreetMap contributors.	59
Figure 13. Lake catchment areas and terrain coverage and habitat data (left) and relative habitat area within each catchment area (right). Note that Llebreta’s catchment area includes all other surrounding delineated catchments. Figure created using data from Servei de Planificació de l’Entorn Natural, Direcció General de Polítiques Ambientals i Medi Natural (Cartografia dels hàbitats d’interès comunitari a Catalunya, versió 2 (2018), last updated 30/11/2018) (Generalitat de Catalunya, Departament de Territori i Sostenibilitat). .	61
Figure 14. Estany Llong (top) and Estany de Llebreta (bottom).....	62
Figure 15. Estanh Redon (top) and Estany de Sarradé (bottom).....	63
Figure 16. Estany de la Collada (top) and Estany de Dellui (bottom).	64
Figure 17. Moving average (48 h) of the air temperatures recorded every 30 min in Estanh Redon (top) and Barcelona (bottom) over the full duration of the study. Figure created using data from Xarxa d’Estacions	

Meteorològiques Automàtiques (XEMA) del Servei Meteorològic de Catalunya (METEOCAT) (Dades meteorològiques de la XEMA, last updated 06/09/2022) (Generalitat de Catalunya, Departament de Territori i Sostenibilitat)..... 66

Figure 18. Wind rose of the average distribution of wind speeds and directions at Estanh Redon (left) and Barcelona (right) between 2010 and 2019. Wind roses from Xarxa d'Estacions Meteorològiques Automàtiques (XEMA) del Servei Meteorològic de Catalunya (METEOCAT) (Dades meteorològiques de la XEMA, last updated 06/09/2022) (Generalitat de Catalunya, Departament de Territori i Sostenibilitat). Base maps: Produced Work by the OpenStreetMap Foundation using OpenStreetMap data under the Open Database License, © OpenStreetMap contributors. 66

Figure 19. Data logger (Tinytag Plus 2, yellow box) deployed at each studied site for registering the ambient temperature and relative humidity for the duration of the sampling periods. 67

Figure 20. Moving averages (48 h) of air temperature (top) and relative humidity (bottom) measured every 30 min during air sampling period PAS I. Figure created using data collected with data loggers. 67

Figure 21. Average temperature at the studied sites as a function of their altitude (left) and daily average temperature profiles (right, shown for sampling period PAS I). Figure created using data collected with data loggers co-deployed at each site with the passive samplers and data from Xarxa d'Estacions Meteorològiques Automàtiques (XEMA) del Servei Meteorològic de Catalunya (METEOCAT) (Dades meteorològiques de la XEMA, last updated 06/09/2022) (Generalitat de Catalunya, Departament de Territori i Sostenibilitat)..... 68

Figure 22. Cluster trajectory analysis (72 h backwards, one trajectory every 6 h from 09/2018 to 08/2019, total of 1444 trajectories) for air trajectories ending at the studied area. The labels indicate cluster number (1 to 5) and percentage of total trajectories grouped. Figure created using NOAA's HYSPLIT transport and dispersion model (National Oceanic and Atmospheric Administration, USA). 70

Figure 23. Examples of air trajectories grouped in the cluster analysis of 09/2018 to 08/2019. Cluster 1 (left) presents a regional component and cluster 4 (right) presents a North-Atlantic component. Calculations performed and figures created using NOAA's HYSPLIT transport and dispersion model (National Oceanic and Atmospheric Administration, USA). 70

Figure 24. Polyurethane foam (PUF) passive air sampler disks..... 71

Figure 25. Diagram of a vertical cross-section of the passive air sampler housing structure..... 72

Figure 26. Passive air samplers deployed at Estany de la Collada. 73

Figure 27. Low-density polyethylene (LDPE, left) and silicone rubber (SR, right) passive water sampler sheets..... 74

Figure 28. Passive water sampler sheets mounted onto a steel grill before (Estany de Dellui, left) and after (Estany de Llebrete, right) deployment. Note that, although oxidation of the grills was inevitable in some lakes, rust does not affect the extraction of the samplers nor the analysis of pollutants in any way. 75

Figure 29. Diagram of the deployed passive water sampling structure under the water surface..... 76

Figure 30. Passive water samplers deployed at Estany de Sarradé. 78

Figure 31. Molecular diffusivities in water (D_{iW}) predicted for several studied PAHs, OCs, and OPEs at v_W 1.5×10^{-2} $\text{cm}^2 \text{s}^{-1}$, represented against their molar volume (V_i) and molar mass (M_i). 82

Figure 32. Variation of the kinematic viscosity of water (ν_W) with temperature (T). Figure created using ν_W and T values from Schwarzenbach et al. (2005). 83

Figure 33. Molecular diffusivities in air (D_{iA}) predicted for several studied PAHs, OCs, and OPEs at 298.15 K and 800 atm, represented against their molar volume (V_i) and molar mass (M_i)..... 84

Figure 34. Variation with lake area (LA, m^2) of the mass transfer coefficient of CO_2 through the stagnant water layer (k_{CO_2W}). Figure created for a fixed space integration value $\text{SIN} = 0.999$ and wind speed $u_{10} = 5$ m s^{-1} using the parametrization shown in Eq. 31 from Klaus and Vachon (2020). 85

- Figure 35. Moving average (48 h) of air temperature (top) and relative humidity (bottom) measured every 30 min during a portion of passive air sampling period PAS II at Estany de Llebreta and Estany de Dellui. Figure created using data collected with data loggers..... 224
- Figure 36. Example NLS regressions of PRC retained fractions in passive water sampling (PWS, top) and passive air sampling (PAS, bottom). The difference between experimental and calculated retained fractions is shown in the charts to the right. 229
- Figure 37. Prediction of OPE K_{PWS-W} using correlations between a) experimental LDPE and SR coefficients and pp-LFER models for b) SR and c) LDPE polymers. Figure created using experimental K_{LDPE-W} and K_{SR-W} values from Smedes (2019, 2018) and Smedes et al. (2009). 232
- Figure 38. Pollutant concentrations in the air of Barcelona before and during lockdown compared to median levels detected in the Pyrenees (the whiskers show maximum and minimum period average concentrations). 235
- Figure 39. Air–surface phase change enthalpies measured in laboratory conditions (black) and estimated from statistically significant temperature regressions of gas-phase concentrations in the Pyrenees (white), regressed against subcooled liquid vapour pressures ($\log p_L^0$). Figure created using $\log p_L^0$ values from Allen et al. (1999), Brommer et al. (2014), Delle Site (1997), and Falconer and Bidleman (1994), and laboratory ΔH_{AS} from Nakajoh et al. (2006), Okeme et al. (2020), Panneerselvam et al. (2007), Roux et al. (2008), and Spijksma et al. (1994). 246
- Figure 40. Sum of PCB, PAH (only gas-phase, low molecular weight –LMW– compounds except for Ret), and OPE (excluding contaminated outliers) atmospheric gas-phase concentrations regressed against the reciprocal of the absolute temperature. 247
- Figure 41. Sum of PCB, PAH (excluding Ret), and OPE atmospheric gas-phase concentrations regressed against the reciprocal of the absolute temperature. Low molecular weight (LMW, Fle to Chr+TriPh) and high molecular weight (HMW, B[b]Flu to B[ghi]pery) PAHs are separated for comparison with atmospheric PAHs in the gas phase. 249
- Figure 42. Temperature correction methods for Henry’s Law constants ($\log H$) of PCB118, HCB, Flu, and TCIPP. Figures created using $\log H$ values and temperature correction relationships from Bamford et al. (1999), Cetin et al. (2006), Hulscher et al. (1992), Paasivirta et al. (1999), Parnis et al. (2015), and Tateya et al. (1988). 257
- Figure 43. A selection of calculation methods reported in the last three decades for mass transfer coefficients in water of CO_2 (k_{CO_2-w}) depending on wind speed (u_{10}). Figure created using relationships from Cole and Caraco (1998), Crusius and Wanninkhof (2003), González-Gaya et al. (2016), Guérin et al. (2007), Klaus and Vachon (2020), MacIntyre et al. (2010), Nightingale et al. (2000), Vachon and Prairie (2013), and Wanninkhof and Bliven (1991). Klaus and Vachon’s (2020) models labelled *a* to *d* are, respectively: linear regression with input variables Lake Area (LA) and space integration (SIN), linear LA, power regression with LA SIN, and power LA..... 258
- Figure 44. Digital elevation model (DEM) of the area of study (ASTGTM2-N42E000) sourced from the Advanced Spaceborne Thermal Emission and Reflection Radiometer (ASTER) global digital elevation model (GDEM) (ASTGTM v002, doi.org/10.5067/ASTER/ASTGTM.002). The image has been brightened for clarity. ASTER GDEM is a product of the Ministry of Economy, Trade, and Industry (METI) of Japan and the United States National Aeronautics and Space Administration (NASA)..... 301
- Figure 45. Flow direction grid for the calculation of water drainage pathways in the area of study. Each colour represents a different slope direction. The lakes and main drainage streams have been superimposed for reference. Calculations performed and figure created using the Arc Hydro data model and toolset in ArcGIS (Esri, Redlands, CA, USA). Calculations performed using ASTER GDEM data (ASTGTM v002, doi.org/10.5067/ASTER/ASTGTM.002). ASTER GDEM is a product of the Ministry of Economy, Trade, and Industry (METI) of Japan and the United States National Aeronautics and Space Administration (NASA)..... 302
- Figure 46. Water drainage pathways displayed over the DEM and used for the calculation of lake catchment areas. The lakes and main drainage streams have been superimposed for reference. Calculations performed and figure created using the Arc Hydro data model and toolset in ArcGIS (Esri, Redlands, CA, USA).

Calculations performed using ASTER GDEM data (ASTGTM v002, doi.org/10.5067/ASTER/ASTGTM.002). ASTER GDEM is a product of the Ministry of Economy, Trade, and Industry (METI) of Japan and the United States National Aeronautics and Space Administration (NASA)..... 303

Figure 47. Lake catchment areas and soil coverage habitats: water (blue), shrubs (light green), forests (dark green), rock (beige), wetlands (brown), urban (maroon), industrial/other (pink). The lakes and main drainage streams have been superimposed for reference. Figure created using the Arc Hydro data model and toolset in ArcGIS (Esri, Redlands, CA, USA). Figure created using data from Servei de Planificació de l'Entorn Natural, Direcció General de Polítiques Ambientals i Medi Natural (Cartografia dels hàbitats d'interès comunitari a Catalunya, versió 2 (2018), last updated 30/11/2018) (Generalitat de Catalunya, Departament de Territori i Sostenibilitat). 304

Figure 48. Average (black), maximum (red), and minimum (blue) temperature recorded every 30 min at Estanh Redon (top, 2247 m), Boí (center, 2535 m), and Barcelona (bottom, 79 m) during all sampling periods. Figure created using data from Xarxa d'Estacions Meteorològiques Automàtiques (XEMA) del Servei Meteorològic de Catalunya (METEOCAT) (Dades meteorològiques de la XEMA, last updated 06/09/2022) (Generalitat de Catalunya, Departament de Territori i Sostenibilitat). 305

Figure 49. Average (black), maximum (red), and minimum (blue) relative humidity recorded every 30 min at Estanh Redon (top, 2247 m), Boí (center, 2535 m), and Barcelona (bottom, 79 m) during all sampling periods. Figure created using data from Xarxa d'Estacions Meteorològiques Automàtiques (XEMA) del Servei Meteorològic de Catalunya (METEOCAT) (Dades meteorològiques de la XEMA, last updated 06/09/2022) (Generalitat de Catalunya, Departament de Territori i Sostenibilitat). 306

Figure 50. Average (black), maximum (red), and minimum (blue) atmospheric pressure recorded every 30 min at Estanh Redon (top, 2247 m) and Barcelona (bottom, 79 m) during all sampling periods. Data from Boí (center) not available. Figure created using data from Xarxa d'Estacions Meteorològiques Automàtiques (XEMA) del Servei Meteorològic de Catalunya (METEOCAT) (Dades meteorològiques de la XEMA, last updated 06/09/2022) (Generalitat de Catalunya, Departament de Territori i Sostenibilitat). 307

Figure 51. Precipitation recorded every 30 min (black) and accumulated precipitation (blue) at Estanh Redon (top, 2247 m), Boí (center, 2535 m), and Barcelona (bottom, 79 m) during all sampling periods. Figure created using data from Xarxa d'Estacions Meteorològiques Automàtiques (XEMA) del Servei Meteorològic de Catalunya (METEOCAT) (Dades meteorològiques de la XEMA, last updated 06/09/2022) (Generalitat de Catalunya, Departament de Territori i Sostenibilitat)..... 308

Figure 52. Snow height recorded every 30 min at Estanh Redon (top, 2247 m) and Boí (center, 2535 m) during all sampling periods. Data from Barcelona (center) not available but assumed to remain at 0 cm. Figure created using data from Xarxa d'Estacions Meteorològiques Automàtiques (XEMA) del Servei Meteorològic de Catalunya (METEOCAT) (Dades meteorològiques de la XEMA, last updated 06/09/2022) (Generalitat de Catalunya, Departament de Territori i Sostenibilitat)..... 309

Figure 53. Average (black) and maximum (red) wind speed recorded every 30 min at Estanh Redon (top, 2247 m), Boí (center, 2535 m), and Barcelona (bottom, 79 m) during all sampling periods. Figure created using data from Xarxa d'Estacions Meteorològiques Automàtiques (XEMA) del Servei Meteorològic de Catalunya (METEOCAT) (Dades meteorològiques de la XEMA, last updated 06/09/2022) (Generalitat de Catalunya, Departament de Territori i Sostenibilitat). 310

Figure 54. Average solar irradiance recorded every 30 min at Estanh Redon (top, 2247 m), Boí (center, 2535 m), and Barcelona (bottom, 79 m) during all sampling periods. Figure created using data from Xarxa d'Estacions Meteorològiques Automàtiques (XEMA) del Servei Meteorològic de Catalunya (METEOCAT) (Dades meteorològiques de la XEMA, last updated 06/09/2022) (Generalitat de Catalunya, Departament de Territori i Sostenibilitat). 311

Figure 55. Wind rose representing the average distribution of wind speeds and directions over the last decade (2010–2019) at Estanh Redon (2247 m). Wind rose from Xarxa d'Estacions Meteorològiques Automàtiques (XEMA) del Servei Meteorològic de Catalunya (METEOCAT) (Dades meteorològiques de la XEMA, last updated 06/09/2022) (Generalitat de Catalunya, Departament de Territori i Sostenibilitat).

Base map: Produced Work by the OpenStreetMap Foundation using OpenStreetMap data under the Open Database License, © OpenStreetMap contributors.	312
Figure 56. Wind rose representing the average distribution of wind speeds and directions over the last decade (2010–2019) at Boi (2535 m). Wind rose from Xarxa d’Estacions Meteorològiques Automàtiques (XEMA) del Servei Meteorològic de Catalunya (METEOCAT) (Dades meteorològiques de la XEMA, last updated 06/09/2022) (Generalitat de Catalunya, Departament de Territori i Sostenibilitat). Base map: Produced Work by the OpenStreetMap Foundation using OpenStreetMap data under the Open Database License, © OpenStreetMap contributors.	313
Figure 57. Wind rose representing the average distribution of wind speeds and directions over the last decade (2010–2019) at Barcelona (79 m). Wind rose from Xarxa d’Estacions Meteorològiques Automàtiques (XEMA) del Servei Meteorològic de Catalunya (METEOCAT) (Dades meteorològiques de la XEMA, last updated 06/09/2022) (Generalitat de Catalunya, Departament de Territori i Sostenibilitat). Base map: Produced Work by the OpenStreetMap Foundation using OpenStreetMap data under the Open Database License, © OpenStreetMap contributors.	314
Figure 58. Moving average (48 h) of air temperature (top) and relative humidity (bottom) measured every 30 min during passive air sampling period PAS I. Figure created using data collected with data loggers co-deployed at each site with the passive samplers.	315
Figure 59. Moving average (48 h) of air temperature (top) and relative humidity (bottom) measured every 30 min during passive air sampling period PAS II. Figure created using data collected with data loggers co-deployed at each site with the passive samplers.	315
Figure 60. Moving average (48 h) of air temperature (top) and relative humidity (bottom) measured every 30 min during passive air sampling period PAS III. Figure created using data collected with data loggers co-deployed at each site with the passive samplers.	316
Figure 61. Moving average (48 h) of air temperature (top) and relative humidity (bottom) measured every 30 min during passive air sampling period PAS IV. Figure created using data collected with data loggers co-deployed at each site with the passive samplers.	316
Figure 62. Moving average (48 h) of air temperature (top) and relative humidity (bottom) measured every 30 min during passive air sampling period PAS V. Figure created using data collected with data loggers co-deployed at each site with the passive samplers.	317
Figure 63. Daily average air temperature profiles at the studied sites over the five passive air sampling periods. Figure created using data collected with data loggers co-deployed at each site with the passive samplers and data from Xarxa d’Estacions Meteorològiques Automàtiques (XEMA) del Servei Meteorològic de Catalunya (METEOCAT) (Dades meteorològiques de la XEMA, last updated 06/09/2022) (Generalitat de Catalunya, Departament de Territori i Sostenibilitat).	318
Figure 64. Trajectory frequency plot (72 h backwards, one trajectory every 6 h from 09/2017 to 08/2018) for air trajectories ending at the studied area (top) and cluster trajectory plot (bottom). Calculations performed and figures created using NOAA’s HYSPLIT transport and dispersion model (National Oceanic and Atmospheric Administration, USA).	319
Figure 65. Trajectory frequency plot (72 h backwards, one trajectory every 6 h from 09/2018 to 08/2019) for air trajectories ending at the studied area (top) and cluster trajectory plot (bottom). Calculations performed and figures created using NOAA’s HYSPLIT transport and dispersion model (National Oceanic and Atmospheric Administration, USA).	320
Figure 66. Trajectory frequency plot (72 h backwards, one trajectory every 6 h from 09/2019 to 08/2020) for air trajectories ending at the studied area (top) and cluster trajectory plot (bottom). Calculations performed and figures created using NOAA’s HYSPLIT transport and dispersion model (National Oceanic and Atmospheric Administration, USA).	321
Figure 67. Backwards (72 h) air trajectories forming each cluster in the cluster trajectory plot from 09/2017 to 08/2018 for air trajectories ending at the studied area. Calculations performed and figures created using NOAA’s HYSPLIT transport and dispersion model (National Oceanic and Atmospheric Administration, USA).	322

Figure 68. Backwards (72 h) air trajectories forming each cluster in the cluster trajectory plot from 09/2018 to 08/2019 for air trajectories ending at the studied area. Calculations performed and figures created using NOAA's HYSPLIT transport and dispersion model (National Oceanic and Atmospheric Administration, USA). 323

Figure 69. Backwards (72 h) air trajectories forming each cluster in the cluster trajectory plot from 09/2019 to 08/2020 for air trajectories ending at the studied area. Calculations performed and figures created using NOAA's HYSPLIT transport and dispersion model (National Oceanic and Atmospheric Administration, USA). 324

Abbreviations and variables

Abbreviations

<i>AAS</i>	Active air sampling
<i>AQUA-GAPS</i>	Global Aquatic Passive Sampling network
<i>ASTER</i>	Advanced Spaceborne Thermal Emission and Reflection Radiometer
<i>BDL</i>	Below detection limits
<i>COVID-19</i>	Coronavirus disease 2019
<i>DDD</i>	Dichlorodiphenyldichloroethane
<i>DDE</i>	Dichlorodiphenyldichloroethylene
<i>DDT</i>	Dichlorodiphenyltrichloroethane
<i>DEM</i>	Digital elevation model
<i>DEQ</i>	Degree of equilibrium
<i>EEA</i>	European Environmental Agency
<i>EPA</i>	Environmental Protection Agency (USA)
<i>EU</i>	Expanded uncertainty
<i>GAPS</i>	Global Atmospheric Passive Sampling network
<i>GC</i>	Gas chromatography
<i>GDEM</i>	Global digital elevation model
<i>GFF</i>	Glass fibre filter
<i>HCB</i>	Hexachlorobenzene
<i>HCH</i>	Hexachlorocyclohexane
<i>HMW</i>	High molecular weight
<i>HOC</i>	Hydrophobic organic compound
<i>HPLC</i>	High-performance liquid chromatography
<i>LDPE</i>	Low-density polyethylene
<i>LMW</i>	Low molecular weight
<i>LOQ</i>	Limit of quantification
<i>MCR-ALS</i>	Multivariate curve resolution–alternating least squares
<i>METEOCAT</i>	Servei Meteorològic de Catalunya (Catalunya)
<i>METI</i>	Ministry of Economy, Trade and Industry (Japan)
<i>MRM</i>	Multiple reaction monitoring
<i>MS</i>	Mass spectrometry
<i>MS/MS</i>	Tandem mass spectrometry
<i>NASA</i>	National Aeronautics and Space Administration (USA)
<i>NCAR</i>	National Center for Atmospheric Research (USA)
<i>NCEP</i>	National Centers for Environmental Prediction (USA)
<i>NLS</i>	Nonlinear least squares
<i>NOAA</i>	National Oceanic and Atmospheric Administration (USA)
<i>OPE</i>	Organophosphate ester
<i>OPFR</i>	Organophosphate flame retardant
<i>P</i>	Phase (e.g., air or water)
<i>PAH</i>	Polycyclic aromatic hydrocarbon
<i>PAS</i>	Passive air sampler
<i>PBDE</i>	Polybrominated diphenyl ether
<i>PCA</i>	Principal component analysis

<i>PCB</i>	Polychlorinated biphenyl
<i>PCDD/PCDF</i>	Polychlorinated dibenzo-p-dioxins and dibenzofurans
<i>PeCB</i>	Pentachlorobenzene
<i>PM</i>	Particulate matter
<i>PMF</i>	Positive matrix factorization
<i>PMOC</i>	Persistent and mobile organic compound
<i>POCIS</i>	Polar organic chemical integrative sampler
<i>POP</i>	Persistent organic pollutant
<i>pp-LFER</i>	Poly-parameter linear free energy relationship
<i>PRC</i>	Performance reference compound
<i>PSM</i>	Passive sampler medium
<i>PUF</i>	Polyurethane foam
<i>PWS</i>	Passive water sampler
<i>RECETOX</i>	Research Centre for Toxic Compounds in the Environment
<i>RSD</i>	Relative standard deviation
<i>SARS-CoV-2</i>	Severe acute respiratory syndrome coronavirus 2
<i>SIM</i>	Selected ion monitoring
<i>SIP</i>	Sorbent impregnated polyurethane foam
<i>SPMD</i>	Semipermeable membrane devices
<i>SPME</i>	Solid phase microextraction
<i>SR</i>	Silicone rubber
<i>SVOC</i>	Semi-volatile organic compound
<i>WHO</i>	World Health Organization
<i>XEMA</i>	Xarxa d'Estacions Meteorològiques Automàtiques (Catalunya)

Variables

Dimensions: L (length), M (mass), T (time), Mol (amount of substance), K (temperature).

a_D	Exponential term for the calculation of air-side mass transfer coefficients	–
A_H	Hydrogen bond acidity	–
A_{PSM}	Area of a PSM	L^2
A_{PUF}	Area of the PUF disk	L^2
a_{Sc}	Exponential term for the calculation of water-side mass transfer coefficients	–
B	Hydrodynamic constant for the calculation of water sampling rates	–
B_H	Hydrogen bond basicity	–
C_A	Concentration in the atmospheric gas phase	$M L^{-3}$
C_{OH}	Concentration of hydroxyl radicals in the atmosphere	$Mol L^{-3}$
C_P	Concentration in a phase	$M L^{-3}$
$C_{PRC,0}$	Amount of PRC in the non-exposed blank	M
$C_{PRC,t}$	Amount of PRC retained by the sampler after exposure	M
C_{PSM}	Concentration in the PSM	$M L^{-3}$
C_S	Concentration in a surface	$M L^{-3}$
C_W	Concentration in the aquatic dissolved phase	$M L^{-3}$

D_A	Molecular diffusivity in air	$L^2 T^{-1}$
D_{film}	Effective film thickness of the PUF disk	L
D_W	Molecular diffusivity in water	$L^2 T^{-1}$
E	Excess molar refraction	–
F_{AW}	Air–water diffusive exchange flux	$M L^{-2} T^{-1}$
F_{deg}	Atmospheric degradation flux	$M L^{-2} T^{-1}$
H	Henry's Law constant	$M L^2 T^{-2} Mol^{-1}$
h_{ABL}	Height of the atmospheric boundary layer	L
j	Diffusive flux	$M L^{-2} T^{-1}$
k_A	Air-side mass transfer coefficient	$L T^{-1}$
K_{AS}	Air–surface partition coefficient	–
k_{AW}	Overall air–water exchange velocity	$L T^{-1}$
K_{AW}	Equilibrium air–water partition coefficient	–
k_e	Exchange rate constant of the uptake of a compound in a PSM over time	T^{-1}
K_{LDPE-W}	LDPE–water partition coefficient	–
k_O	Overall PSM–Phase mass transfer coefficient	$L T^{-1}$
K_{OA}	Octanol–air partition coefficient	–
k_{OH}	Atmospheric hydroxylation rate	$L^3 Mol^{-1} T^{-2}$
K_{OW}	Octanol–water partition coefficient	–
k_P	Phase-side mass transfer coefficient	$L T^{-1}$
k_{PSM}	PSM-side mass transfer coefficient	$L T^{-1}$
K_{PSM-P}	PSM–Phase partition coefficient	–
K_{PUF-A}	PUF–air partition coefficient	$L^3 M^{-1}$
K'_{PUF-A}	Density-corrected PUF–air partition coefficient	–
K_{PWS-W}	PWS–water partition coefficient	–
K_{SR-W}	SR–water partition coefficient	–
k_W	Water-side mass transfer coefficient	$L T^{-1}$
LA	Lake area	L^2
M	Molar mass	$M Mol^{-1}$
m_{PWS}	Mass of a PWS sampler	M
n_{PSM}	Amount of pollutant sequestered by the PSM	M
n_{PUF}	Amount of pollutant sequestered by the PUF	M
n_{PWS}	Amount of pollutant sequestered by the PWS	M
p	Atmospheric pressure	$M L^{-1} T^{-2}$
R	Ideal gas constant	$M L^2 T^{-2} K^{-1}$
R_S	Sampling rate	$L^3 T^{-1}$
S	Dipolarity/polarizability	–
Sc	Schmidt Number	–
SIN	Space integration parameter for the calculation of water-side mass transfer coefficients of CO ₂	–
t	Time	T
T	Temperature	K
u_{10}	Wind speed 10 m above the air–water exchange interface	$L T^{-1}$
u_z	Wind speed z m above the air–water exchange interface	$L T^{-1}$
V	Molar volume	$L^3 Mol^{-1}$
$V_{/100}$	Molar volume divided by 100	–

V_{ef}	Effective sampled volume	L^3
V_{PSM}	Volume of a PSM	L^3
V_{PUF}	Volume of the PUF disk	L^3
z	Altitude of the wind speed measurement	L
δ_{PUF}	Density of the PUF	$M L^{-3}$
ΔH_{AS}	Enthalpy of phase change between air and surfaces	$M L^2 T^{-2}$
ΔU_{AS}	Internal energy of phase change between air and surfaces	$M L^2 T^{-2}$
ν	Coefficient of kinematic viscosity	$L^2 T^{-1}$
ρ	Mass density	$M L^{-3}$
$\phi_{R,P}$	Particle-phase sampling rate as a fraction of the gas-phase sampling rate	—



Estany de Sarradé
(42.564°N, 0.896°E, 2123 m)

Estany de Llebreta
(42.549°N, 0.888°E, 1619 m)

CHAPTER 1

Introduction

1.1 Diffuse pollution

Diffuse pollution is the result of the dispersion through the environment of pollutants that mostly originate from anthropogenic activities. Pollutants are emitted in various ways from a myriad of sources: they are industrial by-products directly released into rivers and oceans, pesticides and other substances that percolate into soils and groundwaters because of agricultural use, fumes dispersed into the air from fuel combustion processes, residues from waste treatment and disposal operations, accidental spills of chemical substances, or manufacturing additives emanating from human-made materials to name a few. Some substances that are also considered pollutants sometimes have a natural origin, as is the case for products of combustion of organic matter in wildfires and volcanic emissions. Pollutant concentrations tend to be highest close to their sources, but many chemicals have the ability to undergo transport at varying distances from their point of origin. The main ways in which the movement of compounds may happen usually involve transport through air and water, the two most prominent and mobile environmental compartments. Some chemical species are more likely to freely diffuse through the atmospheric gas phase and rapidly move with the wind while others do so preferentially bound to airborne particles; dry and wet precipitation events can draw some of these pollutants from the air and deposit them onto surfaces like water bodies and soils, and may then filter through the earth to reach groundwaters; other pollutants more likely to freely dissolve in water or to bind to waterborne particles in aquatic systems also undergo transport via currents in rivers and oceans.

The worldwide spread of many pollutant species is inevitable once they have been released into the environment. This creates a scenario in which a permanent and diffuse background layer of contaminants permeates every known ecosystem. Living organisms find themselves chronically exposed to this ubiquitous and potentially toxic background pollution. Adverse effects linked to diffuse pollution have already been observed in organisms inhabiting remote ecosystems (Jarque et al., 2015, 2014, 2010). Moreover, in addition to currently emitted pollutants, this situation is aggravated by an abundance of substances released in the past which possess a series of physical-chemical properties that facilitate their persistence in the environment (i.e., they do not degrade easily and remain intact for exceptionally long periods of time) and their accumulation in certain

environmental matrices and living organisms. This is the case for persistent organic pollutants (POPs), a group of organic compounds particularly regarded as harmful to life and ecosystems that have an exceptional potential for worldwide dispersion and accumulation (Lohmann et al., 2007). Many POPs have been banned and restricted over the years in international regulations, with the Stockholm Convention (and successive additions to the original resolution) being the most notable regulatory effort to limit the negative impact of these substances.¹ However, although having seen some successful local and global improvements in emissions after the application of this and other national and international actions, regulations and international cooperation efforts fail to keep up with the rhythm at which industries generate new chemicals to substitute restricted ones. In fact, regulations only tend to cover a limited number of compounds in a juncture where polluting emissions consist of an ever-increasing variety of chemical species with POP-like properties (Muir and Howard, 2006; Wang et al., 2021). The scientific evidence needed for establishing policy changes requires years or even decades of research, not even accounting for the additional time needed before policymaker authorities reach an agreement, if any. Thus, producing continued and comprehensive scientific evidence of the extent and effects of diffuse pollution is essential.

The present work tackles the occurrence and distribution of various groups of organic pollutants in the environment, including multiple POPs, with the aim of providing a deeper understanding of the environmental fate of chemicals with different sources, regulatory conditions, and behaviours. This approach includes legacy (i.e., already regulated but still existing in the environment) and emerging (i.e., mostly unregulated and increasing in use and emissions) pollutants of environmental concern. The focus of the research has been placed on lacustrine high-mountain areas as they are vulnerable ecosystems subject mainly to diffuse background pollution by virtue of their remoteness and distance from primary pollutant sources. However, pollutant levels have also been determined at their source in a dense urban environment for comparison, and under particular environmental circumstances that allowed for an assessment of potential pollution abatement scenarios. The evidence presented here will hopefully provide useful insight on the impact of anthropogenic activities on the planet, supplying tools to the

¹ www.pops.int (Accessed June 2022)

scientific community and the regulatory authorities that become helpful in deciding future steps in the pursuit of reducing pollution.

1.1.1 Global distillation effect and mountain cold-trapping

Unexpectedly elevated levels of POPs in polar regions were observed as early as the 1960s (Risebrough et al., 1968; Tatton and Ruzicka, 1967). It was hypothesized that the transport of sufficiently persistent chemicals through the atmosphere and their condensation at colder, higher latitudes was the underlying mechanism causing this global distribution of POPs that would often result in unusually high pollutant concentrations in remote areas of the world. This mechanism received the name “polar cold-trapping”. Moreover, the transport of POPs was observed to cause a fractionation of compounds along their transit towards the poles, which was proposed to occur by differential deposition of each POP (Wania and Mackay, 1993). This fractionation caused by a temperature gradient takes place as different compounds are subject to temperature-dependent condensation and precipitation to varying degrees depending on their physical-chemical properties (Mackay and Wania, 1995; Wania and Mackay, 1995), hence why it was labelled the “global distillation effect”. The result is a relative enrichment of volatile chemicals at the poles because less volatile ones become absorbed in environmental matrices along the way. Moreover, this global migration of pollutants happens in a series of condensation and re-evaporation cycles that has been called the “grasshopper effect” (Gouin et al., 2004; Semeena and Lammel, 2005; Wania and MacKay, 1996) (Figure 1). Overall, these processes result in POPs being distributed through the globe while also partitioning towards soil, water, vegetation, and other environmental compartments with varying efficiency, but ultimately reaching all ecosystems and environmental matrices of the world. Over the years, observations from environmental monitoring studies have generally agreed with this theory (Calamari et al., 1991; Carrera et al., 2002; Grimalt et al., 2001; Iwata et al., 1993; Meijer et al., 2002; Muir et al., 1995; Simonich and Hites, 1995).

Aside from the latitudinal transects from a pollutant’s source location to polar regions, other instances where ambient temperature gradients could drive the distribution of pollutants are mountain slopes in remote alpine sites, where atmospheric transport has been recognized as the main actor in the transport of POPs. Research efforts over the last

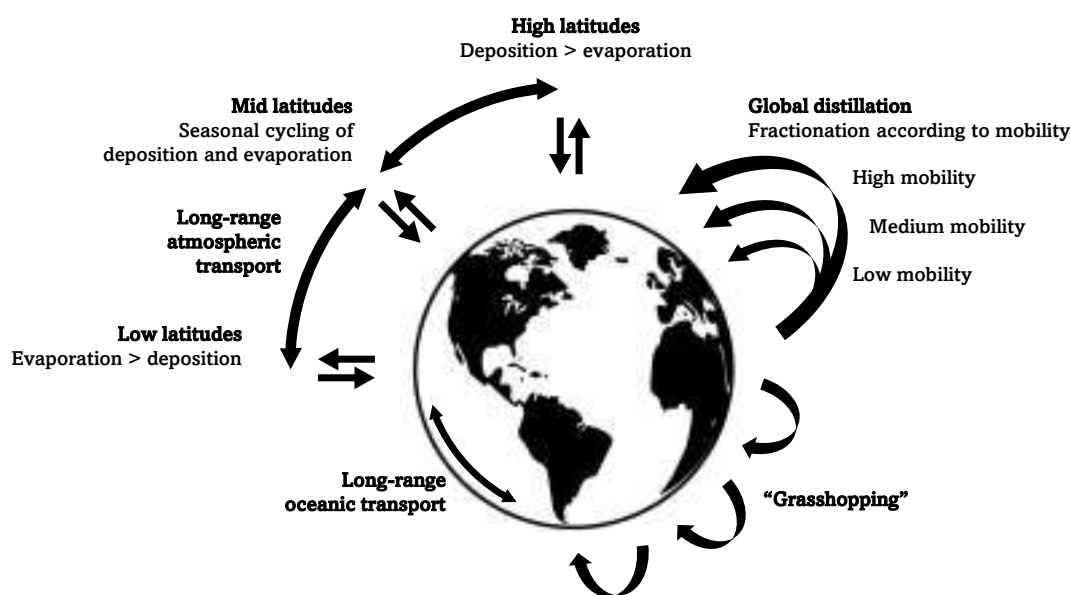


Figure 1. Global distribution of persistent organic pollutants. Reprinted with permission from Wania and Mackay (1996). Copyright 1996 American Chemical Society.

couple of decades have shown selective trapping of organic pollutants in high-elevation sites and cold alpine regions, despite pollutants typically diluting in the environment as the distance from their source increases. The deposition of organochlorine compounds in Canadian mountain snow increased with elevation (Blais et al., 1998), alpine forests in Costa Rica were significantly enriched with pesticides transported through the atmosphere from their application sites (Daly et al., 2007), and soil concentrations of several organochlorine pollutants and pesticides saw significant increases with altitude in mountains from China (Chen et al., 2008), the Alps (Kirchner et al., 2009), and the Andes (Grimalt et al., 2004a). Observations in living organisms from alpine ecosystems showed temperature-dependent accumulation and selective trapping of organochlorine compounds with relatively low volatility in fish and sediment from several European high-altitude lakes (Grimalt et al., 2001). Other increases in the concentration of different organochlorine and organobromine pollutants with altitude were observed in vegetation from Canadian mountains (Davidson et al., 2003), in fish from Pyrenean and Slovakian high-mountain lakes (Gallego et al., 2007; Vives et al., 2004a), in milk from cows in Swiss mountains (Shunthirasingham et al., 2013), and in lichens from the Tibetan Plateau (Zhu et al., 2015).

Wind patterns in alpine regions tend to favour the upwards movement of organic compounds in mountain slopes (Daly and Wania, 2005), driving in part the transport of pollutants towards alpine regions. But other temperature-dependent mechanisms are at play in their selective accumulation along altitudinal transects. Although initially similar to the latitudinal concentration gradients observed due to the global distillation effect, the accumulation of certain organic pollutants in high mountains has been proposed to act under a somewhat different mechanism that explains some dissimilarities in pollutant fractionation patterns. The hypothesis proposed by Wania and Westgate (2008) attributes the mountain cold-trapping effect to differences in the efficiency of precipitation scavenging that are driven by the steep temperature gradients observed in high mountains (Figure 2). That is, the transition from the atmospheric gas and particulate phases to raindrops, snowflakes, and overall environmental surfaces. Thus, low temperatures promoting the condensation of compounds and limiting their re-evaporation may not be the only cause of pollutant accumulation. Instead, a model-based study showed that cold-trapping in mountain slopes is mainly driven by wet deposition, which is enhanced at the lower temperatures and higher precipitation rates typically present at mountaintops (Fowler et al., 1988; Hough, 1987), and less so by dry deposition and wet and dry particle deposition (Westgate and Wania, 2013). This scavenging effect due to enhanced precipitation in mountaintops has also been observed experimentally (Tremolada et al., 2008). Additionally, some compounds are not as efficiently removed or scavenged from

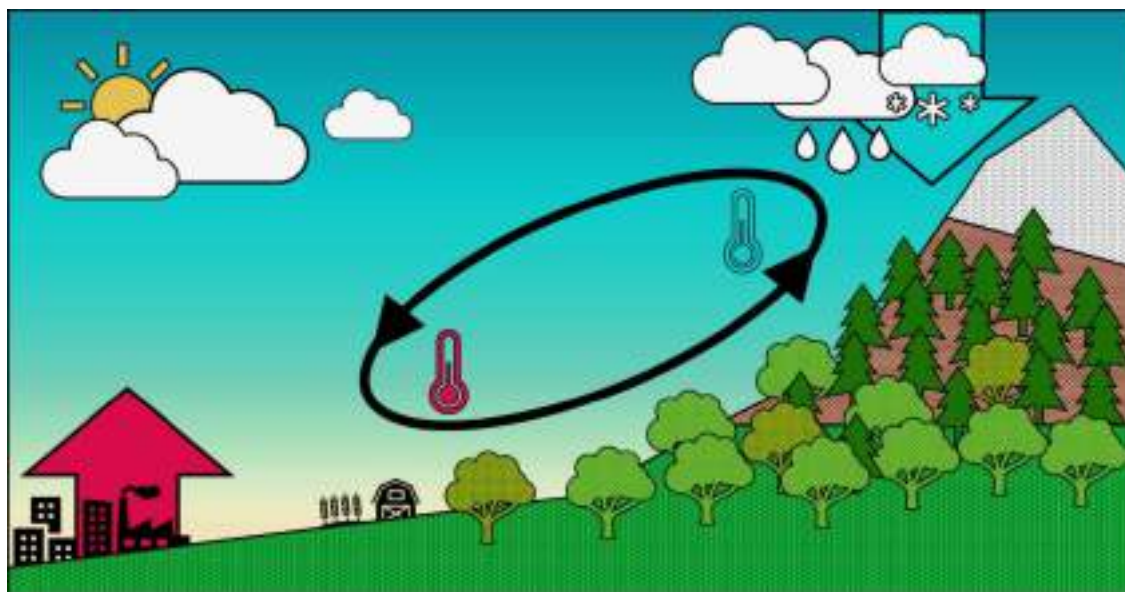


Figure 2. Mountain cold-trapping of persistent organic pollutants and daytime mountain wind cycles. Reprinted with permission from Daly and Wania (2005). Copyright 2005 American Chemical Society.

the atmosphere by precipitation at low-altitude, temperate lowlands as they are at high-altitude, cold mountaintops. This is due to the temperature dependence of the rate of wet deposition of some pollutants (i.e., the partitioning efficiency of a chemical between air and precipitation) (Lei and Wania, 2004), and is thus the cause of an altitudinal distillation effect different in nature to that of the latitudinal (global) distillation model: it is less volatile chemicals that become enriched in alpine areas instead of more volatile ones (Gallego et al., 2007; Grimalt et al., 2001).

All in all, these findings show that alpine regions not only receive organic pollutants through atmospheric transport but are also susceptible to accumulating them after atmospheric deposition, which is usually favoured in these colder sites and effectively increases at higher altitudes. Thus, the fragile ecosystems in these remote regions of the world are particularly subject to chemical stress and are exposed to the potential adverse effects of an increasing number and quantity of toxic substances. In fact, POPs tend to bioaccumulate through food webs in high-altitude ecosystems, reaching significant levels and becoming considerable environmental risk factors (Catalan et al., 2004; Kallenborn, 2006). This has been the driving impulse behind environmental research in mountain areas in recent decades and continues to be so as new pollutants emerge while legacy chemicals persist. The present work adds to this knowledge by assessing some governing factors behind pollutant distribution processes.

1.1.2 High mountains as sentinel ecosystems for the study of diffuse pollution

High mountains are natural areas that share a set of attributes that shape their environment and influence the ecosystems that are found in them. They are high-elevation continental sites with low ambient temperatures and atmospheric pressure, high precipitation rates and amounts, very strong winds, and high solar irradiance. Because of the low temperatures, precipitation typically occurs in the form of snow, which accumulates in these alpine sites for extended periods at the same time that aquatic systems freeze. Vegetation is typically varied and abundant at the mountain valleys but noticeably decreases in diversity, size, and quantity at higher altitudes. Habitats and ecosystems in high mountains are relatively isolated because of their remoteness and tend to be fragile to external perturbations, for example exhibiting an amplified rate of warming due to global climate change (Pepin et al., 2015).

But, as we have seen, no ecosystem is remote enough to escape the influence of diffuse organic pollution. A series of partitioning, kinetic, and phase change effects associated with the nature of pollutants that tend to reach alpine sites and the physical, geographical, and meteorological characteristics of these locations are responsible for the transport and accumulation of pollutants in mountain regions (Wania, 1999). Mountain winds present a cyclic behaviour that aids the transport of pollutants towards higher altitudes (Daly and Wania, 2005): higher temperature contrasts during the day between peaks and valleys create ascending winds in mountain slopes that carry atmospheric pollutants upwards, and lower temperatures along with increased precipitation at the mountaintops facilitate the settling of compounds. Snow, a common form of precipitation in these cold areas, is often more efficient at scavenging organic pollutants than rain (Daly and Wania, 2004; Herbert et al., 2006; Lei and Wania, 2004). At night, wind directions are typically reversed towards the valleys, but the deposited pollutants do not re-volatilize as easily in the colder nights, so they remain trapped in the mountain slopes. All in all, alpine regions present a set of characteristics that emanate from the existence of steep elevation gradients in reduced planar terrain extensions, which is why these areas are a unique subject of study in many scientific fields, including environmental chemistry. This allows for the assessment at a relatively small scale of the fate and behaviour of contaminants transported at long distances, the influence of environmental and physical-chemical variables on their distribution, and the impact they have on remote ecosystems.

Studies on organic pollutants in alpine sites are varied in their scope and target species. As a brief example, POPs and other anthropogenic chemicals have been determined in matrices like air, resolving seasonal and altitudinal variations and studying the partitioning of pollutants with other environmental matrices (Estellano et al., 2008; Fernández et al., 2002; Ren et al., 2014; Riaz et al., 2021b), in water such as lakes and groundwater, with studies on pollutant partitioning between dissolved and particulate phases (Nellier et al., 2015b; Usenko et al., 2005; Vilanova et al., 2001a), soil and the effects of environmental variables on POP accumulation (Tremolada et al., 2012, 2008; van Drooge et al., 2004b), snow and long-term accumulation trends (Carrera et al., 2001; Wang et al., 2014), vegetation and the effects of pollution on mountain forests (Bytnerowicz et al., 2003; Kume et al., 2009; van Drooge, 2006), and organisms and

whole food chains from alpine ecosystems (Bizzotto et al., 2009b; Morselli et al., 2014; Riaz et al., 2021a; Shunthirasingham et al., 2013).

1.1.3 Alpine lakes, continental reservoirs of anthropogenic pollutants

Airborne pollutants are dispersed through the atmosphere because of its high efficiency for transporting compounds, especially in the gas phase but also bound to particles. At the same time, many organic pollutants susceptible to atmospheric transport are also prone to penetrating other environmental compartments to varying degrees, resulting in their ubiquitous presence. Besides air, the other main compartment of global concern regarding environmental pollution is water, as it is fundamental for the sustenance of all ecosystems. Still, the velocity of diffusion of chemicals in water is slower than in air, which can result in increased residence times that cause a trapping effect and the accumulation of pollutants in water bodies.

As a result of the processes described by cold-trapping mechanisms and the global distillation effect, colder regions of the world (i.e., polar regions and high mountains) tend to act as terminal destinations of many pollutants that are transported through the atmosphere, where water bodies are an important sink of compounds. For instance, the accumulation of many POPs has been observed in waters from the Arctic Ocean (Lohmann et al., 2009; Ma et al., 2018), Arctic freshwater ecosystems (Kosek and Ruman, 2021), Antarctic Ocean (Casal et al., 2019), Antarctic freshwater lakes (Vecchiato et al., 2015), and high-mountain glacier streams (Bizzotto et al., 2009a) and lakes (Nellier et al., 2015a; Vilanova et al., 2001a, 2001b). Thus, remote high-mountain lakes also find themselves at the receiving end of the atmospheric pollution that is transported long distances from the original continental sources.

In such a unique position, alpine lakes have been a relevant subject of study for decades. In fact, mountain headwaters have been characterized as witnesses of global pollution (Catalan et al., 2013) and environmental and climate change (Moser et al., 2019). Most studies on anthropogenic organic pollutants in alpine lakes have traditionally focused on the accumulation in compartments other than water itself, such as studies on the occurrence, distribution, accumulation, biological effects, and biotransformation of several groups of anthropogenic organic compounds in fish (Gallego et al., 2007;

Genualdi et al., 2011; Jarque et al., 2010; Vives et al., 2005, 2004a; Yang et al., 2007) and other biota (e.g., plankton, microbial biofilms, lichens, and other links in the aquatic food chain) (Bartrons et al., 2011; Catalan et al., 2004; García-Solorio et al., 2022; Grimalt et al., 2004a; Ren et al., 2017; Usenko et al., 2010). Another environmental compartment typically acting as a sink of pollutants is the sediment at the bottom of alpine lakes, with studies showing evidence of medium- or long-range atmospheric transport of organic pollutants and pointing at differences in sedimentation fluxes across lakes depending on geography, distance to suspected sources, and season (Fernández et al., 1999; Genualdi et al., 2011; Guzzella et al., 2011; Poma et al., 2017; Usenko et al., 2010, 2007).

Studies on water, and specifically the dissolved phase of water, entail additional difficulty regarding sampling procedures in high-altitude sites. As pollutant concentrations in remote waters tend to be low, the volumes of water needed to overcome instrumental and methodological limits of detection are usually higher than in more polluted sites. Thus, grab-sampling and transporting large quantities of water becomes problematic. Still, valuable efforts to this day have shown the presence of anthropogenic POPs in waters of high-altitude and remote lakes around the world, often at environmentally and biologically concerning levels. POPs and organochlorine pesticides were found in Himalayan lakes at concentrations comparable to those in industrialized sites, with observed distributions according to their physical-chemical properties (Galassi et al., 1997), and in water and other compartments from boreal and mountain lakes in Canada (Donald et al., 1998), several North-American remote alpine lakes (Datta et al., 1998; LeNoir et al., 1999; Usenko et al., 2005), and in Himalayan lakes (Guzzella et al., 2011). Some mountain sites in remote and protected areas across the USA including the Rocky Mountain and Sierra Nevada National Parks often showed the highest pollutant concentrations in lake water samples and in other environmental compartments (Landers et al., 2010). Additionally, a mass budget analysis of high-altitude lakes in the French Alps characterized them as POP sinks, pointing at snow deposition, spring thaw, and other atmospheric deposition processes as major pollutant inputs to the water column (Nellier et al., 2015a). This was also observed in other Pyrenean sites (Arellano et al., 2014b, 2011; Carrera et al., 2001; Grimalt et al., 2001). Finally, snow, ice, and glaciers, frequent companions of remote alpine lakes, have often been observed to act as accumulators of

organic pollutants (Arellano et al., 2014b, 2011; Ferrario et al., 2017), becoming predominant pollutant sources to the lakes in their drainage basin with a seasonal behaviour (Meyer and Wania, 2008) and sometimes enhancing pollutant input by up to 70% after ice melt (Piliposian and Appleby, 2003). This was also observed in Canadian (Blais et al., 2001a, 2001b) and Alpine (Schmid et al., 2011) high-altitude lakes. Seasonal pulses in pollution levels were observed in mountain areas in New Zealand following snow and ice melt (Wu et al., 2017).

All in all, the evidence shows that high-altitude lacustrine areas are particularly susceptible to the accumulation of organic pollution transported at long distances. Moreover, these theoretically unperturbed ecosystems and the organisms that inhabit them depend on the preservation of a fragile natural equilibrium that may become disrupted when exposed to anthropogenic pollution and its potentially toxic effects. However, sampling logistics in high mountains have always been complex, hindering the scope and scale of monitoring studies and resulting in the limited attention that has been paid to such locations. The development of alternative sampling techniques in recent decades has allowed for a more accessible approach to environmental assessment in these remote continental sites. The present work employs some of these strategies, which are described in detail in the following sections.

1.2 Semi-volatile and hydrophobic organic pollutants

Semi-volatile organic compounds (SVOCs) are a group of organic chemicals with intermediate volatility and thus relatively high boiling points. The exact definition of SVOCs is ambiguous and non-exclusive to other classifications (e.g., many POPs are SVOCs, but not all SVOCs are POPs). The World Health Organization (WHO) classified them as pollutants with boiling points between 240/260 °C and 380/400 °C (World Health Organization, 1989). They typically encompass compounds with Henry's Law constants between just under 10^{-5} and somewhat over 10^{-7} atm m³ mol⁻¹ and vapour pressures roughly between 10^{-14} and 10^{-4} atm. This makes them less volatile than other organic compounds like organic gasses (e.g., propane, butane) and solvents (e.g., acetone, ethanol, toluene), but more volatile than other typically heavier and more complex organic chemicals (e.g., pharmaceuticals, organic oils). Most SVOCs also are

hydrophobic organic compounds (HOCs) because of the predominance of carbon and hydrogen in their molecular structures. These include relatively insoluble chemicals, with octanol–water coefficients ($\log K_{ow}$) generally greater than 2. Typical groups of SVOCs/HOCs are pollutants like pesticides, fire retardants, and organic combustion products.

SVOCs are perfect candidates for experiencing the global distribution processes described in previous sections. Their intermediate volatility enables them to easily evaporate and migrate through the atmosphere, traveling far from their original emission sources while partitioning to other environmental matrices along the way. Their relative hydrophobicity does not impede them from transferring to aquatic phases to some degree and, from there, spread further to other compartments where they tend to accumulate, like sediment and biota. The continued exposure of the latter to a mixture of these potentially ubiquitous and often toxic compounds is an undeniable risk to their health and to the health of ecosystems, even those located in remote sites. Thus, as long as these risks remain unmitigated, effective monitoring of these substances in the environment is paramount. This section deals with the specific compounds studied in the present work. They are the following: polychlorinated biphenyls (PCBs), other organochlorine compounds, polycyclic aromatic hydrocarbons (PAHs), and organophosphate esters (OPEs). They are a set of both currently emitted and already restricted but still persisting organic compounds representative of a range of pollutant sources and diverse physical-chemical properties. The following pages provide a brief overview of these compounds, their uses and sources, characteristics, and structures. Table 1 contains the complete list of studied compounds and the values of physical-chemical variables used in calculations performed in this work, including parameters pertaining to their partitioning affinity for different phases like air and water as well as to the sampling strategies employed. Note that some compounds often have more than a single denomination in the literature, and a few inconsistencies are present in this work between published articles: TCIPP is sometimes referred to as TCPP, TDCIPP as TDCP, and OPEs are sometimes called organophosphate flame retardants (OPFRs).

Table 1. List of compounds and properties. M: molar mass (g mol^{-1}); V: molar volume ($\text{cm}^3 \text{mol}^{-1}$); H_{298} : Henry's Law constant at 25 °C ($\text{atm m}^3 \text{mol}^{-1}$); partition coefficients at 25 °C: $\log K_{\text{OA}}$ (octanol-air), $\log K_{\text{OW}}$ (octanol-water), $\log K_{\text{PUF-A}}$ (polyurethane foam-air), $\log K_{\text{PUF-W}}$ (polyurethane foam-water), $\log K_{\text{LDPE-W}}$ (low-density polyethylene-water), $\log K_{\text{SR-W}}$ (silicone rubber-water).

Compound	Full name	CAS No.	Formula	M ^a	V ^b	H_{298} ^c	$\log K_{\text{OA}}$	$\log K_{\text{OW}}$	$\log K_{\text{PUF-A}}$	$\log K_{\text{LDPE-W}}$	$\log K_{\text{SR-W}}$
PCB 28	2,4,4'-Trichlorobiphenyl	7012-37-5	C ₁₂ H ₇ Cl ₃	257.547	188.1	2.00E-4	7.93 ^d	5.67 ^h	1.87 ^j	5.56 ^h	5.53 ^h
PCB 52	2,2',5,5'-Tetrachlorobiphenyl	35693-99-3	C ₁₂ H ₆ Cl ₄	291.992	200.8	2.00E-4	8.36 ^d	5.84 ^h	2.14 ^j	5.72 ^h	5.80 ^h
PCB 101	2,2',4,5,5'-Pentachlorobiphenyl	37680-73-2	C ₁₂ H ₅ Cl ₅	326.437	212.4	9.00E-5	8.78 ^d	6.38 ^h	2.41 ^j	6.33 ^h	6.28 ^h
PCB 118	2,3',4,4',5'-Pentachlorobiphenyl	31508-00-6	C ₁₂ H ₅ Cl ₅	326.437	210.9	7.87E-5	8.51 ^d	6.74 ^h	2.24 ^j	6.63 ^h	6.42 ^h
PCB 138	2,2',3,4,4',5'-Hexachlorobiphenyl	35065-28-2	C ₁₂ H ₄ Cl ₆	360.882	223.5	2.10E-5	8.47 ^d	6.83 ^h	2.22 ^j	6.92 ^h	6.67 ^h
PCB 153	2,2',4,4',5,5'-Hexachlorobiphenyl	35065-27-1	C ₁₂ H ₄ Cl ₆	360.882	224.0	2.30E-5	8.51 ^d	6.92 ^h	2.24 ^j	6.96 ^h	6.72 ^h
PCB 180	2,2',3,4,4',5,5'-Heptachlorobiphenyl	35065-29-3	C ₁₂ H ₃ Cl ₇	395.327	235.4	1.00E-5	9.08 ^d	7.36 ^h	2.60 ^j	7.31 ^h	6.99 ^h
HCB	Hexachlorobenzene	118-74-1	C ₆ Cl ₆	284.784	161.2	1.70E-3	7.38 ^e	5.50 ^h	1.52 ^j	5.50 ^h	5.05 ^h
PeCB	Pentachlorobenzene	608-93-5	C ₆ HCl ₅	250.339	149.5	7.03E-4	6.18 ^e	5.18 ^h	0.76 ^j	4.89 ^h	4.61 ^h
α -HCH	α -1,2,3,4,5,6-Hexachlorocyclohexane	319-84-6	C ₆ H ₆ Cl ₆	290.832	178.0	7.34E-6	7.61 ^e	3.72 ^h	1.67 ^j	3.22 ^h	3.27 ^h
γ -HCH	γ -1,2,3,4,5,6-Hexachlorocyclohexane	58-89-9	C ₆ H ₆ Cl ₆	290.832	178.0	7.34E-6	7.84 ^e	3.72 ^h	1.82 ^j	3.18 ^h	3.34 ^h
4,4'-DDE	1,1'-Dichloro-2,2-bis(4-chlorophenyl)ethene	72-55-9	C ₁₄ H ₈ Cl ₄	318.030	222.4	4.16E-5	9.67 ^e	6.51 ^h	2.98 ^j	6.28 ^h	6.27 ^h
Ace	Acenaphthene	83-32-9	C ₁₂ H ₁₀	154.211	142.0	1.84E-4	6.09 ^e	3.92 ^h	0.70 ^j	3.62 ^h	3.26 ^h
Flu	Fluorene	86-73-7	C ₁₃ H ₁₀	166.222	154.8	9.62E-5	6.19 ^e	4.18 ^h	0.76 ^j	3.77 ^h	3.79 ^h
Phe	Phenanthrene	85-01-8	C ₁₄ H ₁₀	178.233	160.6	4.23E-5	7.03 ^e	4.57 ^h	1.30 ^j	4.22 ^h	4.11 ^h
Flu	Fluoranthene	206-44-0	C ₁₆ H ₁₀	202.255	196.1	8.86E-6	8.40 ^e	5.22 ^h	2.17 ^j	4.93 ^h	4.62 ^h
Pyr	Pyrene	129-00-0	C ₁₆ H ₁₀	202.255	182.3	1.19E-5	8.40 ^e	5.18 ^h	2.17 ^j	5.10 ^h	4.68 ^h
Ret	Retene	483-65-8	C ₁₈ H ₁₈	234.341	226.5	2.12E-5	8.70 ^e	6.35 ⁱ	2.36 ^j	6.00 ^f	5.27 ^m
B[a]ant	Benz[a]anthracene	56-55-3	C ₁₈ H ₁₂	228.293	195.1	1.20E-5	9.21 ^e	5.91 ^h	2.68 ^j	5.73 ^h	5.32 ^h
Chr	Chrysene	218-01-9	C ₁₈ H ₁₂	228.293	196.5	5.23E-6	9.21 ^e	5.86 ^h	2.68 ^j	5.78 ^h	5.25 ^h
TriPh	Triphenylene	217-59-4	C ₁₈ H ₁₂	228.293	196.5	6.52E-6	9.21 ^f	5.86 ^f	2.68 ^j	5.78 ^f	5.74 ^m
B[b]flu	Benzo[b]fluoranthene	205-99-2	C ₂₀ H ₁₂	252.315	232.0	6.57E-7	10.59 ^e	5.90 ^h	3.56 ^j	6.66 ^h	5.74 ^f
B[j]flu	Benzo[j]fluoranthene	205-82-3	C ₂₀ H ₁₂	252.315	229.5	7.09E-7	10.59 ^e	5.90 ^h	3.56 ^j	6.66 ^h	5.74 ^f
B[k]flu	Benzo[k]fluoranthene	207-08-9	C ₂₀ H ₁₂	252.315	229.5	5.84E-7	10.59 ^e	5.90 ^h	3.56 ^j	6.66 ^h	5.74 ^h
B[e]pyr	Benzo[e]pyrene	192-97-2	C ₂₀ H ₁₂	252.315	219.6	8.50E-7	10.59 ^f	6.44 ⁱ	3.56 ^j	5.69 ^f	5.63 ^h
B[a]pyr	Benzo[a]pyrene	50-32-8	C ₂₀ H ₁₂	252.315	218.2	4.57E-7	10.59 ^e	6.04 ^h	3.56 ^j	6.75 ^h	5.69 ^f
Pery	Perylene	198-55-0	C ₂₀ H ₁₂	252.315	219.6	8.44E-7	10.59 ^e	6.25 ⁱ	3.56 ^j	6.55 ^f	5.64 ^m
Db[ah]ant	Dibenz[a,h]anthracene	53-70-3	C ₂₂ H ₁₄	278.353	244.2	4.50E-7	11.40 ^e	6.75 ^h	4.08 ^j	7.32 ^h	6.24 ^h
Ind[1,2,3-cd]pyr	Indeno[1,2,3-cd]pyrene	193-39-5	C ₂₂ H ₁₂	276.337	253.7	3.84E-7	11.97 ^e	6.70 ^h	4.44 ^j	7.40 ^h	6.06 ^h
B[ghi]per	Triphenylperylene	191-24-2	C ₂₂ H ₁₂	276.337	241.3	3.31E-7	12.56 ^e	6.63 ^h	4.82 ^j	7.27 ^h	6.02 ^h
TBP	Tributyl phosphate	126-73-8	C ₁₂ H ₂₇ O ₄ P	266.318	265.5	1.13E-6	8.02 ^g	3.82 ⁱ	1.93 ^j	4.90 ^k	4.93 ⁱ
TCEP	Tris(2-chloroethyl) phosphate	115-96-8	C ₆ H ₁₂ Cl ₃ O ₄ P	285.492	196.5	1.28E-7	8.39 ^g	1.63 ⁱ	2.16 ^j	2.80 ^k	3.05 ⁱ
TCIPP	Tris(1-chloro-2-propyl) phosphate	13674-84-5	C ₉ H ₁₈ Cl ₃ O ₄ P	327.572	247.9	2.63E-7	9.76 ^g	2.89 ⁱ	3.04 ^j	3.36 ^k	3.55 ⁱ
TDCIPP	Tris(1,3-dichloro-2-propyl) phosphate	13674-87-8	C ₉ H ₁₅ Cl ₆ O ₄ P	430.907	268.4	1.68E-6	10.55 ^g	3.65 ⁱ	3.54 ^j	3.69 ^k	3.85 ⁱ
TPHP	Triphenyl phosphate	115-86-6	C ₁₈ H ₁₅ O ₄ P	326.288	272.9	1.78E-6	10.76 ^g	4.70 ⁱ	3.68 ^j	4.98 ^k	5.00 ⁱ

^a Reaxys.com (accessed May 2020); ^b archemcalc.com/sparc (accessed May 2020); ^c Williams et al. (2017); ^d Chen et al. (2016); ^e Hamer (2021); ^f Interpolated; ^g Wang et al. (2017); ^h Smedes et al. (2009); ⁱ pubchem.ncbi.nlm.nih.gov (accessed May 2020); ^j Shoenb and Hamer (2002); ^k Extrapolated from Smedes (2018); ^l Smedes (2018); ^m Rusina et al. (2019).

1.2.1 Polychlorinated biphenyls

PCBs are anthropogenic chlorinated hydrocarbons composed of two linked benzene rings substituted with a variable number of chlorine atoms ranging from one to ten (Figure 3). There are 209 possible congeners, the nomenclature of which is defined by the number and position of chlorine substituents. PCBs are relatively volatile (low vapour pressures), hydrophobic, and highly lipophilic. Their volatility decreases and their hydrophobicity increases at higher degrees of chlorination (Abramowitz and Yalkowsky, 1990; Brodsky and Ballschmiter, 1988; Dunnivant et al., 1988). They also show exceptional chemical stability and resistance to degradation, which is the reason behind their remarkable persistence in the environment and accumulation in environmental matrices. The production of PCBs started in 1929 and they gained popularity after World War II. PCBs were generally produced and commercially sold as mixtures of several specific congeners that were thermodynamically favoured in the industrial reaction process. They were used as insulating, heat transfer, and hydraulic fluids in electrical applications such as capacitors and transformers, as well as lubricants, flame retardants, plasticizers, additives in paints, and adhesives (Erickson and Kaley, 2011).

The threat that PCBs pose to the environment has long been recognized. Based on their occurrence in the different environmental compartments and their potential for toxicity, 36 out of the 209 congeners are generally considered the most threatening to life and ecosystems (McFarland and Clarke, 1989). Thirteen congeners exhibit dioxin-like toxicity and have often been used as a toxic equivalent factor approach for the estimation of PCB exposure risk. Dioxin-like toxic effects in animals and humans include weight loss, dermal lesions, hepatotoxicity, reproductive toxicity, immunosuppression, and endocrine disruption (Poland and Knutson, 1982; Safe, 1994). Additionally, PCBs can alter the thyroid function (Chevrier et al., 2008; Sala et al., 2001) and cause neurodevelopmental effects (Grandjean and Landrigan, 2014; Ulbrich and Stahlmann, 2004; Winneke et al., 2002). After observations of their adverse effects and worldwide environmental distribution, the production of PCBs ceased in the late 1970s in North America, while production continued in many places in Europe and Asia at least well into the 1980s. Their worldwide use and production were gradually phased out until the implementation of the Stockholm Convention at the beginning of the 2000s. These

measures led to a significant decrease in emissions, dropping by 73% between 1990 and 2019 in the European Union (EEA, 2021). PCB emissions nowadays may occur mostly from old existing equipment that still contains these chemicals, the use of which is permitted until 2025 by an exception considered in the Stockholm Convention, or from waste disposal and incineration of PCB-containing materials.

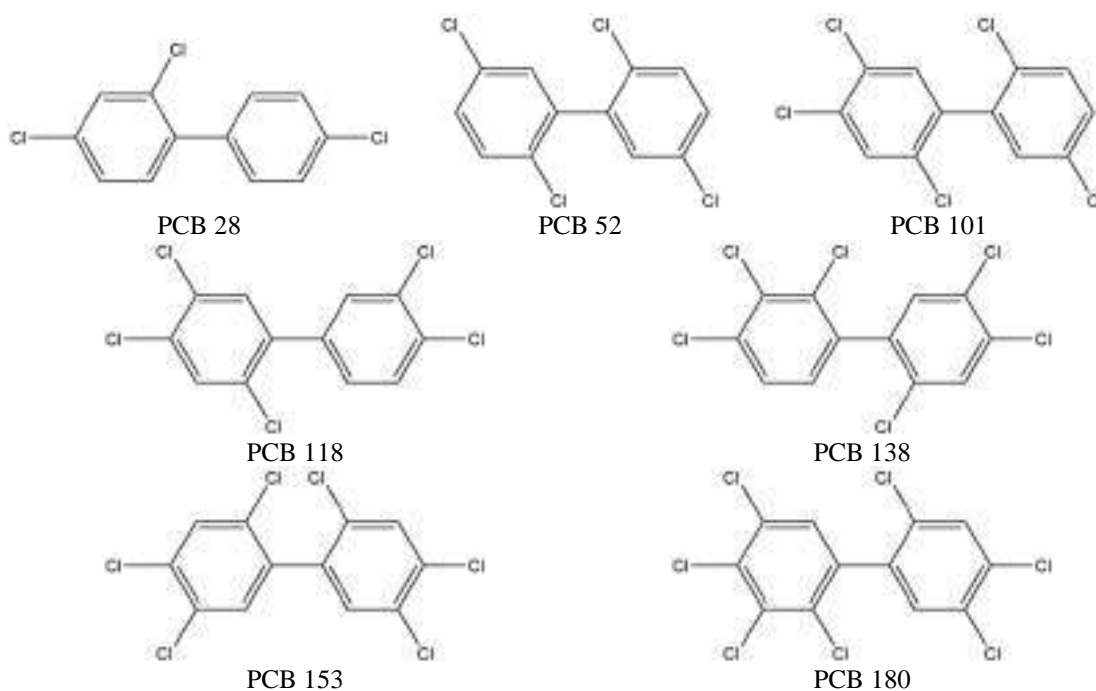


Figure 3. Polychlorinated biphenyls studied in the present work.

1.2.2 Organochlorine compounds

A wide range of compounds can be classified under the broad definition of organochlorine pollutants (i.e., hydrocarbons with chlorine substituents). Here, three main groups were considered: chlorobenzenes (pentachlorobenzene, PeCB, and hexachlorobenzene, HCB), hexachlorocyclohexanes (HCHs), specifically α -HCH and γ -HCH, and dichlorodiphenyltrichloroethanes (DDTs), mainly the main degradation product of DDT, 1,1-dichloro-2,2-bis(4-chlorophenyl)ethene (4,4'-DDE) (Figure 4). Chlorobenzenes are composed of a benzene ring substituted with a variable number of chlorine atoms. HCB was widely used as a fungicide in the 1940s and 1950s, but it also occurs as an industrial by-product in the manufacture of other chlorinated compounds (Courtney, 1979). PeCB was used for the reduction of viscosity in PCB products and in electrical equipment, but can also be released as an industrial by-product and in waste

combustion (Bailey et al., 2009). HCHs consist of a cyclohexane ring with each carbon atom monosubstituted with a chlorine atom. The orientation of the chlorine substituents defines the specific HCH isomer. γ -HCH (often called lindane from the name of the commercial formulation) is an insecticide used since the 1940s (Breivik et al., 1999) with the highest insecticidal activity among all HCHs (Kutz et al., 1991). The α and γ isomers are the most prevalent in the environment, but other isomers such as β -HCH are found more predominantly in biota (Willett et al., 1998). DDTs are a group of compounds originating from a 2,2,2-trichloroethane molecule with two chlorobenzene substituents at C1. The position of the chlorine atoms in the benzene rings defines the specific DDT isomer. The major metabolites and environmental degradation products of DDT are dichlorodiphenyldichloroethylene (DDE) and dichlorodiphenyldichloroethane (DDD). DDT was used worldwide as an insecticide starting in the 1940s and aided in the control of malaria and typhus after World War II (Turusov et al., 2002). While varied in nature due to the different structures grouped under the label of organochlorine compounds, these chemicals are generally lipophilic and hydrophobic, ranging from quite volatile to semi-volatile but often found mostly in the atmospheric gas phase, and remarkably persistent in the environment due to the high degrees of chlorination.

HCB in humans is known to cause porphyria (Starek-Świechowicz et al., 2017), thyroid cancer (Grimalt et al., 1994), and thyroid function disruption (Llop et al., 2017; Sala et al., 2001), as well as decreased foetal development (Lopez-Espinosa et al., 2016). PeCB has shown adverse toxic effects on the liver, kidneys, and thyroid function (den Besten et al., 1991). HCHs primarily affect the central nervous system and liver and renal functions (Willett et al., 1998), but they have also been shown to be teratogenic, mutagenic, and genotoxic, and classified as possible human carcinogens and endocrine disruptors (Nayyar et al., 2014). DDTs have been linked to reproductive toxicity (Bonde and Toft, 2011), neurodevelopmental and neurodegenerative effects (Saeedi Saravi and Dehpour, 2016), and diabetes (Rignell-Hydbom et al., 2009). The 4,4'-DDE isomer is also an androgen receptor antagonist that inhibits male sex development (Kelce et al., 1995). The production and use of most of these chemicals ceased or was gradually reduced due to local restrictions through the second half of the last century. Ultimately, PCBs, HCB, PeCB, and γ -HCH were fully banned by the Stockholm Convention, with additional measures imposed for the control of unintentional releases in industrial

activities. As an example of the effectiveness of regulations, HCB emissions in Europe decreased by 97% between 1990 and 2019 (EEA, 2021). DDTs are mostly banned by the Stockholm Convention, with the only restricted acceptable use as a disease vector control.

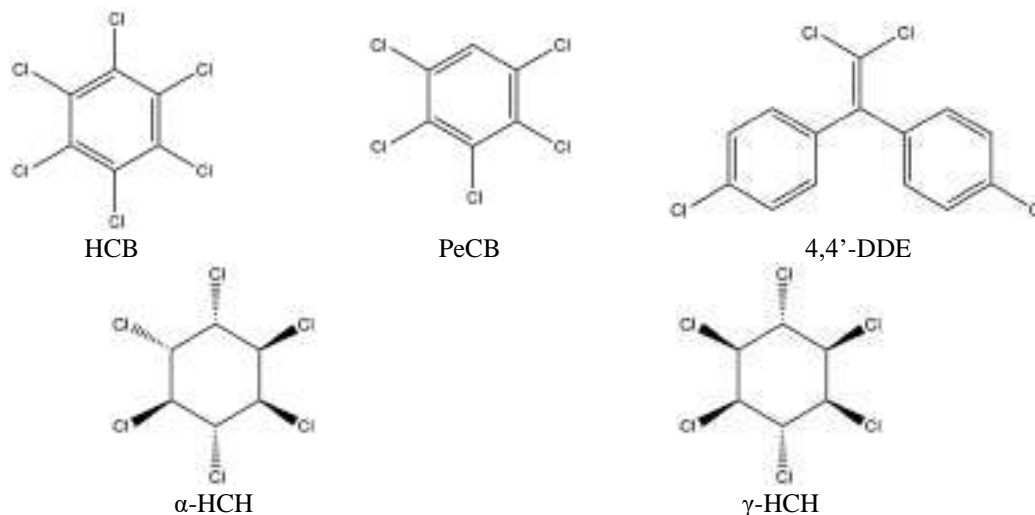


Figure 4. Organochlorine compounds studied in the present work.

1.2.3 Polycyclic aromatic hydrocarbons

PAHs are organic contaminants comprised exclusively of carbon and hydrogen atoms forming at least two fused aromatic rings (Figure 5). PAH-like chemicals containing other heteroatoms and substituents are classified under a broader definition as polycyclic aromatic compounds. PAHs have high melting points, are highly lipophilic, and have relatively low water solubilities and vapour pressures. Their volatility and solubility in water decrease with molecular weight and number of aromatic rings (Achten and Andersson, 2015). They are relatively susceptible to photodegradation in air, water, and soil, bound or not to particulate matter (Fasnacht and Blough, 2002; Kim et al., 2013; Marquès et al., 2017), and also to biodegradation (Premnath et al., 2021). Still, their continued emissions can overcome this susceptibility and allow their global distribution and accumulation in certain environmental matrices. PAHs originate mainly from the incomplete or inefficient combustion of organic matter (i.e., under insufficient supply of oxygen and from low temperature combustion). This includes fossil fuels used in the generation of energy like coal, gas, crude oil, and biomass, the latter being especially relevant in agricultural settings and in house heating in rural sites, but also the combustion of urban and industrial waste and vehicle or traffic emissions (Mastral and Callén, 2000).

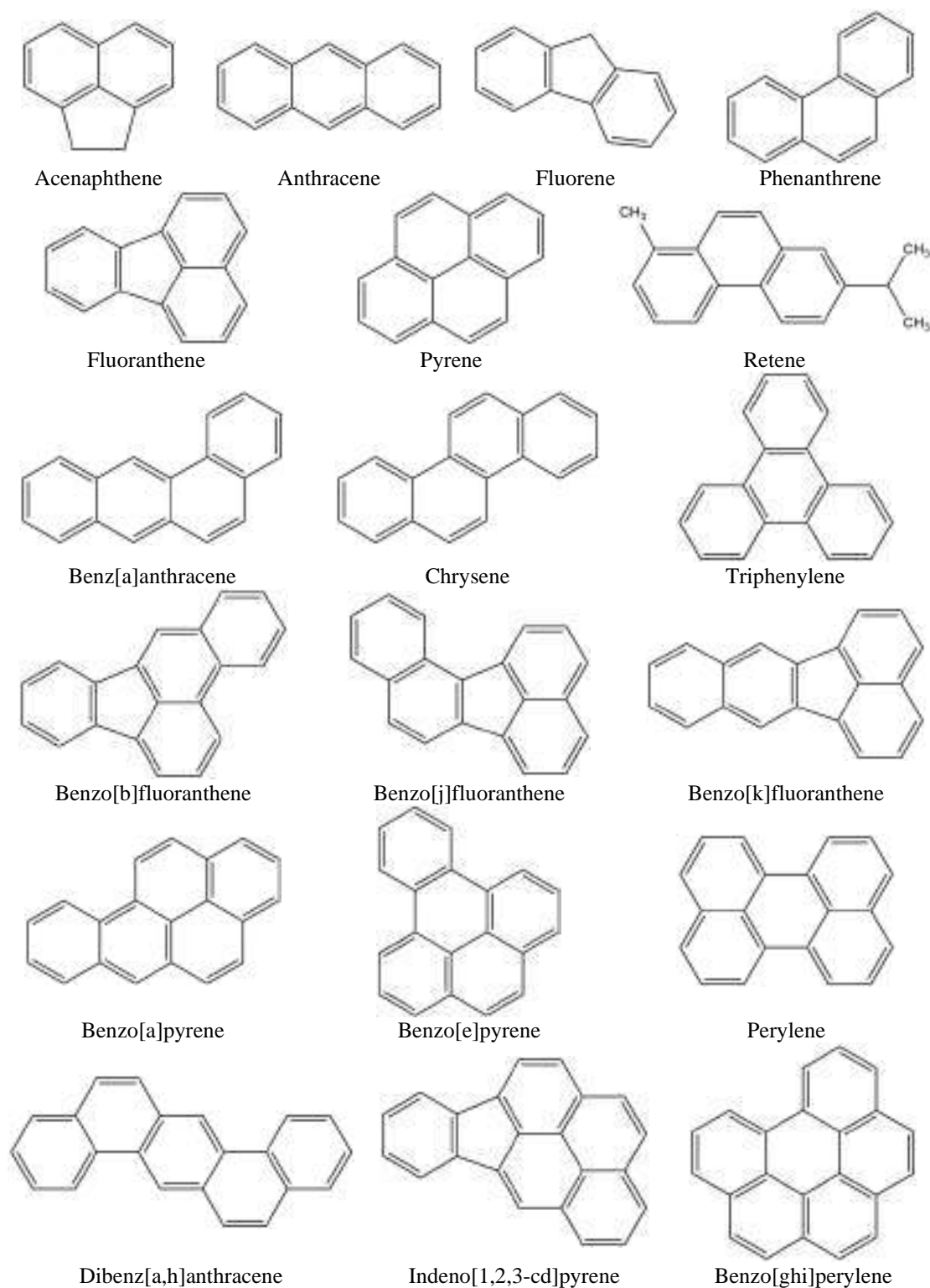


Figure 5. Polycyclic aromatic hydrocarbons studied in the present work.

Thus, urban and industrial areas tend to be predominant sources of PAHs. Natural sources include wildfires, volcanic eruptions, and diagenesis (chemical transformation in sediments), although they are generally less important than anthropogenic ones.

Not all PAHs exhibit the same toxic effects (Mesquita et al., 2014a). Still, PAHs are in general mostly known for being genotoxic, mutagenic, carcinogenic, and teratogenic (Armstrong et al., 2004; Boström et al., 2002; Luch, 2005; Wenger et al., 2009). In fact, benzo[a]pyrene is generally considered to be one of the most carcinogenic PAHs and is frequently used as a tracer of PAH exposure (Agapkina et al., 2018). Other toxic effects on humans and animals include suppression of the immune system (Burchiel and Luster, 2001), oxidative damage, and damage to organs (Abdel-Shafy and Mansour, 2016). The direct regulation of PAH emissions is a difficult endeavour because their sources are multiple, widespread, and in many cases uncontrollable, and because of the large number of compounds released from combustion processes. Instead, the general control over polluting activities related to industrial activity and fuel consumption have steadily reduced PAH emissions in many countries of the world over the last decades (EEA, 2021). Still, some directives have also aimed at limiting the emission of certain PAHs in industrial activities (RPA Europe, 2020). Although PAHs comprise hundreds of possible polycyclic configurations, only a handful of compounds known as EPA's (U.S. Environmental Protection Agency) sixteen PAHs have traditionally been prioritized in environmental monitoring (Keith, 2015). However, the utility of maintaining the focus only on this short list of PAHs has been recently questioned in favour of a longer list of chemicals, including several heterocyclic aromatic compounds (Andersson and Achten, 2015).

1.2.4 Organophosphate esters

OPEs are organic phosphoric acid derivatives composed of a phosphate moiety substituted with aliphatic or aromatic groups that can be halogenated or not (Figure 6). They are sometimes referred to as organophosphate flame retardants (OPFRs) because of their main application in preventing and delaying the combustion of materials. OPEs span a wide range of physical-chemical properties that depends on the size and composition of their substituents. They tend to be more lipophilic than hydrophilic, but they have generally lower $\log K_{ow}$ values than other SVOCs like PCBs or PAHs. Their potential for distribution between environmental matrices is highly variable as a result of the differences in substituents, which is reflected in a broad range of vapour pressures and Henry's Law constants. High molecular mass non-halogen OPEs have a higher tendency

to bioaccumulate than low molecular mass OPEs, but no such relation has been established for chlorinated ones (van der Veen and de Boer, 2012). OPEs are regarded as emerging organic pollutants since their mainstream application is relatively recent compared to other groups of compounds, despite being used in polymers since the 1960s (Kemmllein et al., 2003). Their popularity increased rapidly after polybromodiphenyl ethers (PBDEs) were phased out beginning in the mid-2000s (Blum et al., 2019). Halogenated OPEs are generally used as flame retardants, while non-halogenated OPEs are mostly used as plasticizers (Andresen et al., 2004). Common applications are lubricants, paints, foams, furniture, consumer electronics, building materials, and vehicles (van der Veen and de Boer, 2012). Since they are not chemically bonded to the materials they are added to, they tend to leach and volatilize with relative ease (Chokwe et al., 2020), releasing into the environment and undergoing long-range atmospheric transport predominantly bound to particles, where they exhibit relatively high resistance to degradation (Liu et al., 2014).

The toxicological risk associated with OPE exposure is still not well characterized. Some studies have suggested that OPEs may be neurotoxicants (Wei et al., 2015; Yang et al., 2019), potentially carcinogenic (Li et al., 2019), and have shown adverse toxic impacts in animals and humans such as reproductive and developmental

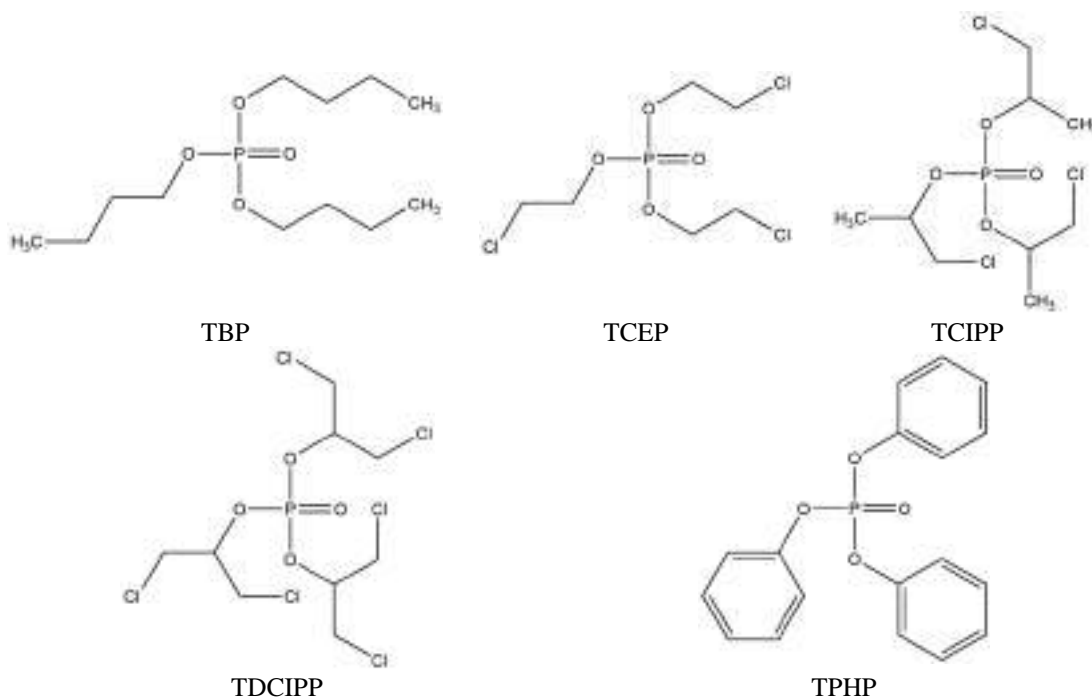


Figure 6. Organophosphate esters studied in the present work.

effects (Alzualde et al., 2018; Oliveri et al., 2015) and disruption of endocrine and hormonal functions (Heindel et al., 2017; Meeker and Stapleton, 2010; Yang et al., 2019). Similarly, because of their relative novelty, there are still no major regulations on OPE use and emissions. Most regulatory action in the European Union and the United States has been introduced for labelling certain OPEs, hazard classification, and banning select compounds or requiring their substitution in certain consumer products, especially those made for children (Blum et al., 2019; European Commission, 2008). Thus, further studies on OPE emissions, distribution through the environment, and toxic effects on animals and humans are needed for the future implementation of informed regulations on the uses and emissions of these compounds.

1.3 Passive sampling as a tool for the global monitoring of pollution

Sample procurement is an essential step in the study of pollutant occurrence in the environment and must be performed to obtain information reliably. Environmental chemistry has typically relied on grab sampling techniques that produce discrete amounts of sample for later extraction and analysis in a laboratory (e.g., collecting soil, sediment, biota, snow, containers of water) or on on-site sample processing using absorbing matrices (e.g., actively pumping large quantities of air or water through solid phase extracting materials) that are then transported to the laboratory. However, these traditional sampling strategies do not always offer a simple and cost-effective solution to every situation. They often involve the transport and use of specialized equipment that can require access to an energy supply, or the acquisition and transport of large amounts of sample to overcome analytical detection limits. Furthermore, the temporal resolution and spatial coverage of the data collected in environmental monitoring depends on the regularity of measurements and the number of sampling operations, which quickly add up to significant economic costs. These shortcomings are especially pronounced in areas difficult to reach, like high mountains. High-altitude alpine regions severely limit the amount of sample that can be collected and carried, as well as the equipment that can be used unless it is transported by air (e.g., via helicopter) along with energy generators and

fuel. But again, this is particularly costly and often not a viable solution for long-term and multi-site monitoring studies.

Instead, passive sampling strategies offer an alternative to the more traditional approaches, which may result in more applicable procedures for specific cases such as environmental monitoring in high mountains. Passive sampling relies on the free transport of pollutant molecules from an environmental compartment, or sampled medium, into a passive sampler device, or sampler medium, as a result of a difference in chemical potential (Górecki and Namieśnik, 2002). Passive sampler devices generally consist of materials permeable to a range of chemicals of interest, such as various polymers and resins, that are deployed in direct contact with the studied environmental compartment for an extended time. They typically rely on diffusive molecular transport mechanics for the gradual uptake of contaminants from the environment, which allows for a time-integrative assessment of pollutant occurrence between sampler deployment and retrieval. Passive samplers are lightweight, inexpensive devices made of materials that are typically commercially available. They are simple to deploy and manipulate and do not require a power source to operate. They can be deployed for extended periods of time and in multiple locations simultaneously or consecutively, providing a viable way of escalating the scope of environmental monitoring programmes. The main difficulty related to passive sampling devices lies in the conversion from amounts of compounds absorbed by the sampler to concentrations in the sampled environmental compartment. Unlike active sampling techniques, these pollutant amounts cannot be directly referenced to a specific volume of air or water or to a specific mass of sediment or soil. Instead, passive sampling relies on the determination of effective sampled volumes or masses by means of diffusive uptake modelling. The models rely on physical-chemical properties of the studied compounds, their different affinities for the sampler material in comparison with the sampled matrix, the passive sampler medium characteristics, and the applied calibration method. This can lead to added uncertainty in the determined environmental concentrations of the studied pollutants if appropriate measures are not taken.

Passive samplers have been used in multiple applications since their introduction several decades ago. Initially, they were developed for monitoring carbon monoxide and other gasses like sulphur dioxide, nitrogen oxides, and ozone, and later expanded to various applications including solid-phase microextraction and monitoring of organic

compounds of varying hydrophobicity and volatility in different environmental matrices (Namieśnik et al., 2005). Common passive sampling devices often make use of polymeric materials: polyurethane foam (Shoeib and Harner, 2002), divinylbenzene–styrene copolymers (Wania et al., 2003), silicone and polyethylene (e.g., semipermeable membrane devices, SPMDs, Huckins et al., 1990), or other ceramic (Martin et al., 2003), fibrous (e.g., solid phase microextraction, SPME, Ouyang et al., 2005), sorbent (e.g., polar organic chemical integrative samplers, POCIS, Alvarez et al., 2004), and other stationary phases (e.g., polymer coated glass, Harner et al., 2003, and C₁₈ phase, Kingston et al., 2000). These sampler materials have served and continue to serve as workplace exposure measuring devices, inorganic and organic chemical monitors and toxicity exposure assessment tools, airborne and waterborne pollutant accumulators, and soil, sediment, and biota samplers, among other applications (Górecki and Namieśnik, 2002; Greenwood et al., 2007; Seethapathy et al., 2008 and references therein). Other publications have presented comprehensive reviews on many of such samplers for air (Tuduri et al., 2012; Wania and Shunthirasingham, 2020) and for water (Seethapathy et al., 2008; Taylor et al., 2021). The following sections provide a brief overview of the most used and better characterized passive air and water samplers, aiming to highlight their main benefits and shortcomings as well as their use in coordinated global pollution monitoring efforts.

1.3.1 Passive air samplers

SPMDs for air sampling were originally adapted from water samplers. They consist of thin low-density polyethylene (LDPE) tubes that enclose a film of triolein, a neutral synthetic lipid that accumulates compounds after they diffuse through the LDPE walls. They were once widely used, especially since comprehensive calibration efforts in the late 1990s and early 2000s (Ockenden et al., 1998; Söderström and Bergqvist, 2004). They are effective and useful for co-deployment with SPMDs in water, but they are also rather complex sampling media and may suffer from some limitations. The LDPE walls are absorptive media by themselves rather than just acting as a limiting phase for the exchange of compounds between air and the triolein, and a completely quantitative interpretation of SPMD-derived results has been put into question based on the complex influence that temperature has on the uptake of compounds (Piccardo et al., 2010). Thus,

SPMDs have gradually seen reduced use in favour of other less complex and more convenient sampling media. Resulting from the realization that LDPE tubing in SPMDs also acts as an accumulating medium for SVOCs, LDPE was also proposed as a suitable material for passive sampling on its own (Booij et al., 1998). The uptake kinetics of this material have been fully characterized (Bartkow et al., 2004) and calibration strategies similar to those used for other sampler types also apply to LDPE samplers (Bartkow et al., 2006). They are among the simplest samplers to use, but their application is not as standardized and widespread, in part due to their relatively low uptake capacity.

Polyurethane foam (PUF) was first used as a material for atmospheric sampling in the 1970s for active air sampling methods (i.e., pumping air through a PUF plug) (Bidleman and Olney, 1974a, 1974b), but its application to passive air sampling did not occur until the 2000s (Shoeib and Harner, 2002). PUF has a reasonably high capacity for absorbing compounds with intermediate volatility. It is a low-cost, commercially available material that is easy to handle and cut to the desired shape depending on the application, and it allows for a straightforward extraction procedure. When coupled with appropriate sampler housings, air sampling rates of PUFs have been observed to increase with wind speed gradually enough to produce time-weighted average air concentrations over a sample collection period (Moeckel et al., 2009; Tuduri et al., 2006). Some sampler designs may also facilitate the absorption of compounds in the particle phase more than others, compared to those strictly in the gas phase (Chaemfa et al., 2009b). When accounting for these effects, passive air sampling using PUFs can yield measurements within the range of those of active sampling techniques (Holt et al., 2017), but the need for tighter control over the uncertainty in such comparisons has still been put forward (Holt et al., 2017; Li and Wania, 2021).

Another widely used passive air sampler is based on divinylbenzene–styrene copolymer resin (XAD). It has a higher uptake capacity for SVOCs and higher stability of absorbed compounds than PUF (Chuang et al., 1987; Dobson et al., 2006), which is an advantage for sampling the more volatile SVOCs or for studying remote areas that may require exceptionally long exposure times. Moreover, because of their large uptake capacity, XAD samplers are assumed to always absorb compounds at a linear rate, eliminating the need for complex modelling for the determination of atmospheric concentrations. A well-established XAD sampler design was introduced in the early

2000s (Wania et al., 2003) and has since seen world-wide application. Some difficulties related to these samplers are the rather expensive cost of the resin and the need for specialized steel mesh housings as XAD is presented in powder form, so their handling can be laborious compared to other alternatives. Notable efforts have been made for bringing the increased uptake capacity of XAD to other more convenient samplers, including XAD-coated PUF (Shoeib et al., 2008). These are known as sorbent-impregnated PUF disks (SIP). However, the introduction of additional steps to the process makes them less attractive as handling becomes more complex, higher error may be induced, uptake kinetics become complicated, and additional contamination may occur.

Besides the passive air sampler types described above, there is a myriad of other sampler materials, configurations, and combinations. These include enclosed sorbent techniques using different polymers, other non-porous sorbents in applications like SPME, materials such as silicone samplers or lipid-coated fibres, and combinations with additional materials like glass fibre filters. However, they are either not as popular as they are limited to very particular applications, or their uptake kinetics have not been as well characterized as for the more common media.

Major developments in passive air sampling technologies have been recognized as potential solutions for overcoming the limitations that other environmental and regulatory assessment approaches traditionally suffered from (Harner et al., 2006a). As a result, their application has become global and international monitoring networks and studies have been established in recent decades, providing a pool of information on the levels and distribution of pollutants across the world. The Global Atmospheric Passive Sampling network (GAPS) was the monitoring effort with the largest scope, encompassing all continents, and provided an evaluation of the feasibility of PUFs as passive samplers on a global scale for the analysis of many SVOCs including PCBs, organochlorine compounds, PBDEs, several pesticides, and novel brominated flame retardants, among others (Harner et al., 2006b; Pozo et al., 2009, 2006; Rauert et al., 2018; Sum et al., 2007). Related efforts used XAD-based samplers for the study of organic pesticides like DDTs, HCHs, and several others across the world (Shunthirasingham et al., 2010). A follow-up initiative to GAPS named GAPS-Megacities aimed at monitoring organic pollutants in twenty major urban areas using PUFs for sampling OPEs, PBDEs, novel flame retardants, and other chemicals of emerging concern (Saini et al., 2020).

Finally, an independent monitoring effort spanning three major continental areas used PUFs for the study of PCBs, organochlorine pesticides like DDTs, and polychlorinated dibenzo-p-dioxins and dibenzofurans (PCDDs/PCDFs) (Bogdal et al., 2013). Additional information on these global networks and other large-scale studies using passive air samplers has been summarized elsewhere (Qu et al., 2018; Wania and Shunthirasingham, 2020).

1.3.2 Passive water samplers

The original application of SPMDs in aquatic environments was described in the early 1990s (Huckins et al., 1990). Their structure consisting of an LDPE tube wall enclosing a triolein film described in Section 1.3.1 was developed to mimic to a certain extent the accumulation of pollutants in biota. SPMDs have arguably been the most widely used passive water samplers to date and helped develop the passive sampling theory and calibration methods to a great extent (Booij et al., 1998; Huckins et al., 2006, 2002). Like with air samplers, the use of only the LDPE membrane as a passive sampling medium was proposed and tested (Adams et al., 2007; Booij et al., 1998; Müller et al., 2001). LDPE on its own is a very cost-effective material, the compound uptake mechanics of which have been studied in detail for aquatic applications (Lohmann, 2012). Additionally, LDPE allows for a simpler sampler treatment and extraction compared to other candidate polymers like silicone rubber (SR), although its resistance to pollutant transport is somewhat higher (Rusina et al., 2007). It is this lower resistance to pollutant diffusion of SR that popularized silicone as an alternative material during the last decade. The compound uptake kinetics of SR have been since characterized (Rusina et al., 2010; Smedes et al., 2009) and put to test against those of LDPE, finding comparable results between materials although advocating for the adoption of SR over LDPE based on simpler data interpretation and higher reliability of the variables involved in the required calculations (Sobotka et al., 2022).

A specific subset of passive water samplers relies on adsorption in a receiving phase as a pollutant uptake mechanism instead of absorption through diffusion. One example is the Chemcatcher[®], a more complex, dual-phase water sampler design based on commercially available particle-loaded solid phase extraction disks typically covered with a membrane through which compounds diffuse (Kingston et al., 2000). The

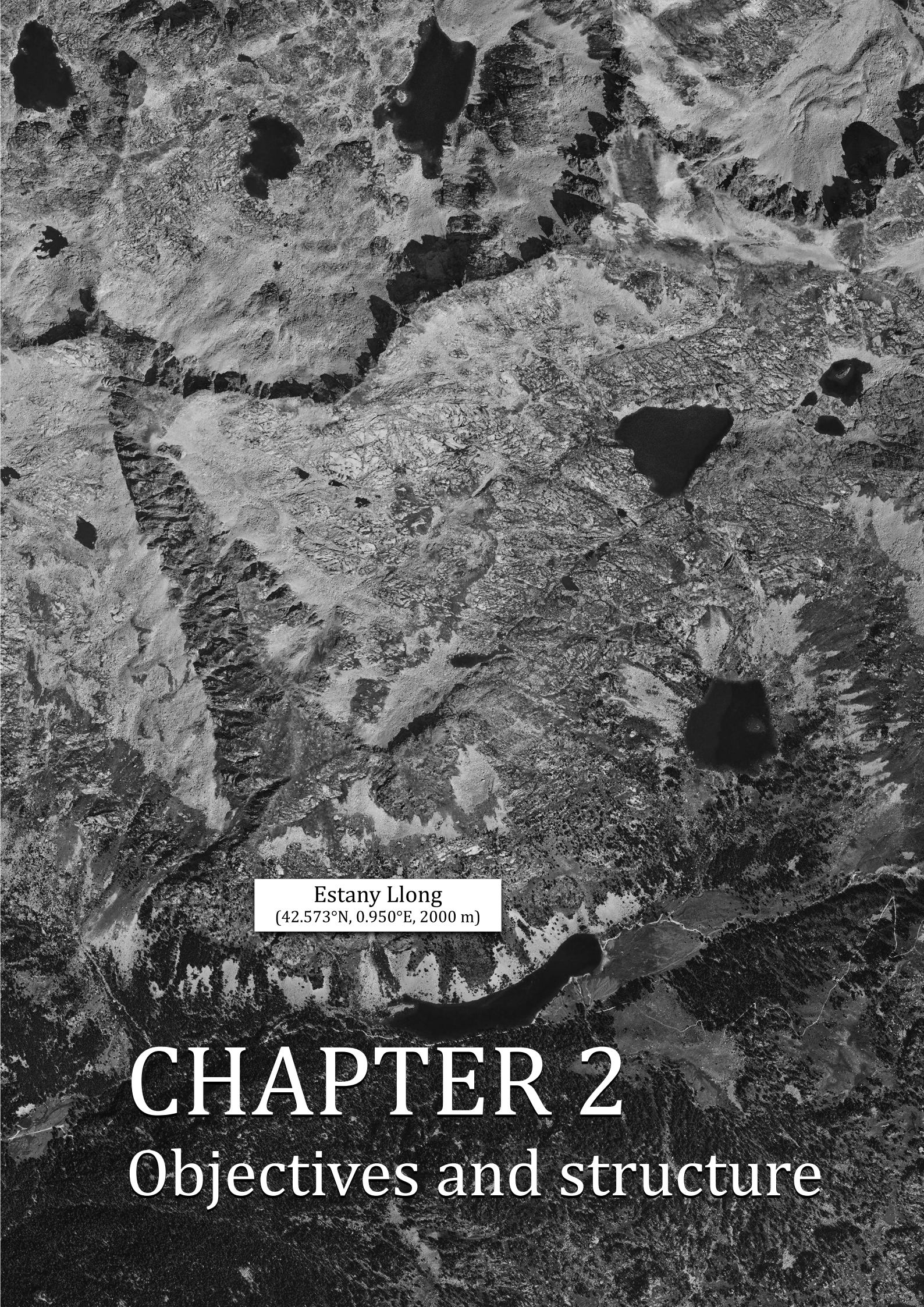
extraction disks and diffusion membrane can be configured using different materials depending on the intended application of the sampler. A similar sampler concept is applied in the commercially available Empore™ and Speedisk™, also varying in configurable materials. However, the most popular multiple-phase sampler is the polar organic chemical integrative sampler (POCIS), specifically targeted at hydrophilic organic contaminants such as pharmaceuticals and some pesticides (Alvarez et al., 2004).

Other alternatives for passive water sampling include polymers like polyurethane, ethylene vinyl acetate, and polyoxymethylene, and techniques like SPME as was also the case with air sampling. Most of these have rather specific applications or do not have fully characterized uptake kinetics, so their popularity is limited in environmental monitoring.

Unlike atmospheric passive sampling, the coordinated application of passive water samplers on a global scale is much more limited and short-lived. The most relevant effort to establish a worldwide monitoring programme is the Global Aquatic Passive Sampling network (AQUA-GAPS). Recognizing the success of the atmospheric GAPS programme, a call to action was made at the beginning of the 2010s for a cooperative deployment of polyethylene samplers in aquatic environments around the world (Lohmann and Muir, 2010). The main aim of the network would be to demonstrate the feasibility of passive water samplers for the study of geographical distribution and changes over time of hydrophobic organic pollutants of concern like PCBs, PBDEs, PAHs, pesticides, and OPEs. The first steps toward establishing the network were made some years later (Lohmann et al., 2017), outlining proof-of-concept studies and setting up the deployment of samplers as a decentralized network. The first results of these concept studies were recently published (Sobotka et al., 2022), testing different sampler materials and their inter-comparability in deployments performed at dozens of locations distributed worldwide. Moving forward, AQUA-GAPS aims to establish a permanent network of networks for oceanic, coastal, riverine, lacustrine, and wastewater effluent environments.

In the present work, passive samplers have a central role in monitoring pollutant levels and trends in remote alpine sites. They have been used for sampling air and water from several high-mountain lacustrine areas, and their capacities and calibration

strategies have been put to the test regarding their ability to produce adequate results and reveal compound distribution patterns in environments with characteristically extreme meteorological conditions and generally low pollutant concentrations. The specifics of sampler uptake mechanics, passive sampler calibration, and deployment conditions are detailed in the following sections.

An aerial photograph of a rugged, mountainous landscape. The terrain is characterized by steep, rocky slopes and a central river valley. The river flows through the valley, surrounded by dense vegetation. The overall scene is a high-altitude, mountainous region.

Estany Llong
(42.573°N, 0.950°E, 2000 m)

CHAPTER 2

Objectives and structure

2.1 Objectives

The exposure of high-altitude alpine areas to environmental pollution regardless of their remoteness has been determined to be considerable. Anthropogenic pollution not only generates a globally distributed background layer of contamination that affects all regions of the world, but also poses a serious threat to cold mountain ecosystems that tend to accumulate pollutants. Persistent legacy pollutants that were once widely used, determined to be highly toxic, and restricted or banned still are a prominent component of this chemical background. Additionally, many substances that are currently used and mostly unregulated are becoming a considerable environmental threat because their production increases year by year despite exhibiting global distribution potential, persistence, and toxicity. The risk is particularly significant for organisms in ecosystems at the mountaintops, but their inaccessibility poses a set of challenges for studying the impact of pollution. These challenges can be overcome using passive samplers, sample collection methodologies that have seen increased use in the last decades but that still present difficulties and uncertainties that may be amplified in the harsh environment of high mountains.

The main aim of the present work is to study the occurrence and distribution of legacy and current semi-volatile and hydrophobic organic pollutants in the air and water of high-elevation lacustrine areas of the Pyrenees and urban areas in Barcelona using passive samplers. To that end, the following objectives were established:

- To assess the performance and applicability of passive samplers to the study of organic compounds in high-altitude areas and to estimate the uncertainty in the calibration of sampling rates and effective sampled volumes.
- To measure the concentrations of semi-volatile organic compounds in the atmospheric gas phase over a high-altitude alpine region using passive air samplers and to determine and explain possible changes in the composition of atmospheric pollution in comparison to measurements performed decades ago in the same area.
- To determine the concentration of a series of legacy and emerging semi-volatile organic compounds in the air of a densely populated urban area, to explain their

changes over time under an unprecedented set of environmental and social conditions caused by the generalized and simultaneous lockdown of multiple countries at the beginning of a global pandemic, and to compare them with measurements in background alpine regions.

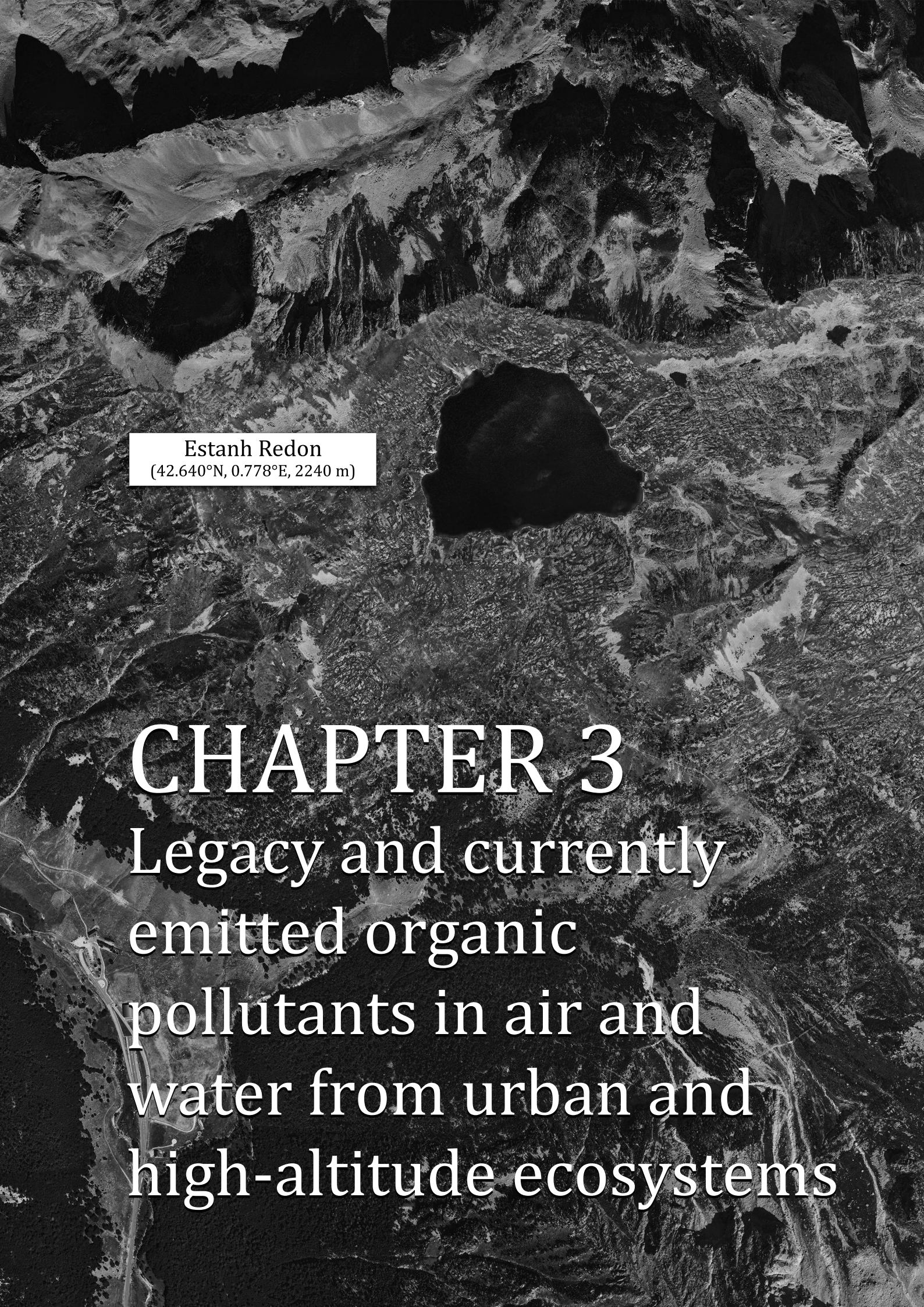
- To assess the environmental fate and behaviour of the selected pollutants by studying the effect of ambient temperature and meteorology on their distribution between air and environmental surfaces, thus characterizing the role of the studied mountains as receivers or emitters of semi-volatile organic pollutants depending on their physical-chemical properties.
- To measure the concentrations of hydrophobic organic compounds in the freely dissolved phase of water of several high-altitude alpine lakes using passive water samplers and to determine the existence of long-term temporal trends in their levels compared to previous measurements from decades ago.
- To determine the direction of the diffusive exchange of compounds between air and water at each studied lake through the application of a boundary layer model that relies on geographical, meteorological, and physical-chemical properties of the compounds, thus identifying the accumulating or emanating behaviour of these high-altitude Pyrenean lakes.

The evidence presented here will hopefully add to the pool of knowledge on the distribution and reach of legacy and, more importantly, emerging pollutants to inform both the scientific community and the pertinent authorities in the event of future regulatory action aimed not only at protecting remote ecosystems, but also human health in urban locations. At the same time, the use and assessment of passive samplers in these remote sites that are scarcely monitored in detail are hoped to provide new insight that becomes useful for the implementation of wider passive sampling networks and for better establishing passive air samplers as an accepted methodology in regulatory monitoring of environmental pollution.

2.2 Structure

The present dissertation is structured as follows:

- CHAPTER 1 introduces the global diffuse occurrence of organic pollutants and the mechanisms behind the worldwide distribution of compounds. The relevance of high mountains as remote ecosystems and their role in the accumulation of pollutants that are transported long distances towards them are highlighted, with special focus on lacustrine areas and their potential for acting as sinks of anthropogenic contamination. The four main groups of studied legacy and emerging chemicals are presented along with their properties and potential health risks. Finally, passive sampling techniques are introduced as proven (but still evolving) tools for the monitoring of pollution that offer solutions to the main issues of sampling in remote and difficult-to-access locations such as high-elevation alpine sites.
- CHAPTER 2 lays the framework of the present thesis, establishes the main research objectives, and describes the structure of the dissertation.
- CHAPTER 3 constitutes the main body of work of this dissertation. Firstly, several aspects relevant to the performed research are introduced, such as a brief review of published literature on anthropogenic pollutants in the area of study, the atypical circumstances in which the measurements in some of the presented studies were performed, key concepts on the sources and distribution of the studied compounds between environmental compartments, and the mechanics of diffusive uptake of pollutants by passive samplers and their calibration. Secondly, the geographical, ecological, and meteorological characteristics of the area of study are described, and the specifics of the sample procurement methodology are detailed for the passive samplers used in air and water. Finally, the results of the research are presented in five scientific articles and an additional discussion of the results, covering the study of the occurrence of organic pollutants and their distribution in the air and water of an urban site and several high-elevation alpine lakes.
- CHAPTER 4 summarizes the general conclusions reached from the work and results presented in this dissertation.

An aerial photograph of a rugged, high-altitude mountain landscape. The terrain is characterized by dark, jagged rock formations and lighter-colored, possibly snow or ice-covered, areas. A prominent, dark, irregularly shaped lake is situated in the center of the image. The overall scene is desolate and mountainous.

Estanh Redon
(42.640°N, 0.778°E, 2240 m)

CHAPTER 3

Legacy and currently
emitted organic
pollutants in air and
water from urban and
high-altitude ecosystems

3.1 Introduction

3.1.1 Background: previous studies and circumstances of the present work

The present work focuses on the study of the occurrence and distribution of atmospheric and aquatic pollutants in a high-elevation area in the Pyrenees. These mountains have been a reference site for the study of ecosystems, biodiversity, and diffuse pollution in the atmosphere and freshwater networks for several decades. The bulk of past research on anthropogenic pollutants in this area dates back to the early 1990s. This section presents a brief overview of the main findings concerning diffuse pollution, with particular focus on pollutants in air and water and the input pathways that lead to pollutant accumulation in alpine lakes like Estanh Redon, possibly the better characterized and most exhaustively studied lake in the whole region.

Additionally, the same atmospheric pollutants that were studied in the Pyrenees were also measured in the city of Barcelona to establish a point of comparison between urban and remote levels. By chance, some of these measurements coincided with major lockdown restrictions imposed at the beginning of the global COVID-19 pandemic that led to an unprecedented drop in pollutant emissions. These unforeseen circumstances allowed for an assessment of short-term changes in the composition of atmospheric pollution in a densely populated city on top of the already planned comparison with alpine levels. A summary of previous research on SVOCs in the city of Barcelona and a detailed description of the consequences of the lockdown restrictions are also provided here.

3.1.1.1 The study of diffuse pollution in the Pyrenean mountains

Atmospheric SVOCs in the Pyrenees have typically been measured using active air sampling techniques. In the late 1990s, the mean gas phase concentrations of the sum of 20 PAHs over the Pyrenees were 1.3–2.6 ng m⁻³, similar to those measured in other European high mountains (Fernández et al., 2002). The highest levels were measured in winter, especially for particle-bound PAHs that revealed a temperature dependence of gas–particle partitioning, and soot carbon was identified as a potential main transport medium for PAHs bound to aerosols. Total PAH concentrations in Estanh Redon were also measured at 1475 pg m⁻³ in the gas phase and 70 pg m⁻³ in the particulate phase in a

different study (van Drooge et al., 2010), which were in the range of other measurements performed in several European and North-Atlantic mountain sites, or on the lower side of that range in the case of particle-bound PAHs. In any case, PAH profiles were indicative of long-range atmospheric transport, and a temperature dependence was observed in their particle partitioning patterns.

PCBs, DDTs, HCB, HCHs, and endosulfans were found predominantly in the atmospheric gas phase at mean total concentrations of 34, 3.3, 49, 30, and 3.0 pg m^{-3} , respectively (van Drooge et al., 2004a). Only the higher molecular weight PCBs showed higher concentrations in the particulate phase according to their lower volatility. The levels of some SVOCs of present use at the time showed seasonal behaviour, such as HCHs and endosulfans due to predominant application in warmer seasons, as did PCBs and DDTs due to a higher occurrence of continental air inputs during summer. On the other hand, HCB always showed uniform concentrations. Aside from the aforementioned application of active sampling techniques, one of the first uses of passive sampling with SPMDs in a high-mountain site was performed in the Central Pyrenees at different altitudes (van Drooge et al., 2005). SPMD performance was adequate, revealing HCB concentrations (10–100 pg m^{-3}) consistent with previous studies and in the range of those found in other remote and alpine regions of the world. The average sum of PCBs was 42 pg m^{-3} , and the levels of individual PCB congeners were quite uniform, for the most part between 1 and 10 pg m^{-3} .

Several reports identified the magnitude of deposition pathways into the lake catchment area for different pollutant groups. Total deposition fluxes of PAHs (1560 $\text{ng m}^{-2} \text{month}^{-1}$) were controlled mainly by particle deposition and precipitation in the case of heavy molecular weight compounds, and temperature in the case of low molecular weight ones (Fernández et al., 2003). The same main drivers of PAH deposition were identified in measurements performed a decade later, with fluxes remaining relatively constant over time (Arellano et al., 2018; Fernández et al., 2021). Bulk deposition fluxes of organochlorine compounds including PCBs, HCHs, HCB, and endosulfans were high at Estanh Redon for compounds of active agricultural use at the time (340 and 430 $\text{ng m}^{-2} \text{month}^{-1}$ for endosulfans and γ -HCH, respectively) (Carrera et al., 2002). Contrarily, already banned compounds like PCBs and HCB showed much lower fluxes. Comparisons with sedimentary deposition showed selective trapping of the less volatile compounds

that increased efficiency at lower temperatures. Deposition fluxes of most organochlorine compounds seemed to increase over time until the mid-2000s, except for HCB, which remained constant, and for pesticides, which showed declining fluxes due to restrictions on their use (Arellano et al., 2015). Re-emission from soils and subsequent precipitation was hypothesized as a possible cause for the observed trend. The input of organochlorine compounds and PAHs into the lake could also be aided by snowmelt since they also accumulate in the snowpack during winter (Carrera et al., 2001; Fernández et al., 2021; Grimalt et al., 2009). Finally, PBDE deposition fluxes into Estanh Redon in the mid-2000s showed distributions consistent with commercial mixtures, and significant correlations were established with air mass inputs of North American origin (Arellano et al., 2014a). This suggested transcontinental pollutant transfer as a main driver of PBDE concentrations, with temperature-dependent re-evaporation as a secondary source of such compounds. Photodegradation was seen to influence PBDE composition significantly, especially during the warmer seasons (Arellano et al., 2014a; Fernández et al., 2021).

Water concentrations of several organochlorine compounds were determined at Estanh Redon at the end of the 1990s (Vilanova et al., 2001b). HCHs were the most abundant organochlorine compounds, with concentrations averaging 2500 pg L⁻¹ for γ -HCH and 410 pg L⁻¹ for α -HCH, which were among the highest concentrations described in lake waters at the time, including urban ones, but in the range of those in a few other remote sites. Endosulfans were found at lower concentrations (α - and β -endosulfan at 60 and 84 pg L⁻¹, respectively), which were at an intermediate level between those found in polar areas and heavily polluted sites. Endosulfan sulfate was the second most abundant organochlorine pollutant at 1000 pg L⁻¹, close to levels in some agricultural tributaries. PCBs at Estanh Redon (62 pg L⁻¹, sum of 7 congeners) were between concentrations from other European alpine lakes but lower than in other continental water bodies, and were observed to be predominantly bound to the particulate phase (generally 72–82%, down to 27% at higher water temperatures) (Vilanova et al., 2001a). The relative abundances of PCB congeners in the dissolved phase were mostly uniform, while lighter PCBs dominated the particulate phase. Total DDT concentrations (16 pg L⁻¹) were close to those in more polluted waters and higher than in other high-altitude lakes. HCB (8.4 pg L⁻¹) was found mainly in the dissolved phase (70–100%,

down to 45–54% at lower temperatures) at concentrations similar to those in other alpine lakes but lower than in some remote polar areas.

PAH concentrations in water from Estanh Redon were also studied over two decades ago (Vilanova et al., 2001c). Low molecular weight PAHs dominated the relative compound distributions in both the dissolved and particulate phases. PAHs in the particulate phase (around 59% of the total PAHs) averaged concentrations of 410 pg L⁻¹, with rather uniform relative abundances of the different compounds except for a lower representation of the more labile PAHs that suffered photooxidation. High molecular weight PAHs were instead more resistant to modifications by water column processes. PAHs in the dissolved phase were found at 270 pg L⁻¹ and were dominated by phenanthrene (around 35% on average) and other low molecular weight PAHs. These concentrations also showed a lower presence of PAHs susceptible to photochemical degradation. Overall, PAH concentrations were much lower than those in water bodies in urban or polluted areas but in the same range or higher than in some other remote sites. Regarding seasonality, higher PAH concentrations were observed in the dissolved phase at lower temperatures, a trend that reflects the increased cold condensation from the atmospheric gas phase into water.

Sediment from Estanh Redon was also analysed for organochlorine compounds and PAHs, showing relatively low concentrations and composition profiles parallel to those observed in atmospheric samples that reflected the remoteness of the lake and the long-range transport nature of the main pollutant input pathways into the lake (Fernández et al., 1999; Grimalt et al., 2004b). Furthermore, air–water–sediment interactions and exchange fluxes were modelled for some compounds, again showing that POP occurrence is mainly driven by atmospheric inputs and diffusive air–water exchange dynamics (Meijer et al., 2006). Seasonal fluxes were determined to control the sink of POPs depending on temperature, especially so for highly chlorinated PCBs (Meijer et al., 2009).

3.1.1.2 The strict lockdown of a country: an opportunity to assess pollution trends at their source

An outbreak of a novel respiratory disease caused by the severe acute respiratory syndrome coronavirus 2 (SARS-CoV-2) and named Coronavirus disease 2019

(COVID-19) by the WHO occurred in China at the end of 2019, and it quickly affected many other countries until being declared a global pandemic in March 2020. The first confirmed COVID-19 positive patient in Spain was registered on 31 January 2020.² Although many cases may have been misidentified due to a lack of information and minimal clinical testing capacity, more than 5000 confirmed cases were detected and over 130 deaths were confirmed to be caused by the virus during the six following weeks. On 14 March 2020, the Spanish government declared a State of Alarm in the whole territory, which became effective the following day, establishing lockdown measures that mandated individuals to remain at home except to fulfil basic needs such as purchasing food and medicines, and forced the temporary closure of schools, universities, and some businesses and shops. On 28 March, further restrictions banned all non-essential activity for 15 days. Some of them were lifted for non-essential workers on 13 April, and further easing of restrictions ensued on 25 May in the city of Barcelona, with a first phase of measures that allowed the opening of small businesses and some freedom of movement during allocated times of the day. A second phase began on 8 June, with less stringent restrictions on businesses and mobility, and a third phase only lasted one day before the lockdown measures were finally lifted on 19 June. Schools remained closed during the whole lockdown period and summer until September 2020.

Personal mobility patterns changed dramatically after lockdown measures came into force. Population movement trends across different categories of activity such as commercial, recreation, and occupational saw reductions between -50 and -90% compared to the period before restrictions, while residential activity increased as people had to stay home (Figure 7). Data reported by local news outlets and authorities in Barcelona during lockdown confirm decreases in urban and industrial activity across many public and commercial sectors, including some of those known to be most impactful on urban air quality. Public transportation traffic (bus and metro) dropped an average of -75 % in March, with the largest drops of -95 to -98% on weekends in April.³ Airborne traffic fell by more than -85% at Barcelona's airport by the end of March.⁴ Cruise and

² www.redaccionmedica.com/secciones/sanidad-hoy/espana-confirma-su-primer-caso-de-positivo-por-coronavirus-de-wuhan-7264 (Accessed October 2020)

³ www.atm.cat/web/ca/covid19.php (Accessed October 2020)

⁴ www.elpuntavui.cat/societat/article/5-societat/1763553-el-traffic-aeri-cau-mes-d-un-85-a-l-aeroport-de-barcelona.html (Accessed October 2020)

ferry traffic at Barcelona’s port dropped by -77 and -56% during March, respectively, while container shipments and transfer operations declined between -19 and -38%.⁵ The first four weeks of lockdown saw average reductions in motorized traffic of -60, -75, -75, and -79%, respectively, up to -93% during the weekends.^{6,7,8,9} Other urban activity indicators showed drops in waste collection of -24%,¹⁰ -9% less water consumption,¹¹ and street noise was reduced by 8.4 dB.¹²

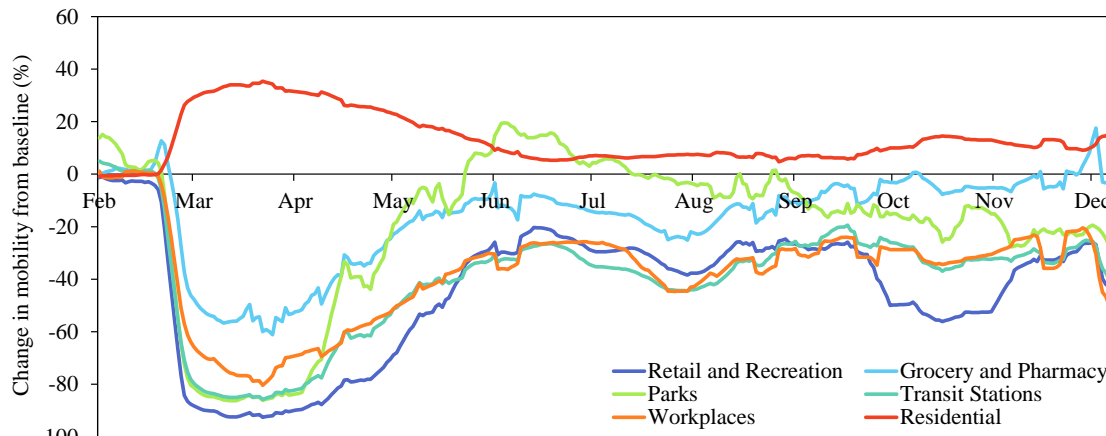


Figure 7. Moving average (7 days) of the changes in population movement trends over time during and after the 2020 lockdown in Barcelona, Spain. Figure created using aggregated location data by Google LLC “Google COVID-19 Community Mobility Reports”.¹³

In our globalized industrial society, this scenario of abrupt cease of commercial, industrial, transport, and social activity in a dense city can be viewed as a unique opportunity for assessing sudden changes in pollutant emissions at their source. Most urban sites nowadays monitor atmospheric contaminants through air quality assessment sensor networks, and satellite measurements are available on a global scale for a number of atmospheric pollutants. Thus, many environmental studies were swiftly published on

⁵ www.elmercantil.com/2020/04/21/el-covid-19-deixa-la-seva-marca-en-les-importacions-i-el-transbord-al-port-de-barcelona/ (Accessed October 2020)

⁶ www.infotransit.blog.gencat.cat/2020/04/03/la-mobilitat-a-larea-metropolitana-de-barcelona-durant-el-confinament/ (Accessed October 2020)

⁷ www.monsostenible.net/catala/noticies/el-transit-de-vehicles-es-reduex-un-63-a-larea-metropolitana-de-barcelona-pel-confinament-demanat-pels-governos-catala-i-espanyol/ (Accessed October 2020)

⁸ www.elpuntavui.cat/societat/article/5-societat/1770111-transit-sota-minims-a-larea-metropolitana-de-barcelona-amb-baixades-de-fins-al-94.html (Accessed October 2020)

⁹ www.ara.cat/societat/transit-Barcelona-respecte-cau-dissabte-confinament-covid-19-coronavirus_0_2433356833.html (Accessed October 2020)

¹⁰ www.amb.cat/ca/web/amb/actualitat/sala-de-premsa/notes-de-premsa/detall/-/notaprensa/covid-19--la-produccio-de-residus-a-larea-metropolitana-de-barcelona-cau/9095832/11696/ (Accessed October 2020)

¹¹ www.govern.cat/govern/docs/2020/03/26/15/34/1e6a600c-c472-49dc-8f9d-1eff51d8e597.pdf (Accessed October 2020)

¹² www.ara.cat/societat/confinament-empremta-ecologica-Barcelona-coronavirus-covid-19_0_2433956597.html (Accessed October 2020)

¹³ <https://www.google.com/covid19/mobility/> (Accessed August 2021)

observed reductions in atmospheric levels of certain contaminants. These usually include volatile species such as CO, NO, NO₂, NO₃, O₃, SO₂, and airborne PM₁₀ (<10 µm particulate matter). Reductions in the levels of most of these contaminants were reported around the world (Fu et al., 2020; Saha et al., 2022), also in Spanish cities (Briz-Redón et al., 2021) including Barcelona (Baldasano, 2020; Tobías et al., 2020), except for ozone, which saw increased levels due to lower reaction capacity with the decreased amounts of NO (Sicard et al., 2020). Overall, these observations pointed to an immediate improvement in air quality in urban sites, which offered a lesson on how effectively some anthropogenic pollutants can be abated (Jevtic et al., 2021; Querol et al., 2021). However, many other anthropogenic pollutants that are continuously released into the environment in urban sites cannot be measured using sensors and automated monitoring equipment. These include SVOCs and POPs emitted from industrial operations, fossil fuel combustion, transport networks (e.g., automobiles, aircraft, and maritime transport), construction activities, waste disposal, energy generation operations, and other sources. As seen in Sections 1.2.1 to 1.2.4, these ubiquitous chemicals have a noteworthy potential for causing adverse health effects and cause harm to ecosystems. But in the context of sudden unannounced restrictions to mobility and a halt of all non-essential occupational activity, the direct measurement of SVOCs became impossible for the duration of the lockdown. That is, unless the sampling was performed with passive samplers that were already deployed before the confinement began.

Although the main objective of the present work is the study of anthropogenic organic pollution in alpine ecosystems, passive air samplers were exposed to the air in the city of Barcelona aiming to obtain a baseline for urban levels of atmospheric contamination. However, the first two planned sampler exposures fortuitously encompassed periods immediately before and during strict lockdown measures, respectively. This allowed for a direct assessment of trends of SVOC concentrations in the city of Barcelona and the determination of potential decreases in their atmospheric levels compared to documented reductions in polluting urban activities. Thus, these results are provided in the present work as a unique evaluation of the behaviours observed in different SVOCs close to their source after experiencing an unprecedented and considerable decline in their potential emissions. To the best of our knowledge and at the date of writing these lines, this is one of the first and very few published reports of

atmospheric SVOC and POP trends during COVID-19 lockdown. Additionally, trends in other typical air quality indicators (CO, PM₁₀, NO, NO₂, and O₃) were also studied and are reported alongside those seen for the organic contaminants. As these measurements were performed in parallel to those in the alpine lakes that are the main focus of this work, pollutant levels observed before and after lockdown were compared to the levels found in the Pyrenees. This provides additional perspective on the difference in magnitude between concentrations at their source and destination, putting the scale of alpine atmospheric pollution into context.

Finally, some background on levels of atmospheric pollutants in the city of Barcelona is provided in the following lines for reference. Many SVOCs considered in the present work have been monitored there in the past, although perhaps not in a way as comprehensive or intensive across the decades as could be expected from a major urban area. The sum of total PAH concentrations in the late 1980s showed very high levels, between 10 and 310 ng m⁻³, with hydrocarbon patterns pointing at gasoline and diesel traffic emissions as predominant PAH sources, as well as heating with diesel stoves (Aceves and Grimalt, 1993). Preferential absorption of high molecular weight PAHs was also observed in small particles in the warm periods, when overall PAH levels were lowest. In the early 2000s, PAH levels in Barcelona measured using passive air samplers were around the median in a study including over sixty sampling sites all across Europe, but polychlorinated naphthalenes were the highest and with the largest contribution of combustion sources (Jaward et al., 2004a). The sum of atmospheric gas-phase PAHs in the mid-2000s was between 3.5 and 7.8 ng m⁻³ in spring and autumn, respectively (Cabrerizo et al., 2011). PAHs in atmospheric particulate matter were between 0.4 and 4.3 ng m⁻³ in the late 2000s, presenting elevated levels in late autumn, and were linked to increased toxicity responses in zebrafish embryos (Mesquita et al., 2014b).

Regarding organochlorinated pollutants, levels of HCHs in Barcelona in the early 2000s were among the highest in Europe, HCB concentrations were very homogenous across all sampling sites, and PCBs were lower compared to other more contaminated sites in Italy, the United Kingdom, France, and Russia (Jaward et al., 2004b). The sum of total PCBs measured by active sampling techniques in the mid-2000s was between 0.08 and 0.30 ng m⁻³ near industrial sites in the city and between 0.06 and 0.13 ng m⁻³ in an urban background site, which was similar to other urban areas at the time (Mari et al.,

2008a). Passive air sampling measurements between 2008 and 2015 found much lower levels in the atmospheric gas phase, where the sum of 12 PCBs in air was around 21 pg m^{-3} (Muñoz-Arnanz et al., 2018). The sum of PBDEs in samples from the same study was 144 pg m^{-3} , the highest among all sampling sites in Spain (Roscales et al., 2018). Finally, measurements of atmospheric OPEs have been very scarce in the city of Barcelona, but individual OPE levels in particle samples were reported between 1 and 1211 pg m^{-3} in the early 2010s (Ramos, 2014), which is much lower than observed in particulate matter from subway stations (sum of 19 OPEs between 6.5 and 156 ng m^{-3}), especially newer ones with plastic components (Olivero-Verbel et al., 2021).

3.1.2 Pollutant sources and partitioning between environmental compartments

Pollutant sources can be divided into primary and secondary. Primary sources result from the direct emission of pollutants into the environment, such as industrial atmospheric emissions and discharge of contaminated residues into rivers and oceans. Secondary sources (not to be confused with secondary formation of new pollutants through chemical reaction in the environment) result from the re-emission of pollutants after these have deposited and accumulated in soils, waters, and other environmental compartments. In alpine regions, the lack of local primary emissions enhances the relative importance of secondary re-evaporation as a pollutant source, although some regional inputs (mid-range atmospheric transport) may also be prominent under certain circumstances as high mountains are closer to continental sources than other more remote sites like the Arctic and Antarctica.

Re-emission plays an important role in the global distribution of pollutants as seen in Section 1.1.1, and is often caused by changes in environmental conditions. For instance, temperature variations may cause the re-volatilization of SVOCs from soils into the atmosphere or the release of compounds trapped in snow and glaciers, hence why the global warming linked to climate change has been identified as a threat that could augment the re-emission of legacy POPs (Gong and Wang, 2022). In fact, the decreasing emissions and atmospheric levels of many POPs (Schuster et al., 2021) and the increasing threat of rising temperatures may significantly boost the relevance of secondary sources of POPs, as has already been observed in the Arctic (Ma et al., 2011). The behaviour that atmospheric concentrations of pollutants exhibit with temperature changes has been

linked to the primary or secondary nature of their sources (Wania et al., 1998), which is of particular interest in mountain slopes with temperature gradients and marked seasonal changes in deposition and evaporation patterns (Daly and Wania, 2005). This will be explored further when discussing the results in the following sections.

We have established that SVOCs tend to volatilize and distribute themselves through the environment by entering different compartments and that this happens after multiple cycles of atmospheric transport in the gas and particle phases, atmospheric removal by wet and dry deposition, re-volatilization, percolation through soils and aquatic transport in rivers and oceans, accumulation in sediments and biota, etc. In this context of pollutants moving between environmental phases, there is an interest in determining the direction of flow of chemicals between compartments and the magnitude of input and output processes and reactions. These determinations usually rely on the assessment of the state of chemical equilibrium in the environmental system, where no net transport, input, or output of substances takes place, even for processes that may never reach actual equilibrium. It is in fact the deviation from a state of equilibrium that provides information on the distribution gradients and the processes taking place. As these states of equilibrium are particular to each chemical, their estimation at specific environmental conditions involves the use of intrinsic physical-chemical variables and empirically determined properties of the compounds. The degree to which a pollutant will enter the atmospheric gas phase depends on its volatility, often measured by its vapour pressure, the partial pressure of a chemical in the gas phase in equilibrium with its liquid or solid form. The capacity of a water body for taking up a compound in its freely dissolved state is determined by the solubility of the compound (i.e., its concentration at equilibrium). The distribution of a pollutant between two environmental phases is determined by partition coefficients, often defined as the ratio of concentrations in both phases in equilibrium conditions. When these phases are the atmospheric gas phase and the dissolved phase of water, the air–water partition coefficient (K_{AW}) often takes the shape of the Henry's Law constant (H), which can be defined as the ratio of the partial pressure of a compound in air to its concentration in water at equilibrium. Partition coefficients can also be derived for any two other compartments, such as air–soil, air–snow, water–sediment, or water–biota. In most cases, however, environmental models rely on proxy partitioning variables that can be determined in a laboratory and that still correlate to the observed behaviour of

pollutants in nature: octanol–air (K_{OA}) and octanol–water (K_{OW}) partition coefficients. These are defined as the ratio of concentrations of a chemical between a phase of n-octanol and air or water, respectively. The octanol fraction thus serves as a reference phase for the study of compound partitioning and allows the extrapolation of behaviours to other matrices. For example, the potential for long-range atmospheric transport of SVOCs is frequently predicted through K_{OA} values (Harner and Bidleman, 1998; Harner and Mackay, 1995; Mackay and Wania, 1995), and the potential of compounds for accumulation in aquatic and lipidic phases can be estimated from K_{OW} values (Armitage and Gobas, 2007; Gossett et al., 1983; Meylan et al., 1996; Miller et al., 1985). The accumulation potential of organic pollutants in remote areas has been proposed to be highest for relatively volatile and hydrophobic compounds with $\log K_{OA}$ between 6.5 and 10 and $\log K_{AW}$ above -3, which roughly corresponds to $\log K_{OW}$ between 5 and 8 (Wania, 2003). This is because chemicals with $\log K_{OA}$ lower than 6.5 are generally too volatile for deposition from the atmosphere, while those with $\log K_{OA}$ greater than 10 tend to accumulate in other compartments before reaching remote locations. Finally, pollutant removal processes are also often described using compound-specific rates and coefficients, like photodegradation rates (Brubaker and Hites, 1998; Keyte et al., 2013; Kwok et al., 1995), and degradation half-lives, sometimes used in biodegradation estimations (Beck and Hansen, 1974; Sinkkonen and Paasivirta, 2000).

Many of these variables play a role in the calculation of environmental fate models and in their interpretation (e.g., Dachs et al., 2000; Gong et al., 2019; Meijer et al., 2006; Palm et al., 2004). These models provide a mechanistic quantitative estimation of the pollutant sources to the environment, transport, and transformation processes based on environmental and physical-chemical variables, and thus aid in the determination of the state of pollution in specific systems. The more complete they are, the more accurate the information they provide on whether pollutant input to any ecosystem is higher than the output, if degradation or accumulation processes are preeminent removal pathways for specific chemicals, or if sites with considerable accumulation of pollutants may be acting as secondary emitters to the environment. In the present work, an air–water exchange model (Deacon, 1977; Schwarzenbach et al., 2016) together with atmospheric degradation estimates were used for establishing the direction of the diffusive transport of pollutants between the gas phase of air and the dissolved phase of water, thus assessing

the general behaviour of the studied high-altitude lakes as accumulators or secondary emitters of SVOCs. The specifics of the model are outlined in Section 3.2.5.

3.1.3 Passive sampling theory: diffusive uptake of pollutants

The transport of pollutants in fluid media like air and water occurs primarily by advection, the bulk transport of mass due to the velocity of the fluid (e.g., wind and aquatic currents). At a narrower scale, convection (i.e., fluid movement due to density gradients) and eddy diffusion (i.e., turbulent fluid dynamics) also affect the transport of mass. However, there is a region of space close to the surface of passive sampler media (PSM) in which molecular diffusion (i.e., the thermal motion of any particle at temperatures above 0 K) dominates the transport of mass. This region is generally known as the diffusion layer, often called air boundary layer for atmospheric samplers and water boundary layer for aquatic samplers. The compounds in the atmospheric gas phase or in the freely dissolved phase of water diffuse through the PSM surface and become absorbed by the sampler material. It is thus necessary for passive samplers to mathematically define the uptake of compounds over time and to predict expected changes in the behaviour of chemicals with different properties.

The exchange of pollutants between an environmental compartment or phase (either air or water, from here on referred to in a general way as just a “phase” or “P”) and a PSM can be described quantitatively in different ways. There are several approaches to modelling passive compound uptake (Salim and Górecki, 2019). The most commonly used models accounting for diffusion boundary layers typically rely on Fick’s first law (Fick, 1855), the fundamental law of diffusion that relates diffusive flux to a gradient in concentration. This can be expressed through a mass transfer coefficient model between the considered phase and the PSM as follows (Huckins et al., 2006):

$$j = k_O \left(C_P - \frac{C_{PSM}}{K_{PSM-P}} \right) \quad \text{Eq. 1}$$

where j is the flux of a compound (mass transferred per unit of area and time), k_O is the overall PSM–phase mass transfer velocity or coefficient, C_P is the concentration of a compound in the phase, C_{PSM} is the concentration of compound absorbed in the PSM, and K_{PSM-P} is the PSM–phase partition coefficient. In the Whitman two-film approach

(Whitman, 1923), which considers the passive sampler as a single and uniform phase in direct contact with the studied environmental phase, the overall mass transfer coefficient can be obtained from individual mass transfer coefficients at each side of the interface between phases. The inverse of k_O , which represents the overall resistance to transport, is equal to the sum of resistances in each phase referenced to the considered environmental compartment:

$$\frac{1}{k_O} = \frac{1}{k_P} + \frac{1}{k_{PSM} K_{PSM-P}} \quad \text{Eq. 2}$$

where k_P is the phase-side (typically air-side or water-side) mass transfer coefficient, and k_{PSM} is the PSM-side mass transfer coefficient.

The rate of change of C_{PSM} over time (t) can be expressed as a function of the flux in Eq. 1 and the sampler's dimensions as:

$$\frac{\partial C_{PSM}}{\partial t} = \frac{A_{PSM}}{V_{PSM}} j = \frac{A_{PSM}}{V_{PSM}} k_O \left(C_P - \frac{C_{PSM}}{K_{PSM-P}} \right) \quad \text{Eq. 3}$$

where A_{PSM} and V_{PSM} are the area and volume of the PSM. The solution for Eq. 3 with initial conditions $C_{PSM} = 0$ at $t = 0$ is:

$$C_{PSM} = K_{PSM-P} C_P [1 - \exp(-k_e t)] \quad \text{Eq. 4}$$

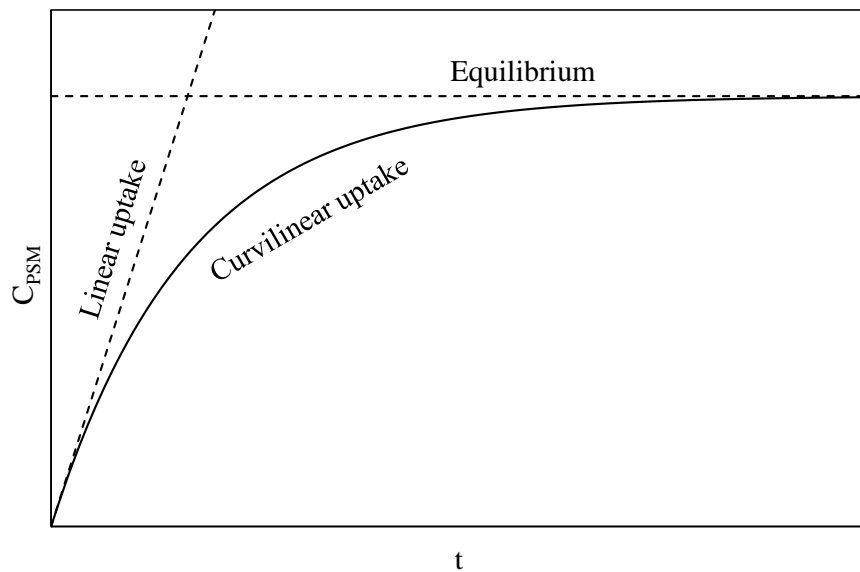


Figure 8. Uptake phases of passive sampling through first-order uptake kinetics, where C_{PSM} is the concentration of compound taken up by the passive sampler medium and t is the exposure time.

which is shaped as a first-order rate equation where k_e is the exchange rate constant. Here, this constant is expressed as:

$$k_e = \frac{A_{PSM} k_O}{V_{PSM} K_{PSM-P}} \quad \text{Eq. 5}$$

Thus, Eq. 4 expresses how the concentration of a compound in the PSM increases over time based on the characteristics of the sampler, the physical-chemical properties of the compound relative to the sampler material, and the initial concentration conditions of the two-phase system. The shape of the accumulation of compounds over time is depicted in Figure 8.

By considering the two extreme cases in these conditions, two distinct sampling regimes are defined. When $k_e t \gg 1$, which can occur with long sampler exposures and for compounds with low K_{PSM-P} (i.e., a lower affinity for the PSM), C_{PSM} reaches its equilibrium value, at which point:

$$C_{PSM} = K_{PSM-P} C_P \quad \text{Eq. 6}$$

which is known as the equilibrium stage of the uptake, where no net absorption of compound occurs in the PSM if its concentration in the environmental phase remains constant. Contrarily, when $k_e t \ll 1$, which can occur with short sampler exposures and for compounds with high K_{PSM-P} (i.e., a higher affinity for the PSM), the expression between brackets in Eq. 4 $\approx k_e t$, leaving:

$$C_{PSM} = K_{PSM-P} C_P k_e t \quad \text{Eq. 7}$$

which is known as the linear stage of the uptake since Eq. 7 describes a linear dependency. The net amount of compound absorbed by the PSM (n_{PSM}) during this linear stage is:

$$n_{PSM} = V_{PSM} K_{PSM-P} C_P k_e t = R_S C_P t = V_{ef} C_P \quad \text{Eq. 8}$$

Note that $V_{PSM} \times K_{PSM-P} \times k_e$ can be condensed under R_S , which is the compound- and sampler-specific sampling rate. R_S gives an indication of the equivalent volume of water or air extracted per unit of time for a specific compound, so it can be directly used for the calculation of effective sampled volumes (V_{ef}) and, therefore, concentrations of compounds in the considered phase for samplers operating under the linear stage of uptake.

However, a more general equation for calculating the amount of absorbed compound can be obtained if the definition of k_e from Eq. 5 is substituted into Eq. 4:

$$n_{PSM} = V_{PSM} K_{PSM-P} C_P \left[1 - \exp\left(-\frac{A_{PSM} k_O}{K_{PSM-P} V_{PSM}} t\right) \right] \quad \text{Eq. 9}$$

The expression between brackets in Eq. 9 is known as the Degree of Equilibrium (DEQ). The DEQ describes the extent of attainment of equilibrium conditions during the exposure of the sampler, taking values from 0 to 1 where 1 represents full equilibrium and 0 the conditions furthest from equilibrium. Thus, Eq. 9 considers all uptake stages indistinctly so no compromises are made regarding the stage achieved by each studied compound. Furthermore, it presents a shape that allows for linking the absorbed amounts during exposure to characteristics of the PSM and its calibration method. Note that this equation depicts a general case, while its application to specific phases like air and water often contains certain variations in how some coefficients are presented in order to better accommodate calibration needs. These specific variations are discussed in the following section.

3.1.3.1 Calibration of passive samplers

Unlike active sampling techniques that commonly involve grab-sampling and pumping operations for the acquisition of samples, the quantity of sampled phase (e.g., air or water) cannot be directly determined in passive sampling. Thus, the conversion from the amount of pollutants found in the samplers to environmental concentrations is not trivial. Different methods for overcoming this issue have been used in the past, from assuming daily uptake rates based on physical-chemical properties and deployment times to co-deployment with active sampling methods. However, this can lead to results with considerable uncertainty as in many cases the conditions in which the sampler is deployed are not optimal for the ideal diffusive behaviour of the studied compounds. For instance, wind speeds, temperature, sampler housing and orientation, water currents, and biofouling growing on samplers deployed underwater can affect sampling rates (Booij et al., 2003; Huckins et al., 2002; Ockenden et al., 2001; Tuduri et al., 2006). Some of these conditions are especially influential in alpine locations where the meteorology and environmental circumstances are usually out of the ordinary (e.g., high wind speeds, low temperatures, and atypical precipitation patterns).

An arguably more quantitative and direct approach to determining sampling rates, and thus more accurate pollutant concentrations, is the use of performance reference compounds (PRCs, sometimes also called depuration compounds), as first suggested in the early 1990s (Huckins et al., 1993) and further tested in following years (Booij et al., 1998). PRCs are analytically non-interfering compounds that do not occur in the natural environment (often isotopically labelled compounds and uncommon PCB congeners) that are added to passive samplers before their deployment into the studied environmental phase. Several PRCs spanning a range of fugacities (i.e., K_{PSM-P}) are typically spiked into PSMs by way of varying techniques depending on the nature of the PSM material. During sampler exposure, PRCs are expected to dissipate over time at differing rates based on their varying physical-chemical properties (affinity for the sampler and sampled phases) as well as exposure time and environmental conditions. The dissipation rates of PRCs are equal but inverse to the uptake rates of equivalent compounds because both uptake and release processes are governed by the same molecular diffusion mechanisms (Booij et al., 2002; Huckins et al., 2002). PRC dissipation rates can thus be used to estimate compound- and sampler-specific sampling rates that account for variation between compounds, sampling sites, periods, and deployment conditions.

The dissipation of PRCs from a PSM is described by:

$$C_{PRC,t} = C_{PRC,0} \exp(-k_e t) \quad \text{Eq. 10}$$

where $C_{PRC,0}$ and $C_{PRC,t}$ are the amount or concentration of a specific PRC in the sampler before and after an exposure time t , respectively. The dissipation profile of a PRC over time is depicted in Figure 9, where the effect of the considered compound and the environmental conditions at the sampling site would produce a value of k_e that adjusts the steepness of the curve. Since $C_{PRC,0}$ cannot be measured in the specific PSM to be deployed, reference blank samplers are prepared, spiked, and analysed in parallel. The release ratio (also known as depletion ratio or retained fraction) of the PRC ($C_{PRC,t}/C_{PRC,0}$) is then calculated, which should take values between 0 and 1, with 0 signifying complete release from the PSM to the environment and 1 complete retention in the PSM. Depending on the affinity of each PRC for the sampler material and for the sampled medium, equilibration may take from days or weeks to months or years, which is why working

with an array of PRCs better represents all possible scenarios. Finally, the dissipation rate is determined as:

$$k_e = \frac{-\ln(C_{PRC,t}/C_{PRC,0})}{t} \quad \text{Eq. 11}$$

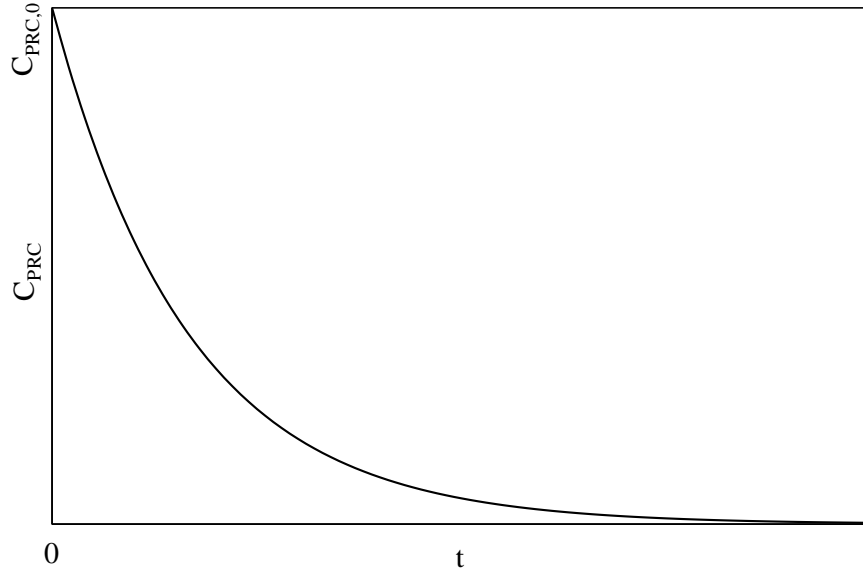


Figure 9. Dissipation profile of a PRC over time through first order release kinetics.

Therefore, the sampling rate of a compound can be estimated from the definition of R_S in Eq. 8 and k_O for the calculation of the sampled volume from Eq. 5. Still, there are several ways in which this concept is typically applied to practical cases. The specific calibration equations for the passive air (PUF disks) and water (LDPE and SR sheets) samplers used in the present work are the following:

a. Calibration of passive air samplers

The retained PRC fractions are related to R_S ($\text{m}^3 \text{d}^{-1}$) through the following equation (Harner, 2021; POZO et al., 2004):

$$R_S = k_A A_{PUF} = \frac{-\ln(C_{PRC,t}/C_{PRC,0}) K'_{PUF-A} D_{film}}{t} \quad \text{Eq. 12}$$

where k_A is the sample-specific air-side mass transfer coefficient (m d^{-1}), K'_{PUF-A} is the density-corrected PUF–air partition coefficient (dimensionless) calculated by multiplying K_{PUF-A} ($\text{m}^3 \text{g}^{-1}$, Table 1) by the density of the PUF (δ_{PUF} , g m^{-3}), A_{PUF} is the area of the PUF disk (m^2), D_{film} is the effective film thickness of the PUF disk (m), and where t is

expressed in days. Note that the practical application of the diffuse uptake theory to atmospheric sampling has led to some important changes. On one hand, k_A is used instead of k_O because for typically monitored compounds ($K_{OA} > 10^7$) the sampler-side velocity term $1/(k_{PUF} \times K_{PUF-A})$ in Eq. 2 is negligible, which means that the mass transfer to the PUF is always air-side controlled and so $k_O \approx k_A$ (Shoeib and Harner, 2002). On the other hand, $D_{film} = V_{PUF}/A_{PUF}$ (where V_{PUF} is the volume of the PUF disk) is used for practical purposes, and K'_{PUF-A} instead of K_{PUF-A} for correcting the PUF partition coefficients to the density of the specific polymer used. K_{PUF-A} values for each PRC can be determined from their temperature-corrected K_{OA} coefficients (Table 1) using the following experimental relationship (Shoeib and Harner, 2002):

$$\log K_{PUF-A} = 0.6366 \log K_{OA} - 3.1774 \quad \text{Eq. 13}$$

Figure 10 shows an example of PRC depletion rates obtained after exposure of a PUF-PAS at one of the studied sites. A different value of R_S can thus be produced from each considered PRC using Eq. 12, which leads to differing values. Typically, an average of these different R_S values is reported, but highly depleted PRCs ($C_{PRC,t}/C_{PRC,0} < 0.2$) and highly retained PRCs ($C_{PRC,t}/C_{PRC,0} > 0.8$) are often left out as small changes in their retained fractions can lead to considerably under or overestimated R_S with high uncertainties. R_S in the present work were obtained as an average of PRCs in the intermediate range of retention.

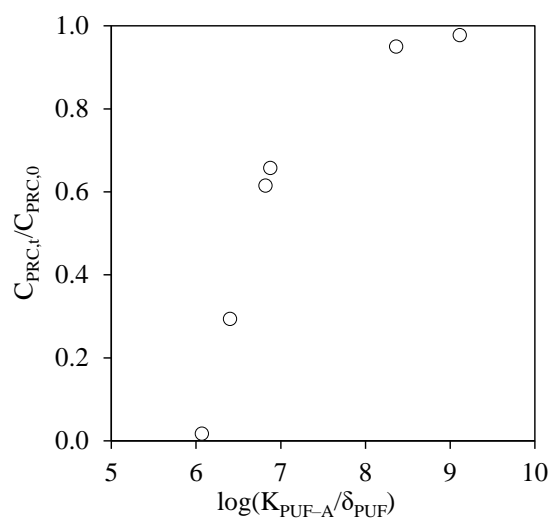


Figure 10. PRC retained fractions as a function of $\log(K'_{PUF-A})$.

Ultimately, concentrations of pollutants in the atmospheric gas phase (C_A , pg m^{-3}) can be calculated for each compound as follows (Poza et al., 2004; Shoeib and Harner, 2002):

$$C_A = \frac{n_{PUF}}{K'_{PUF-A} V_{PUF} \left[1 - \exp\left(-\frac{k_A t}{K'_{PUF-A} D_{film}}\right) \right]} \quad \text{Eq. 14}$$

where n_{PUF} (pg) is the amount of the considered compound found in the PUF disk after analysis and V_{PUF} is expressed in m^3 .

b. Calibration of passive water samplers

The retained PRC fractions in water samplers are related to R_S (L d^{-1}) through the following equation (Huckins et al., 2006, 2002; Smedes and Booij, 2012):

$$R_S = \frac{-\ln(C_{PRC,t}/C_{PRC,0}) K_{PWS-W} m_{PWS}}{t} \quad \text{Eq. 15}$$

where the passive water sampler–water partition coefficient (K_{PWS-W} , in L kg^{-1} , representing either K_{LDPE-W} or K_{SR-W} and often referred to as polymer–water partition coefficient, K_{PW}) takes the place of K_{PSM-P} , m_{PWS} is the combined mass of the sampler sheets (kg), and t is expressed in days. However, much like in passive air sampling calibration, these R_S are specific to each individual PRC. The contributions to the sampling rate of the studied compound and of the hydrodynamic conditions (e.g., water turbulence and sampler geometry) can be separated through the following relationship (Rusina et al., 2010):

$$R_S = \frac{B}{M^{0.47}} \quad \text{Eq. 16}$$

where M is the molar mass of the compound (g mol^{-1}) and B is a proportionality constant that accounts for said hydrodynamic conditions and the conversion of units. Thus, Eq. 15 can be expressed as:

$$\frac{C_{PRC,t}}{C_{PRC,0}} = \exp\left(-\frac{B t}{K_{PWS-W} M^{0.47} m_{PWS}}\right) \quad \text{Eq. 17}$$

A different approach to finding the solution to Eq. 17 is typically used in passive water sampling studies compared to passive air sampling ones. By considering

$C_{PRC,i}/C_{PRC,0}$ as a continuous function of K_{PWS-W} , an unweighted nonlinear least squares (NLS) fit of Eq. 17 with B as an adjustable parameter can be used to estimate compound- and site-specific water boundary layer-controlled uptake sampling rates (Booij and Smedes, 2010). As B has an abstruse practical meaning, R_S for a reference molecule of 300 g mol^{-1} are usually reported for each sample using Eq. 16, allowing for direct comparison between sites or periods. Figure 11 shows an example of NLS fit of PRC fractions as a function of $\log(K_{PWS-W}/M^{0.47})$. Uncertainty estimations for the B coefficient (and thus R_S) are performed from the difference between experimental and modelled values of $C_{PRC,i}/C_{PRC,0}$ and ultimately expressed as standard errors following uncertainty estimations described elsewhere (Billo, 2001) as outlined by Smedes and Booij.¹⁴ This approach to PWS calibration is more developed and tested more in depth in the literature than in the case of PAS. It takes all PRC depletion data into consideration, as opposed to only deriving R_S from selected PRCs. Still, PRCs sitting at the middle of the depletion curve have a higher weight over the NLS fit.

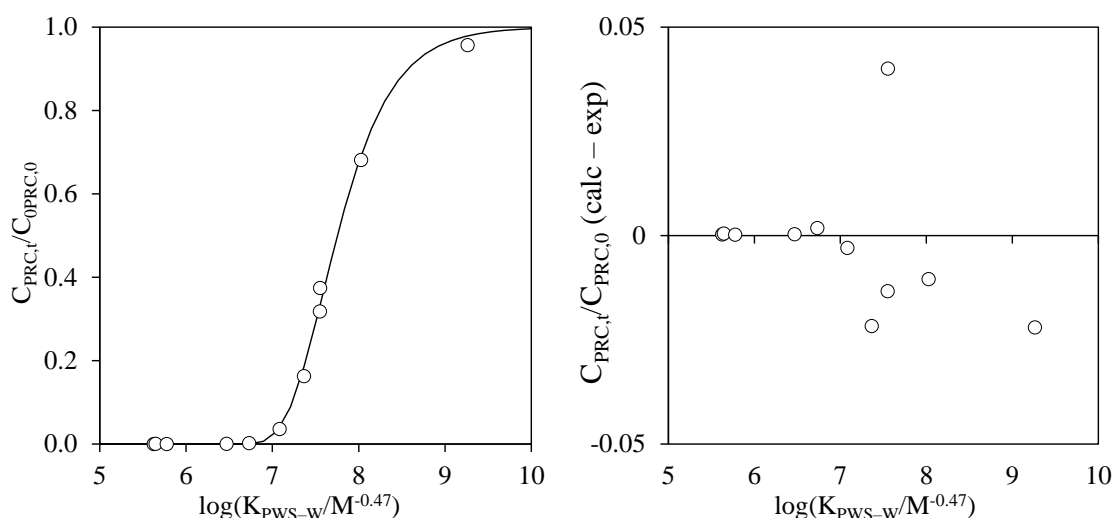


Figure 11. PRC retained fractions as a function of $\log(K_{PWS-W}/M^{0.47})$ (left), where the curved black line is an NLS fit for a water boundary layer-controlled uptake sampling rate, and difference between experimental and calculated retained fractions (right).

Ultimately, concentrations of pollutants in the dissolved phase of water (C_w , pg L^{-1}) can be calculated for each compound as follows (Booij and Smedes, 2010):

$$C_w = \frac{n_{PWS}}{K_{PWS-W} m_{PWS} \left[1 - \exp\left(-\frac{B t}{K_{PWS-W} M^{0.47} m_{PWS}}\right) \right]} \quad \text{Eq. 18}$$

¹⁴ www.passivesampling.net/rs/rs_v3a.xls (Accessed July 2022)

where $npws$ (pg) is the amount of the considered compound in the sampler.

3.2 Methodology

3.2.1 Area of study

Six alpine lakes spanning a range of altitudes in the Central Pyrenees were selected in this work for studying the occurrence, concentration, and distribution of anthropogenic pollution between 2017 and 2020. These were Estany de Llebreta (42.549°N, 0.888°E, 1619 meters above sea level), Estany Llong (42.573°N, 0.950°E, 2000 m), Estany de Sarradé (42.564°N, 0.896°E, 2123 m), Estany Redon (42.640°N, 0.778°E, 2240 m), Estany de Dellui (42.548°N, 0.948°E, 2349 m), and Estany de la Collada (42.544°N, 0.942°E, 2453 m). Figure 12 shows their specific locations. All these lakes are part of the European Union's Natura 2000 network of protected natural areas, and five of them (excluding Estany Redon) are inside of the National Park of Aigüestortes i Estany de Sant Maurici, a reserve for the conservation of natural spaces with restricted access. Thus, they are amongst the most remote and isolated bodies of water in the continent, experiencing reduced anthropogenic influence from distant major roads and



Figure 12. Pyrenean lakes studied in the present work. Base map: Produced Work by the OpenStreetMap Foundation using OpenStreetMap data under the Open Database License, © OpenStreetMap contributors.

population centres. This makes them particularly suitable for the study of global diffuse and background levels of pollution, the influence of long-range atmospheric transport of pollutants, and the accumulation of contaminants in theoretically pristine aquatic ecosystems.

This area of the Pyrenees is well known for its high concentration of small alpine lakes as a result of successive excavation phenomena in the cirques and valleys by glaciers in the Quaternary Period (2.58 million years ago). The lakes are of oligotrophic nature (Catalan et al., 2006), with the highest ones being cirque lakes with small rocky catchments and the lowest ones collecting the drainage of the whole valley. They are subject to especially pronounced seasonal changes. They freeze and remain covered in ice for up to seven months each year, typically starting in November (Catalan et al., 1992). In spring, which is meteorologically short and spans mainly the month of June, an algal bloom occurs as light penetrates the water again and water mixes with the increase of temperature. By summer, the water becomes stratified in two layers of different temperature, which lasts until the end of autumn.

In general, these are small lakes, with only Redon standing out at a larger size, as are their catchment areas compared to those of other continental bodies of water. The size of the lakes and their surrounding catchment areas was determined using the Arc Hydro data model and toolset in ArcGIS (Esri, Redlands, CA, USA) and the global digital elevation model (GDEM) data from the Advanced Spaceborne Thermal Emission and Reflection Radiometer (ASTER; METI, Japan and NASA, USA). For these catchment areas, terrain coverage and habitat data were obtained from the Catalan Government's Department of Territory and Sustainability. This information provides an overview of the type of vegetation (or lack thereof) covering the studied area, which is often relevant in the assessment of the source of certain organic pollutants that can have a natural origin (e.g., some PAHs). The catchments are shown in Figure 13, while additional output from the Arc Hydro model can be seen in Appendix I: Lake catchments (Figure 44 to Figure 46).

The resulting areas were the following: Llebreta (lake area 74,061 m², catchment area 50.91 km²), Llong (72,655 m², 10.95 km²), Sarradé (41,929 m², 4.28 km²), Redon (246,452 m², 1.44 km²), Dellui (51,189 m², 1.51 km²), and Collada (24,102 m², 0.17 km²).

The relative habitat area within each catchment in Figure 13 (see Figure 47 in Appendix I: Lake catchments for an expanded view) shows the presence of forest habitats in the three lowest altitude lakes but not in the highest ones, as is characteristic in alpine altitudinal gradients where the tree line becomes apparent. These forests are typically populated by mountain pine, silver fir, common beech, and Baltic pine. The lowest lakes, Llong and especially Llebreta, are also partially surrounded by fens and wetlands of common sedge. Lakes above the tree line are characterized by sparser vegetation, mainly comprised of grasslands of different fescue species, matgrass, alpine sedge, and common bent, with bushes of alpenrose, junipers, and alpine azalea, and large areas of exposed rock, screes, and glaciers. All these characteristics are noticeable in pictures taken at each lake (Figure 14 to Figure 16).

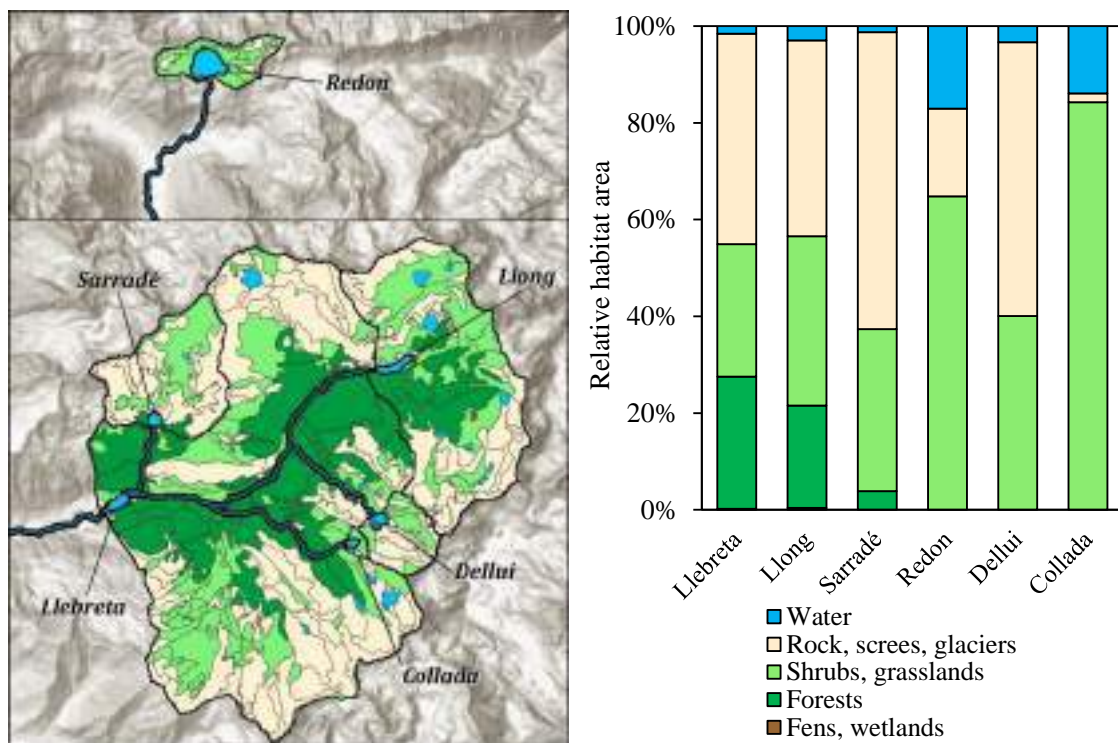


Figure 13. Lake catchment areas and terrain coverage and habitat data (left) and relative habitat area within each catchment area (right). Note that Llebreta's catchment area includes all other surrounding delineated catchments. Figure created using data from Servei de Planificació de l'Entorn Natural, Direcció General de Polítiques Ambientals i Medi Natural (Cartografia dels hàbitats d'interès comunitari a Catalunya, versió 2 (2018), last updated 30/11/2018) (Generalitat de Catalunya, Departament de Territori i Sostenibilitat).



Figure 14. Estany Llong (top) and Estany de Llebre (bottom).



Figure 15. Estanh Redon (top) and Estany de Sarradé (bottom).



Figure 16. Estany de la Collada (top) and Estany de Dellui (bottom).

3.2.2 Meteorology

The present work proposes the study of pollutants in an alpine area along an altitudinal gradient using passive sampling techniques, as well as the determination of their behaviour based on environmental and physical-chemical parameters. All of these rely first and foremost on the accurate determination of the ambient temperature at each specific sampling site, as passive sampling calculations and the environmental fate of chemicals depend directly on temperature and the effect it has on pollutant distribution between environmental compartments. Moreover, other meteorological variables like wind speeds and precipitation can provide additional insight on sampler performance and differences in pollutant levels between periods. Adequately monitoring these variables is especially critical in alpine areas that typically experience much harsher conditions such as lower and more variable temperatures, higher wind speeds, or increased precipitation, often in the form of snow. Here, a series of methods and data sources were used to keep track of the meteorology affecting not only the general area of study but also each specific sampling site individually.

Meteorological data from the area of study were sourced from the Network of Automatic Meteorological Stations (XEMA) from the Catalan Meteorological Service (Meteocat). Values of air temperature, relative humidity, pressure, precipitation, wind speed and direction, and solar irradiance were obtained between September 2017 and October 2020 for three meteorological stations in Estanh Redon (42.63835 °N, 0.77889 °E, 2247 m), la Vall de Boí (42.46602 °N, 0.88405 °E, 2535 m), and Barcelona (41.37919 °N, 2.10540 °E, 79 m) with measurements performed every 30 min. A representation of an example of the data can be seen in Figure 17 as a moving average of air temperature and relative humidity and in Figure 18 as a wind rose of wind speeds and directions. The complete representations of all collected variables are reported in Appendix II: Meteorology (Figure 48 to Figure 57).

As seen in Figure 17 and Figure 18, meteorological conditions in high mountains tend to be much harsher and more pronounced than in other areas. Temperatures are lower on average and reach much lower minimum values (down to -16.6 °C in Estanh Redon compared to only 0.5 °C in Barcelona), with higher average relative humidity (76% compared to 68%) and much higher wind speeds (maximum speed up to 130 km h⁻¹

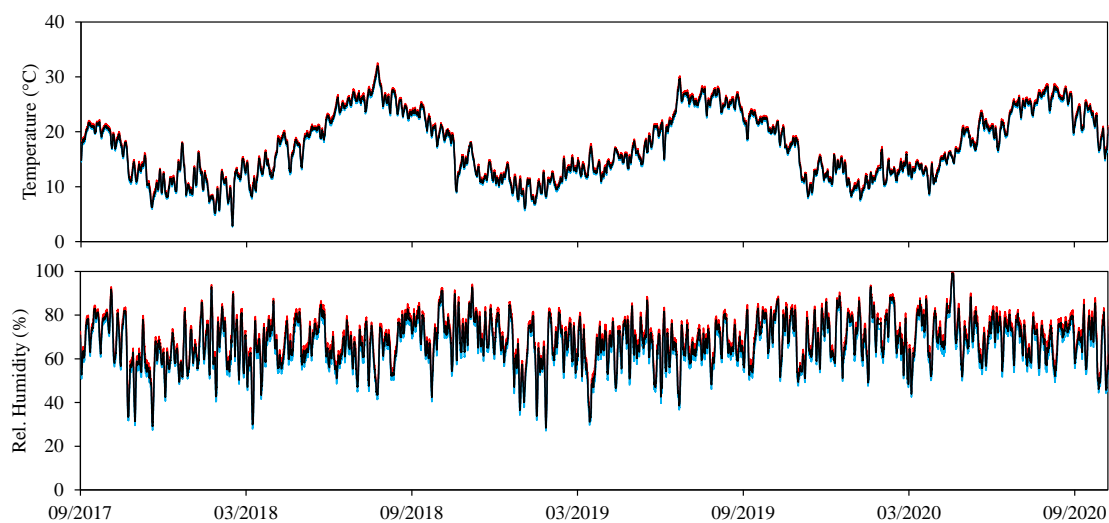


Figure 17. Moving average (48 h) of the air temperatures recorded every 30 min in Estanh Redon (top) and Barcelona (bottom) over the full duration of the study. Figure created using data from Xarxa d'Estacions Meteorològiques Automàtiques (XEMA) del Servei Meteorològic de Catalunya (METEOCAT) (Dades meteorològiques de la XEMA, last updated 06/09/2022) (Generalitat de Catalunya, Departament de Territori i Sostenibilitat).

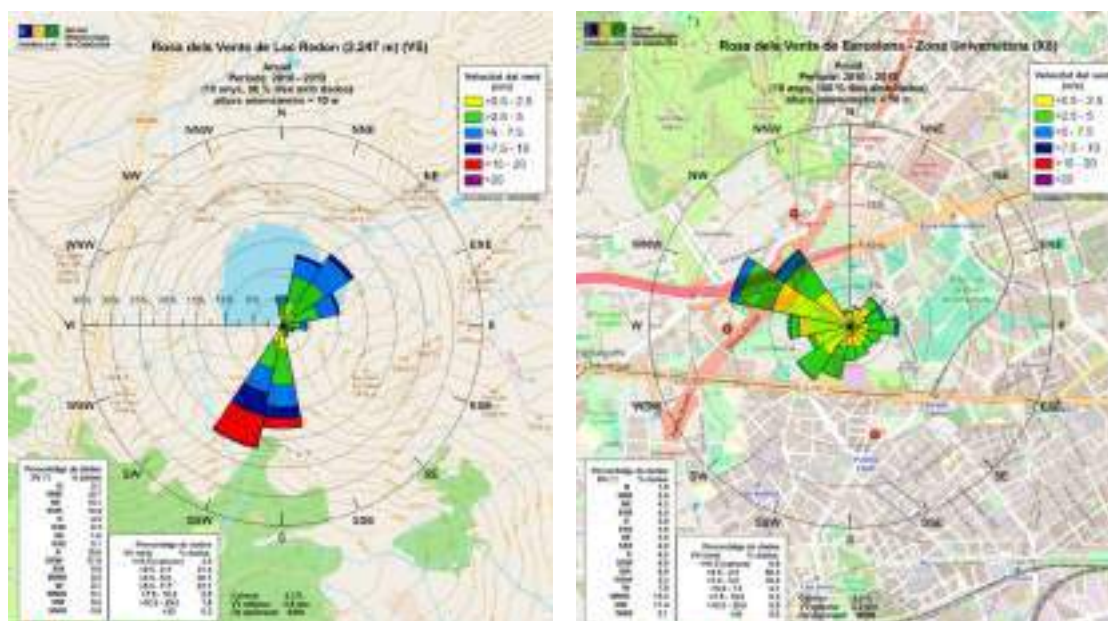


Figure 18. Wind rose of the average distribution of wind speeds and directions at Estanh Redon (left) and Barcelona (right) between 2010 and 2019. Wind roses from Xarxa d'Estacions Meteorològiques Automàtiques (XEMA) del Servei Meteorològic de Catalunya (METEOCAT) (Dades meteorològiques de la XEMA, last updated 06/09/2022) (Generalitat de Catalunya, Departament de Territori i Sostenibilitat). Base maps: Produced Work by the OpenStreetMap Foundation using OpenStreetMap data under the Open Database License, © OpenStreetMap contributors.

compared to 82 km h^{-1}). Precipitation frequency and amounts in alpine environments also tend to be higher, with up to 4991 accumulated mm compared to 2202 mm accumulated in Barcelona. Moreover, this precipitation occurs in the form of snow during a considerable part of the year, reaching heights of accumulated snow of 3.5 m.

Differences in location and altitude between sampling sites lead to significant variations in temperature, but no other automatic meteorological stations were available next to the sites chosen in this work. Thus, temperature-recording devices known as data loggers (Tinytag Plus 2 data logger, Geminy Data Loggers, Chichester, United Kingdom) were deployed with every pair of passive air samplers as shown in Figure 19. Air temperature and relative humidity measurements were performed with a 30 min resolution using data loggers attached to each deployed structure, sheltered from precipitation and direct sunlight inside semi-open opaque plastic boxes. All data loggers were simultaneously calibrated against each other before and after every use at different temperatures in the expected range of the studied sites. An example of the data obtained from data loggers is shown in Figure 20, and additional temperature and humidity measurements can be found in Appendix II: Meteorology (Figure 58 to Figure 62).



Figure 19. Data logger (Tinytag Plus 2, yellow box) deployed at each studied site for registering the ambient temperature and relative humidity for the duration of the sampling periods.

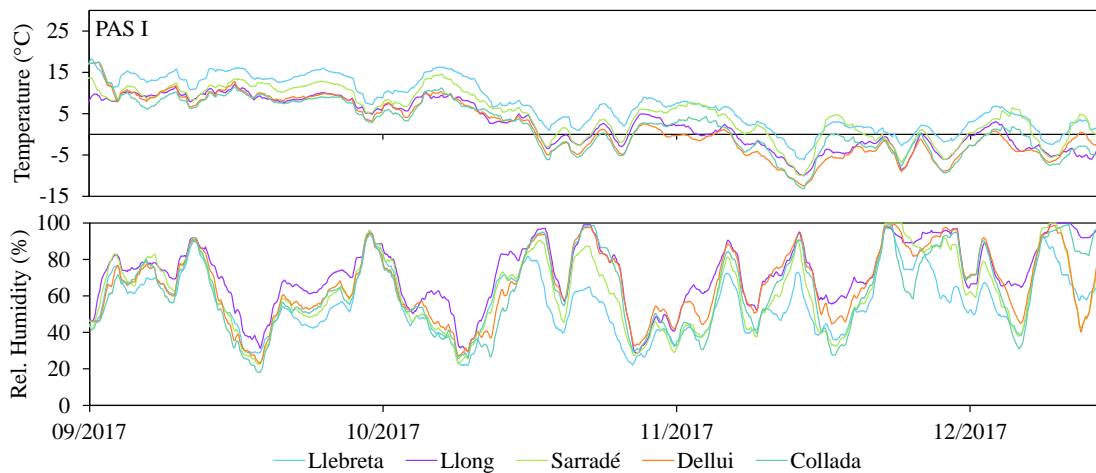


Figure 20. Moving averages (48 h) of air temperature (top) and relative humidity (bottom) measured every 30 min during air sampling period PAS I. Figure created using data collected with data loggers.

The overall mean air temperatures throughout all sampling periods were between 2.6 and 9.8 °C and negatively correlated with altitude ($p < 0.01$) (Figure 21), as is expected with increasing altitudes. As an average, this regression indicates a reduction of 0.87 °C per 100 m, in the range of the globally accepted 0.60 to 0.98 °C per 100 m depending on the meteorological conditions. The average temperatures recorded in this study also depended on the geographical location of the lakes and the characteristics of their catchments, such as the shade that surrounding mountains cast on the sampling sites. Some of these differences can be seen in the average temperature profiles throughout the day shown in Figure 21 (and for additional periods in Figure 63 in Appendix II: Meteorology), with some lakes peaking at higher temperatures than others and at different times of the day.

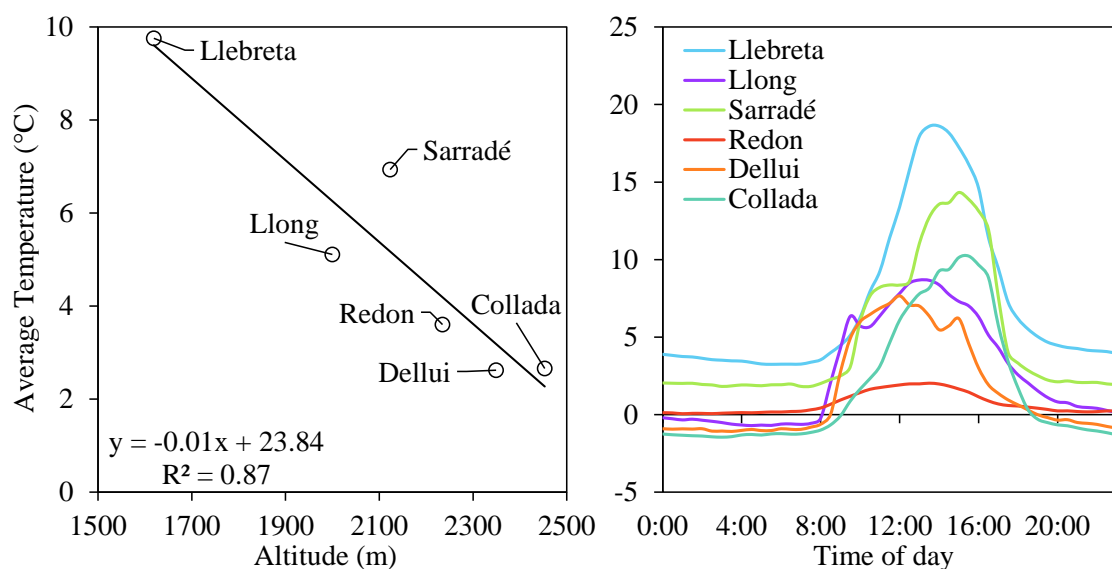


Figure 21. Average temperature at the studied sites as a function of their altitude (left) and daily average temperature profiles (right, shown for sampling period PAS I). Figure created using data collected with data loggers co-deployed at each site with the passive samplers and data from Xarxa d'Estacions Meteorològiques Automàtiques (XEMA) del Servei Meteorològic de Catalunya (METEOCAT) (Dades meteorològiques de la XEMA, last updated 06/09/2022) (Generalitat de Catalunya, Departament de Territori i Sostenibilitat).

Finally, backward air trajectories were modelled to assess the origin of air masses arriving at the area of study and therefore provide insight into the influence of atmospheric transport from regional, continental, and remote sources of pollutants on their concentrations in the Pyrenees. The backward air trajectories were calculated using the HYSPLIT atmospheric transport and dispersion model from the National Oceanic and Atmospheric Administration (NOAA, Washington, D.C., USA) (Stein et al., 2015). The model relies on advection simulations based on archive global meteorology data (wind

speeds and direction components, temperature, humidity, pressure, and several other variables) which are available at different spatial and temporal resolutions. Here, meteorological data were obtained from NOAA's Air Resources Laboratory meteorological archives. The specific data subset was from the NCAR/NCEP (National Centers for Environmental Prediction/National Center for Atmospheric Research) global reanalysis, presented as a 2.5-degree global grid on pressure surface coordinates at six-hour intervals since 1948. The simulations were performed for 72-hour backward trajectories arriving at the coordinates 42.58°N, 0.89°E, and 500 m above ground level (location approximately at the centre of all studied sites and at an altitude representative of the approximate average height of the atmospheric mixing layer). The model only allows for the integrated analysis of 12 months of data, so the trajectories were computed in three one-year periods from the beginning of September 2017 to the end of August 2020. A cluster analysis was performed on the trajectories in order to group them into several average trajectory origins that explained a significant amount of variance between air masses while resulting geographically distinct groups.

Figure 22 shows an example of the output of the cluster analysis for one of the considered periods, and Figure 23 shows the individual air trajectories assembled under some of the resulting clusters. The complete set of figures resulting from the air trajectory analysis can be found in Appendix II: Meteorology (Figure 64 to Figure 69). Generally, the backward air trajectories ending at the central Pyrenees could be decomposed in five to six distinct clusters with average directions and distances indicative of regional, Mediterranean/continental, polar, North-Atlantic, and Central-Atlantic origin. The first and second years showed a high influence of regional sources with origins closer to the studied sites (39–43%), while the analysis of the third year divided these regional trajectories into adjacent clusters with more pronounced Atlantic, Mediterranean, and continental components (Figure 66). North-Atlantic clusters typically grouped 8–20% of the trajectories, while Atlantic clusters originating more to the south were 6–17% of the total (or up to 39% in the third year if two clusters in the Atlantic only differentiated by distance are aggregated). Clusters with a more prominent polar origin were 13–15%, although some of these trajectories could also be grouped with other adjacent clusters with higher continental or North-Atlantic features, which could increase the percentage of true polar air masses. In general, regional air trajectories dominated the distributions,

followed by those arriving from the Atlantic, and with a non-negligible but lower representation of polar and Continental advection of air masses. In the Pyrenees, differences in nature and composition of air masses and precipitation events from different origins (Atlantic or regional) have been observed (Camarero and Catalan, 1996): regional winds typically show more convective and terrene characteristics while Atlantic

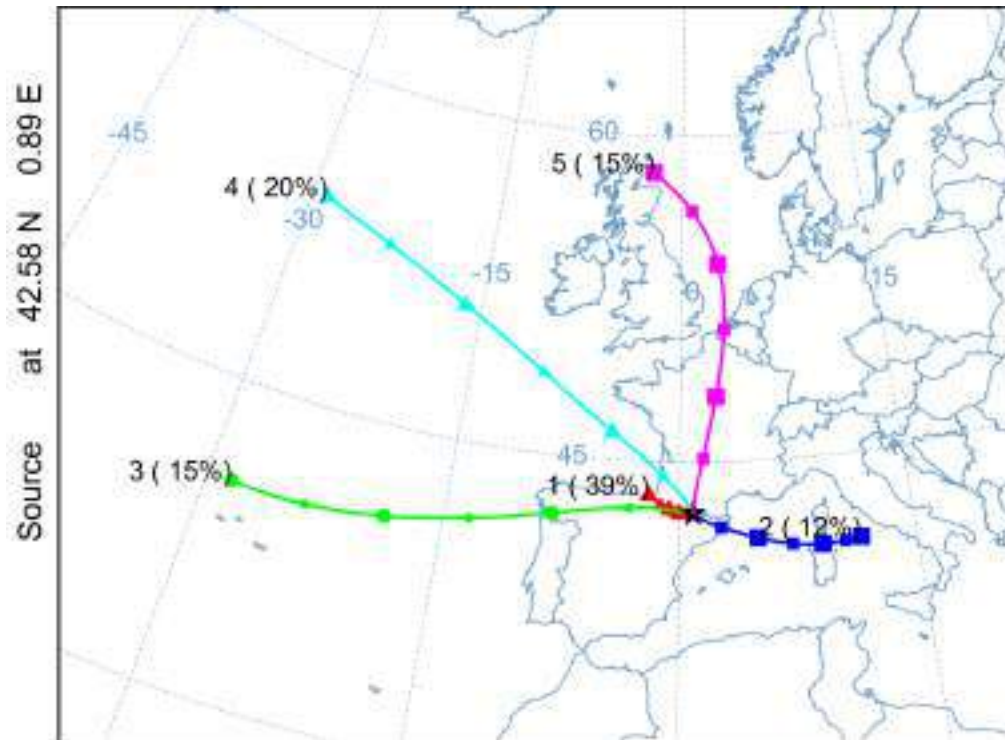


Figure 22. Cluster trajectory analysis (72 h backwards, one trajectory every 6 h from 09/2018 to 08/2019, total of 1444 trajectories) for air trajectories ending at the studied area. The labels indicate cluster number (1 to 5) and percentage of total trajectories grouped. Figure created using NOAA's HYSPLIT transport and dispersion model (National Oceanic and Atmospheric Administration, USA).

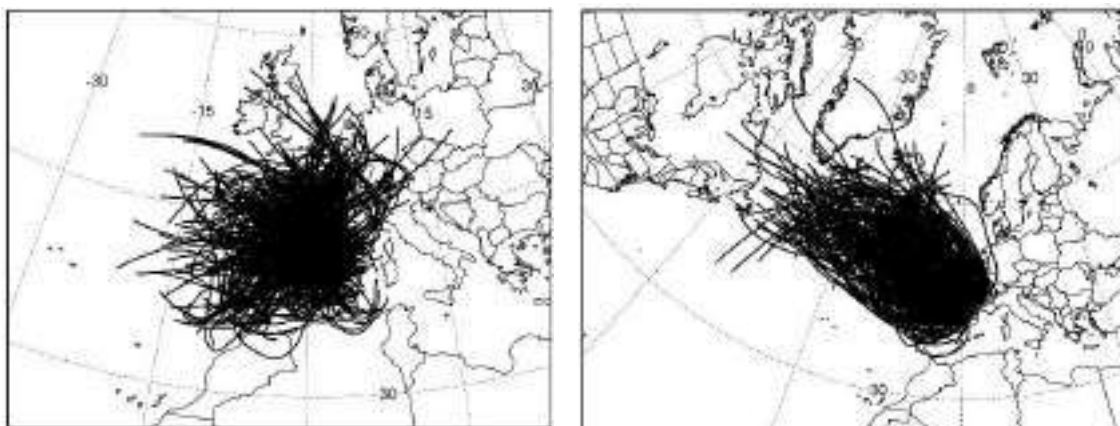


Figure 23. Examples of air trajectories grouped in the cluster analysis of 09/2018 to 08/2019. Cluster 1 (left) presents a regional component and cluster 4 (right) presents a North-Atlantic component. Calculations performed and figures created using NOAA's HYSPLIT transport and dispersion model (National Oceanic and Atmospheric Administration, USA).

winds have higher advective character. These differences can influence the type of pollutants that arrive at certain sites at different moments and can strongly influence discrete measurements as opposed to time-integrated ones.

3.2.3 Passive air sampler configuration and deployment

The passive air samplers (PAS) used in the present work were made of PUF (Figure 24). This type of passive sampler has been widely used in atmospheric studies and global monitoring networks (Pozo et al., 2009, 2006; Saini et al., 2020). The foam was used in the form of porous disks that measured 14 cm in diameter and 1.35 cm in thickness, with a surface area of 369.5 cm² and a density of 0.021 g cm⁻³. Each disk had a perforation in its centre measuring 0.75 cm in diameter that stretched to fit a 1.2 cm circular stainless-steel insert for mounting into the sampler housing structure.



Figure 24. Polyurethane foam (PUF) passive air sampler disks.

Multiple rinses and extractions with water and different organic solvents were performed to strip any contaminants and production by-products from the samplers prior to their exposure. After the extraction, the pre-cleaned stainless-steel inserts were embedded into the disks and each sampler was individually sealed airtight and frozen until deployed.

PUF-PAS housing structures for outdoor use have the objective to shield the samplers from precipitation, direct sunlight, and other environmental interferences, as well as dampening strong winds for a better control of the diffusive exchange of

compounds with the sampler material. The most common housing design is often referred to as the “flying saucer” as it is composed of two opposing stainless-steel domes that enclose the PUF disk in their centre, leaving a circular aperture along the rim that allows the controlled exchange of air between the inside and the outside of the housing. There are several double dome designs with varying shapes (see Melymuk et al., 2021 for visual reference) and they can cause differences in the sampled amounts of contaminants, but they all act on the same principles. The housing design used in the present work is shown in a diagram of the inner supporting structure of the housing in Figure 25 and consists of stainless-steel tubes, washers, and fasteners.

The sampler housings were deployed in duplicate at 1.8 m above ground level, attached through a mounting bracket to a 2 m steel rod supported by three metal wire guylines anchored to the ground (Figure 26). Upon deployment, PRCs for the determination of compound- and site-specific sampling rates were added to the PUF disks by injecting 25 μL of a mixture of selected PCB congeners dissolved in nonane directly onto the foam. The chosen congeners were ^{13}C -PCB3, ^{13}C -PCB9, ^{13}C -PCB15, ^{13}C -PCB32, PCB107, and PCB198 (Cambridge Isotope Laboratories, Tewksbury, MA, USA) at concentrations between 3 and 9 $\text{ng } \mu\text{L}^{-1}$. These PCBs were selected based on their $K'_{\text{PUF-A}}$ values, ranging from 2.1×10^5 to 1.1×10^8 (unitless), which are expected to cover a range of affinities for the sampler material that allows for varying levels of PRC depletion after the period of exposure, encompassing from imperceptible to complete release into the air.

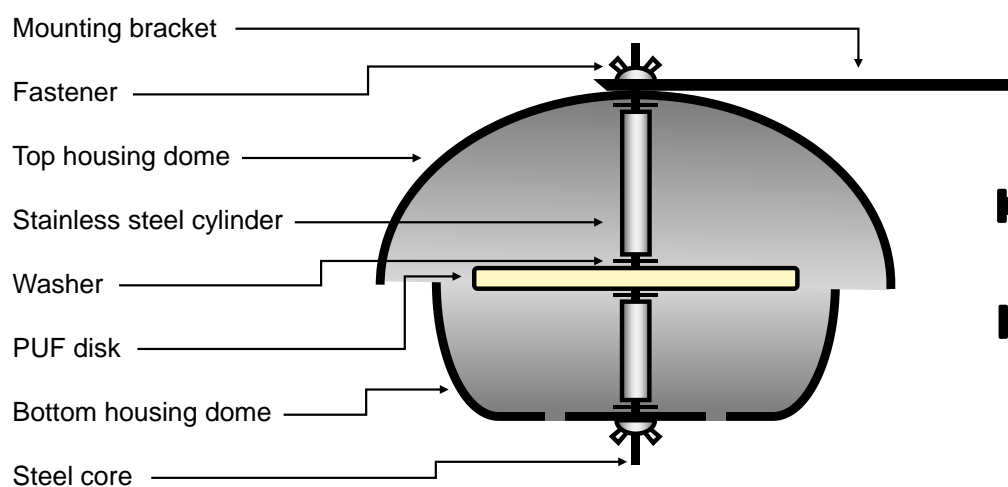


Figure 25. Diagram of a vertical cross-section of the passive air sampler housing structure.



Figure 26. Passive air samplers deployed at Estany de la Collada.

3.2.4 Passive water sampler configuration and deployment

Two types of passive water samplers (PWS) were used in the present work, made of LDPE and SR (Figure 27). These sampler materials have been used in global aquatic monitoring networks in the past (Lohmann et al., 2017). The polymer sheets were used in the form of strips that measured 90×55 mm and with thicknesses of 0.08 mm for LDPE and 0.25 mm for SR, weighing approximately 0.38 and 1.5 g each, respectively. Each strip had two 5.5 mm diameter perforations for mounting onto the sampler structure. Thus, the total exposed area of each sampler sheet was just below 100 cm^2 .

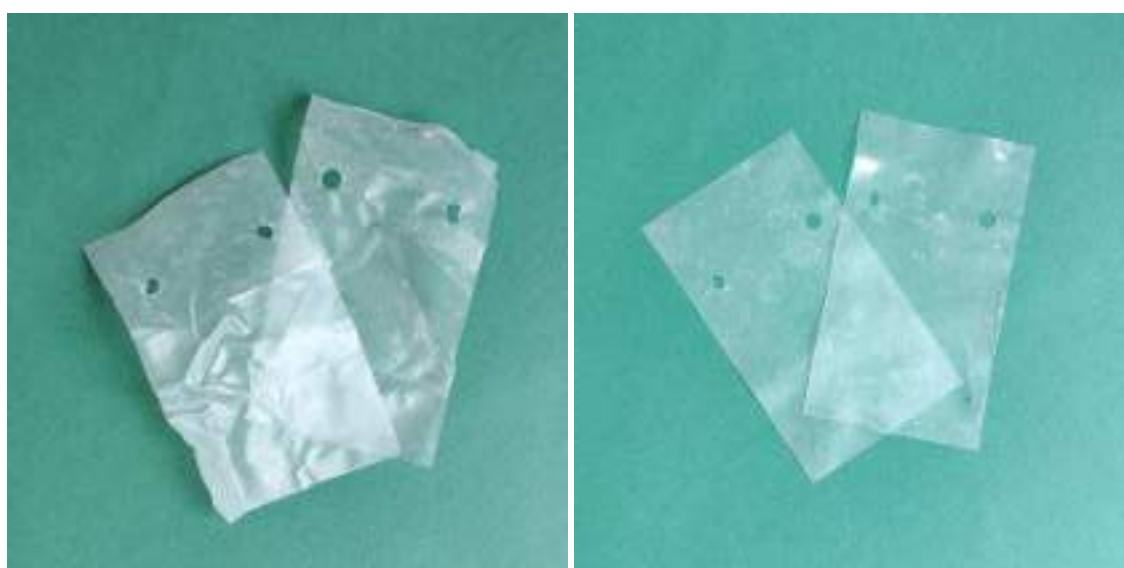


Figure 27. Low-density polyethylene (LDPE, left) and silicone rubber (SR, right) passive water sampler sheets.

The samplers were kindly provided by and pre-treated at the Research Centre for Toxic Compounds in the Environment (RECETOX) from the Masaryk University in Brno, Czech Republic. An extraction using a combination of organic solvents was performed to strip any contaminants from the samplers prior to their exposure, as well as to remove oligomers (short-chain polymers) that may be part of the commercially available material and that can interfere with the analysis. This procedure has been detailed elsewhere (Sobotka et al., 2022). After the extraction, the sampler sheets were spiked with PRCs for the calibration of sampling rates following procedures described elsewhere (Smedes and Booij, 2012). Briefly, the spiking of PRCs is performed by soaking and mixing the sheets in the spiking solution with methanol as solvent and the successive stepwise addition of water to the system, which forces the PCBs into the

polymer. The PRCs were PCBs 1, 2, 3, 10, 14, 21, 50, 55, 78, 104, 145, and 204, with K_{PWS-W} approximately ranging between 4.0 and 7.8 L kg⁻¹ (for both LDPE and SR samplers) (Smedes et al., 2009). Thus, these PRCs span a range of physical-chemical properties such that they are expected to range from complete release from the sampler into the water to almost complete retention by the polymer during exposure. After PRC spiking, the PWS sheets were sealed air-tight in amber glass jars and frozen until deployed.

Several sampler housing structures have been used in the past for the deployment of polymer sheets in water. Some examples are durable stainless-steel cages and tubular steel shrouds (see Sobotka et al., 2022 for visual reference). On many occasions, these are robust structures that enclose the sampler sheets and shield them against extreme water currents, aquatic animals, and other disturbances such as vessel traffic in locations



Figure 28. Passive water sampler sheets mounted onto a steel grill before (Estany de Dellui, left) and after (Estany de Llebreta, right) deployment. Note that, although oxidation of the grills was inevitable in some lakes, rust does not affect the extraction of the samplers nor the analysis of pollutants in any way.

with prominent anthropogenic activity. However, remote alpine lakes are small freshwater bodies without human influence and present weak currents, very low salinity, and are inhabited by very few animal species that are generally uninterested in the sampler material. Complex sampler housing structures are bulky, unwieldy, and heavy, impeding their transport to high-altitude areas of difficult access. Therefore, we opted for lightweight stainless-steel wire frames onto which the LDPE and SR sheets were individually attached using nylon cable ties (Figure 28). This is a much more open design compared to others like the tubular steel shroud, thus allowing for deployment in relatively still and pristine waters without slowing the renewal of water around the samplers.

Typically, twelve sampler sheets are exposed per sampling site and four more are kept as field blanks. The wire frames were suspended four meters below the water surface using an anchor, a submerged buoy, and a nautical cord (Figure 29, Figure 30). Either a steel anchor or a woven polypropylene bag filled with rocks picked on site were used as anchors. Note that the buoy needs to be submerged as the lake surface freezes over winter, which would trap the floating buoy and could drag the whole structure. All deployment and retrieval operations were carried out using an inflatable raft, which was thoroughly cleaned with the biocidal disinfectant Virkon S (Lanxess, Cologne, Germany) between

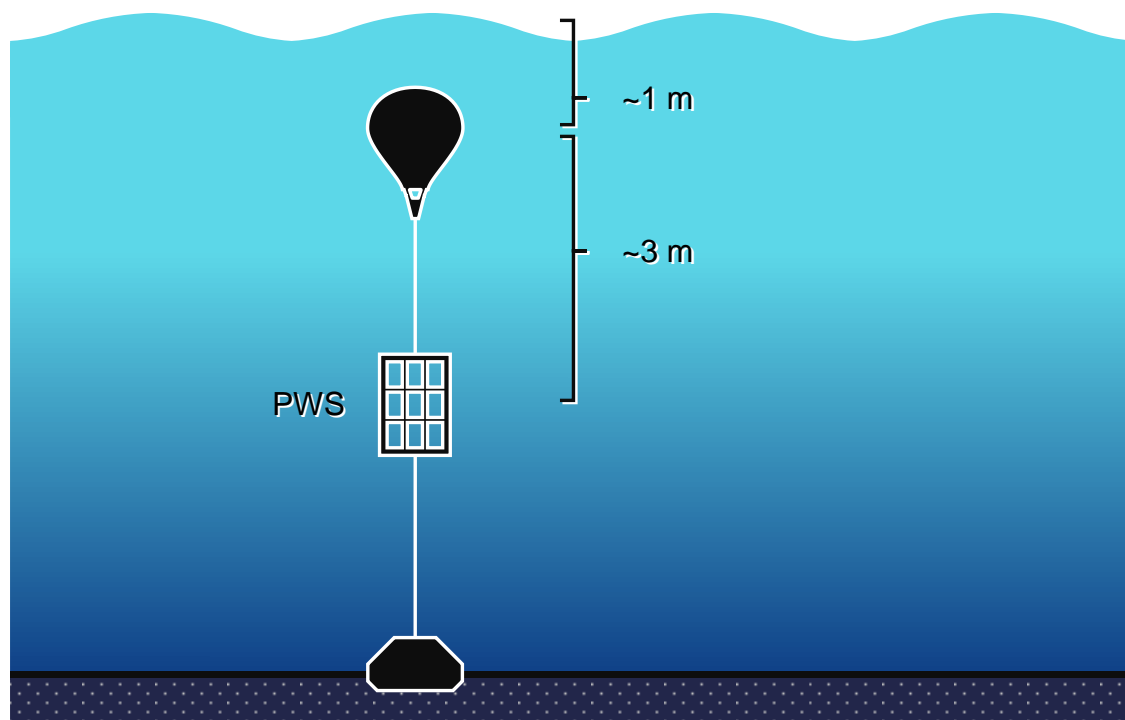


Figure 29. Diagram of the deployed passive water sampling structure under the water surface.

sampling operations to avoid transferring insect eggs, pathogens, or other biotic agents from one lake to another, which is a major concern in pristine ecosystems under the protection of a National Park.

During sampler recovery, any biofouling on the sheets was wiped off on-site with a tissue before sealing them inside an amber jar and refrigerated until stored in a freezer (-20 °C). Biofouling in more eutrophic lakes and marine waters can develop into a problem as the sampler sheets may become overgrown with organisms that impede the exchange of pollutants between water and polymer. Still, the transport of contaminants through the biofilm layer also takes place via molecular diffusion (Huckins et al., 2006), so the uptake of pollutants by the passive samplers would still take place given enough time. The biofouling on sampler sheets in more oligotrophic lakes like the ones considered in this work is usually light and can be easily removed after sampling (see Figure 28 and Figure 30).

3.2.5 Diffusive exchange of pollutants between air and water

Diffusive exchange processes often predominantly define the distribution mechanics of pollutants between environmental compartments such as air and water, which are the main subjects of study in the present work. That is, the transference of compounds between the atmospheric gas phase and the dissolved phase of water often occurs to a preminent degree due to physical diffusion. This was the case for several PCBs in Estanh Redon over two decades ago (Meijer et al., 2006) and has also been determined as an important driver of PAH and organochlorine compound dynamics in other oligotrophic lakes of glacial origin (Luarte et al., 2022; Tucca et al., 2020). The magnitude and effect of this exchange mechanism have also been investigated with the data from atmospheric and aquatic measurements produced in the present work. This section provides an overview of the calculations involved in the assessment of diffusive exchange of pollutants between air and water.

The overall magnitude and direction of diffusive exchange processes between two environmental compartments can be determined through the calculation of exchange fluxes. This exchange occurs at the boundary between phases, in this case, the water surface. A boundary can be defined as the interface at which physical and chemical prop-

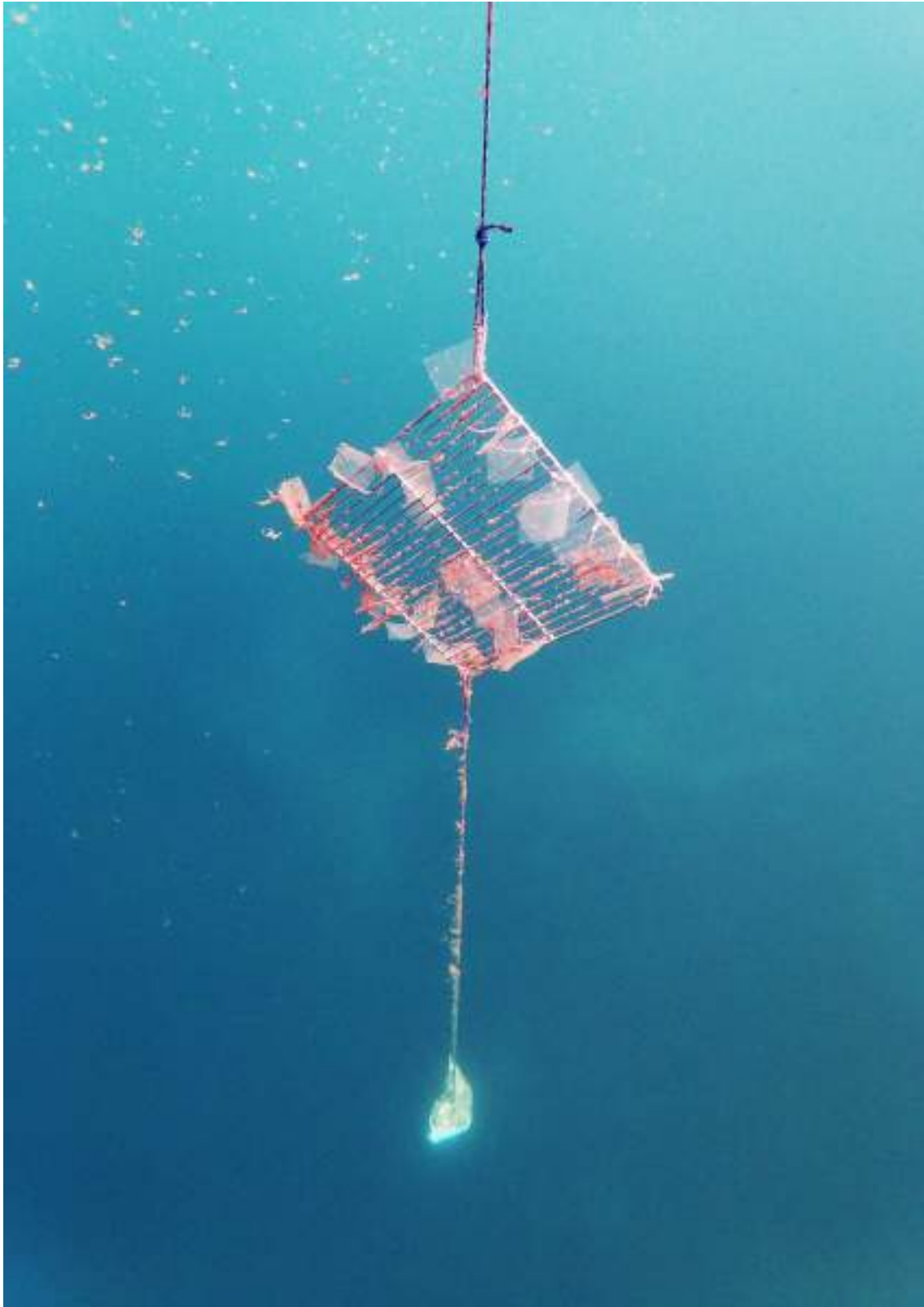


Figure 30. Passive water samplers deployed at Estany de Sarradé.

erties of an environmental system change in a significant way. Some boundaries between phases are clearly defined, such as the interface between air and water at the surface of a lake, or between water and sediment at the bottom of it. Other boundaries are less defined, as is the case between the atmospheric troposphere, stratosphere, and mesosphere, or between the epilimnion and hypolimnion layers in the water from a thermally stratified lake.

Regarding diffusive mass transfer across interfaces, diffusivity profiles (i.e., the ease of diffusion between phases) define three classes of boundary: bottleneck boundaries (e.g., air–water), wall boundaries (e.g., water–sediment), and diffusive boundaries (e.g., epilimnion–hypolimnion). All three describe a different abruptness in the change of properties between phases that governs the nature of the transport of mass through the boundary, and they are influenced differently by molecular diffusion and turbulence of the medium. However, under experimental circumstances, the air–water boundary is often not well defined by any single behaviour and is instead recognized as a complex combination of processes. Several specific air–water exchange models have been proposed in the past. The film model (Whitman, 1923) is the first bottleneck boundary model that considers two turbulent phases such as air and water divided by an interface zone with a steeply decreased diffusivity in which molecular processes control transport between phases. The surface renewal model (Danckwerts, 1951; Higbie, 1935) works under highly turbulent conditions that generate waves and airborne water droplets that act as a diffusive boundary. Finally, the boundary layer model (Deacon, 1977) is a bottleneck model that considers a continuous drop in diffusivity between phases instead of a steep one.

Regardless of the characteristics of the exchange, quantitative descriptions of mass fluxes all share the same general form. In the present work, fluxes were calculated based on the outline proposed by Schwarzenbach et al. (2016). The general flux equation for a specific compound “*i*” presents the following form:

$$F_{iAW} = k_{iAW} \left(C_{iW} - \frac{C_{iA}}{K_{iAW}} \right) \quad \text{Eq. 19}$$

where F_{iAW} is the air–water flux (in $\text{ng m}^{-2} \text{d}^{-1}$), k_{iAW} is the overall air–water exchange velocity (in m d^{-1}), K_{iAW} is the equilibrium air–water partition constant (dimensionless),

and C_{iW} and C_{iA} are the compound concentrations in water and in air, respectively (both in ng m^{-3}). Since the previous equation takes water as the reference phase (note that C_{iA} are transformed by the equilibrium constant), positive values of F_{iAW} indicate a net volatilization flux (from water towards air), while negative values of F_{iAW} indicate a net deposition flux (from air towards water).

K_{iAW} is a compound-specific coefficient that describes its state of partitioning between air and water at equilibrium. It is equivalent to the compound's nondimensional Henry's Law constant:

$$K_{iAW} = \frac{H_{i(T)}}{RT} \quad \text{Eq. 20}$$

where R is the ideal gas constant (in $\text{Pa m}^3 \text{K}^{-1} \text{mol}^{-1}$), T is the mean atmospheric temperature (in K), and $H_{i(T)}$ is the temperature-corrected Henry's Law constant of the compound (in $\text{Pa m}^3 \text{mol}^{-1}$). Thus, K_{iAW} , understood as the theoretical ratio between compound amounts in air and in water in equilibrium conditions, tends to be higher for compounds with higher H_i at a given temperature, which are usually smaller, lighter chemicals with higher volatilities and a higher tendency to remain in the atmospheric gas phase. As with all equilibrium constants, H_i changes with temperature, so it should be regarded more as a coefficient than as a true constant. Thus, when applying H_i to experimental cases, the effect of temperature on its value needs to be considered. Among the different ways to do so, a general method proposed by ten Hulscher et al. (1992) was used in the present work:

$$\log H_{i(T)} = \log H_{i298} + 8.76 - \frac{2611}{T} \quad \text{Eq. 21}$$

This approach is not specific to each compound, unlike other methods. Comprehensive studies reporting compound-specific correction relationships are available for certain groups of compounds, but their application in studies that consider a range of pollutant families that exhibit diverse physical-chemical properties typically results in inconsistencies and systematic differences between groups. The chosen general equation instead compromises the accuracy of experimentally determined, compound-specific temperature correction relationships by extrapolating a constant slope to all studied compounds, but can be applied to any chemicals with a known H_i at 298 K. This

or other general relationships have been used in past studies for correcting H_i of multiple groups of compounds (Baker and Eisenreich, 1990; Hornbuckle et al., 1994). In the same pursuit of consistency, all reference $H_{i\ 298}$ values were obtained from the EPA CompTox Chemistry Dashboard (Williams et al., 2017). A list of all $H_{i\ 298}$ used can be found in Table 1.

The total exchange velocity in Eq. 19, $k_{i\ AW}$, results from an interface exchange between two components: air and water. Using water as the reference phase, $k_{i\ AW}$ can be calculated as:

$$\frac{1}{k_{i\ AW}} = \frac{1}{k_{i\ W}} + \frac{1}{k_{i\ A}K_{i\ AW}} \quad \text{Eq. 22}$$

where $k_{i\ W}$ and $k_{i\ A}$ are the water-side and air-side mass transfer coefficients or single-phase exchange velocities, respectively (both in cm s^{-1} , later converted into m s^{-1} for the calculation of $F_{i\ AW}$). These velocities represent the contribution to the overall transfer velocity of the two extreme cases where the exchange is controlled solely by the water phase and solely by the air phase, respectively.

There are different models that describe these coefficients as a function of environmental variables such as temperature and wind speed. Here, the boundary layer model first proposed by Deacon (1977) has been used. This model is rather complex as it separates the effects of two processes involved in the exchange of compounds at the interface layer between phases: the transport of chemicals (described by molecular diffusivity in a phase, D_i , in $\text{cm}^2 \text{s}^{-1}$) and the transport of turbulence (described by the coefficient of kinematic viscosity of the phase, ν , in $\text{cm}^2 \text{s}^{-1}$). Exchange velocities are proportional to the ratio between both variables, which is defined as the Schmidt Number (Sc_i , unitless):

$$Sc_{i\ A\ or\ W} = \frac{\nu_{A\ or\ W}(T)}{D_{i\ A\ or\ W}} \quad \text{Eq. 23}$$

Exchange velocities thus increase for compounds with large diffusivities and for transfer media with small phase viscosities. In water, Deacon's model for transfer velocities is represented as follows:

$$k_{iW} = k_{CO_2W} \left(\frac{Sc_{iW}}{Sc_{CO_2W}} \right)^{-a_{Sc}} \quad \text{with } a_{Sc} \begin{cases} 2/3 \text{ for } u_{10} \leq 5 \text{ m s}^{-1} \\ 1/2 \text{ for } u_{10} > 5 \text{ m s}^{-1} \end{cases} \quad \text{Eq. 24}$$

where u_{10} is the mean wind speed (in m s^{-1}) measured 10 m above the exchange interface between air and water, and where k_{iW} is calculated relative to a known mass transfer coefficient through the stagnant water layer: that of CO_2 at 20°C (k_{CO_2W} , in cm s^{-1}). Note that, for a boundary layer model like the present one, the exponent a_{Sc} in Eq. 24 changes at wind speeds higher than 5 m s^{-1} (Jähne et al., 1987; Liss and Merlivat, 1986) in response to the perturbation of the water surface. Thus, at higher wind speeds that introduce turbulent regimes into the exchange layer, k_{iW} values become greater reflecting the increase in transfer velocity. Sc_{iW} and Sc_{CO_2W} used in Eq. 24 are calculated at the appropriate temperatures using Eq. 23, where D_{iW} can be estimated using Othmer and Thakar's (1953) expression with coefficients modified by Hayduk and Laudie (1974):

$$D_{iW} = \frac{13.26 \times 10^{-5}}{\nu_W(T)^{1.14} V_i^{0.589}} \quad \text{Eq. 25}$$

where V_i is the molar volume of the studied compound (in $\text{cm}^3 \text{mol}^{-1}$), being $V_{CO_2} = 26.9 \text{ cm}^3 \text{mol}^{-1}$. V_i values in this work were estimated using SPARC's physicochemical calculator (ARChem, Danielsville, GA, USA) (Table 1). Eq. 25 predicts higher molecular diffusivities in water for smaller compounds (Figure 31).

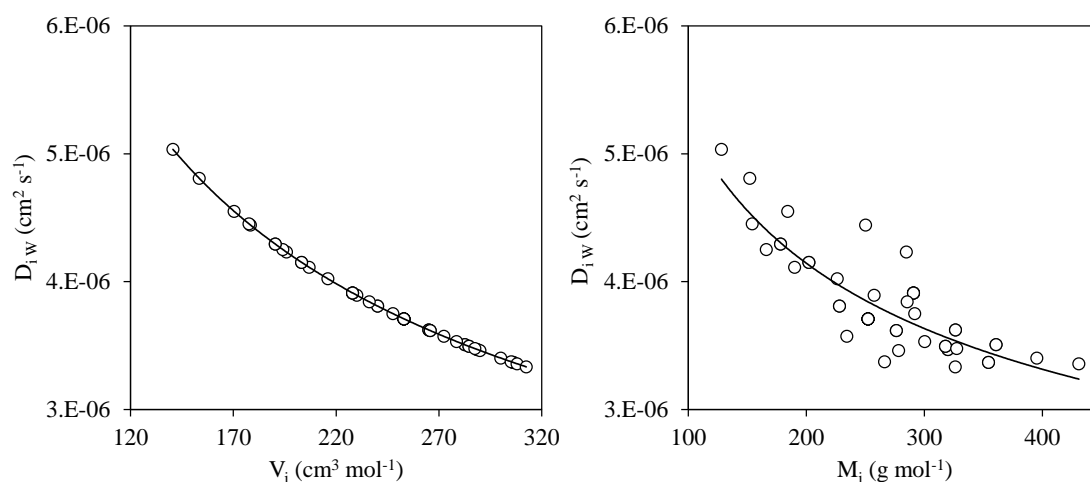


Figure 31. Molecular diffusivities in water (D_{iW}) predicted for several studied PAHs, OCs, and OPEs at $1.5 \times 10^{-2} \text{ cm}^2 \text{ s}^{-1}$, represented against their molar volume (V_i) and molar mass (M_i).

The kinematic viscosity of water used in both Eq. 23 and Eq. 25, ν_W , was determined at specific temperatures using:

$$\nu_W(T) = 6.85 \times 10^{-4} T^2 - 0.427 T + 67.331 \quad \text{Eq. 26}$$

which was fitted to ν_W values given by Schwarzenbach et al. (2005) at temperatures between 273.15 and 298.15 K ($R^2 > 0.999$) as shown in Figure 32.

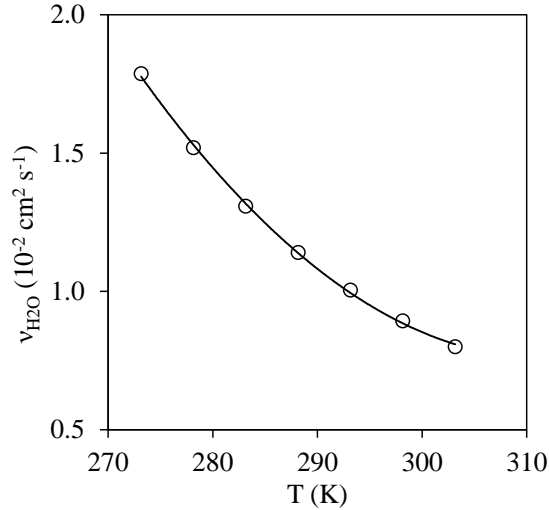


Figure 32. Variation of the kinematic viscosity of water (ν_W) with temperature (T). Figure created using ν_W and T values from Schwarzenbach et al. (2005).

In water, Sc_i accounts for the temperature dependence of the exchange velocity since ν_W decreases at higher T while D_{iW} increases with T . In air, the temperature dependence of Sc_i is small because both ν_A and D_{iA} increase with T , and thus Sc_i values in air show limited variation. Therefore, air-side transfer velocities are instead estimated directly from air diffusivities:

$$k_{iA} = k_{H_2O A} \left(\frac{D_{iA}}{D_{H_2O A}} \right)^{a_D} \quad \text{Eq. 27}$$

where k_{iA} is calculated relative to a known mass transfer coefficient through the stagnant air layer: that of H_2O vapor at air temperatures between 0 and 25 °C ($k_{H_2O A}$, in cm s^{-1}). The optimal value of the exponent a_D has been empirically determined to be 2/3 (Mackay and Yeun, 1983). D_{iA} , including $D_{H_2O A}$, can be estimated as follows (Fuller et al., 1966):

$$D_{iA} = 10^{-3} \frac{T^{1.75} \left(\frac{1}{M_A} + \frac{1}{M_i} \right)^{1/2}}{p \left(V_A^{1/3} + V_i^{1/3} \right)^2} \quad \text{Eq. 28}$$

where T is expressed in K, M_A is the average molar mass of air (28.97 g mol^{-1}), M_i is the molar mass of the studied compound (in g mol^{-1}), p is the average atmospheric pressure

(in atm), V_A is the average molar volume of the gasses in air ($20.1 \text{ cm}^3 \text{ mol}^{-1}$), and V_i is the molar volume of the studied compound (in $\text{cm}^3 \text{ mol}^{-1}$). M_i and V_i values used in this work are listed in Table 1. Eq. 28 is not dimensionally correct, so the result is only valid if the variables are expressed in the aforementioned units. Note that, much like Eq. 23, Eq. 28 predicts larger diffusivities for smaller compounds (Figure 33).

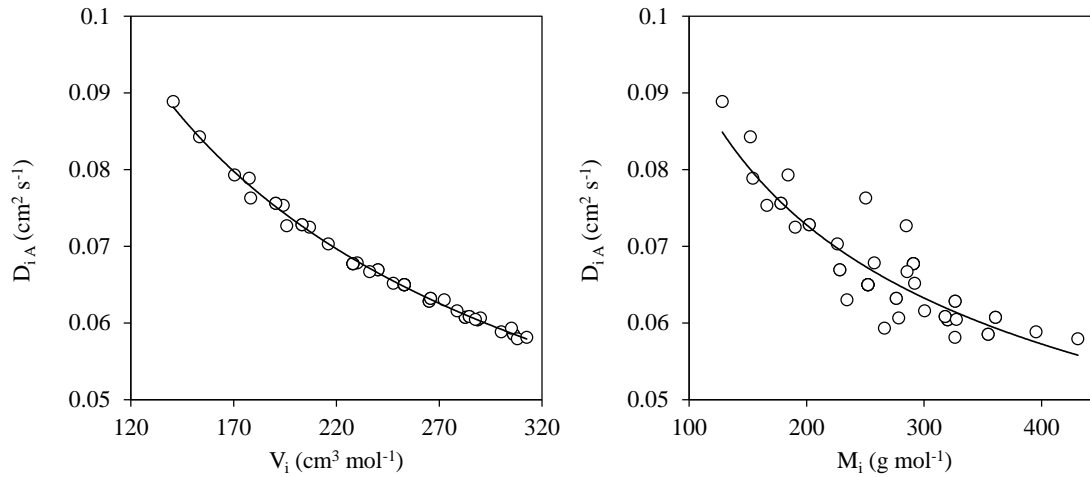


Figure 33. Molecular diffusivities in air ($D_{i,A}$) predicted for several studied PAHs, OCs, and OPEs at 298.15 K and 800 atm, represented against their molar volume (V_i) and molar mass (M_i).

The only values remaining to be determined are the reference mass transfer coefficients of CO_2 in water and H_2O vapor in air, $k_{\text{CO}_2 w}$ and $k_{\text{H}_2\text{O} A}$, respectively. Mass transfer coefficients are positively correlated with wind speed. For $k_{\text{H}_2\text{O} A}$, this correlation is approximately linear, at least at average wind speeds below 10 m s^{-1} (Mackay and Yeun, 1983; Münnich et al., 1978). Here, $k_{\text{H}_2\text{O} A}$ was obtained from the following approximation (Schwarzenbach et al., 2016) with coefficients by Fairall et al. (2011, 2003, 1996) and Johnson (2010):

$$k_{\text{H}_2\text{O} A} = 0.11 u_{10} + 0.1 \quad \text{Eq. 29}$$

In the case that wind speeds have been measured at a distance other than 10 m above the water surface, a common expression for their correction under non-turbulent regimes was proposed by Mackay and Yeun (1983):

$$u_{10} = \left(\frac{10.4}{\ln z + 8.1} \right) u_z \quad \text{Eq. 30}$$

where z is the height of the measurement (in m).

On the other hand, many studies have proposed relationships for the calculation of $k_{CO_2 w}$ (often called k_{600} since Sc of CO_2 in water at $20\text{ }^\circ C$ is equal to 600). Here, we used a parametrization of a compilation of experimental studies specific to air–water exchange fluxes in lakes (as opposed to other models typically applied to open seas and oceans) proposed by Klaus and Vachon (2020):

$$k_{CO_2 w} = (0.328 \log_{10}(LA) + 1.581) u_{10} - 0.066 \text{logit}(SIN) + 1.266 \quad \text{Eq. 31}$$

where LA is the lake area (in m^2), and SIN is a space integration parameter that is equal to 1 if the whole lake is considered instead of just a part of it. This is the best fit linear model between all parametrizations proposed by the authors. Note that $\text{logit}(SIN) = \log_{10}(SIN/(1-SIN))$, so $SIN = 0.999$ was used instead of 1 in order to avoid the undefinition of the expression ($SIN/0$) as recommended (Klaus and Vachon, 2020). Regardless of the abstract nature of this parameter, $k_{CO_2 w}$ values only change by less than 2.5 % between SIN values of 0.001 and 0.999 for the lake areas and wind speeds considered in this study. On the other hand, LA can have a more significant effect on $k_{CO_2 w}$, especially for smaller lakes (Figure 34). As explained by this model, the effect of u_{10} on $k_{CO_2 w}$ increases with LA as a result of increased turbulence due to wave build-up.

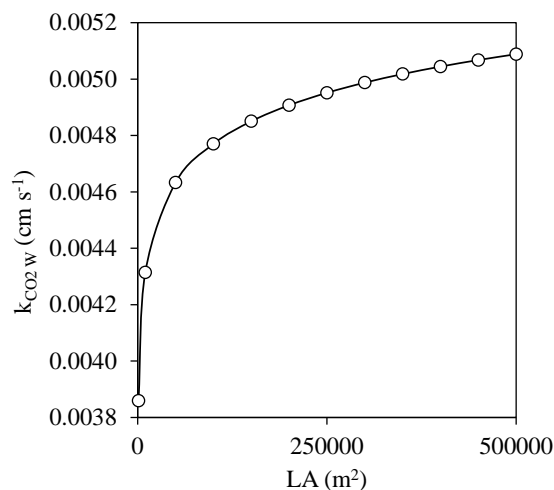


Figure 34. Variation with lake area (LA , m^2) of the mass transfer coefficient of CO_2 through the stagnant water layer ($k_{CO_2 w}$). Figure created for a fixed space integration value $SIN = 0.999$ and wind speed $u_{10} = 5\text{ m s}^{-1}$ using the parametrization shown in Eq. 31 from Klaus and Vachon (2020).

3.3 Results

In this section, the study of the occurrence of PCBs, OCs, PAHs, and OPEs in air and water is presented, both in a dense urban area in Barcelona and in remote high-mountain lakes in the Pyrenees. Passive sampling techniques were used to this end, and their performance, suitability for the study of the considered compounds, and uncertainty in their measurements were assessed in comparison with active sampler techniques and independent measurements of co-deployed samplers. In the urban setting, the unprecedented interruption in pollutant emissions during COVID-19 lockdown was used as an abstraction of the potential short-term effect that strict regulations on contaminant emissions at their source could have on environmental pollution, using background levels in alpine sites as reference. In these alpine areas, passive air samplers were used over five consecutive four to twelve month-long periods (PAS I–PAS V) and water samplers were used over three consecutive one year-long periods (PWS I–PWS III) between 2017 and 2020 (note that, in some of the following publications, some samples may be labelled differently or encompass different periods for convenience). The mean pollutant concentrations observed in the Pyrenean lakes were compared to those reported in previous studies in the same area to observe possible changes over the last couple of decades in relation to their physical-chemical properties and changes in their emissions. Pollutant distribution trends between air and other environmental compartments were studied based on physical-chemical factors, identifying differences between groups of compounds, and analysing the role of environmental factors on the fate of pollutants in these alpine sites. Finally, diffusive exchange fluxes between air and water were estimated based on concentration imbalances in these ecosystems and compared to atmospheric photodegradation fluxes that could compete with them as an atmospheric pollutant removal process for some of the more labile SVOCs.

The results have been described in five articles, which are presented in the following subsections:

- ARTICLE 1 Field Comparison of Passive Polyurethane Foam and Active Air Sampling Techniques for Analysis of Gas-Phase Semi-Volatile Organic Compounds at a Remote High-Mountain Site
Raimon M. Prats, Barend L. van Drooge, Pilar Fernández, Joan O. Grimalt
Science of the Total Environment 803 (2022) 149738
DOI 10.1016/j.scitotenv.2021.149738
- ARTICLE 2 Changes in Urban Gas-Phase Persistent Organic Pollutants During the COVID-19 Lockdown in Barcelona
Raimon M. Prats, Barend L. van Drooge, Pilar Fernández, Esther Marco, Joan O. Grimalt
Frontiers in Environmental Science (2021) 9:650539
DOI 10.3389/fenvs.2021.650539
- ARTICLE 3 Occurrence and Temperature Dependence of Atmospheric Gas-Phase Organophosphate Esters in High-Mountain Areas (Pyrenees)
Raimon M. Prats, Barend L. van Drooge, Pilar Fernández, Joan O. Grimalt
Chemosphere 292 (2022) 133467
DOI 10.1016/j.chemosphere.2021.133467
- ARTICLE 4 Changes and Distribution of Gas-Phase Polycyclic Aromatic Hydrocarbons and Organochlorine Compounds in a High-Mountain Gradient Over a Three-Year Period (Pyrenees, 2017–2020)
Raimon M. Prats, Barend L. van Drooge, Pilar Fernández, Joan O. Grimalt
Science of the Total Environment 829 (2022) 154602
DOI 10.1016/j.scitotenv.2022.154602
- ARTICLE 5 Passive Water Sampling and Air–Water Diffusive Exchange of Long-Range Transported Semi-Volatile Organic Pollutants in High-Mountain Lakes
Raimon M. Prats, Barend L. van Drooge, Pilar Fernández, Joan O. Grimalt
Submitted for publication to Science of the Total Environment



Article 1

FIELD COMPARISON OF PASSIVE POLYURETHANE FOAM AND ACTIVE AIR SAMPLING TECHNIQUES FOR ANALYSIS OF GAS-PHASE SEMI-VOLATILE ORGANIC COMPOUNDS AT A REMOTE HIGH-MOUNTAIN SITE

Raimon M. Prats, Barend L. van Drooge, Pilar Fernández, Joan O. Grimalt
Science of the Total Environment 803 (2022) 149738
DOI 10.1016/j.scitotenv.2021.149738



Contents lists available at ScienceDirect

Science of the Total Environment

journal homepage: www.elsevier.com/locate/scitotenv

Field comparison of passive polyurethane foam and active air sampling techniques for analysis of gas-phase semi-volatile organic compounds at a remote high-mountain site



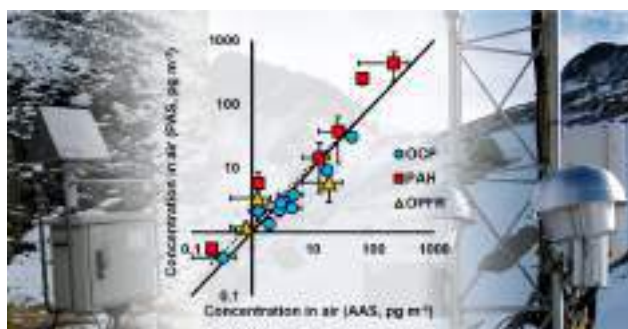
Raimon M. Prats*, Barend L. van Drooge, Pilar Fernández, Joan O. Grimalt

Institute of Environmental Assessment and Water Research (IDAEA-CSIC), Jordi Girona 18, 08034 Barcelona, Catalonia, Spain

HIGHLIGHTS

- Gas-phase SVOC concentrations were determined in a remote high-mountain location.
- Passive sampling rate errors adequately conformed to theoretical uncertainties.
- Passive sampling concentrations showed high agreement with active air sampling ones.

GRAPHICAL ABSTRACT



ARTICLE INFO

Article history:

Received 29 June 2021

Received in revised form 13 August 2021

Accepted 13 August 2021

Available online 21 August 2021

Editor: Shuzhen Zhang

Keywords:

Passive air sampling

Active air sampling

Semi-volatile organic compounds

Performance reference compounds

Calibration

Field comparison

ABSTRACT

Polyurethane foam passive air samplers (PUF-PAS) are good candidates for the determination of gas-phase semi-volatile organic compound (SVOC) air concentrations in high-mountain areas over long periods because they do not require an energy supply. However, the harsh meteorological conditions present in such locations can increase the uncertainties inherently associated to PAS sampling rates due to the many variables involved in their calculation and to the assumptions made regarding PUF diffusive uptake mechanics, which can considerably bias the resulting concentrations. Therefore, we studied the performance of PUF-PASs in a remote location in the Pyrenees mountain range for the analysis of several SVOCs in air, including polychlorobiphenyls (PCBs), hexachlorobenzene, pentachlorobenzene, polycyclic aromatic hydrocarbons (PAHs), and the less studied emerging organophosphate flame retardants (OPFRs). An in-situ PUF-PAS calibration using Performance Reference Compounds (PRCs) provided compound- and sampler-specific sampling rates, showing mean experimental errors (12%) that adequately conformed to an estimate of their expanded theoretical uncertainties (15%). This showcases the suitability of this calibration strategy in an area with conditions beyond those typically considered in calibration efforts available to date. Moreover, gas-phase concentrations of the studied pollutants from PUF-PAS samples showed very good agreement (R^2 up to 0.91, $p < 0.01$) when compared to those obtained using a conventional high-volume active air sampler (PUF-AAS), with some minor deviations observed for PAHs caused by the seasonality in their atmospheric concentrations. No relevant levels of pollutants preferentially bound to the particle phase were detected in the PUF-PASs, the particle infiltration efficiency of the sampler configuration used was found to be low, and compounds typically distributed between the gas and particle phases of AAS samples revealed profiles consistent with their vapor pressures, except for some OPFRs.

© 2021 The Authors. Published by Elsevier B.V. This is an open access article under the CC BY-NC-ND license (<http://creativecommons.org/licenses/by-nc-nd/4.0/>).

* Corresponding author.

E-mail address: raimon.martinez@idaea.csic.es (R.M. Prats).

1. Introduction

1.1. Passive air sampling calibration in high-mountain locations

High mountains and colder regions at higher latitudes tend to accumulate semi-volatile organic compounds (SVOCs), including persistent organic pollutants (POPs), that reach them through long-range atmospheric transport (Wania and MacKay, 1996; Grimalt et al., 2001). This process makes these areas reference sites for the study of the global impact of the use of chemical compounds of anthropogenic origin. At present, polyurethane foam (PUF) disks are commonly used for the analysis of these pollutants in a broad array of locations (Pozo et al., 2006; Shoeib and Harner, 2002). They are simple to use, relatively inexpensive, do not require an energy source, and are convenient for deployment over long periods. These characteristics make them good candidates for atmospheric monitoring programmes in remote and difficult to access locations, compared to the traditional active air sampling (AAS) alternatives. Moreover, they are capable of sampling a wide range of semi-volatile organic compounds; for example, these samplers have been used for the study of polychlorinated biphenyls (PCBs), organochlorine pesticides (OCPs), polybrominated diphenyl ethers (PBDEs), and other SVOCs in remote locations like Antarctica (Li et al., 2012; Pozo et al., 2017), the Tibetan Plateau (Ren et al., 2014), and high-mountain ranges in Brazil (Guida et al., 2018). They have also been shown to collect particle-associated chemicals (Harner et al., 2013; Markovic et al., 2015).

However, the conversion of adsorbed amounts of pollutants to gas-phase concentrations is not trivial, since the sampled air volumes depend on the storage capacity of the PUF, the physical-chemical properties of each SVOC, and the physical conditions of the atmosphere. Although some studies have suggested the dispensability of AAS for the assessment of long-term trends in atmospheric concentrations of certain pollutants (Kalina et al., 2017), parallel AAS measurements are often used to calibrate PAS-PUFs: PAS sampling rates are derived from short AAS sampling periods, where the amount of passively adsorbed compound is normalized to exposure time and divided by its concentration in air determined from AAS (Chaemfa et al., 2009a; Harner et al., 2013; Klánová et al., 2008; Mari et al., 2008). Yet potential problems arise from the assumptions of sampler-independent uptake rates and linear compound uptake conditions that do not always apply for all studied compounds. Moreover, AAS samples used for PAS calibration only account for a very short interval of PAS exposure time (a few hours compared to many weeks or months), bringing into question the representativeness of AAS-derived sampling rates. Secondly, the extent to which particle-phase chemicals are captured by the PUF-PAS sampler configuration can affect the true gas-phase sampling rates. Another practical obstacle is the difficulty, or impossibility, to link PAS measurements to AAS concentrations in remote locations due to difficult access and the lack of an energy supply. Alternatively, PAS sampling rates can be estimated by determining the extent of the linear uptake phase of SVOCs along long sampling periods (Abdollahi et al., 2017; Chaemfa et al., 2008; Evci et al., 2016). Studies using this PAS calibration strategy reported concentrations within a factor of two of AAS measurements for PCBs and OCPs in an urban location in South Korea (Heo and Lee, 2014), and good sampling performances with satisfactory levels of confidence were found for PCBs, OCPs, and PAHs in the Czech Republic (Bohlin et al., 2014).

However, the use of Performance Reference Compounds (PRCs, sometimes referred to as Depuration Compounds, DCs) offers a more reliable PUF-PAS calibration method (Harner et al., 2013). PRCs are a set of compounds representative of a range of physical-chemical properties similar to those of the targeted pollutants. They are spiked into the sampler upon deployment and are diffusively released from the PUF into the air at different rates. The dissipation rate of PRCs is proportional to the uptake of the target compounds (Huckins et al., 2002), and therefore the sampling rates can be estimated, but their calculation is complex

and affected by uncertainties. Nevertheless, this approach eliminates the dependence of PAS on AAS measurements for the determination of compound-specific effective sampled volumes and produces sampling rates distinct for each sampler that account for the variability in physical conditions of each studied location. This is particularly useful in remote areas like high mountains, where calculating site-specific rates is of critical importance due to the extreme weather conditions. A few studies compared the performance of PRC-calibrated PAS with conventional AAS. Atmospheric POP concentrations determined using this approach were within a factor of two or three compared to those obtained by AAS in tropical environments (Gouin et al., 2008; He and Balasubramanian, 2010), and in the Great Lakes basin (Gouin et al., 2005; Hayward et al., 2010). However, to the extent of our knowledge there have been no independent comparison attempts in remote high-mountain areas.

1.2. Uncertainty in passive sampling rates

The determination of sampling rates by PRC calibration often carries considerable uncertainties, mostly associated to the multiple variables involved in the calculation of uptake rates and to the assumptions made regarding the diffusive uptake mechanics of the passive sampler medium (Herker et al., 2018). On one hand, uptake rates have been shown to be influenced by wind speed (Klánová et al., 2008; Moeckel et al., 2009; Tuduri et al., 2006) since the renewal of air inside the sampler housing determines the thickness of the boundary layer of air that is assumed to control uptake and loss of compounds. This can introduce substantial uncertainty depending on the wind speed, the PAS housing design, and its location and orientation (Chaemfa et al., 2009b; Zhang et al., 2015). On the other hand, temperature is the driving force behind molecular diffusivity and uptake or release from the sampler material. PAS applications often benefit from temperate and stable conditions rather than those usually associated with high-mountain locations since PRC calibration takes advantage of moderate and controlled PRC release rates, although diffusivity changes due to temperature variation have been shown to have a relatively smaller impact on sampling rates over a 20 °C range (e.g., from 0 to 20 °C) compared to other factors like wind speed (Shoeib and Harner, 2002). Most PUF-PAS calibration efforts until now have thus been carried out in temperate climates and conditions (Wania and Shunthirasingham, 2020). Moreover, differences between ambient and in-housing registered temperatures can also lead to considerable error in the estimation of sampled volumes (Kennedy et al., 2010).

Therefore, the estimation of sampling rates can lead to non-negligible margins of error in the resulting atmospheric pollutant concentrations, especially in the case of remote locations such as high mountains. Nevertheless, the need for PRC calibration in such places is paramount. Some studies have previously relied on the pool of available data by averaging uptake rates and assuming equal and constant values in their measurements (Mari et al., 2008; Cheng et al., 2013; Jaward et al., 2005; Zhang et al., 2008), but this can induce greater error by not accounting for variability between samples, locations, and sampling periods. Studies in high-mountain sites and other remote areas may be biased from these assumptions more strongly, as the extreme wind velocities, strong solar irradiance, and ample temperature ranges become large sources of uncertainty that need to be accounted for. Other studies have extensively evaluated the use of PRCs and the effect of meteorology on PAS sampling rates, proposing alternative models for the estimation of effective sampled volumes using only publicly available meteorological data (Herker et al., 2018), although it proved more difficult to interpret at higher wind speeds. However, PAS uncertainties are very rarely reported along with sampling rate estimates in the available literature, which is why the need for uncertainty appraisal has been specifically put forward (Wania and Shunthirasingham, 2020).

Accordingly, we deployed PAS and AAS samplers in a high-mountain location in the Pyrenees mountain range for the determination of gas-

phase concentrations of a wide range of SVOCs including PCBs, OCPs, polycyclic aromatic hydrocarbons (PAHs), and organophosphate flame retardants (OPFRs). The effective sampled volumes that allow the conversion of PUF adsorbed amounts to concentrations were calculated by PRC calibration, thus enabling an independent comparison with AAS measurements. The experimental errors in the sampling rates were examined in contrast to an estimate of their theoretical uncertainty in an effort to identify and quantify the main sources of error. Moreover, the agreement between AAS and PAS concentrations was assessed, providing new insight on the reliability of PUF-PAS samplers for the determination of multiple gas-phase semi-volatile pollutants in a remote high-mountain location with characteristics beyond those typically considered in the scope of similar studies (i.e., extreme meteorological conditions and very low pollutant levels).

2. Materials and methods

2.1. Sampling site

All samples were collected near Estanh Redon, a lake located in the Central Catalan Pyrenees (42°38'18.1" N, 0°46'44.1" E, 2240 m.a.s.l.). Estanh Redon is an alpine lake situated above the local tree line, with a hydrology related only to atmospheric precipitation. It has been used as an environmental and biological research site for decades because of its remoteness. The area is characterized by a broad range of temperatures (-16.6–25.1 °C during the deployment of our samples) and periods of extremely high wind speeds (up to 36.2 m s⁻¹, or 130 km h⁻¹). More detailed meteorological conditions have been summarized in Table 1, obtained at a 30 min resolution from an automatic weather station (VS station) from the Catalan Meteorological Service XEMA network located at the exact point of deployment.

2.2. Passive air sampling (PAS)

Polyurethane foam (PUF) passive samplers were deployed in duplicate over four consecutive periods between September 2017 and October 2020 (Table 1). Their durations were 297, 154, 289, and 376 days, respectively. The PUF disks (Techno Spec, Barcelona, Catalonia, Spain) measured 14 cm in diameter, 1.35 cm in thickness, with 369.5 cm² of surface area, and a density of 0.021 g cm⁻³. Prior to deployment, they were thoroughly rinsed with distilled water and acetone (Merck, Darmstadt, Germany), and Soxhlet extracted with acetone and hexane (Merck) for 24 h each. They were further extracted with hexane for another 8 h, dried under vacuum, placed inside acetone-rinsed aluminium foil, sealed air-tight inside of PET/LLDPE bags (Kapak Corporation, St Louis Park, MI, USA), and stored at -20 °C until deployed. They were housed inside stainless steel domes similar to those used in other monitoring programmes (e.g., Pozo et al., 2006) for the entire duration of the sampling campaign (Fig. 1), attached 3 m above ground level to a stainless steel tower structure that holds the equipment of the meteorological station.

PAS sampling rates were determined by PRC calibration (see Section 2.7 below), spiking the PUFs with a mixture of PCB congeners 3, 9, 15, 32 (all labelled), 107, and 198 (Cambridge Isotope Laboratories,

Tewksbury, MA, USA) upon deployment. After their retrieval, the PUFs were sealed again and transported in a refrigerated container and stored at -20 °C until extracted. Two field blanks were performed for each sampling period, being transported with the samples, exposed during deployment and retrieval, spiked with the PRC mixture, and stored at -20 °C for the duration of the sampling until extracted alongside the samples.

2.3. Active air sampling (AAS)

Three AAS samples were obtained in July and September 2017 (Table 1) using a high-volume air sampler (MCV, Collbató, Catalonia, Spain) placed 30 m away from the PAS samplers and connected to a gasoline-fuelled energy generator situated 50 m downwind from both sampler devices. Gas-phase samples were collected with two PUF plugs (6 cm diameter, 10 cm thickness, 0.0285 g cm⁻³ density) inside a Teflon tube, preceded by a 20.3 × 25.4 cm GF/A glass fiber filter (GFF) (Whatman, Maidstone, England) that collected the atmospheric particle phase. Samples between 125 and 242 m³ were collected at 20 m³ h⁻¹. The PUF-AAS plugs were pre-cleaned, transported, and stored as described for the PUF-PAS disks. The GFF filters were pre-treated in a muffle furnace at 450 °C overnight and transported and stored in the same way. Field blanks were also performed for each AAS sample by exposing PUF plugs and filters to the atmosphere during the collection of samples.

Back-trajectories of the air masses arriving at the sampling location during the collection of AAS samples were calculated for 72 h backwards using the NOAA Hysplit model (Stein et al., 2015) (Fig. S1a–c).

2.4. Extraction and clean-up

The PUF-PAS disks and the PUF-AAS plugs were Soxhlet extracted for 8 h with hexane, and the GFF-AAS filters were extracted three times by sonication for 15 min with hexane:dichloromethane 4:1 v/v (all solvents from Merck). The following recovery standards were spiked onto the sampler media before the extraction: 1,2,4,5-tetrabromobenzene, PCB209 (Dr. Ehrenstorfer, Augsburg, Germany), acenaphthene-d₁₀, fluorene-d₁₀, phenanthrene-d₁₀, anthracene-d₁₀, fluoranthene-d₁₀, pyrene-d₁₀, benz[a]anthracene-d₁₂, chrysene-d₁₂, benzo[b]fluoranthene-d₁₂, benzo[ghi]perylene-d₁₂ (National Institute of Standards and Technology, Gaithersburg, MD, USA), tributyl phosphate-d₁₂, tris(2-chloroethyl) phosphate-d₁₂, tris(1-chloro-2-propyl) phosphate-d₁₈, tris(1,3-dichloro-2-propyl) phosphate-d₁₅, and triphenyl phosphate-d₁₅ (Cambridge Isotope Laboratories). The extracts were concentrated to 2 mL with a vacuum rotary evaporator (Büchi, Flawil, Switzerland) and further concentrated to 0.5 mL under a gentle stream of nitrogen gas.

The clean-up of the extracts was performed by HPLC fractionation as described elsewhere (Prats et al., 2021). Briefly, an Agilent 1200 Series system (Agilent Technologies, Santa Clara, CA, USA) equipped with a preparative fraction collector and a Tracer Excel 120 SI HPLC silica column 25 cm × 3 μm × 0.46 cm i.d. (Teknokroma, Sant Cugat del Vallès, Catalonia, Spain) was used for the separation of compounds. Following the injection of 10 μL of extract, two separate fractions were collected

Table 1

Passive (PAS) and active (AAS) air sampling periods and atmospheric conditions.

	PAS I	PAS II	PAS III	PAS IV	AAS I	AAS II	AAS III
Start date	17/09/2017	11/07/2018	12/12/2018	27/09/2019	25/07/2017	26/07/2017	17/09/2017
End date	11/07/2018	12/12/2018	27/09/2019	07/10/2020	25/07/2017	26/07/2017	17/09/2017
Sampled time (d)	297	154	289	376	-	-	-
Sampled volume (m ³)	-	-	-	-	242	125	158
Average temperature (°C)	0.7	6.8	4.1	4.2	6.0	5.6	2.6
(Min–Max)	(-16.6–18.2)	(-9.2–20.3)	(-14.1–25.1)	(-16.6–23.3)	(5.7–6.4)	(5.3–5.9)	(2.4–2.9)
Average wind speed (m s ⁻¹)	4.7	4.4	4.8	4.6	5.4	5.6	6.6
(Min–Max)	(0–36.2)	(0–33.9)	(0–36.0)	(0–35.6)	(2.9–12.1)	(3.9–12.4)	(2.0–13.2)



Fig. 1. PUF-PAS samplers deployed in the Pyrenees (2240 m.a.s.l.) inside dome-shaped stainless steel housings affixed to the structure of an automatic weather station.

after an initial elution of 8 min of 100% hexane at 0.5 mL min^{-1} : a first one for PCBs and OCPs (min 8–15 while performing a solvent composition gradient to 20% dichloromethane) and a second one for PAHs (min 15–20 maintaining solvent composition). The fractions were then concentrated under a stream of nitrogen gas. OPFRs were analysed without requiring HPLC fractionation after drying an aliquot of the original extract through 0.5 g of anhydrous sodium sulphate (Merck) activated at $450 \text{ }^\circ\text{C}$ in a muffle furnace.

2.5. Instrumental analysis

The extract fractions were injected into a gas chromatograph coupled to a mass spectrometer (GC–MS). A targeted analysis was performed for the following compounds: PAHs, acenaphthene (ace), fluorene (fle), phenanthrene (phe), fluoranthene (flu), pyrene (pyr), benz[*a*]anthracene (b[*a*]ant), chrysene+triphenylene (chr + triph), benzo[*b*], [*j*], and [*k*]fluoranthenes (b[*b* + *j* + *k*]flu), benzo[*e*]pyrene (b[*e*]p), benzo[*a*]pyrene (b[*a*]p), indeno[1,2,3-*cd*]pyrene (ind[123 *cd*]pyr), and benzo[*ghi*]perylene (b[*ghi*]peryl); PCB congeners 28, 52, 101, 118, 138, 153, and 180; and OCPs hexachlorobenzene (HCB) and pentachlorobenzene (PeCB). They were identified in SIM mode by retention time and *m/z* ratios (Table S1). A Thermo Trace GC Ultra-DSQ II (Thermo Fisher Scientific, Waltham, MA, USA) GC–MS system was used, with a $60 \text{ m} \times 0.25 \text{ mm i.d.} \times 25 \text{ } \mu\text{m}$ HP-5MS fused capillary column (Agilent Technologies) in electron impact mode at 70 eV. The injector, ion source, quadrupole, and transfer line temperatures were 280, 250, 150, and $270 \text{ }^\circ\text{C}$, respectively. Helium was used as carrier gas (1 mL min^{-1}). The oven program was as follows: $90 \text{ }^\circ\text{C}$ (1 min) to $150 \text{ }^\circ\text{C}$ at $10 \text{ }^\circ\text{C min}^{-1}$ and to $320 \text{ }^\circ\text{C}$ at $6 \text{ }^\circ\text{C min}^{-1}$, with a final holding time of 20 min.

The following OPFRs were analysed by GC coupled to tandem mass spectrometry (GC–MS/MS): tributyl phosphate (TBP), tris(2-chloroethyl) phosphate (TCEP), tris(1-chloro-2-propyl) phosphate (TCPP), tris(1,3-dichloro-2-propyl) phosphate (TDCP), and triphenyl phosphate (TPhP). They were identified in MRM mode by retention time and one quantifier and one qualifier *m/z* transitions (Table S2). An Agilent 7000 Series Triple Quad GC/MS (Agilent Technologies)

system was used, with a $30 \text{ m} \times 0.25 \text{ mm i.d.} \times 0.25 \text{ } \mu\text{m}$ Zebtron ZB-PAH capillary column (Phenomenex, Torrance, CA, USA) in electron impact mode. The injector, ion source, quadrupoles, and transfer line temperatures were 280, 230, 150, and $280 \text{ }^\circ\text{C}$, respectively. Helium was used as a carrier gas at 1.1 mL min^{-1} . The oven program was as follows: $80 \text{ }^\circ\text{C}$ (1.5 min) to $220 \text{ }^\circ\text{C}$ at $10 \text{ }^\circ\text{C min}^{-1}$ and to $315 \text{ }^\circ\text{C}$ at $15 \text{ }^\circ\text{C min}^{-1}$, with a final holding time of 5 min.

2.6. Quality control and assurance

At least one field blank per sampling was performed as described above, taking meticulous measures to avoid contamination of the samplers in the field, during transport, and in the laboratory. They were transported, stored, extracted, and analysed along with each batch of samples. Average blank levels were subtracted from the pollutant amounts in each sampler. Special care was put into avoiding contamination from the exhaust of the energy generator used for AAS sample collection, which was placed over 50 m downwind from the sampler. PAH levels in AAS blanks were compared to PAS blanks in search of increased levels due to exhaust fumes, as observed in previous studies (Fernández et al., 2002), and no influence of such contamination was detected.

Breakthrough of gas-phase pollutants in the PUF-AAS sampling has been previously studied using the same equipment we used, in very similar conditions and at the same site (Fernández et al., 2002; van Drooge et al., 2002). Compounds that can be affected by breakthrough tend to be those with higher volatilities such as naphthalene, acenaphthylene, or pentachlorobenzene, so this was considered when choosing the set of targeted compounds.

The quantification of the target pollutants was performed by internal standard calibration, which accounts for extraction and processing recoveries as well as for analysis variability. Recoveries of most surrogate standards ranged between $73 \pm 24\%$ and $103 \pm 18\%$ for deuterated PAHs, with the more volatile Ace-*d*₁₀ occasionally presenting lower values or non-quantifiable peaks, between $66 \pm 9\%$ and $90 \pm 28\%$ for PCBs and OCPs, and between $48 \pm 11\%$ and $106 \pm 10\%$ for OPFRs, with TDCP occasionally presenting lower values or non-quantifiable peaks due to interferences. In-column limits of quantification ranged between 0.5 and 2.5 pg, or 25 to 125 pg sampler⁻¹ for PAHs and OCPs, and 0.12 to 0.25 pg in-column or 6.25 to 12.5 pg sampler⁻¹ for OPFRs. For average PAS effective sampled volumes, these translate to instrumental LOQs of 0.1–0.4 pg m⁻³ for PAHs and OCPs and 0.01–0.03 pg m⁻³ for OPFRs. For average AAS sampled volumes, they are 0.1–0.7 pg m⁻³ for PAHs and OCPs and 0.04–0.07 pg m⁻³ for OPFRs.

2.7. Determination of PAS concentrations

Concentrations of gas-phase pollutants in air (C_A , pg m⁻³) were calculated by determining compound- and sample-specific effective sampled air volumes (V_A , m³). These are theoretical volumes of air by which the amount of compound found in the PUF-PAS samplers (pg sampler⁻¹) was divided in order to provide an estimate of C_A , accounting for differences both in sampling conditions between periods and in physical-chemical properties between compounds. Here, V_A were calculated as follows (Harner et al., 2013):

$$V_A = V_{PUF} K'_{PUF-A} \left[1 - \exp \left(\frac{-k_A t}{K'_{PUF-A} D_{film}} \right) \right] \quad (1)$$

where V_{PUF} is the volume of the PUF disk (m³), k_A is the sample-specific air-side mass transfer coefficient (m d⁻¹), t is the duration of the sampling campaign (d), D_{film} is the effective film thickness of the PUF disk (0.00567 m), and K'_{PUF-A} is the density-corrected PUF-air partition coefficient (unitless) calculated by multiplying K_{PUF-A} (m³ g⁻¹) by the density of the PUF (g m⁻³). K_{PUF-A} values depend on the sampler material and are compound-specific. They were calculated from octanol-air partition coefficients (K_{OA}) as $\log K_{PUF-A} = 0.6366 \times \log K_{OA}$

– 3.1774 (Shoeib and Harner, 2002). Temperature-corrected K_{OA} values for the studied compounds were obtained from temperature dependence correlations reported in other studies (Chen et al., 2016; Harner, 2021; Odabasi et al., 2006; Wang et al., 2017). Although this $K_{PUF-A}-K_{OA}$ relationship has been extensively used for many SVOCs, recent reports argued that compounds like OPFRs may behave quite differently (therefore making the previous equation not accurate for the estimation of sampled volumes) and proposed a new relationship (Saini et al., 2019). This could lead to added uncertainty on OPFR atmospheric concentrations, so the newly proposed equation ($\log K_{PUF-A} = 0.6087 \times \log K_{OA} + 2.3821$) was also used for comparison.

The calculation of k_A transfer coefficients involves the calibration of each sampler in situ. This is often done by determining sampling rates (R_S , $m^3 d^{-1}$) for each individual sampler using PRCs. The dissipation rate of PRCs is proportional to the uptake of the target compounds, and therefore to their mass transfer coefficients (Huckins et al., 2002). They were calculated as follows:

$$k_A = \frac{R_S}{A_{PUF}} = \frac{\ln(C/C_0) K_{PUF-A} D_{film}}{t} \quad (2)$$

where A_{PUF} is the area of the PUF disk (m^2), and where PRC release ratios are defined as the amount of each PRC left in the exposed sampler after its retrieval (C) divided by the amount found in the field blanks (C_0). These PRC relative amounts were also corrected for recovery and for instrumental variability using the internal standards added before the extraction of the respective exposed and blank PUFs.

The theoretical uncertainty of R_S was estimated through the error propagation of the non-constant variables and coefficients involved in Eq. (2). A more detailed explanation of this calculation can be found in the Supplementary Material (Text S1). Briefly, the main sources of error reside in the calculation of C/C_0 ratios and in the K_{OA} values of PRCs used for the calculation of K_{PUF-A} , the uncertainties of which were reported elsewhere (Harner and Bidleman, 1996). Expanded uncertainties (calculated as twice the regular uncertainty) should then confidently encompass other sources of error such as those inherent to the $K_{PUF-A}-K_{OA}$ and $K_{OA}-T$ correlations.

3. Results and discussion

3.1. PAS sampling rates and uncertainty

Table 2 summarizes the sampling rates calculated by PRC calibration of the PAS samplers for all four passive sampling periods detailed in Table 1. The mean R_S of all samplers was $3.7 \pm 0.5 m^3 d^{-1}$, with individual replicates ranging from 2.6 to $4.5 m^3 d^{-1}$. This is in excellent agreement with most values in the literature and results from global PAS networks using PUF-PAS samplers with the stainless-steel dome design, which typically report R_S of 3 to $4 m^3 d^{-1}$ and standard deviations around 1 to $2 m^3 d^{-1}$ (Herkert et al., 2018; Pozo et al., 2009). Other studies in mountain locations reported PRC-derived R_S of $4.3 \pm 1.6 m^3 d^{-1}$ in the Tibetan plateau (Ren et al., 2014), $2.7 \pm$

$1.1 m^3 d^{-1}$ in the Andes (Estellano et al., 2008), and $3.6 \pm 2.0 m^3 d^{-1}$ in southern Brazil (Meire et al., 2012). Sampling rates have often been correlated with meteorological variables such as wind speed (Klánová et al., 2008; Herkert et al., 2018). However, no significant relationship was found between our results and the average wind speeds or temperatures. This was attributed to a small number of representative sampling periods and to the average values of such variables remaining reasonably stable throughout all sampling campaigns regardless of the time of the year ($0.7-6.8 ^\circ C$, $4.4-4.8 m s^{-1}$), despite temperature and wind speed ranges being characteristically extreme as expected in an alpine site ($-16.6-25.1 ^\circ C$, $0.0-36.2 m s^{-1}$) (Table 1).

The experimental error of R_S was calculated as the relative standard deviation of the replicates. It averaged $12 \pm 11\%$, being as high as 23% for one of the sampled periods (Table 2). R_S could only be calculated for three of the four periods because one of the duplicates was lost due to extreme weather and wind conditions. Nevertheless, an average experimental variability below 20% is adequate considering that all R_S were within the range of typically reported values. Moreover, some differences between samplers may not be solely associated to the inherent uncertainty in the estimation of R_S , but also to differences in air flow through the PUFs due to slight deformations that resulted in tilted sampler housings after heavy snow and intense wind events. This may also explain why the experimental error in the first sampling period (PAS I), when the sampler devices were newly installed, was much smaller ($< 2\%$) than in ensuing periods (Table 2). These differences in air flow are nonetheless accounted for when reporting pollutant concentrations because sampling rates are calculated and used independently for each replicate instead of as a period average.

Theoretical expanded uncertainties of R_S were calculated for each sampler from a rearranged Eq. (2) (see Text S1 in the Supplementary Material). They averaged $15 \pm 4\%$, ranging from 11 to 19% (Table 2). The two main variables contributing to this uncertainty are K_{OA} and the PRC release ratios, C/C_0 . K_{OA} error accounted for 68% of the total unexpanded theoretical uncertainty on average, while C/C_0 error accounted for the remaining 32%. A smaller contribution of the latter term was expected since the determination of C/C_0 does not involve particularly severe error-inducing operations, yet it still amounted to a sizeable fraction of the total uncertainty because small variations in such ratios may render substantial fluctuations in the resulting R_S . On the other hand, uncertainties of PRC K_{OA} values ranging from 2 to 35% (Harner and Bidleman, 1996) are sufficiently large to become the main source of error. This uncertainty is inherent to determining K_{OA} values and is added to that of their temperature dependence relationships and to that of the empirical regression through which K_{PUF-A} is calculated (Shoeib and Harner, 2002), which were indirectly accounted for by calculating the expanded uncertainties.

An additional consideration must be made in regard to sampling rates and effective sampled volumes of OPFRs. As mentioned in Section 2.7, alternative associations between K_{PUF-A} and K_{OA} have been proposed (Saini et al., 2019) arguing that some compound groups may not adequately adhere to the relationship originally described by Shoeib and Harner (2002) due to their different partitioning behavior. Therefore, we compared effective sampled volumes for OPFRs estimated using both equations (Table S3). OPFRs with higher K_{OA} values (i.e., TCPP, TDCP, and TPhP) saw very little or no change in their mean estimated volumes since they remained in the linear phase of uptake by the PUF-PAS. On the other hand, TCEP and TBP, with lower K_{OA} , presented volumes 18 and 30% lower on average using the original relationship, respectively. This is due to one order of magnitude higher K_{PUF-A} values resulting from a higher intercept in the equation proposed by Saini et al. (2019), which undoubtedly adds to the overall uncertainty in OPFR measurements and must be considered when passive sampler-derived concentrations are reported. However, this equation only relies on three non-chlorinated OPFRs, and we did not consider the resulting differences to be large enough to adopt

Table 2

Mean sampling rates (R_S) and standard deviations (SD) of passive air samplers calculated by PRC calibration, and their experimental and theoretical uncertainties.

	Mean $R_S \pm$ SD ($m^3 d^{-1}$)	Experimental error ^b	Expanded theoretical uncertainty ^c
PAS I	3.8 ± 0.1	1.8%	15.5%
PAS II	3.2 ± 0.7	23.0%	19.4%
PAS III	3.6 ± 0.4	11.5%	15.1%
PAS IV	4.5^a	–	10.7%
Mean	3.7 ± 0.5	$12.1 \pm 10.6\%$	$15.2 \pm 3.5\%$

^a One duplicate was lost due to extreme weather conditions.

^b Relative standard deviation of the duplicates.

^c Calculated as twice the error propagated from the uncertainty in the variables used for R_S estimation.

the newest equation just for two compounds. This also allows for direct comparison with other previously reported concentrations.

Overall, the average experimental variability observed in the sampling rates adequately fits within the mean estimated expanded uncertainty. However, this does not always need to be the case. Factors beyond the purely theoretical and analytical ones considered for the calculation of the uncertainty can induce pronounced disagreements between sample replicates (e.g., sampler housing inclination causing differences in wind flux through the samplers). Nevertheless, the fact that they both remained confidently below 20% illustrates the suitability and reliability of our PAS measurements. Still, an uncertainty of up to 20% could potentially translate into misjudgements of effective sampled volumes of 100–200 m³ on average. Therefore, we performed an in-situ field comparison between PUF-PAS and PUF-AAS sampling techniques for further assessing the accuracy of PAS measurements.

3.2. Comparison between PAS and AAS

The degrees of equilibrium (DEQ) reached by the studied compounds during the exposure of each PUF-PAS were calculated as a measure of the performance of these passive samplers across all sampling campaigns in this study and are summarized in Table S4. The DEQ is the magnitude to which the uptake of a compound by the PUF-PAS departed the linear regime and approached equilibrium between air and the PUF. They can be obtained from the components between brackets in Eq. (1). As expected, the more volatile compounds (i.e., PAHs Ace, Fle, and Phe; OCPs PeCB and HCB) reached near or complete equilibrium during all sampling campaigns (DEQ close to 1). They were followed by the low molecular weight PCB28 and the lowest K_{OA} OPFRs TBP and TCEP (mean DEQ between 0.32 and 0.50). All other compounds had low DEQs (below 0.29) signifying a still close-to-linear uptake regime, especially for OPFRs with the highest K_{OA} (DEQ almost 0). This reflects the usefulness of a complete PRC calibration of individual PUF-PASs for studies encompassing a set of compounds with a wide range of physical-chemical properties. Otherwise, the assumption of an invariable linear uptake would lead to a large overestimation of atmospheric concentrations of pollutants that tend to equilibrate more easily.

Table 3 contains the mean gas-phase concentrations obtained using both AAS and PAS methods, along with their standard deviations. The complete results for all replicates can be found in the Supplementary Material (Table S5). Notice that the mean and standard deviation of all samples are presented for AAS, while for PAS they are the mean and standard deviation of the period averages. The agreement between PAS replicates was adequate, averaging relative standard deviations (RSD) between samplers of 23%. These mean differences were consistent for all groups of analysed compounds, with the unique exception of TPhP resulting from a local contamination (see Section 3.4). AAS concentrations were relatively similar between samples, considering their different sampling periods (mean RSD of 41%). Concentrations of OCPs and PCBs were the closest between periods (RSD 33%), while OPFRs were less consistent (59%). It is worth noting that the AAS concentrations of many pollutants in the first sampling period (AAS I) were frequently higher than in the following ones (Table S5). A possible explanation resides in the origin of air mass trajectories computed backwards for each AAS period (Fig. S1). While all of them have a North-Atlantic origin, the trajectories for AAS I have a more pronounced continental component and lower altitudes that may have increased the levels of pollutants they carried.

AAS and PAS mean concentrations were compared to each other to determine the accuracy and suitability of PRC-derived concentrations. Fig. 2 displays the correlation between results from both methods, shown for average PAS results and for the PAS campaign closest to the collection of AAS samples (PAS I). Overall, an adequate linear correlation was observed between measurements (R^2 0.86, $p < 0.01$), showing even better goodness of fit when only PAS I was considered (R^2 0.91, $p < 0.01$). This improvement is a result of PAS campaigns representing

Table 3

Mean gas-phase concentrations and standard deviations (SD) of target organic pollutants determined using passive air sampling (PAS, $n = 4 \times 2$ replicates) and active air sampling (AAS, $n = 3$) methods. Particle-phase concentrations are shown for the active sampling glass fiber filters (GFF-AAS), along with the fraction of compounds distributed in the particle phase over their total concentration (gas + particle) and their log-transformed octanol-air partition coefficients ($\log K_{OA}$) at 25 °C.

	PUF-PAS		PUF-AAS		GFF-AAS		Part %	$\log K_{OA}$
	pg m ⁻³	SD	pg m ⁻³	SD	pg m ⁻³	SD		
HCB	36	16	44	2.5	n.d. ^a	–	–	7.4
PeCB	21	19	17	2.1	n.d.	–	–	6.2
PCB28	4.5	3.5	1.9	0.3	n.d.	–	–	7.9
PCB52	2.5	1.5	1.3	0.4	n.d.	–	–	8.4
PCB101	3.7	1.4	4.8	2.2	n.d.	–	–	8.8
PCB118	2.2	1.1	4.5	2.0	n.d.	–	–	8.5
PCB153	2.5	0.6	2.8	1.1	n.d.	–	–	8.5
PCB138	2.1	1.1	3.0	1.1	n.d.	–	–	8.5
PCB180	1.1	0.7	0.3	0.2	n.d.	–	–	9.1
Σ PCB _{gas}	19		19					
Ace	28	18	11	7.1	n.d.	–	–	6.1
Fle	276	50	65	1.5	4.1	1.8	6%	6.2
Phe	388	102	216	160	n.d.	–	–	7.0
Flu	60	25	26	14	7.7	6.2	24%	8.4
Pyr	24	14	13	6.1	9.1	2.3	33%	8.4
B[a]ant	0.8	0.4	0.2	0.03	1.9	1.7	85%	9.2
Chry + TriPh	9.7	7.0	1.3	0.02	2.6	3.9	42%	9.2
Σ PAH _{gas}	787		332					
B[b + j + k]flu	n.d.	–	n.d.	–	6.3	–	100%	10.6
B[a]pyr	n.d.	–	n.d.	–	1.0	1.5	100%	10.6
B[e]pyr	n.d.	–	n.d.	–	1.2	–	100%	10.6
Pery	n.d.	–	n.d.	–	0.2	–	100%	10.6
Db[ah]ant	n.d.	–	n.d.	–	0.2	–	100%	11.4
Ind[123 cd]pyr	n.d.	–	n.d.	–	2.0	3.0	100%	12.0
B[ghi]peryl	n.d.	–	n.d.	–	4.7	4.0	100%	12.6
Σ PAH _{part}					42			
TBP	1.2	1.0	0.8	0.4	28	26	96%	7.6
TCEP	7.8	10	1.2	0.8	189	125	99%	8.0
TCPP	16	7.0	18	12	32	24	61%	9.7
TDCP	2.1	0.9	n.d.	–	2.9	1.2	99%	10.6
TPhP	2063 ^b	2840 ^b	0.3	0.3	11	5.3	97%	10.9
Σ OPFR _{gas}	27 ^c		20 ^c					
Σ OPFR _{part}					263			

^a Not detected (below detection limit or below blank levels).

^b Affected by a local contamination (see Section 3.4).

^c TPhP not included.

much longer sampling periods that encompassed different seasons, which usually induces higher variability in the results. Alternatively, a power regression was adjusted to the data and is shown in Fig. 2, which better represents the closeness of the data to the identity line. In general, agreement between values factoring in their standard deviations indicates the capability of PUF-PAS samplers to replicate the results of the reference PUF-AAS values.

Total PCB concentrations (Σ PCB_{gas}) were 19 pg m⁻³ for both AAS and PAS samples (Table 3), revealing a very good agreement between methods. Concentrations of individual congeners ranged between 0.3 and 4.8 pg m⁻³, with comparable composition profiles except for a 2.4 times higher PAS concentration of the most volatile PCB28. Nevertheless, this difference is still well within other reported disagreement factors for PCBs (Heo and Lee, 2014; Bohlin et al., 2014; Gouin et al., 2005), and a strong correlation was observed between both methods (Fig. 2). Mean HCB and PeCB concentrations determined using both techniques were also comparable: 36 pg m⁻³ (PAS) and 43 pg m⁻³ (AAS) for HCB, and 21 pg m⁻³ (PAS) and 17 pg m⁻³ (AAS). This level of agreement was similar or better than those reported in other studies (Gouin et al., 2008; Hayward et al., 2010). In general, Σ PCB_{gas} and individual congener concentrations were on the lower range of values reported in the same area two decades ago (16–70 pg m⁻³), while HCB (49 pg m⁻³) did not suffer major changes (van Drooge et al., 2004; van Drooge et al., 2005). This demonstrates the persistence of these compounds in the environment after being banned for decades, especially in remote locations. PeCB concentrations were also similar to

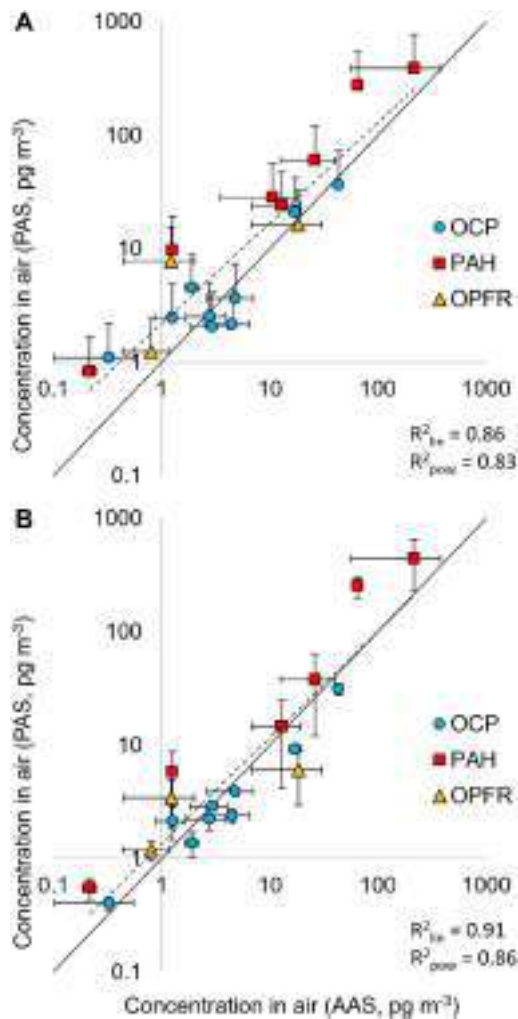


Fig. 2. Comparison of the gas-phase concentrations of organochlorine pesticides (OCP), polycyclic aromatic hydrocarbons (PAH), and organophosphate flame retardants (OPFR) determined using passive air sampling (PAS) and active air sampling (AAS) methods. Regressions are shown for A: mean of four PAS sampling periods; B: sampling period closest to the collection of AAS samples. The error bars represent standard deviations, the dashed line is a power regression for all compounds, and the continuous line represents equal PAS and AAS values.

those found in another remote mountain area in the Tibetan Plateau, 25 pg m^{-3} (Zhu et al., 2014).

The sum of mean PAH concentrations ($\Sigma\text{PAH}_{\text{gas}}$) was 332 pg m^{-3} (AAS) and 787 pg m^{-3} (PAS) (Table 3), with Phe and Fle clearly dominating the concentration profiles (20–35% and 49–65% of total PAHs, respectively). PAS-derived concentrations for all PAHs were consistently greater (3 times on average) than those calculated from AAS samples (note that PAHs fall to the left of the continuous black line that indicates equal PAS and AAS concentrations in Fig. 2). This difference factor is greater than for all other compound groups, and can still be observed even when only the PAS sampling campaign closest to the AAS sampling periods (PAS I) is considered (Fig. 2), albeit less pronounced. The reason for this is the small number of AAS samples that could only be obtained during warmer months due to limited accessibility conditions to the sampling area, and to their short duration compared to the integrative PAS samples, therefore not being able to adequately capture the temporal variability that likely exists for PAHs due to nearby alpine sources. Unlike PCBs and OCPs, PAHs tend to experience marked seasonal changes in rural and mountain regions, with higher concentrations in winter due to intermittent biomass burning

(Van Drooge and Ballesta, 2009; Van Drooge and Grimalt, 2015) and a high impact of seasonal wildfires, both of which will contribute to the integrative nature of PUF-PAS measurements but not be well represented by AAS. Similarly, some disagreement in PAH concentrations was also reported elsewhere (Bohlin et al., 2014), particularly skewed by an underrepresentation of heavier PAHs. Nevertheless, some compounds like Fluo and Pyr still showed close concentrations between both methods, and an overall disagreement factor of 2 to 3 is usually regarded as acceptable for most SVOCs in the literature (e.g., Gouin et al., 2005). Compared to PAH concentrations in high-altitude regions reported elsewhere (Fernández et al., 2002; van Drooge et al., 2010), $\Sigma\text{PAH}_{\text{gas}}$ was 2 to 4 times lower than those previously found in the same location (1442 pg m^{-3} , Tyrolean Alps (1792 pg m^{-3}), and Norwegian Trollheimen (1535 pg m^{-3}), much lower than those found in the Slovakian High Tatras (4421 pg m^{-3}), but higher than in the Canary Islands (187 pg m^{-3}). In any case, the PAH composition profiles generally resembled those reported in these locations.

Finally, total OPFR concentrations ($\Sigma\text{OPFR}_{\text{gas}}$, calculated only for TBP, TCEP, and TCPP) were 20 pg m^{-3} (AAS) and 27 pg m^{-3} (PAS). TDCP and TPHP were not included because the former was not found in AAS samples above detection limits, and the latter suffered from local contamination in the PAS samples (see Section 3.4). Compound profiles were dominated by TCPP (64–90% of total OPFRs). While concentrations of TBP and TCPP between methods were in agreement, that of TCEP was more than 6 times higher in PAS on average due to a particularly high amount observed in one of the sampling periods (PAS II). When treated as an outlier, TCEP PAS concentrations were only 2 times greater on average. Nevertheless, Fig. 2 shows that none of these differences represented a large discrepancy between methods. No AAS–PAS comparison studies for OPFRs were found in the literature, and gas-phase concentrations in remote or high-mountain locations are scarcely reported. Still, our results were reasonably lower than those found in the Great Lakes (Abdollahi et al., 2017; Salamova et al., 2013), in Finland (Marklund et al., 2005), and all across Central and South America (Rauert et al., 2016).

3.3. Particle phase partitioning and PAS infiltration

The GFF-AAS filters that captured the particle phase before passing through the PUF-AAS plugs were analysed for the study of particle-associated SVOCs. PCBs and OCPs were not detected at relevant concentrations above the blanks, which is consistent with the low gas-phase concentrations observed and with previous results showing that these compounds predominantly exist in the gas phase (> 90%) (Yeo et al., 2003). Contrarily, several PAHs and OPFRs were found in the particle phase (Table 3). Detected PAHs included some of those also found in the gas-phase samples, as well as higher molecular weight PAHs usually associated to atmospheric particles. The sum of the average particulate PAH concentrations ($\Sigma\text{PAH}_{\text{part}}$) was 42 pg m^{-3} , which is similar to the one found in a previous study at the same site, 53 pg m^{-3} (van Drooge et al., 2010). However, we could not establish the presence of some more volatile PAHs like Phe and Ant in the particulate phase above blank levels. PAHs only detected in the particulate phase amounted to 37% of $\Sigma\text{PAH}_{\text{part}}$, a somewhat lower proportion than those previously reported (at 39–49%) (van Drooge et al., 2010). Regarding OPFRs, they were prominently found in the particle phase, with a sum of average particulate OPFR concentrations ($\Sigma\text{OPFR}_{\text{part}}$) of 263 pg m^{-3} . This represents a partitioning towards the particulate phase of more than 92% over total OPFR concentrations (gas + particulate), which is consistent with previous considerations indicating that OPFRs mainly exist in the particle-bound form (Abdollahi et al., 2017). The lower proportion of TCEP found in the particulate phase is consistent with the higher vapor pressures of this compound (Okeme et al., 2018), although this distribution was not observed for TCPP which has a similar vapor pressure.

Log-transformed particle to gas concentration ratios were plotted against $\log K_{OA}$ values for compounds detected in both phases (Fig. 3). A linear correlation (R^2 0.85, $p < 0.01$) was observed for most compounds. The slope of the regression (0.74) was very similar to those calculated from reported gas and particle concentrations of pollutants subject to atmospheric transport towards four continental high-mountain locations (0.64–0.75) (van Drooge et al., 2010), including the same area presented in this work (0.72). However, TCPP and TBP exhibited higher concentrations in the particulate phase than expected from their K_{OA} (Table 3), so they were not considered in the regression. Such discrepancies between experimental and K_{OA} -modelled partition ratios have been observed for the more volatile OPFRs before, with suggestions of filter-air partitioning artifacts as a possible cause (Okeme et al., 2018), although we did not observe them for TCEP. Overall, these mixed results should encourage further field studies to experimentally determine OPFR phase distributions based on their physical-chemical properties, since OPFRs are emerging pollutants that encompass a very wide range of volatilities (Sühring et al., 2016).

Finally, the passive sampling theory and all calculations regarding R_S apply only to the fraction of compounds in the gas phase. However, atmospheric particles have been shown to infiltrate into the sampler housings and remain retained by the PUF (Chaemfa et al., 2009b), and there are reports on PUF-PAS sampling of compounds typically bound to particles (Bohlin et al., 2014; Harner et al., 2013; Pozo et al., 2015). The particle infiltration efficiency of passive samplers has been shown to vary greatly for different housing configurations (Markovic et al., 2015). Here, levels of SVOCs typically associated with atmospheric particles, like PAHs with a high number of fused rings, were generally not detected in PAS samples above limits of detection or blank levels, which hints at a low particle infiltration efficiency of the housing configuration used. An approximation of such efficiency was estimated from our experimental data as $\phi_{R,P}$ ($R_{S,part}/R_{S,gas}$), the particle-phase sampling rate as a fraction of the gas-phase sampling rate. It was calculated as outlined elsewhere (Holt et al., 2017). Briefly, the studied compounds were classified as gas-phase compounds if $>70\%$ of their total concentration was found in the atmospheric gas phase of AAS samples, and particle-phase compounds if $>70\%$ was found in AAS filters (Table 3). Compounds that were infrequently detected or close to limits of detection (Ace, TDCP), outside the established thresholds (Pyr, Chr + TriPh), and with contamination (TPhP) were not considered. Average sampling

rates of each group were calculated as the amount of compound in the PUF-PAS sampler divided by the average AAS bulk concentration (gas+particle) and normalized by the sampling duration. The mean $\phi_{R,P}$ was 0.23, or a particle infiltration of 23% compared to the AAS system. This efficiency was 16% if only the PAS campaign closest to the AAS measurements is considered. Note that these values may present substantial uncertainties resulting from a low amount of AAS samples, the disagreement in PAH concentrations between AAS and PAS due to seasonality, and possible artifacts from a small number of particle-phase compounds detected in the PUF-PASs or from PCBs and OCPs not being detected above blank levels in AAS filters. Still, the particle infiltration efficiency calculated only from compounds detected in both gas and particle phases (PAHs in the PAS campaign closest to AAS sampling, and OPFRs) was 18%. While a more comprehensive study would be needed to determine accurate efficiencies, these values indicate a reduced particle infiltration compared to other sampler configurations (Markovic et al., 2015). This suggests that the sampler housing used here may have acted as an effective wind shield, can explain why no correlation was found between average wind speeds and mean sampling rates. Thus, the PUF-PASs performed mainly as gas-phase samplers, which diminishes the need for effective sampled volume correction and is also an advantage in high-mountain areas, ensuring that extremely high wind speeds (up to 36 m s^{-1} , or 130 km h^{-1} , Table 1) did not impact the performance of the sampler.

3.4. Local OPFR contamination

One of the OPFRs (triphenyl phosphate, TPhP) was found in all PUF-PAS replicates at unusually high and fluctuating concentrations, averaging around 2000 pg m^{-3} (Table 3). However, it was never detected above 0.6 pg m^{-3} in AAS samples, the results of which did otherwise generally agree with those of PAS as discussed in Section 3.2. The PAS result was hypothesized to reflect a local contamination, probably due to the presence of a research cabin and meteorological station close (10 m) to the PAS deployment position (Fig. S2). In contrast, the AAS samples were collected further away (nearly 50 m) from the cabin. In order to locate the origin of such contamination, five surface soil samples were collected around the cabin and station, in addition to two samples of different insulating foams used in the interior of the cabin and between the composite metal panels that form its outer walls. They were extracted with acetonitrile after the addition of internal standards and analysed by GC-MS/MS for a quick and qualitative assessment of their OPFR composition.

Abundancies of the targeted OPFRs in each of the samples relative to the internal standards added before their extraction clearly revealed that the origin of TPhP was the insulating material used in the outer wall panels of the cabin (Fig. S3). TPhP was the dominating OPFR in this material ($> 99\%$), while in the soil samples it only amounted to 43% on average. The second main component was TCPP, present at an abundance one to two orders of magnitude higher than in the soil samples, although amounting to only 0.3% of total OPFRs. Contrarily, the sample of inner insulation foam revealed a higher presence of TCPP ($> 99\%$), followed by TDCP and TCEP (both around 0.2%, but still with abundancies two to three orders of magnitude higher than in the soil samples). However, no evidence of TCPP contamination was found in the PAS samples, indicating a small or negligible release rate from the interior of the cabin towards the outside. Finally, TPhP was present in the soil samples in a greater proportion than in the reference AAS samples, indicating the possible influence of this local contamination not only in air but also on the ground, but no clear pattern was observed when factoring in the distance from the source at which each soil sample was taken.

OPFRs are emerging pollutants often used as flame retardants and plasticizers in construction materials and household products. They tend to leach from such materials as they are not chemically bound and are highly susceptible to volatilization (van der Veen and de Boer,

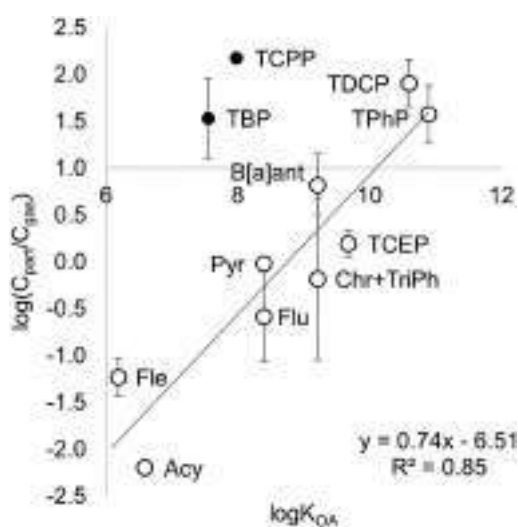


Fig. 3. Correlation between the log-transformed ratio of concentrations between pollutants in particle (C_{part}) and gas (C_{gas}) phases and $\log K_{OA}$, where TCPP and TBP were not included in the regression. Error bars represent standard deviations.

2012). The presence of this local TPhP contamination, although unfortunate for the comparison of AAS and PAS presented in this study, highlights the capacity of the PUF samplers for sequestering this kind of emerging and less studied contaminants in the gas phase notwithstanding their tendency to associate to atmospheric particles (Abdollahi et al., 2017). However, it also exposes the impact that unexpected anthropogenic influences can have on atmospheric pollution studies, especially in areas with low concentrations, and emphasizes the need for adequate treatment of samples and careful data interpretation. It also highlights the importance of adequate site selection and sampler placement for air monitoring studies that include currently used commercial chemicals such as flame retardants and plasticizers, extensively used as material additives, as any nearby objects or structures could greatly influence the results. Although this can be more easily preventable in remote areas such as the one in this work, special attention should be paid to avoiding adjacent sources of contamination in populated and urban environments. Furthermore, studies comparing PAS and AAS measurements should also consider the need for the highest proximity between both samplers, since our results show that cases of local contamination could be inadequately reflected in the samples even by being separated only by a few tens of meters.

4. Conclusions

Polyurethane foam passive air samplers (PUF-PAS) are a useful method for the determination of gas-phase semi-volatile organic compounds in high mountain areas. Their calibration using Performance Reference Compounds (PRCs) produces compound- and sampler-independent sampling rates that account for spatial, temporal, and meteorological differences between samples. The experimental variability observed between the sampling rates of our PAS samples adequately conforms to the estimates of their expanded theoretical uncertainties. On average, sampling rate uncertainties were well below 20%, indicating an adequate precision of the PRC calibration of the PUF-PASs. A comparison of PAS-derived gas-phase concentrations with high-volume active air samples (AAS) showed good agreement between both techniques for different semi-volatile pollutants subject to long-range atmospheric transport at low concentrations. This includes pollutants like PCBs, HCB, PeCB, PAHs, and the less studied emerging OPFRs. These results showcase the suitability of PUF-PAS samplers for the monitoring of SVOCs in remote high-mountain locations with typically low pollutant concentrations and extreme atmospheric and meteorological conditions. Finally, the distribution of most compounds found both in the gas and particle phases of AAS samples revealed profiles consistent with their vapor pressures, except for some OPFRs with higher particle phase concentrations than anticipated. No relevant levels of pollutants typically bound to the particle phase were detected above limits of detection or blank levels in the PUF-PASs.

CRedit authorship contribution statement

RP: sampling, analysis, formal analysis, visualization, and writing – original draft. BD: sampling, analysis, supervision, and writing – review and editing. PF: supervision, writing – review and editing. JG: conceptualization, writing – review and editing, and funding acquisition.

Declaration of competing interest

The authors declare that they have no known competing financial interests or personal relationships that could have appeared to influence the work reported in this paper.

Acknowledgements

Sampling support from Alejandro G. Inarra and Anna Canals-Angerri, and technical assistance from Roser Chalder are acknowledged. The

NOAA Air Resources Laboratory (ARL) is acknowledged for the provision of the HYSPLIT transport and dispersion model and READY website.

Funding

This work was supported by the Spanish Ministry of Science and Innovation (CTM2015-71832-P and PGC2018-102288-B-I00). Raimon M. Prats also acknowledges financial support from the Spanish Ministry of Science and Innovation (BES-2016-076339).

Appendix A. Supplementary data

Supplementary data to this article can be found online at <https://doi.org/10.1016/j.scitotenv.2021.149738>.

References

- Abdollahi, A., Eng, A., Jantunen, L.M., Ahrens, L., Shoeib, M., Parnis, J.M., Harner, T., 2017. Characterization of polyurethane foam (PUF) and sorbent impregnated PUF (SIP) disk passive air samplers for measuring organophosphate flame retardants. *Chemosphere* 167, 212–219. <https://doi.org/10.1016/j.chemosphere.2016.09.111>.
- Bohlin, P., Audy, O., Škrdlíková, L., Kukučka, P., Příbylová, P., Prokeš, R., Vojta, Š., Klánová, J., 2014. Outdoor passive air monitoring of semi volatile organic compounds (SVOCs): a critical evaluation of performance and limitations of polyurethane foam (PUF) disks. *Environ. Sci. Process. Impacts* 16, 433. <https://doi.org/10.1039/c3em00644a>.
- Chaemfa, C., Barber, J.L., Gocht, T., Harner, T., Holoubek, I., Klanova, J., Jones, K.C., 2008. Field calibration of polyurethane foam (PUF) disk passive air samplers for PCBs and OC pesticides. *Environ. Pollut.* 156, 1290–1297. <https://doi.org/10.1016/j.envpol.2008.03.016>.
- Chaemfa, C., Barber, J.L., Kim, K.S., Harner, T., Jones, K.C., 2009a. Further studies on the uptake of persistent organic pollutants (POPs) by polyurethane foam disk passive air samplers. *Atmos. Environ.* 43, 3843–3849. <https://doi.org/10.1016/j.atmosenv.2009.05.020>.
- Chaemfa, C., Wild, E., Davison, B., Barber, J.L., Jones, K.C., 2009b. A study of aerosol entrainment and the influence of wind speed, chamber design and foam density on polyurethane foam passive air samplers used for persistent organic pollutants. *J. Environ. Monit.* 11, 1117–1304. <https://doi.org/10.1039/b823016a>.
- Chen, Y., Cai, X., Jiang, L., Li, Y., 2016. Prediction of octanol-air partition coefficients for polychlorinated biphenyls (PCBs) using 3D-QSAR models. *Ecotoxicol. Environ. Saf.* 124, 202–212. <https://doi.org/10.1016/j.ecoenv.2015.10.024>.
- Cheng, H., Deng, Z., Chakraborty, P., Liu, D., Zhang, R., Xu, Y., Luo, C., Zhang, G., Li, J., 2013. A comparison study of atmospheric polycyclic aromatic hydrocarbons in three Indian cities using PUF disk passive air samplers. *Atmos. Environ.* 73, 16–21. <https://doi.org/10.1016/j.atmosenv.2013.03.001>.
- Estellano, V.H., Pozo, K., Harner, T., Franken, M., Zaballa, M., 2008. Altitudinal and seasonal variations of persistent organic pollutants in the Bolivian Andes mountains. *Environ. Sci. Technol.* 42, 2528–2534. <https://doi.org/10.1021/es702754m>.
- Evcı, Y.M., Esen, F., Tasdemir, Y., 2016. Monitoring of long-term outdoor concentrations of PAHs with passive air samplers and comparison with meteorological data. *Arch. Environ. Contam. Toxicol.* 71, 246–256. <https://doi.org/10.1007/s00244-016-0292-6>.
- Fernández, P., Grimalt, J.O., Vilanova, R.M., 2002. Atmospheric gas-particle partitioning of polycyclic aromatic hydrocarbons in high mountain regions of Europe. *Environ. Sci. Technol.* 36, 1162–1168. <https://doi.org/10.1021/es010190t>.
- Gouin, T., Harner, T., Blanchard, P., Mackay, D., 2005. Passive and active air samplers as complementary methods for investigating persistent organic pollutants in the Great Lakes Basin. *Environ. Sci. Technol.* 39, 9115–9122. <https://doi.org/10.1021/es051397f>.
- Gouin, T., Wania, F., Ruepert, C., Castillo, L.E., 2008. Field testing passive air samplers for current use pesticides in a tropical environment. *Environ. Sci. Technol.* 42, 6625–6630. <https://doi.org/10.1021/es8008425>.
- Grimalt, J.O., Fernandez, P., Berdie, L., Vilanova, R.M., Catalan, J., Psenner, R., Hofer, R., Appleby, P.G., Rosseland, B.O., Lien, L., Massabuau, J.C., Battarbee, R.W., 2001. Selective trapping of organochlorine compounds in mountain lakes of temperate areas. *Environ. Sci. Technol.* 35, 2690–2697. <https://doi.org/10.1021/es000278r>.
- Guida, Y.de S., Meire, R.O., Torres, J.P.M., Malm, O., 2018. Air contamination by legacy and current-use pesticides in Brazilian mountains: an overview of national regulations by monitoring pollutant presence in pristine areas. *Environ. Pollut.* 242, 19–30. <https://doi.org/10.1016/j.envpol.2018.06.061>.
- Harner, T., 2021. 2021 v10 Template for Calculating PUF and SIP Disk Sample Air Volumes. <https://doi.org/10.13140/RG.2.1.3998.8884>.
- Harner, T., Bidleman, T.F., 1996. Measurements of octanol-air partition coefficients for polychlorinated biphenyls. *J. Chem. Eng. Data* 41, 895–899. <https://doi.org/10.1021/je960097y>.
- Harner, T., Su, K., Genualdi, S., Karpowicz, J., Ahrens, L., Mihele, C., Schuster, J., Charland, J.P., Narayan, J., 2013. Calibration and application of PUF disk passive air samplers for tracking polycyclic aromatic compounds (PACs). *Atmos. Environ.* 75, 123–128. <https://doi.org/10.1016/j.atmosenv.2013.04.012>.
- Hayward, S.J., Gouin, T., Wania, F., 2010. Comparison of four active and passive sampling techniques for pesticides in air. *Environ. Sci. Technol.* 44, 3410–3416. <https://doi.org/10.1021/es902512h>.
- He, J., Balasubramanian, R., 2010. A comparative evaluation of passive and active samplers for measurements of gaseous semi-volatile organic compounds in the tropical

- atmosphere. *Atmos. Environ.* 44, 884–891. <https://doi.org/10.1016/j.atmosenv.2009.12.009>.
- Heo, J., Lee, G., 2014. Field-measured uptake rates of PCDDs/Fs and dl-PCBs using PUF-disk passive air samplers in Gyeonggi-do, South Korea. *Sci. Total Environ.* 491–492, 42–50. <https://doi.org/10.1016/j.scitotenv.2014.03.073>.
- Herkert, N.J., Spak, S.N., Smith, A., Schuster, J.K., Harner, T., Martinez, A., Hornbuckle, K.C., 2018. Calibration and evaluation of PUF-PAS sampling rates across the global atmospheric passive sampling (GAPS) network. *Environ. Sci. Process. Impacts* 20, 210–219. <https://doi.org/10.1039/c7em00360a>.
- Holt, E., Bohlin-Nizzetto, P., Boruvková, J., Harner, T., Kalina, J., Melymuk, L., Klánová, J., 2017. Using long-term air monitoring of semi-volatile organic compounds to evaluate the uncertainty in polyurethane-disk passive sampler-derived air concentrations. *Environ. Pollut.* 220, 1100–1111. <https://doi.org/10.1016/j.envpol.2016.11.030>.
- Huckins, J.N., Petty, J.D., Lebo, J.A., Almeida, F.V., Booi, K., Alvarez, D.A., Cranor, W.L., Clark, R.C., Mogensen, B.B., 2002. Development of the permeability/performance reference compound approach for in situ calibration of semipermeable membrane devices. *Environ. Sci. Technol.* 36, 85–91. <https://doi.org/10.1021/es010991w>.
- Jaward, F.M., Zhang, G., Nam, J.J., Sweetman, A.J., Obbard, J.P., Kobara, Y., Jones, K.C., 2005. Passive air sampling of polychlorinated biphenyls, organochlorine compounds, and polybrominated diphenyl ethers across Asia. *Environ. Sci. Technol.* 39, 8638–8645. <https://doi.org/10.1021/es051382h>.
- Kalina, J., Scheringer, M., Boruvková, J., Kukucka, P., Pribylová, P., Bohlin-Nizzetto, P., Klánová, J., 2017. Passive air samplers as a tool for assessing long-term trends in atmospheric concentrations of semivolatile organic compounds. *Environ. Sci. Technol.* 51, 7047–7054. <https://doi.org/10.1021/acs.est.7b02319>.
- Kennedy, K., Hawker, D.W., Bartkow, M.E., Carter, S., Ishikawa, Y., Mueller, J.F., 2010. The potential effect of differential ambient and deployment chamber temperatures on PRC derived sampling rates with polyurethane foam (PUF) passive air samplers. *Environ. Pollut.* 158, 142–147. <https://doi.org/10.1016/j.envpol.2009.07.031>.
- Klánová, J., Èupr, P., Kohoutek, J., Harner, T., 2008. Assessing the influence of meteorological parameters on the performance of polyurethane foam-based passive air samplers. *Environ. Sci. Technol.* 42, 550–555. <https://doi.org/10.1021/es072098o>.
- Li, Y., Geng, D., Liu, F., Wang, T., Wang, P., Zhang, Q., Jiang, G., 2012. Study of PCBs and PBDEs in King George Island, Antarctica, using PUF passive air sampling. *Atmos. Environ.* 51, 140–145. <https://doi.org/10.1016/j.atmosenv.2012.01.034>.
- Mari, M., Schuhmacher, M., Feliubadaló, J., Domingo, J.L., 2008. Air concentrations of PCDD/Fs, PCBs and PCNs using active and passive air samplers. *Chemosphere* 70, 1637–1643. <https://doi.org/10.1016/j.chemosphere.2007.07.076>.
- Marklund, A., Andersson, B., Haglund, P., 2005. Traffic as a source of organophosphorus flame retardants and plasticizers in snow. *Environ. Sci. Technol.* 39, 3555–3562. <https://doi.org/10.1021/es0482177>.
- Markovic, M.Z., Prokop, S., Staebler, R.M., Liggio, J., Harner, T., 2015. Evaluation of the particle infiltration efficiency of three passive samplers and the PS-1 active air sampler. *Atmos. Environ.* 112, 289–293. <https://doi.org/10.1016/j.atmosenv.2015.04.051>.
- Meire, R.O., Lee, S.C., Targino, A.C., Torres, J.P.M., Harner, T., 2012. Air concentrations and transport of persistent organic pollutants (POPs) in mountains of southeast and southern Brazil. *Atmos. Pollut. Res.* 3, 417–425. <https://doi.org/10.5094/APR.2012.048>.
- Moeckel, C., Harner, T., Nizzetto, L., Strandberg, B., Lindroth, A., Jones, K.C., 2009. Use of deuration compounds in passive air samplers: results from active sampling-supported field deployment, potential uses, and recommendations. *Environ. Sci. Technol.* 43, 3227–3232. <https://doi.org/10.1021/es0802897x>.
- Odabasi, M., Cetin, E., Sofuoglu, A., 2006. Determination of octanol-air partition coefficients and supercooled liquid vapor pressures of PAHs as a function of temperature: application to gas-particle partitioning in an urban atmosphere. *Atmos. Environ.* 40, 6615–6625. <https://doi.org/10.1016/j.atmosenv.2006.05.051>.
- Okeme, J.O., Rodgers, T.F.M., Jantunen, L.M., Diamond, M.L., 2018. Examining the gas-particle partitioning of organophosphate esters: how reliable are air measurements? *Environ. Sci. Technol.* 52, 13834–13844. <https://doi.org/10.1021/acs.est.8b04588>.
- Pozo, K., Harner, T., Wania, F., Muir, D.C.G., Jones, K.C., Barrie, L.A., 2006. Toward a global network for persistent organic pollutants in air: results from the GAPS study. *Environ. Sci. Technol.* 40, 4867–4873. <https://doi.org/10.1021/es060447t>.
- Pozo, K., Harner, T., Lee, S.C., Wania, F., Muir, D.C.G., Jones, K.C., 2009. Seasonally resolved concentrations of persistent organic pollutants in the global atmosphere from the first year of the GAPS study. *Environ. Sci. Technol.* 43, 796–803. <https://doi.org/10.1021/es02106a>.
- Pozo, K., Estellano, V.H., Harner, T., Diaz-Robles, L., Cereceda-Balic, F., Etcharren, P., Pozo, Katerine, Vidal, V., Guerrero, F., Vergara-Fernández, A., 2015. Assessing polycyclic aromatic hydrocarbons (PAHs) using passive air sampling in the atmosphere of one of the most wood-smoke-polluted cities in Chile: the case study of Temuco. *Chemosphere* 134, 475–481. <https://doi.org/10.1016/j.chemosphere.2015.04.077>.
- Pozo, K., Martellini, T., Corsolini, S., Harner, T., Estellano, V., Kukucka, P., Mulder, M.D., Lammel, G., Cincinelli, A., 2017. Persistent organic pollutants (POPs) in the atmosphere of coastal areas of the Ross Sea, Antarctica: indications for long-term downward trends. *Chemosphere* 178, 458–465. <https://doi.org/10.1016/j.chemosphere.2017.02.118>.
- Prats, R.M., van Drooge, B.L., Fernández, P., Marco, E., Grimalt, J.O., 2021. Changes in urban gas-phase persistent organic pollutants during the COVID-19 lockdown in Barcelona. *Front. Environ. Sci.* 9, 109. <https://doi.org/10.3389/fenvs.2021.650539>.
- Rauer, C., Harner, T., Schuster, J.K., Quinto, K., Fillmann, G., Castillo, L.E., Fentanes, O., Ibarra, M.V., Miglioranza, K.S.B., Rivadeneira, I.M., Pozo, K., Puerta, A.P., Zuluaga, B.H.A., 2016. Towards a regional passive air sampling network and strategy for new POPs in the GRULAC region: perspectives from the GAPS network and first results for organophosphorus flame retardants. *Sci. Total Environ.* 573, 1294–1302. <https://doi.org/10.1016/j.scitotenv.2016.06.229>.
- Ren, J., Wang, X., Xue, Y., Gong, P., Joswiak, D.R., Xu, B., Yao, T., 2014. Persistent organic pollutants in mountain air of the southeastern Tibetan Plateau: seasonal variations and implications for regional cycling. *Environ. Pollut.* 194, 210–216. <https://doi.org/10.1016/j.envpol.2014.08.002>.
- Saini, A., Clarke, J., Harner, T., 2019. Direct measurements of polyurethane foam (PUF) – air partitioning coefficients for chemicals of emerging concern capable of equilibrating in PUF disk samplers. *Chemosphere* 234, 925–930. <https://doi.org/10.1016/j.chemosphere.2019.06.134>.
- Salamova, A., Ma, Y., Venier, M., Hites, R.A., 2013. High levels of organophosphate flame retardants in the Great Lakes atmosphere. *Environ. Sci. Technol. Lett.* 1, 8–14. <https://doi.org/10.1021/ez400034n>.
- Shoeb, M., Harner, T., 2002. Characterization and comparison of three passive air samplers for persistent organic pollutants. *Environ. Sci. Technol.* 36, 4142–4151. <https://doi.org/10.1021/es020635t>.
- Stein, A.F., Draxler, R.R., Rolph, G.D., Stunder, B.J.B., Cohen, M.D., Ngan, F., 2015. NOAA's Hysplit atmospheric transport and dispersion modeling system. *Bull. Am. Meteorol. Soc.* 96, 2059–2077. <https://doi.org/10.1175/BAMS-D-14-00110.1>.
- Sührling, R., Wolschke, H., Diamond, M.L., Jantunen, L.M., Scheringer, M., 2016. Distribution of organophosphate esters between the gas and particle phase—model predictions vs measured data. *Environ. Sci. Technol.* 50, 6644–6651. <https://doi.org/10.1021/acs.est.6b00199>.
- Tuduri, L., Harner, T., Hung, H., 2006. Polyurethane foam (PUF) disks passive air samplers: wind effect on sampling rates. *Environ. Pollut.* 144, 377–383. <https://doi.org/10.1016/j.envpol.2005.12.047>.
- Van der Veen, I., de Boer, J., 2012. Phosphorus flame retardants: properties, production, environmental occurrence, toxicity and analysis. *Chemosphere* 88, 1119–1153. <https://doi.org/10.1016/j.chemosphere.2012.03.067>.
- Van Drooge, B.L., Ballesta, P.P., 2009. Seasonal and daily source apportionment of polycyclic aromatic hydrocarbon concentrations in PM10 in a semirural European area. *Environ. Sci. Technol.* 43, 7310–7316. <https://doi.org/10.1021/es901381a>.
- Van Drooge, B.L., Grimalt, J.O., 2015. Particle size-resolved source apportionment of primary and secondary organic tracer compounds at urban and rural locations in Spain. *Atmos. Chem. Phys.* 15, 7735–7752. <https://doi.org/10.5194/acp-15-7735-2015>.
- Van Drooge, B.L., Grimalt, J.O., Torres García, C.J., Cuevas, E., 2002. Semivolatile organochlorine compounds in the free troposphere of the Northeastern Atlantic. *Environ. Sci. Technol.* 36, 1155–1161. <https://doi.org/10.1021/es010189u>.
- Van Drooge, B.L., Grimalt, J.O., Camarero, L., Catalan, J., Stuchlík, E., Torres García, C.J., 2004. Atmospheric semivolatile organochlorine compounds in European high-mountain areas (Central Pyrenees and High Tatras). *Environ. Sci. Technol.* 38, 3525–3532. <https://doi.org/10.1021/es030108p>.
- Van Drooge, B.L., Grimalt, J.O., Booi, K., Camarero, L., Catalan, J., 2005. Passive sampling of atmospheric organochlorine compounds by SPMDs in a remote high mountain area. *Atmos. Environ.* 39, 5195–5204. <https://doi.org/10.1016/j.atmosenv.2005.05.020>.
- Van Drooge, B.L., Fernández, P., Grimalt, J.O., Stuchlík, E., García, C.J.T., Cuevas, E., 2010. Atmospheric polycyclic aromatic hydrocarbons in remote European and Atlantic sites located above the boundary mixing layer. *Environ. Sci. Pollut. Res.* 17, 1207–1216. <https://doi.org/10.1007/s11356-010-0296-0>.
- Wang, Q., Zhao, H., Wang, Y., Xie, Q., Chen, J., Quan, X., 2017. Determination and prediction of octanol-air partition coefficients for organophosphate flame retardants. *Ecotoxicol. Environ. Saf.* 145, 283–288. <https://doi.org/10.1016/j.ecoenv.2017.07.040>.
- Wania, F., MacKay, D., 1996. Tracking the distribution of persistent organic pollutants. *Environ. Sci. Technol.* 30, 390A–396A. <https://doi.org/10.1021/es962399q>.
- Wania, F., Shunthirasingham, C., 2020. Passive air sampling for semi-volatile organic chemicals. *Environ. Sci. Process. Impacts* 22, 1919–2134. <https://doi.org/10.1039/d0em00194e>.
- Yeo, H.G., Choi, M., Chun, M.Y., Sunwoo, Y., 2003. Gas/particle concentrations and partitioning of PCBs in the atmosphere of Korea. *Atmos. Environ.* 37, 3561–3570. [https://doi.org/10.1016/S1352-2310\(03\)00361-3](https://doi.org/10.1016/S1352-2310(03)00361-3).
- Zhang, G., Chakraborty, P., Li, J., Sampathkumar, P., Balasubramanian, T., Kathiresan, K., Takahashi, S., Subramanian, A., Tanabe, S., Jones, K.C., 2008. Passive atmospheric sampling of organochlorine pesticides, polychlorinated biphenyls, and polybrominated diphenyl ethers in urban, rural, and wetland sites along the coastal length of India. *Environ. Sci. Technol.* 42, 8218–8223. <https://doi.org/10.1021/es8016667>.
- Zhang, X., Hoang, M., Lei, Y.D., Wania, F., 2015. Exploring the role of the sampler housing in limiting uptake of semivolatile organic compounds in passive air samplers. *Environ. Sci. Process. Impacts* 17, 1995–2136. <https://doi.org/10.1039/c5em00447k>.
- Zhu, N., Schramm, K.W., Wang, T., Henkelmann, B., Zheng, X., Fu, J., Gao, Y., Wang, Y., Jiang, G., 2014. Environmental fate and behavior of persistent organic pollutants in Shergyla Mountain, southeast of the Tibetan Plateau of China. *Environ. Pollut.* 191, 166–174. <https://doi.org/10.1016/j.envpol.2014.04.031>.

FIELD COMPARISON OF PASSIVE POLYURETHANE FOAM AND ACTIVE AIR SAMPLING TECHNIQUES FOR ANALYSIS OF GAS-PHASE SEMI-VOLATILE ORGANIC COMPOUNDS AT A REMOTE HIGH-MOUNTAIN SITE

Raimon M. Prats, Barend L. van Drooge, Pilar Fernández, Joan O. Grimalt

Institute of Environmental Assessment and Water Research (IDAEA-CSIC), Jordi Girona 18, 08034 Barcelona, Catalonia, Spain

ARTICLE 1 – SUPPORTING INFORMATION

Text S1.1	Sampling rate uncertainty.	102
Table S1.1	Ion m/z ratios and collision energies used in GC-MS.	103
Table S1.2	Ion m/z transitions and collision energies used in GC-MS/MS.	104
Table S1.3	Effective sampled volumes of OPFRs calculated from sampling rates.	104
Table S1.4	Degree of equilibrium reached by each compound during exposure.	105
Table S1.5	Atmospheric PAS and AAS (gas and particle phase) replicate concentrations of target pollutants.	106
Figure S1.1	Back-trajectories of air masses during AAS sampling periods.	107
Figure S1.2	Correlation between particle/gas concentration ratio and octanol–air partition coefficient.	110
Figure S1.3	Research cabin at the sampling site.	110
Figure S1.4	Relative abundance of OPFRs in insulation material and soil samples.	111
References S1		112

Text S1.1. Sampling rate uncertainty

Sampling rates (R_S , $\text{m}^3 \text{d}^{-1}$) are used for the calculation of air-side mass transfer coefficients (k_A , $\text{m} \text{d}^{-1}$) in the determination of effective sampled air volumes (V_A , m^3) that allow reporting atmospheric pollutant concentrations instead of just total amounts of compound sequestered per sampler device. They are calculated as follows (Harner, 2021):

$$R_S = \frac{-\ln(C/C_0) K'_{PUF-A} D_{film} A_{PUF}}{t} \quad (\text{Eq. S1.1})$$

where C/C_0 is the ratio of PRC amounts found in the sampler and in the blank, respectively, t is the duration of the sampling campaign (d), D_{film} is the effective film thickness of the PUF disk (m), A_{PUF} is the area of the PUF sampler (m^2), and K'_{PUF-A} is the density-corrected PUF–air partition coefficient (dimensionless) calculated as K_{PUF-A} ($\text{m}^3 \text{g}^{-1}$) multiplied by the PUF density (ρ_{PUF} , $\text{g} \text{m}^{-3}$). K_{PUF-A} values are calculated from temperature-corrected octanol–air partition coefficients ($K_{OA(T)}$) as $\log K_{PUF-A} = 0.6366 \times \log K_{OA(T)} - 3.1774$ (Shoeb and Harner, 2002). Equation S1.1 can be expressed as follows:

$$R_S = \frac{-\ln(C/C_0) D_{film} \rho_{PUF} 10^{(0.6366 \log K_{OA(T)} - 3.1774)} A_{PUF}}{t} = k \ln(C/C_0) 10^{(b \log K_{OA(T)} - a)} \quad (\text{Eq. S1.2})$$

where all constants have been condensed under k , and the numeric parameters of the K_{PUF-A} – K_{OA} regression have been simplified to a and b .

The theoretical error (δ) of the calculation of R_S can be estimated from the propagation of the error of the non-constant variables in Equation S1.2, in this case C/C_0 and $K_{OA(T)}$:

$$\begin{aligned} \delta R_S &= \sqrt{\left(\frac{\partial R_S}{\partial C/C_0}\right)^2 \delta_{C/C_0}^2 + \left(\frac{\partial R_S}{\partial K_{OA(T)}}\right)^2 \delta_{K_{OA(T)}}^2} = \\ &= \sqrt{\left(\frac{10^{-a} k K_{OA(T)}^b}{C/C_0}\right)^2 \delta_{C/C_0}^2 + \left(10^{-a} k b K_{OA(T)}^{b-1} \ln(C/C_0)\right)^2 \delta_{K_{OA(T)}}^2} \end{aligned} \quad (\text{Eq. S1.3})$$

where $\partial R_S / \partial i$ denotes the partial derivative of R_S with respect to a variable i . δR_S can be expressed as percent over the R_S value by calculating $\delta R_S / R_S \times 100$.

The uncertainty of PRC $K_{OA(T)}$ values was estimated from their standard errors, calculated from values reported elsewhere (Harner and Bidleman, 1996), and it averaged 10.1%. The uncertainty of C/C_0 ratios was estimated from the propagation of errors involved in their calculation (i.e., reference material, dilution, instrumental, and peak integration errors), and it averaged 4.7%. Thus, R_S percent uncertainties calculated with Equation S1.3 resulted in an average theoretical uncertainty of $7.6 \pm 1.8\%$, ranging from 5.4 to 9.7%. Expanded uncertainties ($2 \times R_S$ percent uncertainties) therefore averaged $15.2 \pm 3.5\%$, ranging from 10.7 to 19.4%.

Table S1.1. Ion m/z ratios used in GC-MS (SIM mode) for the identification and quantification of target compounds and their recovery standards.

Compound	Abbreviation	m/z (CE 70 eV)
2,4,4'-Trichlorobiphenyl	PCB28	256
2,2',5,5'-Tetrachlorobiphenyl	PCB52	292
2,2',4,5,5'-Pentachlorobiphenyl	PCB101	326
2,3',4,4',5'-Pentachlorobiphenyl	PCB118	326
2,2',3,4,4',5'-Hexachlorobiphenyl	PCB138	360
2,2',4,4',5'-Hexachlorobiphenyl	PCB153	360
2,2',3,4,4',5'-Heptachlorobiphenyl	PCB180	394
Hexachlorobenzene	HCB	284
Pentachlorobenzene	PeCB	250
Acenaphthene	Ace	154
Fluorene	Fle	166
Phenanthrene	Phe	178
Fluoranthene	Flu	202
Pyrene	Pyr	202
Benz[a]anthracene	B[a]ant	228
Chrysene + Triphenylene	Chr + TriPh	228
Benzo[b+j+k]fluoranthene	B[b+j+k]flu	252
Benzo[e]pyrene	B[e]pyr	252
Benzo[a]pyrene	B[a]pyr	252
Indeno[1,2,3-cd]pyrene	Ind[123cd]pyr	276
Benzo[ghi]perylene	B[ghi]pery	276
Decachlorobiphenyl	PCB209	498
1,2,4,5-Tetrabromobenzene	TBB	394
Acenaphthene-d ₁₀	Ace-d ₁₀	164
Fluorene-d ₁₀	Fle-d ₁₀	176
Phenanthrene-d ₁₀	Phe-d ₁₀	188
Anthracene-d ₁₀	Ant-d ₁₀	188
Fluoranthene-d ₁₀	Flu-d ₁₀	212
Pyrene-d ₁₀	Pyr-d ₁₀	212
Benz[a]anthracene-d ₁₂	B[a]ant-d ₁₂	240
Chrysene-d ₁₂	Chr-d ₁₂	240
Benzo[b]fluoranthene-d ₁₂	B[b]flu-d ₁₂	264
Benzo[ghi]perylene-d ₁₂	B[ghi]pery-d ₁₂	288

Table S1.2. Ion m/z transitions and collision energies (CE) used in GC-MS/MS (MRM mode) for the identification and quantification of target compounds and their respective recovery standards.

Compound	Abbr.	Quantifier m/z		Qualifier m/z	
		(CE, eV)		(CE, eV)	
Tributyl phosphate	TBP	99→81	20	99→63	38
Tris(2-chloroethyl) phosphate	TCEP	249→125	10	249→99	32
Tris(1-chloro-2-propyl) phosphate	TCPP	125→81	29	125→99	12
Tris(1,3-dichloro-2-propyl) phosphate	TDCP	191→155	5	191→75	11
Triphenyl phosphate	TPhP	326→215	25	326→169	32
Tributyl phosphate-d ₁₀	TBP-d ₂₇	103→83	20	103→63	43
Tris(2-chloroethyl) phosphate-d ₁₂	TCEP-d ₁₂	261→131	9	261→131	30
Tris(1-chloro-2-propyl) phosphate-d ₁₈	TCPP-d ₁₈	131→83	30	131→103	11
Tris(1,3-dichloro-2-propyl) phosphate-d ₁₅	TDCP-d ₁₅	197→160	4	197→79	12
Triphenyl phosphate-d ₁₅	TPhP-d ₁₅	341→223	26	341→243	11

Table S1.3. Effective air sampled volumes (m³) for all sampling campaigns at Estanh Redon (PAS I–PAS IV) calculated from PUF–air partition coefficients (K_{PUF-A}) obtained using two different proposed relationships with octanol–air partition coefficients (K_{OA}).

$\log K_{\text{PUF-A}} = 0,6366 \times \log K_{\text{OA}} - 3,1774$						
<i>M. Shoeib and T. Harner, Environ. Sci. Technol. 2002, 36, 4142-4151</i>						
	TBP	TCEP	TCIPP	TDCIPP	TPhP	Mean
logK _{OA}	7.6	8.0	9.7	10.6	10.9	
PAS I	791	930	1117	1130	1132	1020
PAS II	390	432	488	492	492	459
PAS III	698	835	1029	1044	1046	930
PAS IV	907	1186	1650	1687	1692	1424
Mean	699	846	1071	1088	1090	

$\log K_{\text{PUF-A}} = 0,6087 \times \log K_{\text{OA}} + 2,3821$						
<i>A. Saini, J. Clarke and T. Harner, Chemosphere 2019, 234, 925-930</i>						
	TBP	TCEP	TCIPP	TDCIPP	TPhP	Mean
logK _{OA}	7.6	8.0	9.7	10.6	10.9	
PAS I	1092	1111	1134	1135	1135	1121
PAS II	481	487	493	493	493	489
PAS III	1005	1025	1048	1050	1050	1035
PAS IV	1587	1637	1698	1702	1703	1666
Mean	1041	1065	1093	1095	1095	

Table S1.4. Degree of equilibrium (DEQ) reached by every compound during exposure in each passive sampling campaign (PAS I – IV). DEQs closer to 1 denote that an equilibrium has been reached between air and sampler material, while DEQs closer to 0 denote that the uptake of the compound is still in the linear phase.

	PAS I	PAS II	PAS III	PAS IV	Mean
Ace	1.00	1.00	1.00	1.00	1.00
Fle	1.00	1.00	1.00	1.00	1.00
Phe	0.97	0.89	0.98	0.96	0.95
Flu	0.30	0.21	0.34	0.29	0.29
Pyr	0.30	0.21	0.34	0.29	0.29
B[a]ant	0.09	0.06	0.10	0.08	0.08
Chr+TriPh	0.09	0.06	0.10	0.08	0.08
PCB28	0.43	0.32	0.49	0.42	0.42
PCB52	0.24	0.18	0.29	0.24	0.24
PCB101	0.14	0.10	0.17	0.14	0.14
PCB118	0.25	0.18	0.29	0.24	0.24
PCB153	0.26	0.19	0.30	0.26	0.25
PCB138	0.25	0.18	0.29	0.24	0.24
PCB180	0.10	0.07	0.12	0.10	0.10
PeCB	1.00	1.00	1.00	1.00	1.00
HCB	0.89	0.73	0.91	0.86	0.85
TBP	0.54	0.38	0.58	0.51	0.50
TCEP	0.34	0.23	0.38	0.32	0.32
TCPP	0.03	0.02	0.04	0.03	0.03
TDCP	0.01	0.01	0.01	0.01	0.01
TPhP	0.01	0.01	0.01	0.01	0.01

Table S1.5. Atmospheric concentrations (pg m^{-3}) of the studied semi-volatile organic compounds in replicate samples collected by passive (PUF-PAS) and active (PUF-AAS) air sampling, as well as in the particulate phase of active samples (GFF-AAS).

	PUF-PAS										PUF-AAS						GFF-AAS								
	PASI 1		PASI 2		PASI 1		PASI 2		PASI 1		PASI 2		PASIV 1		PASIV 2		PASIV 3		AAS I		AAS II		AAS III		
HCB	34	29	54	67	26	26	26	28	42	42	46	42	42	n.d.	n.d.	n.d.	n.d.	n.d.	n.d.	n.d.	n.d.	n.d.	n.d.	n.d.	n.d.
PeCB	9.4	9.1	36	49	n.d. ^a	n.d.	11	19	16	16	16	n.d.	n.d.	n.d.	n.d.	n.d.	n.d.	n.d.	n.d.	n.d.	n.d.	n.d.	n.d.	n.d.	n.d.
PCB28	1.6	1.1	9	7.6	n.d.	n.d.	3.9	2.1	1.6	1.6	2.0	2.0	2.0	n.d.	n.d.	n.d.	n.d.	n.d.	n.d.	n.d.	n.d.	n.d.	n.d.	n.d.	n.d.
PCB52	2.6	1.7	5.2	3.9	3.4	1.0	1.0	1.7	0.9	0.9	1.2	1.2	1.2	n.d.	n.d.	n.d.	n.d.	n.d.	n.d.	n.d.	n.d.	n.d.	n.d.	n.d.	n.d.
PCB101	4.2	3.6	5.2	4.7	n.d.	n.d.	2.1	7.3	3.5	3.5	3.6	3.6	3.6	n.d.	n.d.	n.d.	n.d.	n.d.	n.d.	n.d.	n.d.	n.d.	n.d.	n.d.	n.d.
PCB118	2.6	2.1	3.6	2.6	n.d.	n.d.	1.0	6.8	3.5	3.5	3.3	3.3	3.3	n.d.	n.d.	n.d.	n.d.	n.d.	n.d.	n.d.	n.d.	n.d.	n.d.	n.d.	n.d.
PCB153	2.6	1.9	3.7	3.2	3.0	1.3	2.2	4.1	2.2	2.2	2.0	2.0	2.0	n.d.	n.d.	n.d.	n.d.	n.d.	n.d.	n.d.	n.d.	n.d.	n.d.	n.d.	n.d.
PCB138	2.7	3.1	2.4	2.5	n.d.	n.d.	0.8	4.2	2.4	2.4	2.2	2.2	2.2	n.d.	n.d.	n.d.	n.d.	n.d.	n.d.	n.d.	n.d.	n.d.	n.d.	n.d.	n.d.
PCB180	0.4	0.4	1.2	1.0	n.d.	n.d.	1.8	0.5	0.4	0.4	0.1	0.1	0.1	n.d.	n.d.	n.d.	n.d.	n.d.	n.d.	n.d.	n.d.	n.d.	n.d.	n.d.	n.d.
Ace	n.d.	n.d.	n.d.	n.d.	17	15	41	3.2	17	17	11	11	11	n.d.	n.d.	n.d.	n.d.	n.d.	n.d.	n.d.	n.d.	n.d.	n.d.	n.d.	n.d.
Fle	292	214	350	224	208	238	339	66	63	63	65	65	65	2.4	2.4	3.9	3.9	5.9	5.9	5.9	5.9	5.9	5.9	5.9	5.9
Phe	588	292	524	489	262	344	301	401	137	137	110	110	110	n.d.	n.d.	n.d.	n.d.	n.d.	n.d.	n.d.	n.d.	n.d.	n.d.	n.d.	n.d.
Flu	56	20	114	79	54	52	54	41	14	14	23	23	23	3.2	3.2	5.1	5.1	15	15	15	15	15	15	15	15
Pyr	22	7.2	50	38	22	25	14	20	7.5	7.5	12	12	12	n.d.	n.d.	7.5	7.5	11	11	11	11	11	11	11	11
B[a]ant	0.6	0.5	1.3	0.9	n.d.	n.d.	n.d.	0.2	0.2	0.2	0.3	0.3	0.3	0.7	0.7	1.1	1.1	3.8	3.8	3.8	3.8	3.8	3.8	3.8	3.8
Chr+TriPh	7.9	3.7	18	22	7.6	8.4	4.9	1.2	1.3	1.3	1.3	1.3	1.3	0.6	0.6	0.1	0.1	7.2	7.2	7.2	7.2	7.2	7.2	7.2	7.2
B[b+j+k]flu	n.d.	n.d.	n.d.	n.d.	n.d.	n.d.	n.d.	n.d.	n.d.	n.d.	n.d.	n.d.	n.d.	n.d.	n.d.	n.d.	n.d.	n.d.	6.3	6.3	6.3	6.3	6.3	6.3	6.3
B[e]pyr	n.d.	n.d.	n.d.	n.d.	n.d.	n.d.	n.d.	n.d.	n.d.	n.d.	n.d.	n.d.	n.d.	n.d.	n.d.	n.d.	n.d.	n.d.	1.2	1.2	1.2	1.2	1.2	1.2	1.2
B[a]pyr	n.d.	n.d.	n.d.	n.d.	n.d.	n.d.	n.d.	n.d.	n.d.	n.d.	n.d.	n.d.	n.d.	0	0	0.2	0.2	2.7	2.7	2.7	2.7	2.7	2.7	2.7	2.7
Pery	n.d.	n.d.	n.d.	n.d.	n.d.	n.d.	n.d.	n.d.	n.d.	n.d.	n.d.	n.d.	n.d.	n.d.	n.d.	n.d.	n.d.	n.d.	0.2	0.2	0.2	0.2	0.2	0.2	0.2
Ind[123cd]pyr	n.d.	n.d.	n.d.	n.d.	n.d.	n.d.	n.d.	n.d.	n.d.	n.d.	n.d.	n.d.	n.d.	0.2	0.2	0.4	0.4	5.5	5.5	5.5	5.5	5.5	5.5	5.5	5.5
Db[ah]ant	n.d.	n.d.	n.d.	n.d.	n.d.	n.d.	n.d.	n.d.	n.d.	n.d.	n.d.	n.d.	n.d.	n.d.	n.d.	n.d.	n.d.	n.d.	0.2	0.2	0.2	0.2	0.2	0.2	0.2
B[ghi]pery	n.d.	n.d.	n.d.	n.d.	n.d.	n.d.	n.d.	n.d.	n.d.	n.d.	n.d.	n.d.	n.d.	n.d.	n.d.	n.d.	n.d.	n.d.	8.4	8.4	8.4	8.4	8.4	8.4	8.4
TBP	1.4	1.0	2.7	2.7	1.0	0.9	0.2	0.5	1.2	1.2	0.7	0.7	0.7	8.8	8.8	n.d.	n.d.	46	46	46	46	46	46	46	46
TCEP	4.5	2.3	27	20	2.8	3.1	1.7	2.0	1.3	1.3	0.4	0.4	0.4	301	301	210	210	55	55	55	55	55	55	55	55
TCPP	8.2	3.8	22	21	27	13	18	30	19	19	6.6	6.6	6.6	54	54	36	36	7.1	7.1	7.1	7.1	7.1	7.1	7.1	7.1
TDCCP	1.4	2.6	3.8	2.6	3.0	1.6	0.9	n.d.	n.d.	n.d.	n.d.	n.d.	n.d.	2.1	2.1	4.2	4.2	2.3	2.3	2.3	2.3	2.3	2.3	2.3	2.3
TPhP	1094 ^b	11383 ^b	426 ^b	325 ^b	1516 ^b	1405 ^b	180 ^b	0.3	0.6	0.6	0.1	0.1	0.1	17	17	10	10	6.5	6.5	6.5	6.5	6.5	6.5	6.5	6.5

^a Not detected (below detection limit or below blank levels).^b Affected by a local contamination (see Section 3.4 of the main article).

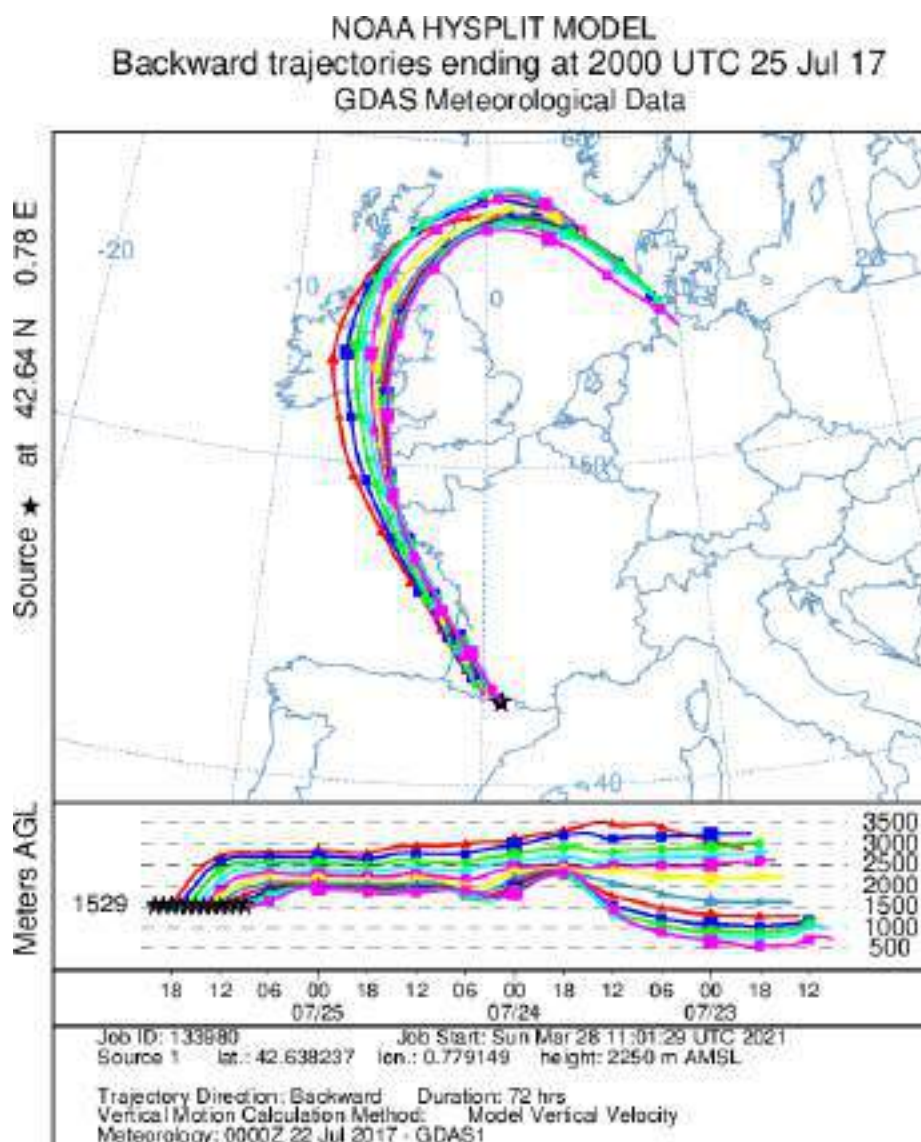


Figure S1.1a. NOAA Hysplit model back-trajectories (72 h backwards, 6 h intervals) of the air masses arriving at the sampling location during the collection of AAS sample I (July 25, 2017).

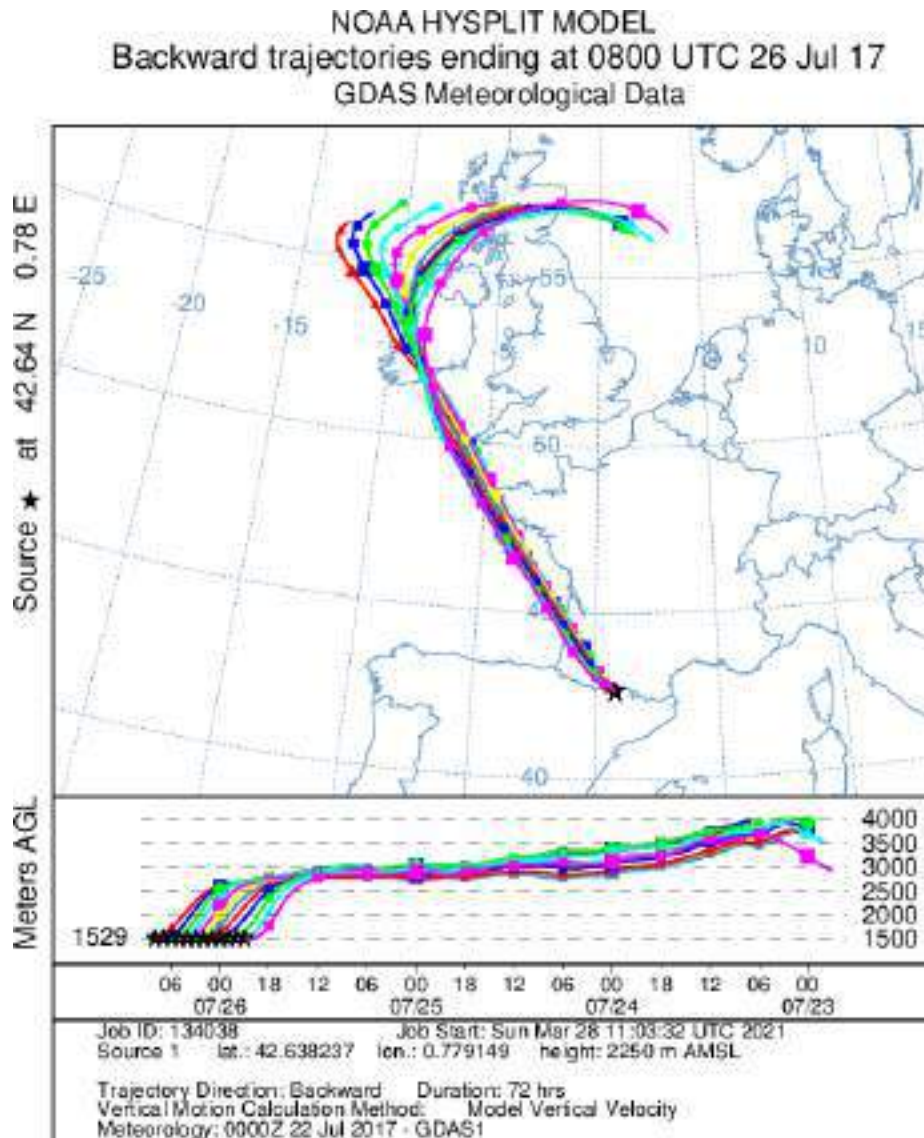


Figure S1.1b. NOAA Hysplit model back-trajectories (72 h backwards, 6 h intervals) of the air masses arriving at the sampling location during the collection of AAS sample II (July 26, 2017).

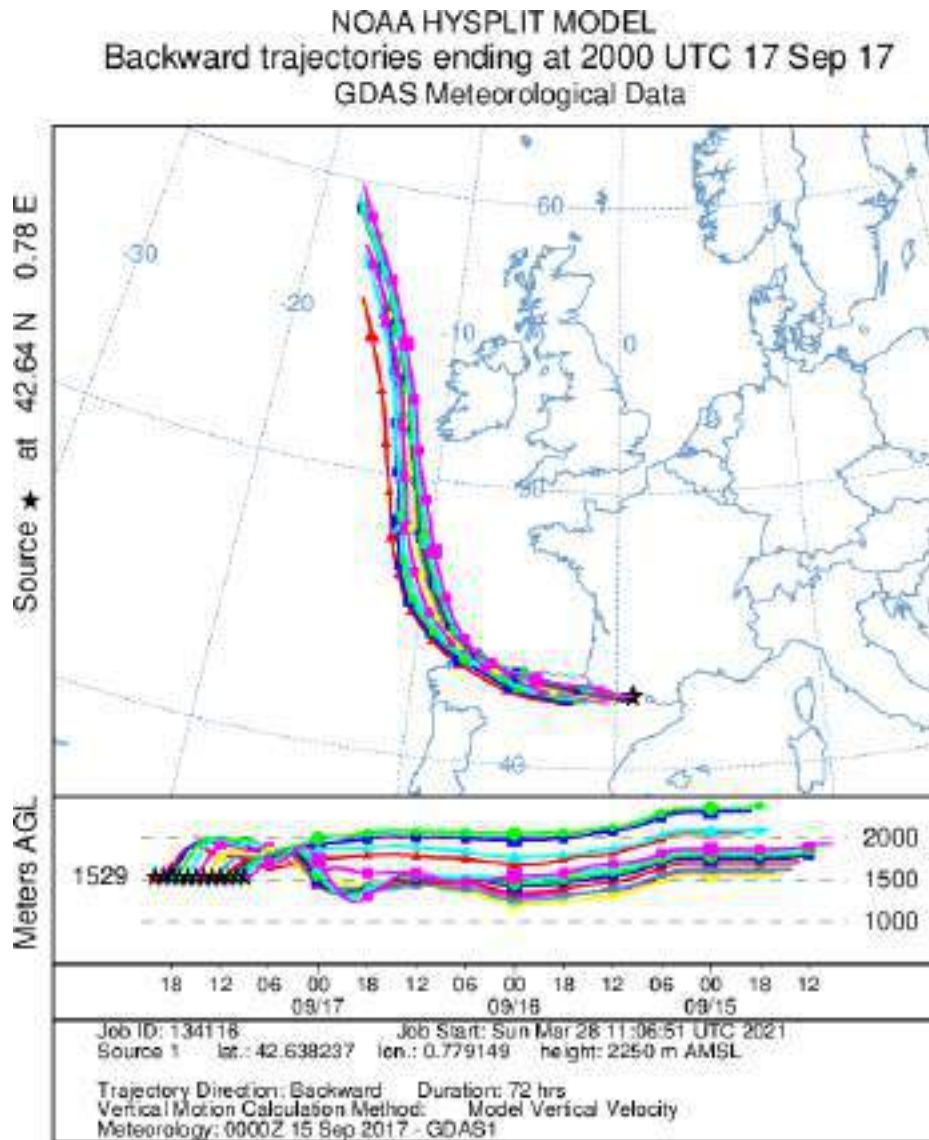


Figure S1.1c. NOAA Hysplit model back-trajectories (72 h backwards, 6 h intervals) of the air masses arriving at the sampling location during the collection of AAS sample III (September 17, 2017).

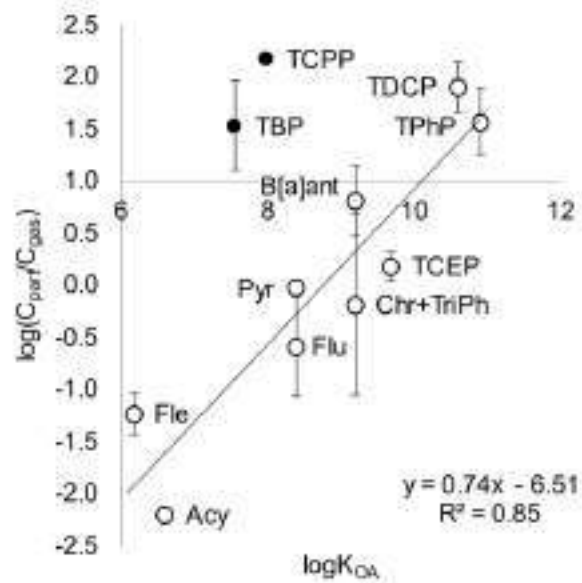


Figure S1.2. Correlation between the log-transformed ratio of concentrations between pollutants in particle (C_{part}) and gas (C_{gas}) phases and $\log K_{OA}$, where TCPP and TBP were not included in the regression. Error bars represent standard deviations.



Figure S1.3. Research cabin and meteorological station at the sampling location (Pyrenees, $42^{\circ}38'18.1''$ N, $0^{\circ}46'44.1''$ E, 2240 m.a.s.l.).

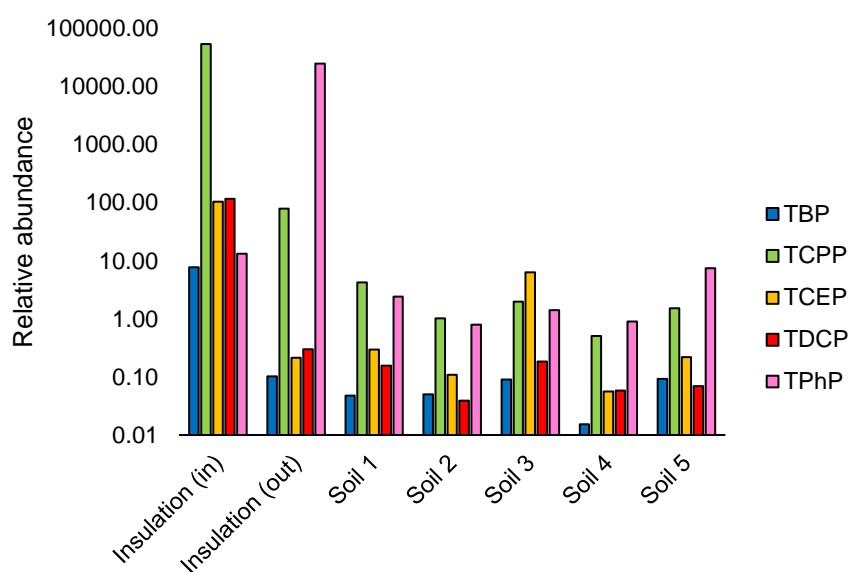


Figure S1.4. Relative abundance (area of GC-MS/MS peak divided by area of deuterated internal standard added during sample extraction) of OPFRs in samples collected as a qualitative assessment of the origin of TPhP contamination in PAS samples: insulating material samples inside (in) and outside (out) of a scientific research cabin located close to the PAS sampling location (10 m), and surface soil samples (1 to 5) at increasing distance from the research cabin and decreasing distance from the PAS deployment location.

References S1

- Harner, T., 2021. 2021 v10 Template for calculating PUF and SIP disk sample air volumes. <https://doi.org/https://doi.org/10.13140/RG.2.1.3998.8884>
- Shoeib, M., Harner, T., 2021. Characterization and comparison of three passive air samplers for persistent organic pollutants. *Environ. Sci. Technol.* 36, 4142–4151. <https://doi.org/10.1021/es020635t>
- Harner, T., Bidleman, T.F., 1996. Measurements of octanol-air partition coefficients for polychlorinated biphenyls, *J. Chem. Eng. Data.* 41, 895–899. <https://doi.org/10.1021/je960097y>



Article 2

CHANGES IN URBAN GAS-PHASE PERSISTENT ORGANIC POLLUTANTS DURING THE COVID-19 LOCKDOWN IN BARCELONA

Raimon M. Prats, Barend L. van Drooge,
Pilar Fernández, Esther Marco, Joan O. Grimalt
Frontiers in Environmental Science (2021) 9:650539
DOI 10.3389/fenvs.2021.650539



Changes in Urban Gas-Phase Persistent Organic Pollutants During the COVID-19 Lockdown in Barcelona

Raimon M. Prats*, Barend L. van Drooge, Pilar Fernández, Esther Marco and Joan O. Grimalt

Institute of Environmental Assessment and Water Research (IDAEA-CSIC), Barcelona, Spain

OPEN ACCESS

Edited by:

Dimitris G. Kaskaoutis,
National Observatory of Athens,
Greece

Reviewed by:

Umesh Dumka,
Aryabhatta Research Institute
of Observational Sciences, India
Suvarna Sanjeev Fadnavis,
Indian Institute of Tropical
Meteorology, India

*Correspondence:

Raimon M. Prats
raimon.martinez@idaea.csic.es

Specialty section:

This article was submitted to
Atmosphere and Climate,
a section of the journal
Frontiers in Environmental Science

Received: 07 January 2021

Accepted: 23 March 2021

Published: 13 April 2021

Citation:

Prats RM, van Drooge BL,
Fernández P, Marco E and Grimalt JO
(2021) Changes in Urban Gas-Phase
Persistent Organic Pollutants During
the COVID-19 Lockdown
in Barcelona.
Front. Environ. Sci. 9:650539.
doi: 10.3389/fenvs.2021.650539

The composition of polycyclic aromatic hydrocarbons (PAHs), polychlorobiphenyls (PCBs), hexachlorobenzene (HCB), pentachlorobenzene (PeCB), and organophosphate flame retardants (OPFRs) present in the gas-phase fraction of the atmosphere of Barcelona was analyzed during the SARS-CoV-2 coronavirus disease (COVID-19) lockdown and prior to this period. The changes in daily concentrations of CO, NO, NO₂, O₃ and particulate matter smaller than 10 μm (PM₁₀) were considered for comparison. Bayesian analysis considering serial dependencies and seasonality showed statistically significant decreases of CO, NO, NO₂, and PM₁₀ (between –28 and –76%) and O₃ increases (+45%) during lockdown. However, the lockdown concentration decreases of PeCB (–90.5%, from 8.5 to 0.8 pg m^{–3}), HCB (–79%, 25.5–5.4 pg m^{–3}) and some PAHs, such as benz[a]anthracene (–87%, 120–17 pg m^{–3}) and pyrene (–81%, 3,500–680 pg m^{–3}), were even stronger. The PAH depletion ranged between –68 and –87% that could be primarily associated with the strong reduction of traffic mobility during this period (–80%). Besides traffic reduction, the observed air quality improvements could be related to lower generation of solid urban residues (–25%) and the subsequent decrease of urban waste incineration (between –25 and –28%). Tributyl phosphate also showed a reduction in concentration during lockdown but the other OPFRs were seemingly not affected by this restriction, possibly as a result of the uniform release from the emission sources, e.g., construction material, industrial applications, and household products.

Keywords: COVID-19, semi-volatile air pollutants, organic contaminants, passive air sampling, lockdown, air quality

INTRODUCTION

The outbreak of a novel respiratory disease in China, caused by the SARS-CoV-2 virus and named coronavirus disease (COVID-19) by the World Health Organization (WHO), was quickly extended to many other countries generating a global pandemic (Sohrabi et al., 2020). On March 14, a lockdown was set in all Spain which mandated individuals to remain home except for needs such as purchasing food and medicines. These measures also included the temporary closure of schools, universities, some businesses and shops.

In general, lockdown measures have led to unprecedented reductions of air pollutant concentrations in many regions of the world, including several of the most polluted areas

(Berman and Ebisu, 2020; Cameletti, 2020; Le Quéré et al., 2020; Li et al., 2020; Venter et al., 2020; Zhang R. et al., 2020; Zhang Z. et al., 2020). Most reports in urban and industrial areas have only focused on air quality gas pollutants such as nitrogen oxides (NO and NO₂), carbon monoxide (CO), and carbon dioxide (CO₂), and particulate matter (PM₁₀ and PM_{2.5}). The same is the case for satellite imaging methods that can estimate the concentrations of these gases over large geographical areas (Kaufman et al., 1997; Krotkov et al., 2016). However, pollution assessment also requires the measurement of other contaminants that are deleterious for human health, such as organochlorine compounds (OCs) and polycyclic aromatic hydrocarbons (PAHs), among others.

Most OCs and PAHs are persistent organic pollutants (POPs), a group of compounds that are notorious for their resistance to degradation, potential for long-range atmospheric transport, and toxicity. They are recognized as a threat to human and wildlife health (De Voogt et al., 1990; Grimalt et al., 1994; Boström et al., 2002; Lauby-Secretan et al., 2013). PAHs are of great environmental concern, since several parent (non-methylated) compounds of these hydrocarbons are human carcinogens and priority pollutants (Baek et al., 1991; Armstrong et al., 2004). Hexachlorobenzene (HCB) has been related with obesity (Smink et al., 2008; Valvi et al., 2014), low fetal growth (Lopez-Espinosa et al., 2016), disruption of thyroid metabolism (Sala et al., 2001; Llop et al., 2017), and higher incidence of thyroid cancer (Grimalt et al., 1994). Polychlorobiphenyls (PCBs) have also been related with low fetal growth (Casas et al., 2015; Lopez-Espinosa et al., 2016), obesity (Valvi et al., 2012) or alterations of the thyroid function (Chevrier et al., 2008). In addition, they have been associated with metabolic disturbances of 25-hydroxy-vitamin D3 (Morales et al., 2013) and neurotoxicity (Grandjean and Landrigan, 2014). The production and use of these compounds have been restricted in many industrialized countries, resulting in significant endeavors to gradually reduce and prevent their release and diffusion in the environment. A culminating protocol for the elimination and monitoring of POPs was elaborated in 2001 during the Stockholm Convention¹ and has since been amended to include more compounds.

In addition, organophosphate flame retardants (OPFRs) are emerging pollutants that are currently used and produced in increasing amounts to meet the demand for flame retardants and plasticizers in construction material, industrial applications, and household products, including electronic devices (Van der Veen and de Boer, 2012; Du et al., 2019). OPFRs are neurotoxic, may cause haemolysis, and some of them are carcinogenic (Dishaw et al., 2011; Van der Veen and de Boer, 2012). Compared to historical POPs, OPFRs tend to show relatively high concentrations in outdoor air from urban and industrial areas (Salamova et al., 2014; Liu et al., 2016; van Drooge et al., 2018b).

Barcelona is one of the most densely populated cities of Europe, 16,000 inhabitants/km². Its metropolitan area lacks significant atmospheric emissions from industries and domestic heating is generally powered by natural gas. The high traffic intensity, 13,000–85,000 vehicles/day downtown in 2018, is the main pollution source (van Drooge and Grimalt, 2015; van

Drooge et al., 2018a). Other reports (UNEP, 2010) also point at transport, housing, and related activities as important sources of emissions of pollutants and products of environmental concern in Spain (e.g., around 60% of CO₂ and greenhouse gasses are emitted from transport and housing-related activities). Air pollution is therefore closely related to the activities of its inhabitants. Comparison of the air pollution levels during regular days and the lockdown period may provide guidelines for the ultimate achievable air quality standards, namely POPs, upon ideal management of urban pollution sources. Air samples were collected in the atmosphere of the city of Barcelona by means of passive air sampling (PAS) during regular conditions and lockdown. The results were used to determine possible changes in gas-phase POP concentrations during both periods. These pollutants were also analyzed in a remote continental background location in the Pyrenees for PAS calibration and comparison with the lockdown atmospheric conditions.

MATERIALS AND METHODS

Air Sampling

Two passive gas-phase air samplers for POP analysis were deployed during two periods: B1 (15 October 2019–9 January 2020, 86 days) and B2 (9 January 2020–15 July 2020, 188 days). B1 provided a reference time interval of typical air pollution conditions in the city. B2 was deployed during lockdown, although this period was larger than the specific lockdown time (March 15–June 22, 2020, 100 days). The samples were obtained using GAPS-style polyurethane foam passive air samplers (PUF-PASs) as employed in other studies (e.g., Pozo et al., 2009). The PUF disks (14 cm diameter, 1.35 cm thickness, 369.5 cm² surface area, and 0.021 g cm⁻³ density) were previously cleaned with acetone, Soxhlet-extracted with hexane for 6 h, dried under vacuum, and stored in a sealed PET/LLDPE bag at -20°C. Upon deployment, they were spiked with a Performance Reference Compound (PRC) mixture of PCBs 3, 9, 15, 32 (all ¹³C-labeled), 107, and 198 (unlabeled) (Cambridge Isotope Laboratories, Tewksbury, United States). One field blank was performed for each sample. These blanks were also doped with the PRCs, sealed, and stored at -20°C for the entire duration of the sampling period. The PUFs were immediately extracted after retrieval at the end of the sampling period. The recovery of PRCs from each sample was used for the assessment of the specific sampling rates as explained in the “Theory and Calculations” section below.

Polyurethane foam passive air samplers were also deployed in duplicate, in four 4–10-month periods, at six remote locations in the Pyrenees (September 2017–September 2019). Because of the minimal local contaminant sources, these sites constitute continental background reference regions for air pollution levels. The results obtained with the PUF-PASs were evaluated by comparison with those from active air sampling (AAS) with a high-volume pump (MCV, Collbató; van Drooge et al., 2004) which was used in one of these Pyrenean sites between July and September 2017. The PUF-AAS plugs (6 cm diameter, 5 cm thickness, 0.028 g cm⁻³ density) used for this purpose were

¹www.pops.int

located behind glass fiber filters that collected the atmospheric particle phase. One field blank was performed for every two duplicate samplers, both for PAS and AAS. All PUFs were cleaned and stored until extraction as described above.

Meteorological and air quality data were obtained for the whole B1 and B2 periods, including the pre- and lockdown intervals within them. Data corresponding to analogous periods in the previous 2 years were also collected for reference and description of seasonal variations. **Table 1** summarizes temperature, accumulated precipitation, and wind speed average values recorded on-site in all locations with Tinytag Plus 2 data loggers (Gemini Data Loggers, Chichester, United Kingdom) and from the automatic meteorological network (XEMA stations VS, Z2, X8, and X4) of the Catalan Meteorological Service. The concentrations of CO, NO, NO₂, PM₁₀, and O₃ in Barcelona were obtained for the same periods from the stations of the Air Quality Network (XVPCA 08019043 and 08019057) of the Catalan Government.

Extraction and Clean-Up

Both the PUF-PAS disks and the PUF-AAS plugs were subjected to Soxhlet extraction with hexane (Merck, Darmstadt, Germany) for 6 h after being spiked with a mixture of recovery standards containing: tetrabromobenzene, PCB209, fluorene-d₁₀, phenanthrene-d₁₀, fluoranthene-d₁₀, pyrene-d₁₀, benz[a]anthracene-d₁₂, and chrysene-d₁₂ (Dr. Ehrenstorfer) as well as an alkyl/aryl phosphate mixture containing tributyl phosphate-d₁₂, tris(2-chloroethyl) phosphate-d₁₂, tris(1-chloro-2-propyl) phosphate-d₁₈, tris(1,3-dichloro-2-propyl) phosphate-d₁₅ and triphenyl phosphate-d₁₅ (Cambridge Isotope Laboratories). The extracts were concentrated down to 2 mL with a rotary evaporator (Büchi, Flawil, Switzerland), quantitatively transferred into gas chromatography vials, and further evaporated to 0.5 mL under a gentle stream of nitrogen.

Fifty μL of each extract were cleaned-up and fractionated using an Agilent 1200 Series Gradient HPLC system (Agilent Technologies, Santa Clara, United States) equipped with a quaternary pump, a vacuum degasser, an autosampler, a thermostated column compartment (set at 30°C), and a preparative fraction collector. A Tracer Excel 120 SI HPLC silica column (25 cm \times 3 μm \times 0.46 cm i.d.; Teknokroma, Sant Cugat del Vallès) was used for the chromatographic separation. The elution program was as follows: 100% hexane at 0.5 mL min⁻¹ flow rate for 8 min, then a linear gradient to 100% dichloromethane at 0.5 mL min⁻¹ in 7 min, held until min 20. It was additionally changed to (80:20%) dichloromethane:methanol in order to elute more polar compounds remaining in the column before performing the next fractionation, with a linear flow rate increase from 0.5 to 1 mL min⁻¹ in 10 min, and a final holding time of 15 min. The fractions containing the target compounds were collected between minutes 8–15 (PCBs and other OCs) and 15–20 (PAHs). These fractions were evaporated under a gentle nitrogen gas stream, transferred into gas chromatography vials, and further evaporated to 0.5 mL. The OPFRs were analyzed from another extract aliquot, not requiring HPLC fractionation, but dried by elution through 0.5 g of anhydrous sodium sulfate previously activated overnight at 450°C.

Instrumental Analysis

The OC and PAH HPLC fractions were run separately by gas chromatography coupled to mass spectrometry (GC-MS) with a Thermo Trace GC Ultra-DSQ II (Thermo Fisher Scientific, Waltham, United States) equipped with a 60 m \times 0.25 mm i.d. \times 25 μm film thickness HP-5MS fused capillary column (Agilent Technologies). The MS was operated in electron impact mode (70 eV). The injector, ion source, quadrupole, and transfer line temperatures were 280, 250, 150, and 270°C, respectively. The oven program started at 90°C with a hold time of 1 min, then heated to 150°C at 10°C min⁻¹ and to 320°C at 6°C min⁻¹, where it was held for 20 min. Helium was used as a carrier gas at 1 mL min⁻¹. The targeted compounds were the following: polychlorobiphenyls (PCB28, PCB52, PCB101, PCB118, PCB138, PCB153, and PCB180), HCB, pentachlorobenzene (PeCB), α - and γ -hexachlorocyclohexanes (α - and γ -HCH), fluorene (fle), phenanthrene (phe), fluoranthene (flu), pyrene (pyr), benz[a]anthracene (b[a]ant), and chrysene+triphenylene (chr+triph). They were identified by their m/z values and retention times recorded in selected ion monitoring (SIM) mode (**Supplementary Table 1**).

The PUF extract aliquots were run for OPFR analysis by gas chromatography coupled to tandem mass spectrometry (GC-MS/MS) into an Agilent 7000 Series Triple Quad GC/MS (Agilent Technologies) equipped with a 30 m \times 0.25 mm i.d. \times 0.25 μm film thickness Zebtron ZB-PAH capillary column (Phenomenex, Torrance, CA, United States). The MS/MS was operated in electron impact ionization mode. The injector, ion source, quadrupoles, and transfer line temperatures were 280, 230, 150, and 280°C, respectively. The oven temperature program started at 80°C with a hold time of 1.5 min, then heated to 220°C at 10°C min⁻¹ and to 315°C at 15°C min⁻¹, where it was held for 5 min. Helium was used as a carrier gas at 1.1 mL min⁻¹. The targeted compounds were the following: tributylphosphate (TBP), tris(2-chloroethyl) phosphate (TCEP), tris(1-chloro-2-propyl) phosphate (TCPP), tris(1,3-dichloro-2-propyl) phosphate (TDCP) and triphenyl phosphate (TPhP). They were identified by their m/z transitions and retention times recorded in multiple reaction monitoring mode (**Supplementary Table 2**).

Quantification was performed with internal standard calibration curves, accounting for extraction and analysis recoveries. The field blank values were subtracted. LOQ values ranged between 0.5 and 2.5 pg in column, or 125–625 pg/sampler for PAHs, OCs, and PCBs, and 250–1,250 pg/sampler for OPFRs. For average effective sampled air volumes, these correspond to 0.3–1.6 pg m⁻³ of air for PAHs, 0.4–2.1 pg m⁻³ for OCs, 0.2–1.2 pg m⁻³ for PCBs, and 0.5–2.4 pg m⁻³ for OPFRs.

Theory and Calculations

As shown in Equation 1 (Harner et al., 2013), the calculation of gas-phase concentrations (C_A , pg m⁻³) from the pollutant amounts obtained with PAS (N_A) requires the determination of effective sampled volumes (V_A , m³) that are compound- and location-specific for each sampling period:

TABLE 1 | Sampling locations, periods of study, and average meteorological conditions (\pm standard deviation).

Location	Altitude (m.a.s.l.)	Period	Temperature (°C)	Precipitation (mm)	Wind speed (m s ⁻¹)			
Barcelona (urban site)	41.388° N, 2.115° E	108	Mean 2018–2019	B1	14.3 \pm 0.2	197 \pm 114	1.21 \pm 0.21	
				B2	16.5 \pm 0.1	257 \pm 155	1.23 \pm 0.02	
				Pre-lockdown	11.8 \pm 0.2	90 \pm 91	1.30 \pm 0.19	
				Lockdown	17.4 \pm 0.6	166 \pm 73	1.25 \pm 0.03	
				2020	B1	14.7 \pm 3.6	225	1.99 \pm 1.46
					B2	17.3 \pm 5.0	513	2.15 \pm 1.39
					Pre-lockdown	13.1 \pm 2.6	124	2.12 \pm 1.62
					Lockdown	18.0 \pm 4.0	373	2.15 \pm 1.26
Aigüestortes (continental background)	42.572° N, 0.932° E	1,619–2,453	2017–2019	Range of averages ^a	4.7 \pm 0.2–8.3 \pm 0.7	484 \pm 330–1,832 \pm 389	3.70 \pm 1.00–4.27 \pm 0.05	

^aValues for temperature, accumulated precipitation, and wind speed for the sampling site of Aigüestortes are shown as a range spanning the lowest and highest average values (\pm standard deviation) registered over four consecutive 4–10-month sampling periods from six studied mountain locations.

$$C_A = \frac{N_A}{V_A} = \frac{N_A}{V_{PUF} K'_{PUF-A} \left[1 - \exp\left(\frac{-k_A t}{K'_{PUF-A} D_{film}}\right) \right]} \quad (1)$$

where N_A is the amount of compound accumulated in the PUF disk during the sampling time (pg sampler⁻¹), V_{PUF} is the volume of the PUF disk (0.00021 m³), K'_{PUF-A} is the dimensionless PUF density-corrected PUF-Air partition coefficient K_{PUF-A} (K_{PUF-A} multiplied by the PUF density, $\delta_{PUF} = 21,000 \text{ g m}^{-3}$), k_A is the air-side mass transfer coefficient (m d⁻¹), t is the sampling time (d), and D_{film} is the PUF's effective film thickness (0.00567 m).

The sample-specific k_A values needed for V_A estimation can be derived from the PRC calibration of sampling rates (R_S , m³ d⁻¹):

$$k_A = \frac{R_S}{A_{PUF}} = \frac{\ln(C/C_0) K'_{PUF-A} D_{film}}{t} \quad (2)$$

where A_{PUF} is the PUF's surface area (0.0365 m²) and C/C_0 is the PCR ratio of amounts (g sampler⁻¹) between exposed and non-exposed (field blanks) PUFs.

Compound-specific K_{PUF-A} values for this type of PUFs are correlated to octanol-air partition coefficients (K_{OA}) through the following relationship (Shoeib and Harner, 2002):

$$\log K_{PUF-A} = 0.6366 \log K_{OA} - 3.1774 \quad (3)$$

The $\log K_{OA}$ values were corrected for the average temperature of each sampling site over the sampling period using temperature-dependent relationships reported elsewhere (Odabasi et al., 2006; Chen et al., 2016; Harner, 2016; Wang et al., 2017).

RESULTS AND DISCUSSION

Passive Gas-Phase Air Sampling for POP Analysis

The performance of the PUF-PAS samplers and reliability of the pollutant concentrations obtained with this system were assessed by comparison of the results from simultaneous deployment of these PAS and AAS between September 2017 and September

2019 in Aigüestortes, a continental background location in remote high mountains. The quantitative results obtained with both methods were in good agreement (Table 2). Thus, the AAS/PAS ratio differences were 0.7–2.1 for PCBs, 1.1 for HCB, 0.3–0.8 for PAHs and 0.3–1.5 for OPFRs. These ratios have to be compared considering that AAS involves much more variability than PAS, as the former is only collected over a few hours and the latter represents average values of several months of deployment. Therefore, variations in day-to-day meteorological and atmospheric conditions greatly affect the resulting AAS levels, especially for compounds like PAHs that could be influenced by local sources from nearby rural areas that are much more season dependent. Thus, the differences between sampling methods were deemed to be within acceptable ranges, especially at the low observed concentrations, for all compounds < 50 pg m⁻³ except for Fle and Phe. These results concur with other studies that established a strong agreement or no statistical difference between AAS- and PAS-obtained concentrations, even in urban sites with generally higher POP concentrations (He and Balasubramanian, 2012; Kalina et al., 2019). Furthermore, PAS duplicates showed low average relative standard deviations (RSD), between 9.4 and 23.3% for most compounds, with values above 30% only observed for the less volatile compounds such as PCB180, TCPP, TCEP, and TDCP, 34.2, 30.8, 36.3, and 60.1%, respectively (Supplementary Table 3).

Urban Concentrations of Organochlorine Compounds, PAHs, and Organophosphate Flame Retardants

The concentrations of HCB found in the B1 and B2 periods in Barcelona, 25.5 and 5.4 pg m⁻³, respectively (Table 2), were generally lower than those found in other urban areas from India: average values of 120–260 pg m⁻³ (Chakraborty et al., 2010), Bangladesh: 70–685 pg m⁻³ (Nost et al., 2015), Bosnia Herzegovina: 34 pg m⁻³ (Lammel et al., 2011), Nepal: 6.3–1,500 pg m⁻³ (Pokhrel et al., 2018), or China: 261 pg m⁻³ (Zhang et al., 2010). The concentrations of PeCB, 8.5 and 0.8 pg m⁻³ in B1 and B2, respectively, were

TABLE 2 | Average compound concentrations in air (gas phase, $\text{pg m}^{-3} \pm$ standard deviation) in the mountain background (Aigüestortes) and in the urban (Barcelona) locations, obtained using passive air sampling (PAS), and active air sampling (AAS) methods.

Compounds		Aigüestortes (background)				Barcelona PAS (urban)		
		PAS (n = 20)		AAS (n = 3)		B1	B2	Variation %
PCBs	PCB28	2.9	± 1.0	2.4	± 1.5	6.8	2.8	-59
	PCB52	2.1	± 0.7	1.4	± 0.3	11	3.4	-68
	PCB101	2.7	± 1.0	5.7	± 1.9	15	6.1	-59
	PCB118	2.5	± 0.3	4.8	± 1.6	13	3.9	-69.5
	PCB138	1.6	± 0.7	3.0	± 0.9	6.7	4.4	-34
	PCB153	2.3	± 0.2	3.2	± 0.9	5.8	2.6	-56
	PCB180	0.5	± 0.2	0.5	± 0.1	b.d.l. ^a	b.d.l.	
	Σ PCBs	14.6		21.0		58.3	23.2	-60
OCs	HCB	45	± 8.4	49	± 4.9	25.5	5.4	-79
	PeCB	25	± 3.2	b.d.l.		8.5	0.8	-90.5
	α -HCH	1.6	± 0.3	b.d.l.		3.5	0.5	-86
	γ -HCH	1.0	± 0.4	b.d.l.		12.9	3.9	-70
	Σ OCs	72.6		49.0		50.4	10.6	-79
PAHs	Flu	250	± 38	72	± 3.6	10,000	2,600	-75
	Phe	300	± 88	230	± 170	18,000	5,800	-68
	Flu	39	± 16	28	± 14	4,000	1,000	-75
	Pyr	18	± 7.6	15	± 6.7	3,500	680	-81
	B[a]ant	0.7	± 0.5	0.3	± 0.1	120	17	-87
	Chr+TriPh	5.3	± 2.8	1.4	± 0.1	240	63.5	-74
	Σ PAHs	613		347		35,860	10,160	-72
OPFRs	TBP	1.5	± 0.3	0.8	± 0.4	260	94	-64
	TCEP	6.1	± 1.9	2.1	± 1.4	230	270	19
	TCPP	14	± 16	20.5	± 15	4,800	4,700	-3.3
	TDCP	1.5	± 0.5	b.d.l.		129	187	45
	TPhP	7.2	± 3.5	b.d.l.		284	268	-5.6
	Σ OPFRs	30.3		23.4		5,703	5,519	-3.2

^ab.d.l. Below detection limit.

similar to those described in Bosnia Herzegovina, 9.9 pg m^{-3} (Lammel et al., 2011). The respective α - and γ -HCH concentrations, 3.5 and 12.9 pg m^{-3} during B1 and 0.5 and 3.9 pg m^{-3} during B2, were lower than those reported in other urban areas of Spain: 37 pg m^{-3} for their sum (de la Torre et al., 2016).

The concentrations of total PCBs in B1 and B2, 58 and 23 pg m^{-3} , respectively (sum of congeners reported in Table 2), were again generally lower than those found in other urban areas from Italy: 117 pg m^{-3} (Estellano et al., 2012), Spain: 122 pg m^{-3} (Poza et al., 2009), France: $3,100 \text{ pg m}^{-3}$ (Poza et al., 2009), Turkey: $153\text{--}376 \text{ pg m}^{-3}$ (Kuzu, 2016), Argentina: $146\text{--}200 \text{ pg m}^{-3}$ (Tombesi et al., 2014; Astoviza et al., 2016), Chile: 160 pg m^{-3} (Poza et al., 2012), Canada: 481 pg m^{-3} (Motelay-Massei et al., 2005), Pakistan: $37\text{--}293 \text{ pg m}^{-3}$ (Nasir et al., 2014), India: 278 pg m^{-3} (Poza et al., 2011), China: $600\text{--}7,600 \text{ pg m}^{-3}$ (Cui et al., 2017), and Bangladesh: $7\text{--}1,800 \text{ pg m}^{-3}$ (Nost et al., 2015). They were similar to those reported in Nepal: $1.2\text{--}47 \text{ pg m}^{-3}$ (Pokhrel et al., 2018).

Total PAHs in B1 and B2, approximately $36,000$ and $10,000 \text{ pg m}^{-3}$, respectively (sum of the compounds reported in Table 2), were found in lower concentrations than those found in Strasbourg: $51,000 \text{ pg m}^{-3}$ (Morville et al., 2011) and

Istanbul, $21,000\text{--}290,000 \text{ pg m}^{-3}$ (Kuzu, 2016) and higher than those found in the United States: $4,100\text{--}12,000 \text{ pg m}^{-3}$ (Pratt et al., 2018).

The concentrations of TBP in B1 and B2, 260 and 94 pg m^{-3} , were lower than those found in urban areas of Germany, $1,550 \text{ pg m}^{-3}$ (Zhou et al., 2017) and those of TCPP, $4,800$ and $4,700 \text{ pg m}^{-3}$, respectively, were higher than those found in these urban areas, $2,700 \text{ pg m}^{-3}$ (Zhou et al., 2017). The concentrations of TDCP, 129 pg m^{-3} in B1 and 187 pg m^{-3} in B2, and of TPhP, 284 pg m^{-3} in B1 and 268 pg m^{-3} in B2, were higher than those reported in urban air in Sweden, 7.6 and 47 pg m^{-3} , respectively (Wong et al., 2018).

The concentrations of PCBs in Barcelona in the B1 period, 58 pg m^{-3} , were about four times higher than in the continental background station 14.6 pg m^{-3} (Table 2), whereas those of PAHs, $36,000 \text{ pg m}^{-3}$, were about 60 times higher than in Aigüestortes, 613 pg m^{-3} , and those of the OPFRs were between 38 and 340 times higher (Table 2). The concentrations of HCHs were two to twelve times higher in Barcelona during the B1 period compared to the background location (Table 2). In contrast, HCB and PeCB in the continental background station were nearly two and three times higher than in the B1 period in Barcelona. The differences in PCB, HCB and PeCB air concentrations between

urban and remote sites compared to PAHs and OPFRs could be explained by fundamental differences in emission sources. The production and use of PCBs and most OCs have been restricted for several decades, but they are present in urban waste at low amounts (Wegiel et al., 2011; Neuwahl et al., 2019) which constitute a potential source in cities such as Barcelona. However, these legacy POPs may still be released to the atmosphere from diffusive secondary sources, including other environmental compartments (Grimalt et al., 2009), especially so in cold and remote areas that now might act as repositories for persistent contaminants such as HCB (Meijer et al., 2003). Contrarily, PAHs are still emitted from many primary combustion sources, such as traffic and domestic emissions in urban areas, while OPFRs are widely applied as flame retardants in construction material, household products and electronic equipment.

Assessment of the Lockdown Changes on Airborne POPs and OPFRs

One of the main features of **Table 2** is the strong decrease of HCB and PeCB between B1 and B2 periods, -79 and -90.5% , respectively (**Table 2**). At present, the occurrence of these compounds in the atmosphere of urban areas without industrial activity is mainly related to waste treatment, including incineration (EPA, 1986; Martens et al., 1998; Bailey, 2001; Wegiel et al., 2011). The lockdown period in Barcelona involved a -24.6% reduction of urban waste generation (a reduction of almost 20,000 tons of solid waste) which, in turn, represented incineration decreases between -25 and -28% when quantified as CO_2 emission (Montlleo et al., 2020; State of the City, 2020). These reductions may have contributed to the decrease in the concentrations of these compounds. Other processes, e.g., less transport of materials, may also have been relevant for the observed decrease.

Polycyclic aromatic hydrocarbons also showed high reduction of atmospheric concentrations, between -68 and -87% (**Table 2**). Atmospheric PAHs in urban areas are primarily generated as by-products of motorized transport. Therefore, the

observed differences are in agreement with the strong reduction of traffic in Barcelona, -80% , during the lockdown period (Montlleo et al., 2020; State of the City, 2020).

The atmospheric concentrations of PCBs and other OCs like the HCHs were also strongly depleted, between -34 and -69.5% , and between -70 and -86% , respectively. These decreases were probably related with the -24.6% reduction in waste generation during lockdown (Montlleo et al., 2020; State of the City, 2020) as incineration of urban waste is one main PCB source in the air of urban areas (Neuwahl et al., 2019; Arp et al., 2020) due to the presence of such compounds in urban waste and their high resistance to combustion (Neuwahl et al., 2019).

The OPFRs showed different trends (**Table 2**). TBP was the only compound following the concentration differences of OCs and PAHs, which were reflected in a large reduction in concentration, -64% , between the B1 and B2 periods. In contrast, the other OPFRs showed small decreases or even increases in atmospheric concentrations. This is probably related with the fundamentally different sources of OPFRs, e.g., being related with construction material, household products and electronic equipment over time, thus being less susceptible to variations in urban and industrial activities.

Changes in Atmospheric Gases and Particles

The average concentrations of CO , PM_{10} , NO , and NO_2 in Barcelona in the B2 period of 2020 show lower values than those of the 2018–2019 average, whereas these differences are not observed for B1 (**Supplementary Figure 1**). Similarly, the concentrations of these gases and PM_{10} in the lockdown period of 2020 are much lower than those in the equivalent time interval of the 2018–2019 average. This difference is the opposite in the case of O_3 , which is consistent with the lack of NO during lockdown and higher insolation during spring months. An initial study encompassing the first lockdown weeks (March 14–March 30) showed consistent changes (Tobias et al., 2020). In the present study, comparison of the data encompassing

TABLE 3 | Results of the Bayesian model for the air pollutant concentrations in the pre-lockdown/lockdown and B1/B2 periods.

Compound	Period	Average concentration			Effect of lockdown		Causality	
		Measured	Predicted \pm SD	95% CI	Effect \pm SD	95% CI	p-value	Probability (%)
CO (mg m^{-3})	Pre/lock	0.22	0.30 \pm 0.02	[0.26, 0.34]	$-28\% \pm 6.4\%$	[-40%, -16%]	0.0011	99.89
	B1/B2	0.25	0.37 \pm 0.02	[0.33, 0.41]	$-32\% \pm 5.4\%$	[-43%, -22%]	0.0011	99.89
PM_{10} ($\mu\text{g m}^{-3}$)	Pre/lock	19	31 \pm 2.2	[26, 35]	$-37\% \pm 7\%$	[-50%, -23%]	0.0011	99.89
	B1/B2	24	30 \pm 1.8	[27, 34]	$-20\% \pm 5.9\%$	[-32%, -8.8%]	0.0010	99.90
NO ($\mu\text{g m}^{-3}$)	Pre/lock	7.4	31 \pm 4.3	[23, 40]	$-76\% \pm 14\%$	[-103%, -51%]	0.0011	99.89
	B1/B2	18	31 \pm 4.1	[23, 39]	$-41\% \pm 13\%$	[-66%, -14%]	0.0033	99.67
NO_2 ($\mu\text{g m}^{-3}$)	Pre/lock	22	47 \pm 2.0	[43, 51]	$-52\% \pm 4.2\%$	[-61%, -44%]	0.0011	99.89
	B1/B2	33	52 \pm 1.8	[49, 56]	$-38\% \pm 3.4\%$	[-44%, -31%]	0.0012	99.88
O_3 ($\mu\text{g m}^{-3}$)	Pre/lock	56	38 \pm 2.9	[33, 44]	$45\% \pm 7.4\%$	[31%, 59%]	0.0010	99.90
	B1/B2	45	45 \pm 3.0	[39, 51]	$-0.12\% \pm 6.7\%$	[-13%, 12%]	0.4985	50.00

The average concentrations measured during the periods after lockdown restrictions (i.e., lockdown and B2) are compared to the concentrations (\pm standard deviation, SD) predicted by the model from data including the two previous years. Confidence intervals (95%), p-values, and probability of the observed concentration changes caused by lockdown measures are provided.

the whole lockdown period using a Bayesian structured time-series model (CausalImpact 1.2.4 R package, Brodersen et al., 2015) also allowed to account for the influence of seasonal effects on the concentration changes. Accordingly, the pollutant concentrations of 2020 were used as the response series and the average pollutant data of 2018–2019 as the control series, which was assumed not affected by the lockdown measures, consistently with the absence of restrictions in 2018–2019. The applicability of this model to these data was supported by comparison of the time series and dummy causal impact analyses performed with imaginary intervention periods which provided reasonable predictions and low causality probabilities.

The Bayesian analysis of the whole lockdown period showed noticeable concentration reductions of CO, NO, and NO₂ coinciding with the lockdown measures of March 2020, which picked up slightly after lockdown easing at the end of May 2020 and finally returned to ordinary levels at the end of lockdown (Figure 1). The same representations showing the predictions calculated for the B1/B2 sampling periods can be found in Supplementary Figure 2. The causal impact analysis of CO, NO, and NO₂ concentrations for the pre-lockdown/lockdown periods yielded statistically significant average variations of −28, −76, and −52%, respectively ($p = 0.0011$; Table 3). Despite the B2 sampling period included some weeks before and after lockdown, similar (−32% CO) or slightly lower (−41% NO, −38% NO₂) but still significant reductions were observed for the same compounds, $p = 0.0011$, 0.0033, and 0.0012, respectively (Table 3). These differences indicated a direct influence of lockdown restrictions as consequence of the steep decline in motor vehicle traffic, the main contributing source of CO and NO through direct emissions (EEA, 2019) as well as NO₂ formation by reaction of NO with atmospheric O₃.

The decrease between the usual polluting conditions and the lockdown period is more intense in areas with a lot of traffic such as downtown Barcelona, although it is also noticeable in the north and west forested areas, as shown in Figure 2 where the atmospheric NO₂ concentrations are displayed for the B1, B2, and specific lockdown periods. Comparison of the average NO₂ concentrations in the B2 and specific lockdown periods from this figure shows very similar distributions which support the representativeness of the sampled B2 interval concerning lockdown conditions.

Reductions in NO concentrations usually lead to increasing O₃ concentrations (Leighton, 1961), which are also observed in Figure 1. However, O₃ levels usually increase in the months leading up to the summer (with higher temperatures and increased solar radiation), which can lead to misidentification of an effect of lockdown on O₃ concentrations. The Bayesian time-series prediction model used here corrects for seasonal effects by taking into account data from the previous 2 years and shows a statistically significant increase of O₃ concentrations in the lockdown period (+45%; $p = 0.001$) which overcomes these effects. The increases in O₃ during the B2 and lockdown periods are also documented in Figure 2. In this case, the increases in O₃ are greater in the forested areas because downtown the NO from traffic still decreases the concentrations of this oxidant. Again, the differences between the B2 and lockdown periods are small.

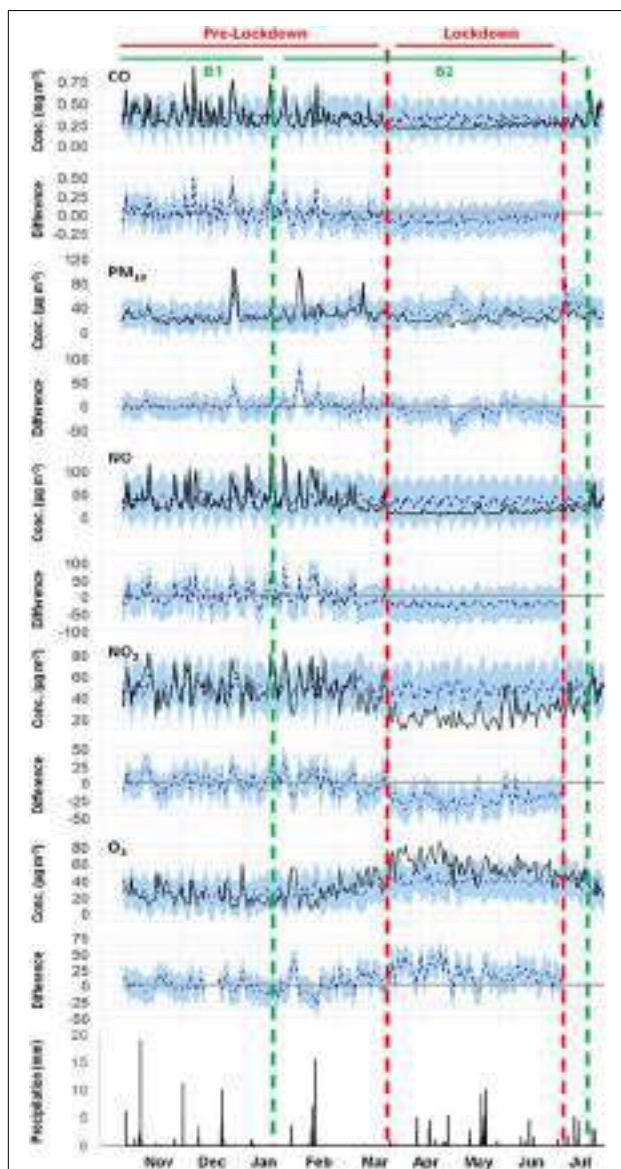


FIGURE 1 | Representation of the concentrations of atmospheric pollutants in Barcelona during the lockdown of 2020 and the corresponding Bayesian model predictions. The pre-lockdown/lockdown and the PAS-sampled B1/B2 periods are delimited by dashed, vertical, red and green lines, respectively. For each compound, the top graphs show daily average concentrations recorded in 2020 (black continuous line) against a counterfactual prediction based on 2018–2019 average values (blue dashed line). The bottom graphs show the difference between the observed data and the counterfactual predictions if lockdown had not occurred. From data of the air monitoring stations of the Catalan Government.

Concerning PM₁₀, the concentration decrease was noticed both for the lockdown (−37%; $p = 0.0011$) and the B2 periods (−20%; $p = 0.001$). This change is small in comparison with those observed for the gases except in the case of CO, which suggest that besides traffic other

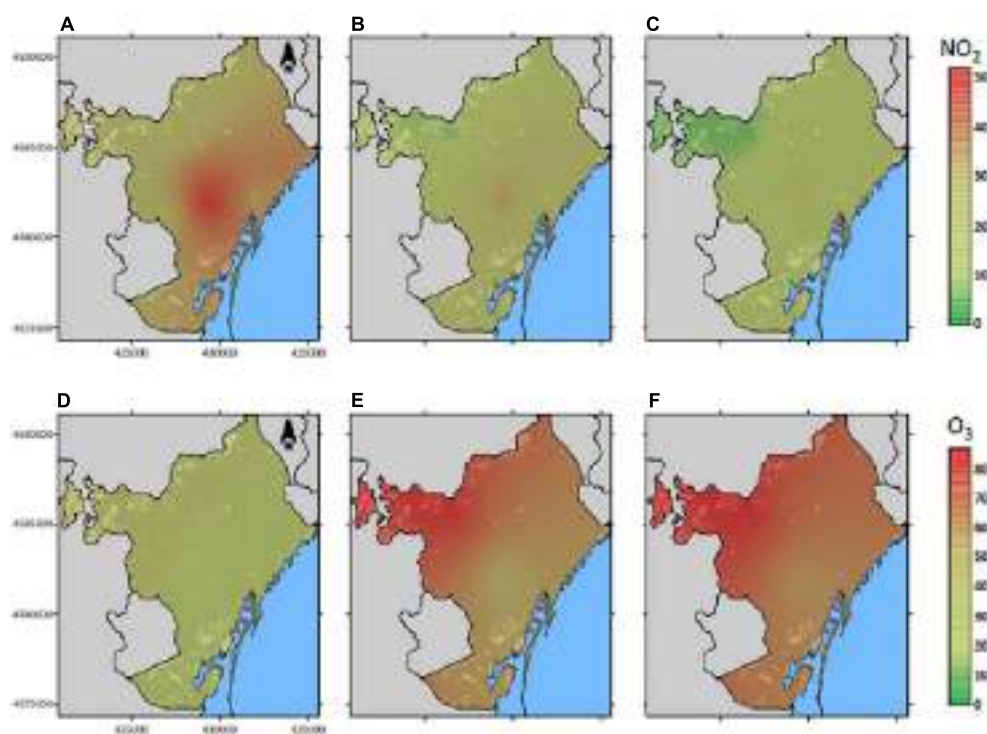


FIGURE 2 | Spatial distributions of airborne NO_2 (A–C) and O_3 (D–F) Barcelona, averaging in the B1 [15 October 2019–9 January 2020; (A,D)], B2 [9 January 2020–15 July 2020; (B,E)] and specific lockdown [15 March 2020–22 June 2020; (C,F)] periods. The plotted values ($\mu\text{g m}^{-3}$) are the averages of the daily measurements between 7 and 20 h. Note that the north and west zones are forested. From data of the air monitoring stations of the Catalan Government.

sources contributed to the atmospheric concentrations of PM_{10} in the city.

These results are in the range of those reported in other studies from several European and Mediterranean urban areas that also experienced lockdown conditions during the first half of 2020. Other studies in the city of Barcelona reported NO_2 reductions in concentration of -50% (Baldasano, 2020), -47% to -61% (Petetin et al., 2020), and -51% (Tobias et al., 2020). These values are similar to those reported in Madrid, -39% to -59% (Petetin et al., 2020), -62% (Baldasano, 2020), and -35% to -50% (Shi et al., 2021), and also to the average meteorology-normalized Spanish average of -50% (Petetin et al., 2020). Other European cities also presented comparable NO_2 reductions like -61% in Milan (Collivignarelli et al., 2020), -39% in Lucca and -39% in Florence (Donzelli et al., 2020), -32% in Athens (Grivas et al., 2020), and somewhat larger than -16 , -27 , -8 , -26 , and -11% in Milan, Rome, London, Paris, and Berlin, respectively (Shi et al., 2021). Our results for other pollutants are also similar to those reported for PM_{10} : -31% in Barcelona (Tobias et al., 2020), -48% in Milan (Collivignarelli et al., 2020), and -31% in Florence (Donzelli et al., 2020); for CO: -58% in Milan (Collivignarelli et al., 2020) and -35% in Athens (Grivas et al., 2020); and for NO: -42% in Pisa (Donzelli et al., 2020). Finally, compared to our results, other reports show similar O_3 variations in Barcelona: $+33\%$ increase during the first lockdown weeks (Tobias et al., 2020); slightly lower variations of -2% to

$+30\%$ in several European cities (Shi et al., 2021); and much higher variations of $+252\%$ in Milan (Collivignarelli et al., 2020).

Moreover, air pollutant concentration reductions over the first weeks of lockdown have also been reported in a broader scale through satellite imaging techniques. The European Space Agency reported central and southern European reductions of NO_2 concentrations in Madrid (-48%), Rome (-49%), Milan (-47%), and Paris (-54%) (ESA, 2020a,b). These values are well in agreement with the values summarized in the paragraph above, as well as in the range of those reported here for the city of Barcelona (Table 3).

Finally, daily precipitation episodes are also represented in Figure 1. Comparison with the daily concentrations of all gases (i.e., CO, NO, NO_2 , and O_3) and PM_{10} evidences that rain events generally do not coincide with noticeable drops in their atmospheric concentrations. This is consistent with results presented by other studies assessing changes in air pollution during lockdown in several cities in Spain, which found no correlation between precipitation values and air pollutant concentrations (Briz-Redón et al., 2021). Contrarily, the overall trend in concentration differences was consistent with the lockdown period, leaving wet precipitation as a minor driving factor in reducing air pollutant concentrations. This observation can be extrapolated to the atmospheric POP distributions. Rainfall rates averaged by sampled time can be derived from Table 1 and are sufficiently similar for both PAS-sampled periods

(2.6 and 2.7 mm day⁻¹ for B1 and B2, respectively) as to not expect considerable differences in washout, leaving the lockdown as the main cause for pollutant reductions.

CONCLUSION

All examined airborne pollutants showed lower concentrations during lockdown than in the regular period. PeCB was the compound displaying the highest lockdown decrease, -90.5%, followed by HCB and some PAHs such as b[a]ant and pyr, -79, -87, and -81%, respectively. In general, PAHs were the pollutants with higher reduction, -68 to -87%. Other compounds such as PCBs decreased by -37 to -69.5%.

The drops in atmospheric PAH concentrations can be associated with the strong traffic decrease during lockdown, -80% on average, and the significant reduction of harbor activities in this time interval, in the order of -65%. The present results regarding atmospheric PAHs indicate that the observed improvement of urban atmospheric quality related with lockdown restrictions was even better than recorded in the changes of nitrogen oxides and CO, providing a more holistic approach.

The study of other pollutants such as HCB, PeCB, and PCBs also evidences other atmospheric improvements related with the lockdown period such as the beneficial effects of reduction in the generation of solid residues and the subsequent reduction of urban waste incineration. The concentrations of PCBs during the B2 period in Barcelona were very close to those of remote sites such as the Pyrenees, with HCB and PeCB showing lower levels than those in these remote areas even during the pre-lockdown period.

Concerning the OPFRs, TBP also showed a decrease during lockdown but the other compounds of this group were seemingly not affected by the restrictions, possibly as a result of distinct and uniform release from their emission sources, e.g., construction material, industrial applications, household products, and others.

All in all, a significant decrease on the gas phase concentrations of atmospheric pollutants with current sources linked with anthropogenic urban activity was observed as consequence of the lockdown restrictions. O₃ is an exception related to processes other than traffic. The present work evidences the effectiveness of reducing overall anthropogenic emissions on a relatively short time span, not only in air quality indicator pollutants but also in many POPs. This highlights the potential of much needed policies that tackle air quality in a more stringent and broader way, which should stem from reports like the one

we present. A sustained improvement on air quality, especially in densely populated areas, would contribute to reduce the over four million deaths attributed every year to ambient air pollution (WHO, 2018), as well as improve the health of many more.

DATA AVAILABILITY STATEMENT

The raw data supporting the conclusions of this article will be made available by the authors, without undue reservation.

AUTHOR CONTRIBUTIONS

RP: sampling, analysis, formal analysis, visualization, and writing – original draft. BD: sampling, analysis, supervision, and writing – review and editing. PF: supervision, writing – review and editing. EM: Formal analysis and visualization. JG: conceptualization, writing – review and editing, and funding acquisition. All authors contributed to the article and approved the submitted version.

FUNDING

This work was supported by the Spanish Ministry of Science and Innovation (Projects: CUANTOX CTM2015-71832-P and INTEMPOL PGC2018-10228-B-I00). RP also acknowledges financial support from the Spanish Ministry of Science and Innovation (BES-2016-076339).

ACKNOWLEDGMENTS

Sampling support from Alejandro G. Inarra and Anna Canals-Angerri, and technical assistance from Roser Chaler are acknowledged. Part of this work was performed in the Parc Nacional d'Aiguestortes i Estany de Sant Maurici, in Catalonia, with collaboration from the Department of Territory and Sustainability of the Catalan Government.

SUPPLEMENTARY MATERIAL

The Supplementary Material for this article can be found online at: <https://www.frontiersin.org/articles/10.3389/fenvs.2021.650539/full#supplementary-material>

REFERENCES

- Armstrong, B., Hutchinson, E., Unwin, J., and Fletcher, T. (2004). Lung cancer risk after exposure to polycyclic aromatic hydrocarbons: a review and meta-analysis. *Environ. Health Perspect.* 112, 970–978. doi: 10.1289/ehp.6895
- Arp, H. P. H., Morin, N. A. O., Andersson, P. L., Hale, S. E., Wania, F., Breivik, K., et al. (2020). The presence, emission and partitioning behavior of polychlorinated biphenyls in waste, leachate and aerosols from Norwegian waste-handling facilities. *Sci. Total Environ.* 715:136824. doi: 10.1016/j.scitotenv.2020.136824
- Astoviza, M. J., Cappelletti, N., Bilos, C., Migoya, M. C., and Colombo, J. C. (2016). Airborne PCB patterns and urban scale in the Southern Río de la Plata Basin, Argentina. *Sci. Total Environ.* 572, 16–22. doi: 10.1016/j.scitotenv.2016.07.101
- Baek, S. O., Field, R. A., Goldstone, M. E., Kirk, P. W., Lester, J. N., and Perry, R. (1991). A review of atmospheric polycyclic hydrocarbons: sources, fate and behavior. *Water Air Soil Pollut.* 60, 279–300. doi: 10.1007/BF00282628
- Bailey, R. E. (2001). Global hexachlorobenzene emissions. *Chemosphere* 43, 167–182. doi: 10.1016/S0045-6535(00)00186-7

- Baldasano, J. M. (2020). COVID-19 lockdown effects on air quality by NO₂ in the cities of Barcelona and Madrid (Spain). *Sci. Total Environ.* 741:140353. doi: 10.1016/j.scitotenv.2020.140353
- Berman, J. D., and Ebisu, K. (2020). Changes in U.S. air pollution during the COVID-19 pandemic. *Sci. Total Environ.* 739:139864. doi: 10.1016/j.scitotenv.2020.139864
- Boström, C. E., Gerde, P., Hanberg, A., Jernström, B., Johansson, C., Kyrklund, T., et al. (2002). Cancer risk assessment, indicators, and guidelines for polycyclic aromatic hydrocarbons in the ambient air. *Environ. Health Perspect.* 110, 451–488. doi: 10.1289/ehp.110-1241197
- Brodersen, K. H., Galluser, F., Koehler, J., Remy, N., and Scott, S. L. (2015). *CausalImpact 1.2.4*. *Ann. Appl. Stat.* Available online at: <http://google.github.io/CausalImpact/> (accessed October 15, 2020).
- Briz-Redón, Á., Belenguer-Sapiña, C., and Serrano-Aroca, Á. (2021). Changes in air pollution during COVID-19 lockdown in Spain: a multi-city study. *J. Environ. Sci.* 101, 16–26. doi: 10.1016/j.jes.2020.07.029
- Cameletti, M. (2020). The effect of corona virus lockdown on air pollution: evidence from the city of Brescia in Lombardia Region (Italy). *Atmos. Environ.* 239:117794. doi: 10.1016/j.atmosenv.2020.117794
- Casas, M., Nieuwenhuijsen, M., Martínez, D., Ballester, F., Basagaña, X., Barterrechea, M., et al. (2015). Prenatal exposure to PCB-153, p,p'-DDE and birth outcomes in 9000 mother-child pairs: Exposure-response relationship and effect modifiers. *Environ. Int.* 74, 23–31. doi: 10.1016/j.envint.2014.09.013
- Chakraborty, P., Zhang, G., Li, J., Xu, Y., Liu, X., Tanabe, S., et al. (2010). Selected organochlorine pesticides in the atmosphere of major Indian cities: levels, regional versus local variations, and sources. *Environ. Sci. Technol.* 44, 8038–8043. doi: 10.1021/es102029t
- Chen, Y., Cai, X., Jiang, L., and Li, Y. (2016). Prediction of octanol-air partition coefficients for polychlorinated biphenyls (PCBs) using 3D-QSAR models. *Ecotoxicol. Environ. Saf.* 124, 202–212. doi: 10.1016/j.ecoenv.2015.10.024
- Chevrier, J., Eskenazi, B., Holland, N., Bradman, A., and Barr, D. B. (2008). Effects of exposure to polychlorinated biphenyls and organochlorine pesticides on thyroid function during pregnancy. *Am. J. Epidemiol.* 168, 298–310. doi: 10.1093/aje/kwn136
- Collivignarelli, M. C., Abbà, A., Bertanza, G., Pedrazzani, R., Ricciardi, P., and Miino, M. C. (2020). Lockdown for CoViD-2019 in Milan: what are the effects on air quality? *Sci. Total Environ.* 732:139280. doi: 10.1016/j.scitotenv.2020.139280
- Cui, S., Fu, Q., Li, Y.-F., Li, T.-X., Liu, D., Dong, W.-C., et al. (2017). Spatial-temporal variations, possible sources and soil-air exchange of polychlorinated biphenyls in urban environments in China. *RSC Adv.* 7:14797. doi: 10.1039/C6RA26864A
- de la Torre, A., Sanz, P., Navarro, I., and Martínez, M. A. (2016). Time trends of persistent organic pollutants in Spanish air. *Environ. Pollut.* 217, 26–32. doi: 10.1016/j.envpol.2016.01.040
- De Voogt, P., Wells, D. E., Reutergardh, L., and Brinkman, U. A. T. (1990). Biological activity, determination and occurrence of planar, mono- and di-ortho PCBs. *Int. J. Environ. Anal. Chem.* 40, 1–46. doi: 10.1080/03067319008030516
- Dishaw, L. V., Powers, C. M., Ryde, I. T., Roberts, S. C., Seidler, F. J., Slotkin, T. A., et al. (2011). Is the PentaBDE replacement, tris (1,3-dichloro-2-propyl) phosphate (TDCPP), a developmental neurotoxicant? Studies in PC12 cells. *Toxicol. Appl. Pharmacol.* 256, 281–289. doi: 10.1016/j.taap.2011.01.005
- Donzelli, G., Cioni, L., Cancellieri, M., Morales, A. L., and Suárez-Varela, M. M. M. (2020). The Effect of the Covid-19 lockdown on air quality in three Italian medium-sized cities. *Atmosphere* 11:1118. doi: 10.3390/atmos11101118
- Du, J., Li, H., Xu, S., Zhou, Q., Jin, M., and Tang, J. (2019). A review of organophosphorus flame retardants (OPFRs): occurrence, bioaccumulation, toxicity, and organism exposure. *Environ. Sci. Pollut. Res.* 26, 22126–22136. doi: 10.1007/s11356-019-05669-y
- EEA (2019). *Air Quality in Europe – EEA Report No 10/2019*. Available online at: <https://www.eea.europa.eu/publications/air-quality-in-europe-2019> (accessed November 15, 2020).
- EPA (1986). *Exposure Assessment for Hexachlorobenzene*. Washington, DC: U.S. Environmental Protection Agency, Office of Pesticides and Toxic Substances.
- ESA (2020a). *Nitrogen Dioxide Concentrations Over Spain*. Available online at: http://www.esa.int/ESA_Multimedia/Images/2020/03/Nitrogen_dioxide_concentrations_over_Spain (accessed November 15, 2020).
- ESA (2020b). *Air Pollution Remains Low as Europeans Stay at Home*. Available online at: http://www.esa.int/Applications/Observing_the_Earth/Copernicus/Sentinel-5P/Air_pollution_remains_low_as_Europeans_stay_at_home (accessed November 15, 2020).
- Estellano, V. H., Pozo, K., Harner, T., Carsolini, S., and Focardi, S. (2012). Using PUF disk passive samplers to simultaneously measure air concentrations of persistent organic pollutants (POPs) across the Tuscany Region, Italy. *Atmos. Pollut. Res.* 3, 88–94. doi: 10.5094/APR.2012.008
- Grandjean, P., and Landrigan, P. J. (2014). Neurobehavioural effects of developmental toxicity. *Lancet Neurol.* 13, 330–338. doi: 10.1016/S1474-4422(13)70278-3
- Grimalt, J. O., Sunyer, J., Moreno, V., Amaral, O. C., Sala, M., Rosell, A., et al. (1994). Risk excess of soft-tissue sarcoma and thyroid cancer in a community exposed to airborne organochlorinated compound mixtures with a high hexachlorobenzene content. *Int. J. Cancer.* 56, 200–203. doi: 10.1002/ijc.2910560209
- Grimalt, J. O., Fernandez, P., and Quiroz, R. (2009). Input of organochlorine compounds by snow to European high mountain lakes. *Freshwater Biol.* 54, 2533–2542. doi: 10.1111/j.1365-2427.2009.02302.x
- Grivas, G., Athanasopoulou, E., Kakouri, A., Bailey, J., Liakakou, E., Stavroulas, I., et al. (2020). Integrating in situ measurements and city scale modelling to assess the COVID-19 lockdown effects on emissions and air quality in Athens, Greece. *Atmosphere* 11:1174. doi: 10.3390/atmos11111174
- Harner, T., Su, K., Genualdi, S., Karpowicz, J., Ahrens, L., Mihele, C., et al. (2013). Calibration and application of PUF disk passive air samplers for tracking polycyclic aromatic compounds (PACs). *Atmos. Environ.* 75, 123–128. doi: 10.1016/j.atmosenv.2013.04.012
- Harner, T. (2016). 2016 v1 3 Template for Calculating PUF and SIP Disk Sample Air Volumes. doi: 10.13140/RG.2.1.3998.8884
- He, J., and Balasubramanian, R. (2012). Passive sampling of gaseous persistent organic pollutants in the atmosphere. *Energy Proc.* 16, 494–500. doi: 10.1016/j.egypro.2012.01.080
- Kalina, J., White, K. B., Scheringer, M., Poibylvá, P., Kukučková, P., Audy, O., et al. (2019). Comparability of long-term temporal trends of POPs from co-located active and passive air monitoring networks in Europe. *Environ. Sci. Processes Impacts* 21, 1132–1142. doi: 10.1039/C9EM00136K
- Kaufman, Y. J., Tanré, D., Remer, L. A., Vermote, E. F., Chu, A., and Holben, B. N. (1997). Operational remote sensing of tropospheric aerosol over land from EOS moderate resolution imaging spectroradiometer. *J. Geophys. Res. Atmos.* 102, 17051–17067. doi: 10.1029/96jd03988
- Krotkov, N. A., McLinden, C. A., Li, C., Lamsal, L. N., Celarier, E. A., Marchenko, S. V., et al. (2016). Aura OMI observations of regional SO₂ and NO₂ pollution changes from 2005 to 2015. *Atmos. Chem. Phys.* 16, 4605–4629. doi: 10.5194/acp-16-4605-2016
- Kuzu, S. L. (2016). Compositional variation of PCBs, PAHs, and OCPs at Gas phase and size segregated particle phase during dust incursion from the Saharan desert in the Northwestern Anatolian peninsula. *Adv. Meteorol.* 2016:7153286. doi: 10.1155/2016/7153286
- Lammel, G., Klanova, J., Eric, L., Ilic, P., Kohoutek, J., and Kovacic, I. (2011). Sources of organochlorine pesticides in air in an urban Mediterranean environment: volatilization from soil. *J. Environ. Monit.* 13, 3358–3364. doi: 10.1039/C1EM10479A
- Lauby-Secretan, B., Loomis, D., Grosse, Y., El Ghissassi, F., Bouvard, V., Benbrahim-Tallaa, L., et al. (2013). Carcinogenicity of polychlorinated biphenyls and polybrominated biphenyls. *Lancet Oncol.* 14, 287–288. doi: 10.1016/S1470-2045(13)70104-9
- Le Quéré, C., Jackson, R. B., Jones, M. W., Smith, A. J. P., Abernethy, S., Andrew, R. M., et al. (2020). Temporary reduction in daily global CO₂ emissions during the COVID-19 forced confinement. *Nat. Clim. Chang.* 10, 647–653. doi: 10.1038/s41558-020-0797-x
- Leighton, P. A. (1961). *Photochemistry of Air Pollution*. New York, NY: Academic Press.
- Li, L., Li, Q., Huang, L., Wang, Q., Zhu, A., Xu, J., et al. (2020). Air quality changes during the COVID-19 lockdown over the Yangtze River Delta Region: an insight into the impact of human activity pattern changes on air pollution variation. *Sci. Total Environ.* 732:139282. doi: 10.1016/j.scitotenv.2020.139282
- Liu, D., Lin, T., Shen, K., Li, J., Yu, Z., and Zhang, G. (2016). Occurrence and concentrations of halogenated flame retardants in the atmospheric fine particles in Chinese cities. *Environ. Sci. Technol.* 50, 9846–9854. doi: 10.1021/acs.est.6b01685
- Llop, S., Murcia, M., Alvarez-Pedrerol, M., Grimalt, J. O., Santa Marina, L., Julvez, J., et al. (2017). Association between exposure to organochlorine compounds

- and maternal thyroid status: Role of the iodothyronine deiodinase 1 gene. *Environ. Int.* 104, 83–90. doi: 10.1016/j.envint.2016.12.013
- Lopez-Espinosa, M. J., Murcia, M., Iniguez, C., Vizcaíno, E., Costa, O., Fernández-Somoano, A., et al. (2016). Organochlorine compounds and ultrasound measurements of fetal growth in the INMA Cohort (Spain). *Environ. Health Perspect.* 124, 157–163. doi: 10.1289/ehp.1408907
- Martens, D., Balta-Brouma, K., Brotsack, R., Michalke, B., Schramel, P., Klimm, C., et al. (1998). Chemical impact of uncontrolled solid waste combustion to the vicinity of the Kouroupitos Ravine, Crete, Greece. *Chemosphere* 36, 2855–2866. doi: 10.1016/S0045-6535(97)10242-9
- Meijer, S. N., Ockenden, W. A., Sweetman, A., Breivik, K., Grimalt, J. O., and Jones, K. C. (2003). Global distribution and budget of PCBs and HCB in Background surface soils: implications for sources and environmental processes. *Environ. Sci. Technol.* 37, 667–672. doi: 10.1021/es010322i
- Montlleo, M., Rodriguez, G., Tavares, N., Masvidal, M., Lao, J., Coral, A., et al. (2020). *Observatori COVID-19. Metabolisme de la Ciutat. City Hall of Barcelona*. Available online at: https://www.barcelona.cat/barcelona-pel-clima/sites/default/files/documents/20200729-observatori_covid-19-metabolisme_de_la_ciutat.pdf (accessed November 15, 2020).
- Morales, E., Gascon, M., Martinez, D., Casas, M., Ballester, F., Rodriguez-Bernal, C. L., et al. (2013). Associations between blood persistent organic pollutants and 25-hydroxyvitamin D3 in pregnancy. *Environ. Int.* 57–58, 34–41. doi: 10.1016/j.envint.2013.03.011
- Morville, S., Delhomme, O., and Millet, M. (2011). Seasonal and diurnal variations of atmospheric PAH concentrations between rural, suburban and urban areas. *Atmos. Pollut. Res.* 2, 366–373. doi: 10.5094/APR.2011.041
- Motelay-Massei, A., Harner, T., Shoeib, M., Diamond, M., Stern, G., and Rosenbreg, B. (2005). Using passive air samplers to assess urban-rural trends for persistent organic pollutants and polycyclic aromatic hydrocarbons. 2. Seasonal trends for PAHs, PCBs, and organochlorine pesticides. *Environ. Sci. Technol.* 39, 5763–5773. doi: 10.1021/es0504183
- Nasir, J., Wang, X., Xu, B., Wang, C., Joswiak, D. R., Rehman, S., et al. (2014). Selected organochlorine pesticides and polychlorinated biphenyls in urban atmosphere of Pakistan: concentration, spatial variation and sources. *Environ. Sci. Technol.* 48, 2610–2618. doi: 10.1021/es404711n
- Neuwahl, F., Cusano, G., Gomez-Benavides, J., Holbrook, S., and Roudier, S. (2019). *Best Available Techniques (BAT). Reference Document for waste incineration. Industrial Emission Directive 2010/75/EU. Integrated Pollution Prevention and Control*. Luxembourg: Publications Office of the European Union.
- Nost, T. H., Halse, A. K., Randall, S., Borgen, A. R., Schlabach, M., Paul, A., et al. (2015). High concentrations of organic contaminants in air from ship breaking activities in Chittagong, Bangladesh. *Environ. Sci. Technol.* 49, 11372–11380. doi: 10.1021/acs.est.5b03073
- Odabasi, M., Cetin, E., and Sofuoğlu, A. (2006). Determination of octanol-air partition coefficients and supercooled liquid vapor pressures of PAHs as a function of temperature: Application to gas-particle partitioning in an urban atmosphere. *Atmos. Environ.* 40, 6615–6625. doi: 10.1016/j.atmosenv.2006.05.051
- Petin, H., Bowdalo, D., Soret, A., Guevara, M., Jorba, O., Serradell, K., et al. (2020). Meteorology-normalized impact of the COVID-19 lockdown upon NO₂ pollution in Spain. *Atmos. Chem. Phys.* 20, 11119–11141. doi: 10.5194/acp-20-11119-2020
- Pokhrel, B., Gong, P., Wang, X., Khanal, S. N., Ren, J., Wang, C., et al. (2018). Atmospheric organochlorine pesticides and polychlorinated biphenyls in urban areas of Nepal: spatial variation, sources, temporal trends, and long-range transport potential. *Atmos. Chem. Phys.* 18, 1325–1336. doi: 10.5194/acp-18-1325-2018
- Pozo, K., Harner, T., Lee, S. C., Wania, F., Muir, D. C. G., and Jones, K. C. (2009). Seasonally resolved concentrations of persistent organic pollutants in the global atmosphere from the first year of the GAPS Study. *Environ. Sci. Technol.* 43, 796–803. doi: 10.1021/es802106a
- Pozo, K., Harner, T., Lee, S. C., Sinha, R. K., Sengupta, B., Loewen, M., et al. (2011). Assessing seasonal and spatial trends of persistent organic pollutants (POPs) in Indian agricultural regions using PUF disk passive air samplers. *Environ. Pollut.* 159, 646–653. doi: 10.1016/j.envpol.2010.09.025
- Pozo, K., Harner, T., Rudolph, A., Oyola, G., Estellano, V. H., Ahumada-Rudolph, R., et al. (2012). Survey of persistent organic pollutants (POPs) and polycyclic aromatic hydrocarbons (PAHs) in the atmosphere of rural, urban and industrial areas of Concepción, Chile, using passive air samplers. *Atmos. Poll. Res.* 3, 426–434. doi: 10.5094/APR.2012.049
- Pratt, G. C., Herbrandson, C., Krause, M. J., Schmitt, C., Lippert, C. J., McMahon, C. R., et al. (2018). Measurements of gas and particle polycyclic aromatic hydrocarbons (PAHs) in air at urban, rural and near-roadway sites. *Atmos. Environ.* 179, 268–278. doi: 10.1016/j.atmosenv.2018.02.035
- Sala, M., Sunyer, J., Herrero, C., Xu, J., and Grimalt, J. O. (2001). Association between serum concentration of hexachlorobenzene and polychlorobiphenyls with thyroid hormone and liver enzymes in a sample of the general population. *Occup. Environ. Med.* 58, 172–177. doi: 10.1136/oem.58.3.172
- Salamova, A., Hermanson, M. H., and Hites, R. A. (2014). Organophosphate and halogenated flame retardants in atmospheric particles from a European Arctic site. *Environ. Sci. Technol.* 48, 6133–6140. doi: 10.1021/es500911d
- Shi, Z., Song, C., Liu, B., Lu, G., Xu, J., Vu, T. V., et al. (2021). Abrupt but smaller than expected changes in surface air quality attributable to COVID-19 lockdowns. *Sci. Adv.* 7:eabd6696. doi: 10.1126/sciadv.abd6696
- Shoeb, M., and Harner, T. (2002). Characterization and comparison of three passive air samplers for persistent organic pollutants. *Environ. Sci. Technol.* 36, 4142–4151. doi: 10.1021/es020635t
- Smink, A., Ribas-Fito, N., Garcia, R., Torrent, M., Mendez, M. A., Grimalt, J. O., et al. (2008). Exposure to hexachlorobenzene during pregnancy increases the risk of overweight in children aged 6 years. *Acta Paediatr.* 97, 1465–1469. doi: 10.1111/j.1651-2227.2008.00937.x
- Sohrabi, C., Alsafi, Z., O'Neill, N., Khan, M., Kerwan, A., Al-Jabir, A., et al. (2020). World Health Organization declares global emergency: A review of the 2019 novel coronavirus (COVID-19). *Int. J. Surg.* 76, 71–76. doi: 10.1016/j.ijvsu.2020.02.034
- State of the City (2020). *State of the City. Barcelona City Hall Report. 2020*. Available online at: <https://ajuntament.barcelona.cat/premsa/wp-content/uploads/2020/06/200626-Informe-Estat-de-la-ciutat-2019-Document-complementari.pdf> (accessed November 15, 2020).
- Tobias, A., Carnerero, C., Reche, C., Massagué, J., Via, M., Minguillón, M. C., et al. (2020). Changes in air quality during the lockdown in Barcelona (Spain) one month into the SARS-CoV-2 epidemic. *Sci. Total Environ.* 726:138540. doi: 10.1016/j.scitotenv.2020.138540
- Tombesi, N., Pozo, K., and Harner, T. (2014). Persistent organic pollutants (POPs) in the atmosphere of agricultural and urban areas in the Province of Buenos Aires in Argentina using PUF disk passive air samplers. *Atmos. Pollut. Res.* 5, 170–178. doi: 10.5094/APR.2014.021
- UNEP (2010). *United Nations Environment Programme. Assessing the Environmental Impacts of Consumption and Production. Priority Products and Materials*. Nairobi: UNEP.
- Valvi, D., Mendez, M. A., Martinez, D., Grimalt, J. O., Torrent, M., Sunyer, J., et al. (2012). Prenatal concentrations of polychlorinated biphenyls, DDE, and DDT and overweight in children. A prospective birth cohort study. *Environ. Health Persp.* 120, 451–457. doi: 10.1289/ehp.1103862
- Valvi, D., Mendez, M. A., Garcia-Esteban, R., Ballester, F., Ibarluzea, J., Goñi, F., et al. (2014). Prenatal exposure to persistent organic pollutants and rapid weight gain and overweight in infancy. *Obesity* 22, 488–496. doi: 10.1002/oby.20603
- Van der Veen, I., and de Boer, J. (2012). Phosphorus flame retardants: Properties, production, environmental occurrence, toxicity and analysis. *Chemosphere* 88, 1119–1153. doi: 10.1016/j.chemosphere.2012.03.067
- van Drooge, B. L., Grimalt, J. O., Camarero, L., Catalan, J., Stuchlik, E., and Torres García, C. J. (2004). Atmospheric semivolatile organochlorine compounds in European high-mountain areas (Central Pyrenees and High Tatras). *Environ. Sci. Technol.* 38, 3525–3532. doi: 10.1021/es030108p
- van Drooge, B. L., and Grimalt, J. O. (2015). Particle size-resolved source apportionment of primary and secondary organic tracer compounds at urban and rural locations in Spain. *Atmos. Chem. Phys.* 15, 7735–7752. doi: 10.5194/acp-15-7735-2015
- van Drooge, B. L., Fontal, M., Fernández, P., Fernández, M. A., Muñoz-Arnanz, J., Jiménez, B., et al. (2018a). Organic molecular tracers in atmospheric PM₁ at urban intensive traffic and background sites in two high-insolation European cities. *Atmos. Environ.* 188, 71–81. doi: 10.1016/j.atmosenv.2018.06.024

- van Drooge, B. L., Ramos García, D., and Lacorte, S. (2018b). Analysis of organophosphorus flame retardants in submicron atmospheric particulate matter (PM₁). *AIMS Environ. Sci.* 5, 294–304. doi: 10.3934/envirosci.2018.4.294
- Venter, Z. S., Aunan, K., Chowdhury, S., and Lelieveld, J. (2020). COVID-19 lockdowns cause global air pollution declines. *Proc. Natl. Acad. Sci. U.S.A.* 117, 18984–18990. doi: 10.1073/pnas.2006853117
- Wang, Q., Zhao, H., Wang, Y., Xie, Q., Chen, J., and Quan, X. (2017). Determination and prediction of octanol-air partition coefficients for organophosphate flame retardants. *Ecotoxicol. Environ. Saf.* 145, 283–288. doi: 10.1016/j.ecoenv.2017.07.040
- Wegiel, M., Chrzaszcz, R., Maslanka, A., and Grochowalski, A. (2011). Study on the determination of PCDDs/Fs and HCB in exhaust gas. *Chemosphere* 85, 481–486. doi: 10.1016/j.chemosphere.2011.07.079
- WHO (2018). *Ambient (outdoor) Air Pollution*. Geneva: WHO.
- Wong, F., de Wit, C. A., and Newton, S. R. (2018). Concentrations and variability of organophosphate esters, halogenated flame retardants, and polybrominated diphenyl ethers in indoor and outdoor air in Stockholm, Sweden. *Environ. Pollut.* 240, 514–522. doi: 10.1016/j.envpol.2018.04.086
- Zhang, R., Zhang, Y., Lin, H., Feng, X., Fu, T. M., and Wang, Y. (2020). NO_x emission reduction and recovery during COVID-19 in East China. *Atmosphere* 11:433. doi: 10.3390/ATMOS11040433
- Zhang, W., Ye, Y., Hu, D., Qu, L., and Wang, X. (2010). Characteristics and transport of organochlorine pesticides in urban environment: air, dust, rain, canopy, throughfall, and runoff. *J. Environ. Monit* 12, 2153–2160. doi: 10.1039/C0EM00110D
- Zhang, Z., Arshad, A., Zhang, C., Hussain, S., and Li, W. (2020). Unprecedented temporary reduction in global air pollution associated with COVID-19 forced confinement: A continental and city scale analysis. *Remote Sens.* 12:2420. doi: 10.3390/RS12152420
- Zhou, L., Hiltcher, M., Gruber, D., and Püttmann, W. (2017). Organophosphate flame retardants (OPFRs) in indoor and outdoor air in the Rhine/Main area, Germany: comparison of concentrations and distribution profiles in different microenvironments. *Environ. Sci. Pollut. Res.* 24, 10992–11005. doi: 10.1007/s11356-016-6902-z

Conflict of Interest: The authors declare that the research was conducted in the absence of any commercial or financial relationships that could be construed as a potential conflict of interest.

Copyright © 2021 Prats, van Drooge, Fernández, Marco and Grimalt. This is an open-access article distributed under the terms of the Creative Commons Attribution License (CC BY). The use, distribution or reproduction in other forums is permitted, provided the original author(s) and the copyright owner(s) are credited and that the original publication in this journal is cited, in accordance with accepted academic practice. No use, distribution or reproduction is permitted which does not comply with these terms.

CHANGES IN URBAN GAS-PHASE PERSISTENT ORGANIC POLLUTANTS DURING THE COVID-19 LOCKDOWN IN BARCELONA

Raimon M. Prats, Barend L. van Drooge, Pilar Fernández, Joan O. Grimalt

Institute of Environmental Assessment and Water Research (IDAEA-CSIC), Jordi Girona 18, 08034 Barcelona, Catalonia, Spain

ARTICLE 2 – SUPPORTING INFORMATION

Table S2.1	Ion m/z ratios and collision energies used in GC-MS.	128
Table S2.2	Ion m/z transitions and collision energies used in GC-MS/MS.	129
Table S2.3	Average relative standard deviations of PAS replicates.	129
Figure S2.1	Distribution of the concentrations of gas pollutants measured in the city of Barcelona before and during lockdown.	130
Figure S2.2	Causal impact analysis representations of concentrations of air quality indicators measured in Barcelona during lockdown of 2020.	131

Table S2.1. Ion m/z ratios used for the identification and quantification in selective ion monitoring GC-MS of polychlorinated biphenyls, polycyclic aromatic hydrocarbons, other organohalogen compounds, and their recovery standards.

Compound	Abbreviation	m/z (CE 70 eV)
2,4,4'-Trichlorobiphenyl	PCB28	256
2,2',5,5'-Tetrachlorobiphenyl	PCB52	292
2,2',4,5,5'-Pentachlorobiphenyl	PCB101	326
2,3',4,4',5-Pentachlorobiphenyl	PCB118	326
2,2',3,4,4',5'-Hexachlorobiphenyl	PCB138	360
2,2',4,4',5,5'-Hexachlorobiphenyl	PCB153	360
2,2',3,4,4',5,5'-Heptachlorobiphenyl	PCB180	394
Decachlorobiphenyl	PCB209	498
Tetrabromobenzene	TBB	394
Hexachlorobenzene	HCB	284
Pentachlorobenzene	PeCB	250
α -Hexachlorocyclohexane	α -HCH	181
γ -Hexachlorocyclohexane	γ -HCH	181
Fluorene	Fle	166
Phenanthrene	Phe	178
Fluoranthene	Flu	202
Pyrene	Pyr	202
Benz[a]anthracene	B[a]ant	228
Chrysene + Triphenylene	Chr + TriPh	228
Fluorene-d ₁₀	Fle-d ₁₀	176
Phenanthrene-d ₁₀	Phe-d ₁₀	188
Fluoranthene-d ₁₀	Flu-d ₁₀	212
Pyrene-d ₁₀	Pyr-d ₁₀	212
Benz[a]anthracene-d ₁₂	B[a]ant-d ₁₂	240
Chrysene-d ₁₂	Chr-d ₁₂	240

Table S2.2. Ion m/z transitions and collision energies (CE) used for the identification and quantification in GC-MS/MS MRM of organophosphate flame retardants (OPFRs) and their respective recovery standards.

Compound	Abbr.	Quantifier		Qualifier	
		Transition (m/z)	CE (eV)	Transition (m/z)	CE (eV)
Tributyl phosphate	TBP	99→81	20	99→63	38
Tris(2-chloroethyl) phosphate	TCEP	249→125	10	249→99	32
Tris(1-chloro-2-propyl) phosphate	TCPP	125→81	29	125→99	12
Tris(1,3-dichloro-2-propyl) phosphate	TDCP	191→155	5	191→75	11
Triphenyl phosphate	TPhP	326→215	25	326→169	32
Tributyl phosphate-d ₁₀	TBP-d ₂₇	103→83	20	103→63	43
Tris(2-chloroethyl) phosphate-d ₁₂	TCEP-d ₁₂	261→131	9	261→131	30
Tris(1-chloro-2-propyl) phosphate-d ₁₈	TCPP-d ₁₈	131→83	30	131→103	11
Tris(1,3-dichloro-2-propyl) phosphate-d ₁₅	TDCP-d ₁₅	197→160	4	197→79	12
Triphenyl phosphate-d ₁₅	TPhP-d ₁₅	341→223	26	341→243	11

Table S2.3. Average relative standard deviations (RSD%) of passive air sampling (PAS) replicates for each target compound. These values were calculated from the concentrations analyzed in samplers deployed in duplicate at six different sites over four consecutive sampling periods between 2017 and 2019 in Aigüestortes, a high-mountain continental background location.

Compound	Abbreviation	RSD %
2,4,4'-Trichlorobiphenyl	PCB28	18.1
2,2',5,5'-Tetrachlorobiphenyl	PCB52	14.6
2,2',4,5,5'-Pentachlorobiphenyl	PCB101	11.5
2,3',4,4',5'-Pentachlorobiphenyl	PCB118	23.3
2,2',3,4,4',5'-Hexachlorobiphenyl	PCB138	16.2
2,2',4,4',5,5'-Hexachlorobiphenyl	PCB153	15.7
2,2',3,4,4',5,5'-Heptachlorobiphenyl	PCB180	34.2
Hexachlorobenzene	HCB	12.8
Pentachlorobenzene	PeCB	9.4
Fluorene	Fle	13.5
Phenanthrene	Phe	11.2
Fluoranthene	Flu	16.5
Pyrene	Pyr	18.7
Benz[a]anthracene	B[a]ant	17.8
Chrysene + Triphenylene	Chr + TriPh	20.4
Tributyl phosphate	TBP	22.6
Tris(2-chloroethyl) phosphate	TCEP	36.3
Tris(1-chloro-2-propyl) phosphate	TCPP	30.8
Tris(1,3-dichloro-2-propyl) phosphate	TDCP	60.1
Triphenyl phosphate	TPhP	22.3

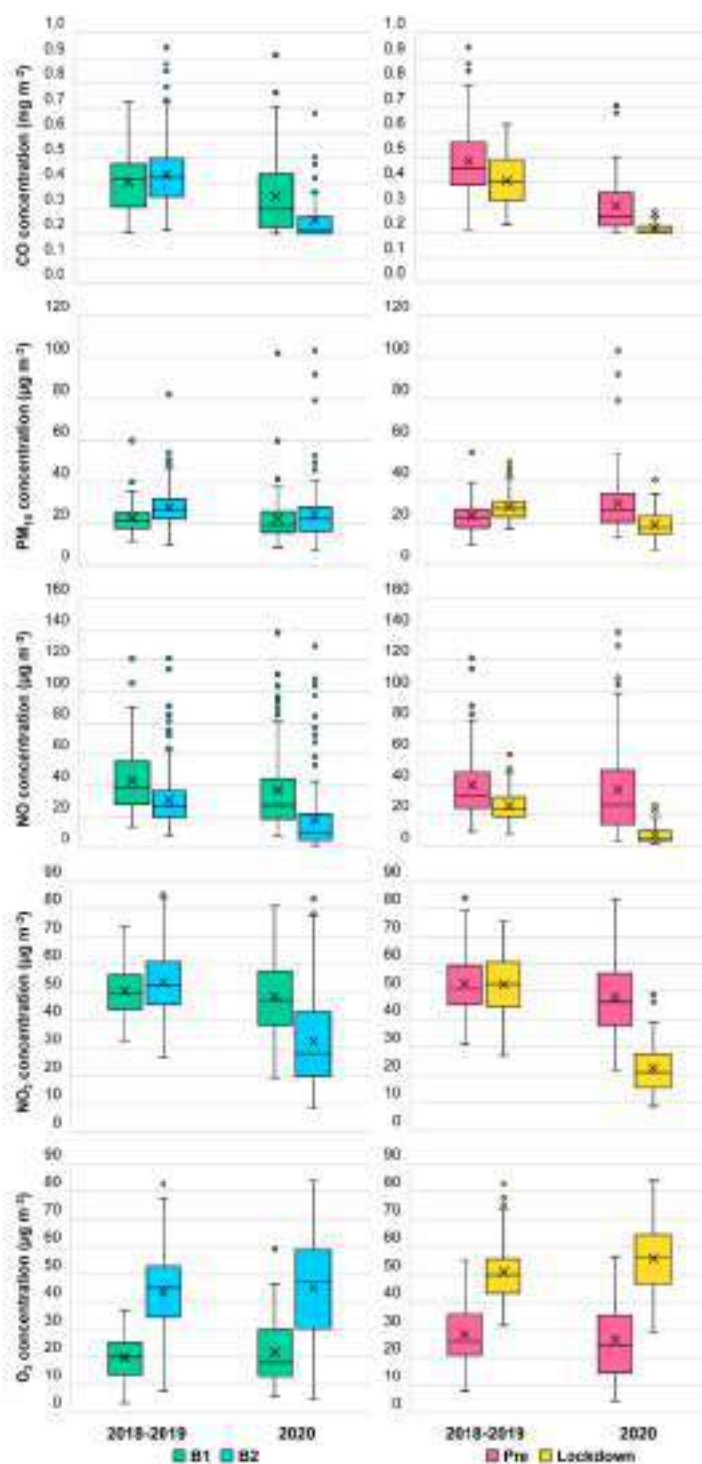


Figure S2.1. Distribution of the concentrations of gas pollutants measured in the city of Barcelona during the following periods: B1: 15/10/2019–9/1/2020; B2: 9/1/2020–15/7/2020; pre-lockdown: 1/1/2020–14/3/2020; lockdown: 15/3/2020–22/6/2020. The median value is represented by the horizontal line inside the box and the mean value by an x. They are compared to the concentrations in the same periods of the previous two years (2018 and 2019, averaged).

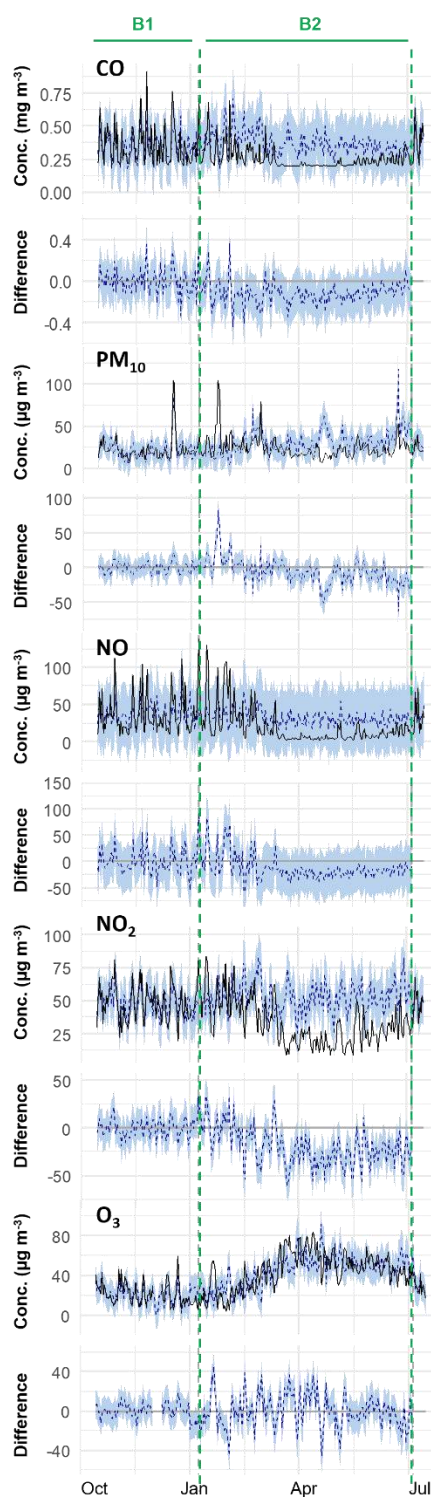


Figure S2.2. Causal impact analysis representations of concentrations of air quality indicators measured in Barcelona during lockdown of 2020. The passive air sampled (PAS) B1/B2 periods are delimited by vertical, green, dashed lines. For each compound, the top charts show daily average concentrations recorded in 2020 (black continuous line) against a counterfactual prediction based on 2018–2019 average values (blue dashed line, based on B1/B2 sampling dates). The bottom charts show the difference between the observed data and the counterfactual predictions.



Article 3

OCCURRENCE AND TEMPERATURE DEPENDENCE OF ATMOSPHERIC GAS-PHASE ORGANOPHOSPHATE ESTERS IN HIGH-MOUNTAIN AREAS (PYRENEES)

Raimon M. Prats, Barend L. van Drooge, Pilar Fernández, Joan O. Grimalt
Chemosphere 292 (2022) 133467
DOI 10.1016/j.chemosphere.2021.133467



Contents lists available at ScienceDirect

Chemosphere

journal homepage: www.elsevier.com/locate/chemosphere



Occurrence and temperature dependence of atmospheric gas-phase organophosphate esters in high-mountain areas (Pyrenees)

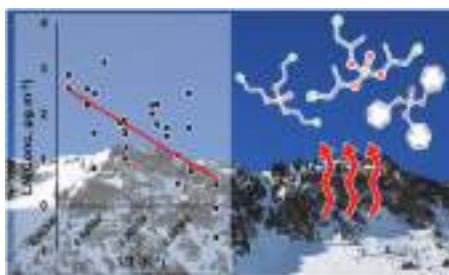
Raimon M. Prats^{*}, Barend L. van Drooge, Pilar Fernández, Joan O. Grimalt

Institute of Environmental Assessment and Water Research (IDAEA-CSIC), Jordi Girona 18, 08034, Barcelona, Catalonia, Spain

HIGHLIGHTS

- Organophosphate esters (OPEs) in air of continental regions are lowest in mountains.
- Air tris(1-chloro-2-propyl) phosphate, the most used, predominates at low altitudes.
- Tris(2-chloroethyl) phosphate in air predominates at altitudes above 2300 m
- The air levels of abundant OPEs are correlated with the reciprocal of temperature.
- OPEs are adsorbed on mountain snow and released into the atmosphere during snowmelt.

GRAPHICAL ABSTRACT



ARTICLE INFO

Handling Editor: R Ebinghaus

Keywords:

Organophosphate flame retardants
Passive air sampling
Remote sites
Secondary emission
Temperature trends

ABSTRACT

The air concentrations of organophosphate esters (OPEs) were studied in a network of six remote high-mountain areas of the Pyrenees located along an altitudinal profile between 1619 m and 2453 m above sea level on a restricted planar surface to assess their vertical distribution based on long-range atmospheric transport and temperature gradients. Polyurethane foam passive samplers were used in five periods spanning over three years (September 2017–October 2020). The sum of concentrations of five OPEs were between 5.3 and 100 pg m^{-3} , averaging 16–53 pg m^{-3} across campaigns at the different locations. These concentrations were much lower than those observed in areas under anthropogenic influence but also than those found in low altitude remote continental sites. A significant progressive change in predominant compounds was observed along the altitudinal gradient, with prevalence of tris(1-chloro-2-propyl) phosphate (TCIPP) or tris(2-chloroethyl) phosphate (TCEP) below or above 2300 m above sea level, respectively. This trend was consistent with the higher volatility of TCEP, which was retained at greater extent at lower environmental temperatures (higher altitude).

A significant temperature dependence of the gas phase concentrations was observed for TCEP, TCIPP and triphenyl phosphate (TPHP), which could be explained by retention in the cold periods, predominantly adsorbed in snow, and their release to the atmosphere during snowmelt. This mechanism was consistent with the good agreement found between the vaporization enthalpies measured under laboratory conditions and the experimental values obtained from the slopes of the significant linear regressions when representing the vertical gradients.

^{*} Corresponding author.

E-mail address: raimon.martinez@idaea.csic.es (R.M. Prats).

<https://doi.org/10.1016/j.chemosphere.2021.133467>

Received 3 September 2021; Received in revised form 26 December 2021; Accepted 27 December 2021

Available online 30 December 2021

0045-6535/© 2021 Elsevier Ltd. All rights reserved.

1. Introduction

Organophosphate esters (OPEs) are synthetic compounds used as flame retardants, plasticizers, and antifoaming agents in a myriad of industrial processes and consumer products (e.g., foams, paints, lubricants, hydraulic fluids, furniture, building materials, vehicles, and electronics) (van der Veen and de Boer, 2012). Exposure to various OPEs has been documented in adults and children (Hou et al., 2016; Wei et al., 2015). Endocrine disruption effects and developmental toxicity upon exposure to OPEs has been observed in animal experiments (Yang et al., 2019). These compounds are suspected neurotoxicants because of their structural similarities with the organophosphorus pesticides (Wei et al., 2015; Yang et al., 2019) and the chlorinated OPEs are suspected carcinogens (World Health Organization, 1998). Human incidence of sick house syndrome (Kanazawa et al., 2010), contact dermatitis (Camarasa and Serra-Baldrich, 1992), and disrupted hormone levels, such as reduced thyroid hormone, and decreased semen quality among human males have been associated with OPE exposure (Meeker and Stapleton, 2010). Despite these unwanted properties, their production has steadily increased because they are used to replace other restricted compounds (Blum et al., 2019), e.g., in 2005 the estimated world production was 186,000 tons and in 2018 it exceeded one million, which represents more than 30% of flame retardants worldwide (Chokwe et al., 2020; Du et al., 2019).

OPEs are not chemically bound to the materials where they are added, which facilitates their release into the environment by volatilization and leaching (Chokwe et al., 2020). They have been found in urban and industrial sites close to their potential sources (Kurt-Karakus et al., 2018; Saini et al., 2020; Shoeib et al., 2014; van Drooge et al., 2018). However, OPEs have also been identified in environmental matrices from remote areas like the Arctic (Gustavsson et al., 2019; Salamova et al., 2014a; Sühling et al., 2021; Sun et al., 2020), Antarctica (Fu et al., 2020; Cheng et al., 2017; Xie et al., 2020), and the global oceanic atmosphere (Castro-Jiménez et al., 2016). Although the modeled atmospheric lifespan of OPEs is low, they exhibit high resistance to degradation while attached to particles, which may explain their observed capacity for long-range atmospheric transport (Liu et al., 2014). These properties and the massive use of these compounds require an understanding of the impact of global pollution associated with their occurrence, with a focus on remote sites.

The high mountains are the most remote regions of the continents. These environments can be used as sentinel ecosystems for assessment of the overall background pollution resulting from the anthropogenic activities on land. This assessment also requires understanding the processes that determine the fate of long-range atmospheric transported compounds in these areas and the influence of the vertical transport processes between lower and higher elevation. Unfortunately, these sites present great difficulties for sampling given their reduced accessibility, especially during winter, and limited access to energy supply. Polyurethane foam passive air samplers (PUF-PASs) have the ability to overcome these obstacles that could otherwise preclude studies in such remote locations, especially when long periods of time are considered. These samplers have been used successfully to determine gas-phase concentrations of OPEs in urban areas (Abdollahi et al., 2017; Khairy and Lohmann, 2019).

Here, we present a study of the gas-phase concentrations of five of the most widely used and ubiquitous OPEs: tributyl phosphate (TBP), tris(2-chloroethyl) phosphate (TCEP), tris(1-chloro-2-propyl) phosphate (TCIPP), tris(1,3-dichloro-2-propyl) phosphate (TDCIPP), and triphenyl phosphate (TPHP), in several high-mountain background sites in the Catalan Pyrenees. The dependences between gas-phase concentrations and temperature were also assessed to determine the influence of this parameter on the occurrence and release of OPEs from possible environmental reservoirs (e.g., snow, soils, particles, vegetation). The atmospheric concentrations of these ubiquitous pollutants in mountain areas have scarcely and sparsely been considered to date.

The present study provides a novel approach in which OPE data were measured over three years (September 2017–October 2020; Table 1) in a network of six high-mountain sites distributed along an altitudinal profile, between 1619 m and 2453 m above sea level (asl; Table 1; Fig. 1). These sites are far from human-populated areas and located over a restricted space in which the maximal planar projection distance between the component sites is 17.5 km (Redon and Collada). Therefore, the sites are subject to the same type of air-transported diffuse pollution, thus providing a description of the distribution of the OPEs at various altitudes as a consequence of long-range atmospheric transport and temperature gradients.

2. Materials and methods

2.1. Air sampling, extraction, and analysis

A total of 43 atmospheric gas-phase samples were collected in five sampling campaigns between September 2017 and October 2020 at six high-mountain sites in the Catalan Pyrenees encompassing an altitudinal gradient between 1619 and 2453 m asl. The sampling sites were located near alpine lakes (Fig. 1), which are distributed between Vall d'Aran and the National Park of Aiguestortes i Estany de Sant Maurici. This restricted natural reserve is included in the European Union's Natura 2000 protected natural network and is considerably distant from populated areas. Sampling durations and meteorological conditions are summarized in Table 1. The latter were obtained using in-situ Tinytag Plus 2 data loggers (Gemini Data Loggers, Chichester, United Kingdom) and from the XEMA network automatic weather stations of the Catalan Meteorological Service.

The sampling and analytical procedures were described in detail elsewhere (Prats et al., 2021a, 2021b). Briefly, the samples were obtained using PUF-PASs deployed in duplicate at each location inside stainless steel dome housings suspended at 1.8 m above ground by a steel pole supported by three metal wire ropes anchored to the ground (Figure S1). The PUF disks (Techno Spec, Barcelona, Catalonia, Spain: 14 cm diameter, 1.35 cm thickness, 369.5 cm² surface area, 0.021 g cm⁻³ density, and 0.00567 m effective film thickness) were pre-cleaned in distilled water and acetone baths and extracted by Soxhlet with acetone and hexane for 24 h each (all solvents from Merck, Darmstadt, Germany). Prior to deployment, they were further extracted during 8 h with hexane, dried under vacuum, wrapped in rinsed aluminum foil, and stored and transported at -20 °C inside air-tight PET/LLDPE bags (Kapak Corporation, St Louis Park, MI, USA). At the sampling site, a mixture of Performance Reference Compounds (PRCs) consisting of polychlorobiphenyl congeners (PCBs) 3, 9, 15, 32 (all isotopically labeled), 107, and 198 (Cambridge Isotope Laboratories, Tewksbury, MA, USA) was spiked into the exposed and blank PUF-PASs to calculate the sampler-specific sampling rates. After exposure, the samplers were sealed, transported, and stored in the aforementioned conditions until extraction, usually less than 48 h after retrieval.

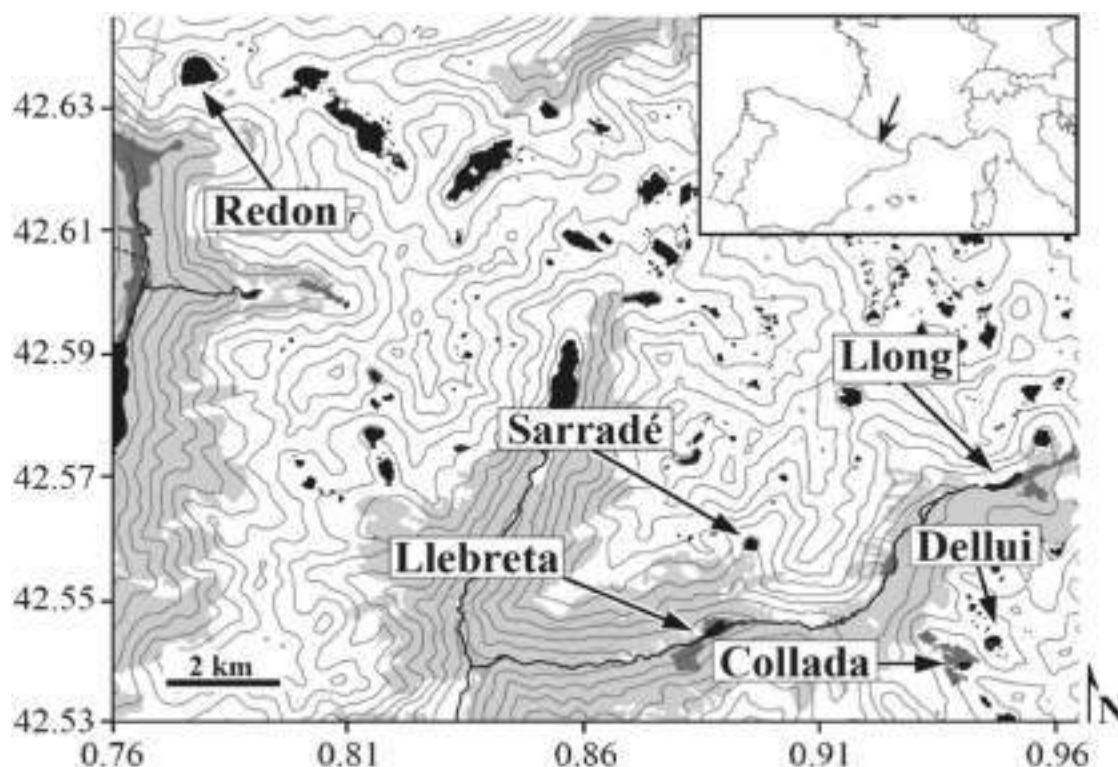
The compounds adsorbed by the PUF disks were Soxhlet-extracted for 8 h with hexane (Merck) immediately after spiking the material by injecting 25 µL of a mixture of recovery standards consisting of TBP-d₁₂, TCEP-d₁₂, TCIPP-d₁₈, TDCIPP-d₁₅, and TPHP-d₁₅ (ES-5529 standard mixture from Cambridge Isotope Laboratories). The resulting extracts were concentrated to 2 mL by vacuum rotary evaporation (Büchi, Flawil, Switzerland), dried by elution through 0.5 g of pre-cleaned anhydrous sodium sulphate (Merck) activated at 450 °C overnight, and further concentrated to 50 µL under a gentle stream of nitrogen.

The extracts were analyzed by gas chromatography coupled to tandem mass spectrometry (GC-MS/MS) using an Agilent 7000 Series Triple Quad GC/MS (Agilent Technologies, Santa Clara, CA, United States) in electron impact mode with a Zebron ZB-PAH capillary column (30 m, 0.25 mm i.d., 0.25 µm from Phenomenex, Torrance, CA, USA). The injector, ion source, quadrupoles, and transfer line temperatures were 280, 230, 150, and 280 °C, respectively. Helium was used as a carrier gas

Table 1

Sampling times (d), average air temperatures (°C), and meteorological conditions at the mountain sites in the sampled periods (I–V; September 2017–October 2020).

		I	II	III	IV	V
		09/17–01/18	01/18–07/18	07/18–12/18	12/18–09/19	09/19–10/20
Llebreta (1619 m)	Time	132	162	154	287	376
	Temperature	7.1	7.6	12.3	10.6	10.0
Llong (2000 m)	Time	135	161	154	–	–
	Temperature	2.5	3.5	9.0	–	–
Sarradé (2123 m)	Time	133	162	155	286	376
	Temperature	4.8	4.3	9.9	7.2	7.4
Redon (2240 m)	Time	–	297 ^a	154	289	376
	Temperature	0.7	0.7	6.8	4.1	4.2
Dellui (2349 m)	Time	130	163	154	–	–
	Temperature	1.4	–0.7	7.2	–	–
Collada (2453 m)	Time	129	163	154	–	–
	Temperature	1.6	–0.7	7.1	–	–
Meteo stations^b	Temperature (°C) ^c	0.3 (-16–15)	0.1 (-17–18)	6.1 (-11–20)	3.6 (-16–25)	3.4 (-13–23)
	Precipitation (mm)	250–717	976–1038	573–659	581–1058	1176–1605
	Wind speed (m s ⁻¹) ^d	4.3	4.1	3.7	4.2	4.1
	Snow height (mm) ^d	303	1616	99	422	604

^a Samples collected during sampling period II at Redon encompass sampling periods I and II.^b Data from XEMA meteorological stations in the studied region: Redon VS (2247 m), Boi Z2 (2535 m).^c Average value, range in parentheses.^d Average value during each sampling period.**Fig. 1.** Sampling sites, located next to six high-mountain lakes between 1619 and 2453 m above sea level in the Pyrenees.

at 1.1 mL min⁻¹. The oven temperatures were programmed from 80 °C (held for 1.5 min) to 220 °C at 10 °C min⁻¹ and then to 315 °C at 15 °C min⁻¹ (held for 5 min). The target compounds were identified in MRM mode by their retention times and by the *m/z* transitions summarized in Table S1. Matrix effect was only observed for the TDCIPP qualifier transition, but not for the quantifier one. Nevertheless, qualifier chromatographic peaks were still generally easily identifiable above background noise and did not suffer any coelutions. Data treatment, visualization, and statistical analyses were performed in R 4.1.0 (R Core Team, 2021) and Microsoft Excel (Microsoft, Redmond, WA, USA).

2.2. Recoveries

An internal standard calibration method was used for the quantification of the targeted compounds, accounting for surrogate standard recovery correction and instrumental variability. Recoveries of the surrogate standards in three spiked matrix recovery extractions were 86 ± 19% for TBP-d₁₂, 53 ± 14% for TCEP-d₁₂, 86 ± 23% for TCIPP-d₁₈, 53 ± 9% for TDCIPP-d₁₅, and 89 ± 15% for TPHP-d₁₅. The chromatographic peaks could be identified and quantified with ease. The recovery standard mixture also contained tripropyl phosphate-d₂₁ and triethyl

phosphate-d₁₅, but the corresponding OPEs were not included in the analyses because the former was never detected in environmental samples nor blanks, and the latter was too volatile (logK_{OA} around 5) for an accurate determination of passive sampling rates. Instrumental LOQs (10 times the signal-to-noise ratio, s/n) were between 0.12 and 0.25 pg in-column, or 6.25–12.5 pg sampler⁻¹, which correspond to 0.01–0.03 pg m⁻³ for mean PAS effective sampled volumes.

2.3. Blanks

Field and laboratory blanks were analyzed with the samples of each campaign for controlling background, transport, and processing contamination as well as for estimating sampling rates. The PUF blanks were cleaned, stored, and transported in the same conditions as the samples, both before and after exposure. In order to avoid any contamination of the PUF-PASs, pre-cleaned handling equipment, tools, and wrapping material were used as well as air-tight sealing bags for transport and storage. The blanks were spiked with PRCs and exposed to the ambient air during deployment and retrieval operations, and then resealed and stored at -20 °C for the duration of the sampling campaign and until extraction. Blank levels were on average 36% of the sample amounts for TBP, 42% for TCEP, 25% for TCIPP, 19% for TDCIPP, and 27% for TPHP, and were subtracted from the sample concentrations. The TPHP atmospheric concentrations at the Redon sampling site showed a local contamination.

2.4. Sampling rates (R_S)

Effective sampled air volumes (V_A, m³) for the conversion from OPE amounts per sampler to air concentrations were calculated using Equation (1) (Harner et al., 2013):

$$V_A = V_{PUF} K'_{PUF-A} \left[1 - \exp\left(\frac{-k_A t}{K'_{PUF-A} D_{film}}\right) \right] \quad (1)$$

where K' _{PUF-A} (unitless) is the density-corrected sampler-air partition coefficient (K_{PUF-A} × PUF density) of the pollutant, k_A (m d⁻¹) is the air-side mass transfer coefficient, t (d) is the duration of the sampling campaign, and V_{PUF} (m³) and D_{film} (m) are the volume and effective film thickness of the PUF disk, respectively. This is a degree-of-equilibrium model that accounts for all stages of the uptake of compounds (i.e., linear, curvilinear, and equilibrium).

The K_{PUF-A} values were determined for each compound using the relationship proposed by Shoeib and Harner (2002) (logK_{PUF-A} = 0.6366 × logK_{OA(T)} - 3.1774) from octanol-air partition coefficients (K_{OA}) calculated at the average temperature of each sampling campaign (Wang et al., 2017). The k_A values were determined from the in-situ calibration of each sampler by PRC depletion using Equation (2):

$$k_A = \frac{R_S}{A_{PUF}} = \frac{\ln(C/C_0) K'_{PUF-A} D_{film}}{t} \quad (2)$$

where C/C₀ is the ratio between PRC amounts found in exposed samplers after their retrieval and in non-exposed blanks, A_{PUF} (m²) is the total surface area of the sampler disk, and K' _{PUF-A} references the partition coefficient of the PRCs calculated from their temperature-corrected K_{OA} (Harner, 2021).

2.5. R_S uncertainties

Uncertainties in PAS sampling rates are a matter of concern and need to be monitored. Potential sources of uncertainty for the sampler configuration used in the context of the present study area have been discussed elsewhere (Prats et al., 2021b). The R_S experimental errors were determined as relative standard deviation of the replicates (RSD, %), and estimated theoretical expanded uncertainties (EU, %). The EUs were measured as propagated uncertainties of the sampling rates (δR_S)

calculated with the PRCs by propagation of the errors of the variables involved in the calculations.

Substituting K_{PUF-A} for its temperature-corrected octanol-air partition coefficient (K_{OA(T)}) dependence relationship (Shoeib and Harner, 2002) in a rearranged Equation (2), we obtain:

$$R_S = \frac{-\ln\left(\frac{C}{C_0}\right) D_{film} \rho_{PUF} 10^{(0.6366 \log K_{OA(T)} - 3.1774) A_{PUF}}}{t} = k \ln\left(\frac{C}{C_0}\right) 10^{(b \log K_{OA(T)} - a)} \quad (3)$$

where ρ_{PUF} is the density of the PUF, and where simplifications can be made by grouping all constants (k) and renaming the coefficients in the exponential term (a and b). Thus, the δR_S can be calculated as the square root of the sum of squares of the partial derivatives of R_S with respect to the non-constant variables, C/C₀ and K_{OA}, multiplied by their respective squared uncertainties:

$$\begin{aligned} \delta R_S &= \sqrt{\left(\frac{\partial R_S}{\partial C/C_0}\right)^2 \delta_{C/C_0}^2 + \left(\frac{\partial R_S}{\partial K_{OA(T)}}\right)^2 \delta_{K_{OA(T)}}^2} = \\ &= \sqrt{\left(\frac{10^{-a} k K_{OA(T)}^b}{C/C_0}\right)^2 \delta_{C/C_0}^2 + \left(10^{-a} k b K_{OA(T)}^{b-1} \ln\left(\frac{C}{C_0}\right)\right)^2 \delta_{K_{OA(T)}}^2} \end{aligned} \quad (4)$$

The uncertainties of the variables can be estimated from further propagation of C/C₀ calculation error (from instrumental and quantification standard errors) and from PRC K_{OA(T)} standard errors reported elsewhere (Harner and Bidleman, 1996). Finally, the EUs are calculated as twice the resulting propagated uncertainty to account for other undefined sources of error such as in temperature correction relationships.

3. Results and discussion

3.1. Average R_S

The overall average R_S calculated by PRC calibration of all campaigns at each site was 3.2 ± 0.7 m³ d⁻¹ (n = 43), ranging from 1.6 to 4.5 m³ d⁻¹ for individual samples (Table S2). These rates were in the range of previous reports in remote mountain regions (Estellano et al., 2008; Meire et al., 2012; Ren et al., 2014), and close to the general estimate of 4 m³ d⁻¹ in most PUF-PAS studies (Herkert et al., 2018).

The RSD of the R_S replicates were between 1.5 and 33% (Table S2) and averaged 14%, generally staying within an acceptable RSD of 25% with only two higher exceptions in the longest running campaigns. Most RSDs for each site across campaigns were between 6 and 15% with one exception at 25% (corresponding to the highest and coldest site), while campaign means across sites were between 12 and 23% with the exception of the longest campaign (40%).

The overall average EU was 19%, ranging between 11 and 34% (Table S2). Therefore, the experimental RSDs and the theoretical EUs were close to each other, indicating limited overall experimental errors and good performance of PUF-PASs for monitoring semi-volatile organic compounds in remote high-mountains despite the meteorological conditions of these areas being outside the typical range of application of these samplers.

3.2. Effective sampled air volumes

The average effective sampled air volumes calculated from the R_S ranged from 475 to 662 m³ depending on the compound (Table S3), with values increasing with K_{OA}. Individual replicate volumes were as low as 284 m³ and as high as 1692 m³ depending on the sampling site and

period. However, it has been argued that the widely-used $K_{PUF-A-K_{OA}}$ relationship from [Shoeib and Harner \(2002\)](#) may not hold true for all compound classes such as OPEs, proposing a new OPE-specific regression similar in slope but with a higher intercept ($\log K_{PUF-A} = 0.6087 \times \log K_{OA(T)} + 2.3821$) ([Saini et al., 2019a](#)). This difference was attributed to the higher polarity and hydrophilicity of OPEs generating additional interactions with the PUF material that enhance their partitioning between air and sampler. Enhanced partitioning towards the particle phase relative to their K_{OA} has also been observed for some OPEs ([Salamova et al., 2014a](#); [Sühring et al., 2016b](#)), possibly driven by molecular interactions that could also explain the increased partitioning towards PUFs ([Saini et al., 2019a](#)). Still, PUF-PASs have been shown to perform well for OPEs and other compounds with high K_{OA} and particle association tendency ([Harner et al., 2013](#); [Markovic et al., 2015](#); [Rauert et al., 2016](#)). Moreover, smaller partition ratios towards the particle phase have been suggested for some OPEs based on K_{OA} models ([Sühring et al., 2016b](#)), so a similar argument could be made for their PUF-air partitioning capabilities.

We used both proposed $K_{PUF-A-K_{OA}}$ relationships to calculate effective sampled volumes for comparison. The newer one yielded K_{PUF-A} values one-log units higher than the original equation, which resulted in PUF-air partitioning conditions farther from equilibrium and closer to strictly linear exchange than the original one. This change was moderately noticeable for OPEs with lower K_{OA} like TBP and TCEP, resulting in increased sampled volumes (34 and 26% higher on average, respectively) ([Table S3](#)). However, OPEs with $\log K_{OA}$ well above 9 like TCIPP, TDCIPP, and TPHP already presented partitioning conditions distant from equilibrium. Therefore, their sampled volumes were not dependent on K_{OA} , being instead only proportional to the length of the sampling period and the measured sampling rate. Thus, the application of the newer $K_{PUF-A-K_{OA}}$ relationship yielded only 0–10% higher volumes ([Table S3](#)). Although these differences were somewhat relevant for TBP

and TCEP and worth discussing since they add to the overall uncertainty of PAS-derived OPE concentrations in air, they were of an acceptable magnitude, so the original relationship proposed by [Shoeib and Harner](#) was chosen for consistency and comparability with previous studies, as recommended in the most recent calculation template available at the time of this analysis ([Harner, 2021](#)). Furthermore, the equation proposed by [Saini et al. \(2019a\)](#) only relies on modeled K_{OA} values of three aliphatic OPEs, so future work in passive OPE monitoring should focus on further studying PUF-air partitioning and equilibrium including chlorinated compounds regardless of the assumed linearity of their uptake.

3.3. OPEs in the atmospheric gas phase

Most OPEs are prominently bound to the atmospheric particle phase. PUF-PAS samplers have occasionally been shown to collect particle-bound pollutants at rates similar to gas-phase compounds, with particle infiltration efficiencies of the sampler housing configurations up to 100% compared to air outside the sampler ([Markovic et al., 2015](#)). Thus, OPE concentrations measured by PUF-PAS are often reported as total atmospheric OPEs instead of gas-phase concentrations. However, we have previously shown that the sampler configuration used in this study and in this location performed mainly as a gas phase sampler through the estimation of low (16–23%) experimental particle infiltration efficiencies ([Prats et al., 2021b](#)). Moreover, PAS OPE concentrations agreed with high-volume gas-phase measurements, while particle-phase OPE concentrations were up to two orders of magnitude higher ([Prats et al., 2021b](#)). Therefore, concentrations in this work will be presented as gas-phase OPE levels, although a limited contribution of particle-bound OPEs could still be expected.

The mean OPE gas-phase concentrations for each sampling period at each studied site are summarized in [Table 2](#). The sums of OPE

Table 2
Mean organophosphate ester (OPE) concentrations (pg m^{-3}) for each sampling period at each site (\pm standard deviation of the replicates).

Site	Period ^a	Temperature	TBP	TCEP	TCIPP	TDCIPP	TPHP	Σ OPE
Llebreta (1619 m)	I	7.1	3.3 ± 2.6	1.2 ± 0.1	16 ± 6	2.7 ± 0.9	4.8 ± 1.7	28 ± 12
	II	7.6	1.2 ± 0.2	1.5 ± 0.7	23 ± 1	0.3	6.1 ± 0.1	32 ± 0.5
	III	12.3	2.4 ± 0.2	13 ± 1	69 ± 19	1.5 ± 0.9	15 ± 3.0	101 ± 23
	IV	10.6	0.8 ± 0.4	2.9 ± 0.8	56 ± 7	0.3 ± 0.2	11 ± 3.0	71 ± 11
	V	10.0	0.2	3.4 ± 0.7	28 ± 0.2	0.3 ± 0.1	3.6 ± 1.9	35 ± 1.4
	Mean			1.6 ± 1.2	4.4 ± 4.9	38 ± 23	1.0 ± 1.1	8.1 ± 4.9
Llong (2000 m)	I	2.5	1.8 ± 0.3	0.4	3.9 ± 0.4	BDL ^b	2.3 ± 1.0	8.2 ± 1.4
	II	3.5	1.0 ± 0.3	1.4 ± 0.7	8.9 ± 1.9	0.6 ± 0.6	5.1 ± 0.7	17 ± 2.8
	III	9.0	2.1 ± 0.3	14 ± 0.1	11 ± 0.4	2.2 ± 0.5	23 ± 0.1	53 ± 1.1
	Mean		1.6 ± 0.6	5.4 ± 7.8	8.0 ± 3.7	1.4 ± 1.1	10 ± 11	26 ± 24
	Sarradé (2123 m)	I	4.8	2.9 ± 1.5	BDL	4.9 ± 5.7	4.3 ± 4.1	8.3 ± 1.1
II	4.3	1.0 ± 0.3	2.8 ± 0.2	5.3 ± 3.6	0.4 ± 0.4	7.6 ± 2.3	17 ± 6.8	
III ^c	9.9	1.4	8.7	3.2	0.9	12	26	
IV ^c	7.2	1.2	5.1	10	1.0	6.5	24	
V	7.4	0.2 ± 0.01	4.0 ± 1.0	11 ± 2	0.3 ± 0.2	3.2 ± 0.02	19 ± 1.6	
Mean			1.3 ± 1.0	5.2 ± 2.5	6.9 ± 3.5	1.4 ± 1.6	7.5 ± 3.1	20 ± 3.6
Redon (2240 m)	II	0.7	1.2 ± 0.2	3.4 ± 1.5	6.0 ± 3.1	2.0 ± 0.9	1094 ^d	13 ± 4 ^e
	III	6.8	2.7 ± 0.02	23 ± 5	21 ± 1	3.2 ± 0.9	376 ± 71 ^d	50 ± 6.7 ^c
	IV	4.1	0.9 ± 0.1	3.0 ± 0.2	20 ± 10	2.3 ± 1.0	1460 ± 78 ^d	26 ± 11 ^c
	V ^c	4.2	0.2	1.7	18	0.9	180 ^d	20 ^e
	Mean			1.2 ± 1.0	7.8 ± 10	16 ± 7	2.1 ± 0.9	777 ± 601 ^d
Dellui (2349 m)	I	1.4	2.4 ± 0.7	6.3 ± 6.1	11 ± 8	0.9 ± 1.0	2.3 ± 0.2	23 ± 16
	II	-0.7	0.3 ± 0.1	1.4 ± 0.4	1.3 ± 0.3	0.7 ± 0.4	1.6 ± 0.1	5.3 ± 0.5
	III	7.2	0.8 ± 0.03	11 ± 2	2.0 ± 1.2	1.3 ± 1.3	4.1 ± 1.7	19 ± 6.1
	Mean		1.2 ± 1.1	6.1 ± 4.6	4.9 ± 5.6	0.9 ± 0.3	2.7 ± 1.3	16 ± 9.4
Collada (2453 m)	I	1.6	2.6 ± 0.6	0.3 ± 0.1	8.4 ± 4.0	1.4 ± 0.5	8.6 ± 4.4	21 ± 0.7
	II	-0.7	0.4 ± 0.1	4.7 ± 2.4	3.7 ± 1.4	2.3 ± 1.9	0.7 ± 0.3	12 ± 2.3
	III	7.1	1.1 ± 0.3	16 ± 3	1.9 ± 0.3	2.5 ± 0.1	3.8 ± 1.4	26 ± 1.9
	Mean		1.4 ± 1.1	7.1 ± 8.4	4.7 ± 3.3	2.1 ± 0.6	4.4 ± 4.0	20 ± 7.2

^a Sampling periods: I, 09/17–01/18; II, 01/18–07/18; III, 07/18–12/18; IV, 12/18–09/19; V, 09/19–10/20.

^b Below detection limit.

^c Replicates lost due to extreme weather conditions.

^d Sampling site affected by local contamination.

^e Not including TPHP.

concentrations were between 5.3 and 100 pg m^{-3} , averaging 16–53 pg m^{-3} across campaigns at the different locations. The concentrations of individual OPEs ranged between below detection limits (BDL, $3 \times \text{s/n}$) and 69 pg m^{-3} , except for samples from Redon site that was found to have a local source of TPHP. The average concentrations and ranges were 15 ± 17 (1.3–69) pg m^{-3} (TCIPP), 6.8 ± 5.5 (0.7–23) pg m^{-3} (TPHP, not including Redon sampling site), 5.9 ± 6.1 (BDL–23) pg m^{-3} (TCEP), 1.5 ± 1.1 (BDL–4.3) pg m^{-3} (TDCIPP), and 1.4 ± 0.9 (0.2–3.3) pg m^{-3} (TBP) (Table 2).

The TPHP atmospheric concentrations at the Redon site were unusually high in all samples, 777 ± 601 pg m^{-3} , compared to those from the other studied sites, 2.7–10 pg m^{-3} (Table 2). These high concentrations were comparable to those found in urban sites in Canada (Saini et al., 2019b), China (Liang et al., 2020), and other megacities (Saini et al., 2020) (Table 3). These unusual results suggested a local source of TPHP contamination. Lake Redon has a small cabin built in the 1990s for storage purposes, basic research operations, and shelter whose wall panels are filled with insulating foam. Samples from this foam were extracted with acetonitrile and analyzed. TPHP contributed to 99.7% of the total OPEs in the insulation material, followed by TCIPP at 0.3% (Figure S2). On the other hand, TPHP averaged 94% of total OPEs in air samples at the Redon sampling site, while in the other locations it ranged between 15 and 35% (Figure S2). The concentrations of TPHP in Redon were therefore not considered.

All OPE results from the Pyrenean mountains were much lower than those reported in land areas under anthropogenic influence (Table 3). Comparison of the results from the present study with those available from continental remote sites (Rauert et al., 2018b; Wang et al., 2019; Wang et al., 2020, Table 3) showed that the results from the mountain areas were also lower than or in the range of those in these remote regions. The Pyrenean mountain values of TBP, TCEP, TCIPP, TDCIPP and TPHP showed ranges of 0.2–3.3, BDL–23, 1.3–69, BDL–4.3, and 0.7–23 pg m^{-3} , respectively, whereas those reported in continental remote regions were in ranges of BDL–107, 1.4–580, BDL–1400, BDL–30, and BDL–250 pg m^{-3} , respectively (Table 3).

In general, the concentrations of these compounds did not exhibit significant correlations. Such correlations are often reported in atmospheric studies in urban sites or at an intermediate distance from

primary OPE sources (Saini et al., 2019; Wu et al., 2020). In contrast, non-significant correlations have been reported between atmospheric OPE concentrations in some highly industrialized sites (Kurt-Karakus et al., 2018), which could be due to the use of individual compounds instead of mixtures in applications and products (van der Veen and de Boer, 2012). Additionally, no correlations between gaseous OPEs were reported in remote sites such as Antarctica and the Arctic (Wang et al., 2020; Han et al., 2020). More than source emission strength, this could reflect different fates of OPEs due to long-range transportation, deposition, and degradation potential. Thus, the lack of significant correlations we report may be a result of the remoteness of the studied area.

TCIPP dominated the concentration profiles ($46 \pm 23\%$), followed by TPHP ($25 \pm 13\%$), TCEP ($21 \pm 18\%$), TDCIPP ($7 \pm 9\%$), and TBP ($6 \pm 5\%$). This is consistent with TCIPP often being reported as the dominant OPE in most studies, both in particle phase (Clark et al., 2017; Salamova et al., 2014b; van Drooge et al., 2018; Wu et al., 2020) including samples from oceanic transects (Castro-Jiménez et al., 2016), and in gas-phase samples from global passive sampling monitoring programs (Rauert et al., 2016, 2018b) and outdoor air samples from Germany (Zhou et al., 2017), China (Cao et al., 2019; Wang et al., 2018, 2020b), Egypt (Khairy and Lohmann, 2019), and Canada (Saini et al., 2019b). TCIPP was also dominant in all OPE distributions from sites under anthropogenic influence in Table 3 except for one case (Costa Rica, Wang et al., 2019), and in some remote areas (e.g., polar Arctic, Rauert et al., 2018b). In other remote areas, TBP (Uganda, Wang et al., 2019) or TCEP (western Antarctic Peninsula; Wang et al., 2020) dominated the concentration profiles (Table 3). TCIPP is widely used as a foam and polymer additive since the phase-out of previously available flame retardant commercial mixtures (Dodson et al., 2012), constituting one of the OPEs of highest production (van der Veen and de Boer, 2012). TCIPP has also progressively replaced other OPEs like TCEP in many applications (Quednow and Püttmann, 2009), mainly for toxicity considerations (Sühling et al., 2016a; Wang et al., 2020). Moreover, TCIPP, as a chlorinated OPE, has a stronger persistence potential than alkyl and aryl OPEs (Reemtsma et al., 2008) and has been characterized as a persistent and mobile organic compound (Li et al., 2017; Rodgers et al., 2018).

TCIPP was also the first or second OPE in highest absolute and relative concentration in all Pyrenean mountain sites (Table 2;

Table 3
Continental atmospheric gas-phase OPE concentration ranges (pg m^{-3}) reported in the recent years, sampled using polyurethane foam passive air sampling (PUF) and high-volume active air sampling (HiVol).

Site	Sampling	TBP	TCEP	TCIPP	TDCIPP	TPHP	Reference
Remote and protected regions							
Pyrenees	PUF	0.2–3.3	BDL ^a -23	1.3–69	BDL-4.3	0.7–23 ^b	This study
Polar Arctic ^c	PUF	BDL-8.8	6–580	BDL-1400	BDL-30	BDL-250	Rauert et al. (2018b)
Uganda (protected area)	PUF	44–107	36–150	30–69	–	–	Wang et al. (2019)
W Antarctic Peninsula	HiVol	1.7–92	1.4–272	1.2–174	BDL-4.8	0.6–25	Wang et al. (2020)
Urban and other sites, including global monitoring networks							
Latin America and Caribbean ^d	PUF	BDL-2100	BDL-1924	BDL-2800	BDL-252	BDL-1475	Rauert et al. (2016), 2018a, 2018b
Asia Pacific	PUF	–	BDL-350	BDL-1570	–	BDL-115	Rauert et al. (2018a)
Europe	PUF	–	BDL-390	BDL-1170	–	BDL-65	
North America	PUF	–	BDL-430	BDL-1140	–	BDL-210	
South Africa	PUF	–	BDL-120	BDL-180	–	BDL-23	
Turkey (industrial)	PUF	–	BDL-136	214–4918	–	130–302	Kurt-Karakus et al. (2018)
Turkey (background)	PUF	–	45–112	100–385	–	66–147	
Canada (urban)	PUF	53–1030	BDL-732	98–2180	5.3–773	BDL-1120	Saini et al. (2019)
Costa Rica (rural and protected land)	PUF	162–5667	55–1392	55–396	–	–	Wang et al. (2019)
China (Tianjin)	PUF	BDL-146	BDL-53	BDL-3053	0.8–53	BDL-1278	Liang et al. (2020)
GAPS Megacities ^e	PUF	16–165	74–2660	88–10500	4.3–978	24–2100	Saini et al. (2020)
China (Dalian)	PUF	12–337	55–794	157–3045	17–1070	10–164	Wang et al. (2020)
Great Lakes	HiVol	BDL-218	BDL-423	BDL-572	BDL-42	BDL-228	Wu et al. (2020)

^a Below detection level.

^b Not including samples from Redon (see the main article).

^c Samples from Alert (NU, Canada), Barrow (AK, USA), St. Lawrence Island (AK, USA), and Ny-Ålesund (Norway).

^d Samples from Mexico, Costa Rica, Colombia, Brazil, Bolivia, Chile, and Argentina.

^e Samples from Toronto, New York, Sydney, Istanbul, London, Madrid, São Paulo, Bogotá, Ciudad de México, Santiago de Chile, Buenos Aires, Warsaw, Kolkata, Beijing, Bangkok, Tokyo, New Delhi, Lagos, and Cairo.

Figure S2), presenting the highest concentration in Llebre (1619 m). However, the sites located at higher altitudes (>2300 m) showed an OPE distribution dominated by TCEP. This compound has a lower volatilization enthalpy, 81.5 kJ mol⁻¹, than TCIPP, 84.7 kJ mol⁻¹ (Table 4), entailing lower octanol-air and air-water partition coefficients (logK_{OA} and logK_{AW}), 8.39 and -2.69, respectively, than TCIPP, 9.75 and -1.53. TCIPP therefore has a weaker tendency to remain in the gas phase than TCEP. Consequently, TCEP would be less affected by retention and accumulation on surfaces at lower temperatures and thus remain in the gas phase in greater proportion compared to TCIPP. Accordingly, a regression of TCEP/TCIPP ratios in each mountain site, excluding the locally contaminated Redon, against the reciprocal of the average temperature for the sampling periods (Fig. 2) shows a significant correlation, R² = 0.9153, p < 0.02, indicating that the colder sites contained a higher proportion of TCEP than TCIPP.

3.4. Temperature dependence

Fig. 3 shows the temperature trends of OPE concentrations in the atmospheric gas phase. All compounds except TDCIPP showed negative slopes when regressed against the reciprocal of the absolute temperature, indicating increased gas-phase concentrations at higher temperatures. TCEP, TCIPP, and TPHP presented statistically significant regressions (p < 0.05, Table 4). Contrarily, TBP and TDCIPP did not. The squared Spearman's correlation coefficients (R²) for the significant regressions were moderate, between 0.17 and 0.38 (Table 4). Note that samples below detection limits were not included in the regressions, and neither were the OPE levels from the Redon site. It must also be noted that these correlations are set in a somewhat narrow mean temperature range (-0.7 to 12.3 °C), which may be a source of uncertainty. Finally, a higher uncertainty in the low concentrations of TBP and TDCIPP compared to the other OPEs should not be excluded as a contributing factor to the lack of temperature correlations observed for these two compounds.

Similar statistically significant associations that imply higher atmospheric gas-phase OPE concentrations at higher temperatures have also been observed in some studies in sites under anthropogenic influence (Kerric et al., 2021; Saini et al., 2019b; Wong et al., 2018) which were mostly attributed to changes in primary emissions. They were also consistent with other studies showing increased OPE concentrations in the warmer seasons of the year (Ohura et al., 2006; Salamova et al., 2014b, 2016; Wang et al., 2018; Wu et al., 2020). However, no correlations with temperature were found for many OPEs in urban air in Canada (Shoeb et al., 2014) or areas receiving human inputs in the Great Lakes (Ma et al., 2021). Temperature dependences of opposite sign were observed for TBP in Canadian urban areas (Saini et al., 2019b). Concerning remote sites, a correlation between TBP concentrations and temperature was observed in the western Antarctica Peninsula but not for the other OPEs (Wang et al., 2020). The observed correlation was attributed to the inputs of an airport located at 3 km from the sampling site.

In remote high-mountain areas, located away both in distance and in altitude from primary pollutant sources, direct temperature

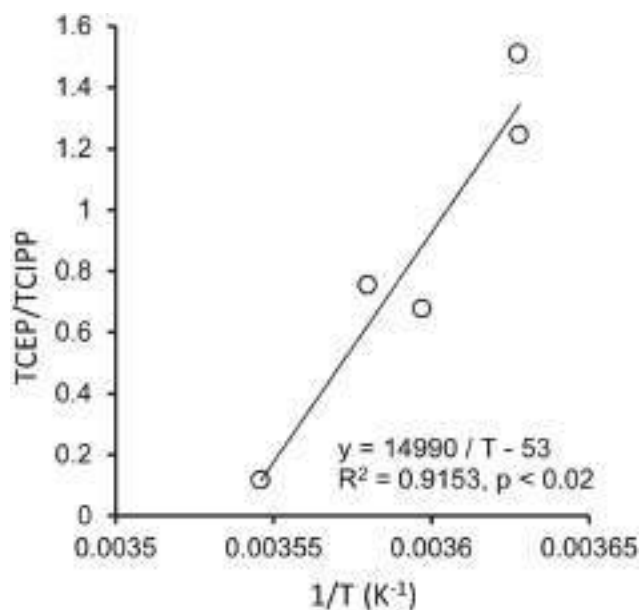


Fig. 2. Correlation of the average TCEP/TCIPP ratios in each site with average temperatures of the sampling periods.

dependences may be explained by secondary emissions (i.e., re-evaporation from surfaces at higher temperatures). However, increases in atmospheric concentrations near emission sources and advection of air masses towards the remote sampling sites cannot a priori be discarded. The slopes of the observed correlations can provide information to discriminate between these two possible options. They afford the calculation of the experimental enthalpies of vaporization, $\Delta_{\text{vap}}H$, which has been proposed to elucidate between long-range atmospheric transport and secondary volatilization in the vicinity of the sampling location because $\Delta_{\text{vap}}H$ values close to laboratory measurements are characteristic of the second option (Wania et al., 1998; Raurert et al., 2014).

Internal energies of phase change ($\Delta_{\text{vap}}U$, J mol⁻¹) were estimated from the linear regression of $\ln C_a$ (expressed on a mass per volume basis instead of partial pressure) against $1/T$ (K⁻¹) since slope = $-\Delta_{\text{vap}}U/R$ (where R is the ideal gas constant, J K⁻¹ mol⁻¹), and were transformed into enthalpies following $\Delta H = \Delta U - RT$ (Atkinson and Curthoys, 1978). The calculated enthalpy values were 93, 117, and 94 kJ mol⁻¹ for TCEP, TCIPP, and TPHP respectively (Table 4). The enthalpies of TCEP and TPHP were very close to those obtained in laboratory conditions, and that of TCIPP slightly higher, but still within the confidence interval. This agreement is consistent with a dominance of secondary sources in the control of gas-phase concentration trends with temperature.

3.5. Secondary sources

Snow, soil, vegetation, water, and deposited atmospheric particles are some of the possible secondary sources in remote areas when

Table 4

Linear regression of the natural logarithm-transformed gas-phase OPE concentrations against the reciprocal of the absolute temperature, and experimental enthalpies of phase change ($\Delta_{\text{vap}}H$) calculated from the regression slopes.

	lnC _a vs. 1/T (K ⁻¹)			Experimental enthalpies		Reference enthalpies of volatilization		
	Slope (K)	R ² (Spearman)	p ^a	$\Delta_{\text{vap}}H$ (KJ mol ⁻¹)	95% CI	$\Delta_{\text{vap}}H$ (KJ mol ⁻¹)	Standard error	Reference
TBP	-2510	0.002	0.823	-	-	80.6	±1.6	Panneerselvam et al. (2007)
TCEP	-11467	0.222	0.004	93	±58	81.5	±10	Okeme et al. (2020)
TCIPP	-14326	0.388	5E-5	117	±54	84.7	±11	Okeme et al. (2020)
TDCIPP	1625	0.021	0.407	-	-	91.2	±3.2	Okeme et al. (2020)
TPHP	-11603	0.380	1E-4	94	±36	92.8	±3.2	Okeme et al. (2020)

^a Statistically significant correlations (p < 0.05) marked in bold.

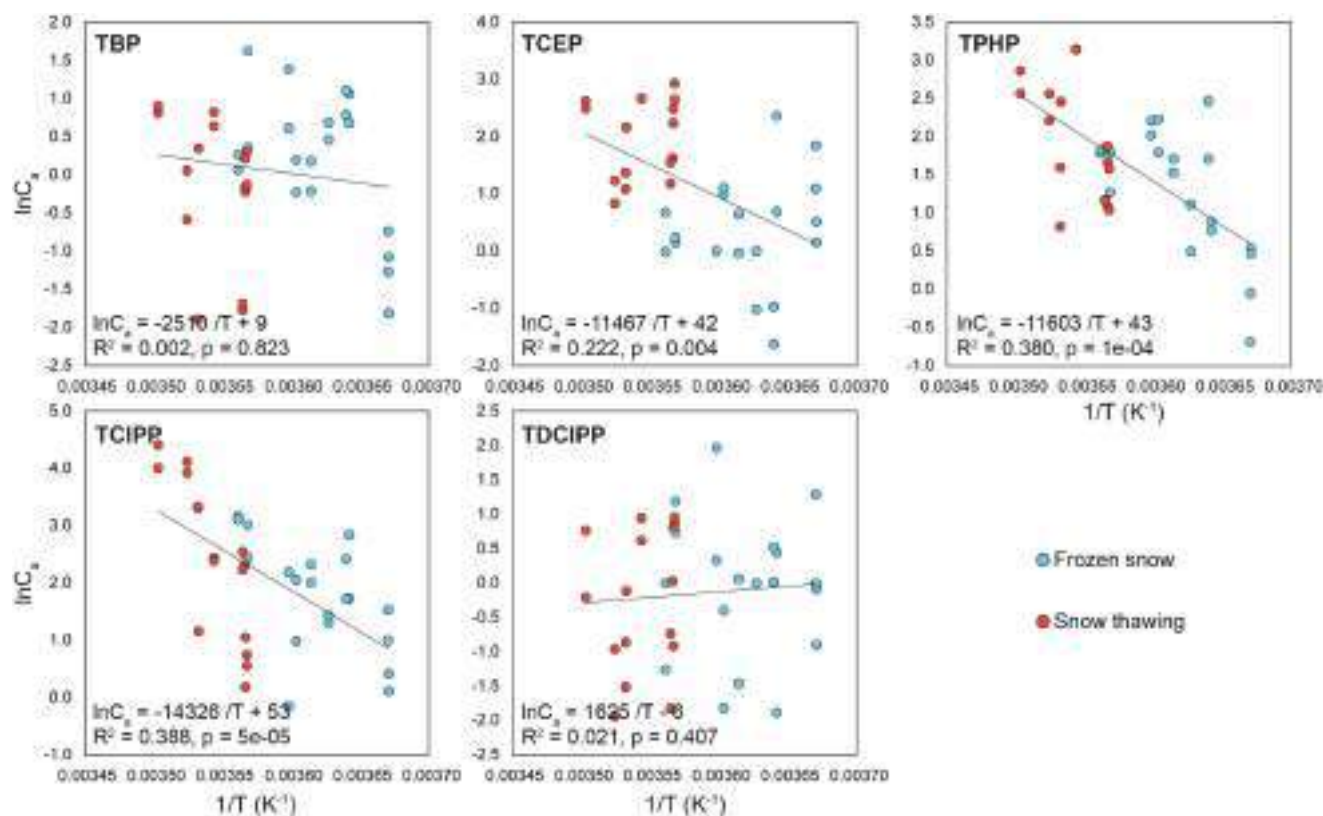


Fig. 3. Representation of the atmospheric gas-phase OPE concentrations of all air sample replicates ($\ln C_a$) against average temperature of the sampled period ($1/T$). The TPHP concentrations from Redon are not included.

significant correlations involving higher atmospheric concentrations at higher temperature are observed. Temperature trends similar to those reported in this study were attributed to volatilization of chlorinated OPEs from water bodies in the Canadian Arctic (Sühring et al., 2016a), by secondary emissions and gas-particle partitioning of TCEP, TCIPP, and TDCIPP in China (Wang et al., 2020a), and secondary TBP emissions from soil and water bodies in the Great Lakes (Ma et al., 2021). However, the high-mountain areas in the Pyrenees are covered with snow most of the year and, therefore, snow is a preliminary source to consider. In addition, the sampling sites above 2000 m (Sarradé, Redon, Dellui,

and Collada) were located above the tree line, so the vegetation was very scarce.

The snow thawing or freezing conditions of the measured concentrations are represented in Fig. 3. This information was obtained from the snow heights recorded at the Redon site throughout the studied period (Fig. 4). Samplings I and II (“frozen snow” periods) had different conditions than samplings III, IV, and V (“snow thawing” periods). Period III had practically no snow, and in IV and V the samplers were deployed after a long period of thaw. In contrast, sampling II was characterized by a large accumulation of snow, and sampling I started at

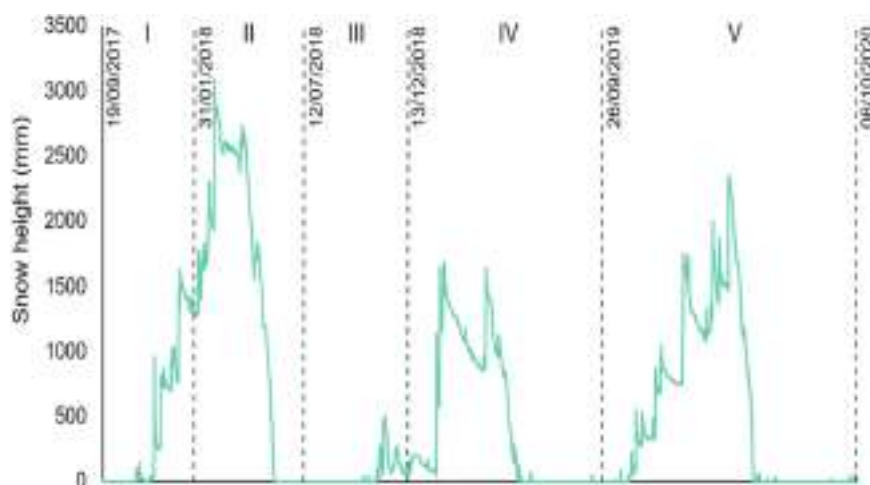


Fig. 4. Snow heights measured in Redon station during the whole sampling period.

the end of summer after a long period of potential OPE evaporation from snow and soils and ended in a period of frozen snow, hence why it was also considered a “frozen snow” period. As seen in Fig. 3, almost all measurements showing high atmospheric OPE concentrations were recorded under snowmelt conditions. The difference between measurements obtained in thawing or freezing conditions is especially clear for OPEs that showed a significant correlation with temperature. This difference suggests that the snow may have played a role as a reservoir for long-range atmospheric transported OPEs, including the fraction associated with particles, which may have been subsequently released into the atmospheric gas phase when the snow thawed and the soils were uncovered at higher temperatures.

Accumulation of OPEs in snow has been reported both in low and high elevation urban areas (Regnery and Püttmann, 2009; You et al., 2022) and in remote sites (Li et al., 2017; Xie et al., 2020). Furthermore, snow melting has been shown to be a main driver of OPE transport between environmental compartments in the Arctic (Gustavsson et al., 2019), and several studies have documented that snow can accumulate long-range atmospheric transported organic pollutants in high-mountain areas that can be released upon seasonal thawing in spring or even summer (Arellano et al., 2011, 2015, 2018; Grimalt et al., 2009).

This implies that OPEs can reach these remote mountain areas after long-range atmospheric transport, partly bound to atmospheric particles, and settle onto surfaces by means of dry and wet deposition. Most available surfaces in the studied area during low-temperature seasons are covered by snow, which may accumulate a significant portion of pollutants and subsequently release them into the gaseous phase as the temperature increases and the snow thaws. Moreover, as snow melts and uncovers soil surfaces, an important fraction of pollutants becomes trapped in soils and may also evaporate directly towards the atmospheric gas phase. Therefore, future studies should consider a broader approach by including the analysis of snow, soil, and atmospheric deposition samples that complement atmospheric measurements in remote areas.

4. Conclusions

The gas-phase concentrations of OPEs (Σ OPEs 2.2–120 pg m^{-3}) in high mountain sites (>1600 m asl) were much lower than those observed in areas under anthropogenic influence, but also than those found in some low altitude remote continental sites (Σ OPEs 4.9–2300 pg m^{-3}). The altitudinal gradient formed by the sampling locations showed a significant and progressive change in the predominant OPE distribution that implies the prevalence of TCIPP or TCEP below or above 2300 m asl, respectively. This trend is consistent with the volatilization enthalpies, $\log K_{\text{OA}}$ and $\log K_{\text{AW}}$ of these compounds, entailing a lower volatility for TCIPP, which is retained by surfaces to a greater extent at lower temperatures and thus decreasing in proportion in the gas phase relative to TCEP.

The concentrations of the OPEs, i.e., TCEP, TCIPP, and TPHP showed statistically significant dependences with temperature, being higher at warm values. These trends can be explained by the retention of these compounds in the colder periods, predominantly in snow, and release into air during snowmelt. In this respect, a good agreement was found between their vaporization enthalpies measured under laboratory conditions and the experimental values obtained from the slopes of the significant linear regressions with temperature.

Author contribution statement

Raimon M. Prats: sampling, analysis, Formal analysis, Visualization, and Writing – original draft. Barend L. van Drooge: sampling, analysis, Supervision, and Writing – review & editing. Pilar Fernandez: Supervision, Conceptualization, and Writing – review & editing. Joan O. Grimalt: Writing – review & editing, Conceptualization, and funding acquisition.

Funding support

This work was supported by the Spanish Ministry of Science and Innovation (CTM2015-71832-P and PGC2018-102288-B-I00). Raimon M. Prats also acknowledges financial support from the Spanish Ministry of Science and Innovation (BES-2016-076339).

Declaration of competing interest

The authors declare that they have no known competing financial interests or personal relationships that could have appeared to influence the work reported in this paper.

Acknowledgements

Sampling support from Alejandro G. Inarra and technical assistance from Roser Chaler are acknowledged. Part of this work was performed in the National Park of Aigüestortes i Estany de Sant Maurici, in Catalonia, with collaboration from the Department of Territory and Sustainability of the Government of Catalonia.

Appendix A. Supplementary data

Supplementary data to this article can be found online at <https://doi.org/10.1016/j.chemosphere.2021.133467>.

References

- Abdollahi, A., Eng, A., Jantunen, L.M., Ahrens, L., Shoeib, M., Parnis, J.M., Harner, T., 2017. Characterization of polyurethane foam (PUF) and sorbent impregnated PUF (SIP) disk passive air samplers for measuring organophosphate flame retardants. *Chemosphere* 167, 212–219. <https://doi.org/10.1016/j.chemosphere.2016.09.111>.
- Arellano, L., Fernandez, P., Tatosova, J., Stuchlik, E., Grimalt, J.O., 2011. Long-Range transported atmospheric pollutants in snowpacks accumulated at different altitudes in the Tatra Mountains (Slovakia). *Environ. Sci. Technol.* 45, 9268–9275. <https://doi.org/10.1021/es202111n>.
- Arellano, L., Fernández, P., Fonts, R., Rose, N.L., Nickus, U., Thies, H., Stuchlík, E., Camarero, L., Catalan, J., Grimalt, J.O., 2015. Increasing and decreasing trends of the atmospheric deposition of organochlorine compounds in European remote areas during the last decade. *Atmos. Chem. Phys.* 15, 6069–6085. <https://doi.org/10.5194/acp-15-6069-2015>.
- Arellano, L., Fernández, P., van Drooge, B.L., Rose, N.L., Nickus, U., Thies, H., Stuchlík, E., Camarero, L., Catalan, J., Grimalt, J.O., 2018. Drivers of atmospheric deposition of polycyclic aromatic hydrocarbons at European high-altitude sites. *Atmos. Chem. Phys.* 18, 16081–16097. <https://doi.org/10.5194/acp-18-16081-2018>.
- Atkinson, D., Curthoys, G., 1978. The determination of heats of adsorption by gas-solid chromatography. *J. Chem. Educ.* 55, 564–566. <https://doi.org/10.1021/ed055p564>.
- Blum, A., Behl, M., Birnbaum, L.S., Diamond, M.L., Phillips, A., Singla, V., Sipes, N.S., Stapleton, H.M., Venier, M., 2019. Organophosphate ester flame retardants: are they a regrettable substitution for polybrominated diphenyl ethers? *Environ. Sci. Technol. Lett.* 6, 638–649. <https://doi.org/10.1021/acs.estlett.9b00582>.
- Camarasa, J.G., Serra-Baldrich, E., 1992. Allergic contact dermatitis from triphenyl phosphate. *Contact Dermatitis* 26, 264–265. <https://doi.org/10.1111/J.1600-0536.1992.tb00241.x>.
- Cao, D., Lv, K., Gao, W., Fu, Jie, Wu, J., Fu, Jianjie, Wang, Y., Jiang, G., 2019. Presence and human exposure assessment of organophosphate flame retardants (OPEs) in indoor dust and air in Beijing, China. *Ecotoxicol. Environ. Saf.* 169, 383–391. <https://doi.org/10.1016/j.ecoenv.2018.11.038>.
- Castro-Jiménez, J., González-Gaya, B., Pizarro, M., Casal, P., Pizarro-Álvarez, C., Dachs, J., 2016. Organophosphate ester flame retardants and plasticizers in the global oceanic atmosphere. *Environ. Sci. Technol.* 50, 12831–12839. <https://doi.org/10.1021/acs.est.6b04344>.
- Cheng, W., Blais, J.M., Xie, Z., Liu, Y., Li, M., Sun, L., 2017. Response of polar regions to emerging organic pollutant organophosphorus esters (OPEs), a review. *Adv. Polar Sci.* 28, 13–22. <https://doi.org/10.13679/j.advps.2017.1.00013>.
- Chokwe, T.B., Abafe, O.A., Mbelu, S.P., Okonkwo, J.O., Sibali, L.L., 2020. A review of sources, fate, levels, toxicity, exposure and transformations of organophosphorus flame-retardants and plasticizers in the environment. *Emerg. Contam.* 6, 345–366. <https://doi.org/10.1021/j.emcon.2020.08.004>.
- Clark, A.E., Yoon, S., Sheesley, R.J., Usenko, S., 2017. Spatial and temporal distributions of organophosphate ester concentrations from atmospheric particulate matter samples collected across houston, TX. *Environ. Sci. Technol.* 51, 4239–4247. <https://doi.org/10.1021/acs.est.7b00115>.
- Dodson, R.E., Perovich, L.J., Covaci, A., Van den Eede, N., Ionas, A.C., Dirtu, A.C., Brody, J.G., 2012. Rudel, R.A. After the PBDE phase-out: a broad suite of flame

- retardants in repeat house dust samples from California. *Environ. Sci. Technol.* 46, 13056–13066. <https://doi.org/10.1021/ES303879N>.
- Du, J., Li, H., Xu, S., Zhou, Q., Jin, M., Tang, J., 2019. A review of organophosphorus flame retardants (OPFRs): occurrence, bioaccumulation, toxicity, and organism exposure. *Environ. Sci. Pollut. Res.* 26, 22126–22136. <https://doi.org/10.1007/s11356-019-05669-y>.
- Estellano, V.H., Pozo, K., Harner, T., Franken, M., Zaballa, M., 2008. Altitudinal and seasonal variations of persistent organic pollutants in the Bolivian Andes mountains. *Environ. Sci. Technol.* 42, 2528–2534. <https://doi.org/10.1021/es702754m>.
- Fu, J., Fu, K., Gao, K., Li, H., Xue, Q., Chen, Y., Wang, L., Shi, J., Fu, J., Zhang, Q., Zhang, A., Jiang, G., 2020. Occurrence and trophic magnification of organophosphate esters in an antarctic ecosystem: insights into the shift from legacy to emerging pollutants. *J. Hazard Mater.* 396, 122742. <https://doi.org/10.1016/j.jhazmat.2020.122742>.
- Grimalt, J.O., Fernandez, P., Quiroz, R., 2009. Input of organochlorine compounds by snow to European high mountain lakes. *Freshw. Biol.* 54, 2533–2542. <https://doi.org/10.1111/j.1365-2427.2009.02302.x>.
- Gustavsson, J., Wiberg, K., Nguyen, M.A., Josefsson, S., Laudon, H., Ahrens, L., 2019. Seasonal trends of legacy and alternative flame retardants in river water in a boreal catchment. *Sci. Total Environ.* 692, 1097–1105. <https://doi.org/10.1016/j.scitotenv.2019.07.158>.
- Han, X., Hao, Y., Li, Y., Yang, R., Wang, P., Zhang, G., Zhang, Q., Jiang, G., 2020. Occurrence and distribution of organophosphate esters in the air and soils of Ny-Ålesund and London Island, Svalbard, Arctic. *Environ. Pollut.* 263, 114495. <https://doi.org/10.1016/j.envpol.2020.114495>.
- Harner, T., 2021. 2021 V10 Template for Calculating PUF and SIP Disk Sample Air Volumes. <https://doi.org/10.13140/RG.2.1.3998.8884>.
- Harner, T., Bidleman, T.F., 1996. Measurements of octanol-air partition coefficients for polychlorinated biphenyls. *J. Chem. Eng. Data* 41, 895–899. <https://doi.org/10.1021/je960097y>.
- Harner, T., Su, K., Genualdi, S., Karpowicz, J., Ahrens, L., Mihele, C., Schuster, J., Charland, J., Narayan, J., 2013. Calibration and application of PUF disk passive air samplers for tracking polycyclic aromatic compounds. *PACs* 75, 123–128. <https://doi.org/10.1016/j.atmosenv.2013.04.012>.
- Herkert, N.J., Spak, S.N., Smith, A., Schuster, J.K., Harner, T., Martinez, A., Hombuckle, K.C., 2018. Calibration and evaluation of PUF-PAS sampling rates across the global atmospheric passive sampling (GAPS) network. *Environ. Sci. Process. Impacts* 20, 210–219. <https://doi.org/10.1039/c7em00360a>.
- Hou, R., Xu, Y., Wang, Z., 2016. Review of OPFRs in animals and humans: absorption, bioaccumulation, metabolism, and internal exposure research. *Chemosphere* 153, 78–90. <https://doi.org/10.1016/j.chemosphere.2016.03.003>.
- Kanazawa, A., Saito, I., Araki, A., Takeda, M., Ma, M., Saijo, Y., Kishi, R., 2010. Association between indoor exposure to semi-volatile organic compounds and building-related symptoms among the occupants of residential dwellings. *Indoor Air* 20, 72–84. <https://doi.org/10.1111/j.1600-0668.2009.00629.x>.
- Kerric, A., Okeme, J., Jantunen, L., Giroux, J.F., Diamond, M.L., Verreault, J., 2021. Spatial and temporal variations of halogenated flame retardants and organophosphate esters in landfill air: potential linkages with gull exposure. *Environ. Pollut.* 271, 116396. <https://doi.org/10.1016/j.envpol.2020.116396>.
- Khairy, M.A., Lohmann, R., 2019. Organophosphate flame retardants in the indoor and outdoor dust and gas-phase of Alexandria, Egypt. *Chemosphere* 220, 275–285. <https://doi.org/10.1016/j.chemosphere.2018.12.140>.
- Kurt-Karakus, P., Alegria, H., Birgul, A., Gungormus, E., Jantunen, L., 2018. Organophosphate ester (OPEs) flame retardants and plasticizers in air and soil from a highly industrialized city in Turkey. *Sci. Total Environ.* 625, 555–565. <https://doi.org/10.1016/j.scitotenv.2017.12.307>.
- Li, C., Chen, J., Xie, H., Bin, Zhao, Y., Xia, D., Xu, T., Li, X., Qiao, X., 2017. Effects of atmospheric water on -OH-initiated oxidation of organophosphate flame retardants: a DFT investigation on TCPP. *Environ. Sci. Technol.* 51, 5043–5051. <https://doi.org/10.1021/acs.est.7b00347>.
- Li, J., Xie, Z., Mi, W., Lai, S., Tian, C., Emeis, K.C., Ebinghaus, R., 2017. Organophosphate esters in air, snow, and seawater in the North Atlantic and the Arctic. *Environ. Sci. Technol.* 51, 6887–6896. <https://doi.org/10.1021/acs.est.7b01289>.
- Liang, Y., Wang, H., Yang, Q., Cao, S., Yan, C., Zhang, L., Tang, N., 2020. Spatial distribution and seasonal variations of atmospheric organophosphate esters (OPEs) in Tianjin, China based on gridded field observations. *Environ. Pollut.* 263, 114460. <https://doi.org/10.1016/j.envpol.2020.114460>.
- Liu, Y., Liggio, J., Harner, T., Jantunen, L., Shoenib, M., Li, S.M., 2014. Heterogeneous OH initiated oxidation: a possible explanation for the persistence of organophosphate flame retardants in air. *Environ. Sci. Technol.* 48, 1041–1048. <https://doi.org/10.1021/est404515k>.
- Ma, Y., Vojta, S., Becanova, J., Habtemichael, A.Z., Adelman, D.A., Muir, D., Lohmann, R., 2021. Spatial distribution and air–water exchange of organophosphate esters in the lower Great Lakes. *Environ. Pollut.* 286, 117349. <https://doi.org/10.1016/j.envpol.2021.117349>.
- Markovic, M.Z., Prokop, S., Staebler, R.M., Liggio, J., Harner, T., 2015. Evaluation of the particle infiltration efficiency of three passive samplers and the PS-1 active air sampler. *Atmos. Environ.* 112, 289–293. <https://doi.org/10.1016/j.atmosenv.2015.04.051>.
- Meeker, J.D., Stapleton, H.M., 2010. House dust concentrations or organophosphate flame retardants in relation to hormone levels and semen quality parameters. *Environ. Health Perspect.* 118, 318–323.
- Meire, R.O., Lee, S.C., Targino, A.C., Torres, J.P.M., Harner, T., 2012. Air concentrations and transport of Persistent Organic Pollutants (POPs) in mountains of southeast and southern Brazil. *Atmos. Pollut. Res.* 3, 417–425. <https://doi.org/10.5094/APR.2012.048>.
- Ohura, T., Amagai, T., Senga, Y., Fusaya, M., 2006. Organic air pollutants inside and outside residences in Shimizu, Japan: levels, sources and risks. *Sci. Total Environ.* 366, 485–499. <https://doi.org/10.1016/j.scitotenv.2005.10.005>.
- Okeme, J.O., Rodgers, T.F.M., Parnis, J.M., Diamond, M.L., Bidleman, T.F., Jantunen, L.M., 2020. Gas chromatographic estimation of vapor pressures and octanol-air partition coefficients of semivolatile organic compounds of emerging concern. *J. Chem. Eng. Data* 65, 2467–2475. <https://doi.org/10.1021/acs.jced.9b01126>.
- Panneerselvam, K., Antony, M.P., Srinivasan, T.G., Rao, P.R.V., 2007. Measurement of enthalpies of vaporization of trialkyl phosphates using correlation gas chromatography. *Thermochim. Acta* 466, 49–56. <https://doi.org/10.1016/j.tca.2007.10.007>.
- Prats, R.M., van Drooge, B.L., Fernández, P., Marco, E., Grimalt, J.O., 2021a. Changes in urban gas-phase persistent organic pollutants during the COVID-19 lockdown in Barcelona. *Front. Environ. Sci.* 9, 109. <https://doi.org/10.3389/fenvs.2021.650539>.
- Prats, R.M., van Drooge, B.L., Fernández, P., Grimalt, J.O., 2021b. Field comparison of passive polyurethane foam and active air sampling techniques for analysis of gas-phase semi-volatile organic compounds at a remote high-mountain site. *Sci. Total Environ.* 149738. <https://doi.org/10.1016/j.scitotenv.2021.149738>.
- Quednow, K., Püttmann, W., 2009. Temporal concentration changes of DEET, TCEP, terbutryn, and nonylphenols in freshwater streams of hesse, Germany: possible influence of mandatory regulations and voluntary environmental agreements. *Environ. Sci. Pollut. Res. Int.* 16, 630–640. <https://doi.org/10.1007/S11356-009-0169-6>.
- R Core Team, 2021. A Language and Environment for Statistical Computing. R Foundation for Statistical Computing, Vienna, Austria. <https://www.R-project.org>.
- Rauert, C., Harner, T., Schuster, J.K., Eng, A., Fillmann, G., Castillo, L.E., Fentanes, O., Villa Ibarra, M., Miglioranza, K.S.B., Moreno Rivadeneira, I., Pozo, K., Aristizábal Zuluaga, B.H., 2018a. Atmospheric concentrations of new persistent organic pollutants and emerging chemicals of concern in the group of Latin America and Caribbean (GRULAC) region. *Environ. Sci. Technol.* 52, 7240–7249. <https://doi.org/10.1021/acs.est.8b00995>.
- Rauert, C., Harner, T., Schuster, J.K., Quinto, K., Fillmann, G., Castillo, L.E., Fentanes, O., Ibarra, M.V., Miglioranza, K.S.B., Rivadeneira, I.M., Pozo, K., Puerta, A.P., Zuluaga, B.H.A., 2016. Towards a regional passive air sampling network and strategy for new POPs in the GRULAC region: perspectives from the GAPS Network and first results for organophosphorus flame retardants. *Sci. Total Environ.* 573, 1294–1302. <https://doi.org/10.1016/j.scitotenv.2016.06.229>.
- Rauert, C., Lazarov, B., Harrad, S., Covaci, A., Stranger, M., 2014. A review of chamber experiments for determining specific emission rates and investigating migration pathways of flame retardants. *Atmos. Environ.* 82, 44–45. <https://doi.org/10.1016/j.atmosenv.2013.10.003>.
- Rauert, C., Schuster, J.K., Eng, A., Harner, T., 2018b. Global atmospheric concentrations of brominated and chlorinated flame retardants and organophosphate esters. *Environ. Sci. Technol.* 52, 2777–2789. <https://doi.org/10.1021/acs.est.7b06239>.
- Reemtsma, T., García-López, M., Rodríguez, I., Quintana, J.B., Rodil, R., 2008. Organophosphorus flame retardants and plasticizers in water and air I. Occurrence and fate. *TRAC Trends Anal. Chem. (Reference Ed.)* 27, 727–737. <https://doi.org/10.1016/j.trac.2008.07.002>.
- Regnery, J., Püttmann, W., 2009. Organophosphorus flame retardants and plasticizers in rain and snow from middle Germany. *Clean* 37, 334–342. <https://doi.org/10.1002/clen.200900050>.
- Ren, J., Wang, X., Xue, Y., Gong, P., Joswiak, D.R., Xu, B., Yao, T., 2014. Persistent organic pollutants in mountain air of the southeastern Tibetan Plateau: seasonal variations and implications for regional cycling. *Environ. Pollut.* 194, 210–216. <https://doi.org/10.1016/j.envpol.2014.08.002>.
- Rodgers, T.F.M., Truong, J.W., Jantunen, L.M., Helm, P.A., Diamond, M.L., 2018. Organophosphate ester transport, fate, and emissions in Toronto, Canada, estimated using an updated multimedia urban model. *Environ. Sci. Technol.* 52, 12465–12474. <https://doi.org/10.1021/acs.est.8b02576>.
- Saini, A., Clarke, J., Harner, T., 2019a. Direct measurements of polyurethane foam (PUF) – air partitioning coefficients for chemicals of emerging concern capable of equilibrating in PUF disk samplers. *Chemosphere* 234, 925–930. <https://doi.org/10.1016/j.chemosphere.2019.06.134>.
- Saini, A., Clarke, J., Jariyasopit, N., Rauert, C., Schuster, J.K., Halappanavar, S., Evans, G.J., Su, Y., Harner, T., 2019b. Flame retardants in urban air: a case study in Toronto targeting distinct source sectors. *Environ. Pollut.* 247, 89–97. <https://doi.org/10.1016/j.envpol.2019.01.027>.
- Saini, A., Harner, T., Chinnadhurai, S., Schuster, J.K., Yates, A., Sweetman, A., Aristizábal-Zuluaga, B.H., Jiménez, B., Manzano, C.A., Gaga, E.O., Stevenson, G., Falandysz, J., Ma, J., Miglioranza, K.S.B., Kannan, K., Tominaga, M., Jariyasopit, N., Rojas, N.Y., Amador-Muñoz, O., Sinha, R., Alani, R., Suresh, R., Nishino, T., Shoenib, T., 2020. GAPS-megacities: a new global platform for investigating persistent organic pollutants and chemicals of emerging concern in urban air. *Environ. Pollut.* 267, 115416. <https://doi.org/10.1016/j.envpol.2020.115416>.
- Salamova, A., Hermanson, M.H., Hites, R.A., 2014a. Organophosphate and halogenated flame retardants in atmospheric particles from a European Arctic site. *Environ. Sci. Technol.* 48, 6133–6140. <https://doi.org/10.1021/es500911d>.
- Salamova, A., Ma, Y., Venier, M., Hites, R.A., 2014b. High levels of organophosphate flame retardants in the great lakes atmosphere. *Environ. Sci. Technol. Lett.* 1, 8–14. <https://doi.org/10.1021/ez400034n>.
- Salamova, A., Pevery, A.A., Venier, M., Hites, R.A., 2016. Spatial and temporal trends of particle phase organophosphate ester concentrations in the atmosphere of the great lakes. *Environ. Sci. Technol.* 50, 13249–13255. <https://doi.org/10.1021/acs.est.6b04789>.
- Shoenib, M., Ahrens, L., Jantunen, L., Harner, T., 2014. Concentrations in air of organobromine, organochlorine and organophosphate flame retardants in Toronto,

- Canada. *Atmos. Environ.* 99, 140–147. <https://doi.org/10.1016/j.atmosenv.2014.09.040>.
- Shoeb, M., Harner, T., 2002. Characterization and comparison of three passive air samplers for persistent organic pollutants. *Environ. Sci. Technol.* 36, 4142–4151. <https://doi.org/10.1021/es020635t>.
- Sühring, R., Diamond, M.L., Bernstein, S., Adams, J.K., Schuster, J.K., Fernie, K., Elliott, K., Stern, G., Jantunen, L.M., 2021. Organophosphate esters in the Canadian arctic ocean. *Environ. Sci. Technol.* 55, 304–312. <https://doi.org/10.1021/acs.est.0c04422>.
- Sühring, R., Diamond, M.L., Scheringer, M., Wong, F., Pućko, M., Stern, G., Burt, A., Hung, H., Fellin, P., Li, H., Jantunen, L.M., 2016a. Organophosphate esters in Canadian Arctic air: occurrence, levels and trends. *Environ. Sci. Technol.* 50, 7409–7415. <https://doi.org/10.1021/acs.est.6b00365>.
- Sühring, R., Wolschke, H., Diamond, M.L., Jantunen, L.M., Scheringer, M., 2016b. Distribution of organophosphate esters between the gas and particle phase-model predictions vs measured data. *Environ. Sci. Technol.* 50, 6644–6651. <https://doi.org/10.1021/acs.est.6b00199>.
- Sun, Y., De Silva, A.O., St Pierre, K.A., Muir, D.C.G., Spencer, C., Lehnerr, I., MacInnis, J.J., 2020. Glacial melt inputs of organophosphate ester flame retardants to the largest high Arctic lake. *Environ. Sci. Technol.* 54, 2734–2743. <https://doi.org/10.1021/acs.est.9b06333>.
- van der Veen, I., de Boer, J., 2012. Phosphorus flame retardants: properties, production, environmental occurrence, toxicity and analysis. *Chemosphere* 88, 1119–1153. <https://doi.org/10.1016/j.chemosphere.2012.03.067>.
- van Drooge, B.L., García, D.R., Lacorte, S., 2018. Analysis of organophosphorus flame retardants in submicron atmospheric particulate matter (PM1). *AIMS Environ. Sci.* 5, 294–304. <https://doi.org/10.3934/environsci.2018.4.294>.
- Wang, C., Wang, P., Zhao, J., Fu, M., Zhang, L., Li, Y., Yang, R., Zhu, Y., Fu, J., Zhang, Q., Jiang, G., 2020. Atmospheric organophosphate esters in the Western Antarctic Peninsula over 2014–2018: occurrence, temporal trend and source implication. *Environ. Pollut.* 267, 115428. <https://doi.org/10.1016/j.envpol.2020.115428>.
- Wang, Q., Zhao, H., Wang, Y., Xie, Q., Chen, J., Quan, X., 2017. Determination and prediction of octanol-air partition coefficients for organophosphate flame retardants. *Ecotoxicol. Environ. Saf.* 145, 283–288. <https://doi.org/10.1016/j.ecoenv.2017.07.040>.
- Wang, S., Steiniche, T., Romanak, K.A., Johnson, E., Quirós, R., Mutegeki, R., Wasserman, M.D., Venier, M., 2019. Atmospheric occurrence of legacy pesticides, current use pesticides, and flame retardants in and around protected areas in Costa Rica and Uganda. *Environ. Sci. Technol.* 53, 6171–6181. <https://doi.org/10.1021/acs.est.9b00649>.
- Wang, Y., Bao, M., Tan, F., Qu, Z., Zhang, Y., Chen, J., 2020a. Distribution of organophosphate esters between the gas phase and PM2.5 in urban Dalian, China. *Environ. Pollut.* 259, 113882. <https://doi.org/10.1016/j.envpol.2019.113882>.
- Wang, Y., Li, Z., Tan, F., Xu, Y., Zhao, H., Chen, J., 2020b. Occurrence and air-soil exchange of organophosphate flame retardants in the air and soil of Dalian, China. *Environ. Pollut.* 265, 114850. <https://doi.org/10.1016/j.envpol.2020.114850>.
- Wang, Y., Wu, X., Zhang, Q., Zhao, H., Hou, M., Xie, Q., Chen, J., 2018. Occurrence, distribution, and air-water exchange of organophosphorus flame retardants in a typical coastal area of China. *Chemosphere* 211, 335–344. <https://doi.org/10.1016/j.chemosphere.2018.07.062>.
- Wania, F., Haugen, J.E., Lei, Y.D., Mackay, D., 1998. Temperature dependence of atmospheric concentrations of semivolatile organic compounds. *Environ. Sci. Technol.* 32, 1013–1021. <https://doi.org/10.1021/es970856c>.
- Wei, G.L., Li, D.Q., Zhuo, M.N., Liao, Y.S., Xie, Z.Y., Guo, T.L., Li, J.J., Zhang, S.Y., Liang, Z.Q., 2015. Organophosphorus flame retardants and plasticizers: sources, occurrence, toxicity and human exposure. *Environ. Pollut.* 196, 29–46. <https://doi.org/10.1016/j.envpol.2014.09.012>.
- Wong, F., de Wit, C.A., Newton, S.R., 2018. Concentrations and variability of organophosphate esters, halogenated flame retardants, and polybrominated diphenyl ethers in indoor and outdoor air in Stockholm, Sweden. *Environ. Pollut.* 240, 514–522. <https://doi.org/10.1016/j.envpol.2018.04.086>.
- World Health Organization, 1998. *Environmental Health Criteria 209. Flame Retardants: Tris(chloropropyl) Phosphate and Tris(2-Chloroethyl) Phosphate*. WHO, Geneva, Switzerland. https://apps.who.int/iris/bitstream/handle/10665/42148/WHO_EH_C_209.pdf.
- Wu, Y., Venier, M., Salamova, A., 2020. Spatiotemporal variations and partitioning behavior of organophosphate esters in the Great Lakes atmosphere. *Environ. Sci. Technol.* 54, 5400–5408. <https://doi.org/10.1021/acs.est.9b07755>.
- Xie, Z., Wang, Z., Magand, O., Thollot, A., Ebinghaus, R., Mi, W., Dommergue, A., 2020. Occurrence of legacy and emerging organic contaminants in snow at Dome C in the Antarctic. *Sci. Total Environ.* 741, 140200. <https://doi.org/10.1016/j.scitotenv.2020.140200>.
- Yang, J., Zhao, Y., Li, M., Du, M., Li, X., Li, Y., 2019. A review of a class of emerging contaminants: the classification, distribution, intensity of consumption, synthesis routes, environmental effects and expectation of pollution abatement to organophosphate flame retardants (OPFRs). *Int. J. Mol. Sci.* 20, 2874. <https://doi.org/10.3390/ijms20122874>.
- You, J., Chen, Z., man, Hou, X. yu, Guo, J. song, chen, Wang C., Gao, J. min, 2022. Occurrence, potential sources and risks of organophosphate esters in the high-elevation region, Tibet, China. *Sci. Total Environ.* 806, 151348. <https://doi.org/10.1016/j.scitotenv.2021.151348>.
- Zhou, L., Hiltcher, M., Gruber, D., Pittmann, W., 2017. Organophosphate flame retardants (OPFRs) in indoor and outdoor air in the Rhine/Main area, Germany: comparison of concentrations and distribution profiles in different microenvironments. *Environ. Sci. Pollut. Res.* 24, 10992–11005. <https://doi.org/10.1007/s11356-016-6902-z>.

OCCURRENCE AND TEMPERATURE DEPENDENCE OF ATMOSPHERIC GAS-PHASE ORGANOPHOSPHATE ESTERS IN HIGH-MOUNTAIN AREAS (PYRENEES)

Raimon M. Prats, Barend L. van Drooge, Pilar Fernández, Joan O. Grimalt

*Institute of Environmental Assessment and Water Research (IDAEA-CSIC), Jordi Girona
18, 08034 Barcelona, Catalonia, Spain*

ARTICLE 3 – SUPPORTING INFORMATION

Table S3.1	Ion m/z transitions and collision energies used in GC-MS/MS.	148
Table S3.2	Mean sampling rates and standard deviations of the replicates, experimental errors, and estimated theoretical expanded uncertainties.	148
Table S3.3	Effective sampled air volumes calculated from sampling rates using two different $K_{\text{PUF-A}}-K_{\text{OA}}$ relationships in the literature.	149
Figure S3.1	Polyurethane foam passive air samplers (PUF-PAS).	150
Figure S3.2	Relative OPE composition of atmospheric and insulation material samples.	150

Table S3.1. Ion transitions (m/z) and collision energies (CE) used in GC-MS/MS (MRM mode) for the identification and quantification of target compounds and their respective recovery standards.

	Abbreviation	Quantifier m/z (CE, eV)		Qualifier m/z (CE, eV)	
Tributyl phosphate	TBP	99→81	20	99→63	38
Tris(2-chloroethyl) phosphate	TCEP	249→125	10	249→99	32
Tris(1-chloro-2-propyl) phosphate	TCIPP	125→81	29	125→99	12
Tris(1,3-dichloro-2-propyl) phosphate	TDCIPP	191→155	5	191→75	11
Triphenyl phosphate	TPHP	326→215	25	326→169	32
Tributyl phosphate-d ₁₀	TBP-d ₂₇	103→83	20	103→63	43
Tris(2-chloroethyl) phosphate-d ₁₂	TCEP-d ₁₂	261→131	9	261→131	30
Tris(1-chloro-2-propyl) phosphate-d ₁₈	TCIPP-d ₁₈	131→83	30	131→103	11
Tris(1,3-dichloro-2-propyl) phosphate-d ₁₅	TDCIPP-d ₁₅	197→160	4	197→79	12
Triphenyl phosphate-d ₁₅	TPHP-d ₁₅	341→223	26	341→243	11

Table S3.2. Mean sampling rates (R_s , m³ d⁻¹) ± standard deviations of the replicates (SD), experimental errors calculated as relative standard deviation of the replicates (RSD, %), and estimated theoretical expanded uncertainties (EU, %).

	Sampling period						Mean
		I	II	III	IV	V	
Llebreta	$R_s \pm SD$	2.7 ± 0.3	2.7 ± 0.1	2.4 ± 0.04	2.2 ± 0.7	2.0 ± 0.7	2.4 ± 0.3
	RSD	10	4.8	1.5	30	33	12
	EU	22	19	18	15	12	17
Llong	$R_s \pm SD$	3.4 ± 0.7	3.8 ± 0.7	3.7 ± 0.1	-	-	3.6 ± 0.2
	RSD	21	17	2.1	-	-	5.9
	EU	23	18	16	-	-	19
Sarradé	$R_s \pm SD$	3.5 ± 0.7	3.2 ± 0.3	3.5 ^a	3.1 ^a	2.8 ± 0.5	3.2 ± 0.3
	RSD	18	7.9	-	-	18	9.3
	EU	20	20	16	15	11	16
Redon	$R_s \pm SD$	- ^a	3.8 ± 0.1	3.2 ± 0.7	3.6 ± 0.4	4.5 ^a	3.7 ± 0.5
	RSD	-	1.8	23	12	-	15
	EU	-	16	19	15	11	15
Dellui	$R_s \pm SD$	3.7 ± 0.4	3.3 ± 0.2	3.6 ± 0.3	-	-	3.5 ± 0.2
	RSD	10	6.0	8.6	-	-	6.3
	EU	23	24	17	-	-	21
Collada	$R_s \pm SD$	3.5 ± 0.8	2.1 ± 0.1	3.0 ± 0.7	-	-	2.9 ± 0.7
	RSD	22	4.7	24	-	-	25
	EU	24	34	19	-	-	26
Mean	$R_s \pm SD$	3.4 ± 0.4	3.1 ± 0.7	3.2 ± 0.5	3.0 ± 0.7	3.1 ± 1.2	-
	RSD	12	21	15	23	40	-
	EU	22	22	18	15	11	-

^a Replicate lost or sample not collected due to extreme weather conditions.

Table S3.3. Effective sampled air volumes (m³, average of the replicates) calculated from sampling rates using two different K_{PUF-A}-K_{OA} relationships in the literature.

logK _{OA} ^c	Shoeib and Harner, 2002 ^a						Saini et al., 2019 ^b					
	logK _{PUF-A} = 0.6366 × logK _{OA(T)} - 3.1774						logK _{PUF-A} = 0.6087 × logK _{OA(T)} + 2.3821					
	TBP	TCEP	TCIPP	TDCIPP	TPHP	Mean	TBP	TCEP	TCIPP	TDCIPP	TPHP	Mean
Sampling period I												
Llebreta	302	326	357	359	359	341	353	356	359	360	360	358
Llong	391	423	462	464	464	441	457	460	465	465	465	462
Sarradé	389	426	472	475	476	448	467	471	476	477	477	474
Dellui	410	443	482	484	485	461	477	481	485	485	485	483
Collada	390	420	455	458	458	436	451	454	458	459	459	456
	376	408	446	448	448		441	445	449	449	449	
Sampling period II												
Llebreta	359	395	442	446	446	418	437	442	447	447	447	444
Llong	487	543	614	618	619	576	605	612	620	620	621	616
Sarradé	423	466	519	523	523	491	513	518	524	524	524	521
Redon	791	930	1117	1130	1132	1020	1092	1111	1134	1135	1135	1121
Dellui	460	496	538	541	541	515	533	537	542	542	542	539
Collada	309	324	341	342	343	332	339	341	343	343	343	342
	472	526	595	600	601		586	593	601	602	602	
Sampling period III												
Llebreta	297	330	374	377	378	351	370	374	379	379	379	376
Llong	429	490	574	580	581	531	565	573	582	583	583	577
Sarradé	404	460	537	544	545	498	529	537	546	546	546	541
Redon	390	432	488	492	492	459	481	487	493	493	493	489
Dellui	434	489	562	567	568	524	554	561	569	570	570	565
Collada	374	414	466	469	470	439	460	465	471	471	471	467
	388	436	500	505	506		493	499	507	507	507	
Sampling period IV												
Llebreta	478	569	705	716	718	637	691	704	720	721	722	712
Sarradé	615	744	936	951	953	840	913	932	956	957	958	943
Redon	698	835	1029	1044	1046	930	1005	1025	1048	1050	1050	1035
	597	716	890	904	906		869	887	908	910	910	
Sampling period V												
Llebreta	537	654	837	853	855	747	817	836	858	860	860	846
Sarradé	655	810	1050	1069	1072	931	1021	1046	1076	1078	1078	1060
Redon	907	1186	1650	1687	1692	1424	1587	1637	1698	1703	1703	1666
	700	883	1179	1203	1207		1142	1173	1211	1214	1214	
Mean	475	548	652	660	662		640	650	663	664	664	

^a Shoeib, M. and Harner, T. 2002. Environ. Sci. Technol. 36, 4142–4151.

^b Saini, A. et al. 2019. Chemosphere 234, 925–930.

^c logK_{OA} (25 °C) from Wang, Q. et al. 2017. Ecotoxicol. Environ. Saf. 145, 283–288.



Figure S3.1. Polyurethane foam passive air samplers (PUF-PAS) were deployed in duplicate inside of steel dome housings held 1.8 m above ground. In the picture, samplers deployed during winter 2017-2018 near lake Collada in the Catalan Pyrenees (2,453 m.a.s.l.).

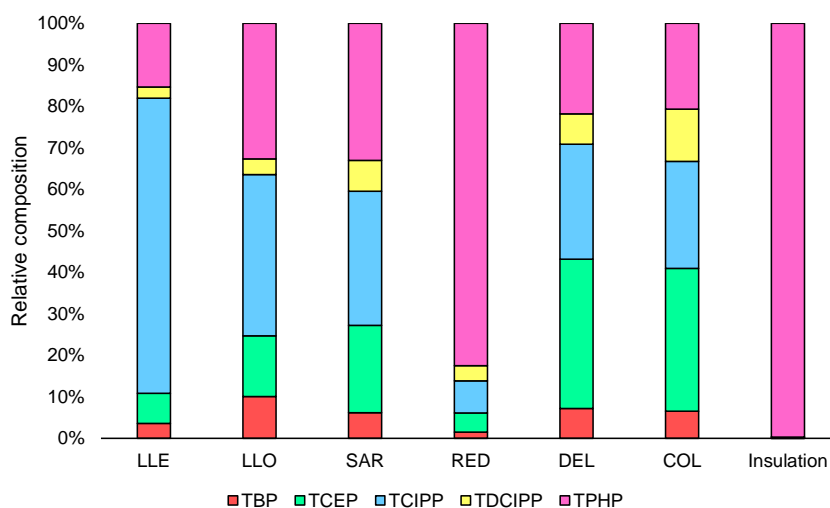


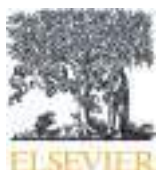
Figure S3.2. Mean relative OPE composition (%) of atmospheric samples compared to insulation material samples taken at the Redon (RED) sampling site.



Article 4

CHANGES AND DISTRIBUTION OF GAS-PHASE POLYCYCLIC AROMATIC HYDROCARBONS AND ORGANOCHLORINE COMPOUNDS IN A HIGH-MOUNTAIN GRADIENT OVER A THREE-YEAR PERIOD (PYRENEES 2017–2020)

Raimon M. Prats, Barend L. van Drooge, Pilar Fernández, Joan O. Grimalt
Science of the Total Environment 829 (2022) 154602
DOI 10.1016/j.scitotenv.2022.154602



Contents lists available at ScienceDirect

Science of the Total Environment

journal homepage: www.elsevier.com/locate/scitotenv

Changes and distribution of gas-phase polycyclic aromatic hydrocarbons and organochlorine compounds in a high-mountain gradient over a three-year period (Pyrenees, 2017–2020)

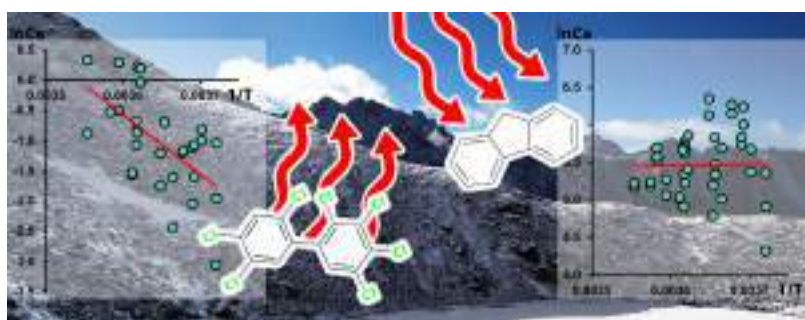
Raimon M. Prats^{*}, Barend L. van Drooge, Pilar Fernández, Joan O. Grimalt

Institute of Environmental Assessment and Water Research (IDAEA-CSIC), Jordi Girona 18, 08034 Barcelona, Catalonia, Spain

HIGHLIGHTS

- Atmospheric gas-phase concentrations of PAHs were lower than two decades ago.
- PCB and HCB concentrations were the same due to persistence and continued emissions.
- Most SVOCs showed significantly higher concentrations with increasing temperatures.
- Phase-change enthalpies suggest air advection as a main driver of concentrations.
- Less volatile SVOCs presented higher re-volatilization from secondary sources.

GRAPHICAL ABSTRACT



ARTICLE INFO

Article history:

Received 7 February 2022
 Received in revised form 11 March 2022
 Accepted 12 March 2022
 Available online 17 March 2022

Editor: Shuzhen Zhang

Keywords:

Polychlorinated biphenyls
 Hexachlorobenzene
 Passive air sampling
 Long-range atmospheric transport
 Diffuse exchange

ABSTRACT

The atmospheric gas-phase concentrations of several polychlorinated biphenyls (PCBs), polycyclic aromatic hydrocarbons (PAHs), hexachlorobenzene (HCB), and pentachlorobenzene (PeCB) were measured in six high-mountain sites in the Pyrenees (1619–2453 m). Polyurethane foam passive air samplers were used for this purpose, providing continuous records spanning over three years (2017–2020). The mean concentrations of Σ PCBs, HCB, and PeCB, $13 \pm 4 \text{ pg m}^{-3}$, $44 \pm 18 \text{ pg m}^{-3}$, and $23 \pm 20 \text{ pg m}^{-3}$, respectively, were of the order of those reported in other mountain sites and similar to those measured 20 years ago in the same area, evidencing the persistence of these compounds despite the international regulatory actions. The mean concentration of Σ PAHs was $631 \pm 238 \text{ pg m}^{-3}$, representing between two- and three-times lower values than 20 years ago in the same area, but still in the range of other mountain regions. Statistically significant increases in gas-phase concentrations at higher temperatures were observed for most compounds. The experimental phase-change pseudo-enthalpies calculated from the slopes of the regressions between the natural logarithm of the concentrations and the reciprocal of temperature were lower than the reference values for nearly all compounds. This difference suggested a main contribution of long-range atmospheric transport of the gas-phase PAH and organochlorine concentrations in this mountain area. However, the less volatile compounds such as benz[a]anthracene, PCB138, and PCB180 showed a closer similarity between experimental and laboratory enthalpies, indicating that a significant portion of the variations in concentration of these compounds originated from temperature-dependent diffusive exchange by re-volatilization from local surfaces. The concentrations found in these sentinel ecosystems demonstrate that long-range transport of organic pollutants remains a risk in remote continental environments.

^{*} Corresponding author at: Institute of Environmental Assessment and Water Research (IDAEA-CSIC).
 E-mail address: raimon.martinez@idaea.csic.es (R.M. Prats).

1. Introduction

Semi-volatile organic compounds (SVOCs) have been of concern in the last decades. They include pollutants such as polychlorobiphenyls (PCBs), hexachlorobenzene (HCB), pentachlorobenzene (PeCB), and other organochlorine compounds. Many of these were banned or severely restricted in the past because of toxic effects on humans and wildlife. PCBs have been linked to altered thyroid function (Sala et al., 2001; Chevrier et al., 2008), neurotoxicity (Ribas-Fito et al., 2003; Álvarez-Pedrerol et al., 2008; Grandjean and Landrigan, 2014), and reproductive and developmental toxicity (Ulbrich and Stahlmann, 2004 and references therein). HCB has also been associated with thyroid metabolism disruption (Llop et al., 2017; Sala et al., 2001) and thyroid cancer (Grimalt et al., 1994), as well as decreased fetal development (Lopez-Espinosa et al., 2015). Despite decades of prohibition, many organochlorines continue to be released into the environment from waste disposal and incineration, as byproducts in industrial processes, and from energy production and distribution operations, among others (EEA, 2021). Re-emission from local surfaces (e.g., particulate matter, soils, snow, vegetation) is also a relevant source of these compounds to the atmosphere (Cabrerizo et al., 2011), even in remote locations (Grimalt et al., 2009; Becker et al., 2012; Arellano et al., 2011, 2015, 2018).

Polycyclic aromatic hydrocarbons (PAHs) are SVOCs generated during the incomplete combustion of organic matter. They are currently emitted to the atmosphere from many sources, such as wood combustion, controlled field burnings, wildfires, and fossil fuel combustion in industrial processes or in residential or commercial activities (EEA, 2021). PAHs have characteristic carcinogenic and mutagenic properties (Armstrong et al., 2004; Boström et al., 2002; Wenger et al., 2009). Chronic exposure to these compounds may lead to decreased immune function, abnormalities in lung function, and damage to other organs (Abdel-Shafy and Mansour, 2016 and references therein).

SVOCs exhibit intermediate volatility and, in many cases, remarkable environmental persistence, with many of them being classified as persistent organic pollutants (POPs) by the Stockholm Convention (UNEP, 2022). Due to these characteristics, SVOCs have a unique potential for long-range atmospheric transport through condensation and re-volatilization cycles, while accumulating in remote environments due to their limited degradation or continuous input in the case of PAHs. Many of the physical-chemical properties that determine the environmental fate of SVOCs are temperature-dependent, leading to a selective buildup of pollutant concentrations in cold regions (i.e., high latitudes and mountains). In addition, these physical-chemical properties lead to selective transport processes, as described by the Global Distillation Effect (Wania and Mackay, 1993; Fernández and Grimalt, 2003; Grimalt et al., 2001).

High mountains are reference sites for understanding the global effects of these parameters and the influence of environmental variables on SVOC distributions, especially temperature along altitudinal transects. Despite previous studies in different high-mountain environments (Abdul Hussain et al., 2019; Ali et al., 2018; Choi et al., 2009; Fernández et al., 2002), the transport and distribution of these pollutants still has many aspects to be elucidated, such as the influence of local re-emission vs. transport from distant sources, association to snow, particles, and others. One important aspect for the understanding of the significance of these processes is the comparison of atmospheric concentrations over long time periods (i.e., decades). In the present study, we report concentrations of several SVOCs in the Pyrenees between 2017 and 2020. This area was previously sampled and analyzed in 1996–1998 and 2000–2002. Thus, the present study provides a comparison of data in periods 21 and 17 years apart, respectively. To the best of our knowledge, there is no other remote high-mountain site where atmospheric pollutant concentrations have been studied over such long time periods.

The assessment of atmospheric pollution in remote locations involves great difficulties, such as limited accessibility, reduced capacity for transportation and installation of sampling equipment, harsh weather conditions, lack of access to power supply, and thus costly sampling campaigns.

Polyurethane foam passive air samplers (PUF-PASs) offer a way to overcome many of these challenges. They have been used over the past two decades to monitor PAHs, organochlorine compounds, and pesticides in remote locations and mountainous regions (e.g., Abdul Hussain et al., 2019; Daly et al., 2007; Li et al., 2012; Ren et al., 2014). Accordingly, we present a study of atmospheric gas-phase concentrations of several of the aforementioned SVOCs over a three-year period (September 2017–October 2020) in a remote high-mountain area in the Pyrenees mountain range. The PAS-PUFs were deployed during five sampling periods at six sites spanning an altitudinal gradient between 1619 and 2453 m above sea level (asl) and a maximum planar projection distance from each other of 17.5 km.

Therefore, the temperature-dependent concentration trends have been studied with limited interference from other variables, as all sites are probably under the same input sources, long-range atmospheric transport, and meteorological conditions. The dominance of primary emission or secondary sources (re-emission from surfaces) of pollutants in the atmospheric gas phase, including possible differences between compound groups, has been related to the physical-chemical properties of the compounds. Finally, the comparison of concentrations in the present study with those measured some two decades ago provides a benchmark test for the effects of ban regulations in remote regions, which in turn provides guidelines for the overall decrease of exposure to these compounds in the environment. In this sense, the use of PAS-PUF devices allows continuous sampling over long periods, offering a more complete evaluation of SVOC concentrations in the mountain atmosphere than active sampling techniques at limited time intervals.

2. Materials and methods

2.1. Sampling

The studied area comprises six remote high-mountain sites between 1619 and 2453 m asl in a European Union's Natura 2000 protected area in the Central Pyrenees. They were located next to alpine lakes from Val d'Aran and the National Park of Aiguestortes i Estany de Sant Maurici (Fig. 1). A total of 43 atmospheric gas-phase samples were obtained using polyurethane foam passive air samplers (PUF-PAS) in five sampling periods between September 2017 and October 2020: I (09/17–01/18), II (02/18–07/18), III (07/18–12/18), IV (12/18–09/19), and V (09/19–10/20). Further site information, specific deployment and retrieval dates, and sampling durations are included in Table S1 along with mean air temperatures registered in situ using Tinytag Plus 2 data loggers (Gemini Data Loggers, Chichester, United Kingdom). Complementary meteorological data obtained from the Catalan Meteorological Service network of automatic weather stations has been summarized in Table S2.

The PUF-PAS configuration used, assessment of its performance in high mountains, and sampling and procedure details have been described elsewhere (Prats et al., 2022a). Briefly, PUF disks (14 cm diameter, 1.35 cm thickness, 369.5 cm² surface area, 0.021 g cm⁻³ density, 0.00567 m effective film thickness) (Techno Spec, Barcelona, Catalonia, Spain) were deployed in duplicate at 1.8 m above ground inside dome-shaped, stainless steel housings (Fig. S1). They were pre-conditioned by rinsing with distilled water and acetone and extracted by Soxhlet with acetone and hexane for 24 h each (all solvents from Merck, Darmstadt, Germany). They were further extracted with hexane for 8 h, dried under vacuum, wrapped in pre-cleaned aluminum foil, sealed airtight inside PET/LLDPE bags (Kapak Corporation, St Louis Park, MI, USA), and stored and transported at -20 °C. Upon deployment, both samplers and blanks were spiked with a mixture of Performance Reference Compounds (PRCs, sometimes called Depuration Compounds) containing polychlorinated biphenyl (PCB) congeners 3, 9, 15, 32 (all ¹³C labeled), 107, and 198 (Cambridge Isotope Laboratories, Tewksbury, MA, USA). The blanks were stored at -20 °C for the duration of the respective sampling periods, and then transported and stored along with the exposed PUF-PASs after their retrieval until extraction.

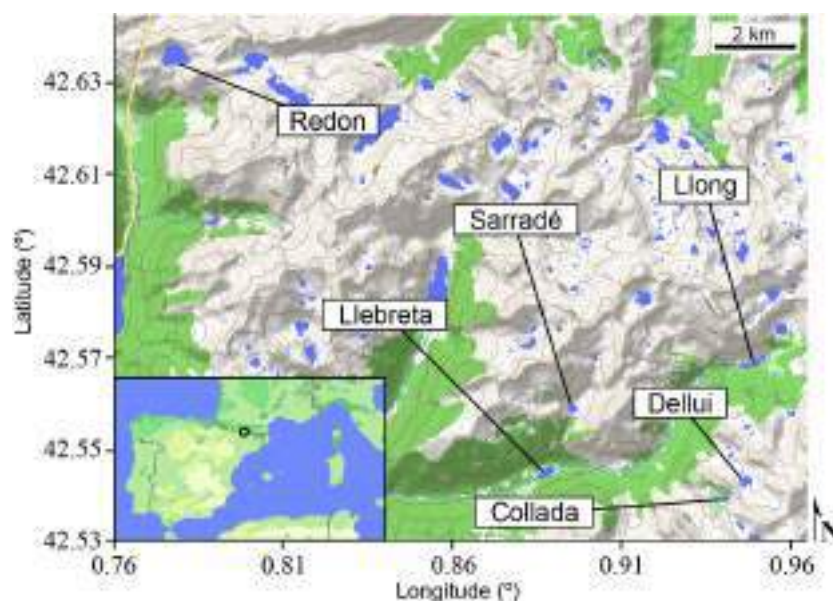


Fig. 1. Area of study and location of the six sampling sites, next to alpine lakes encompassing altitudes between 1619 and 2453 m asl.

2.2. Extraction and clean-up

The PUF-PASs and blanks were extracted for 8 h with hexane (Merck) after being spiked with a mixture of recovery standards containing 1,2,4,5-tetrabromobenzene (TBB), PCB209 (Dr. Ehrenstorfer, Augsburg, Germany), fluorene- d_{10} , phenanthrene- d_{10} , fluoranthene- d_{10} , pyrene- d_{10} , benz[*a*]anthracene- d_{12} , and chrysene- d_{12} (National Institute of Standards and Technology, Gaithersburg, MD, USA). The extracts were concentrated to 2 mL by vacuum rotary evaporation and then to 0.5 mL under a gentle nitrogen gas stream. An aliquot of 10 μ L of extract was cleaned-up and fractionated by HPLC using an Agilent 1200 Series system (Agilent Technologies, Santa Clara, CA, USA) with a preparative fraction collector and a Tracer Excel 120 SI HPLC silica column (25 cm \times 3 μ m \times 0.46 cm i.d.) (Teknokroma, Sant Cugat del Vallès, Catalonia, Spain). The elution was performed at a flow rate of 0.5 mL min^{-1} with a solvent composition of 100% hexane between 0 and 8 min, then linearly changed to 20% dichloromethane at 15 min, and maintained at this last composition for 5 more min. A first fraction containing the organochlorine compounds (PCBs, PeCB, and HCB) was collected between 8 and 15 min, and a second one containing the PAHs was collected between 15 and 20 min. These fractions were concentrated to 50 μ L under a nitrogen gas stream.

2.3. Instrumental analysis

PAHs and organochlorine compounds were analyzed by gas chromatography coupled to a single quadrupole mass spectrometer (GC-MS) (Thermo Trace GC Ultra-DSQ II, Thermo Fisher Scientific, Waltham, MA, USA). The extracts were injected into a 60 m \times 0.25 mm i.d. \times 25 μ m HP-5MS fused capillary column (Agilent Technologies) in electron impact mode (70 eV). The injector, ion source, quadrupole, and transfer line temperatures were 280, 250, 150, and 270 $^{\circ}\text{C}$, respectively. Helium was used as carrier gas (1 mL min^{-1}). The oven program started at 90 $^{\circ}\text{C}$ and was held for 1 min, then increased to 150 $^{\circ}\text{C}$ at 10 $^{\circ}\text{C} \text{ min}^{-1}$ and to 320 $^{\circ}\text{C}$ at 6 $^{\circ}\text{C} \text{ min}^{-1}$, finishing with a holding time of 20 min. The following compounds were targeted and identified in SIM mode by retention time and m/z ratio (Table S3): PAHs fluorene (Flu), phenanthrene (Phe), fluoranthene (Flu), pyrene (Pyr), benz[*a*]anthracene (B[*a*]ant), and chrysene + triphenylene (Chr + Triph); PCB congeners 28, 52, 101, 118, 138, 153, and 180; and HCB and PeCB.

2.4. Quality control and assurance

The performance of the PUF-PAS configuration used in high mountains has been described elsewhere (Prats et al., 2022a). Multiple field and procedural blanks were obtained for each sampling period. Blank PUFs were pre-cleaned, stored, transported, extracted, and analyzed with the rest of the samples. Average blank levels were less than 11.2% of the average amounts of compound per sampler and were subtracted from the amounts detected in the samples. They were also spiked with PRCs during the deployment of each campaign and then used for the calculation of sampling rates. An internal standard calibration method was used for the quantification, accounting for procedural recoveries and instrumental variability. The recoveries were between $73 \pm 24\%$ and $103 \pm 18\%$ for deuterated PAHs, $66 \pm 9\%$ for TBB, and $90 \pm 28\%$ for PCB209. Limits of quantification ($10 \times s/n$) were between 0.5 and 2.5 pg in column, or 25 to 125 pg sampler $^{-1}$. For average PAS effective sampled volumes, they were 0.1–0.4 pg m^{-3} .

2.5. Effective sampled air volumes

The calculation of effective sampled air volumes (V_A , m^3) was performed using a degree-of-equilibrium model based on the sampler-specific calibration with PRCs that accounts for all phases of pollutant uptake (i.e., linear, curvilinear, and equilibrium) (Harner et al., 2013):

$$V_A = V_{\text{PUF}} K'_{\text{PUF-A}} \left[1 - \exp \left(\frac{-k_A t}{K'_{\text{PUF-A}} D_{\text{film}}} \right) \right] \quad (1)$$

where $K'_{\text{PUF-A}}$ (unitless) is the sampler-air partition coefficient of each studied compound ($K_{\text{PUF-A}}$, $\text{m}^3 \text{ g}^{-1}$) multiplied by the PUF density, k_A (m d^{-1}) is the air-side mass transfer coefficient, t (d) is the duration of the sampling campaign, V_{PUF} (m^3) is the volume of the PUF disk, and D_{film} (m) is its effective film thickness. $K_{\text{PUF-A}}$ were calculated as $\log K_{\text{PUF-A}} = 0.6366 \times \log K_{\text{OA(T)}} - 3.1774$ (Shoeb and Harner, 2002) using octanol-air partition coefficients at the average temperature of each sampling campaign (Table S1) (Chen et al., 2016; Harner, 2021; Odabasi et al., 2006). The calculation of the expression between brackets in Eq. (1) results in a value between 0 and 1 known as degree of equilibrium (DEQ), which measures the degree of attainment of equilibrium conditions determined for each compound and each individual sampler. Compounds with $\text{DEQ} = 1$ after exposure

are in equilibrium conditions between the atmospheric gas phase and the PUF-PAS, while compounds with $DEQ < 1$ are still in the net uptake phase at the moment of retrieval. Thus, by not assuming the uptake stage of each compound at each location, the V_A calculation yields air volumes from which period average concentrations can be obtained. The accuracy of these measurements was tested in the studied area against active air sampling methods (Prats et al., 2022a).

The PRC calibration of each sampler was used to determine the average k_A at each site and for each period as follows:

$$k_A = \frac{R_S}{A_{PUF}} = \frac{\ln(C/C_0) K'_{PUF-A} D_{film}}{t} \quad (2)$$

where R_S is the sampling rate ($m^3 d^{-1}$), A_{PUF} (m^2) is the total surface area of the PUF disk, and C/C_0 is the ratio between the recovery-corrected amounts of PRC in exposed samplers and non-exposed blanks. Here, K'_{PUF-A} is the partition coefficient of the PRCs calculated from their temperature-corrected K_{OA} (Harner, 2021).

The theoretical uncertainties of the sampling rates were estimated from the propagation of the error in the variables involved in Eq. (2) as explained elsewhere (Prats et al., 2022b), which has been summarized in Text S1 of the Supplementary Material.

2.6. Statistical analysis

A Multivariate Curve Resolution-Alternating Least Squares (MCR-ALS) under non-negativity constraint method was applied for the analysis of pollutant source contributions in MATLAB R2021a (MathWorks, Natick, MA, USA). Briefly, the model is based on a bilinear decomposition of the original matrix (Jaumot et al., 2005; Tauler, 1995; Tauler et al., 1995): $D(I \times J) = U(I \times N) V^T(N \times J) + E(I \times J)$, where D is the original data array (I rows or samples, J columns or compounds), U is the matrix of scores of dimensions $I \times N$ (N reduced number of components), V^T is the matrix of loadings (dimension $N \times J$), and E is the matrix of residuals (not modeled by the N components). A data matrix containing scaled (normalized by standard deviation) compound concentrations for the different samples ($n = 33$, including replicates from the first three complete sampling campaigns) was fed into the model, which resolved different components described by their loadings (compound profiles) and their contribution to each sample (scores).

3. Results and discussion

3.1. Sampling rates and effective sampled volumes

The average sampling rates calculated for every sampling period at each site are summarized in Table S4. The rates varied between 2.1 and 4.5 $m^3 d^{-1}$, with mean \pm standard deviation (sd) values for each site across sampling periods between 2.5 ± 0.2 and $3.7 \pm 0.5 m^3 d^{-1}$. These rates are in the range of the 3 to 4 $m^3 d^{-1}$ rates typically reported for the PUF-PAS configuration used in this study (Herkert et al., 2018; Pozo et al., 2009), confirming that harsh environmental conditions such as high wind speeds (Table S2) had limited effect on the sampling rates with the sampler configuration used here (Prats et al., 2022a). The relative standard deviations (RSD) of the sampling rate from the duplicate samplers at each site and period ranged between 1.5 and 24.6% (Table S4). Average RSDs at each site were below 15%, with only one site up to 25%. To contrast these values, theoretical expanded uncertainties (EU) were estimated for each pair of replicates. They depend on the errors involved in quantifying PRC amounts, K_{OA} values, and temperature correction relationships, among other sources of uncertainty (Text S1). EUs ranged from 5.4 to 17.1% (Table S4), which is in very good agreement with the experimental RSDs. This indicates that the experimental errors outside of those inherent to the calibration method were well constrained and did not significantly affect the resulting sampling rates.

The different compounds reached varying degrees of equilibrium (DEQ) (Table S5), depending on the exposure time and meteorological conditions at each site. Fle and PeCB, the most volatile among the analyzed pollutants, reached almost complete uptake equilibrium, followed by Phe at 89% and HCB at 76%, on average. The rest of PAHs and PCBs remained much closer to the linear uptake phase, with lower DEQs between 7 and 36%, due to their lower volatilities. Samples from periods IV and V presented higher DEQs due to their longer durations, but only by up to a difference of 20–30% with respect to the shorter ones. Mean effective sampled volumes calculated using Eq. 1 ranged between 51 and 1123 m^3 , with averages per compound between 60 and 634 m^3 (Table S5).

It must be noted that two of the sampling campaigns (IV and V) were exceptionally long (Table S1) due to logistics and accessibility conditions. However, this had limited effect on the DEQs reached by the studied compounds. The more volatile SVOCs that reached equilibrium conditions between sampler and air in the shortest periods (e.g., Fle, Phe, PeCB) did so again in these longer periods, while less volatile compounds either remained in the linear uptake stage (e.g., B[a]ant, Chr + TriPh, PCB180) or started to transition towards curvilinear uptake (e.g., PCB28, Flu, Pyr) (Table S5). But regardless of the uptake phase reached, the compound- and site-specific DEQ estimation allowed for an accurate determination of period average concentrations.

3.2. Gas-phase concentrations

The mean gas-phase concentrations of the studied compounds by sampling site and period are shown in Table 1. The average concentrations of each pair of replicate samples can be found in Table S6.

3.2.1. PAHs

The mean \pm sd of the sum of gas-phase PAH concentrations (Σ PAH) was $631 \pm 238 \text{ pg m}^{-3}$, ranging between 409 ± 208 and $764 \pm 201 \text{ pg m}^{-3}$ in different sites and between 495 ± 233 and $884 \pm 203 \text{ pg m}^{-3}$ in different periods (Table 1). Phe ($49 \pm 7\%$, with concentrations between 81 and 588 pg m^{-3}) and Fle ($41 \pm 9\%$, between 75 and 571 pg m^{-3}) were the dominant compounds, followed by Flu ($6 \pm 2\%$) and Pyr ($3 \pm 2\%$). B[a]ant, Chr and TriPh weighed much less in the relative PAH composition as expected from their lower volatility and greater tendency to partially adhere to the atmospheric particle phase. Hence, the less volatile PAHs (i.e., more than five ring PAHs) were not detected in the PUF-PAS. The gas-phase concentrations of PAHs reported during the last two decades in other high-mountain areas all over the world are shown in Table S7. Direct comparisons can be misleading since PAH concentrations are not always reported for individual compounds and total PAH amounts are calculated as the sum of a varying number of compounds. Still, the Σ PAH concentrations of the current study was generally in the range of those reported in the Rocky Mountains (Choi et al., 2009), in mountainous areas of national parks in Brazil (Meire et al., 2019), and in several mountains in Canada (Abdul Hussain et al., 2019). Conversely, they were slightly lower than those found in Mauna Loa (Zhang et al., 2017) and in the Nyainqêntanglha mountains, in the Tibetan Plateau (Ren et al., 2017), and up to one or two orders of magnitude lower than those from the Tibetan Plateau (Jin et al., 2020) and the Western Hubei Mountain in China (Hu et al., 2021). For reference, both lower (58 pg m^{-3}) and higher (2.4–31 ng m^{-3}) Σ_{9-15} PAH concentrations were observed in the atmospheric gas phase of the Arctic and Antarctica (Cao et al., 2018; Ding et al., 2007; Na et al., 2020; Wang et al., 2013).

Comparison of the present PAH concentrations, 631 pg m^{-3} (Table 1), with those measured in the same area two decades ago, 1690 pg m^{-3} in 1996–1997 (Fernández et al., 2002) and 1441 pg m^{-3} in 2000–2002 (Van Drooge et al., 2010), show a decrease of two to three times (Table S7). However, comparing only the Σ PAH observed at the Estanh Redon (764 pg m^{-3} , Table 1), which is the same location studied in the aforementioned reports, Σ PAH was half of the values reported twenty years ago. It must be noted that in the present study the observed concentrations correspond to the average values over long deployment periods

Table 1
Means and standard deviations of gas-phase atmospheric concentrations of PAHs, PCBs, PeCB, and HCB from the six high-mountain sites studied in the Pyrenees.

	Overall mean (pg m ⁻³)	Mean concentration by site (pg m ⁻³)						Mean concentration by period (pg m ⁻³)				
		Llebretra	Llong	Sarradé	Redon	Dellui	Collada	I	II	III	IV	V
Fle	261 ± 118	221 ± 66	299 ± 164	288 ± 158	266 ± 60	296 ± 141	211 ± 117	421 ± 100	171 ± 72	229 ± 60	190 ± 38	296 ± 27
Phe	306 ± 120	309 ± 43	317 ± 126	367 ± 107	400 ± 130	238 ± 110	167 ± 81	389 ± 93	274 ± 150	277 ± 136	298 ± 31	288 ± 14
Flu	41 ± 21	46 ± 6	34 ± 14	48 ± 21	61 ± 29	28 ± 13	17 ± 8	49 ± 17	31 ± 19	41 ± 31	46 ± 8	41 ± 10
Pyr	18 ± 12	25 ± 16	14 ± 5	16 ± 8	25 ± 14	12 ± 6	12 ± 8	18 ± 6	12 ± 7	28 ± 18	20 ± 4	10 ± 7
B[a]ant	0.70 ± 0.58	1.7 ± 0.5	0.52 ± 0.18	0.57 ± 0.15	0.83 ± 0.36	0.31 ± 0.08	0.29 ± 0.18	0.60 ± 0.41	0.70 ± 0.56	0.81 ± 0.75	n.d. ^a	n.d.
Chr + TriPh	5.3 ± 4.4	5.0 ± 3.0	4.4 ± 2.2	5.1 ± 4.2	10 ± 7	3.9 ± 2.8	2.6 ± 0.9	5.7 ± 1.6	6.2 ± 3.0	6.1 ± 7.3	4.4 ± 3.4	1.6 ± 1.9
ΣPAH	631 ± 238	607 ± 101	669 ± 297	724 ± 272	764 ± 201	578 ± 261	409 ± 208	884 ± 203	495 ± 233	582 ± 214	558 ± 69	636 ± 54
PCB28	2.4 ± 1.2	2.1 ± 1.0	3.0 ± 1.5	2.8 ± 0.5	3.2 ± 2.2	1.6 ± 0.6	2.2 ± 0.9	1.7 ± 0.6	2.7 ± 1.3	2.7 ± 1.3	^b	-
PCB52	1.8 ± 0.8	1.4 ± 0.3	1.5 ± 0.6	2.7 ± 1.1	2.4 ± 0.5	1.3 ± 0.2	1.6 ± 0.7	1.3 ± 0.4	2.2 ± 0.9	1.7 ± 0.7	-	-
PCB101	2.7 ± 1.1	2.9 ± 0.8	2.5 ± 0.6	3.4 ± 1.5	4.3 ± 0.5	1.8 ± 0.5	2.0 ± 0.6	1.8 ± 0.5	3.2 ± 1.2	3.0 ± 1.0	-	-
PCB118	2.2 ± 0.9	2.3 ± 1.3	2.0 ± 0.8	2.1 ± 0.9	2.3 ± 0.3	2.1 ± 0.9	2.1 ± 0.9	1.7 ± 0.5	1.8 ± 0.7	2.9 ± 0.9	-	-
PCB153	1.6 ± 0.6	1.8 ± 0.5	1.4 ± 0.3	2.2 ± 1.1	2.0 ± 0.4	1.3 ± 0.3	1.2 ± 0.4	1.4 ± 0.2	1.8 ± 0.9	1.7 ± 0.4	-	-
PCB138	2.2 ± 1.2	2.5 ± 1.4	1.9 ± 0.8	2.4 ± 1.2	2.9 ± 0.4	1.9 ± 1.2	1.7 ± 1.6	1.2 ± 0.3	1.9 ± 0.9	3.4 ± 0.9	-	-
PCB180	0.47 ± 0.36	0.52 ± 0.44	0.47 ± 0.46	0.41 ± 0.17	0.74 ± 0.41	0.31 ± 0.13	0.43 ± 0.48	0.29 ± 0.10	0.28 ± 0.16	0.82 ± 0.41	-	-
ΣPCB	13 ± 4	14 ± 4	13 ± 3	16 ± 5	18 ± 3	10 ± 3	11 ± 4	9.5 ± 1.8	14 ± 4	16 ± 4	-	-
PeCB	23 ± 20	19 ± 10	25 ± 20	20 ± 16	23 ± 19	29 ± 28	27 ± 30	16 ± 4	8.0 ± 1.5	51 ± 15	16 ± 7	16 ± 3
HCB	44 ± 18	40 ± 15	45 ± 16	40 ± 10	38 ± 17	60 ± 20	43 ± 31	42 ± 16	35 ± 7	65 ± 19	31 ± 5	31 ± 7

^a Not detected above detection limits or blank levels.

^b PCB concentrations were only measured in sampling periods I-III.

(129–376 days; Table S1) whereas the previous results were obtained with active sampling over short periods. This difference generates some uncertainty when comparing the data from these current and past samplings. Furthermore, the seasonal behavior and partially natural origin of PAHs (i.e., increased emissions in colder seasons, wildfires, etc.) are factors that may influence the observed levels at any given time, which also complicates the assessment of the evolution of concentrations in the absence of continuous monitoring in the past. Still, the PAH concentrations that we observed were precisely half of those in the mid-to-late 1990s, which matches the overall decrease of 53% in total PAH emissions recorded in Europe between 1990 and 2019 (EEA, 2021). Furthermore, these results are also in line with the decrease observed in average PAH deposition fluxes at Estanh Redon between 1997 and 2006 (0.05 μg m⁻² d⁻¹ to 0.02 μg m⁻² d⁻¹, respectively) (Arellano et al., 2018).

3.2.2. PCBs

PCB concentrations were only determined for the first three sampling periods. The mean ± sd sum of PCB concentrations (ΣPCB) was 13 ± 4 pg m⁻³, ranging between 10 ± 3 and 18 ± 3 pg m⁻³ in different sites, and between 9.5 ± 1.8 and 16 ± 4 pg m⁻³ in different periods (Table 1, Table S6). The relative PCB composition was much more homogenous than that of PAHs, with all congeners accounting for 12 to 20% of the sum of all PCBs, except for the least volatile PCB180 at 3 ± 2%. Individual congener concentrations were between 0.7 and 5.6 pg m⁻³, with only PCB180 showing lower values between 0.3 and 0.7 pg m⁻³. Like PAHs, total PCB concentrations in the literature encompass different numbers of congeners, so comparisons should be made with care (Table S7). Still, the average ΣPCB concentrations of the present study are similar to those from other high-mountain sites in Canada (Abdul Hussain et al., 2019), slightly higher than in the Bolivian Andes (Estellano et al., 2008), Mt. Everest (Wang et al., 2010), and the Tibetan Plateau (Gong et al., 2019; Ren et al., 2017, 2014), and lower than in the Slovakian High Tatras (Van Drooge et al., 2004), Brazilian mountains (Meire et al., 2012), and Lower Himalaya (Riaz et al., 2021). For reference, the sum of the seven PCB congeners considered in this study was reported in the atmospheric gas phases of the Arctic and Antarctica at both lower and somewhat higher levels (0.5–26 pg m⁻³) (Cabrerizo et al., 2018; Hao et al., 2019; Wong et al., 2021; Wu et al., 2020).

The mean ΣPCB of all lakes (13 pg m⁻³, Table 1) was lower than those measured in the same area in the past (averaging approximately 21 pg m⁻³, ranging from 10 to 43 pg m⁻³) (Van Drooge et al., 2005; Van Drooge et al., 2004). However, the mean ΣPCB at Estanh Redon, the same site sampled in these previous studies, was 18 pg m⁻³ (Table 1), pointing at a minimal or nonexistent decrease in atmospheric PCB concentrations over the past

two decades. This result contrasts with the 73% decrease in PCB emissions in Europe in recent decades (EEA, 2021). Although this reduction was somewhat gradual (from over 4500 kg of overall emissions in Europe in 1990 to over 2500 kg in 2002, to remain generally stable at around 1500 kg between 2013 and 2019), the lack of noticeable reductions in atmospheric concentrations of PCBs in a remote area away from any local sources such as urban areas, agricultural fields, and anthropogenic influence highlights the persistence of these organochlorine compounds in the environment. Other studies performed at the same site even noted an increase in PCB deposition fluxes over a decade of measurements (Arellano et al., 2015).

3.2.3. Hexachlorobenzene and pentachlorobenzene

The mean ± sd HCB concentration was 44 ± 18 pg m⁻³, ranging from 17 to 90 pg m⁻³ (Tables 1 and S6). Average HCB concentrations remained fairly stable across sites (38–60 pg m⁻³) and periods (31–65 pg m⁻³). The mean ± sd PeCB concentration was 23 ± 20 pg m⁻³, ranging from 5.3 to 69 pg m⁻³. The site averages showed limited variation (19–29 pg m⁻³), but greater differences were observed across periods (8–51 pg m⁻³). The HCB concentrations of the present study were in the range of those reported in other high-mountain areas (Table S7), e.g., the Rocky Mountains (Daly et al., 2007), the Shergyla Mountain in the Tibetan Plateau (Zhu et al., 2014), and Serra do Mar in Brazil (Guida et al., 2018), but they were two to three times lower than in the Western Hubei Mountain in China (Qu et al., 2015), the Alps (Kirchner et al., 2016), and Mauna Loa in Hawaii (Zhang et al., 2017), and between fivefold and up to two orders of magnitude higher than in other mountain sites in the Himalayas and the Tibetan Plateau (Ali et al., 2018; Riaz et al., 2021; Sheng et al., 2013; Ullah et al., 2019). For reference, HCB was found at similar concentrations in the Arctic (6–78 pg m⁻³) and Antarctic (BDL–61 pg m⁻³) atmospheric gas phases (Bidleman et al., 1993; Cabrerizo et al., 2018; Dickhut et al., 2004; Galbán-Malagón et al., 2013a and Galbán-Malagón et al., 2013b; Su et al., 2006; Wong et al., 2021), but also at higher (129–222 pg m⁻³) and lower (2.6 pg m⁻³) concentrations (Hao et al., 2019; Wu et al., 2020).

PeCB atmospheric concentrations have been scarcely reported in high-mountain areas. The present results are very similar to those found in the Tibetan Plateau (mean of 23 pg m⁻³, ranging from 14 to 62 pg m⁻³) (Zhu et al., 2014), but somewhat lower than in multiple sites across North America including the Rocky Mountains (mean of 45 pg m⁻³, from 17 to 138 pg m⁻³) (Shen et al., 2005) and in the Alps (means from 75.9 to 96.0 pg m⁻³, ranging from 14.3 to 126 pg m⁻³) (Kirchner et al., 2016), although the latter also included PeCB in the particle phase.

The HCB gas-phase concentrations (44 ± 18 pg m⁻³ all samples, 38 ± 17 pg m⁻³ only in Estanh Redon, Table 1) were very similar to those

reported 20 years ago in the same site (49 pg m^{-3} , ranging from 36 to 98 pg m^{-3}) (Van Drooge et al., 2004). This result is in contrast with the reported 97% emission decrease in Europe between 1990 and 2019, especially considering that the sharpest decrease was produced after the measurements of 2000–2001 from Van Drooge et al. (2004), from around 4000 kg emitted overall in 2001 to just 500 kg in 2002 (EEA, 2021). As in the case of PCBs, in the absence of local primary sources of pollution, this result reflects the persistence and resistance to degradation of HCB in the atmosphere, particularly in colder areas like high mountains.

3.3. Multivariate analysis

A multivariate analysis by MCR-ALS was applied to the complete dataset from sampling periods I, II, and III in order to observe similarities and differences in behavior among the compound concentrations in the different periods and sites. If compound concentrations are scaled by normalizing by their standard deviations, results obtained with this method are equivalent to principal component analysis (PCA) and positive matrix factorization (PMF) (Tauler et al., 2009). ALS bilinearly decomposes the data into different components described by compound profiles and their contributions to each sample, but the calculations are performed under a non-negativity constraint. Models with two, three and four components were tested. The variance explained by the addition of successive components and the meaning behind such components did not increase in a relevant way after two (56% of the variance explained). A relatively low percent of explained variance is nonetheless not unexpected since the remoteness of the studied area homogenizes the possible sources and transport modes of pollutants. This is different than other studies in urban areas with primary sources, where the MCR-ALS method successfully resolved distinct components that explained over 95% of the variance (Jaén et al., 2021).

For the high-mountain sites, the first component (C1) accounted for main contributions of PAHs and the lower molecular weight PCBs (Fig. 2a). This responds to the significant correlations observed between concentrations of most PAHs ($p < 0.05$) with R^2 values ranging between 0.19 and 0.74 (Table S8). The compound pairs Phe–Flu, Flu–Chr + TriPh, and Pyr–B[a]Ant show the strongest associations ($R^2 > 0.51$). Furthermore, PCB28, PCB52 and PCB101 are significantly correlated with Chr + TriPh with $R^2 > 0.20$. The second component (C2) was characterized by prominent loadings of the higher molecular weight PCBs, PeCB, and HCB (Fig. 2a). This is again consistent with the significant ($p < 0.05$) correlations of PeCB and HCB with PCB118, PCB138, and PCB180 ($R^2 > 0.20$ and 0.30 for PeCB and HCB, respectively), and the strong significant correlation between PeCB and HCB ($R^2 = 0.63$) (Table S8). Note that the association of the more volatile PeCB and HCB with the heavier PCBs, while not expected a priori, may be related to their higher degree of chlorination, involving lower susceptibility to photodegradation compared to PAHs and lighter PCBs, and more similar to heavier PCBs. Therefore, an environmental fate more comparable to the one shown by the less volatile compounds could be explained by a combination of re-volatilization from surfaces and higher concentrations during warmer seasons (with higher solar irradiance and atmospheric oxidizing agents) due to their resistance to degradation.

As shown in Fig. 2b, C1 contributed more to the samples collected during the colder periods (periods I and II, 61 and 57% on average, respectively), while C2 was clearly dominant in the warmest one (period III, 74% on average), especially in samples from the two highest sites (Dellui and Collada). Moreover, C2 scores showed a statistically significant ($p < 0.05$) increase in relevance with temperature (Fig. 2c). This possibly reflects differences in sources and volatility of the studied compounds that result in contrasting behaviors and environmental fates. However, the remoteness of the sampling sites limits the differences that can be observed in a source apportionment analysis that treats the dataset as a whole. Therefore, since the variations in gas-phase concentrations seemed to be affected by air temperature, they were studied in further detail by plotting concentrations against ambient temperatures individually for each compound.

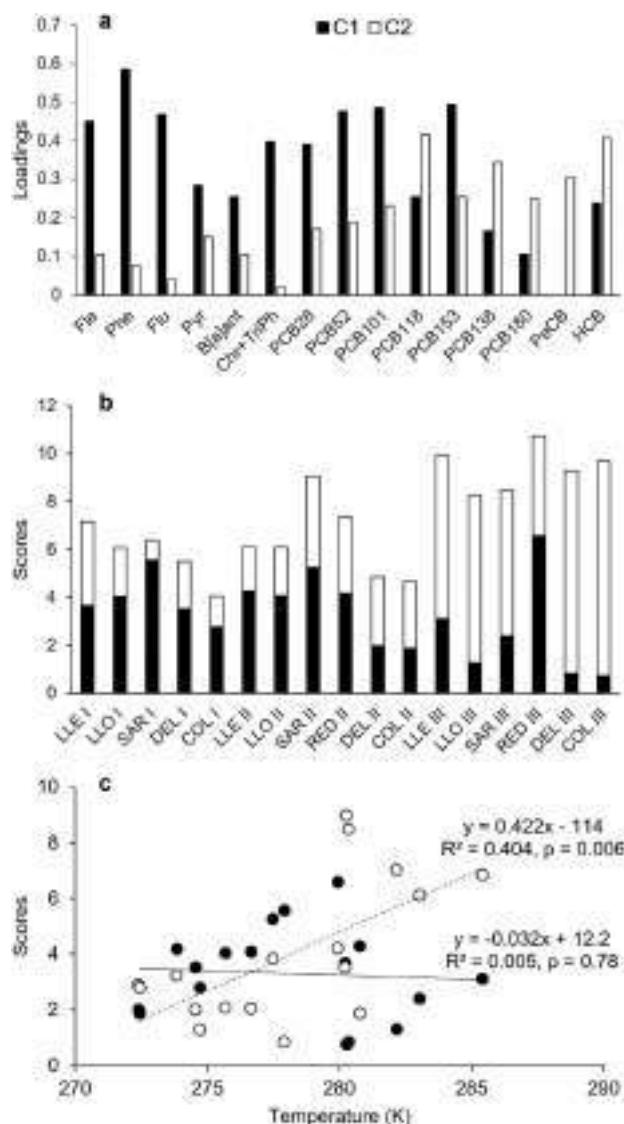


Fig. 2. Loadings (a), scores (b), and temperature correlations (c) of the component C1 and C2 scores obtained by MCR-ALS analysis for the samples obtained in periods I (09/17–01/18), II (01/18–07/18), and III (07/18–12/18) at sites LLE (Llebreta), LLO (Llong), SAR (Sarradé), RED (Redon), DEL (Dellui), and COL (Collada).

3.4. Temperature dependence

The correlations between the natural logarithm of gas-phase air concentrations ($\ln C_a$) and the mean air temperatures during the sampling period ($1/T, \text{K}^{-1}$) are shown in Fig. 3. The plots indicate a general trend towards higher concentrations at higher temperatures (12 of 15 compounds), and in 8 of them the correlations were statistically significant ($p < 0.05$). This is the case of Flu, Pyr, B[a]ant, PCB101, PCB118, PCB138, PCB180, and PeCB. Most of these compounds are grouped into the second component of the multivariate analysis, which is consistent with the statistically significant dependence of this component with temperature (Fig. 2c). The steepest slopes in the regressions of Fig. 3 were observed for B[a]ant, PCB138, PCB180, and PeCB, indicating a stronger temperature dependence that points at a pollution source distinctly different from that of other SVOCs with no temperature association such as Flu, Phe, or PCB52. In the absence of primary sources of pollutants, as is the case for the remote mountain region studied here, the different trends that result in these slopes can

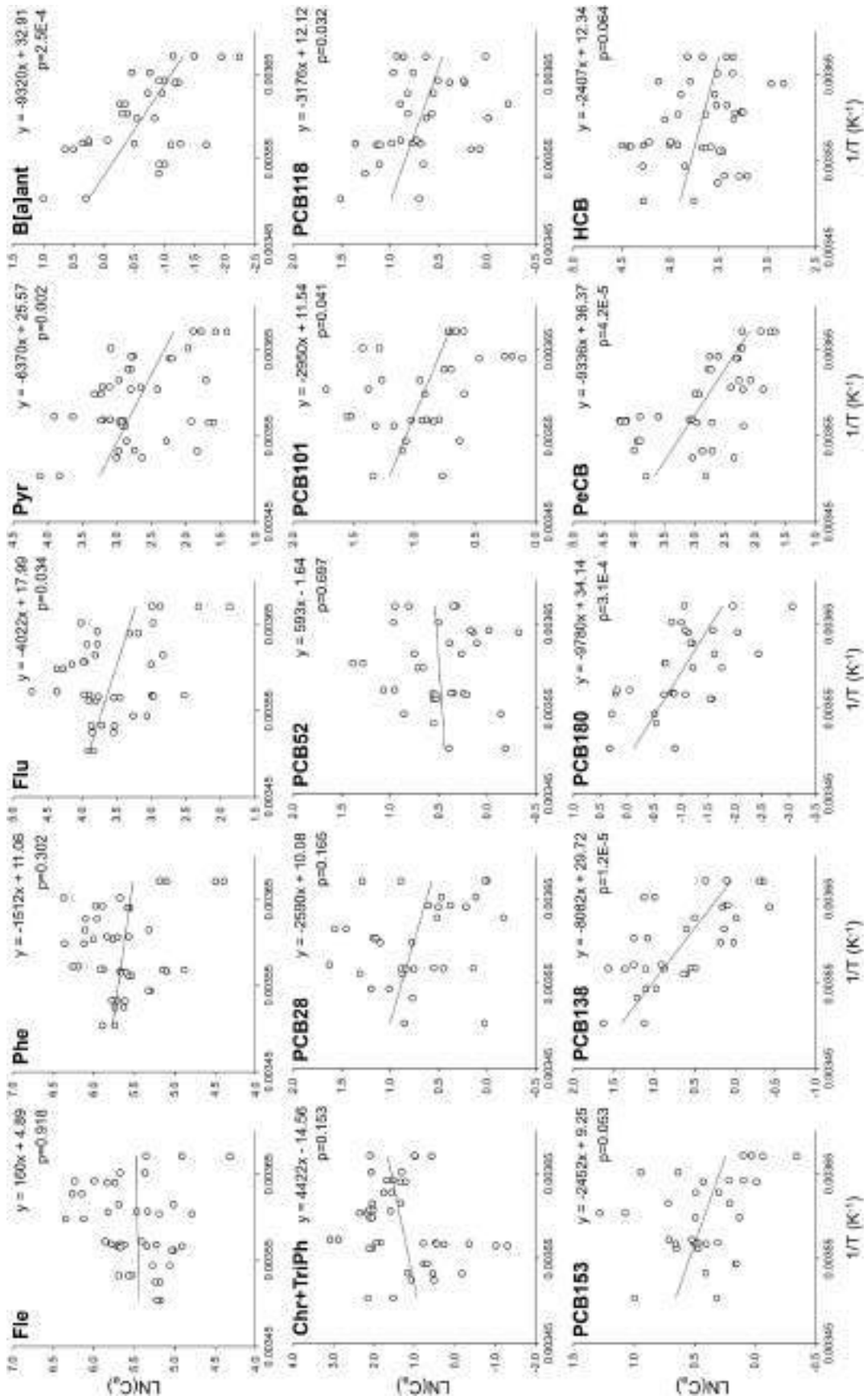


Fig. 3. Linear regressions of the natural logarithm of atmospheric gas-phase concentrations against the reciprocal of the absolute temperatures.

offer additional information on the immediate sources of pollution as these trends depend on the physical-chemical properties of each compound. This analysis is performed in Section 3.5.

Previous studies in the Pyrenees also showed significant correlations between gas-phase atmospheric concentrations of SVOCs and temperature. An increase in organochlorine compounds concentrations was observed at higher temperatures in Estanh Redon in the Pyrenees (Van Drooge et al., 2004), which was proposed to partially reflect re-emission from soils and melting ice and snow (Arellano et al., 2015). In addition, lower gas-phase PCB concentrations were observed at higher (colder) altitudes along an altitudinal transect in the valley of Estanh Redon (1600–2600 m; Van Drooge et al., 2005).

Other studies that reported similar temperature or elevation trends in mountain regions for PCBs were performed in Teide, Spain (Van Drooge et al., 2002), the Italian Alps (Jaward et al., 2005), northern Italy (Castro-Jiménez et al., 2009), South-Eastern Brazil (Meire et al., 2012), British Columbia, Canada (Abdul Hussain et al., 2019), the Tibetan Plateau (Zhu et al., 2014; Wang et al., 2017), and Central Himalayas (Gong et al., 2019). Contrarily, no significant dependences were observed for PCBs, HCB, and PeCB in the Bolivian Andes (Estellano et al., 2008), the Tibetan Plateau (Zhu et al., 2014; Ren et al., 2014), two National Parks in Brazil (Meire et al., 2016), and the Lesser Himalaya (Ali et al., 2018). Finally, trends of opposite sign were observed for HCB in the Italian Alps (Jaward et al., 2005) and in central China (Qu et al., 2015).

Volatile PAHs increased at lower temperatures in Brazilian National Parks reflecting long-range atmospheric transport (Meire et al., 2019). However, in the case of PAH temperature trends in remote areas, the influence of primary emissions and transport from regional and seasonal sources is often more prevalent than transport from long-distance sources. PAHs in remote European mountain sites showed strong gas-particle partitioning that led to higher concentrations and deposition fluxes in colder periods dependent on the proximity of active regional emission sources such as biomass combustion (Fernández et al., 2003; Van Drooge et al., 2010). PAHs in high elevation sites showed higher concentrations at lower altitudes (higher temperatures) linked to primary sources like coal and wood combustion in the Taurus Mountains, Turkey (Turgut et al., 2017), and other anthropogenic sources in Mauna Loa, Hawaii (Zhang et al., 2017) and Canada (Choi et al., 2009). On the other hand, no clear trends were observed in British Columbia, Canada (Abdul Hussain et al., 2019).

3.5. Long-range atmospheric transport and diffusive surface exchange

Pseudo-enthalpies of phase change between the atmosphere and surfaces (ΔH_{AS}) were calculated for the statistically significant correlations. The slopes of the linear regressions between $\ln C_a$ and $1/T$ equal $-\Delta U_{AS}/R$ when the concentrations are expressed on a mass per volume basis instead of partial pressure, where ΔU_{AS} ($J mol^{-1}$) is the internal energy of phase change and R is the ideal gas constant ($J K^{-1} mol^{-1}$) (Wania et al., 1998). ΔU_{AS} were then converted into ΔH_{AS} at 298 K as $\Delta H = \Delta U - RT$ (Atkinson and Curthoys, 1978). The resulting values ranged between 22 and 79 $KJ mol^{-1}$, and their confidence intervals between 21 and 38 $KJ mol^{-1}$ (Table 2). Steep slopes in $\ln C_a$ against $1/T$ regressions that yield greater ΔH_{AS} reflect increased diffusive exchange between surfaces and air at higher temperatures, while less pronounced temperature dependences indicate a higher influence of long-range atmospheric transport (Wania et al., 1998). This is a result of the loss of seasonal variation after long distance transport of pollutants on one hand, and the temperature dependence of diffusive exchange mechanics between surfaces and air on the other. A clear example of the dependence of the relative contribution of long-range atmospheric transport to local re-volatilization can be observed for the studied PCBs in Fig. S2 as a function of their tendency for partitioning to the gas phase, which is related to the volatility of the compounds: the PCBs with higher degree of chlorination, and therefore less volatile, present lower regression slopes, and therefore ΔH_{AS} .

Volatility can be represented by the subcooled liquid vapor pressures ($\log P_L^0$; Allen et al., 1999; Falconer and Bidleman, 1994). The

Table 2

Experimental phase change enthalpies (ΔH_{AS} , $KJ mol^{-1}$) and their confidence intervals (CI) estimated from the slopes of the statistically significant associations between compound concentrations and the reciprocal of the absolute temperature. Laboratory-determined reference enthalpies and relative magnitudes of experimental enthalpies compared to reference values are provided.

	$\ln C_a$ vs. $1/T$ (K^{-1})			Experimental enthalpy		Reference enthalpy		Exp/Ref
	Slope	R^2	p^a	ΔH_{AS}	95% CI	ΔH_{AS}	Error	
Fle	160	2.6E-4	0.918	–	–	72.1 ^c	1.9	–
Phe	–1512	0.026	0.302	–	–	78.3 ^c	1.8	–
Flu	–4022	0.105	0.034 *	31 ^b	28	87.1 ^c	3.6	36%
Pyr	–6370	0.209	0.002 *	50 ^b	30	89.4 ^c	3.1	57%
B[a]ant	–9320	0.355	2.5E-4 *	75	36	105.8 ^c	3.8	71%
Chr + TriPh	4422	0.049	0.153	–	–	106.2 ^c	8.6	–
PCB28	–2590	0.061	0.165	–	–	79.4 ^d	0.9	–
PCB52	593	0.005	0.697	–	–	81.3 ^d	0.5	–
PCB101	–2950	0.128	0.041 *	22 ^b	21	87.1 ^d	4.6	25%
PCB118	–3176	0.139	0.032 *	24 ^b	22	87.0 ^d	3.9	28%
PCB153	–2452	0.116	0.053	–	–	99.4 ^d	4.2	–
PCB138	–8082	0.465	1.2E-5*	65 ^b	24	94.5 ^d	0.9	69%
PCB180	–9780	0.356	3.1E-4*	79	38	99.4 ^d	2.5	79%
PeCB	–9336	0.361	4.2E-5*	75	31	67.7 ^e	–	111%
HCB	–2407	0.081	0.064	–	–	76.8 ^c	–	–

^a Values with an asterisk indicate statistically significant ($p < 0.05$) correlations.

^b Significantly different (95% confidence) from the theoretical enthalpy.

^c Roux et al., 2008.

^d Nakajoh et al., 2006.

^e Spieksma et al., 1994.

representation of ΔH_{AS} against $\log P_L^0$ results in linear correlations showing lower enthalpies for compounds with higher vapor pressures (Goss and Schwarzenbach, 1999; Macleod et al., 2007), as shown in Fig. 4 for laboratory measurements (Nakajoh et al., 2006; Roux et al., 2008; Spieksma et al., 1994). This trend was also observed for the experimental pseudo-enthalpies measured on site. However, the experimental enthalpies obtained from the temperature regressions showed significant differences compared to their respective laboratory counterparts. Such differences between measured and reference values can be regarded as a semi-quantitative assessment of the relative contribution of long-range atmospheric transport to the behavior and fate observed for each compound. Experimental enthalpies

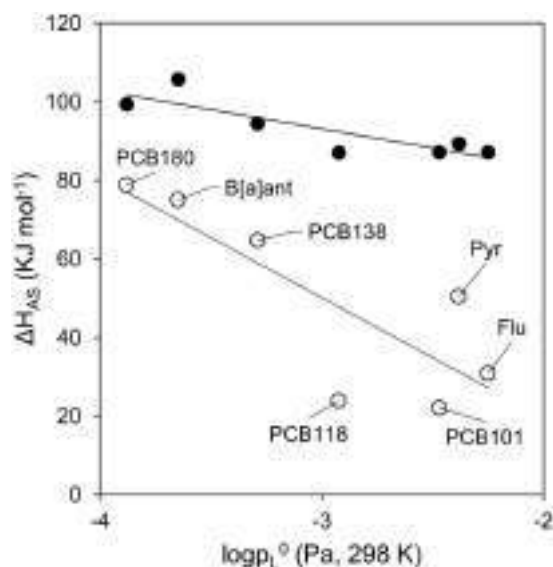


Fig. 4. Mountain (white) and laboratory-measured (black) phase change enthalpies of the PAH and PCB compounds that showed statistically significant correlations with temperature, regressed against subcooled liquid vapor pressures.

amounted to between 25 and 79% of their reference values, with the exception of PeCB at 111% (Table 2). Moreover, five out of the eight compounds with significant temperature correlations presented enthalpies confidently lower (95% confidence interval) than their reference ones. As values close to 100% would indicate a completely evaporative origin as in laboratory conditions, the overall smaller experimental pseudo-enthalpies suggest that the gas-phase concentrations of most compounds were generally dominated by long-range atmospheric transport and less by local surface exchange dynamics. This distant origin includes the rest of compounds with no significant temperature dependences, which in most cases comprise the more volatile compounds.

Furthermore, as shown in Fig. 4, the larger disagreements between enthalpy values were observed for the more volatile compounds (i.e., Flu, Pyr, PCB101, and PCB118), while the differences were smaller for the less volatile ones (i.e., B[a]ant, PCB138, and PCB180). This difference suggests that the former group was less dependent on temperature-driven partitioning than the latter. That is, the occurrence of the more volatile compounds was more influenced by contributions from distant sources, like rural sources (Van Drooge and Ballesta, 2009; Van Drooge and Grimalt, 2015), either in gas phase or adsorbed to particles. In fact, a greater decrease of enthalpies for the more volatile PCBs can be observed in Fig. 4 compared to the more volatile PAHs, which may reflect the greater adsorption by particulate matter of PAHs compared to PCBs, which tend to exist predominantly in the atmospheric gas phase (Yeo et al., 2003). Conversely, the higher agreement between theoretical and experimental enthalpies is consistent with a higher influence of local secondary sources (e.g., compounds adsorbed to soils, snow, vegetation) and re-volatilization at higher temperatures, which was also observed in the same area for other compounds with high tendency to become adsorbed onto surfaces, like organophosphate esters (Prats et al., 2022b).

4. Conclusions

The mean gas-phase concentrations of Σ PAH were in the range of those found in other mountain regions but two to three times lower than those reported in the same area two decades ago, which is consistent with the decreasing trend in PAH emissions over Europe. Σ PCB, HCB, and PeCB also showed similar mean concentrations to those reported in other remote high-mountain sites, but PCBs and HCB remained at essentially the same levels as those found twenty years ago, evidencing the persistence of these compounds in the environment despite the international regulatory actions. Increases in gas-phase concentrations at higher temperatures were observed for most studied compounds, with statistically significant correlations for eight of them. Experimental phase-change enthalpies derived from regressions against the reciprocal of the absolute temperature suggested a predominant long-range atmospheric transport over a temperature-dependent re-emission from local surfaces. However, the close similarity between field-calculated and laboratory-measured enthalpies of the least volatile compounds (B[a]ant, PCB 138, PCB 180) pointed to a higher influence of re-emission from local surfaces (e.g., particulate matter, soils, snow, vegetation) for these compounds. This behavior was also consistent with the degree of chlorination of PCBs, involving higher phase-change enthalpies at higher number of chlorine substituents. Finally, PAHs showed experimental enthalpies somewhat closer to the reference values compared to PCBs, probably as a result of a greater affinity for bonding with particulate matter and continuous active primary emission sources.

CRedit authorship contribution statement

RP: Sampling, Analysis, Formal analysis, Visualization, and Writing – original draft. BD: Sampling, Analysis, Supervision, and Writing – review and editing. PF: Supervision, Conceptualization, and Writing – review and editing. JG: Writing – review and editing, Conceptualization, and Funding acquisition.

Funding support

This work was supported by the Spanish Ministry of Science and Innovation through projects CTM2015-71832-P and PGC2018-102288-B-I00. IDAEA-CSIC is a Severo Ochoa Centre of Research Excellence, grant CEX2018-000794-S funded by MCIN/AEI/10.13039/501100011033. Raimon M. Prats also acknowledges financial support from the Spanish Ministry of Science and Innovation (BES-2016-076339).

Declaration of competing interest

The authors declare that they have no known competing financial interests or personal relationships that could have appeared to influence the work reported in this paper.

Acknowledgements

Sampling support from Alejandro G. Inarra and technical assistance from Roser Chaler are acknowledged. Part of this work was performed in the National Park of Aiguestortes i Estany de Sant Maurici, in Catalonia, with collaboration from the Department of Vice Presidency and Digital and Territorial Policies of the Government of Catalonia.

Appendix A. Supplementary data

Supplementary data to this article can be found online at <https://doi.org/10.1016/j.scitotenv.2022.154602>.

References

- Abdel-Shafy, H.I., Mansour, M.S.M., 2016. A review on polycyclic aromatic hydrocarbons: source, environmental impact, effect on human health and remediation. *Egypt. J. Pet.* 25, 107–123. <https://doi.org/10.1016/J.EJPE.2015.03.011>.
- Abdul Hussain, B., Westgate, J.N., Hayward, S.J., Shunthirasingham, C., Brown, T.N., Hung, H., Lei, Y.D., Wania, F., 2019. Polycyclic aromatic hydrocarbons and polychlorinated biphenyls in soils and atmosphere of Western Canadian mountains: the role of source proximity, precipitation, forest cover and mountain cold-trapping. *Atmos. Environ. X* 1, 100004. <https://doi.org/10.1016/j.aeaoa.2018.100004>.
- Ali, U., Sweetman, A.J., Jones, K.C., Malik, R.N., 2018. Higher atmospheric levels and contribution of black carbon in soil-air partitioning of organochlorines in lesser Himalaya. *Chemosphere* 191, 787–798. <https://doi.org/10.1016/j.chemosphere.2017.10.021>.
- Allen, J.O., Sarofim, A.F., Smith, K.A., 1999. Thermodynamic properties of polycyclic aromatic hydrocarbons in the subcooled liquid state. *Polycycl. Aromat. Compd.* 13, 261–283. <https://doi.org/10.1080/10406639908020550>.
- Álvarez-Pedrerol, M., Ribas-Fitó, N., Torrent, M., Carrizo, D., Grimalt, J.O., Sunyer, J., 2008. Effects of PCBs, p, p'-DDT, p, p'-DDE, HCB and β -HCH on thyroid function in preschool children. *Occup. Environ. Med.* 65, 452–457. <https://doi.org/10.1136/oem.2007.032763>.
- Arellano, L., Fernández, P., Tatosova, J., Stuchlík, E., Grimalt, J.O., 2011. Long-range transported atmospheric pollutants in snowpacks accumulated at different altitudes in the Tatra Mountains (Slovakia). *Environ. Sci. Technol.* 45, 9268–9275. <https://doi.org/10.1021/es202111n>.
- Arellano, L., Fernández, P., Fonts, R., Rose, N.L., Nickus, U., Thies, H., Stuchlík, E., Camarero, L., Catalan, J., Grimalt, J.O., 2015. Increasing and decreasing trends of the atmospheric deposition of organochlorine compounds in European remote areas during the last decade. *Atmos. Chem. Phys. Discuss.* 15, 6069–6085. <https://doi.org/10.5194/acpd-15-3415-2015>.
- Arellano, L., Fernández, P., van Drooge, B.L., Rose, N.L., Nickus, U., Thies, H., Stuchlík, E., Camarero, L., Catalan, J., Grimalt, J.O., 2018. Drivers of atmospheric deposition of polycyclic aromatic hydrocarbons at European high-altitude sites. *Atmos. Chem. Phys.* 18, 16081–16097. <https://doi.org/10.5194/acp-18-16081-2018>.
- Armstrong, B., Hutchinson, E., Unwin, J., Fletcher, T., 2004. Lung cancer risk after exposure to polycyclic aromatic hydrocarbons: a review and meta-analysis. *Environ. Health Perspect.* 112, 970–978. <https://doi.org/10.1289/EHP.6895>.
- Atkinson, D., Curthoys, G., 1978. The determination of heats of adsorption by gas-solid chromatography. *J. Chem. Educ.* 55, 564–566. <https://doi.org/10.1021/ed055p564>.
- Becker, S., Halsall, C.J., Tych, W., Kallenborn, R., Schlabach, M., Manø, S., 2012. Changing sources and environmental factors reduce the rates of decline of organochlorine pesticides in the Arctic atmosphere. *Atmos. Chem. Phys.* 12, 4033–4044. <https://doi.org/10.5194/ACP-12-4033-2012>.
- Bidleman, T.F., Walla, M.D., Roura, R., Carr, E., Schmidt, S., 1993. Organochlorine pesticides in the atmosphere of the Southern Ocean and Antarctica, January–March, 1990. *Mar. Pollut. Bull.* 26, 258–262. [https://doi.org/10.1016/0025-326X\(93\)90064-Q](https://doi.org/10.1016/0025-326X(93)90064-Q).
- Boström, C.E., Gerde, P., Hanberg, A., Jernström, B., Johansson, C., Kyrklund, T., Rannug, A., Törnqvist, M., Victorin, K., Westerholm, R., 2002. Cancer risk assessment, indicators, and guidelines for polycyclic aromatic hydrocarbons in the ambient air. *Environmental*

- Health Perspectives. Public Health Services, US Dept of Health and Human Services <https://doi.org/10.1289/ehp.110-1241197>.
- Cabrero, A., Dachs, J., Moeckel, C., Ojeda, M.J., Caballero, G., Barceló, D., Jones, K.C., 2011. Factors influencing the soil-air partitioning and the strength of soils as a secondary source of polychlorinated biphenyls to the atmosphere. *Environ. Sci. Technol.* 45, 4785–4792. <https://doi.org/10.1021/es200400e>.
- Cabrero, A., Muir, D.C.G., De Silva, A.O., Wang, X., Lamoureux, S.F., Lafrenière, M.J., 2018. Legacy and emerging persistent organic pollutants (POPs) in terrestrial compartments in the high Arctic: sorption and secondary sources. *Environ. Sci. Technol.* 52, 14187–14197. <https://doi.org/10.1021/acs.est.8b05011>.
- Cao, S., Na, G., Li, R., Ge, L., Gao, H., Jin, S., Hou, C., Gao, Y., Zhang, Z., 2018. Fate and deposition of polycyclic aromatic hydrocarbons in the Bransfield Strait, Antarctica. *Mar. Pollut. Bull.* 137, 533–541. <https://doi.org/10.1016/j.marpolbul.2018.10.045>.
- Castro-Jiménez, J., Dueri, S., Eisenreich, S.J., Mariani, G., Skejo, H., Umlauf, G., Zaldívar, J.M., 2009. Polychlorinated biphenyls (PCBs) in the atmosphere of sub-alpine northern Italy. *Environ. Pollut.* 157, 1024–1032. <https://doi.org/10.1016/j.envpol.2008.10.007>.
- Chen, Y., Cai, X., Jiang, L., Li, Y., 2016. Prediction of octanol-air partition coefficients for polychlorinated biphenyls (PCBs) using 3D-QSAR models. *Ecotoxicol. Environ. Saf.* 124, 202–212. <https://doi.org/10.1016/j.ecoenv.2015.10.024>.
- Chevrier, J., Eskenazi, B., Holland, N., Bradman, A., Barr, D.B., 2008. Effects of exposure to polychlorinated biphenyls and organochlorine pesticides on thyroid function during pregnancy. *Am. J. Epidemiol.* 168, 298–310. <https://doi.org/10.1093/AJE/KWN136>.
- Choi, S.D., Shunthirasingham, C., Daly, G.L., Xiao, H., Lei, Y.D., Wania, F., 2009. Levels of polycyclic aromatic hydrocarbons in Canadian mountain air and soil are controlled by proximity to roads. *Environ. Pollut.* 157, 3199–3206. <https://doi.org/10.1016/j.envpol.2009.05.032>.
- Daly, G.L., Lei, Y.D., Teixeira, C., Muir, D.C.G., Wania, F., 2007. Pesticides in western Canadian Mountain air and soil. *Environ. Sci. Technol.* 41, 6020–6025. <https://doi.org/10.1021/es070848o>.
- Dickhut, R.M., Cincinelli, A., Cochran, M., Ducklow, H.W., 2004. Atmospheric concentrations and air–water flux of organochlorine pesticides along the Western Antarctic peninsula. *Environ. Sci. Technol.* 39, 465–470. <https://doi.org/10.1021/ES048648P>.
- Ding, X., Wang, X.M., Xie, Z.Q., Xiang, C.H., Mai, B.X., Sun, L.G., Zheng, M., Sheng, G.Y., Fu, J.M., Pöschl, U., 2007. Atmospheric polycyclic aromatic hydrocarbons observed over the North Pacific Ocean and the Arctic area: spatial distribution and source identification. *Atmos. Environ.* 41, 2061–2072. <https://doi.org/10.1016/J.ATMOSENV.2006.11.002>.
- EEA, 2021. European Union Emission Inventory Report 1990–2019 Under the UNECE Convention on Long-range Transboundary Air Pollution (Air Convention). <https://doi.org/10.2800/701303>.
- Estellano, V.H., Pozo, K., Harner, T., Franken, M., Zaballa, M., 2008. Altitudinal and seasonal variations of persistent organic pollutants in the Bolivian Andes mountains. *Environ. Sci. Technol.* 42, 2528–2534. <https://doi.org/10.1021/es072754m>.
- Falconer, R.L., Bidleman, T.F., 1994. Vapor pressures and predicted particle/gas distributions of polychlorinated biphenyl congeners as functions of temperature and ortho-chlorine substitution. *Atmos. Environ.* 28, 547–554. [https://doi.org/10.1016/1352-2310\(94\)90130-9](https://doi.org/10.1016/1352-2310(94)90130-9).
- Fernández, P., Grimalt, J.O., 2003. On the global distribution of persistent organic pollutants. *Chimia* 57, 514–521. <https://doi.org/10.2533/00094290377679000>.
- Fernández, P., Grimalt, J.O., Vilanova, R.M., Fernández, P., Grimalt, J.O., Vilanova, R.M., 2002. Atmospheric gas-particle partitioning of polycyclic aromatic hydrocarbons in high mountain regions of Europe. *Environ. Sci. Technol.* 36, 1162–1168. <https://doi.org/10.1021/es010190t>.
- Fernández, P., Carrera, G., Grimalt, J.O., Ventura, M., Camarero, L., Catalan, J., Nickus, U., Thies, H., Psenner, R., 2003. Factors governing the atmospheric deposition of polycyclic aromatic hydrocarbons to remote areas. *Environ. Sci. Technol.* 37, 3261–3267. <https://doi.org/10.1021/es020137k>.
- Galbán-Malagón, C., Cabrero, A., Caballero, G., Dachs, J., 2013a. Atmospheric occurrence and deposition of hexachlorobenzene and hexachlorocyclohexanes in the Southern Ocean and Antarctic peninsula. *Atmos. Environ.* 80, 41–49. <https://doi.org/10.1016/j.atmosenv.2013.07.061>.
- Galbán-Malagón, C.J., Berrojalbiz, N., Gioia, R., Dachs, J., 2013b. The “degradative” and “biological” pumps controls on the atmospheric deposition and sequestration of hexachlorocyclohexanes and hexachlorobenzene in the North Atlantic and Arctic oceans. *Environ. Sci. Technol.* 47, 7195–7203. <https://doi.org/10.1021/es4011256>.
- Gong, P., Wang, X., Pokhrel, B., Wang, H., Liu, Xiande, Liu, Xiaobo, Wania, F., 2019. Trans-Himalayan transport of organochlorine compounds: three-year observations and model-based flux estimation. *Environ. Sci. Technol.* 53, 6773–6783. <https://doi.org/10.1021/acs.est.9b01223>.
- Goss, K.U., Schwarzenbach, R.P., 1999. Empirical prediction of heats of vaporization and heats of adsorption of organic compounds. *Environ. Sci. Technol.* 33, 3390–3393. <https://doi.org/10.1021/es980812j>.
- Grandjean, P., Landrigan, P.J., 2014. Neurobehavioural effects of developmental toxicity. *Lancet Neurol.* 13, 330–338. [https://doi.org/10.1016/S1474-4422\(13\)70278-3](https://doi.org/10.1016/S1474-4422(13)70278-3).
- Grimalt, J.O., Sunyer, J., Moreno, V., Amaral, O.C., Sala, M., Rosell, A., Anto, J.M., Albaiges, J., 1994. Risk excess of soft-tissue sarcoma and thyroid cancer in a community exposed to airborne organochlorinated compound mixtures with a high hexachlorobenzene content. *Int. J. Cancer* 56, 200–203. <https://doi.org/10.1002/ijc.2910560209>.
- Grimalt, J.O., Fernández, P., Berdié, L., Vilanova, R.M., Catalan, J., Psenner, R., Hofer, R., Appleby, P.G., Rosseland, B.O., Lien, L., Massabuau, J.C., Battarbee, R.W., 2001. Selective trapping of organochlorine compounds in mountain lakes of temperate areas. *Environ. Sci. Technol.* 35, 2690–2697. <https://doi.org/10.1021/es000278r>.
- Grimalt, J.O., Fernández, P., Quiroz, R., 2009. Input of organochlorine compounds by snow to european high mountain lakes. *Freshw. Biol.* 54, 2533–2542. <https://doi.org/10.1111/j.1365-2427.2009.02302.x>.
- Guida, Y.de S., Meire, R.O., Torres, J.P.M., Malm, O., 2018. Air contamination by legacy and current-use pesticides in Brazilian mountains: an overview of national regulations by monitoring pollutant presence in pristine areas. *Environ. Pollut.* 242, 19–30. <https://doi.org/10.1016/j.envpol.2018.06.061>.
- Hao, Y., Li, Y., Han, X., Wang, T., Yang, R., Wang, P., Xiao, K., Li, W., Lu, H., Fu, J., Wang, Y., Shi, J., Zhang, Q., Jiang, G., 2019. Air monitoring of polychlorinated biphenyls, polybrominated diphenyl ethers and organochlorine pesticides in West Antarctica during 2011–2017: concentrations, temporal trends and potential sources. *Environ. Pollut.* 249, 381–389. <https://doi.org/10.1016/J.ENVPOL.2019.03.039>.
- Harner, T., 2021. 2021 v10 Template for Calculating PUF and SIP Disk Sample Air Volumes. <https://doi.org/10.13140/RG.2.1.3998.8884>.
- Harner, T., Su, K., Genualdi, S., Karpowicz, J., Ahrens, L., Mihele, C., Schuster, J., Charland, J.P., Narayan, J., 2013. Calibration and application of PUF disk passive air samplers for tracking polycyclic aromatic compounds (PACs). *Atmos. Environ.* 75, 123–128. <https://doi.org/10.1016/j.atmosenv.2013.04.012>.
- Herbert, N.J., Spak, S.N., Smith, A., Schuster, J.K., Harner, T., Martinez, A., Hornbuckle, K.C., 2018. Calibration and evaluation of PUF-PAS sampling rates across the global atmospheric passive sampling (GAPS) network. *Environ Sci Process Impacts* 20, 210–219. <https://doi.org/10.1039/c7em00360a>.
- Hu, T., Mao, Y., Ke, Y., Liu, W., Cheng, C., Shi, M., Zhang, Z., Zhang, J., Qi, S., Xing, X., 2021. Spatial and seasonal variations of PAHs in soil, air, and atmospheric bulk deposition along the plain to mountain transect in Hubei province, Central China: air–soil exchange and long-range atmospheric transport. *Environ. Pollut.* 291, 118139. <https://doi.org/10.1016/j.envpol.2021.118139>.
- Jaén, C., Villascasas, P., Fernández, P., Grimalt, J.O., Udina, M., Bedia, C., van Drooge, B.L., 2021. Source apportionment and toxicity of PM in urban, sub-urban, and rural air quality network stations in Catalonia. *Atmosphere* 12, 744. <https://doi.org/10.3390/ATMOS12060744>.
- Jaumot, J., Gargallo, R., De Juan, A., Tauler, R., 2005. A graphical user-friendly interface for MCR-ALS: a new tool for multivariate curve resolution in MATLAB. *Chemom. Intell. Lab. Syst.* 76, 101–110. <https://doi.org/10.1016/J.CHEMOLAB.2004.12.007>.
- Jaward, F.M., Di Guardo, A., Nizzetto, L., Cassani, C., Raffaele, F., Ferretti, R., Jones, K.C., 2005. PCBs and selected organochlorine compounds in Italian mountain air: the influence of altitude and forest ecosystem type. *Environ. Sci. Technol.* 39, 3455–3463. <https://doi.org/10.1021/es048160o>.
- Jin, R., Bu, D., Liu, G., Zheng, M., Lammel, G., Fu, J., Yang, L., Li, C., Habib, A., Yang, Y., Liu, X., 2020. New classes of organic pollutants in the remote continental environment – chlorinated and brominated polycyclic aromatic hydrocarbons on the Tibetan Plateau. *Environ. Int.* 137, 105574. <https://doi.org/10.1016/j.envint.2020.105574>.
- Kirchner, M., Jakobi, G., Körner, W., Levy, W., Moche, W., Niedermoser, B., Schaub, M., Ries, L., Weiss, P., Anritter, F., Fischer, N., Henkelmann, B., Schramm, K.W., 2016. Ambient air levels of organochlorine pesticides at three high Alpine monitoring stations: trends and dependencies on geographical origin. *Aerosol Air Qual. Res.* 16, 738–751. <https://doi.org/10.4209/AAQR.2015.04.0213>.
- Li, Y., Geng, D., Liu, F., Wang, T., Wang, P., Zhang, Q., Jiang, G., 2012. Study of PCBs and PBDEs in King George Island, Antarctica, using PUF passive air sampling. *Atmos. Environ.* 51, 140–145. <https://doi.org/10.1016/j.atmosenv.2012.01.034>.
- Llop, S., Murcia, M., Alvarez-Pedrerol, M., Grimalt, J.O., Santa-Marina, L., Julvez, J., Goñi-Irigoyen, F., Espada, M., Ballester, F., Rebagliato, M., Lopez-Espinosa, M.J., 2017. Association between exposure to organochlorine compounds and maternal thyroid status: role of the iodothyronine deiodinase 1 gene. *Environ. Int.* 104, 83–90. <https://doi.org/10.1016/J.ENVINT.2016.12.013>.
- Lopez-Espinosa, M.J., Murcia, M., Iñiguez, C., Vizcaino, E., Costa, O., Fernández-Somoano, A., Basterrechea, M., Lertxundi, A., Guxens, M., Gascon, M., Goñi-Irigoyen, F., Grimalt, J.O., Tardón, A., Ballester, F., 2015. Organochlorine compounds and ultrasonid measurements of fetal growth in the INMA cohort (Spain). *Environ. Health Perspect.* 124, 157–163. <https://doi.org/10.1289/EHP.1408907>.
- Macleod, M., Scheringer, M., Hungerbühler, K., 2007. Estimating enthalpy of vaporization from vapor pressure using Trouton’s rule. *Environ. Sci. Technol.* 41, 2827–2832. <https://doi.org/10.1021/es0608186>.
- Meire, R.O., Lee, S.C., Targino, A.C., Torres, J.P.M., Harner, T., 2012. Air concentrations and transport of persistent organic pollutants (POPs) in mountains of southeast and southern Brazil. *Atmos. Pollut. Res.* 3, 417–425. <https://doi.org/10.5094/APR.2012.048>.
- Meire, R.O., Khairy, M., Targino, A.C., Galvão, P.M.A., Torres, J.P.M., Malm, O., Lohmann, R., 2016. Use of passive samplers to detect organochlorine pesticides in air and water at wet-land mountain region sites (S-SE Brazil). *Chemosphere* 144, 2175–2182. <https://doi.org/10.1016/j.chemosphere.2015.10.133>.
- Meire, R.O., Khairy, M., Aldeman, D., Galvão, P.M.A., Torres, J.P.M., Malm, O., Lohmann, R., 2019. Passive sampler-derived concentrations of PAHs in air and water along Brazilian mountain transects. *Atmos. Pollut. Res.* 10, 635–641. <https://doi.org/10.1016/j.apr.2018.10.012>.
- Na, G., Gao, Y., Li, R., Gao, H., Hou, C., Ye, J., Jin, S., Zhang, Z., 2020. Occurrence and sources of polycyclic aromatic hydrocarbons in atmosphere and soil from 2013 to 2019 in the Fildes Peninsula, Antarctica. *Mar. Pollut. Bull.* 156, 111173. <https://doi.org/10.1016/J.MARPOLBUL.2020.111173>.
- Nakajoh, K., Shibata, E., Todoroki, T., Ohara, A., Nishizawa, K., Nakamura, T., 2006. Measurement of temperature dependence for the vapor pressures of twenty-six polychlorinated biphenyl congeners in commercial Kanechlor mixtures by the knudsen effusion method. *Environ. Toxicol. Chem.* 25, 327–336. <https://doi.org/10.1897/05-215R.1>.
- Odabasi, M., Cetin, E., Sofuoglu, A., 2006. Determination of octanol-air partition coefficients and supercooled liquid vapor pressures of PAHs as a function of temperature: application to gas-particle partitioning in an urban atmosphere. *Atmos. Environ.* 40, 6615–6625. <https://doi.org/10.1016/j.atmosenv.2006.05.051>.
- Pozo, K., Harner, T., Lee, S.C., Wania, F., Muir, D.C.G., Jones, K.C., 2009. Seasonally resolved concentrations of persistent organic pollutants in the global atmosphere from the first year of the GAPS study. *Environ. Sci. Technol.* 43, 796–803. <https://doi.org/10.1021/es802106a>.
- Prats, R.M., van Drooge, B.L., Fernández, P., Grimalt, J.O., 2022a. Field comparison of passive polyurethane foam and active air sampling techniques for analysis of gas-phase semi-

- volatile organic compounds at a remote high-mountain site. *Sci. Total Environ.* 803, 149738. <https://doi.org/10.1016/j.scitotenv.2021.149738>.
- Prats, R.M., van Drooge, B.L., Fernández, P., Grimalt, J.O., 2022b. Occurrence and temperature dependence of atmospheric gas-phase organophosphate esters in high-mountain areas (Pyrenees). *Chemosphere* 292, 133467. <https://doi.org/10.1016/j.chemosphere.2021.133467>.
- Qu, C., Xing, X., Albanese, S., Doherty, A., Huang, H., Lima, A., Qi, S., De Vivo, B., 2015. Spatial and seasonal variations of atmospheric organochlorine pesticides along the plain-mountain transect in Central China: regional source vs. long-range transport and air-soil exchange. *Atmos. Environ.* 122, 31–40. <https://doi.org/10.1016/j.atmosenv.2015.09.008>.
- Ren, J., Wang, X., Xue, Y., Gong, P., Joswiak, D.R., Xu, B., Yao, T., 2014. Persistent organic pollutants in mountain air of the southeastern tibetan plateau: seasonal variations and implications for regional cycling. *Environ. Pollut.* 194, 210–216. <https://doi.org/10.1016/j.envpol.2014.08.002>.
- Ren, J., Wang, X., Wang, C., Gong, P., Yao, T., 2017. Atmospheric processes of organic pollutants over a remote lake on the central Tibetan Plateau: implications for regional cycling. *Atmos. Chem. Phys.* 17, 1401–1415. <https://doi.org/10.5194/acp-17-1401-2017>.
- Riaz, R., Malik, R.N., de Wit, C.A., 2021. Soil-air partitioning of semivolatile organic compounds in the lesser Himalaya region: influence of soil organic matter, atmospheric transport processes and secondary emissions. *Environ. Pollut.* 291, 118006. <https://doi.org/10.1016/j.envpol.2021.118006>.
- Ribas-Fito, N., Cardo, E., Sala, M., de Muga, M.E., Mazon, C., Verdu, A., Kogevinas, M., Grimalt, J.O., Sunyer, J., 2003. Breastfeeding, exposure to organochlorine compounds, and neurodevelopment in infants. *Pediatrics* 111, 580–585. <https://doi.org/10.1542/peds.111.5.e580>.
- Roux, M.V., Tempardo, M., Chickos, J.S., Nagano, Y., 2008. Critically evaluated thermochemical properties of polycyclic aromatic hydrocarbons. *J. Phys. Chem. Ref. Data* 37, 1855–1996. <https://doi.org/10.1063/1.2955570>.
- Sala, M., Sunyer, J., Herrero, C., To-Figueras, J., Grimalt, J.O., 2001. Association between serum concentrations of hexachlorobenzene and polychlorobiphenyls with thyroid hormone and liver enzymes in a sample of the general population. *Occup. Environ. Med.* 58, 172–177. <https://doi.org/10.1136/OEM.58.3.172>.
- Shen, L., Wania, F., Lei, Y.D., Teixeira, C., Muir, D.C.G., Bidleman, T.F., 2005. Atmospheric distribution and long-range transport behavior of organochlorine pesticides in North America. *Environ. Sci. Technol.* 39, 409–420. <https://doi.org/10.1021/es049489c>.
- Sheng, J., Wang, X., Gong, P., Joswiak, D.R., Tian, L., Yao, T., Jones, K.C., 2013. Monsoon-driven transport of organochlorine pesticides and polychlorinated biphenyls to the Tibetan Plateau: three year atmospheric monitoring study. *Environ. Sci. Technol.* 47, 3199–3208. <https://doi.org/10.1021/es305201s>.
- Shoeb, M., Harner, T., 2002. Characterization and comparison of three passive air samplers for persistent organic pollutants. *Environ. Sci. Technol.* 36, 4142–4151. <https://doi.org/10.1021/es020635t>.
- Spiekma, W., Luijk, R., Govers, H.A.J., 1994. Determination of the liquid vapour pressure of low-volatility compounds from the Kováts retention index. *J. Chromatogr. A* 672, 141–148. [https://doi.org/10.1016/0021-9673\(94\)80602-0](https://doi.org/10.1016/0021-9673(94)80602-0).
- Su, Y., Hung, H., Blanchard, P., Patton, G.W., Kallenborn, R., Konoplev, A., Fellin, P., Li, H., Geen, C., Stern, G., Rosenberg, B., Barrie, L.A., 2006. Spatial and seasonal variations of hexachlorocyclohexanes (HCHs) and hexachlorobenzene (HCB) in the Arctic atmosphere. *Environ. Sci. Technol.* 40, 6601–6607. <https://doi.org/10.1021/es061065q>.
- Tauler, R., 1995. Multivariate curve resolution applied to second order data. *Chemom. Intell. Lab. Syst.* 30, 133–146. [https://doi.org/10.1016/0169-7439\(95\)00047-X](https://doi.org/10.1016/0169-7439(95)00047-X).
- Tauler, R., Smilde, A., Kowalski, B., 1995. Selectivity, local rank, three-way data analysis and ambiguity in multivariate curve resolution. *J. Chemom.* 9, 31–58. <https://doi.org/10.1002/CEM.1180090105>.
- Tauler, R., Viana, M., Querol, X., Alastuey, A., Flight, R.M., Wentzell, P.D., Hopke, P.K., 2009. Comparison of the results obtained by four receptor modelling methods in aerosol source apportionment studies. *Atmos. Environ.* 43, 3989–3997. <https://doi.org/10.1016/j.atmosenv.2009.05.018>.
- Turgut, C., Mazmanci, M.A., Mazmanci, B., Yalçın, M., Karakuş, P.B.K., Atatanir, L., Keski, M., Henkelmann, B., Pfister, G., Schramm, K.W., 2017. Polycyclic aromatic hydrocarbons (PAHs) determined by pine needles and semipermeable membrane devices along an altitude profile in Taurus Mountains, Turkey. *Environ. Sci. Pollut. Res.* 24, 7077–7087. <https://doi.org/10.1007/s11356-017-8363-4>.
- Ulbrich, B., Stahlmann, R., 2004. Developmental toxicity of polychlorinated biphenyls (PCBs): a systematic review of experimental data. *Arch. Toxicol.* 78, 252–268. <https://doi.org/10.1007/s00204-003-0519-Y>.
- Ullah, R., Asghar, R., Baqar, M., Mahmood, A., Ali, S.N., Sohail, M., Schäfer, R.B., Eqani, S.A.M.A.S., 2019. Assessment of organochlorine pesticides in the Himalayan riverine ecosystems from Pakistan using passive sampling techniques. *Environ. Sci. Pollut. Res.* 26, 6023–6037. <https://doi.org/10.1007/s11356-018-3987-6>.
- UNEP, 2022. Stockholm convention. Protecting human health and the environment from persistent organic pollutants [WWW document] URL <http://www.pops.int/TheConvention/ThePOPs/AllPOPs> (accessed 1.2.22).
- Van Drooge, B.L., Ballesta, P.P., 2009. Seasonal and daily source apportionment of polycyclic aromatic hydrocarbon concentrations in PM10 in a semirural European area. *Environ. Sci. Technol.* 43, 7310–7316. <https://doi.org/10.1021/es901381a>.
- Van Drooge, B.L., Grimalt, J.O., 2015. Particle size-resolved source apportionment of primary and secondary organic tracer compounds at urban and rural locations in Spain. *Atmos. Chem. Phys.* 15, 7735–7752. <https://doi.org/10.5194/acp-15-7735-2015>.
- Van Drooge, B.L., Grimalt, J.O., Torres García, C.J., Cuevas, E., 2002. Semivolatile organochlorine compounds in the free troposphere of the Northeastern Atlantic. *Environ. Sci. Technol.* 36, 1155–1161. <https://doi.org/10.1021/es010189u>.
- Van Drooge, B.L., Grimalt, J.O., Camarero, L., Catalan, J., Stuchlík, E., Torres García, C.J., 2004. Atmospheric semivolatile organochlorine compounds in European high-mountain areas (Central Pyrenees and high Tatras). *Environ. Sci. Technol.* 38, 3525–3532. <https://doi.org/10.1021/es030108p>.
- Van Drooge, B.L., Grimalt, J.O., Booi, K., Camarero, L., Catalan, J., 2005. Passive sampling of atmospheric organochlorine compounds by SPMDs in a remote high mountain area. *Atmos. Environ.* 39, 5195–5204. <https://doi.org/10.1016/j.atmosenv.2005.05.020>.
- Van Drooge, B.L., Fernández, P., Grimalt, J.O., Stuchlík, E., García, C.J.T., Cuevas, E., 2010. Atmospheric polycyclic aromatic hydrocarbons in remote European and Atlantic sites located above the boundary mixing layer. *Environ. Sci. Pollut. Res.* 17, 1207–1216. <https://doi.org/10.1007/s11356-010-0296-0>.
- Wang, X.P., Gong, P., Yao, T.D., Jones, K.C., 2010. Passive air sampling of organochlorine pesticides, polychlorinated biphenyls, and polybrominated diphenyl ethers across the Tibetan plateau. *Environ. Sci. Technol.* 44, 2988–2993. <https://doi.org/10.1021/es9033759>.
- Wang, Z., Na, G., Ma, X., Fang, X., Ge, L., Gao, H., Yao, Z., 2013. Occurrence and gas/particle partitioning of PAHs in the atmosphere from the North Pacific to the Arctic Ocean. *Atmos. Environ.* 77, 640–646. <https://doi.org/10.1016/j.atmosenv.2013.05.052>.
- Wang, C., Wang, X., Ren, J., Gong, P., Yao, T., 2017. Using a passive air sampler to monitor air-soil exchange of organochlorine pesticides in the pasture of the central Tibetan plateau. *Sci. Total Environ.* 580, 958–965. <https://doi.org/10.1016/j.scitotenv.2016.12.046>.
- Wania, F., Mackay, D., 1993. Global fractionation and cold condensation of low volatility organochlorine compounds in polar regions. *Ambio* 22, 10–18. <https://doi.org/10.2307/4314030>.
- Wania, F., Haugen, J.E., Lei, Y.D., Mackay, D., 1998. Temperature dependence of atmospheric concentrations of semivolatile organic compounds. *Environ. Sci. Technol.* <https://doi.org/10.1021/es970856c>.
- Wenger, D., Gerecke, A.C., Heeb, N.V., Hueglin, C., Seiler, C., Haag, R., Naegeli, H., Zenobi, R., 2009. Aryl hydrocarbon receptor-mediated activity of atmospheric particulate matter from an urban and a rural site in Switzerland. *Atmos. Environ.* 43, 3556–3562. <https://doi.org/10.1016/j.atmosenv.2009.04.012>.
- Wong, F., Hung, H., Dryfhout-Clark, H., Aas, W., Bohlin-Nizzetto, P., Breivik, K., Mastrodonato, M.N., Lundén, E.B., Ólafsdóttir, K., Sigurðsson, Á., Vorkamp, K., Bossi, R., Skov, H., Hakola, H., Barresi, E., Sverko, E., Fellin, P., Li, H., Vlasenko, A., Zapevalov, M., Samsonov, D., Wilson, S., 2021. Time trends of persistent organic pollutants (POPs) and Chemicals of Emerging Arctic Concern (CEAC) in Arctic air from 25 years of monitoring. *Sci. Total Environ.* 775, 145109. <https://doi.org/10.1016/j.scitotenv.2021.145109>.
- Wu, X., Chen, A., Yuan, Z., Kang, H., Xie, Z., 2020. Atmospheric organochlorine pesticides (OCPs) and polychlorinated biphenyls (PCBs) in the Antarctic marginal seas: distribution, sources and transportation. *Chemosphere* 258, 127359. <https://doi.org/10.1016/j.chemosphere.2020.127359>.
- Yeo, H.G., Choi, M., Chun, M.Y., Sunwoo, Y., 2003. Gas/particle concentrations and partitioning of PCBs in the atmosphere of Korea. *Atmos. Environ.* 37, 3561–3570. [https://doi.org/10.1016/S1352-2310\(03\)00361-3](https://doi.org/10.1016/S1352-2310(03)00361-3).
- Zhang, X., Barnes, J., Lei, Y.D., Wania, F., 2017. Semivolatile organic contaminants in the Hawaiian atmosphere. *Environ. Sci. Technol.* 51, 11634–11642. <https://doi.org/10.1021/acs.est.7b03841>.
- Zhu, N., Schramm, K.W., Wang, T., Henkelmann, B., Zheng, X., Fu, J., Gao, Y., Wang, Y., Jiang, G., 2014. Environmental fate and behavior of persistent organic pollutants in Shergyla Mountain, southeast of the Tibetan Plateau of China. *Environ. Pollut.* 191, 166–174. <https://doi.org/10.1016/j.envpol.2014.04.03>.

CHANGES AND DISTRIBUTION OF GAS-PHASE POLYCYCLIC AROMATIC HYDROCARBONS AND ORGANOCHLORINE COMPOUNDS IN A HIGH-MOUNTAIN GRADIENT OVER A THREE-YEAR PERIOD (PYRENEES, 2017-2020)

Raimon M. Prats, Barend L. van Drooge, Pilar Fernández, Joan O. Grimalt

Institute of Environmental Assessment and Water Research (IDAEA-CSIC), Jordi Girona 18, 08034 Barcelona, Catalonia, Spain

ARTICLE 4 – SUPPORTING INFORMATION

Text S4.1	Theoretical uncertainty of the sampling rates.	166
Table S4.1	Sampling sites, duration of the sampler exposures, and mean temperatures.	167
Table S4.2	Complimentary meteorological conditions registered in the studied area.	168
Table S4.3	Ion m/z ratios and collision energies used in GC-MS.	168
Table S4.4	Mean sampling rates, experimental errors, and theoretical expanded uncertainties.	169
Table S4.5	Mean effective sampled air volumes and degrees of equilibrium.	170
Table S4.6	Gas-phase atmospheric concentrations of PAHs, PCBs, PeCB, and HCB.	171
Table S4.7	Comparison of gas-phase atmospheric concentrations of the present study with literature data.	172
Table S4.8	Correlation matrix between concentrations of target pollutants.	173
Figure S4.1	Polyurethane foam passive air samplers (PUF-PAS).	174
Figure S4.2	Slope of PCB temperature dependence regression against degree of chlorination.	174
References S4		175

Text S4.1. Theoretical uncertainty of the sampling rates

The theoretical expanded uncertainties (EU , %) of the sampling rates (R_S) were estimated as propagated uncertainties (δR_S) from the variables involved in Performance Reference Compound (PRC) calculations. A rearranged Equation 2 with K_{PUF-A} substituted for its temperature-corrected octanol-air partition coefficient ($K_{OA(T)}$) dependence relationship (Shoeib and Harner, 2002) yields:

$$R_S = \frac{-\ln(C/C_0) D_{film} \rho_{PUF} 10^{(0.6366 \log K_{OA(T)} - 3.1774)} A_{PUF}}{t} = k \ln(C/C_0) 10^{(b \log K_{OA(T)} - a)} \quad (\text{Eq. S4.1})$$

where ρ_{PUF} is the density of the PUF, k is a value grouping all constants, and a and b are the renamed coefficients in the exponential term. The square root of the sum of squares of the partial derivatives of R_S with respect to the non-constant variables (C/C_0 and K_{OA}) multiplied by their respective squared uncertainties is equal to δR_S :

$$\begin{aligned} \delta R_S &= \sqrt{\left(\frac{\partial R_S}{\partial C/C_0}\right)^2 \delta_{C/C_0}^2 + \left(\frac{\partial R_S}{\partial K_{OA(T)}}\right)^2 \delta_{K_{OA(T)}}^2} = \\ &= \sqrt{\left(\frac{10^{-a} k K_{OA(T)}^b}{C/C_0}\right)^2 \delta_{C/C_0}^2 + \left(10^{-a} k b K_{OA(T)}^{b-1} \ln(C/C_0)\right)^2 \delta_{K_{OA(T)}}^2} \quad (\text{Eq. S4.2}) \end{aligned}$$

The uncertainties of the variables C/C_0 and $K_{OA(T)}$ were estimated from further propagation of the error made in the calculation of C/C_0 (peak integration and quantification standard errors) and from PRC $K_{OA(T)}$ standard errors (Harner and Bidleman, 1996). EUs were finally calculated as twice the propagated uncertainty, which accounts for other undefined sources of error (e.g., uncertainty in temperature correction relationships).

Table S4.1. Sampling sites, duration of the sampler exposures, and mean temperatures recorded on-site during each period.

Sampling site	Latitude, Longitude	Period	Deployed	Retrieved	Duration (d)	Mean T (°C)
Llebreta 1,619 m	42.55063, 0.88728	I	21/9/2017	31/1/2018	132	7.1
		II	31/1/2018	12/7/2018	162	7.6
		III	12/7/2018	13/12/2018	154	12.3
		IV	13/12/2018	26/9/2019	287	10.6
		V	26/9/2019	6/10/2020	376	10.0
Llong 2,000 m	42.57308, 0.95176	I	19/9/2017	1/2/2018	135	2.5
		II	1/2/2018	12/7/2018	161	3.5
		III	12/7/2018	13/12/2018	154	9.0
Sarradé 2,123 m	42.56232, 0.89669	I	20/9/2017	31/1/2018	133	4.8
		II	31/1/2018	12/7/2018	162	4.3
		III	12/7/2018	14/12/2018	155	9.9
		IV	14/12/2018	26/9/2019	286	7.2
		V	26/9/2019	6/10/2020	376	7.4
Redon 2,240 m	42.63836, 0.77890	I+II	17/9/2017	11/7/2018	297	0.7
		III	11/7/2018	12/12/2018	154	6.8
		IV	12/12/2018	27/9/2019	289	4.1
		V	27/9/2019	7/10/2020	376	4.2
Dellui 2,349 m	42.54637, 0.94799	I	22/9/2017	30/1/2018	130	1.4
		II	30/1/2018	12/7/2018	163	-0.7
		III	12/7/2018	13/12/2018	154	7.2
Collada 2,453 m	42.54437, 0.94312	I	23/9/2017	30/1/2018	129	1.6
		II	30/1/2018	12/7/2018	163	-0.7
		III	12/7/2018	13/12/2018	154	7.1

Table S4.2. Meteorological conditions registered in the studied area by two automatic weather stations from the XEMA network of the Catalan Meteorological Service.

Period	Start date	End date	Mean T (°C)	Max. T (°C)	Min. T (°C)	Rel.Humidity (%)	Accumulated precipitation (mm)	Mean snow height (mm)	Mean wind speed (m/s)	Max. wind speed (m/s)	Mean solar irradiance (W/m ²)
Redon VS (2,247 m asl)											
I	17/9/2017	31/1/2018	0.7 ± 6.0	15.0	-14.2	70 ± 26	717	431 ± 544	4.3 ± 2.6	30.7	109 ± 192
II	31/1/2018	11/7/2018	0.7 ± 6.9	18.2	-16.6	85 ± 17	1038	1438 ± 1041	5.0 ± 3.6	36.2	194 ± 286
III	11/7/2018	12/12/2018	6.8 ± 6.1	20.3	-9.2	78 ± 23	573	49 ± 99	4.4 ± 3	33.9	172 ± 273
IV	12/12/2018	27/9/2019	4.1 ± 7.5	25.1	-14.1	70 ± 28	1058	436 ± 528	4.8 ± 3.2	36.0	203 ± 302
V	27/9/2019	7/10/2020	4.2 ± 6.3	23.3	-12.6	77 ± 26	1605	494 ± 632	4.6 ± 3.3	35.6	169 ± 270
Boí Z2 (2,535 m asl)											
I	17/9/2017	31/1/2018	-0.1 ± 6.0	14.2	-16.1	61 ± 27	250	175 ± 227	4.2 ± 3.6	33.9	126 ± 202
II	31/1/2018	12/7/2018	-0.6 ± 6.9	16.1	-16.5	82 ± 18	976	1794 ± 941	3.2 ± 3	32.1	204 ± 284
III	12/7/2018	13/12/2018	5.4 ± 5.9	19.7	-11.2	75 ± 24	659	149 ± 232	3.0 ± 2.5	29.5	165 ± 249
IV	13/12/2018	26/9/2019	3.1 ± 7.2	22.3	-15.9	63 ± 28	581	409 ± 383	3.5 ± 3.2	39.2	213 ± 297
V	26/9/2019	6/10/2020	2.7 ± 6.2	20.7	-12.6	72 ± 29	1176	714 ± 746	3.6 ± 3.1	35.7	173 ± 258

Table S4.3. Mass-to-charge (m/z) ratios used for the identification and quantification of target compounds and recovery standards in GC-MS (SIM mode).

Compound	Abbreviation	m/z (CE 70 eV)
2,4,4'-Trichlorobiphenyl	PCB28	256
2,2',5,5'-Tetrachlorobiphenyl	PCB52	292
2,2',4,5,5'-Pentachlorobiphenyl	PCB101	326
2,3',4,4',5-Pentachlorobiphenyl	PCB118	326
2,2',3,4,4',5'-Hexachlorobiphenyl	PCB138	360
2,2',4,4',5,5'-Hexachlorobiphenyl	PCB153	360
2,2',3,4,4',5,5'-Heptachlorobiphenyl	PCB180	394
Hexachlorobenzene	HCB	284
Pentachlorobenzene	PeCB	250
Fluorene	Fle	166
Phenanthrene	Phe	178
Fluoranthene	Flu	202
Pyrene	Pyr	202
Benz[a]anthracene	B[a]ant	228
Chrysene + Triphenylene	Chr + TriPh	228
Decachlorobiphenyl	PCB209	498
1,2,4,5-Tetrabromobenzene	TBB	394
Fluorene-d ₁₀	Fle-d ₁₀	176
Phenanthrene-d ₁₀	Phe-d ₁₀	188
Fluoranthene-d ₁₀	Flu-d ₁₀	212
Pyrene-d ₁₀	Pyr-d ₁₀	212
Benz[a]anthracene-d ₁₂	B[a]ant-d ₁₂	240
Chrysene-d ₁₂	Chr-d ₁₂	240

Table S4.4. Mean sampling rates ($R_S \pm SD$, $m^3 d^{-1}$) at each site for each sampling period, experimental error (RSD, %), and theoretical expanded uncertainties (EU, %).

Sampling period		I	II	III	IV	V	Mean
Llebreta 1,619 m	R_S	2.7 ± 0.3	2.7 ± 0.1	2.4 ± 0.04	2.5 ± 0.5	2.3 ± 0.6	2.5 ± 0.2
	RSD	10.1	4.8	1.5	18.5	24.6	7.7
	EU	11.0	9.4	8.9	6.6	5.4	-
Llong 2,000 m	R_S	3.4 ± 0.7	3.8 ± 0.7	3.7 ± 0.1	-	-	3.6 ± 0.2
	RSD	20.7	17.2	2.1	-	-	5.9
	EU	11.3	9.2	8.1	-	-	-
Sarradé 2,123 m	R_S	3.5 ± 0.7	3.2 ± 0.3	3.5^a	3.3^a	2.8 ± 0.4	3.3 ± 0.3
	RSD	18.5	7.9	-	-	13.9	8.6
	EU	10.1	9.8	8.1	6.9	5.6	-
Redon 2,240 m	R_S	$-^a$	3.8 ± 0.1	3.2 ± 0.7	3.6 ± 0.4	4.5^a	3.7 ± 0.5
	RSD	-	1.8	23.0	11.5	-	14.6
	EU	-	7.8	9.7	7.5	5.4	-
Dellui 2,349 m	R_S	3.7 ± 0.4	3.3 ± 0.2	3.6 ± 0.3	-	-	3.5 ± 0.2
	RSD	10.5	6.0	8.6	-	-	6.3
	EU	11.6	11.9	8.5	-	-	-
Collada 2,453 m	R_S	3.5 ± 0.8	2.1 ± 0.1	3.0 ± 0.7	-	-	2.9 ± 0.7
	RSD	22.1	4.7	23.7	-	-	25.4
	EU	12.0	17.1	9.3	-	-	-

^a Sample not collected or replicate lost due to extreme meteorological conditions.

Table S4.5. Mean effective sampled air volumes (V_A) and degrees of equilibrium (DEQ) for each compound during each sampling period (Green = full or nearby equilibrium; Yellow to Red = linear uptake phase).

Period	V_A (m ³) ^a						DEQ ^b					
	I	II	III	IV	V	Mean	I	II	III	IV	V	Mean
Fle	65	69	51	55	55	60	1.00	1.00	1.00	1.00	1.00	1.00
Phe	216	238	183	213	217	213	0.81	0.85	0.92	0.98	0.98	0.89
Flu	412	535	442	733	912	559	0.16	0.19	0.24	0.36	0.37	0.24
Pyr	412	535	442	733	912	559	0.16	0.19	0.24	0.36	0.37	0.24
B[a]ant	439	584	489	858	1123	634	0.04	0.05	0.07	0.11	0.12	0.07
Chr+TriPh	439	584	489	858	1123	634	0.04	0.05	0.07	0.11	0.12	0.07
PCB28	392	501	404	642	771	506	0.24	0.28	0.37	0.52	0.53	0.36
PCB52	419	547	450	757	952	574	0.13	0.16	0.21	0.32	0.33	0.21
PCB101	433	572	476	824	1064	614	0.07	0.09	0.12	0.18	0.19	0.12
PCB118	419	546	453	761	958	576	0.13	0.16	0.20	0.31	0.32	0.20
PCB153	417	543	450	754	946	571	0.14	0.17	0.21	0.32	0.33	0.21
PCB138	419	547	453	762	959	576	0.13	0.16	0.20	0.31	0.31	0.20
PCB180	437	580	485	848	1105	628	0.05	0.06	0.09	0.13	0.14	0.09
PeCB	105	113	73	82	82	93	0.98	0.98	1.00	1.00	1.00	0.99
HCB	283	327	261	336	353	305	0.63	0.69	0.77	0.92	0.92	0.76

^a Calculated using Equation 1 in the main text.

^b Calculated from the expression between brackets in Equation 1 in the main text. A DEQ of 1 indicates full equilibrium conditions have been reached.

Table S4.6. Gas-phase atmospheric concentrations (pg m^{-3}) of PAHs, PCBs, pentachlorobenzene, and hexachlorobenzene in six high-mountain sites in the Pyrenees between 2017 and 2020, measured by means of polyurethane foam passive air samplers (PUF-PAS). Note that sampling period II at Redon encompasses both periods I and II in all other sites, and that PCB concentrations were only measured in the first three sampling periods.

Site	Period	Flu	Phe	File	Pyr	B[a]ant	Chr+TriPh	Σ PAH	PCB28	PCB52	PCB101	PCB118	PCB153	PCB138	PCB180	Σ PCB	PeCB	HCB
Liebreta	I	309 ± 23	366 ± 9	51 ± 3	23 ± 2	1.4 ± 0.1	6.6 ± 0.5	758 ± 13	1.4 ± 0.4	1.4 ± 0.03	2.3 ± 0.2	2.4 ± 0.4	1.5 ± 0.2	1.7 ± 0.1	0.43 ± 0.00011 ± 1	21 ± 1	53 ± 3	
	II	152 ± 2	258 ± 7	47 ± 3	18 ± 1	1.8 ± 0.2	8.0 ± 0.3	486 ± 13	3.1 ± 0.9	1.7 ± 0.04	3.5 ± 0.4	1.1 ± 0.1	1.8 ± 0.2	1.9 ± 0.04	0.21 ± 0.0003	13 ± 1	9.0 ± 0.01	32 ± 1
	III	181 ± 6	338 ± 37	48 ± 3	53 ± 11	2.0 ± 1.0	6.6 ± 2.8	629 ± 19	1.7 ± 0.9	1.2 ± 0.5	3.0 ± 1.2	3.3 ± 1.8	2.0 ± 0.9	4.1 ± 1.4	0.90 ± 0.69	16 ± 7	31 ± 20	58 ± 21
Lllong	IV	183 ± 8	296 ± 23	41 ± 9	17 ± 5	n.d. ^a	2.3 ± 0.9	540 ± 45	-	-	-	-	-	-	-	16 ± 7	34 ± 0.04	
	V	280 ± 24	289 ± 19	41 ± 10	13 ± 9	n.d.	1.3 ± 0.6	624 ± 61	-	-	-	-	-	-	-	-	16 ± 2	26 ± 2
2,000 m	I	498 ± 42	419 ± 42	48 ± 5	17 ± 1	0.44 ± 0.07	5.3 ± 0.7	987 ± 91	1.3 ± 0.6	1.3 ± 0.3	2.1 ± 0.1	2.0 ± 0.4	1.5 ± 0.2	1.3 ± 0.5	0.30 ± 0.01	9.8 ± 0.1	16 ± 1	42 ± 10
	II	224 ± 103	328 ± 175	31 ± 20	13 ± 10	0.74 ± 0.05	5.8 ± 2.8	602 ± 311	4.6 ± 0.4	1.7 ± 0.6	3.1 ± 0.7	1.6 ± 1.2	1.6 ± 0.6	1.5 ± 0.5	0.14 ± 0.08	14 ± 3	8.8 ± 1.2	32 ± 3
	III	176 ± 26	203 ± 4	24 ± 3	14 ± 5	0.38 ± 0.03	2.1 ± 0.1	419 ± 25	3.0 ± 0.4	1.6 ± 1.1	2.4 ± 0.7	2.5 ± 0.8	1.2 ± 0.003	2.8 ± 0.3	0.97 ± 0.52	15 ± 3	51 ± 2	60 ± 18
Sarradé	I	516 ± 79	518 ± 88	75 ± 5	27 ± 2	0.51 ± 0.10	8.0 ± 0.3	1144 ± 174	2.6 ± 0.6	2.0 ± 0.1	2.2 ± 0.5	1.4 ± 0.6	1.4 ± 0.4	1.1 ± 0.1	0.24 ± 0.09	11 ± 1	19 ± 1	43 ± 21
	II	150 ± 43	362 ± 601	42 ± 30	14 ± 4	0.71 ± 0.04	9.7 ± 1.2	578 ± 51	3.2 ± 0.1	3.8 ± 0.3	4.8 ± 1.2	2.0 ± 0.4	3.3 ± 0.5	3.2 ± 0.4	0.50 ± 0.003	21 ± 2	7.8 ± 1.8	44 ± 9
2,123 m	III ^b	252	324	41	16	0.4	3.2	636	2.2	1.7	3	3.5	1.5	3.4	0.59	16	54	31
	IV ^b	136	291	43	19	n.d.	1.3	490	-	-	-	-	-	-	-	n.d.	n.d.	36
Redon	V	291 ± 4	280 ± 12	33 ± 2	5.2 ± 0.3	n.d.	0.32 ± 0.06	610 ± 18	-	-	-	-	-	-	-	-	17 ± 3	39 ± 1
	II	253 ± 55	440 ± 209	38 ± 26	15 ± 10	0.55 ± 0.11	5.8 ± 3.0	752 ± 303	1.4 ± 0.3	2.1 ± 0.7	3.9 ± 0.4	2.4 ± 0.4	2.2 ± 0.5	2.9 ± 0.3	0.40 ± 0.05	15 ± 2	9.2 ± 0.2	31 ± 4
	III	287 ± 89	507 ± 25	96 ± 24	44 ± 8	1.1 ± 0.2	20 ± 3	955 ± 144	5.1 ± 0.002	2.8 ± 0.2	4.7 ± 0.1	2.3 ± 0.3	1.9 ± 0.3	3.0 ± 0.7	1.1 ± 0.2	21 ± 2	43 ± 9	61 ± 10
2,240 m	IV	223 ± 21	303 ± 57	53 ± 1	24 ± 2	n.d.	8.0 ± 0.6	610 ± 80	-	-	-	-	-	-	-	-	n.d.	26 ± 0.4
	V ^b	339	301	54	14	n.d.	4.9	714	-	-	-	-	-	-	-	-	11	28
Dellui	I	458 ± 78	379 ± 24	44 ± 0.1	16 ± 0.4	0.39 ± 0.03	5.0 ± 0.5	903 ± 102	1.6 ± 0.3	1.1 ± 0.2	1.3 ± 0.1	1.5 ± 0.3	1.2 ± 0.1	1.1 ± 0.01	0.27 ± 0.10	8.0 ± 0.9	15 ± 2	53 ± 12
	II	174 ± 54	171 ± 10	19 ± 2	6.3 ± 0.5	0.27 ± 0.07	5.4 ± 3.9	376 ± 66	1.0 ± 0.01	1.4 ± 0.03	1.9 ± 0.1	1.8 ± 1.1	1.1 ± 0.1	1.3 ± 0.2	0.24 ± 0.15	8.7 ± 0.7	8.0 ± 1.7	42 ± 5
2,349 m	III	256 ± 66	164 ± 0.3	20 ± 0.1	13 ± 9	0.26 ± 0.10	1.1 ± 0.6	455 ± 57	2.2 ± 0.1	1.5 ± 0.3	2.3 ± 0.003	3.1 ± 0.1	1.7 ± 0.3	3.5 ± 0.6	0.42 ± 0.12	15 ± 2	65 ± 4	83 ± 2
	I	326 ± 23	263 ± 5	26 ± 2	9.2 ± 0.2	0.30 ± 0.01	3.6 ± 0.3	628 ± 31	1.5 ± 0.3	0.94 ± 0.31	1.4 ± 0.3	1.4 ± 0.2	1.3 ± 0.4	0.91 ± 0.36	0.23 ± 0.14	7.5 ± 2.0	10 ± 0.2	18 ± 2
2,453 m	II	75 ± 0.1	85 ± 6	8.3 ± 2.6	4.5 ± 0.5	0.12 ± 0.03	2.2 ± 0.6	175 ± 9	3.0 ± 0.9	2.4 ± 0.2	2.0 ± 0.03	2.1 ± 0.4	0.82 ± 0.16	0.72 ± 0.02	0.05	11 ± 1	5.5 ± 0.3	30 ± 2
	III	231 ± 63	152 ± 28	16 ± 5	22 ± 5	0.44 ± 0.23	1.9 ± 0.4	423 ± 102	2.0 ± 0.6	1.5 ± 0.3	2.7 ± 0.2	2.9 ± 1.4	1.6 ± 0.02	3.6 ± 1.7	0.83 ± 0.58	15 ± 4	65 ± 5	81 ± 13

^a Not detected above detection limits or blank levels. ^b Duplicates lost due to extreme meteorological conditions.

Table S4.7. Gas-phase atmospheric concentrations of hexachlorobenzene (HCB), the sum of polychlorinated biphenyl congeners (Σ PCB), and the sum of polycyclic aromatic hydrocarbons (Σ PAH) measured in mountainous regions and altitudinal transects in the last two decades by means of passive air sampling (PAS) and active air sampling (AAS).

Site	Altitude (m)	Sampler ¹	R _s ²	HCB (pg m ⁻³)			Σ PCB (pg m ⁻³)			Σ PAH (ng m ⁻³)			Reference
				Average	Range	n	Average	Range	n	Average	Range	n	
Central Pyrenees, Aigüestortes NP ^a , Spain (2017-2020)	1619-2453	PUF-PAS	PRC	44	18-81	7	13	7.5-21	7	0.63	0.18-1.14	This study	
Central Pyrenees, Spain (1996-1997)	2240	PUF-AAS	-	-	-	-	-	-	7	1.69 ^b	1.24-2.30 ^b	Fernández et al. 2002	
									14	2.12 ^b	1.31-3.34 ^b	Fernández et al. 2002	
Central Pyrenees, Spain (1996-1998)	2240	PUF-AAS	-	-	-	-	-	-	7	1.44 ^c	-	van Drooge et al. 2010	
Central Pyrenees, Spain (2000-2002)	2240	PUF-AAS	-	49	36-98	7	21 ^b	10-43 ^b	8	1.48	1.18-2.21	van Drooge et al. 2010	
												van Drooge et al. 2004	
Several remote areas and NPs, Chile ^d	Octe-20	PUF-PAS	PRC	-	-	48	2.2-8.9	1.9-11.4	-	-	-	Pozo et al. 2004	
High Tatras, Slovakia	1778	PUF-AAS	-	85	62-119	10	38	23-64	-	-	-	van Drooge et al. 2004	
Alps, Italy	700-1790	PUF-PAS	3.5	- ^e	- ^e	29	- ^e	25-52	-	-	-	Jaward et al. 2005	
Alps, Italy	700-1790	PUF-AAS	-	- ^e	40-53	29	- ^e	35-125	-	-	-	Jaward et al. 2005	
Mt. Everest, Dingri and Rongbuk Valley, Tibet	4400-4976	PUF-AAS	-	8.9	4.8-12.6	-	-	-	-	-	-	Li et al. 2006	
Rocky Mountains, Revelstoke, Yoho and Banff NPs, Canada	570-2902	XAD-PAS	Assumed	39-50 ^f	21-149	-	-	-	-	-	-	Daly et al. 2007	
Andes, Bolivia	1820-5200	PUF-PAS	PRC	-	-	48	BDL ^g -7.2 ^c	BDL-12	-	-	-	Estellano et al. 2008	
Rocky Mountains, Revelstoke, Yoho and Banff NPs, Canada	570-2902	XAD-PAS	Assumed	-	-	-	-	-	4	0.03-0.23	0.02-1.03	Choi et al. 2009	
Several European remote high-mountain areas	728-2413	PUF-AAS	-	-	-	-	-	-	8	190-4443	56-11950	van Drooge et al. 2010	
Several remote areas near Mt. Everest, Tibetan Plateau	2720-4740	XAD-PAS	Meeteo	25-28	2.8-80	15	4.4-4.4	1.8-8.2	-	-	-	Wang et al. 2010	
Serra do Mar, Serra dos Orgãos NP, Brazil ^d	400-2200	PUF-PAS	PRC	-	-	30	84-305	68-430	-	-	-	Meire et al. 2012	
Serra Geral, São Joaquim NP, Brazil ^d	600-1800	PUF-PAS	PRC	-	-	30	25-177	25-230	-	-	-	Meire et al. 2012	
Lulang, Tibetan Plateau	3330	PUF-AAS	-	7.9	0.1-27.1	6	1.9	BDL-16.7	-	-	-	Sheng et al. 2013	
Sygera Mountain, Tibetan Plateau	3800-4400	PUF-PAS	PRC	12.4	BDL-42	6	1.4	0.1-9.5	-	-	-	Ren et al. 2014	
Sheryla Mountain, Tibetan Plateau	1983-4553	XAD-PAS	Assumed	56	-	25	0.86	0.2-2.2	-	-	-	Zhu et al. 2014	
Western Hubei Mountain, China ^d	1792	PUF-PAS	3.5	82-139	-	-	-	-	-	-	-	Qu et al. 2015	
Serra do Mar, Itatiaia NP, Brazil	700-2400	LDPE-PAS	PRC	25	21-29	-	-	-	-	-	-	Meire et al. 2016	
Serra Geral, São Joaquim NP, Brazil	900-1700	LDPE-PAS	PRC	8	4.3-9.9	-	-	-	-	-	-	Meire et al. 2016	
Nyainqentangha Mountains, Tibetan Plateau	4718	PUF-AAS	-	20	11.4-40.5	6	2.5 ^c	0.2-13.7	15	2.2	0.5-13	Ren et al. 2017	
Nyainqentangha Mountains, Tibetan Plateau	4718	PUF-PAS	PRC	27.8	11.5-40.7	-	-	-	4	0.9-5.2 ^f	0.4-7.8	Zhang et al. 2017	
Mauna Loa, Hawaii, USA	0-3400	FTS-PAS	Meeteo	102.6-131.2 ^f	51.7-135.1	-	-	-	-	-	-	Ali et al. 2018	
Lesser Himalaya, Pakistan	357-2324	PUF-PAS	3.5	2.47	0.17-7.01	36	133	8.5-458	-	-	-	Guida et al. 2018	
Serra do Mar, Itatiaia NP, Brazil	2470	PUF-PAS	Assumed	35	19-67	-	-	-	-	-	-	Guida et al. 2018	
Serra do Mar, Serra dos Órdagos NP, Brazil	2200	PUF-PAS	Assumed	60	43-87	-	-	-	-	-	-	Guida et al. 2018	
Central Himalayas, Nepal ^d	1475-5806	XAD-PAS	Meeteo	9.5-31 ^c	3.6-148.9	7	0.21-1.8 ^c	0.002-6.3	-	-	-	Gong et al. 2019	
Several mountains in British Columbia, Canada	1100-1500	XAD-PAS	Assumed	-	-	27	14	0.4-76	10	0.14-0.92 ^c	0.11-1.40 ^c	Hussain et al. 2019	
Serra Geral, São Joaquim NP, Brazil	990-1700	LDPE-PAS	PRC	-	-	-	-	-	20	41.4 ^c	0.74-90.8	Meire et al. 2019	
Serra do Mar, Itatiaia NP, Brazil	700-2400	LDPE-PAS	PRC	-	-	-	-	-	20	1.17 ^c	0.74-1.61	Meire et al. 2019	
Lesser Himalaya, Pakistan	851-6200	PUF-PAS	3.5	0.31	0.12-0.53	-	-	-	-	-	-	Ullah et al. 2019	
Sheryla Mountain, Tibetan Plateau	859-4217	XAD-PAS	Assumed	-	-	-	-	-	17	- ^e	0.75-9.39	Lin et al. 2020	
Western Hubei Mountain, China	1792	PUF-PAS	3.5	-	-	-	-	-	16	83.8	13.2-426	Hu et al. 2021	
Lesser Himalaya, Pakistan	357-3970	PUF-PAS	3.5	1.3-10.2	0.35-9.8	19	3.5-176	0.01-191	-	-	-	Riaz et al. 2021	

¹ Sampler configurations: PAS (passive air sampler); AAS (active air sampler); PUF (polyurethane foam); XAD (XAD resin); LDPE (low-density polyethylene); FTS (flow through sampler). ² Sampling rates used in the conversion to concentrations: PRC (rates experimentally determined from in situ Performance Reference Compound calibration); 3.5 (m³ day⁻¹, assumed by general consensus as an average value to be used in absence of calibration); Assumed (rate assumed based on previous studies, measurements, and calibrations); Meeteo (rate derived from meteorological variables, e.g., temperature and wind speed).

^a National Park; ^b Detailed data kindly provided by the authors; ^c Partly or completely calculated from data in tables or in the supplementary material of the original reference; ^d Data selected only from sites categorized as remote and mountain areas; ^e Measured but not reported, or reported results in amounts per sampler or in non-numerical form; ^f Median; ^g Below detection limits.

Table S4.8. Correlation matrix between concentrations of target pollutants (Spearman R^2). Values in bold indicate statistical significance ($p < 0.05$).

Phe	Flu	Pyr	B[a]ant	Chr+ TriPh	PCB28	PCB52	PCB101	PCB118	PCB153	PCB138	PCB180	PeCB	HCB	
0.40	0.23	0.03	0.02	0.02	0.06	0.07	0.10	0.03	0.01	0.10	0.01	0.00	0.00	Flu
	0.74	0.26	0.07	0.42	0.01	0.07	0.14	0.01	0.16	0.00	0.01	0.05	0.03	Phe
		0.46	0.19	0.58	0.09	0.09	0.19	0.00	0.11	0.00	0.05	0.00	0.00	Flu
			0.51	0.31	0.04	0.01	0.16	0.14	0.13	0.23	0.35	0.09	0.11	Pyr
				0.20	0.04	0.00	0.20	0.02	0.17	0.12	0.11	0.00	0.01	B[a]ant
					0.27	0.24	0.39	0.02	0.16	0.01	0.09	0.01	0.00	Chr+TriPh
						0.29	0.30	0.00	0.05	0.02	0.07	0.01	0.00	PCB28
							0.57	0.02	0.39	0.05	0.05	0.01	0.01	PCB52
								0.08	0.66	0.28	0.19	0.01	0.00	PCB101
									0.10	0.52	0.41	0.38	0.23	PCB118
										0.33	0.10	0.00	0.01	PCB153
											0.58	0.43	0.37	PCB138
												0.42	0.29	PCB180
													0.63	PeCB



Figure S4.1. Polyurethane foam passive air samplers (PAS-PUFs) inside stainless steel dome housings near lake Collada (2,453 m asl) during January 2018.

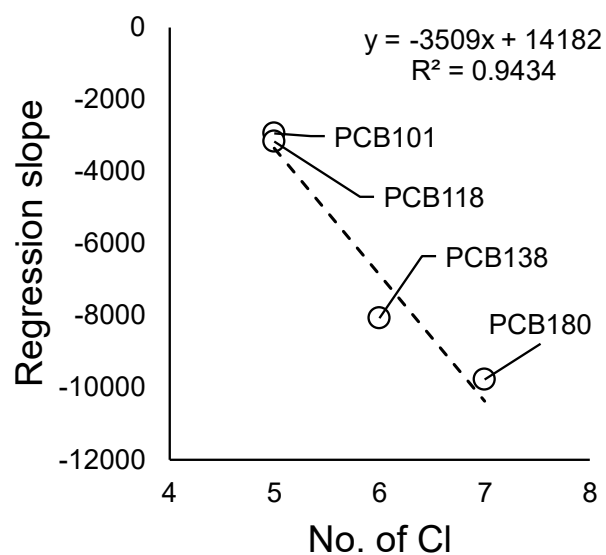


Figure S4.2. Slope of the temperature dependence regression against the number of chlorine substituents of the PCBs.

References S4

- Ali, U., Sweetman, A.J., Jones, K.C., Malik, R.N., 2018. Higher atmospheric levels and contribution of black carbon in soil-air partitioning of organochlorines in Lesser Himalaya. *Chemosphere* 191, 787–798. <https://doi.org/10.1016/j.chemosphere.2017.10.021>
- Choi, S.D., Shunthirasingham, C., Daly, G.L., Xiao, H., Lei, Y.D., Wania, F., 2009. Levels of polycyclic aromatic hydrocarbons in Canadian mountain air and soil are controlled by proximity to roads. *Environ. Pollut.* 157, 3199–3206. <https://doi.org/10.1016/j.envpol.2009.05.032>
- Daly, G.L., Lei, Y.D., Teixeira, C., Muir, D.C.G.G., Wania, F., 2007. Pesticides in Western Canadian Mountain Air and Soil. *Environ. Sci. Technol.* 41, 6020–6025. <https://doi.org/10.1021/es070848o>
- Estellano, V.H., Pozo, K., Harner, T., Franken, M., Zaballa, M., 2008. Altitudinal and seasonal variations of persistent organic pollutants in the Bolivian Andes mountains. *Environ. Sci. Technol.* 42, 2528–2534. <https://doi.org/10.1021/es702754m>
- Fernández, P., Grimalt, J.O., Vilanova, R.M., Fernández, P., Grimalt, J.O., Vilanova, R.M., 2002. Atmospheric gas-particle partitioning of polycyclic aromatic hydrocarbons in high mountain regions of Europe. *Environ. Sci. Technol.* 36, 1162–1168. <https://doi.org/10.1021/es010190t>
- Gong, P., Wang, X., Pokhrel, B., Wang, H., Liu, X.X., Liu, X.X., Wania, F., 2019. Trans-Himalayan Transport of Organochlorine Compounds: Three-Year Observations and Model-Based Flux Estimation. *Environ. Sci. Technol.* 53, 6773–6783. <https://doi.org/10.1021/acs.est.9b01223>
- Guida, Y. de S., Meire, R.O., Torres, J.P.M., Malm, O., 2018. Air contamination by legacy and current-use pesticides in Brazilian mountains: An overview of national regulations by monitoring pollutant presence in pristine areas. *Environ. Pollut.* 242, 19–30. <https://doi.org/10.1016/j.envpol.2018.06.061>
- Harner, T., Bidleman, T.F., 1996. Measurements of octanol-air partition coefficients for polychlorinated biphenyls. *J. Chem. Eng. Data* 41, 895–899. <https://doi.org/10.1021/je960097y>
- Hu, T., Mao, Y., Ke, Y., Liu, W., Cheng, C., Shi, M., Zhang, Z., Zhang, J., Qi, S., Xing, X., 2021. Spatial and seasonal variations of PAHs in soil, air, and atmospheric bulk deposition along the plain to mountain transect in Hubei province, central China: Air-soil exchange and long-range atmospheric transport. *Environ. Pollut.* 291, 118139. <https://doi.org/10.1016/j.envpol.2021.118139>
- Hussain, B.A., Westgate, J.N., Hayward, S.J., Shunthirasingham, C., Brown, T.N., Hung, H., Lei, Y.D., Wania, F., 2019. Polycyclic aromatic hydrocarbons and polychlorinated biphenyls in soils and atmosphere of Western Canadian mountains: The role of source proximity, precipitation, forest cover and mountain cold-trapping. *Atmos. Environ.* X 1, 100004. <https://doi.org/10.1016/j.aeaoa.2018.100004>
- Jaward, F.M., Di Guardo, A., Nizzetto, L., Cassani, C., Raffaele, F., Ferretti, R., Jones, K.C., 2005. PCBs and selected organochlorine compounds in Italian mountain air: The influence of altitude and forest ecosystem type. *Environ. Sci. Technol.* 39, 3455–3463. <https://doi.org/10.1021/es048160o>
- Jin, R., Bu, D., Liu, G., Zheng, M., Lammel, G., Fu, J., Yang, L., Li, C., Habib, A., Yang, Y., Liu, X., 2020. New classes of organic pollutants in the remote continental environment – Chlorinated and

- brominated polycyclic aromatic hydrocarbons on the Tibetan Plateau. *Environ. Int.* 137, 105574. <https://doi.org/10.1016/j.envint.2020.105574>
- Li, J., Zhu, T., Wang, F., Qiu, X.H., Lin, W.L., 2006. Observation of organochlorine pesticides in the air of the Mt. Everest region. *Ecotoxicol. Environ. Saf.* 63, 33–41. <https://doi.org/10.1016/j.ecoenv.2005.04.001>
- Meire, R.O., Khairy, M., Aldeman, D., Galvão, P.M.A., Torres, J.P.M., Malm, O., Lohmann, R., 2019. Passive sampler-derived concentrations of PAHs in air and water along Brazilian mountain transects. *Atmos. Pollut. Res.* 10, 635–641. <https://doi.org/10.1016/j.apr.2018.10.012>
- Meire, R.O., Khairy, M., Targino, A.C., Galvão, P.M.A., Torres, J.P.M., Malm, O., Lohmann, R., 2016. Use of passive samplers to detect organochlorine pesticides in air and water at wetland mountain region sites (S-SE Brazil). *Chemosphere* 144, 2175–2182. <https://doi.org/10.1016/j.chemosphere.2015.10.133>
- Meire, R.O., Lee, S.C., Targino, A.C., Torres, J.P.M., Harner, T., 2012. Air concentrations and transport of Persistent Organic Pollutants (POPs) in mountains of southeast and southern Brazil. *Atmos. Pollut. Res.* 3, 417–425. <https://doi.org/10.5094/APR.2012.048>
- Pozo, K., Harner, T., Shoeib, M., Urrutia, R., Barra, R., Parra, O., Focardi, S., 2004. Passive-sampler derived air concentrations of persistent organic pollutants on a north-south transect in Chile. *Environ. Sci. Technol.* 38, 6529–6537. <https://doi.org/10.1021/es049065i>
- Qu, C., Xing, X., Albanese, S., Doherty, A., Huang, H., Lima, A., Qi, S., De Vivo, B., 2015. Spatial and seasonal variations of atmospheric organochlorine pesticides along the plain-mountain transect in central China: Regional source vs. long-range transport and air-soil exchange. *Atmos. Environ.* 122, 31–40. <https://doi.org/10.1016/j.atmosenv.2015.09.008>
- Ren, J., Wang, X., Wang, C., Gong, P., Yao, T., 2017. Atmospheric processes of organic pollutants over a remote lake on the central Tibetan Plateau: Implications for regional cycling. *Atmos. Chem. Phys.* 17, 1401–1415. <https://doi.org/10.5194/acp-17-1401-2017>
- Ren, J., Wang, X., Xue, Y., Gong, P., Joswiak, D.R., Xu, B., Yao, T., 2014. Persistent organic pollutants in mountain air of the southeastern Tibetan Plateau: Seasonal variations and implications for regional cycling. *Environ. Pollut.* 194, 210–216. <https://doi.org/10.1016/j.envpol.2014.08.002>
- Riaz, R., Malik, R.N., de Wit, C.A., 2021. Soil-air partitioning of semivolatile organic compounds in the Lesser Himalaya region: Influence of soil organic matter, atmospheric transport processes and secondary emissions. *Environ. Pollut.* 291, 118006. <https://doi.org/10.1016/j.envpol.2021.118006>
- Sheng, J., Wang, X., Gong, P., Joswiak, D.R., Tian, L., Yao, T., Jones, K.C., 2013. Monsoon-driven transport of organochlorine pesticides and polychlorinated biphenyls to the tibetan plateau: Three year atmospheric monitoring study. *Environ. Sci. Technol.* 47, 3199–3208. <https://doi.org/10.1021/es305201s>
- Shoeib, M., Harner, T., 2002. Characterization and comparison of three passive air samplers for persistent organic pollutants. *Environ. Sci. Technol.* 36, 4142–4151. <https://doi.org/10.1021/es020635t>
- Ullah, R., Asghar, R., Baqar, M., Mahmood, A., Ali, S.N., Sohail, M., Schäfer, R.B., Eqani, S.A.M.A.S., 2019. Assessment of organochlorine pesticides in the Himalayan riverine ecosystems from Pakistan

- using passive sampling techniques. *Environ. Sci. Pollut. Res.* 26, 6023–6037. <https://doi.org/10.1007/s11356-018-3987-6>
- Van Drooge, B.L., Fernández, P., Grimalt, J.O., Stuchlík, E., García, C.J.T., Cuevas, E., 2010. Atmospheric polycyclic aromatic hydrocarbons in remote European and Atlantic sites located above the boundary mixing layer. *Environ. Sci. Pollut. Res.* 17, 1207–1216. <https://doi.org/10.1007/s11356-010-0296-0>
- Van Drooge, B.L., Grimalt, J.O., Camarero, L., Catalan, J., Stuchlík, E., Torres García, C.J., 2004. Atmospheric semivolatile organochlorine compounds in European high-mountain areas (Central Pyrenees and High Tatras). *Environ. Sci. Technol.* 38, 3525–3532. <https://doi.org/10.1021/es030108p>
- Wang, C., Wang, X., Ren, J., Gong, P., Yao, T., 2017. Using a passive air sampler to monitor air–soil exchange of organochlorine pesticides in the pasture of the central Tibetan Plateau. *Sci. Total Environ.* 580, 958–965. <https://doi.org/10.1016/j.scitotenv.2016.12.046>
- Wang, X.P., Gong, P., Yao, T.D., Jones, K.C., 2010. Passive air sampling of organochlorine pesticides, polychlorinated biphenyls, and polybrominated diphenyl ethers across the tibetan plateau. *Environ. Sci. Technol.* 44, 2988–2993. <https://doi.org/10.1021/es9033759>
- Zhang, X., Barnes, J., Lei, Y.D., Wania, F., 2017. Semivolatile Organic Contaminants in the Hawaiian Atmosphere. *Environ. Sci. Technol.* 51, 11634–11642. <https://doi.org/10.1021/acs.est.7b03841>
- Zhu, N., Schramm, K.W., Wang, T., Henkelmann, B., Zheng, X., Fu, J., Gao, Y., Wang, Y., Jiang, G., 2014. Environmental fate and behavior of persistent organic pollutants in Shergyla Mountain, southeast of the Tibetan Plateau of China. *Environ. Pollut.* 191, 166–174. <https://doi.org/10.1016/j.envpol.2014.04.031>



Article 5

PASSIVE WATER SAMPLING AND AIR-WATER DIFFUSIVE EXCHANGE OF LONG-RANGE TRANSPORTED SEMI-VOLATILE ORGANIC POLLUTANTS IN HIGH-MOUNTAIN LAKES

Raimon M. Prats, Barend L. van Drooge, Pilar Fernández, Joan O. Grimalt
Submitted for publication to Science of the Total Environment

Article 5

Submitted for publication to *Science of the Total Environment*

Passive water sampling and air–water diffusive exchange of long-range transported semi-volatile organic pollutants in high-mountain lakes

Raimon M. Prats*, Barend L. van Drooge, Pilar Fernández, Joan O. Grimalt

Institute of Environmental Assessment and Water Research (IDAEA-CSIC), Jordi Girona 18, 08034 Barcelona, Catalonia, Spain

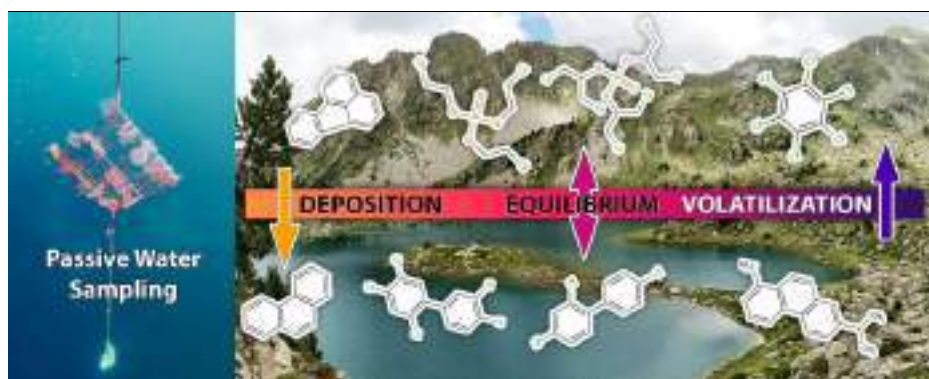
HIGHLIGHTS

- LDPE and SR passive water samplers were used to analyze HOCs in high-mountain lakes.
- PCB concentrations were lower than 20 years ago, while HCB remained the same.
- PAH concentrations were reduced by half, as did atmospheric emissions in Europe.
- OPEs were detected for the first time in these lakes at environmentally relevant levels.
- Air-water fluxes revealed generalized deposition or near-equilibrium conditions.

KEYWORDS

Passive sampling
Polycyclic aromatic hydrocarbons
Organophosphate esters
Polychlorinated biphenyls
Freely dissolved

GRAPHICAL ABSTRACT



ABSTRACT

The concentrations of several legacy and currently emitted organic pollutants were determined in the freely dissolved phase of water from six high-mountain lakes in the Pyrenees (1619–2453 m) by means of passive water sampling. Low-density polyethylene (LDPE) and silicone rubber (SR) sheets were exposed for three consecutive periods lasting each one year between 2017 and 2020 for the study of polychlorinated biphenyls (PCBs), hexachlorobenzene (HCB), organophosphate esters (OPEs), and polycyclic aromatic hydrocarbons (PAHs), pentachlorobenzene (PeCB) and dichlorodiphenyldichloroethylene (4,4'-DDE). Σ PCB concentrations ($1.2\text{--}2.2\text{ pg L}^{-1}$) were substantially lower than measured with pumping systems over two decades ago in the same area, while HCB ($1.0\text{--}14\text{ pg L}^{-1}$) remained essentially the same. Σ PAHs ($35\text{--}920\text{ pg L}^{-1}$) were around half of those observed in the past, which agrees with reports of reductions in atmospheric emissions over Europe. Σ OPEs ($139\text{--}2849\text{ pg L}^{-1}$) were measured for the first time in this area and were found at high concentrations, but the resulting levels suffer from higher uncertainties in their partition coefficients than the other compounds, which hindered the assessment of spatial and temporal trends. Concentrations of most compounds obtained with LDPE and SR samplers agreed with each other by ratios generally lower than three or four times, except for a few PAHs and OPEs. Diffusive exchange flux calculations between the atmospheric gas phase and the freely dissolved water phase revealed net deposition of pollutants from air to water, except for some OPEs and PCBs presenting equilibrium conditions, and HCB with volatilization fluxes. Atmospheric degradation fluxes of PAHs and OPEs point at competing removal mechanisms that further support the air-to-water direction of their diffusive exchange, while PCBs and HCB were not affected by photodegradation. In their current state, these remote lakes seem to act on average as accumulators of many emerging and legacy pollutants subject to long-range atmospheric transport.

* Corresponding author.

E-mail address: raimon.martinez@idaea.csic.es (R.M. Prats).

1. Introduction

Hydrophobic organic compounds (HOCs) are ubiquitous pollutants present in all environmental compartments, including the freely dissolved phase of water from oceans, rivers, and lakes. Many HOCs are semi-volatile and persistent. Their intermediate volatility allows them to disperse through the global atmosphere but also accumulate in water bodies and most environmental matrices, and their persistence provides them with a remarkable resistance to degradation. HOCs of major concern include currently emitted pollutants such as polycyclic aromatic hydrocarbons (PAHs) and organophosphate esters (OPEs), the latter included in the lists of emerging contaminants, and banned legacy pollutants such as polychlorinated biphenyls (PCBs), hexachlorobenzene (HCB), and pentachlorobenzene (PeCB).

Exposure to these compounds has been related to different toxic effects both in humans and in organisms. PCBs have been observed to cause neurotoxicity and endocrine dysfunction, also in human infants (Darvill et al., 2000; Forns et al., 2012a and 2012b; Grandjean and Landrigan, 2014; Tan et al., 2004; Winneke et al., 2002), decreased fetal growth (Casas et al., 2015; Lopez-Espinosa et al., 2016), and disruption of the thyroid function (Alvarez-Pedrerol et al., 2008; Chevrier et al., 2008; Sala et al., 2001). HCB has been linked to disruption of thyroid metabolism and cancer (Grimalt et al., 1994; Llop et al., 2017; Sala et al., 2001) and low prenatal growth (Lopez-Espinosa et al., 2016). DDT and its metabolites were related to oxidative damage and increased apoptosis (Pérez-Maldonado et al., 2006, 2005), genotoxicity (Gerić et al., 2012), deleterious effects on the nervous system (Van Wendel De Joode et al., 2001), and increased risk of cancer (Eskenazi et al., 2009 and references therein). Many PAHs have been associated to organ damage and abnormalities in immune and lung functions (Abdel-Shafy and Mansour, 2016 and references therein) as well as to carcinogenicity and mutagenicity (Armstrong et al., 2004; Boström et al., 2002; Wenger et al., 2009). Finally, OPEs are endocrine disruptors (Hu et al., 2022), suspected neurotoxicants (Wei et al., 2015; Yang et al., 2019) and carcinogens (WHO, 1998).

Diffusive air-water exchange processes have been identified as a globally dominating deposition pathway for many HOCs in lakes and oceans (Bidleman and McConnell, 1995; Wania et al., 1998). Since temperature plays a principal role in determining the direction of the exchange (Mackay and Wania, 1995), alpine lakes in cold high-mountain areas tend to act as sinks of HOCs after long-range atmospheric transport (Grimalt et al., 2001; Nellier et al., 2015a; Ren et al., 2017a; Vilanova et al., 2001b). As such, these sites have become reference ecosystems for the study of the environmental fate of anthropogenic pollutants (e.g., Fernández et al., 2005; Nellier et al., 2015b; Schmid et al., 2011; Vilanova et al., 2001c) and risk for aquatic organisms related to their exposure and toxicity (e.g., Bartrons et al., 2011; Gallego et al., 2007; Vives et al., 2005). Still, re-volatilization from water to air has also been observed in oligotrophic and high-altitude lakes (Blais et al., 2001; Luarte et al., 2022), with seasonal changes being an important driver of variability in water concentrations and thus exchange fluxes between environmental compartments (Meijer et al., 2009, 2006).

Alpine lakes distant from primary sources of atmospheric contaminants are thus valuable sentinel regions for the assessment of the distribution, accumulation, and impact of diffuse background pollution. Previously reported water monitoring studies consisted of discrete sampling operations (Vilanova et al., 2001a, 2001b, and 2001c), but the inaccessibility of remote mountain lakes renders them infeasible over extended periods of time when several sites are considered. Instead, passive samplers offer a cost-effective, simple-to-use alternative as they absorb HOCs over extended exposure periods. This alternative approach has been implemented in recent decades by using low-density polyethylene (LDPE) and silicone rubber (SR) polymers for the uptake of nonpolar compounds in global monitoring networks (Lohmann et al., 2017; Lohmann and Muir, 2010; Sobotka et al., 2022). The partitioning properties of many HOCs between the freely dissolved phase of water and these polymers have been assessed (Smedes et al., 2009; Smedes, 2018) and, together with diffusive uptake models and in situ sampler calibration strategies, they allow accurate determinations of HOC concentrations in water (Booij et al., 2007; Booij and Smedes, 2010; Huckins et al., 2006). However, under changing weather conditions, uncertainties in polymer uptake, calibration of the samplers, and physical-chemical properties of the studied compounds introduce uncertainties into the concentration calculations. These errors may be particularly relevant for the assessment of trace-level concentrations from high-mountain areas, so further study on the performance of this approach in such locations is still needed.

Here, we present a study of the occurrence of different groups of organic pollutants emitted from distant sites in waters of high-altitude mountain lakes in the Pyrenees (Fig. 1) by means of passive sampling. LDPE and SR passive water samplers (PWS) were deployed during three consecutive periods lasting one year each between 2017 and 2020 at six lakes encompassing an altitudinal gradient between 1619 and 2453 m above sea level in a National Park area within a radius of less than 9 km. The concentrations obtained using both polymer types were compared for the assessment of accuracy and precision of the measurements. The results from the present work were also compared to pollutant levels determined in the area two decades ago by water-pumping sampling, which could provide valuable indications on whether regulations had noticeable consequences on pollutant levels in remote ecosystems. Moreover, the present measurements were performed simultaneously with the determination of the same compounds in the atmospheric gas phase surrounding the lakes, which allows the determination of diffusive air-water exchange fluxes and, therefore, of the role of alpine lakes as sentinel ecosystems of the impact of long-range transported pollutants into remote continental areas. Atmospheric degradation fluxes were also calculated in order to determine the gas-phase removal rates of pollutants in comparison with possible deposition into the lakes.

2. Materials and methods

2.1. Sampling site

The waters of six remote Pyrenean alpine lakes were sam-



Fig. 1. Location of the studied lakes in the Central Pyrenees, between the National Park of Aigüestortes and Val d'Aran.

pled and analyzed during three yearly periods (2017–2020): Lakes Llebreta (1619 m), Llong (2000 m), Sarradé (2123 m), Redon (2240 m), Dellui (2349 m), and Collada (2453 m) (Fig. 1). They are located in a European Union's Natura 2000 protected area in the Central Pyrenees encompassing the National Park of Aigüestortes i Estany de Sant Maurici and Val d'Aran (Catalonia, Spain). They are oligotrophic lakes of glacial origin (Catalan et al., 2006) with catchments generally characterized by rocky slopes. All lakes except Redon belong to the National Park and are located in the same main catchment (50.9 km²), while Lake Redon lies in a separate valley with its own catchment (1.4 km²). The lowest lakes (Llebreta, Llong, and to a lesser degree, Sarradé) are surrounded by subalpine meadows and forests, while the higher lakes (Redon, Dellui, and Collada) are cirque lakes in small rocky catchments above the tree line, covered by alpine meadows and bare rock. They are relatively small, shallow lakes (0.02–0.07 km², <15 m maximum depth, while Sarradé has 24 m maximum depth) but Lake Redon has an extension of 0.25 km² and maximum depth of 73 m. All lakes freeze between November and December and remain ice covered for up to seven months (Catalan et al., 1992). Thus, most of the water input into the lakes comes from snowmelt.

2.2. Water sampling

LDPE-PWS were deployed at all lakes for a year-long sampling period between 2017 and 2018, followed up by two additional yearly periods, 2018–2019 and 2019–2020 in Lakes Llebreta, Sarradé, and Redon (Table 1). SR-PWS were deployed in these three lakes along with LDPE-PWS during the last sampling period. The specifications of both sampler types were the same as those used in the Aquatic Global Passive Sampling (AQUA-GAPS/MONET, from here on just AQUA-GAPS) monitoring network (Lohmann et al., 2017; Lohmann and Muir, 2010). Sampler preparations were performed at RECETOX facilities (Masaryk University,

Brno, Czech Republic) as detailed elsewhere (Sobotka et al., 2022) following standard guidelines (Smedes and Booij, 2012). Briefly, 90 × 55 mm LDPE (0.08 mm thickness, 0.924 g cm⁻³ density, Alto-Rego Corporation, Etobicoke, ON, Canada) and translucent SR sheets (0.25 mm thickness, 1.14 g cm⁻³ density, Shielding Solution LTD) were Soxhlet-extracted for 100 h with ethyl acetate and hexane:acetone 1:1 (v/v), respectively. The sheets were spiked with a Performance Reference Compound (PRC) mixture consisting of PCB congeners 1, 2, 3, 10, 14, 21, 50, 55, 78, 104, 145, and 204 by soaking in methanol with stepwise addition of water until 50% (v/v) content. The sampler sheets were packed into amber glass jars and transported at -20 °C until deployment.

Twelve sampler sheets were deployed per lake and period. The punctured sheets were fixed to stainless steel grills using nylon cable ties and suspended 4 m below the water surface with a submerged buoy and an anchor (Fig. 2). The samplers were retrieved after approximately one year of exposure. Any biofouling was wiped off on site, and the samplers were stored in clean amber glass jars, sealed airtight inside PET/LLDPE bags (Kapak Corporation, St. Louis Park, MI, USA), and stored at -20 °C until extracted. Four unexposed sampler sheets per site were used as reference blanks for PRC calibration. These blanks were exposed to the air during sampler deployment and retrieval operations and stored in separate amber glass jars at -20 °C during the remainder of the sampling period.

Meteorological conditions of the sampling periods such as air temperature, atmospheric pressure, and wind speed were recorded by an automatic weather station from the XEMA network of the Catalan Meteorological Service (see Table S1 for a summary). Additionally, the site-specific air temperatures were continuously measured using Tinytag Plus 2 data loggers (Gemini Data Loggers, Chichester, UK) (Table 1).

Table 1

Passive water sampling campaigns (PWS) and calibration output for each site. Proportionality constants (B, Eq. 3), sampling rates (R_s, Eq. 2), effective water sampled volumes (V_w, Eq. 1) and standard errors (SE) are shown for a reference molecular weight of 300 g mol⁻¹.

	PWS I (LDPE ^a)				PWS II (LDPE)				PWS III (LDPE)				PWS III (SR ^b)					
	Lliebreta	Llong	Sarradé	Redon	Dellui	Collada	Lliebreta	Sarradé	Redon	Lliebreta	Sarradé	Redon	Lliebreta	Sarradé	Redon	Lliebreta	Sarradé	Redon
Deployed	21/9/2017	19/9/2017	24/11/2017	17/9/2017	22/9/2017	23/9/2017	18/10/2018	18/10/2018	25/9/2018	26/9/2019	26/9/2019	27/9/2019	26/9/2019	26/9/2019	27/9/2019	26/9/2019	26/9/2019	27/9/2019
Retrieved	26/9/2018	26/9/2018	26/9/2018	25/9/2018	27/9/2018	27/9/2018	26/9/2019	26/9/2019	27/9/2019	6/10/2020	6/10/2020	7/10/2020	6/10/2020	6/10/2020	7/10/2020	6/10/2020	6/10/2020	7/10/2020
Exposure, d	370	372	306	373	370	369	343	343	367	376	376	376	376	376	376	376	376	376
Mean T, °C	9.1	5.2	6.3	2.9	2.8	2.8	9.9	7.2	3.7	10.4	7.6	4.2	10.4	7.6	4.2	10.4	7.6	4.2
Air T October ^c , °C	13.1±2.7	8.4±1.8	10.5±2.3	6.8±1.1	8.2±2.0	7.7±2.1	9.9±4.6	–	3.5±4.7	11.2±3.0	9.1±3.1	5.6±2.6	11.2±3.0	9.1±3.1	5.6±2.6	11.2±3.0	9.1±3.1	5.6±2.6
B	306.5	216.1	78.5	274.3	200.9	134	77.2	73.2	98.8	145.9	112	138.3	143	52.3	156.4	143	52.3	156.4
SE (B)	7.1	4.5	3.6	21.4	10.9	7.2	6.9	9.3	19.6	35.9	13	23.3	21.9	17.1	26.6	21.9	17.1	26.6
R _s 300, L d ⁻¹	21	14.8	5.4	18.8	13.8	9.2	5.3	5	6.8	10	7.7	9.5	9.8	3.6	10.7	9.8	3.6	10.7
SE (R _s 300), L d ⁻¹	0.5	0.3	0.2	1.5	0.7	0.5	0.5	0.6	1.3	2.5	0.9	1.6	1.5	1.2	1.8	1.5	1.2	1.8
V _w 300, L	7769	5507	1647	7008	5092	3387	1815	1721	2484	3757	2885	3562	3684	1349	4028	3684	1349	4028
SE (V _w 300), %	2.3	2.1	4.6	7.8	5.4	5.4	8.9	12.7	19.8	24.6	11.6	16.8	15.3	32.6	17	15.3	32.6	17

^a Low-density polyethylene; ^b silicone rubber; ^c average values and standard deviations of the semi-hourly measurements recorded between 1 Oct and 2 Nov.



Fig. 2. Low-density polyethylene passive water samplers (LDPE-PWS) after a year of deployment below the water surface. The LDPE sheets were mounted onto a stainless-steel rack held four meters below the surface by a buoy and a heavy weight.

2.3. Extraction and clean-up

The sampler sheets were Soxhlet-extracted in batch for 8 h with acetonitrile (all solvents from Merck, Darmstadt, Germany) after spiking them with a mixture of recovery standards containing fluorene-d₁₀, phenanthrene-d₁₀, anthracene-d₁₀, fluoranthene-d₁₀, pyrene-d₁₀, benz[a]anthracene-d₁₂, chrysene-d₁₂, benzo[b]fluoranthene-d₁₂, benzo[k]fluoranthene-d₁₂, benzo[a]pyrene-d₁₂, benzo[ghi]perylene-d₁₂, indeno[1,2,3-cd]pyrene-d₁₂ (National Institute of Standards and Technology, Gaithersburg, MD, USA), tributyl phosphate-d₂₇, tris(2-chloroethyl) phosphate-d₁₂, tris(1-chloro-2-propyl) phosphate-d₁₈, tris(1,3-dichloro-2-propyl) phosphate-d₁₅, triphenyl phosphate-d₁₅ (Cambridge Isotope Laboratories, Tewksbury, MA, USA), 1,2,4,5-tetrabromobenzene, and decachlorobiphenyl (Dr. Ehrenstorfer, Augsburg, Germany). It must be noted that the samplers from the first period (PWS I) were extracted with acetonitrile:methanol 2:1 (v/v) as in Smedes and Booij (2012), but subsequent batches were treated as recommended in updated procedures (Sobotka et al., 2022). After the extraction, the sampler sheets were dried and weighted for the determination of the exact sampler masses. The extracts were concentrated down to 2 mL by vacuum rotary evaporation, liquid/liquid extracted with hexane, and both fractions were separately dried over 1 g of anhydrous Na₂SO₄ (Merck) activated overnight in an oven at 450 °C, concentrated in the rotary evaporator down to 2 mL, and further concentrated to 0.5 mL under a gentle stream of nitrogen gas.

An additional clean-up step was performed for the hexane phase, which was separated into two fractions, respectively containing PAHs and organochlorine compounds. The separation was performed with an Agilent 1200 Series HPLC system (Agilent Technologies, Santa Clara, CA, USA) equipped with a fraction collector module and a 25 cm × 3 mm × 0.46 cm i.d. Tracer Excel 120 SI HPLC silica column (Teknokroma, Sant Cugat del Vallès). The detailed fractionation procedure has been described elsewhere (Prats et al., 2021). The eluted fractions were concentrated under nitrogen gas down to 0.5 mL.

2.4. Instrumental analysis

PAHs, PCBs, and OCs were analyzed by gas chromatography–single quadrupole mass spectrometry (GC-MS) using a Thermo Trace GC Ultra–DSQ II (Thermo Fisher Scientific, Waltham, MA, USA) with a HP-5MS fused capillary column (60 m × 0.25 mm i.d. × 25 μm, Agilent Technologies). The extracts were injected in electron impact mode (EI, 70 eV) with injector, ion source, quadrupole, and transfer line temperatures of 280, 250, 150, and 270 °C, respectively. The carrier gas was helium at 1 mL min⁻¹, and the oven program was as follows: 90 °C held for 1 min, then increased to 150 °C (10 °C min⁻¹) and to 320 °C (6 °C min⁻¹), finally held at 320 °C for 20 min. The target compounds were identified and quantified in SIM mode by retention time and m/z fragments. The target compounds, PRCs, and recovery standards are listed in Table S2 along with their abbreviations and m/z fragments.

OPEs were analyzed in the acetonitrile fraction of the extracts by gas chromatography–triple quadrupole tandem mass spectrometry (GC-MS/MS) using an Agilent 7000 Series Triple Quad GC/MS (Agilent Technologies) with a Zebron ZB-PAH capillary column (30 m × 0.25 mm i.d. × 0.25 μm, Phenomenex, Torrance, CA, USA). The extracts were injected in EI mode with injector, ion source, quadrupoles, and transfer line temperatures of 280, 230, 150, and 280 °C, respectively. The carrier gas was helium at 1.1 mL min⁻¹, and the oven program was as follows: 80 °C held for 1.5 min, then increased to 220 °C (10 °C min⁻¹) and to 315 °C (15 °C min⁻¹), finally held at 315 °C for 5 min. The analyzed compounds were identified and quantified in multiple reaction monitoring (MRM) mode by retention time and m/z qualifier and quantifier transitions. The target compounds and recovery standards are listed in Table S3 along with their abbreviations, m/z transitions, and collision energies.

2.5. Quality control and assurance

Internal standard calibration was used for the quantification of compounds, accounting for instrumental variability and method recoveries. Recoveries were 66–90 % for PCBs and organochlorines, 73–103 % for PAHs, and 48–106 % for OPEs. Limits of quantification in column (10 × s/n) were 0.5–2.5 pg for PAHs, PCBs, and organochlorines, and 0.12–0.25 pg for OPEs, or 25–125 and 6.25–12.5 pg per sample, respectively. These correspond to 0.03–5.1 pg L⁻¹ for PAHs, PCBs, and organochlorine compounds, and 0.03–4.8 pg L⁻¹ for OPEs, where the average water sampled volumes were calculated for each compound (see Section 2.6).

Field blanks were used for subtracting contamination absorbed by the sampler sheets during storage, transport, and manipulation of the sheets and extracts. However, the contamination in exposed samplers can be overestimated if full blank levels are subtracted. Part of the contaminants absorbed before sampler deployment are released into the water while staying absorbed into the unexposed blank sheets. This difference between sheets is relevant when sampling takes place in relatively clean surface waters, as is the case for alpine lakes. Therefore, average contaminant amounts per sampler were subtracted in two steps: 50% of the blank amounts (corresponding to contamination absorbed between retrieval and analysis) were entirely subtracted from the analyzed amounts per exposed sampler, while the other 50% (corresponding to contamination absorbed between sampler pre-cleaning and deployment) was subtracted based on the achievement of equilibrium conditions during exposure (i.e., multiplying half of the blank amounts per sampler by 1-DEQ, the Degree of Equilibrium). The DEQ is a measure of the attainment of equilibrium during sampler exposure in the water, and its calculation is performed as described in Section 2.6. This step corrects sampler contamination proportionally to the state of partitioning equilibrium between sampler and water of each compound, therefore accounting for the partial release of contaminants present in the sampler sheets before exposure. Compounds that reached equilibrium between sampler and water during exposure (DEQ=1, or 1-DEQ=0) will not need subtraction of the pre-exposure half of the blanks since the amounts of target compound per sampler directly represent concentrations in water. Contrarily, compounds still in the uptake phase (DEQ<1, 1-DEQ>0) will be affected by possible contamination present before deployment. Blank levels were most relevant for OPEs in LDPE samplers (present in 100% of blanks, 19–55% of exposed sampler amounts on average), but less so for PAHs (47% of blanks, below detection level, BDL–29%) and not relevant for PCBs and organochlorines (13% of blanks, BDL–18%).

2.6. Effective sampled water volumes

Compound- and site-specific effective sampled water volumes (V_w , in L), necessary for reporting concentrations in the freely dissolved phase of water, were calculated as described in Equation 1 (Booij et al., 2007; Huckins et al., 2006):

$$V_w = K_{PWS-w} m_{PWS} \left[1 - \exp\left(\frac{-R_s t}{K_{PWS-w} m_{PWS}}\right) \right] \quad (1)$$

where K_{PWS-w} is the passive water sampler–water partition coefficient of each studied compound (L kg⁻¹), m_{PWS} is the combined sampler mass (kg), R_s is the sampling rate (L d⁻¹), and t is the exposure time (d). The part of the equation between brackets represents the degree of equilibrium (DEQ), a value between 0 and 1 that measures the degree of attainment of equilibrium conditions during exposure. K_{PWS-w} values for the studied compounds were obtained from the literature (Rusina et al., 2019; Smedes et al., 2009; Smedes, 2018) and are listed in Table S4. Since no K_{PWS-w} were available for OPEs, they were extrapolated from silicone values (Fig. S1). R_s were obtained from the following

relationship with molar mass (M , g mol⁻¹) (Rusina et al., 2010):

$$R_S = \frac{B}{M^{0.47}} \quad (2)$$

where B is a proportionality constant that accounts for hydrodynamic conditions such as turbulence, sampler geometry, and unit conversion. B is determined from the PRC calibration of the samplers as follows:

$$C/C_0 = \exp\left(\frac{-B t}{K_{PWS-W} M^{0.47} m_{PWS}}\right) \quad (3)$$

where C/C_0 is the fraction of retained PRCs, calculated as the ratio between the amount of each PRC present in the exposed sheets after sampling and the amount in the unexposed reference blanks. Sampling site-specific B values were adjusted by fitting C/C_0 as a function of $K_{PWS-W} M^{0.47}$ using an unweighted nonlinear least-squares (NLS) method (Booij and Smedes, 2010). K_{PWS-W} values for the PRCs were obtained from Smedes et al. (2009) and are listed in Table S4.

2.7. Air–water exchange and atmospheric degradation fluxes

Freely dissolved pollutant concentrations in water from the first sampling period (PWS I) were used for the estimation of net air–water exchange fluxes (F , ng m⁻² d⁻¹) along with atmospheric gas phase concentrations measured simultaneously at each site during three passive air sampling periods (PAS I–III) presented elsewhere (Prats et al., 2022b, 2022a). These air concentrations have been summarized in Table S5. The exchange fluxes were calculated as outlined in Schwarzenbach et al. (2016):

$$F = k_{AW} \left(C_W - \frac{C_A}{K_{AW}} \right) \quad (4)$$

where k_{AW} is the overall air–water exchange velocity (m d⁻¹), C_W is the concentration of the compound in the freely dissolved phase of water (ng m⁻³), C_A is the concentration of the compound in the atmospheric gas phase (ng m⁻³), and K_{AW} is the equilibrium air–water partition constant (dimensionless). K_{AW} is equivalent to H/RT , the non-dimensional Henry's Law constant, where R is the ideal gas constant (Pa m³ K⁻¹ mol⁻¹) and T is the average temperature of the sampling period (K) (Table 1). Henry's law constants at 298 K (Williams et al., 2017) were temperature-corrected as proposed elsewhere (Hulscher et al., 1992).

The calculation of k_{AW} was performed as follows:

$$\frac{1}{k_{AW}} = \frac{1}{k_W} + \frac{1}{k_A K_{AW}} \quad (5)$$

where k_W and k_A are the water-side and air-side single-phase exchange velocities, respectively (in cm s⁻¹, later converted into m s⁻¹ for the calculation of F). Both coefficients depend on meteorological conditions like wind speed and temperature (Table 1, Table S1), and the physical-chemical properties of each compound (Table S4). They were calculated using a boundary layer model first proposed by Deacon (1977) and outlined in Schwarzenbach et al. (2016).

Full details on the complete exchange flux calculation are provided in Text S1. Theoretical uncertainties were estimated individually for each compound through propagation of the error from the variables involved in the calculation of the flux. Further description of the calculation of theoretical flux uncertainties is provided in Text S2.

Additionally, atmospheric degradation fluxes due to oxidation by free hydroxyl radicals in the atmospheric mixing layer were calculated as follows:

$$F_{deg} = h_{ABL} k_{OH} C_{OH} C_A \quad (6)$$

where h_{ABL} is the average height of the atmospheric boundary layer (m), k_{OH} is the compound-specific atmospheric hydroxylation rate (cm³ molec⁻¹ s⁻¹), C_{OH} is the concentration of hydroxyl radicals in the atmospheric layer (molec cm⁻³), and C_A is the measured gas-phase concentration of the compound (ng m⁻³). Additional details on the calculation of these variables are provided in Text S3.

3. Results and discussion

3.1. Sampling rates and effective sampled volumes

Table 1 summarizes the sampler deployment conditions and calibration output for all studied sites and periods. Effective sampled water volumes (V_W) were determined individually for each compound and sampling site from sampling rates derived by means of PRC calibration. The PRC depletion ratios and best NLS fit curves are shown in Fig. S2. The sampling rates are compound-specific, so R_S and V_W are shown for a reference molecule of molecular weight 300 g mol⁻¹. $R_{S\ 300}$ for LDPE-PWS ranged between 5.4 and 21.0 L d⁻¹ in the first sampling period, PWS I, between 5.0 and 6.8 L d⁻¹ in PWS II, and between 7.7 and 10.0 L d⁻¹ in PWS III, while it varied between 3.6 and 10.7 L d⁻¹ for SR-PWS in PWS III (Table 1). Some differences between lakes and their exposure conditions become apparent from $R_{S\ 300}$, such as samplers in Lake Sarradé consistently presenting rates lower than the other lakes. $V_{W\ 300}$ were 1647–7769 L and 1349–4028 L for the LDPE and SR samplers, respectively. Estimated relative standard errors of $V_{W\ 300}$ ranged from 2.1 to 24.6% for LDPE and from 15.3 to 32.6% for SR. The standard error associated to the NLS fit was noticeably lower for PWS I (2.1–7.8%) than for the two following periods (8.9–32.6%), as can be seen by how the NLS curves adjust to individual PRC fractions in Fig. S2.

$R_{S\ 300}$ at some sampling sites for PWS I were also larger than in the following periods (e.g., LDPE in Llebrete 21.0 L d⁻¹ in PWS I, but 5.3 and 10.0 L d⁻¹ in PWS II and III, respectively), although not for all of them (e.g., LDPE in Sarradé 5.4 L d⁻¹ in PWS I, and 5.0 and 7.7 L d⁻¹ in PWS II and III, respectively). These differences in R_S are reflected in the volumes effective sampled volumes. Thus, in Redon, the volumes sampled in the PWS I, II and III periods were 7769, 2484, and 4028 L, respectively (Table 1). These differences paralleled the measured water precipitation in these periods, 2030, 1348, and 1605 mm (Table S1). Calculation of the average and standard deviation of the semi-hourly air temperatures in the month prior to freezing (October), 6.8±1.1, 3.5±0.5, and 5.6±2.6 °C for PWS I, II and III, respectively (Table 1), also show parallelism with sampling volumes, resulting in larger volumes at higher temperatures.

These recorded average temperatures in October were significantly different ($p < 0.001$). Similarly, in Lake Llebreta, the sampled volumes in PWS I, II, and III, 7769, 1815, and 3684 L, respectively, were also parallel to their corresponding averaged October air temperatures, 13.1 ± 2.7 , 9.9 ± 4.6 , and 11.2 ± 3.0 °C, respectively. Again, these average temperatures were significantly different ($p < 0.001$). Higher water precipitation and temperatures in the period before freezing lead to freezing delays and therefore longer times in which the deployed passive sampler may exchange chemical compounds with the lake waters at temperatures above 4 °C, which is the water temperature under the ice once the lakes are frozen. Previous experimental setups under controlled flow conditions showed that the amounts of organochlorine compounds and polycyclic aromatic hydrocarbons absorbed by LDPE dropped significantly at water temperatures of 2 °C in comparison to 13 °C, which also resulted in lower sampling rates at lower temperatures (Booij et al., 2003).

Table S6 contains the DEQs of the studied compounds at each lake, while the resulting V_w are presented in Table S7. It takes longer for compounds with greater K_{PWS-w} to achieve equilibrium, which typically are compounds with lower water solubility. Thus, most low molecular weight PAHs, all OPEs, PeCB, HCB, and the lowest molecular weight PCBs reached near or full equilibrium conditions ($DEQ > 0.95$) during most LDPE sampler exposures, and therefore lower water volumes were effectively sampled. On the other hand, high molecular weight PAHs and PCBs were those furthest away from reaching equilibrium, staying in the linear or integrative uptake phase ($DEQ < 0.20$) instead. Compounds in the curvilinear phase of uptake were closer to equilibrium in PWS I than in the following periods due to the higher R_S . In general, around half of the studied compounds reached near-equilibrium conditions, which is often the case during long exposures (approximately one year long). However, lengthy exposure times are preferred in waters where expected pollutant levels are low and compound diffusivities are reduced, as is the case for cold, remote high-mountain lakes, as higher amounts of pollutant sequestered by the samplers are less likely to slip under the detection limits. Different compound affinities for the silicone rubber material (K_{PWS-w}) resulted in somewhat decreased DEQs for the SR-PWS that were co-deployed with the LDPE-PWS during PWS III. This was mainly noticeable for compounds in the curvilinear uptake phase and for the non-chlorinated OPEs.

3.2. Freely dissolved water concentrations

The compound concentrations in the freely dissolved phase of water (C_w) for each lake and sampling period are shown in Table 2. Additionally, Table S8 contains a compilation of pollutant concentrations measured 20 or more years ago using active sampling methods at Lake Redon. Furthermore, the results of freely dissolved PAHs, organochlorine compounds and OPEs obtained from other studies using LDPE-PWS are also included in Table S8 for comparison.

3.2.1. PCBs

PCB concentrations were only determined in the first sampling period, PWS I. The observed Σ_7 PCB

concentrations in PWS I were similar across all lakes, ranging between 1.2 and 2.2 $\mu\text{g L}^{-1}$ and showing no clear trends with altitude (Table 2). The relative abundance of PCBs decreased with the water solubility of each congener from 25% for PCB28 to 3.5% for PCB180, except for PCB153, which had the second highest abundance at 19%. It is expected that the less water soluble congeners could instead be more prominently bound to other compartments such as the suspended particulate phase. No relevant trends were observed between lakes regarding PCB relative composition, aside from a slight increase in PCB153 and decrease in PCB118 at higher altitudes.

Σ_7 PCB concentrations in the freely dissolved phase of water at Estanh Redon were six times lower than those measured in 1996–1998 (removing outliers) (Vilanova et al., 2001a, 2001b) and ten to twenty times lower than in 2000 (Fernández et al., 2005) (Table S8). While a decrease in freely dissolved PCB concentrations could have happened as these compounds have been banned for an extended period of time, the observed decrease seems too steep for the expected persistence of PCBs. The measurements from over two decades ago were performed by single active sampling measurements instead of time-averaged passive samplers, which are more susceptible to seasonal changes related to increased input to the lakes after snowmelt periods or increased atmospheric deposition. This effect can be observed in the unlikely sharp increase of Σ_7 PCB observed between 1998 and 2000 (Arellano et al., 2015). In the same way, part of the reduction in PCB levels that is now apparent from our measurements could be due to the comparison of our yearly average measurements to active sampling values performed during different PCB distribution stages in the lake. On the other hand, part of the PCBs present in water may be associated to the colloidal organic matter (e.g., humic and fulvic acids), which may be collected to a larger extent by active sampling methodologies, such as those using XAD-2 or polyurethane foam (Gómez-Belinchón et al., 1988), compared to LDPE-PWS, which mostly accumulates freely dissolved organic molecules.

A comparison of the PCB concentrations found in the present study with active sampling measurements in the literature show that our results are lower than those observed in the Great Lakes (Boesen et al., 2020; Venier et al., 2014), Lake Maggiore in the Italian Alps (Nizzetto et al., 2012), and high-altitude lakes in the French Alps (Nellier et al., 2015b). However, the Σ_7 PCB concentrations in the present study were in the range of those reported in oligotrophic lakes such as Lake Panguipulli in Patagonia (Luarte et al., 2022) and Lake Nam Co in the Tibetan Plateau (Ren et al., 2017b).

In comparison to other studies that used LDPE-PWS, the Σ_7 PCB concentrations were in the same range as samples from background areas like the North and Tropical Atlantic Ocean (Sun et al., 2016). They were in the lower side of concentration ranges reported in the Great Lakes (Khairy et al., 2015; Liu et al., 2016; Ruge et al., 2018; Zhang et al., 2020) and much lower than in many other surface and ocean waters closer to emission sources like several bays in Puerto Rico (Rodríguez-Sierra et al., 2019) and contaminated waterways and treatment facilities in Seattle (Apell and Gschwend, 2017) and California (Fernandez et al., 2014, 2012), USA (Table S8), with the exception of river waters from an industrialized area in Bosnia and Herzegovina (Harman et al., 2018).

Table 2
Concentrations (pg L⁻¹) in the freely dissolved phase of water at each lake for each sampling period (PWS I–III), measured using low-density polyethylene (LDPE) and silicone rubber (SR) samplers.

Compound	PWS I (LDPE)			PWS II (LDPE)			PWS III (LDPE)			PWS III (SR)			
	Llebreta	Llong	Sarradé Redon	Dellui	Collada	Llebreta	Sarradé Redon	Llebreta	Sarradé Redon	Llebreta	Sarradé Redon	Llebreta	Sarradé Redon
PCB28	0.21	0.69	0.48	0.39	0.38	na	na	na	na	na	na	na	na
PCB52	0.25	0.16	0.53	0.43	0.1	0.37	na	na	na	na	na	na	na
PCB101	0.31	0.22	0.34	0.43	0.17	0.23	na	na	na	na	na	na	na
PCB118	0.19	0.34	0.26	0.1	0.12	0.15	na	na	na	na	na	na	na
PCB138	0.14	0.07	0.11	0.07	0.06	0.13	na	na	na	na	na	na	na
PCB153	0.23	0.14	0.44	0.26	0.32	0.47	na	na	na	na	na	na	na
PCB180	0.08	0.05	0.02	0.06	0.05	0.06	na	na	na	na	na	na	na
Σ ₇ PCB	1.4	1.7	2.2	1.7	1.2	1.8	na	na	na	na	na	na	na
4,4'-DDE	0.13	0.12	0.1	0.02	0.01	0.02	0.65	0.07	0.51	0.05	0.02	nd	nd
HCB	8.5	8.3	4	7	6.2	3.4	14	8.8	11	2.5	1	1.5	3.1
PeCB	2.4	0.5	0.84	0.59	3.1	0.6	4.5	3.1	4.1	2.2	0.81	2.3	4.7
Flu	9.1	2.8	nd	nd	11	nd	71	32	67	65	41	86	9.7
Phe	71	61	47	26	28	44	97	74	58	93	92	80	105
Ant	2	1.7	2.8	1.1	1.3	3.4	nd	1.7	nd	nd	11	nd	nd
Flu	60	74	12	3.3	1.9	11	64	8.7	8.9	42	9.9	14	13
Pyr	nd	nd	nd	1.6	0.76	4.9	nd	nd	3.6	nd	nd	nd	9.2
Ret	760	259	352	0.13	0.2	0.54	246	53	0.54	180	24	0.26	201
B[a]ant	1.8	1.3	0.06	0.06	0.05	0.11	2.8	2.9	nd	1.8	0.48	0.15	0.55
Chr+TriPh	12	16	6.1	2.3	1.3	2.2	8.4	2.3	5.3	4.5	0.74	0.2	2.3
B[b]fluo	1.3	2.1	0.2	0.05	0.08	0.06	2.6	0.15	1.9	4.2	1.8	1.5	2.6
B[j+k]fluo	0.33	0.8	0.51	0.4	0.43	0.34	4.6	0.83	2	nd	nd	nd	nd
B[e]pyr	2.1	3	nd	nd	nd	nd	2.5	1	0.23	4.5	0.65	1.1	1.3
B[a]pyr	0.09	0.11	0.1	nd	nd	nd	0.44	0.24	nd	0.39	nd	0.09	0.09
Pery	0.16	0.71	0.19	nd	nd	nd	0.91	0.1	0.12	2.4	0.06	0.04	nd
Ind[123cd]pyr	0.18	0.29	nd	nd	nd	nd	0.16	0.14	0.35	nd	nd	0.33	nd
B[ghi]pery	0.27	0.77	nd	nd	nd	0.35	nd	nd	0.11	nd	nd	nd	nd
Σ ₁₇ PAH	920	424	420	35	45	66	500	177	147	397	181	184	344
TBP	0.96	1.5	0.32	2.1	3.8	1.2	4.5	1.1	1.9	1.8	0.6	1.7	3.5
TCEP	563	758	118	na	408	633	907	267	171	305	211	393	47
TCIPP	31	291	nd	489	26	327	106	51	16	778	955	2448	509
TDCIPP	24	47	20	288	46	39	20	1.8	20	1.83	18	6.4	215
TPhP	2.2	2.6	0.35	6.6	1.6	3.4	7.1	8.2	9.8	5	14	0.58	41
Σ ₅ OPE	621	1099	139	786	486	1004	1044	330	218	1092	1199	2849	815

na: not analyzed; nd: not detected above limits of detection or blank levels.

3.2.2. HCB, PeCB, and 4,4'-DDE

HCB concentrations measured using LDPE-PWS ranged from 1.0 to 14 pg L⁻¹ (Table 2), while averages of the three lakes sampled across all periods were between 4.6 and 8.4 pg L⁻¹. PeCB concentrations ranged from 0.5 to 4.5 pg L⁻¹ (Table 2), with averages of the three lakes for the three studied periods between 1.6 and 3.0 pg L⁻¹. Finally, 4,4'-DDE

concentrations ranged from 0.01 and 0.65 pg L⁻¹ (Table 2), with averages of the three lakes ranging between 0.06 and 0.28 pg L⁻¹. DDT and its other degradation products were not detected above blank levels. HCB and PeCB concentrations remained generally constant with altitude, while 4,4'-DDE showed lower levels at the three highest lakes during PWS I. HCB and PeCB concentrations derived from SR samplers were slightly higher than those obtained from LDPE

samplers in PWS III, but within acceptable ratios of 1.4–2.6. On the other hand, 4,4'-DDE was not detected above blank levels in the SR samplers.

HCB in the freely dissolved phase of water at Estanh Redon in the present study remained at essentially the same concentration as the one observed with active sampling over twenty years ago (Fernández et al., 2005; Vilanova et al., 2001b) (Table S8). This lack of variability reflects the exceptionally high persistence of HCB in different environmental compartments of remote sites. Although expected, this contrasts with the changes over time observed for PCBs discussed in the previous section that could be a result of the integrative nature of passive samples compared to active measurements. Still, HCB typically shows a remarkable uniformity and invariability in its background environmental concentrations, as measured in air in the same area over the same twenty-year period (Prats et al. 2022a). On the other hand, 4,4'-DDE concentrations in the present work are over an order of magnitude lower than previous measurements (Fernández et al., 2005; Vilanova et al., 2001b) (Table S8). This could be a result of the lower persistence in surface waters of 4,4'-DDE compared to HCB (Howard et al., 1991) or the higher affinity of this compound of higher K_{ow} for colloidal matter.

Compared to other studies using direct or active sampling methodologies, HCB average concentrations were somewhat higher than in Patagonian and Tibetan oligotrophic lakes (Luarte et al., 2022; Ren et al., 2017b), similar or in the lower side of concentration ranges reported in several Canadian lakes including high-altitude ones (Venier et al., 2014; Wilkinson et al., 2005), and lower than in other Great Lakes (Venier et al., 2014). Concentrations in water of 4,4'-DDE were similar to those in Nam Co Lake (Ren et al., 2017b), somewhat lower than in Lake Superior (Venier et al., 2014), and much lower than in most other Great Lakes (Venier et al., 2014). Freely dissolved PeCB concentrations are more scarcely reported in the literature. They were in the lower range compared to measurements in multiple freshwater sites spread across the Netherlands, Slovakia, Czech Republic, Norway, and Russia (Allan et al., 2021).

Other studies that used LDPE-PWS showed HCB concentrations in the same range in the Atlantic Ocean (Sun et al., 2016) and the Great Lakes (Khairy et al., 2014; Ruge et al., 2018), on the lower side of levels in rivers from Bosnia and Herzegovina (Harman et al., 2018), and higher than in wetlands of Brazilian National Parks (Meire et al., 2016) (Table S8). PeCB concentrations were lower than in the Bosnian rivers (Harman et al., 2018), and 4,4-DDE concentrations were in the range of those in Brazil (Meire et al., 2016), lower than in the Atlantic (Sun et al., 2016) and the Great Lakes (Zhang et al., 2020; Ruge et al., 2018), and much lower than near a Californian wastewater facility (Fernandez et al., 2012) and Puerto Rican bays (Rodríguez-Sierra et al., 2019) (Table S8).

3.2.3. PAHs

Σ_{17} PAH concentrations ranged from 35 to 920 $\mu\text{g L}^{-1}$ (Table 2), with averages of the lakes sampled in all periods between 127 and 611 $\mu\text{g L}^{-1}$. Phe was the most abundant PAH on average (33–39% across all lakes). However, retene was consistently much more abundant in samples from the three

lower altitude lakes (30–84% in all sampling periods except for Lake Sarradé in PWS III at 13%). These three lower lakes, surrounded by forests, presented retene concentrations more than three orders of magnitude higher than the lakes situated above the tree line. This compound has also been identified in the waters of high-mountain lakes when using pumping sampling (Vilanova et al., 2001c). In some studies, it has been considered a marker of wood combustion (Aceves and Grimalt, 1993; Ramdahl, 1983; van Drooge et al., 2016). However, it is also a product of diagenetic degradation of abietic acid in lake sediments, a diterpene resin acid produced by conifers (Keeling and Bohlmann, 2006; Simoneit et al., 1986; Wakeham et al., 1980). To qualitatively confirm diagenesis as its origin, 25 samples of aquatic plants, algae, submerged mountain pine tree bark, and nearshore lake sediment were collected at the studied lakes, freeze-dried, extracted by sonication with hexane:dichloromethane 4:1 (v/v), and processed and analyzed like the PWS samples. Retene was detected in large abundance in sediment samples of the lower lakes, especially from Lake Sarradé, along with three common degradation products of abietic acid: dehydroabietic aldehyde, fichtelite, and 1,2,3,4-tetrahydroretene (Simoneit et al., 1986; Wakeham et al., 1980). These findings support the in-situ origin of retene in the lower lakes.

Without considering retene, the mean relative abundance of Phe increased to 46–59% and was followed by Fle (5–34%) and Flu (11–22%). The less volatile and less water soluble high molecular weight PAHs that are typically more associated to particulate matter (B[b]flu to B[ghi]pery) showed abundances only as high as 1.3% and were detected most frequently and at often higher concentrations in the lowest altitude lakes. Overall, SR-derived concentrations of PAHs were within an acceptable ratio of two to four times those measured with LDPE, except for a few exceptions mainly including Fle, Phe, and Ret (Table 2).

Σ_{17} PAH concentrations at Estanh Redon were approximately half of those measured over two decades ago at the same site (Vilanova et al., 2001c) or less than half than measured a few years later although more PAHs were included in the sum (Fernández et al., 2005) (Table S8), which is in accordance with the 53% decrease of estimated PAH emissions in the European continent over the last three decades (EEA, 2021). Σ PAH concentrations in the freely dissolved water phase in the mountain lakes were in the range of those in a Chilean oligotrophic lake (Tucca et al., 2020), slightly lower than in a subalpine lake in Italy (Olivella, 2006) and high-altitude Himalayan lakes (Guzzella et al., 2011), and much lower than in a Tibetan oligotrophic lake (Ren et al., 2017a) and other Chinese lakes (Qin et al., 2014, 2013; Zhao et al., 2015).

Compared to other LDPE-PWS measurements, Σ PAH concentrations in this study were in the range of those in the Atlantic Ocean (Sun et al., 2016) and in Brazilian mountain range freshwaters (Meire et al., 2019), but much lower than in the Great Lakes (McDonough et al., 2014), rivers in Oregon, USA, and Bosnia and Herzegovina (Harman et al., 2018; Paulik et al., 2016), the Plymouth harbor area, UK (Aminot et al., 2017), and freshwater lakes in Antarctica (Yao et al., 2016) (Table S8).

3.2.4. OPEs

Σ_5 OPE concentrations in the freely dissolved phase of water ranged between 139 and 2849 $\mu\text{g L}^{-1}$ (Table 2). TCEP was the most abundant OPE (78–82% on average), followed by TCIPP (11–14%) except in PWS III where TCIPP amounted to 79% and TCEP to 20%. The other three OPEs presented mean relative abundances below 6%. While not showing clear trends with altitude, some compounds presented high variability between sampling sites and periods. A clear example is TCIPP, with levels ranging between below blank levels and 2.4 ng L^{-1} , apparently changing in concentration by a considerable margin between exposure periods in lakes like Redon (489 $\mu\text{g L}^{-1}$ in PWS I to 16 $\mu\text{g L}^{-1}$ in PWS II, and back up to 2448 $\mu\text{g L}^{-1}$ in PWS III).

Such substantial changes in a limited time are not expected in a remote alpine area without primary pollutant sources. This variability could have two main causes: a poor performance of LDPE for the reproducible uptake of OPEs and uncertainty in the effective sampled volumes derived from sampling rates. OPEs, particularly the chlorinated ones, have relatively low K_{ow} (Table S4) that results in a lower affinity for LDPE than other HOCs, which implies a limited uptake capacity of the polymer that can become a source of error and turn into a higher susceptibility to being negatively impacted by blank levels. To the best of our knowledge, reliable measurements of the affinity of OPEs for LDPE are not available as experimentally measured K_{PWS-W} values have not been reported in the literature. Other LDPE-PWS studies presenting OPE concentrations in water have performed K_{PWS-W} estimations from water solubility or vapor pressure (Ma et al., 2021; McDonough et al., 2018), although they can result in much lower values than reasonable for some OPEs. In the present study, K_{PWS-W} were estimated from known OPE partition coefficients for SR passive samplers linearly correlated with those for LDPE (Fig. S1, $R^2=0.991$). This approach is based on the regression of experimental values instead of just physical-chemical properties, assuming that relative affinities for the polymer phase remain relatively the same between compounds. Similar extrapolations have been used before for other polymers, matrices, and compounds (Smedes et al., 2020). However, its application to OPEs may suppose a larger leap of physical-chemical properties between predictor and predicted compounds that results in higher K_{PWS-W} uncertainties. Slight variations in the low effective sampled volumes resulting from the low K_{PWS-W} values of OPEs could have developed into the substantial differences in concentration observed in Table 2. Still, we argue that while individual OPE levels suffering from these uncertainties may not be suitable for the assessment of short-range altitudinal and short-term temporal trends, the overall average LDPE-derived OPE concentrations for the studied area are good indicators of the current magnitude of OPE pollution in such remote locations.

SR K_{PWS-W} values for OPEs are available in the literature (Smedes, 2018), ranging between 0.02 and 0.25 log units higher than our LDPE predictions. OPE concentrations measured using the SR samplers during PWS III were on average about half of those measured with the LDPE samplers, which is an acceptable margin, although differences varied largely between compounds and sampling

sites (Table 2). SR-derived concentrations of TBP, TDCIPP, and TPhP were generally higher than LDPE ones by ratios of 0.8–120, while SR-derived concentrations of TCEP and TCIPP were lower by ratios of 0.2–0.9. Excluding obvious outliers, differences between SR and LDPE values were all within a maximum difference ratio of 8. In general, the SR relative amounts were relatively close to those of the LDPE but with a slightly higher representation of TDCIPP, TBP, and TPhP at the expense of the two most abundant OPEs (TCIPP and TCEP). In general, the SR polymers may provide data that are more easily comparable to those reported in the waters of other locations, but most LDPE measurements were deemed to be acceptable.

OPE concentrations ranged from slightly lower to considerably lower than in high Arctic lakes (Sun et al., 2020) and were generally below those reported in Italian volcanic lakes (Bacaloni et al., 2008), German alpine reservoirs (Regnery and Püttmann, 2010), Lake Victoria in Uganda (Nantaba et al., 2021), and the Great Lakes (except for similar concentrations of TCEP at some sites) (Ma et al., 2021; Venier et al., 2014). Σ_5 OPE concentrations in the present work were also similar to those reported in other studies using LDPE-PWS samplers in Canadian Arctic lakes, but higher than in the Arctic Ocean (McDonough et al., 2018), and lower than in the Great Lakes (Ma et al., 2021) and the Plymouth harbor marina (Aminot et al., 2017) by up to two orders of magnitude (Table S8).

3.3. Accuracy of measurements and adequacy of sampler material

Some compound concentrations showed variations between sampling periods (e.g., OPEs and the organochlorines) that likely arose from higher uncertainty in the PRC-derived sampling rates or K_{PWS-W} values. The overall concentration averages were deemed suitable for comparing pollutant levels with other locations and for establishing long-term concentration trends, but in some cases short-term temporal trends and small-scale spatial distributions could be hindered as a result of data variability. PWS concentrations can carry uncertainties linked to the modelled nature of their determination, as uptake models rely on an array of variables that are highly dependent on physical-chemical properties, deployment conditions, and error in their measurement. Compounds with a tendency to quickly reach equilibrium are most affected by uncertainty in K_{PWS-W} values and insensitive to sampling rate uncertainties (e.g., OPEs), while compounds in the integrative uptake stage suffer most from uncertainties in sampling rates through PRC K_{PWS-W} error (e.g., high molecular weight PCBs and PAHs). Furthermore, the material chosen for the uptake of pollutants can significantly determine the magnitude to which these uncertainties affect the results.

Additional LDPE and SR samplers to those analyzed in the present study were co-deployed at Lake Redon for all sampling periods as part of the Aquatic Global Passive Sampling network (AQUA-GAPS/MONET, www.aqua-gaps.passivesampling.net). These samplers were independently extracted and analyzed at RECETOX (Masaryk University, Czech Republic) as described elsewhere (Sobotka et al., 2022). Comparison of AQUA-GAPS and the results of the present study, together with a

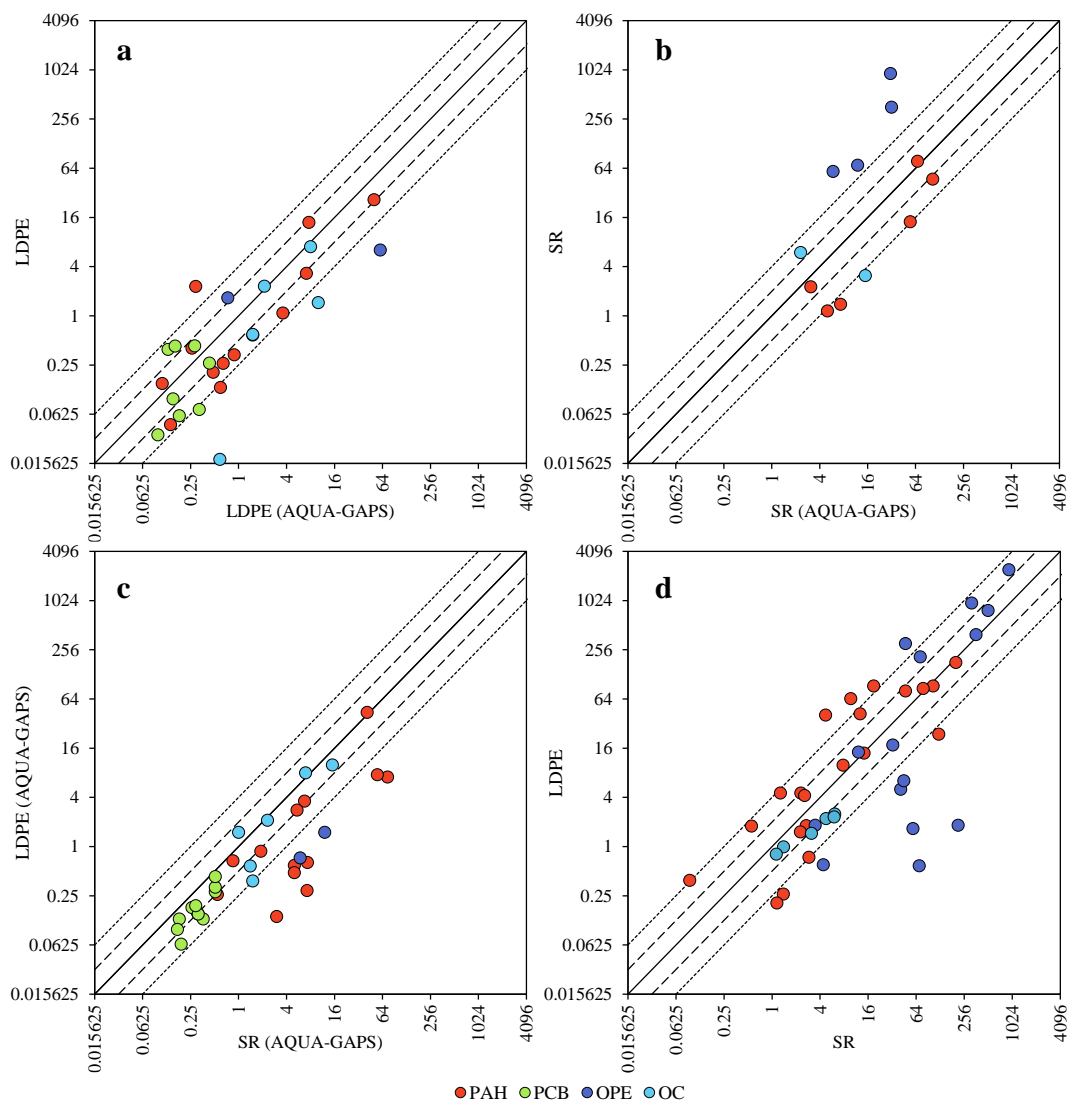


Fig 3. Pollutant concentrations in the freely dissolved phase of water ($\mu\text{g L}^{-1}$) measured using low-density polyethylene (LDPE) and silicone rubber (SR) passive samplers. Results are compared for: a) LDPE from this study vs AQUA-GAPS measurements performed at Masaryk University from lake Redon during PWS I and III; b) SR from this study vs AQUA-GAPS at lake Redon during PWS III; c) LDPE and SR from AQUA-GAPS at lake Redon during PWS I and III; and d) LDPE and SR from this study at lakes Llebreta, Sarradé, and Redon during PWS III. The continuous, dashed, and dotted lines represent equality and difference ratio of 2 and 4 between measurements, respectively.

comparison between sampler materials, are shown in Fig. 3.

LDPE-derived concentrations in our study were generally within a ratio of up to two to four of AQUA-GAPS ones (Fig. 3a), which is somewhat disperse but centered around the equality line for all compound groups. No systematic deviations of the data between both independent variables were observed. The main observed outliers concerned concentrations of 4,4'-DDE in PWS I and HCB and TDCIPP in PWS III, which were more than four times lower in the present study than in AQUA-GAPS, and the concentration of Chr+TriPh, which was over four times higher in PWS I from the present study than in AQUA-GAPS. Since such differences in these few compounds were not observed in other periods, the cause of these discrepancies could be related to analytical differences like blank levels and higher uncertainties due to overall low environmental concentrations.

Regarding the SR-derived concentrations in PWS III, PAHs and OCs showed results within the same margins of

agreement as with the LDPE samplers. However, the concentrations of OPEs show deviations by ratios of 6 to 30 between both laboratories (Fig. 3b) as well as between LDPE and SR (Fig. 3c and 3d). These differences were particularly noticeable for TBP, TDCIPP, and TPhP in PWS I and III. It seems clear that some OPE values might have been under or overestimated by either or both analyses, probably due to uncertainties related to effective sampled volume determination. These uncertainties originate from the experimental determination of $K_{\text{PWS-w}}$ values. Because partitioning constants of OPEs are low, they reach equilibrium conditions between water and sampler with ease (Table S6), so their effective sampled volumes are low (Table S7) and errors in their concentration are thus amplified. For SR, the relatively higher water solubility of OPEs was hypothesized to somewhat hamper the accurate determination of $K_{\text{PWS-w}}$ (Smedes, 2018). For LDPE, the lack of experimentally determined $K_{\text{PWS-w}}$ calls for the approximation of their values, thus introducing additional

uncertainty. Although SR $K_{\text{PWS-W}}$ for OPEs are slightly higher than for LDPE, which would lead to larger effective sampled volumes, the theoretical benefit of this choice of material is only marginal and further assessment on the performance of these and other sampler materials for the analysis of OPEs would be needed for future studies.

3.4. Air–water diffusive exchange

The freely dissolved water concentrations determined using LDPE-PWS samplers during sampling period PWS I and the mean gas-phase atmospheric concentrations determined in parallel at each site over three passive air sampling periods (PAS I–III, 09/2017–12/2018) (Table S5) (Prats et al., 2022b, 2022a) can be used to determine the diffusive exchange fluxes of the studied compounds at several mountain altitudes (Fig. 4). The calculations resulted in positive and negative fluxes, which indicate net volatilization and deposition, respectively, and include the theoretical uncertainty of the fluxes. The largest contributing factors to the uncertainty were the atmospheric gas-phase concentrations (49% of the overall uncertainty on average) and the Henry's Law constants (39%) due to the wide range of values available in the literature for every single compound (Sander, 2015). The other variables involved amounted to smaller fractions of the average theoretical uncertainty (combined contribution <13%).

In general, most compounds exhibited net deposition fluxes from air to water (flux < 0), or fluxes with either standard deviations or estimated uncertainties large enough that do not allow their differentiation from equilibrium (Fig. 4). PAH average net deposition fluxes were between 0.07 and 70.4 ng m⁻² d⁻¹, higher than those of most PCBs (0.07 to 0.85 ng m⁻² d⁻¹), OPEs (0.06 to 7.8 ng m⁻² d⁻¹), and PeCB (1.9 to 4.1 ng m⁻² d⁻¹). The air-to-water direction of both PAH and PCB fluxes agrees with the dominance of long-range atmospheric transport as their main source in this area (Prats et al., 2022b, 2022a), and the larger magnitude of PAH fluxes is consistent with the continued emission of PAHs to the atmosphere, especially in rural areas and over colder seasons (Van Drooge and Grimalt, 2015). Still, some PCBs like PCB28, PCB52, and PCB180 often showed net fluxes less differentiated from equilibrium, as is also the case for PeCB. While average OPE fluxes were mainly deposition ones, the uncertainty in the fluxes was often large enough as to not reject equilibrium conditions unequivocally, except for TBP and TPhP in several lakes. No general correlations with temperature or altitude were observed, as was the case in alpine lakes in the Rocky Mountains (Wilkinson et al., 2005).

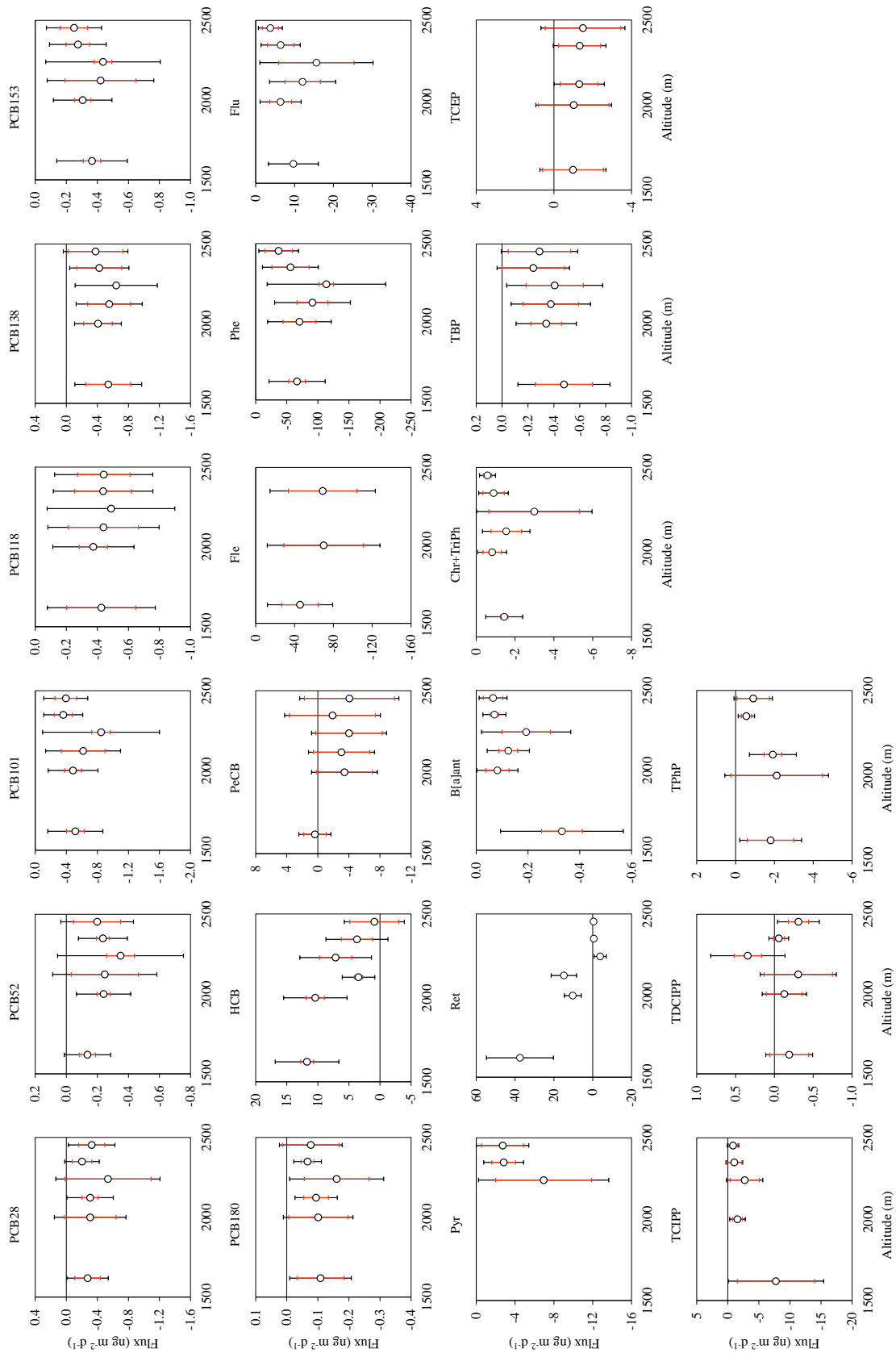
The main exceptions showing net volatilization fluxes from water to air were retene at the three lowest lakes, TCEP and TDCIPP at Estanh Redon, and HCB at most lakes. The large retene fluxes at Lakes Llebreta, Llong, and Sarradé (10.3 to 37.5 ng m⁻² d⁻¹) are explained by the exceptionally high concentrations in water resulting from diagenetic processes discussed in previous sections. Retene presented the highest volatilization flux at Lake Llebreta as a result of both higher concentration in water (Table 2) and higher mean ambient temperature (Table 1), which facilitates volatilization. Many OPEs seemed to behave differently at Estanh Redon, which could be due to a difference in sources as it is located the furthest from all other lakes (Fig. 1).

Finally, HCB showed volatilization fluxes that became progressively lower at higher, colder lakes, even transitioning towards equilibrium conditions (Fig. 4). This trend is to be expected since condensation increases (or volatilization decreases) at lower temperatures. However, HCB being the only compound that consistently presents volatilization fluxes is more puzzling in a context where most other legacy organochlorine pollutants showed net deposition or equilibrium conditions. Low HCB concentrations in air due to atmospheric degradation by free hydroxyl radicals is an unlikely cause of this air–water imbalance because of the remarkable persistence of HCB. Still, volatilization fluxes of HCB while other organochlorines presented net deposition were also observed in other Russian and Canadian mountain lakes (McConnell et al., 1996; Wilkinson et al., 2005).

Modelling studies at Estanh Redon using data from over two decades ago determined annually integrated net volatilization fluxes for PCBs and showed that diffusive air–water exchange dominated PCB dynamics in the lake (Meijer et al., 2009, 2006). This contrasts with the present study, where most PCBs showed near-equilibrium conditions or small deposition fluxes, which probably responds to the decrease in freely dissolved PCB concentrations in water (Table S8). PCBs and other organochlorine pollutants presented deposition fluxes in Swiss and North American lakes (Bogdal et al., 2010; Dachs et al., 2000), ranged from deposition to volatilization in the Great Lakes (Liu et al., 2016), and showed mostly volatilization fluxes in North Patagonian, Canadian, Russian, and arctic and subarctic lakes (Blais et al., 2001; Diamond et al., 2005; Luarte et al., 2022; McConnell et al., 1996). PAHs showed mainly deposition fluxes in a Chinese urban lake (Li et al., 2009) and at some sites from Lake Superior (Ruge et al., 2015), but the direction of exchange fluxes of PAHs was much more dependent on molecular weight and season of the year in several Chinese and North Patagonian lakes (Qin et al., 2013; Tao et al., 2017; Tucca et al., 2020; Wu and Tao, 2021). Estimations of OPE exchange fluxes in lakes are scarce, but they mostly showed deposition fluxes at the Great Lakes (Ma et al., 2021).

3.5. Atmospheric photodegradation

Air–water diffusive exchange has been identified as a main driver of pollutant distribution between the atmosphere and water bodies, especially in background areas (González-Gaya et al., 2016; Jurado et al., 2005). However, photooxidation due to reaction with free hydroxyl radicals in the atmospheric gas phase can also be a relevant removal mechanism for many semi-volatile organic compounds transported at long distances (Berrojalbiz et al., 2014). Here, degradation fluxes were calculated for all studied compounds based on their concentrations in air. These fluxes are presented in Table 3. All PCBs, HCB, and PeCB showed very low estimated degradation fluxes, between 0.01 and 0.26 ng m⁻² d⁻¹, as expected from their characteristic environmental persistence. On the other hand, PAHs showed much higher fluxes, between 0.3 and 15 ng m⁻² d⁻¹ for the heavier compounds (Ret, B[a]ant, Chr+TriPh, outliers removed) and between 22 and 232 ng m⁻² d⁻¹ for the more labile ones (Fle, Phe, Flu, and Pyr). These higher PAH



degradation fluxes were similar to others found in background areas (Nizzetto et al., 2008). OPE degradation fluxes were somewhere in the middle, between 0.8 and 38 $\text{ng m}^{-2} \text{d}^{-1}$ (outliers removed).

Compared to the air-water diffusive fluxes, PCB and organochlorine degradation fluxes were on average 3 to 14 times lower, meaning that diffusive exchange from the atmospheric gas phase into the lakes is a much more prominent removal process than photodegradation. On the

Fig. 4. Average air-water diffusive exchange fluxes at each lake by altitude (from lowest to highest, lakes Lebreña, Long, Sarradé, Redon, Dellui, and Collada). Negative fluxes describe net deposition of pollutants, positive fluxes describe net volatilization, and a flux equal to zero describes a state of equilibrium. The red whiskers represent flux standard deviations from all air sampling periods considered, and the black whiskers represent theoretical uncertainties calculated from error propagation.

Table 3
Mean degradation fluxes ($\text{ng m}^{-2} \text{d}^{-1}$) in the atmospheric gas phase by reaction with OH radicals over periods PAS I–III.

	Llebretra	Llong	Sarradé	Redon	Dellui	Collada
PCB28	0.10	0.13	0.12	0.13	0.07	0.09
PCB52	0.05	0.05	0.08	0.07	0.04	0.05
PCB101	0.08	0.06	0.08	0.09	0.04	0.04
PCB118	0.07	0.05	0.06	0.06	0.05	0.05
PCB138	0.08	0.05	0.07	0.07	0.05	0.04
PCB153	0.05	0.04	0.06	0.05	0.03	0.03
PCB180	0.02	0.01	0.01	0.02	0.01	0.01
HCB	0.06	0.05	0.04	0.05	0.06	0.04
PeCB	0.21	0.23	0.26	0.22	0.25	0.23
Fle	126	157	167	132	144	103
Phe	189	167	219	232	116	81
Flu	111	69	111	126	52	32
Pyr	72	29	39	55	22	22
Ret	– ^a	8.7	15	13	1.9	1.6
B[a]ant	2.2	0.59	0.64	0.88	0.32	0.31
Chr+TriPh	9.0	5.0	8.2	14	4.1	2.7
TBP	1.9	1.2	1.4	1.3	0.81	1.0
TCEP	6.9	6.3	7.0	15	6.7	7.8
TCIPP	38	7.6	4.4	12	4.3	4.1
TDCIPP	1.6	1.4	1.8	2.3	0.83	1.8
TPhP	8.4	8.7	8.2	– ^a	2.1	3.5

^a Affected by outliers.

other hand, degradation fluxes of PAHs and OPEs were 2 to 9 times higher than diffusive exchange ones. Nevertheless, the calculated exchange fluxes for these two later groups of compounds were predominantly air-to-water directed or close to equilibrium. Considering the magnitude of PAH and OPE degradation fluxes, this direction of the diffusive exchange at the air–water interface is reinforced, meaning that gas-phase concentrations were high enough to cause net deposition even when appreciable atmospheric degradation took place. Still, other atmospheric removal mechanisms like dry and wet deposition and removal processes in the lakes like biodegradation should be accounted for in a complete determination of the net direction of compound fluxes, which is nevertheless likely to remain from air towards water as deposition processes can be substantial in alpine settings (Carrera et al., 2002; Fernández et al., 2003, 2021).

4. Conclusions

Passive water samplers are simple and effective alternatives for sampling hydrophobic organic compounds in the freely dissolved phase of water in alpine lakes. Their use overcomes the difficulties associated with sampling logistics in remote areas over long periods of time. While HCB concentrations were essentially the same as those from two decades ago, sampled with active pumping systems, the observed PCB and 4,4'-DDE concentrations were considerably lower. Despite a possible reduction over the years, such a steep decrease of remarkably persistent pollutants could in part be a result of comparing yearly averages from this study with single measurements in the past affected by temporary changes in the lake (e.g., snowmelt and stratification), as well as differences between the freely soluble fraction sampled with PWS and that retained in XAD-2 or other polymers, which could

incorporate colloidal organic matter. PAH concentrations were relatively high due to their continued release into the atmosphere and long-range atmospheric transport inputs into the lakes, with a lower presence of high molecular weight PAHs typically bound to the particle phase. PAH levels were around half of those found over 20 years ago at the same site, agreeing with reports on the decrease of atmospheric PAH emissions over Europe of around 50%. OPEs were found at even higher concentrations than the other compounds, although the data presented high variability and method uncertainties. In general, most studied compounds showed levels similar to or around the same order of those reported in other oligotrophic, high-altitude, alpine and subalpine lakes.

There was an acceptable agreement between independent measurements and different sampler materials for most compounds, albeit within moderately wide margins of uncertainty. The main outliers were mostly OPEs, which often showed disagreements and variation between sites and periods that were linked to uncertainties of the predicted $K_{\text{PWS-W}}$ values that are otherwise unavailable for LDPE. Furthermore, the lower hydrophobicity of OPEs could place them at the limit of adequacy of the sampler materials used in this work.

Finally, diffusive exchange fluxes between atmospheric gas phase and freely dissolved water concentrations revealed net diffusive flux of pollutants from air to water, except for some OPEs and PCBs presenting equilibrium conditions, and HCB with volatilization fluxes (water to air). Diffusive exchange fluxes of PAHs (air to water) were the highest, as expected from their continuous emission and transport towards colder areas like high mountains. Atmospheric degradation by photooxidation due to free hydroxyl radicals was identified as a relevant mechanism of pollutant removal in air for PAHs and OPEs. This further supports the air-to-water direction of the exchange fluxes for these compounds as the higher proportion of pollutants in air with respect to equilibrium conditions exists despite having photodegradation competing for their removal from the atmosphere. As expected, persistent PCBs and organochlorines are not as affected by degradation processes. Thus, these lakes in their current state most probably act as accumulators of many emerging and legacy pollutants subject to long-range atmospheric transport.

CRedit authorship contribution statement

RP: Sampling, Analysis, Formal analysis, Visualization, and Writing – original draft. BD: Sampling, Analysis, Supervision, and Writing – review and editing. PF: Supervision, Conceptualization, and Writing – review and editing. JG: Writing – review and editing, Conceptualization, and Funding acquisition.

Declaration of competing interest

The authors declare that they have no known competing financial interests or personal relationships that could have appeared to influence the work reported in this paper.

Acknowledgements

Sampling support from Alejandro G. Inarra and technical assistance from Roser Chaler are acknowledged. Part of this work was carried out with the support of RECETOX Research Infrastructure (ID LM2018121, MEYS CR, 2020-2022). Foppe Smedes, Branislav Vrana, and Jaromír Sobotka (RECETOX, Masaryk University, Brno, Czech Republic) are acknowledged for providing sampler materials, counselling, and complementary analyses. Part of this work was performed in the National Park of Aigüestortes i Estany de Sant Maurici with collaboration from the Department of Vice Presidency and Digital and Territorial Policies of the Government of Catalonia.

Funding

This work was supported by the Spanish Ministry of Science and Innovation through projects CTM2015-71832-P and PGC2018-102288-B-I00. IDAEA-CSIC is a Severo Ochoa Centre of Research Excellence, grant CEX2018-000794-S funded by MCIN/AEI/ 10.13039/501100011033. Raimon M. Prats also acknowledges financial support from the Spanish Ministry of Science and Innovation (BES-2016-076339).

Appendix A. Supplementary data

Supplementary data to this article can be found in the following pages.

References

- Abdel-Shafy, H.I., Mansour, M.S.M., 2016. A review on polycyclic aromatic hydrocarbons: Source, environmental impact, effect on human health and remediation. *Egypt. J. Pet.* 25, 107–123. <https://doi.org/10.1016/J.EJPE.2015.03.011>
- Aceves, M., Grimalt, J.O., 1993. Large and small particle size screening of organic compounds in urban air. *Atmos. Environ.* 27, 251–263. [https://doi.org/10.1016/0957-1272\(93\)90010-4](https://doi.org/10.1016/0957-1272(93)90010-4)
- Allan, I.J., Vrana, B., de Weert, J., Kringstad, A., Ruus, A., Christensen, G., Terentjev, P., Green, N.W., 2021. Passive sampling and benchmarking to rank HOC levels in the aquatic environment. *Sci. Reports* 2021 111 11, 1–12. <https://doi.org/10.1038/S41598-021-90457-3>
- Álvarez-Pedrerol, M., Ribas-Fito, N., Torrent, M., Carrizo, D., Grimalt, J.O., Sunyer, J., 2008. Effects of PCBs, p,p'-DDT, p,p'-DDE, HCB and β -HCH on thyroid function in preschool children. *Occup. Environ. Med.* 65, 452–457. <http://dx.doi.org/10.1136/oem.2007.032763>
- Aminot, Y., Belles, A., Alary, C., Readman, J.W., 2017. Near-surface distribution of pollutants in coastal waters as assessed by novel polyethylene passive samplers. *Mar. Pollut. Bull.* 119, 92–101. <https://doi.org/10.1016/J.MARPOLBUL.2017.03.022>
- Apell, J.N., Gschwend, P.M., 2017. The atmosphere as a source/sink of polychlorinated biphenyls to/from the Lower Duwamish Waterway Superfund site. *Environ. Pollut.* 227, 263–270. <https://doi.org/10.1016/J.ENVPOL.2017.04.070>
- Arellano, L., Fernández, P., Fonts, R., Rose, N.L., Nickus, U., Thies, H., Stuchlík, E., Camarero, L., Catalan, J., Grimalt, J.O., 2015. Increasing and decreasing trends of the atmospheric deposition of organochlorine compounds in European remote areas during the last decade. *Atmos. Chem. Phys. Discuss.* 15, 6069–6085. <https://doi.org/10.5194/acpd-15-3415-2015>
- Armstrong, B., Hutchinson, E., Unwin, J., Fletcher, T., 2004. Lung cancer risk after exposure to polycyclic aromatic hydrocarbons: A review and meta-analysis. *Environ. Health Perspect.* 112, 970–978. <https://doi.org/10.1289/EHP.6895>
- Bacaloni, A., Cucci, F., Guarino, C., Nazzari, M., Samperi, R., Laganà, A., 2008. Occurrence of Organophosphorus Flame Retardant and Plasticizers in Three Volcanic Lakes of Central Italy. *Environ. Sci. Technol.* 42, 1898–1903. <https://doi.org/10.1021/ES702549G>
- Bartrons, M., Grimalt, J.O., Catalan, J., 2011. Altitudinal distributions of BDE-209 and other polybromodiphenyl ethers in high mountain lakes. *Environ. Pollut.* 159, 1816–1822. <https://doi.org/10.1016/J.ENVPOL.2011.03.027>
- Berrojalbiz, N., Castro-Jiménez, J., Mariani, G., Wollgast, J., Hanke, G., Dachs, J., 2014. Atmospheric occurrence, transport and deposition of polychlorinated biphenyls and hexachlorobenzene in the Mediterranean and Black seas. *Atmos. Chem. Phys.* 14, 8947–8959. <https://doi.org/10.5194/acp-14-8947-2014>
- Bidleman, T.F., McConnell, L.L., 1995. A review of field experiments to determine air-water gas exchange of persistent organic pollutants. *Sci. Total Environ.* 159, 101–117. [https://doi.org/10.1016/0048-9697\(95\)04255-Y](https://doi.org/10.1016/0048-9697(95)04255-Y)
- Blais, J.M., Schindler, D.W., Sharp, M., Braekvelt, E., Lafrenière, M., McDonald, K., Muir, D.C.G., Strachan, W.M.J., 2001. Fluxes of semivolatile organochlorine compounds in Bow Lake, a high-altitude, glacier-fed, subalpine lake in the Canadian rocky mountains. *Limnol. Oceanogr.* 46, 2019–2031. <https://doi.org/10.4319/lo.2001.46.8.2019>
- Boesen, A.C., Martinez, A., Hornbuckle, K.C., 2020. Air-water PCB fluxes from southwestern Lake Michigan revisited. *Environ. Sci. Pollut. Res.* 27, 8826–8834. <https://doi.org/10.1007/S11356-019-05159-1>
- Bogdal, C., Scheringer, M., Schmid, P., Bläuenstein, M., Kohler, M., Hungerbühler, K., 2010. Levels, fluxes and time trends of persistent organic pollutants in Lake Thun, Switzerland: Combining trace analysis and multimedia modeling. *Sci. Total Environ.* 408, 3654–3663. <https://doi.org/10.1016/J.SCITOTENV.2010.04.038>
- Booij, K., Hofmans, H.E., Fischer, C.V., van Weerlee, E.M., 2003. Temperature-dependent uptake rates of nonpolar organic compounds by semipermeable membrane devices and low-density polyethylene membranes. *Environ. Sci. Technol.* 37, 361–366. <https://doi.org/10.1021/es025739i>
- Booij, K., Smedes, F., 2010. An improved method for estimating in situ sampling rates of nonpolar passive samplers. *Environ. Sci. Technol.* 44, 6789–6794. <https://doi.org/10.1021/es101321v>
- Booij, K., Vrana, B., Huckins, J.N., 2007. Chapter 7. Theory, modelling and calibration of passive samplers used in water monitoring. *Compr. Anal. Chem.* [https://doi.org/10.1016/S0166-526X\(06\)48007-7](https://doi.org/10.1016/S0166-526X(06)48007-7)
- Boström, C.E., Gerde, P., Hanberg, A., Jernström, B., Johansson, C., Kyrklund, T., Rannug, A., Törnqvist, M., Victorin, K., Westerholm, R., 2002. Cancer risk assessment, indicators, and guidelines for polycyclic aromatic hydrocarbons in the ambient air. *Environmental Health Perspectives. Public Health Services, US Dept of Health and Human Services.* <https://doi.org/10.1289/ehp.110-1241197>
- Carrera, G., Fernández, P., Grimalt, J.O., Ventura, M., Camarero, L., Catalan, J., Nickus, U., Thies, H., Psenner, R., Guillem Carrera, Pilar Fernández, and, Grimalt*, J.O., Marc Ventura, Lluís Camarero, and, Catalan, J., Nickus, U., and, H.T., Psenner, R., 2002. Atmospheric deposition of organochlorine compounds to remote high mountain lakes of Europe. *Environ. Sci. Technol.* 36, 2581–2588. <https://doi.org/10.1021/es0102585>
- Casas, M., Nieuwenhuijsen, M., Martínez, D., Ballester, F., Basagaña, X., Basterrechea, M., Chatzi, L., Chevrier, C., Eggesbø, M., Fernandez, M.F., Govarts, E., Guxens, M., Grimalt, J.O., Hertz-Picciotto, I., Iszatt, N., Kasper-Sonnenberg, M., Kiviranta, H., Kogevinas, M., Palkovicova, L., Ranft, U., Schoeters, G., Patelarou, E., Petersen, M.S., Torrent, M., Trnovec, T., Valvi, D., Toft, G.V., Weihe, P., Weisglas-

- Kuperus, N., Wilhelm, M., Wittsiepe, J., Vrijheid, M., Bonde, J.P., 2015. Prenatal exposure to PCB-153, p,p'-DDE and birth outcomes in 9000 mother-child pairs: Exposure-response relationship and effect modifiers. *Environ. Int.* 74, 23–31. <https://doi.org/10.1016/j.envint.2014.09.013>
- Catalan, J., Ballesteros, E., Camarero, L., Felip, M., Gacia, E., 1992. Limnology in the Pyrenean Lakes. *Limnetica* 8, 27–38.
- Catalan, J., Camarero, L., Felip, M., Pla, S., Ventura, M., Buchaca, T., Bartumeus, F., De Mendoza, G., Miró, A., Casamayor, E.O., Medina-Sánchez, J.M., Bacardit, M., Altuna, M., Bartrons, M., De Quijano, D.D., 2006. High mountain lakes: Extreme habitats and witnesses of environmental changes. *Limnetica* 25, 551–584. <https://doi.org/10.23818/limn.25.38>
- Chevrier, J., Eskenazi, B., Holland, N., Bradman, A., Barr, D.B., 2008. Effects of Exposure to Polychlorinated Biphenyls and Organochlorine Pesticides on Thyroid Function during Pregnancy. *Am. J. Epidemiol.* 168, 298–310. <https://doi.org/10.1093/AJE/KWN136>
- Dachs, J., Eisenreich, S.J., Hoff, R.M., 2000. Influence of Eutrophication on Air-Water Exchange, Vertical Fluxes, and Phytoplankton Concentrations of Persistent Organic Pollutants. *Environ. Sci. Technol.* 34, 1095–1102. <https://doi.org/10.1021/ES990759E>
- Darvill, T., Lonky, E., Reihman, J., Stewart, P., Pagano, J., 2000. Prenatal exposure to PCBs and infant performance on the fagan test of infant intelligence. *Neurotoxicology* 21, 1029–1038.
- Deacon, E.L., 1977. Gas transfer to and across an air-water interface. *Tellus* 29, 363–374. <https://doi.org/10.3402/tellusa.v29i4.11368>
- Diamond, M.L., Bhavsar, S.P., Helm, P.A., Stern, G.A., Alaei, M., 2005. Fate of organochlorine contaminants in arctic and subarctic lakes estimated by mass balance modelling. *Sci. Total Environ.* 342, 245–259. <https://doi.org/10.1016/J.SCITOTENV.2004.12.045>
- EEA, 2021. European Union emission inventory report 1990-2019 under the UNECE Convention on Long-range Transboundary Air Pollution (Air Convention). <https://doi.org/10.2800/701303>
- Eskenazi, B., Chevrier, J., Rosas, L.G., Anderson, H.A., Bomman, M.S., Bouwman, H., Chen, A., Cohn, B.A., de Jager, C., Henshel, D.S., Leipzig, F., Leipzig, J.S., Lorenz, E.C., Snedeker, S.M., Stapleton, D., 2009. The Pine River Statement: Human Health Consequences of DDT Use. *Environ. Health Perspect.* 117, 1359–1367. <https://doi.org/10.1289/EHP.11748>
- Fernandez, L.A., Lao, W., Maruya, K.A., Burgess, R.M., 2014. Calculating the diffusive flux of persistent organic pollutants between sediments and the water column on the palos verdes shelf superfund site using polymeric passive samplers. *Environ. Sci. Technol.* 48, 3925–3934. <https://doi.org/10.1021/es404475c>
- Fernandez, L.A., Lao, W., Maruya, K.A., White, C., Burgess, R.M., 2012. Passive sampling to measure baseline dissolved persistent organic pollutant concentrations in the water column of the Palos Verdes shelf superfund site. *Environ. Sci. Technol.* 46, 11937–11947. <https://doi.org/10.1021/es302139y>
- Fernández, P., Carrera, G., Grimalt, J.O., 2005. Persistent organic pollutants in remote freshwater ecosystems. *Aquat. Sci.* 2005 673 67, 263–273. <https://doi.org/10.1007/S00027-005-0747-8>
- Fernández, P., Carrera, G., Grimalt, J.O., Ventura, M., Camarero, L., Catalan, J., Nickus, U., Thies, H., Psenner, R., 2003. Factors governing the atmospheric deposition of polycyclic aromatic hydrocarbons to remote areas. *Environ. Sci. Technol.* 37, 3261–3267. <https://doi.org/10.1021/es020137k>
- Fernandez, P., van Drooge, B.L., Arellano, L., Grimalt, J.O., 2021. Atmospheric deposition of semivolatile organic pollutants in European high mountains: Sources, settling and chemical degradation. *Sci. Total Environ.* 784, 147099. <https://doi.org/10.1016/j.scitotenv.2021.147099>
- Forns, J., Lertxundi, N., Aranbarri, A., Murcia, M., Gascon, M., Martinez, D., Grellier, J., Lertxundi, A., Julvez, J., Fano, E., Goñi, F., Grimalt, J.O., Ballester, F., Sunyer, J., Ibarluzea, J., 2012a. Prenatal exposure to organochlorine compounds and neuropsychological development up to two years of life. *Environ. Int.* 45, 72–77. <https://doi.org/10.1016/j.envint.2012.04.009>
- Forns, J., Torrent, M., Garcia-Esteban, R., Grellier, J., Gascon, M., Julvez, J., Guxens, M., Grimalt, J.O., Sunyer, J., 2012b. Prenatal exposure to polychlorinated biphenyls and child neuropsychological development in 4-year-olds: An analysis per congener and specific cognitive domain. *Sci. total Environ.* 432, 338–343. <https://doi.org/10.1016/j.scitotenv.2012.06.012>
- Gallego, E., Grimalt, J.O., Bartrons, M., Lopez, J.F., Camarero, L., Catalan, J., Stuchlik, E., Battarbee, R., 2007. Altitudinal gradients of PBDEs and PCBs in fish from European high mountain lakes. *Environ. Sci. Technol.* 41, 2196–2202. <https://doi.org/10.1021/es062197m>
- Gerić, M., Ceraj-Cerić, N., Gajski, G., Vasilčić, Ž., Capuder, Ž., Garaj-Vrhovac, V., 2012. Cytogenetic status of human lymphocytes after exposure to low concentrations of p,p'-DDT, and its metabolites (p,p'-DDE, and p,p'-DDD) in vitro. *Chemosphere* 87, 1288–1294. <https://doi.org/10.1016/j.chemosphere.2012.01.037>
- González-Gaya, B., Fernández-Pinos, M.C., Morales, L., Méjanelle, L., Abad, E., Piña, B., Duarte, C.M., Jiménez, B., Dachs, J., 2016. High atmosphere-ocean exchange of semivolatile aromatic hydrocarbons. *Nat. Geosci.* 9, 438–442. <https://doi.org/10.1038/ngeo2714>
- Grandjean, P., Landrigan, P.J., 2014. Neurobehavioural effects of developmental toxicity. *Lancet Neurol.* 13, 330–338. [https://doi.org/https://doi.org/10.1016/S1474-4422\(13\)70278-3](https://doi.org/https://doi.org/10.1016/S1474-4422(13)70278-3)
- Gómez-Belinchón, J.I., Grimalt, J. O., Albaigés, J., 1988. Intercomparison study of liquid-liquid extraction and adsorption on polyurethane and amberlite XAD-2 for the analysis of hydrocarbons, PCBs and fatty acids dissolved in seawater. *Environ. Sci. Technol.* 22, 677–685. <https://doi.org/10.1021/es00171a010>
- Grimalt, J.O., Sunyer, J., Moreno, V., Amaral, O.C., Sala, M., Rosell, A., Anto, J.M., Albaiges, J., 1994. Risk excess of soft-tissue sarcoma and thyroid cancer in a community exposed to airborne organochlorinated compound mixtures with a high hexachlorobenzene content. *Int. J. Cancer.* <https://doi.org/10.1002/ijc.2910560209>
- Grimalt, J.O., Fernandez, P., Berdić, L., Vilanova, R.M., Catalan, J., Psenner, R., Hofer, R., Appleby, P.G., Rosseland, B.O., Lien, L., Massabuau, J.C. Battarbee, R.W., 2001. Selective trapping of organochlorine compounds in mountain lakes of temperate areas. *Environ. Sci. Technol.* 35, 2690–2697. <https://doi.org/10.1021/es000278r>
- Guzzella, L., Poma, G., De Paolis, A., Roscioli, C., Viviano, G., 2011. Organic persistent toxic substances in soils, waters and sediments along an altitudinal gradient at Mt. Sagarmatha, Himalayas, Nepal. *Environ. Pollut.* 159, 2552–2564. <https://doi.org/10.1016/J.ENVPOL.2011.06.015>
- Harman, C., Grung, M., Djedjibegovic, J., Marjanovic, A., Fjeld, E., Braaten, H.F.V., Sober, M., Larssen, T., Ranneklev, S.B., 2018. The organic pollutant status of rivers in Bosnia and Herzegovina as determined by a combination of active and passive sampling methods. *Environ. Monit. Assess.* 190, 1–10. <https://doi.org/10.1007/s10661-018-6667-6>
- Howard, P.H., Boethling, R.S., Jarvis, W.F., Meylan, W.M., Michalenko, E.M., Printup, H.T., 1991. *Handbook of Environmental Degradation Rates*. CRC Press. <https://doi.org/10.1201/9780203719329>
- Hu, W., Gao, P., Wang, L., Hu, J., 2022. Endocrine disrupting toxicity of aryl organophosphate esters and mode of action. *Crit. Rev. Environ. Sci. Technol.* 1–18. <https://doi.org/10.1080/10643389.2022.2050147>
- Huckins, J.N., Petty, J.D., Booij, K., 2006. *Monitors of organic chemicals in the environment: Semipermeable membrane devices*. Springer US. <https://doi.org/10.1007/0-387-35414-X>
- Hulscher, T.E.M. Ten, Van Der Velde, L.E., Bruggeman, W.A.,

1992. Temperature dependence of Henry's law constants for selected chlorobenzenes, polychlorinated biphenyls and polycyclic aromatic hydrocarbons. *Environ. Toxicol. Chem.* 11, 1595–1603. <https://doi.org/10.1002/etc.5620111109>
- Jurado, E., Jaward, F., Lohmann, R., Jones, K.C., Simó, R., Dachs, J., 2005. Wet deposition of persistent organic pollutants to the global oceans. *Environ. Sci. Technol.* 39, 2426–2435. <https://doi.org/10.1021/es048599g>
- Keeling, C.I., Bohlmann, J., 2006. Diterpene resin acids in conifers. *Phytochemistry* 67, 2415–2423. <https://doi.org/10.1016/J.PHYTOCHEM.2006.08.019>
- Khairy, M., Muir, D., Teixeira, C., Lohmann, R., 2015. Spatial Distribution, Air-Water Fugacity Ratios and Source Apportionment of Polychlorinated Biphenyls in the Lower Great Lakes Basin. *Environ. Sci. Technol.* 49, 13787–13797. <https://doi.org/10.1021/acs.est.5b00186>
- Khairy, M., Muir, D., Teixeira, C., Lohmann, R., 2014. Spatial trends, sources, and air-water exchange of organochlorine pesticides in the Great Lakes basin using low density polyethylene passive samplers. *Environ. Sci. Technol.* 48, 9315–9324. <https://doi.org/10.1021/es501686a>
- Li, J., Cheng, H., Zhang, G., Qi, S., Li, X., 2009. Polycyclic aromatic hydrocarbon (PAH) deposition to and exchange at the air-water interface of Luhu, an urban lake in Guangzhou, China. *Environ. Pollut.* 157, 273–279. <https://doi.org/10.1016/J.ENVPOL.2008.06.039>
- Liu, Y., Wang, S., McDonough, C.A., Khairy, M., Muir, D.C.G., Helm, P.A., Lohmann, R., 2016. Gaseous and Freely-Dissolved PCBs in the Lower Great Lakes Based on Passive Sampling: Spatial Trends and Air-Water Exchange. *Environ. Sci. Technol.* 50, 4932–4939. <https://doi.org/10.1021/acs.est.5b04586>
- Llop, S., Murcia, M., Alvarez-Pedrerol, M., Grimalt, J.O., Santamarina, L., Julvez, J., Goñi-Irigoyen, F., Espada, M., Ballester, F., Rebagliato, M., Lopez-Espinosa, M.J., 2017. Association between exposure to organochlorine compounds and maternal thyroid status: Role of the iodothyronine deiodinase 1 gene. *Environ. Int.* 104, 83–90. <https://doi.org/10.1016/J.ENVINT.2016.12.013>
- Lohmann, R., Muir, D., 2010. Global aquatic passive sampling (AQUA-GAPS): Using passive samplers to monitor POPs in the waters of the world. *Environ. Sci. Technol.* 44, 860–864. <https://doi.org/10.1021/es902379g>
- Lohmann, R., Muir, D., Zeng, E.Y., Bao, L.-J.J., Allan, I.J., Arinaitwe, K., Booij, K., Helm, P., Kaserzon, S., Mueller, J.F., Shibata, Y., Smedes, F., Tsapakis, M., Wong, C.S., You, J., 2017. Aquatic Global Passive Sampling (AQUA-GAPS) Revisited: First Steps toward a Network of Networks for Monitoring Organic Contaminants in the Aquatic Environment. *Environ. Sci. Technol.* 51, 1060–1067. <https://doi.org/10.1021/acs.est.6b05159>
- Lopez-Espinosa, M.J., Murcia, M., Iñiguez, C., Vizcaino, E., Costa, O., Fernández-Somoano, A., Basterrechea, M., Lertxundi, A., Guxens, M., Gascon, M., Goñi-Irigoyen, F., Grimalt, J.O., Tardón, A., Ballester, F., 2016. Organochlorine compounds and ultrasound measurements of fetal growth in the INMA cohort (Spain). *Environ. Health Perspect.* 124, 157–163. <https://doi.org/10.1289/ehp.1408907>
- Luarte, T., Tucca, F., Nimptsch, J., Woelfl, S., Casas, G., Dachs, J., Chiang, G., Pozo, K., Barra, R., Galbán-Malagón, C., 2022. Occurrence and air-water diffusive exchange legacy persistent organic pollutants in an oligotrophic north Patagonian lake. *Environ. Res.* 204, 112042. <https://doi.org/10.1016/J.ENVRES.2021.112042>
- Ma, Y., Vojta, S., Becanova, J., Habtemichael, A.Z., Adelman, D.A., Muir, D., Lohmann, R., 2021. Spatial distribution and air-water exchange of organophosphate esters in the lower Great Lakes. *Environ. Pollut.* 286, 117349. <https://doi.org/10.1016/j.envpol.2021.117349>
- Mackay, D., Wania, F., 1995. Transport of contaminants to the Arctic: partitioning, processes and models. *Sci. Total Environ.* 160–161, 25–38. [https://doi.org/10.1016/0048-9697\(95\)04342-X](https://doi.org/10.1016/0048-9697(95)04342-X)
- McConnell, L.L., Kucklick, J.R., Bidleman, T.F., Ivanov, G.P., Chernyak, S.M., 1996. Air-water gas exchange of organochlorine compounds in Lake Baikal, Russia. *Environ. Sci. Technol.* 30, 2975–2983. <https://doi.org/10.1021/es9509487>
- McDonough, C.A., De Silva, A.O., Sun, C., Cabrerizo, A., Adelman, D., Soltwedel, T., Bauerfeind, E., Muir, D.C.G., Lohmann, R., 2018. Dissolved Organophosphate Esters and Polybrominated Diphenyl Ethers in Remote Marine Environments: Arctic Surface Water Distributions and Net Transport through Fram Strait. *Environ. Sci. Technol.* 52, 6208–6216. <https://doi.org/10.1021/acs.est.8b01127>
- McDonough, C.A., Khairy, M.A., Muir, D.C.G., Lohmann, R., 2014. Significance of population centers as sources of gaseous and dissolved PAHs in the lower Great Lakes. *Environ. Sci. Technol.* 48, 7789–7797. <https://doi.org/10.1021/es501074r>
- Meijer, S.N., Dachs, J., Fernandez, P., Camarero, L., Catalan, J., Del Vento, S., Van Drooge, B., Jurado, E., Grimalt, J.O., 2006. Modelling the dynamic air-water-sediment coupled fluxes and occurrence of polychlorinated biphenyls in a high altitude lake. *Environ. Pollut.* 140, 546–560. <https://doi.org/10.1016/j.envpol.2005.06.015>
- Meijer, S.N., Grimalt, J.O., Fernandez, P., Dachs, J., 2009. Seasonal fluxes and temperature-dependent accumulation of persistent organic pollutants in lakes: The role of internal biogeochemical cycling. *Environ. Pollut.* 157, 1815–1822. <https://doi.org/10.1016/J.ENVPOL.2009.01.024>
- Meire, R.O., Khairy, M., Aldeman, D., Galvão, P.M.A., Torres, J.P.M., Malm, O., Lohmann, R., 2019. Passive sampler-derived concentrations of PAHs in air and water along Brazilian mountain transects. *Atmos. Pollut. Res.* 10, 635–641. <https://doi.org/10.1016/j.apr.2018.10.012>
- Meire, R.O., Khairy, M., Targino, A.C., Galvão, P.M.A., Torres, J.P.M., Malm, O., Lohmann, R., 2016. Use of passive samplers to detect organochlorine pesticides in air and water at wetland mountain region sites (S-SE Brazil). *Chemosphere* 144, 2175–2182. <https://doi.org/10.1016/j.chemosphere.2015.10.133>
- Nantaba, F., Palm, W.U., Wasswa, J., Bouwman, H., Kylin, H., Kümmerer, K., 2021. Temporal dynamics and ecotoxicological risk assessment of personal care products, phthalate ester plasticizers, and organophosphorus flame retardants in water from Lake Victoria, Uganda. *Chemosphere* 262, 127716. <https://doi.org/10.1016/J.CHEMOSPHERE.2020.127716>
- Nellier, Y.M., Perga, M.E., Cottin, N., Fanget, P., Malet, E., Naffrechoux, E., 2015a. Mass budget in two high altitude lakes reveals their role as atmospheric PCB sinks. *Sci. Total Environ.* 511, 203–213. <https://doi.org/10.1016/J.SCITOTENV.2014.12.052>
- Nellier, Y.M., Perga, M.E., Cottin, N., Fanget, P., Naffrechoux, E., 2015b. Particle-Dissolved Phase Partition of Polychlorinated Biphenyls in High Altitude Alpine Lakes. *Environ. Sci. Technol.* 49, 9620–9628. <https://doi.org/10.1021/acs.est.5b01274>
- Nizzetto, L., Gioia, R., Li, J., Borgå, K., Pomati, F., Bettinetti, R., Dachs, J., Jones, K.C., 2012. Biological pump control of the fate and distribution of hydrophobic organic pollutants in water and plankton. *Environ. Sci. Technol.* 46, 3204–3211. <https://doi.org/10.1021/es204176q>
- Nizzetto, L., Lohmann, R., Gioia, R., Jahnke, A., Temme, C., Dachs, J., Herckes, P., Di Guardo, A., Jones, K.C., 2008. PAHs in air and seawater along a North-South Atlantic transect: Trends, processes and possible sources. *Environ. Sci. Technol.* 42, 1580–1585. <https://doi.org/10.1021/es0717414>
- Olivella, M.À., 2006. Polycyclic aromatic hydrocarbons in rainwater and surface waters of Lake Maggiore, a subalpine lake in Northern Italy. *Chemosphere* 63, 116–131. <https://doi.org/10.1016/J.CHEMOSPHERE.2005.07.045>
- Paulik, L.B., Smith, B.W., Bergmann, A.J., Sower, G.J., Forsberg,

- N.D., Teeguarden, J.G., Anderson, K.A., 2016. Passive samplers accurately predict PAH levels in resident crayfish. *Sci. Total Environ.* 544, 782–791. <https://doi.org/10.1016/j.scitotenv.2015.11.142>
- Pérez-Maldonado, I.N., Athanasiadou, M., Yáñez, L., González-Amaro, R., Bergman, A., Díaz-Barriga, F., 2006. DDE-induced apoptosis in children exposed to the DDT metabolite. *Sci. Total Environ.* 370, 343–351. <https://doi.org/10.1016/J.SCITOTENV.2006.06.026>
- Pérez-Maldonado, I.N., Herrera, C., Batres, L.E., González-Amaro, R., Díaz-Barriga, F., Yáñez, L., 2005. DDT-induced oxidative damage in human blood mononuclear cells. *Environ. Res.* 98, 177–184. <https://doi.org/10.1016/J.ENVRES.2004.11.001>
- Prats, R.M., van Drooge, B.L., Fernández, P., Grimalt, J.O., 2022a. Changes and distribution of gas-phase polycyclic aromatic hydrocarbons and organochlorine compounds in a high-mountain gradient over a three-year period (Pyrenees, 2017–2020). *Sci. Total Environ.* 829, 154602. <https://doi.org/10.1016/J.SCITOTENV.2022.154602>
- Prats, R.M., van Drooge, B.L., Fernández, P., Grimalt, J.O., 2022b. Occurrence and temperature dependence of atmospheric gas-phase organophosphate esters in high-mountain areas (Pyrenees). *Chemosphere* 292, 133467. <https://doi.org/10.1016/J.CHEMOSPHERE.2021.133467>
- Prats, R.M., van Drooge, B.L., Fernández, P., Marco, E., Grimalt, J.O., 2021. Changes in Urban Gas-Phase Persistent Organic Pollutants During the COVID-19 Lockdown in Barcelona. *Front. Environ. Sci.* 9, 109. <https://doi.org/10.3389/fenvs.2021.650539>
- Qin, N., He, W., Kong, X.Z., Liu, W.X., He, Q.S., Yang, B., Ouyang, H.L., Wang, Q.M., Xu, F.L., 2013. Atmospheric partitioning and the air–water exchange of polycyclic aromatic hydrocarbons in a large shallow Chinese lake (Lake Chaohu). *Chemosphere* 93, 1685–1693. <https://doi.org/10.1016/J.CHEMOSPHERE.2013.05.038>
- Qin, N., He, W., Kong, X.Z., Liu, W.X., He, Q.S., Yang, B., Wang, Q.M., Yang, C., Jiang, Y.J., Jorgensen, S.E., Xu, F.L., Zhao, X.L., 2014. Distribution, partitioning and sources of polycyclic aromatic hydrocarbons in the water–SPM–sediment system of Lake Chaohu, China. *Sci. Total Environ.* 496, 414–423. <https://doi.org/10.1016/J.SCITOTENV.2014.07.045>
- Ramdahl, T., 1983. Retene—a molecular marker for wood combustion in ambient air. *Nature.* 306, 580–583. <https://doi.org/10.1038/306580a0>
- Regnery, J., Püttmann, W., 2010. Occurrence and fate of organophosphorus flame retardants and plasticizers in urban and remote surface waters in Germany. *Water Res.* 44, 4097–4104. <https://doi.org/10.1016/J.WATRES.2010.05.024>
- Ren, J., Wang, X., Wang, C., Gong, P., Yao, T., 2017a. Atmospheric processes of organic pollutants over a remote lake on the central Tibetan Plateau: Implications for regional cycling. *Atmos. Chem. Phys.* 17, 1401–1415. <https://doi.org/10.5194/acp-17-1401-2017>
- Ren, J., Wang, Xiaoping, Wang, C., Gong, P., Wang, Xiruo, Yao, T., 2017b. Biomagnification of persistent organic pollutants along a high-altitude aquatic food chain in the Tibetan Plateau: Processes and mechanisms. *Environ. Pollut.* 220, 636–643. <https://doi.org/10.1016/J.ENVPOL.2016.10.019>
- Rodríguez-Sierra, C.J., Adelman, D., Vojta, Š., Mansilla-Rivera, I., Lohmann, R., 2019. Passive Sampling of Persistent Organic Pollutants in Four Coastal Aquatic Systems of Puerto Rico: A Pilot Study. *Bull. Environ. Contam. Toxicol.* 103, 770–775. <https://doi.org/10.1007/s00128-019-02731-w>
- Ruge, B.Z., Muir, D., Helm, P., Lohmann, R., 2018. Concentrations, Trends, and Air–Water Exchange of PCBs and Organochlorine Pesticides Derived from Passive Samplers in Lake Superior in 2011. *Environ. Sci. Technol.* 52, 14061–14069. <https://doi.org/10.1021/acs.est.8b04036>
- Ruge, Z., Muir, D., Helm, P., Lohmann, R., 2015. Concentrations, Trends, and Air–Water Exchange of PAHs and PBDEs Derived from Passive Samplers in Lake Superior in 2011. *Environ. Sci. Technol.* 49, 13777–13786. <https://doi.org/10.1021/acs.est.5b02611>
- Rusina, T.P., Smedes, F., Brborić, M., Vrana, B., 2019. Investigating levels of organic contaminants in Danube River sediments in Serbia by multi-ratio equilibrium passive sampling. *Sci. Total Environ.* 696, 1–10. <https://doi.org/10.1016/j.scitotenv.2019.133935>
- Rusina, T.P., Smedes, F., Koblizkova, M., Klanova, J., 2010. Calibration of silicone rubber passive samplers: Experimental and modeled relations between sampling rate and compound properties. *Environ. Sci. Technol.* 44, 362–367. <https://doi.org/10.1021/es900938r>
- Sala, M., Sunyer, J., Herrero, C., To-Figueras, J., Grimalt, J.O., 2001. Association between serum concentrations of hexachlorobenzene and polychlorobiphenyls with thyroid hormone and liver enzymes in a sample of the general population. *Occup. Environ. Med.* 58, 172–177. <https://doi.org/10.1136/OEM.58.3.172>
- Sander, R., 2015. Compilation of Henry’s law constants (version 4.0) for water as solvent. *Atmos. Chem. Phys.* 15, 4399–4981. <https://doi.org/10.5194/acp-15-4399-2015>
- Schmid, P., Bogdal, C., Blüthgen, N., Anselmetti, F.S., Zwysig, A., Hungerbühler, K., 2011. The missing piece: Sediment records in remote mountain lakes confirm glaciers being secondary sources of persistent organic pollutants. *Environ. Sci. Technol.* 45, 203–208. <https://doi.org/10.1021/es1028052>
- Schwarzenbach, R.P., Gschwend, P.M., Imboden, D.M., 2016. *Environmental Organic Chemistry*, 3rd Edition. John Wiley & Sons, Ltd.
- Simoneit, B.R.T., Grimalt, J.O., Wang, T.G., Cox, R.E., Hatcher, P.G., Nissenbaum, A., 1986. Cyclic terpenoids of contemporary resinous plant detritus and of fossil woods, ambers and coals. *Org. Geochem.* 10, 877–889. [https://doi.org/10.1016/S0146-6380\(86\)80025-0](https://doi.org/10.1016/S0146-6380(86)80025-0)
- Smedes, F., 2018. Silicone–water partition coefficients determined by cosolvent method for chlorinated pesticides, musks, organo phosphates, phthalates and more. *Chemosphere* 210, 662–671. <https://doi.org/10.1016/j.chemosphere.2018.07.054>
- Smedes, F., Booij, K., 2012. Guidelines for passive sampling of hydrophobic contaminants in water using silicone rubber samplers. *ICES Tech. Mar. Environ. Sci.* 52.
- Smedes, F., Geertsma, R.W., Van Der Zande, T., Booij, K., 2009. Polymer-water partition coefficients of hydrophobic compounds for passive sampling: Application of cosolvent models for validation. *Environ. Sci. Technol.* 43, 7047–7054. <https://doi.org/10.1021/es9009376>
- Smedes, F., Sobotka, J., Rusina, T.P., Fialová, P., Carlsson, P., Kopp, R., Vrana, B., 2020. Unraveling the Relationship between the Concentrations of Hydrophobic Organic Contaminants in Freshwater Fish of Different Trophic Levels and Water Using Passive Sampling. *Environ. Sci. Technol.* 54, 7942–7951. <https://doi.org/10.1021/acs.est.9b07821>
- Sobotka, J., Smedes, F., Vrana, B., 2022. Performance comparison of silicone and low-density polyethylene as passive samplers in a global monitoring network for aquatic organic contaminants. *Environ. Pollut.* 119050. <https://doi.org/10.1016/j.envpol.2022.119050>
- Sun, C., Soltwedel, T., Bauerfeind, E., Adelman, D.A., Lohmann, R., 2016. Depth Profiles of Persistent Organic Pollutants in the North and Tropical Atlantic Ocean. *Environ. Sci. Technol.* 50, 6172–6179. <https://doi.org/10.1021/acs.est.5b05891>
- Sun, Y., De Silva, A.O., St Pierre, K.A., Muir, D.C.G., Spencer, C., Lehnher, I., MacInnis, J.J., 2020. Glacial Melt Inputs of Organophosphate Ester Flame Retardants to the Largest High Arctic Lake. *Environ. Sci. Technol.* 54, 2734–2743. <https://doi.org/10.1021/acs.est.9b06333>
- Tan, Y., Song, R., Lawrence, D., Carpenter, D.O., 2004. Ortho-Substituted but Not Coplanar PCBs Rapidly Kill Cerebellar Granule Cells. *Toxicol. Sci.* 79, 147–156. <https://doi.org/>

- 10.1093/TOXSCI/KFH108
- Tao, Y., Yu, J., Lei, G., Xue, B., Zhang, F., Yao, S., 2017. Indirect influence of eutrophication on air – water exchange fluxes, sinking fluxes, and occurrence of polycyclic aromatic hydrocarbons. *Water Res.* 122, 512–525. <https://doi.org/10.1016/j.watres.2017.06.026>
- Tucca, F., Luarte, T., Nimptsch, J., Woelfl, S., Pozo, K., Casas, G., Dachs, J., Barra, R., Chiang, G., Galbán-Malagón, C., 2020. Sources and diffusive air–water exchange of polycyclic aromatic hydrocarbons in an oligotrophic North–Patagonian lake. *Sci. Total Environ.* 738. <https://doi.org/10.1016/j.scitotenv.2020.139838>
- van Drooge, B.L., Grimalt, J.O., 2015. Particle size-resolved source apportionment of primary and secondary organic tracer compounds at urban and rural locations in Spain. *Atmos. Chem. Phys.* 15, 7735–7752. <https://doi.org/10.5194/acp-15-7735-2015>
- van Drooge, B.L., Sicard, M., Stohl, A., Fontal, M., Bravo, N., Muñoz, A., Lange, D., Fernández, P., Grimalt, J.O., 2016. Detection and simulation of wildfire smoke impacting a Mediterranean urban atmosphere. *Atmos. Poll. Res.* 7, 494–502. <https://doi.org/10.1016/j.apr.2015.12.003>
- van Wendel De Joode, B., Wesseling, C., Kromhout, H., Monge, P., García, M., Mergler, D., 2001. Chronic nervous-system effects of long-term occupational exposure to DDT. *Lancet* 357, 1014–1016. [https://doi.org/10.1016/S0140-6736\(00\)04249-5](https://doi.org/10.1016/S0140-6736(00)04249-5)
- Venier, M., Dove, A., Romanak, K., Backus, S., Hites, R., 2014. Flame retardants and legacy chemicals in Great Lakes’ water. *Environ. Sci. Technol.* 48, 9563–9572. <https://doi.org/10.1021/es501509r>
- Vilanova, R.M., Fernández, P., Grimalt, J.O., 2001a. Polychlorinated biphenyl partitioning in the waters of a remote mountain lake. *Sci. Total Environ.* 279, 51–62. [https://doi.org/10.1016/S0048-9697\(01\)00725-2](https://doi.org/10.1016/S0048-9697(01)00725-2)
- Vilanova, R.M., Fernández, P., Martínez, C., Grimalt, J.O., 2001b. Organochlorine Pollutants in Remote Mountain Lake Waters. *J. Environ. Qual.* 30, 1286–1295. <https://doi.org/10.2134/jeq2001.3041286x>
- Vilanova, R.M., Fernández, P., Martínez, C., Grimalt, J.O., 2001c. Polycyclic aromatic hydrocarbons in remote mountain lake waters. *Water Res.* 35, 3916–3926. [https://doi.org/10.1016/S0043-1354\(01\)00113-0](https://doi.org/10.1016/S0043-1354(01)00113-0)
- Vives, I., Grimalt, J.O., Ventura, M., Catalan, J., Rosseland, B.O., 2005. Age dependence of the accumulation of organochlorine pollutants in brown trout (*Salmo trutta*) from a remote high mountain lake (Redó, Pyrenees). *Environ. Pollut.* 133, 343–350. <https://doi.org/10.1016/j.envpol.2004.05.027>
- Wakeham, S.G., Schaffner, C., Giger, W., 1980. Poly cyclic aromatic hydrocarbons in Recent lake sediments-II. Compounds derived from biogenic precursors during early diagenesis. *Geochim. Cosmochim. Acta* 44, 415–429. [https://doi.org/10.1016/0016-7037\(80\)90041-1](https://doi.org/10.1016/0016-7037(80)90041-1)
- Wania, F., Axelman, J., Broman, D., 1998. A review of processes involved in the exchange of persistent organic pollutants across the air–sea interface. *Environ. Pollut.* 102, 3–23. [https://doi.org/10.1016/S0269-7491\(98\)00072-4](https://doi.org/10.1016/S0269-7491(98)00072-4)
- Wei, G.L., Li, D.Q., Zhuo, M.N., Liao, Y.S., Xie, Z.Y., Guo, T.L., Li, J.J., Zhang, S.Y., Liang, Z.Q., 2015. Organophosphorus flame retardants and plasticizers: Sources, occurrence, toxicity and human exposure. *Environ. Pollut.* 196, 29–46. <https://doi.org/10.1016/j.envpol.2014.09.012>
- Wenger, D., Gerecke, A.C., Heeb, N. V., Hueglin, C., Seiler, C., Haag, R., Naegeli, H., Zenobi, R., 2009. Aryl hydrocarbon receptor-mediated activity of atmospheric particulate matter from an urban and a rural site in Switzerland. *Atmos. Environ.* 43, 3556–3562. <https://doi.org/10.1016/J.ATMOSENV.2009.04.012>
- WHO, 1998. Environmental Health Criteria 209. Flame retardants: tris (chloropropyl) phosphate and tris (2-chloroethyl) phosphate. World Health Organization, Geneva, Switzerland.
- Wilkinson, A.C., Kimpe, L.E., Blais, J.M., 2005. Air-water gas exchange of chlorinated pesticides in four lakes spanning a 1,205 meter elevation range in the Canadian Rocky Mountains. *Environ. Toxicol. Chem.* 24, 61–69. <https://doi.org/10.1897/04-071R.1>
- Williams, A.J., Grulke, C.M., Edwards, J., McEachran, A.D., Mansouri, K., Baker, N.C., Patlewicz, G., Shah, I., Wambaugh, J.F., Judson, R.S., Richard, A.M., 2017. The CompTox Chemistry Dashboard: A community data resource for environmental chemistry. *J. Cheminform.* 9, 61. <https://doi.org/10.1186/s13321-017-0247-6>
- Winneke, G., Walkowiak, J., Lilienthal, H., 2002. PCB-induced neurodevelopmental toxicity in human infants and its potential mediation by endocrine dysfunction. *Toxicology* 181–182, 161–165. [https://doi.org/10.1016/S0300-483X\(02\)00274-3](https://doi.org/10.1016/S0300-483X(02)00274-3)
- Wu, Z., Tao, Y., 2021. Occurrence, sources, bioaccumulation, and air–water exchange fluxes of polycyclic aromatic hydrocarbons in Lake Hongze, China. *J. Soils Sediments* 2021 218 21, 2969–2980. <https://doi.org/10.1007/S11368-021-02982-3>
- Yang, J., Zhao, Y., Li, M., Du, M., Li, X., Li, Y., 2019. A review of a class of emerging contaminants: The classification, distribution, intensity of consumption, synthesis routes, environmental effects and expectation of pollution abatement to organophosphate flame retardants (opfrs). *Int. J. Mol. Sci.* 20. <https://doi.org/10.3390/ijms20122874>
- Yao, Y., Meng, X.Z., Wu, C.C., Bao, L.J., Wang, F., Wu, F.C., Zeng, E.Y., 2016. Tracking human footprints in Antarctica through passive sampling of polycyclic aromatic hydrocarbons in inland lakes. *Environ. Pollut.* 213, 412–419. <https://doi.org/10.1016/J.ENVPOL.2016.02.035>
- Zhang, X., Robson, M., Jobst, K., Pena-Abaurrea, M., Muscalu, A., Chaudhuri, S., Marvin, C., Brindle, I.D., Reiner, E.J., Helm, P., 2020. Halogenated organic contaminants of concern in urban-influenced waters of Lake Ontario, Canada: Passive sampling with targeted and non-targeted screening. *Environ. Pollut.* 264, 114733. <https://doi.org/10.1016/j.envpol.2020.114733>
- Zhao, Z., Zhang, L., Deng, J., Wu, J., 2015. The potential effects of phytoplankton on the occurrence of organochlorine pesticides (OCPs) and polycyclic aromatic hydrocarbons (PAHs) in water from Lake Taihu, China. *Environ. Sci. Process. Impacts* 17, 1150–1156. <https://doi.org/10.1039/C5EM00025D>

PASSIVE WATER SAMPLING AND AIR–WATER DIFFUSIVE EXCHANGE OF LONG-RANGE TRANSPORTED SEMI-VOLATILE ORGANIC POLLUTANTS IN HIGH-MOUNTAIN LAKES

Raimon M. Prats, Barend L. van Drooge, Pilar Fernández, Joan O. Grimalt

Institute of Environmental Assessment and Water Research (IDAEA-CSIC), Jordi Girona 18, 08034 Barcelona, Catalonia, Spain

ARTICLE 5 – SUPPORTING INFORMATION

Text S5.1	Calculation of air–water exchange fluxes.	202
Text S5.2	Calculation of flux theoretical uncertainties.	204
Text S5.3	Calculation of atmospheric degradation fluxes.	205
Table S5.1	Meteorological conditions for the passive air (PAS) and water (PWS) sampling periods.	206
Table S5.2	Ion m/z ratios for the quantification of PCBs, OCs, and PAHs in GC-MS.	207
Table S5.3	Ion m/z transitions for the quantification of OPEs in GC-MS/MS.	208
Table S5.4	Physical-chemical properties of target compounds and PRCs used for calculations.	209
Table S5.5	Degrees of equilibrium reached during the PWS periods.	210
Table S5.6	Effective sampled water volumes used in the calculation of water concentrations.	211
Table S5.7	Gas-phase atmospheric concentrations at each lake, measured using PUF-PAS samplers.	212
Table S5.8	Literature comparison of freely dissolved water concentrations measured using LDPE-PWS.	213
Figure S5.1	Polymer–water partition coefficients for LDPE and SR samplers.	215
Figure S5.2	PRC fractions and NLS fit for the calibration of passive water samplers.	216
References S5		217

Text S5.1. Calculation of air–water exchange fluxes

Air–water diffusive exchange fluxes were calculated considering the first passive water sampling period (PWS I) and the three passive air sampling periods coinciding in time with the water sampling (PAS I–III; Prats et al., 2022a, 2022b). Fluxes for each specific compound “*i*” were calculated at each sampling site using a boundary layer model first proposed by Deacon (1977) as outlined in Schwarzenbach et al. (2016):

$$F_i = k_{iAW} \left(C_{iW} - \frac{C_{iA}}{K_{iAW}} \right) \quad (\text{Eq. S5.1})$$

where k_{iAW} is the overall air–water exchange velocity (m d^{-1}), C_{iW} and C_{iA} are the concentrations of the compound in the freely dissolved phase of water and in the atmospheric gas phase, respectively (ng m^{-3}), and K_{iAW} is the equilibrium air–water partition constant (dimensionless). K_{iAW} is equivalent to the nondimensional Henry’s Law constant:

$$K_{iAW} = \frac{H_{i(T)}}{RT} \quad (\text{Eq. S5.2})$$

where R is the ideal gas constant ($\text{Pa m}^3 \text{K}^{-1} \text{mol}^{-1}$), T is the average temperature (K), and $H_{i(T)}$ is the compound’s Henry’s Law constant corrected for temperature from $H_{i(298K)}$ values (Williams et al., 2017) as proposed elsewhere (Hulscher et al., 1992).

The calculation of k_{iAW} was as follows:

$$\frac{1}{k_{iAW}} = \frac{1}{k_{iW}} + \frac{1}{k_{iA}K_{iAW}} \quad (\text{Eq. S5.3})$$

where k_{iW} and k_{iA} are the water-side and air-side single-phase exchange velocities, respectively (in cm s^{-1} , later converted into m s^{-1} for the calculation of F_i).

In water, k_{iW} was determined relative to that of CO_2 (k_{CO_2W}) through the following equation:

$$k_{iW} = k_{\text{CO}_2W} \left(\frac{Sc_{iW}}{Sc_{\text{CO}_2W}} \right)^{-a_{Sc}} \quad \text{with } a_{Sc} \begin{cases} 2/3 \text{ for } u_{10} \leq 5 \text{ m s}^{-1} \\ 1/2 \text{ for } u_{10} > 5 \text{ m s}^{-1} \end{cases} \quad (\text{Eq. S5.4})$$

where u_{10} is the average wind speed (m s^{-1}) measured 10 m above the surface (which determines the value of the coefficient a_{Sc}) (Table S5.1) and Sc_{iW} and Sc_{CO_2W} are the Schmidt numbers (unitless) of the compound of interest and of CO_2 , respectively. The calculation of k_{CO_2W} was performed using a lake-specific parametrization of measurements from multiple literature sources (Klaus and Vachon, 2020):

$$k_{\text{CO}_2W} = (0.328 \log_{10}(LA) + 1.581) u_{10} - 0.066 \log_{10}(SIN) + 1.266 \quad (\text{Eq. S5.5})$$

where LA is the lake area and SIN is a space integration parameter equal to 1 when the whole lake is considered. LA were determined in km^2 using ArcGIS (Esri, Redlands, CA, USA): 0.074 Llebreta, 0.073 Llong, 0.042 Sarradé, 0.246 Redon, 0.051 Dellui, 0.024 Collada. $SIN=0.999$ was used as in Klaus and Vachon (2020) to avoid a mathematical undefinition. Sc_{iW} and Sc_{CO_2W} were calculated as $\nu_{W(T)}/D_{iW}$, where $\nu_{W(T)}$ is the kinematic viscosity of water at the average exposure temperature (obtained from interpolation

of values in Schwarzenbach et al., 2005) and D_{iW} is the molecular diffusivity of each compound in water ($\text{cm}^2 \text{s}^{-1}$). D_{iW} and D_{CO_2W} values were calculated as (Hayduk and Laudie, 1974; Othmer and Thakar, 1953):

$$D_{iW} = \frac{13.26 \times 10^{-5}}{\nu_{H_2O}(T)^{1.14} V_i^{0.589}} \quad (\text{Eq. S5.6})$$

where V_i is the molar volume of the compound ($\text{cm}^3 \text{mol}^{-1}$), with $V_{CO_2} = 26.9 \text{ cm}^3 \text{mol}^{-1}$. V_i were estimated using the SPARC physicochemical calculator (ARChem, Danielsville, GA, USA) (Table S5.4).

In air, k_{iA} was determined relative to that of H_2O (k_{H_2OA}) through the following equation:

$$k_{iA} = k_{H_2OA} \left(\frac{D_{iA}}{D_{H_2OA}} \right)^{a_D} \quad (\text{Eq. S5.7})$$

where the exponent $a_D = 2/3$ (Mackay and Yeun, 1983) and D_{iA} is the molar diffusivity of each compound in air ($\text{cm}^2 \text{s}^{-1}$). The calculation of k_{H_2OA} was performed as proposed by Schwarzenbach et al. (2016) with coefficients from Fairall et al. (2011, 2003, 1996) and Johnson (2010):

$$k_{H_2OA} = 0.11 u_{10} + 0.1 \quad (\text{Eq. S5.8})$$

D_{iA} and D_{H_2OA} were calculated as (Fuller et al., 1966):

$$D_{iA} = 10^{-3} \frac{T^{1.75} \left(\frac{1}{M_A} + \frac{1}{M_i} \right)^{1/2}}{p \left(V_A^{1/3} + V_i^{1/3} \right)^2} \quad (\text{Eq. S5.9})$$

where M_i and M_A are the molar mass of the studied compound (g mol^{-1}) (Table S5.4) and average molar mass of air (28.97 g mol^{-1}), p is the average atmospheric pressure (atm) (Table S5.1), and V_A is the average molar volume of air ($20.1 \text{ cm}^3 \text{mol}^{-1}$).

Text S5.2. Calculation of flux theoretical uncertainties

The air–water exchange flux theoretical uncertainties (δF_i) were calculated individually for each compound at each sampling site by propagation of the error in the non-constant variables involved in the following flux equation:

$$F_i = k_{iAW} \left(C_{iW} - \frac{C_{iA}RT}{H_i(T)} \right) \quad (\text{Eq. S5.10})$$

Thus, δF_i is calculated as the square root of the sum of squares of the partial derivatives of F_i with respect to each variable “ x ” ($\partial F_i / \partial x$), multiplied in turn by the square of their respective errors:

$$\delta F_i = \sqrt{\left(\frac{\partial F_i}{\partial k_{iAW}} \right)^2 \delta_{k_{iAW}}^2 + \left(\frac{\partial F_i}{\partial H_i} \right)^2 \delta_{H_i}^2 + \left(\frac{\partial F_i}{\partial T} \right)^2 \delta_T^2 + \left(\frac{\partial F_i}{\partial C_{iA}} \right)^2 \delta_{C_{iA}}^2 + \left(\frac{\partial F_i}{\partial C_{iW}} \right)^2 \delta_{C_{iW}}^2} \quad (\text{Eq. S5.11})$$

The solution to the previous equation is:

$$\frac{\delta F_i}{F_i} = \sqrt{\left(\frac{\delta_{k_{iAW}}}{k_{iAW}} \right)^2 + \left(\frac{k_{iAW} C_{iA} RT}{F_i H_i} \frac{\delta_{H_i}}{H_i} \right)^2 + \left(\frac{k_{iAW} C_{iA} R}{F_i H_i} \delta T \right)^2 + \left(\frac{k_{iAW} RT}{F_i H_i} \delta_{C_{iA}} \right)^2 + \left(\frac{k_{iAW}}{F_i} \delta_{C_{iW}} \right)^2} \quad (\text{Eq. S5.12})$$

where $\delta F_i / F_i$ is the relative flux uncertainty. Given the difficulty for determining errors for k_{iAW} and H_i , their relative errors were assumed as 0.3 (30%) and 0.5 (50%), respectively, based on other analyses of error (Blanchard et al., 2008; Hoff, 1994), as recommended by (Rowe and Perlinger, 2012). The errors of T and C_{iA} were determined as the standard deviation of the temperature measured in situ over the sampling period (Table 1) and the standard deviation of the concentrations from the three PAS periods (Table S5.5), respectively. The error of C_{iW} was calculated from PWS I concentrations by assuming a relative error of 0.2 (20%) as recommended for determinations with less than three replicates (Rowe and Perlinger, 2012).

Text S5.3. Calculation of atmospheric degradation fluxes

Atmospheric degradation fluxes due to hydroxyl radical ($\cdot\text{OH}$) oxidation were calculated as outlined elsewhere (Gioia et al., 2010; Luarte et al., 2022; Nizzetto et al., 2008). Briefly, the degradation flux ($F_{i\text{ deg}}$, $\text{ng m}^{-2} \text{d}^{-1}$) of a specific compound “ i ” was calculated as:

$$F_{i\text{ deg}} = h_{ABL} k_{i\text{ OH}} C_{OH} C_{iA} \quad (\text{Eq. S5.13})$$

where h_{ABL} is the average height of the atmospheric boundary layer (m), $k_{i\text{ OH}}$ is the compound-specific atmospheric hydroxylation rate ($\text{cm}^3 \text{ molec}^{-1} \text{ s}^{-1}$), C_{OH} is the concentration of hydroxyl radicals in the atmospheric layer (molec cm^{-3}), and C_{iA} is the measured gas-phase concentration of the compound (ng m^{-3} , Table S5.5). Here, h_{ABL} was considered at an average height of 700 m above ground level based on other studies (Fernández et al. 2021). Values for $k_{i\text{ OH}}$ were mostly modelled and obtained from a single source (Williams et al., 2017) for maintaining consistency between compound groups. Nevertheless, they were generally of the same order as other values considered elsewhere (Brubaker and Hites, 1998; Keyte et al., 2013; Kwok et al., 2002). C_{OH} were calculated as an average of tabulated estimations at latitude 42° N between atmospheric pressures of 700 and 800 hPa (Spivakovsky et al., 2000) and values calculated as a function of the average ambient temperature (T in °C, Table 1) following (Beyer et al., 2003):

$$C_{OH} = [0.5 + 0.4 \times T(^{\circ}\text{C})] \times 10^5 \quad (\text{Eq. S5.14})$$

Table S5.1. Meteorological conditions for the passive air (PAS) and water (PWS) sampling periods recorded by an automatic weather station from the XEMA network of the Catalan Meteorological Service at Estanh Redon.

	Start date	End date	Air temperature (range) °C	Rel. Humidity %	Pressure atm	Acc. Precipitation mm	Average wind speed (max) m s ⁻¹	Average solar irradiance (max) W m ⁻²
PAS I	19/9/2017	31/1/2018	0.6 ± 6.0 (-14.2–15.0)	69.5 ± 26.2	778.4 ± 7.2	709	4.3 (30.7)	109.6 (839)
PAS II	31/1/2018	12/7/2018	0.8 ± 7.0 (-16.6–18.2)	85.3 ± 16.7	772.6 ± 8.4	1051	5.0 (36.2)	194.8 (1203)
PAS III	12/7/2018	13/12/2018	6.7 ± 6.1 (-9.2–20.3)	78.2 ± 22.3	779.4 ± 6.7	600	4.4 (33.9)	170.4 (1073)
PAS I+II+III	19/9/2017	13/12/2018	2.8 ± 7.0 (-16.6–20.3)	78.2 ± 22.8	776.7 ± 8.1	2359	4.6 (36.2)	160.9 (1203)
PWS I	21/9/2017	26/9/2018	2.9 ± 7.4 (-16.6–20.3)	78.2 ± 21.9	776.8 ± 8.2	2030	4.6 (36.2)	173.1 (1203)
PWS II	26/9/2018	27/9/2019	3.7 ± 7.1 (-14.0–25.1)	71.6 ± 27.2	778.0 ± 7.2	1348	4.8 (36.0)	182.3 (1302)
PWS III	27/9/2019	7/10/2020	4.2 ± 6.3 (-12.6–23.1)	76.9 ± 24.6	777.6 ± 6.9	1605	4.6 (35.6)	169.2 (1224)

Table S5.2 Ion m/z ratios (70 eV, SIM mode) for the quantification of target compounds, performance reference compounds (PRCs), and recovery standards in GC-MS.

Compound	Abbreviation	m/z
2,4,4'-Trichlorobiphenyl	PCB28	256
2,2',5,5'-Tetrachlorobiphenyl	PCB52	292
2,2',4,5,5'-Pentachlorobiphenyl	PCB101	326
2,3',4,4',5-Pentachlorobiphenyl	PCB118	326
2,2',3,4,4',5'-Hexachlorobiphenyl	PCB138	360
2,2',4,4',5,5'-Hexachlorobiphenyl	PCB153	360
2,2',3,4,4',5,5'-Heptachlorobiphenyl	PCB180	394
1,1-Dichloro-2,2-bis(4-chlorophenyl)ethene	4,4'-DDE	246
Hexachlorobenzene	HCB	284
Pentachlorobenzene	PeCB	250
Fluorene	Fle	166
Phenanthrene	Phe	178
Anthracene	Ant	188
Fluoranthene	Flu	202
Pyrene	Pyr	202
Retene	Ret	219
Benz[a]anthracene	B[a]ant	228
Chrysene + Triphenylene	Chr + TriPh	228
Benzo[b]fluoranthene	B[b]flu	252
Benzo[j+k]fluoranthene	B[j+k]flu	252
Benzo[e]pyrene	B[e]pyr	252
Benzo[a]pyrene	B[a]pyr	252
Perylene	Pery	252
Indeno[1,2,3-cd]pyrene	Ind[123cd]pyr	276
Benzo[ghi]perylene	B[ghi]pery	276
2-Chlorobiphenyl	PCB1	188
3-Chlorobiphenyl	PCB2	188
4-Chlorobiphenyl	PCB3	188
2,6-Dichlorobiphenyl	PCB10	222
3,5-Dichlorobiphenyl	PCB14	222
2,3,4-Trichlorobiphenyl	PCB21	256
2,2',4,6-Tetrachlorobiphenyl	PCB50	290
2,3,3',4-Tetrachlorobiphenyl	PCB55	290
3,3',4,5-Tetrachlorobiphenyl	PCB78	290
2,2',4,6,6'-Pentachlorobiphenyl	PCB104	326
2,2',3,4,6,6'-Hexachlorobiphenyl	PCB145	360
2,2',3,4,4',5,6,6'-Octachlorobiphenyl	PCB204	428
Decachlorobiphenyl	PCB209	498
Tetrabromobenzene	TBB	394
Fluorene-d ₁₀	Fle-d ₁₀	176
Phenanthrene-d ₁₀	Phe-d ₁₀	188
Anthracene-d ₁₀	Ant-d ₁₀	198
Fluoranthene-d ₁₀	Flu-d ₁₀	212
Pyrene-d ₁₀	Pyr-d ₁₀	212
Benz[a]anthracene-d ₁₂	B[a]ant-d ₁₂	240
Chrysene-d ₁₂	Chr-d ₁₂	240
Benzo[b]fluoranthene-d ₁₂	B[b]flu-d ₁₂	264
Benzo[k]fluoranthene-d ₁₂	B[k]flu-d ₁₂	264
Benzo[a]pyrene-d ₁₂	B[a]pyr-d ₁₂	264
Indeno[1,2,3-cd]pyrene-d ₁₂	Ind[123cd]pyr-d ₁₂	288
Benzo[ghi]perylene-d ₁₂	B[ghi]pery-d ₁₂	288

Table S5.3. Ion m/z transitions and collision energies (CE) for the quantification of organophosphate esters (OPEs) and their recovery standards (GC-MS/MS).

Compound	Abbreviation	Quantifier		Qualifier	
		Transition (m/z)	CE (eV)	Transition (m/z)	CE (eV)
Tributyl phosphate	TBP	99→81	20	99→63	38
Tris(2-chloroethyl) phosphate	TCEP	249→125	10	249→99	32
Tris(1-chloro-2-propyl) phosphate	TCIPP	125→81	29	125→99	12
Tris(1,3-dichloro-2-propyl) phosphate	TDCIPP	191→155	5	191→75	11
Triphenyl phosphate	TPhP	326→215	25	326→169	32
Tributyl phosphate-d ₂₇	TBP-d ₂₇	103→83	20	103→63	43
Tris(2-chloroethyl) phosphate-d ₁₂	TCEP-d ₁₂	261→131	9	261→131	30
Tris(1-chloro-2-propyl) phosphate-d ₁₈	TCIPP-d ₁₈	131→83	30	131→103	11
Tris(1,3-dichloro-2-propyl) phosphate-d ₁₅	TDCIPP-d ₁₅	197→160	4	197→79	12
Triphenyl phosphate-d ₁₅	TPhP-d ₁₅	341→223	26	341→243	11

Table S5.4. Compound properties: molar mass (M), molar volume (V), Henry's Law constant (H), octanol–water partition coefficient (logK_{ow}), and polymer–water partition coefficients (logK_{PWS-w}) for the low-density polyurethane (LDPE) and silicone rubber (SR) samplers (Rusina et al., 2019; Smedes, 2018a, 2018b; Smedes et al., 2009; Williams et al., 2017).

Compounds	M	V	H, 25 °C	logK _{ow} , 25 °C	logK _{PWS-w} , 25 °C	logK _{PWS-w} , 25 °C
	g mol ⁻¹	cm ³ mol ⁻¹	atm m ³ mol ⁻¹		(LDPE)	(SR)
PCB28	257.55	188.1	2.00E-4	5.67	5.56	5.53
PCB52	291.99	200.8	2.00E-4	5.84	5.72	5.80
PCB101	326.44	212.4	9.00E-5	6.38	6.33	6.28
PCB118	326.44	210.9	7.87E-5	6.74	6.63	6.42
PCB138	360.88	223.5	2.10E-5	6.83	6.92	6.67
PCB153	360.88	224.0	2.30E-5	6.92	6.96	6.72
PCB180	395.33	235.4	1.00E-5	7.36	7.31	6.99
4,4'-DDE	318.03	222.4	4.16E-5	6.51	6.28	6.27
HCB	284.78	161.2	1.70E-3	5.50	5.50	5.05
PeCB	250.34	149.5	7.03E-4	5.18	4.89	4.61
Flu	166.22	154.8	9.62E-5	4.18	3.77	3.79
Phe	178.23	160.6	4.23E-5	4.57	4.22	4.11
Ant	178.23	159.1	5.56E-5	4.54	4.33	4.21
Fluo	202.26	196.1	8.86E-6	5.22	4.93	4.62
Pyr	202.26	182.3	1.19E-5	5.18	5.10	4.68
Ret	234.34	226.5	2.12E-5	6.35	6.00	5.27
B[a]ant	228.29	195.1	1.20E-5	5.91	5.73	5.32
Chr/TriPh	228.29	196.5	5.23E-6	5.86	5.78	5.25
B[b/j/k]fluo	252.32	232.0	6.57E-7	5.90	6.66	5.74
B[e]pyr	252.32	219.6	8.50E-7	6.44	5.69	5.63
B[a]pyr	252.32	218.2	4.57E-7	6.04	6.75	5.69
Pery	252.32	219.6	8.44E-7	6.25	6.55	5.64
Ind[123cd]pyr	276.34	253.7	3.84E-7	6.70	7.40	6.06
B[ghi]pery	276.34	241.3	3.31E-7	6.63	7.27	6.02
TBP	266.32	265.5	1.13E-6	3.82	4.90 ^a	4.93
TCEP	285.49	196.5	1.28E-7	1.63	2.80 ^a	3.05
TCIPP	327.57	247.9	2.63E-7	2.89	3.36 ^a	3.55
TDCIPP	430.91	268.4	1.68E-6	3.65	3.69 ^a	3.85
TPhP	326.29	272.9	1.78E-6	4.70	4.98 ^a	5.00
PCB1	188.65	-	-	4.46	4.08	4.22
PCB2	188.65	-	-	4.69	4.36	4.41
PCB3	188.65	-	-	4.69	4.38	4.36
PCB10	223.10	-	-	4.84	4.47	4.57
PCB14	223.10	-	-	5.28	5.16	5.04
PCB21	257.55	-	-	5.51	5.40	5.34
PCB50	291.99	-	-	5.63	5.72	5.70
PCB55	291.99	-	-	6.11	6.01	5.93
PCB78	291.99	-	-	6.35	6.19	5.97
PCB104	326.44	-	-	5.81	6.17	6.15
PCB145	360.88	-	-	6.25	6.63	6.62
PCB204	429.77	-	-	7.30	7.82	7.35

^a Derived from a linear regression between SR (Smedes, 2018a) and LDPE (Smedes et al., 2009) logK_{PWS-w} for PCBs (n=23, R²=0.991, see Figure S5.1).

Table S5.5. Concentrations (pg m^{-3}) in the atmospheric gas phase at each lake for each sampling period (PAS I–III), measured using polyurethane foam (PUF) passive samplers. Data from Prats et al. (2022a) and Prats et al. (2022b), except for retene (Ret, new data).

Compound	PAS I					PAS II					PAS III							
	Liebreta	Llong	Sarradé	Redon	Dellui	Collada	Liebreta	Llong	Sarradé	Redon ^a	Dellui	Collada	Liebreta	Llong	Sarradé	Redon	Dellui	Collada
PCB28	1.4	1.3	2.6	na	1.7	1.5	3.1	4.6	3.2	1.4	1.0	3.0	1.7	3.0	2.2	5.1	2.2	2.0
PCB52	1.4	1.3	2.0	na	1.1	0.94	1.7	1.7	3.8	2.1	1.4	2.4	1.2	1.6	1.7	2.8	1.5	1.5
PCB101	2.3	2.1	2.2	na	1.3	1.4	3.5	3.1	4.8	3.9	1.9	2.0	3.0	2.4	3.0	4.7	2.3	2.7
PCB118	2.4	2.0	1.4	na	1.5	1.4	1.1	1.6	2.0	2.4	1.8	2.1	3.3	2.5	3.5	2.3	3.1	2.9
PCB138	2.7	1.3	1.1	na	1.1	0.91	1.9	1.5	3.2	2.9	1.3	0.72	4.1	2.8	3.4	3.0	3.5	3.6
PCB153	1.5	1.5	1.4	na	1.2	1.3	1.8	1.6	3.3	2.2	1.1	0.82	2.0	1.2	1.5	1.9	1.7	1.6
PCB180	0.43	0.30	0.24	na	0.27	0.23	0.21	0.14	0.50	0.40	0.24	0.03	0.90	0.97	0.59	1.1	0.42	0.83
Σ_7 PCB	11	9.8	11	na	8.0	7.5	13	14	21	15	8.7	11	16	15	16	21	15	15
HCB	53	42	43	na	53	18	32	32	44	31	42	30	58	60	31	61	83	81
PeCB	21	16	19	na	15	10	9.0	8.8	7.8	9.2	8.0	5.5	31	51	54	43	65	65
Fle	309	498	516	na	458	326	152	224	150	253	174	75	181	176	252	287	256	231
Phe	366	419	518	na	379	263	258	328	362	440	171	85	338	203	324	507	164	152
Flu	51	48	75	na	44	26	47	31	42	38	19	8.3	48	24	41	96	20	16
Pyr	23	17	27	na	16	9.2	18	13	14	15	6.3	4.5	53	14	16	44	13	22
Ret	na	na	na	na	na	na	na	na	na	na	na	na	52	11	18	17	2.5	2.1
B[a]ant	1.4	0.44	0.51	na	0.39	0.30	1.8	0.74	0.71	0.55	0.27	0.12	2.0	0.38	0.40	1.1	0.26	0.44
Chr+TriPh	6.6	5.3	8.0	na	5.0	3.6	8.0	5.8	9.7	5.8	5.4	2.2	6.6	2.1	3.2	20	1.1	1.9
Σ_8 PAH ^b	758	987	1144	na	903	628	486	602	578	752	376	175	629	419	636	955	455	423
TBP	3.3	1.8	2.9	na	2.4	2.6	1.2	1.0	1.0	1.2	0.25	0.38	2.4	2.1	1.4	2.7	0.83	1.1
TCEP	1.2	0.36	nd	na	6.3	0.29	1.5	1.4	2.9	3.4	1.4	4.7	13	14	8.7	23	11	16
TCIPP	16	3.9	4.9	na	11	8.4	23	8.9	5.3	6.0	1.3	3.7	69	11	3.2	21	2.0	1.9
TDCIPP	2.7	nd	4.3	na	0.86	1.4	0.28	0.65	0.42	2.0	0.66	2.3	1.5	2.2	0.89	3.2	1.3	2.5
TPhP	4.8	2.3	8.3	na	2.3	8.6	6.1	5.1	7.6	1094 ^c	1.7	0.72	15	23	12	375 ^c	4.1	3.8
Σ_5 OPE	28	8.4	20	na	23	21	32	17	17	1107 ^c	5.3	12	101	53	26	426 ^c	19	26

na: not analyzed; nd: not detected above limits of detection or blank levels; ^a Sample spans periods PAS I+II; ^b Not including Ret; ^c Contaminated sample.

Table S5.7. Effective sampled water volumes (in L) for each compound at each sampling site during all passive water sampling (PWS) periods. The volumes depend on the partitioning affinity of compounds between the freely dissolved phase of water and the sampler material, as well as on the degree of equilibrium (DEQ) reached during exposure.

	PWS I (LDPE)			PWS II (LDPE)			PWS III (LDPE)			PWS III (SR)					
	Llebreta	Llong	Sarradé	Redon	Dellui	Collada	Llebreta	Sarradé	Redon	Llebreta	Sarradé	Redon	Llebreta	Sarradé	Redon
	PCB28	1656	1329	986	1719	1559	1274	1057	1007	1321	1787	1600	1773	2946	1293
PCB52	2315	1833	1120	2365	2074	1628	1211	1152	1552	2162	1859	2121	3200	1288	3492
PCB101	5242	3870	1436	4949	3831	2682	1575	1494	2118	3133	2480	2998	3371	1272	3683
PCB118	6211	4499	1506	5741	4314	2947	1656	1570	2246	3358	2620	3199	3417	1279	3734
PCB138	6491	4652	1473	5929	4382	2954	1621	1537	2209	3322	2571	3157	3313	1227	3621
PCB153	6553	4691	1476	5978	4411	2969	1626	1541	2216	3334	2579	3168	3320	1228	3629
PCB180	6578	4683	1432	5963	4362	2917	1578	1496	2156	3253	2506	3087	3207	1180	3506
4,4'-DDE	5067	3759	1434	4810	3753	2645	1572	1491	2109	3110	2472	2980	3407	1287	3722
HCB	1446	1163	896	1504	1371	1128	959	913	1191	1601	1447	1593	1764	1010	1914
PeCB	354	286	286	370	342	291	299	286	350	444	436	451	759	643	821
Flu	27	22	22	28	26	22	23	22	27	34	34	35	116	113	125
Phe	75	61	61	79	73	62	64	61	74	94	93	96	241	237	261
Ant	99	80	80	103	96	81	84	80	98	124	122	126	304	297	328
Flu	390	315	315	407	377	320	330	315	385	489	480	497	779	674	842
Pyr	577	466	460	603	559	474	483	462	567	722	706	733	891	741	963
Ret	3891	2999	1455	3855	3208	2391	1585	1505	2081	2986	2464	2893	2424	1224	2636
B[a]ant	2391	1901	1213	2454	2170	1720	1309	1245	1670	2311	2004	2272	2572	1264	2798
Chr+TriPh	2632	2083	1265	2687	2353	1845	1368	1301	1754	2445	2100	2398	2385	1224	2593
B[b]fluo	6939	5033	1696	6423	4836	3309	1865	1768	2528	3777	2949	3599	3314	1363	3616
B[j+k]fluo	6939	5033	1696	6423	4836	3309	1865	1768	2528	3777	2949	3599	3314	1363	3616
B[e]pyr	2193	1746	1137	2255	2002	1593	1226	1167	1560	2153	1874	2120	3145	1334	3430
B[a]pyr	7179	5187	1711	6616	4950	3370	1882	1785	2556	3827	2979	3643	3240	1350	3534
Pery	6577	4800	1671	6130	4659	3213	1835	1741	2481	3695	2898	3526	3163	1338	3449
Ind[123cd]pyr	7806	5556	1697	7075	5173	3458	1870	1773	2555	3856	2969	3659	3510	1357	3833
B[ghi]pery	7707	5494	1691	6997	5128	3434	1863	1766	2544	3836	2958	3642	3481	1353	3801
TBP	364	294	294	380	352	299	308	294	360	456	448	464	1456	936	1578
TCEP	3	2	2	3	3	2	2	2	3	4	4	4	21	21	23
TCIPP	10	8	8	11	10	9	9	8	10	13	13	13	66	65	72
TDCIPP	23	18	18	24	22	19	19	18	22	28	28	29	133	130	143
TPhP	436	352	349	455	422	358	366	350	429	546	534	554	1591	930	1726

Table S5.8. Polychlorinated biphenyl (PCB), hexachlorobenzene (HCB), pentachlorobenzene (PeCB), 4,4'-dichlorodiphenyldichloroethylene (4,4'-DDE), polycyclic aromatic hydrocarbon (PAH), and organophosphate ester (OPE) concentrations (pg L⁻¹) reported in the literature, measured in the freely dissolved phase of water by means of LDPE passive water sampling. Literature values were either directly reported by the referenced study or calculated from data provided in their respective supplementary materials.

Region	Site	ΣPCB			HCB, PeCB			4,4'-DDE			ΣPAH			ΣOPE			References
		n	Range	Average	n	Range	Average	n	Range	Average	n	Range	Average	n	Range	Average	
Catalonia, Spain	Pyrenees, NP ^a , remote high mountain	Lake	7	1.2-2.2	1.7	HCB 1.0-1.4	6.4	BDL ^b -0.65	0.17	16 ^c	35-254	150	5 ^c	139-2849	978	This study	
						PeCB 0.50-4.5	2.3			17	35-920	282					
	Estanh Redon, remote high mountain	Lake	7	-	1.7	HCB 1.5-1.1	6.5	BDL-0.51	0.26	17	35-184	122	5 ^c	218-2849	1284		
						PeCB 0.59-4.1	2.3										
Catalonia, Spain	Estanh Redon, remote high mountain	Lake	7	9.0-10.7 ^b	9.9 ^c	HCB 1.9-2.3	7.3	5.4-12	6.9							Vilanova et al., 2001b, 2001a	
Catalonia, Spain	Estanh Redon, remote high mountain	Lake								22	-	270				Vilanova et al., 2001c	
Catalonia, Spain	Estanh Redon, remote high mountain	Lake	13	28-58	44	HCB 3.3-8.8	6.0	2.2-8.8	6.8	26	344-962	678				Fernández et al., 2005	
			7	16-36	26												
California, USA	Palos Verdes Peninsula, wastewater	Ocean	43	50-316	164			37-2200	1271							Fernandez et al., 2012	
			7	7.2-121	52			3.1-24	13							Fernandez et al., 2014	
			13	108-457	268												
			7	86-331	199												
Great Lakes	Lake Ontario, Lake Erie	Lake				HCB 3.7-2.3	9.3-11	3.6-57	11-19							Khairy et al., 2014	
Great Lakes	Lake Ontario, Lake Erie	Lake								18	2380-3.0E4	2700-1.3E4				McDonough et al., 2014	
Oregon, USA	Willamette river, Portland Harbor	River								34	3.8E6-2.0E7	1.0E7				Paulik et al., 2016	
Great Lakes	Lake Ontario, Lake Erie	Lake	29	1.5-105	31-34											Liu et al., 2016	
			7	1.7-44	13-14												
Brazil	Serra do Mar and Serra Geral, NPs	Wetland				HCB 1.2-2.3	1.6-2.2	0.12-0.24	0.16-0.21							Meire et al., 2016	
Atlantic	North and Tropical Atlantic, deep mooring	Ocean	7	0.2-1.3	0.63-9.1	HCB 2.7-1.4	7.9-8.3	0.26-1.3	0.55-4.4	6	10-254	80-142				Sun et al., 2016	
Antarctica	Larsemann Hills, ice-free freshwater	Lake								17	1.4E4-3.6E5	2.1E5				Yao et al., 2016	

Table S5.8 (continued)

Region	Site	ΣPCB			HCB, PeCB			4,4'-DDE			ΣPAH			ΣOPE			References
		Samples	n	Average	n	Range	Average	Range	Average	n	Range	Average	n	Range	Average		
Plymouth, UK	Sutton harbor marina	Ocean								10	-	1.60E+04	7	-	1.0E5	Aminot et al., 2017	
Seattle, USA	Lower Duwamish Waterway, contamin.	River	27	106-960	318											Apell and Gschwend, 2017	
Bosnia and Herzegovina	Bosna and Neretva rivers, industrialized	River	7	BDL-0.24	0.12	HCB	6.0-27	8.8-11	BDL-23	13-14	19	526-5.8E4	2535-2.6E4			Harman et al., 2018	
Arctic	Canadian Arctic, surface waters	Lake				PeCBBDL-18	BDL-6.0									McDonough et al., 2018	
	Fran Strait, deep mooring	Ocean															
Puerto Rico	Jobsos and Guánica bays, Condado lagoon and Laguna Grande	Ocean	7	BDL-2101	1221											Rodriguez-Sierra et al., 2019	
			29	BDL-4000	2370												
Great Lakes	Lake Ontario, Toronto area	Lake	73	3.8-4121	542											Zhang et al., 2020	
			6	BDL-835	112												
Great Lakes Erie	Lake Ontario, Lake Erie	Lake															
			9	2600-6.4E5	1.9E5											Ma et al., 2021	
			5	2400-6.3E5	1.8E5												

^a National Park; ^b Below detection limit; ^c Outliers not included; ^d XAD-2 active water sampling; ^e Outliers removed.

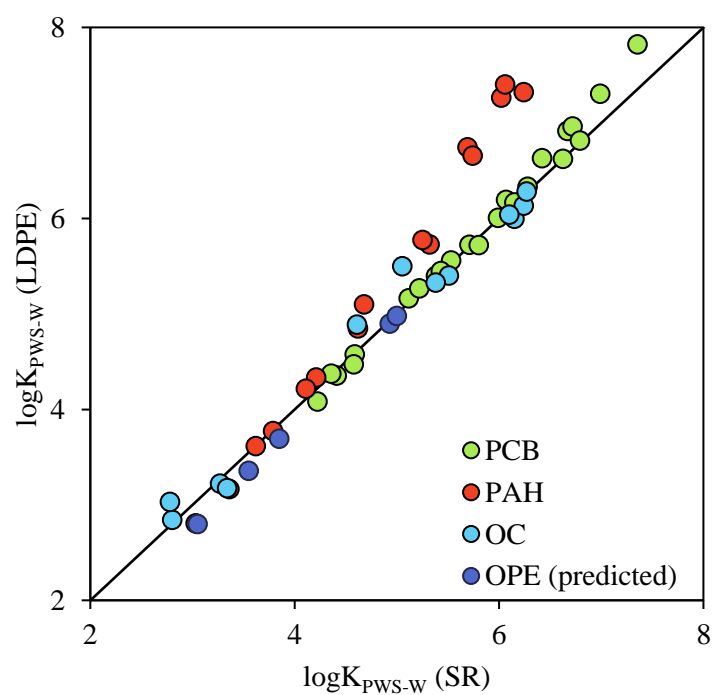


Figure S5.1. Polymer–water partition coefficients (K_{pws-w}) of semi-volatile organic compounds reported in the literature for silicone rubber (SR) (Smedes, 2018a) and low-density polyethylene (LDPE) (Smedes et al., 2009). K_{pws-w} for organophosphate esters (OPE) were predicted from published SR values through a LDPE–SR regression ($n = 24$, $R^2 = 0.991$, $SE = 0.10$, prediction error < 3%).

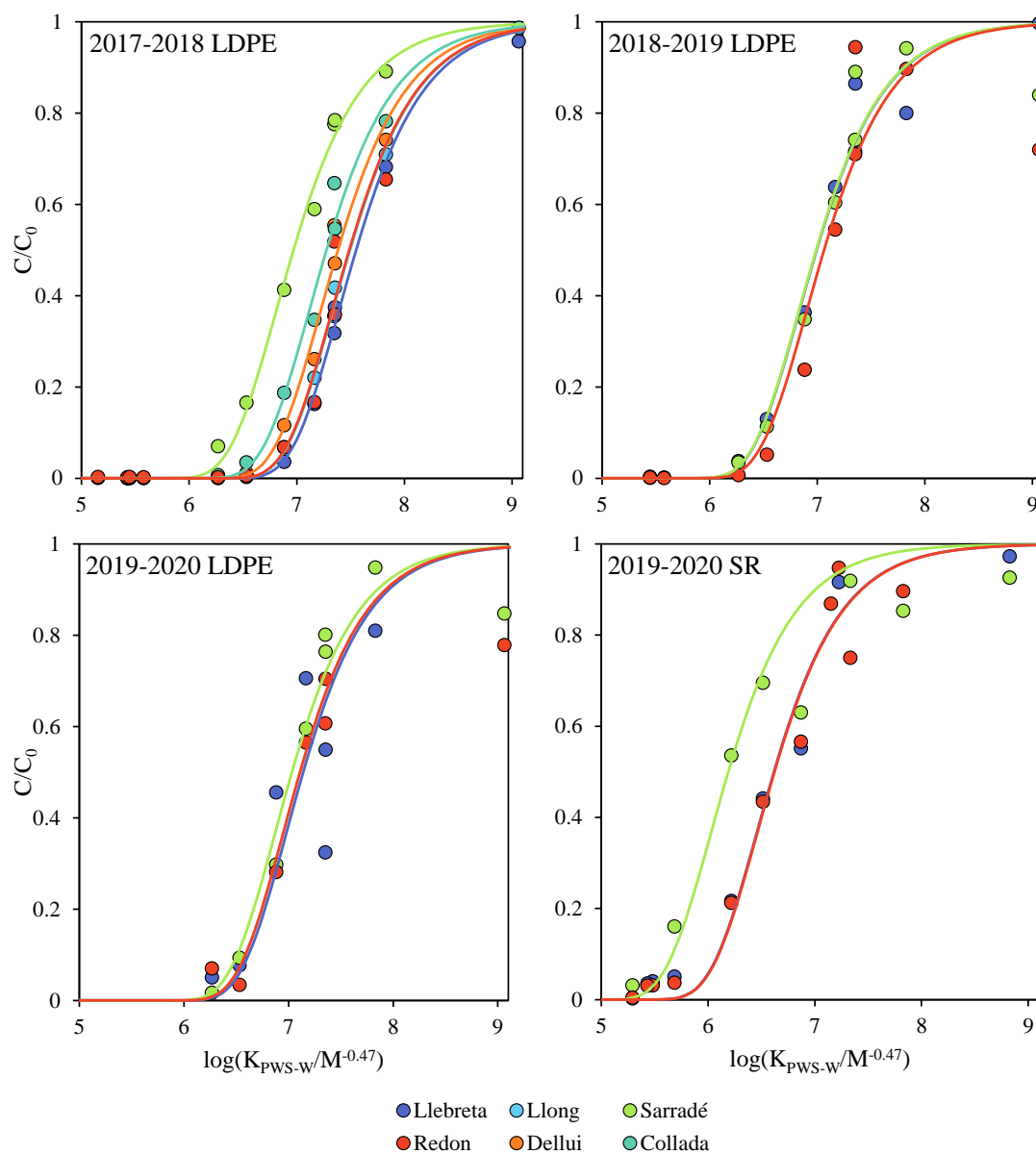


Figure S5.2. Fraction of Performance Reference Compound (PRC) retained in the samplers after exposure (C/C_0) as a function of its molar mass-normalized partition coefficient ($K_{PWS-W}/M^{-0.47}$). The curved lines represent the best unweighted nonlinear least-squares fit for each site.

References S5

- Aminot, Y., Belles, A., Alary, C., Readman, J.W., 2017. Near-surface distribution of pollutants in coastal waters as assessed by novel polyethylene passive samplers. *Mar. Pollut. Bull.* 119, 92–101. <https://doi.org/10.1016/J.MARPOLBUL.2017.03.022>
- Apell, J.N., Gschwend, P.M., 2017. The atmosphere as a source/sink of polychlorinated biphenyls to/from the Lower Duwamish Waterway Superfund site. *Environ. Pollut.* 227, 263–270. <https://doi.org/10.1016/J.ENVPOL.2017.04.070>
- Beyer, A., Wania, F., Gouin, T., Mackay, D., Matthies, M., 2003. Temperature dependence of the characteristic travel distance. *Environ. Sci. Technol.* 37, 766–771. <https://doi.org/10.1021/es025717w>
- Blanchard, P., Hulting, M.L., Brice, K.A., Backus, S.M., Dryfhout-Clark, H., Hites, R.A., 2008. Atmospheric deposition of toxic substances to the Great Lakes: IADN results through 2005, EPA-905-R-08-001. US EPA and Environment Canada.
- Brubaker, W.W., Hites, R.A., 1998. OH reaction kinetics of gas-phase α - and γ -hexachlorocyclohexane and hexachlorobenzene. *Environ. Sci. Technol.* 32, 766–769. <https://doi.org/10.1021/es970650b>
- Deacon, E.L., 1977. Gas transfer to and across an air-water interface. *Tellus* 29, 363–374. <https://doi.org/10.3402/tellusa.v29i4.11368>
- Fairall, C.W., Bradley, E.F., Hare, J.E., Grachev, A.A., Edson, J.B., 2003. Bulk Parameterization of Air–Sea Fluxes: Updates and Verification for the COARE Algorithm. *J. Clim.* 16, 571–591. [https://doi.org/10.1175/1520-0442\(2003\)016<0571:BPOASF>2.0.CO;2](https://doi.org/10.1175/1520-0442(2003)016<0571:BPOASF>2.0.CO;2)
- Fairall, C.W., Bradley, E.F., Rogers, D.P., Edson, J.B., Young, G.S., 1996. Bulk parameterization of air-sea fluxes for Tropical Ocean-Global Atmosphere Coupled-Ocean Atmosphere Response Experiment. *J. Geophys. Res. Ocean.* 101, 3747–3764. <https://doi.org/10.1029/95JC03205>
- Fairall, C.W., Yang, M., Bariteau, L., Edson, J.B., Helmig, D., McGillis, W., Pezoa, S., Hare, J.E., Huebert, B., Blomquist, B., 2011. Implementation of the Coupled Ocean-Atmosphere Response Experiment flux algorithm with CO₂, dimethyl sulfide, and O₃. *J. Geophys. Res. Ocean.* 116, 0–09. <https://doi.org/10.1029/2010JC006884>
- Fernandez, L.A., Lao, W., Maruya, K.A., Burgess, R.M., 2014. Calculating the diffusive flux of persistent organic pollutants between sediments and the water column on the palos verdes shelf superfund site using polymeric passive samplers. *Environ. Sci. Technol.* 48, 3925–3934. <https://doi.org/10.1021/es404475c>
- Fernandez, L.A., Lao, W., Maruya, K.A., White, C., Burgess, R.M., 2012. Passive sampling to measure baseline dissolved persistent organic pollutant concentrations in the water column of the Palos Verdes shelf superfund site. *Environ. Sci. Technol.* 46, 11937–11947. <https://doi.org/10.1021/es302139y>
- Fernández, P., Carrera, G., Grimalt, J.O., 2005. Persistent organic pollutants in remote freshwater ecosystems. *Aquat. Sci.* 2005 673 67, 263–273. <https://doi.org/10.1007/S00027-005-0747-8>

- Fernandez, P., van Drooge, B.L., Arellano, L., Grimalt, J.O., 2021. Atmospheric deposition of semivolatile organic pollutants in European high mountains: Sources, settling and chemical degradation. *Sci. Total Environ.* 784, 147099. <https://doi.org/10.1016/j.scitotenv.2021.147099>
- Fuller, E.N., Schettler, P.D., Giddings, J.C., 1966. A new method for prediction of binary gas-phase diffusion coefficients. *Ind. Eng. Chem.* 58, 18–27. <https://doi.org/10.1021/ie50677a007>
- Gioia, R., Jones, K.C., Lohmann, R., Nizzetto, L., Dachs, J., 2010. Field-derived Henry's law constants for polychlorinated biphenyls in oceanic waters. *J. Geophys. Res. Ocean.* 115, 5024. <https://doi.org/10.1029/2008JC005054>
- Harman, C., Grung, M., Djedjibegovic, J., Marjanovic, A., Fjeld, E., Braaten, H.F.V., Sober, M., Larssen, T., Ranneklev, S.B., 2018. The organic pollutant status of rivers in Bosnia and Herzegovina as determined by a combination of active and passive sampling methods. *Environ. Monit. Assess.* 190, 1–10. <https://doi.org/10.1007/s10661-018-6667-6>
- Hayduk, W., Laudie, H., 1974. Prediction of diffusion coefficients for nonelectrolytes in dilute aqueous solutions. *AIChE J.* 20, 611–615. <https://doi.org/10.1002/aic.690200329>
- Hoff, R.M., 1994. An Error Budget for the Determination of the Atmospheric Mass Loading of Toxic Chemicals in the Great Lakes. *J. Great Lakes Res.* 20, 229–239. [https://doi.org/10.1016/S0380-1330\(94\)71143-6](https://doi.org/10.1016/S0380-1330(94)71143-6)
- Hulscher, T.E.M. Ten, Van Der Velde, L.E., Bruggeman, W.A., 1992. Temperature dependence of Henry's law constants for selected chlorobenzenes, polychlorinated biphenyls and polycyclic aromatic hydrocarbons. *Environ. Toxicol. Chem.* 11, 1595–1603. <https://doi.org/10.1002/etc.5620111109>
- Johnson, M.T., 2010. A numerical scheme to calculate temperature and salinity dependent air-water transfer velocities for any gas. *Ocean Sci.* 6, 913–932. <https://doi.org/10.5194/os-6-913-2010>
- Keyte, I.J., Harrison, R.M., Lammel, G., 2013. Chemical reactivity and long-range transport potential of polycyclic aromatic hydrocarbons—a review. *Chem. Soc. Rev.* 42, 9333–9391. <https://doi.org/10.1039/c3cs60147a>
- Khairy, M., Muir, D., Teixeira, C., Lohmann, R., 2014. Spatial trends, sources, and air-water exchange of organochlorine pesticides in the Great Lakes basin using low density polyethylene passive samplers. *Environ. Sci. Technol.* 48, 9315–9324. <https://doi.org/10.1021/es501686a>
- Klaus, M., Vachon, D., 2020. Challenges of predicting gas transfer velocity from wind measurements over global lakes. *Aquat. Sci.* 82, 53. <https://doi.org/10.1007/s00027-020-00729-9>
- Kwok, E.S.C., Atkinson, R., Arey, J., 2002. Rate Constants for the Gas-Phase Reactions of the OH Radical with Dichlorobiphenyls, 1-Chlorodibenzo-p-dioxin, 1,2-Dimethoxybenzene, and Diphenyl Ether: Estimation of OH Radical Reaction Rate Constants for PCBs, PCDDs, and PCDFs. *Environ. Sci. Technol.* 29, 1591–1598. <https://doi.org/10.1021/ES00006A024>
- Liu, Y., Wang, S., McDonough, C.A., Khairy, M., Muir, D.C.G., Helm, P.A., Lohmann, R., 2016. Gaseous and Freely-Dissolved PCBs in the Lower Great Lakes Based on Passive Sampling: Spatial Trends and Air-Water Exchange. *Environ. Sci. Technol.* 50, 4932–4939. <https://doi.org/10.1021/acs.est.5b04586>

- Luarte, T., Tucca, F., Nimptsch, J., Woelfl, S., Casas, G., Dachs, J., Chiang, G., Pozo, K., Barra, R., Galbán-Malagón, C., 2022. Occurrence and air-water diffusive exchange legacy persistent organic pollutants in an oligotrophic north Patagonian lake. *Environ. Res.* 204, 112042. <https://doi.org/10.1016/J.ENVRES.2021.112042>
- Ma, Y., Vojta, S., Becanova, J., Habtemichael, A.Z., Adelman, D.A., Muir, D., Lohmann, R., 2021. Spatial distribution and air-water exchange of organophosphate esters in the lower Great Lakes. *Environ. Pollut.* 286, 117349. <https://doi.org/10.1016/j.envpol.2021.117349>
- Mackay, D., Yeun, A.T.K., 1983. Mass Transfer Coefficient Correlations for Volatilization of Organic Solutes from Water. *Environ. Sci. Technol.* 17, 211–217. <https://doi.org/10.1021/es00110a006>
- McDonough, C.A., De Silva, A.O., Sun, C., Cabrerizo, A., Adelman, D., Soltwedel, T., Bauerfeind, E., Muir, D.C.G., Lohmann, R., 2018. Dissolved Organophosphate Esters and Polybrominated Diphenyl Ethers in Remote Marine Environments: Arctic Surface Water Distributions and Net Transport through Fram Strait. *Environ. Sci. Technol.* 52, 6208–6216. <https://doi.org/10.1021/acs.est.8b01127>
- McDonough, C.A., Khairy, M.A., Muir, D.C.G., Lohmann, R., 2014. Significance of population centers as sources of gaseous and dissolved PAHs in the lower Great Lakes. *Environ. Sci. Technol.* 48, 7789–7797. <https://doi.org/10.1021/es501074r>
- Meire, R.O., Khairy, M., Targino, A.C., Galvão, P.M.A., Torres, J.P.M., Malm, O., Lohmann, R., 2016. Use of passive samplers to detect organochlorine pesticides in air and water at wetland mountain region sites (S-SE Brazil). *Chemosphere* 144, 2175–2182. <https://doi.org/10.1016/j.chemosphere.2015.10.133>
- Nizzetto, L., Lohmann, R., Gioia, R., Jahnke, A., Temme, C., Dachs, J., Herckes, P., Di Guardo, A., Jones, K.C., 2008. PAHs in air and seawater along a North-South Atlantic transect: Trends, processes and possible sources. *Environ. Sci. Technol.* 42, 1580–1585. <https://doi.org/10.1021/es0717414>
- Othmer, D.F., Thakar, M.S., 1953. Correlating Diffusion Coefficient in Liquids. *Ind. Eng. Chem.* 45, 589–593. <https://doi.org/10.1021/ie50519a036>
- Paulik, L.B., Smith, B.W., Bergmann, A.J., Sower, G.J., Forsberg, N.D., Teeguarden, J.G., Anderson, K.A., 2016. Passive samplers accurately predict PAH levels in resident crayfish. *Sci. Total Environ.* 544, 782–791. <https://doi.org/10.1016/j.scitotenv.2015.11.142>
- Prats, R.M., van Drooge, B.L., Fernández, P., Grimalt, J.O., 2022a. Changes and distribution of gas-phase polycyclic aromatic hydrocarbons and organochlorine compounds in a high-mountain gradient over a three-year period (Pyrenees, 2017–2020). *Sci. Total Environ.* 829, 154602. <https://doi.org/10.1016/J.SCITOTENV.2022.154602>
- Prats, R.M., van Drooge, B.L., Fernández, P., Grimalt, J.O., 2022b. Occurrence and temperature dependence of atmospheric gas-phase organophosphate esters in high-mountain areas (Pyrenees). *Chemosphere* 292, 133467. <https://doi.org/10.1016/J.CHEMOSPHERE.2021.133467>
- Rodríguez-Sierra, C.J., Adelman, D., Vojta, Š., Mansilla-Rivera, I., Lohmann, R., 2019. Passive Sampling of Persistent Organic Pollutants in Four Coastal Aquatic Systems of Puerto Rico: A Pilot Study. *Bull. Environ. Contam. Toxicol.* 103, 770–775. <https://doi.org/10.1007/s00128-019-02731-w>

- Rowe, M.D., Perlinger, J.A., 2012. Micrometeorological measurement of hexachlorobenzene and polychlorinated biphenyl compound air-water gas exchange in Lake Superior and comparison to model predictions. *Atmos. Chem. Phys.* 12, 4607–4617. <https://doi.org/10.5194/acp-12-4607-2012>
- Rusina, T.P., Smedes, F., Brborić, M., Vrana, B., 2019. Investigating levels of organic contaminants in Danube River sediments in Serbia by multi-ratio equilibrium passive sampling. *Sci. Total Environ.* 696, 1–10. <https://doi.org/10.1016/j.scitotenv.2019.133935>
- Schwarzenbach, R.P., Gschwend, P.M., Imboden, D.M., 2016. *Environmental Organic Chemistry*, 3rd Edition. John Wiley & Sons, Ltd.
- Schwarzenbach, R.P., Gschwend, P.M., Imboden, D.M., 2005. *Environmental Organic Chemistry*, 2nd Edition. John Wiley & Sons, Ltd.
- Smedes, F., 2018a. Silicone–water partition coefficients determined by cosolvent method for chlorinated pesticides, musks, organo phosphates, phthalates and more. *Chemosphere* 210, 662–671. <https://doi.org/10.1016/j.chemosphere.2018.07.054>
- Smedes, F., 2018b. Corrigendum to “Silicone–water partition coefficients determined by cosolvent method for chlorinated pesticides, musks, organo phosphates, phthalates and more” [*Chemosphere* 210 (2018) 662–671]. *Chemosphere* 212, 1180. <https://doi.org/10.1016/j.chemosphere.2018.09.094>
- Smedes, F., Geertsma, R.W., Van Der Zande, T., Booij, K., 2009. Polymer-water partition coefficients of hydrophobic compounds for passive sampling: Application of cosolvent models for validation. *Environ. Sci. Technol.* 43, 7047–7054. <https://doi.org/10.1021/es9009376>
- Spivakovsky, C.M., Logan, J.A., Montzka, S.A., Balkanski, Y.J., Foreman-Fowler, M., Jones, D.B.A., Horowitz, L.W., Fusco, A.C., Brenninkmeijer, C.A.M., Prather, M.J., Wofsy, S.C., McElroy, M.B., 2000. Three-dimensional climatological distribution of tropospheric OH: Update and evaluation. *J. Geophys. Res. Atmos.* 105, 8931–8980. <https://doi.org/10.1029/1999JD901006>
- Sun, C., Soltwedel, T., Bauerfeind, E., Adelman, D.A., Lohmann, R., 2016. Depth Profiles of Persistent Organic Pollutants in the North and Tropical Atlantic Ocean. *Environ. Sci. Technol.* 50, 6172–6179. <https://doi.org/10.1021/acs.est.5b05891>
- Vilanova, R.M., Fernández, P., Grimalt, J.O., 2001a. Polychlorinated biphenyl partitioning in the waters of a remote mountain lake. *Sci. Total Environ.* 279, 51–62. [https://doi.org/10.1016/S0048-9697\(01\)00725-2](https://doi.org/10.1016/S0048-9697(01)00725-2)
- Vilanova, R.M., Fernández, P., Martínez, C., Grimalt, J.O., 2001b. Organochlorine Pollutants in Remote Mountain Lake Waters. *J. Environ. Qual.* 30, 1286–1295. <https://doi.org/10.2134/jeq2001.3041286x>
- Vilanova, R.M., Fernández, P., Martínez, C., Grimalt, J.O., 2001c. Polycyclic aromatic hydrocarbons in remote mountain lake waters. *Water Res.* 35, 3916–3926. [https://doi.org/10.1016/S0043-1354\(01\)00113-0](https://doi.org/10.1016/S0043-1354(01)00113-0)
- Williams, A.J., Grulke, C.M., Edwards, J., McEachran, A.D., Mansouri, K., Baker, N.C., Patlewicz, G., Shah, I., Wambaugh, J.F., Judson, R.S., Richard, A.M., 2017. The CompTox Chemistry Dashboard: A community data resource for environmental chemistry. *J. Cheminform.* 9, 61. <https://doi.org/10.1186/s13321-017-0247-6>

- Yao, Y., Meng, X.Z., Wu, C.C., Bao, L.J., Wang, F., Wu, F.C., Zeng, E.Y., 2016. Tracking human footprints in Antarctica through passive sampling of polycyclic aromatic hydrocarbons in inland lakes. *Environ. Pollut.* 213, 412–419. <https://doi.org/10.1016/J.ENVPOL.2016.02.035>
- Zhang, X., Robson, M., Jobst, K., Pena-Abaurrea, M., Muscalu, A., Chaudhuri, S., Marvin, C., Brindle, I.D., Reiner, E.J., Helm, P., 2020. Halogenated organic contaminants of concern in urban-influenced waters of Lake Ontario, Canada: Passive sampling with targeted and non-targeted screening. *Environ. Pollut.* 264, 114733. <https://doi.org/10.1016/j.envpol.2020.114733>

3.4 Discussion

3.4.1 Performance and uncertainty of passive air and water sampling

a. Uncertainty of PRC-derived sampling rates and accuracy of concentrations

Passive samplers for monitoring organic pollutants have grown in popularity in recent decades and have seen worldwide application as new materials become available and their interaction with environmental matrices and chemicals becomes better understood. Remote and inaccessible locations have long been a subject of interest regarding their potential for accumulating pollutants, and passive samplers found an ideal niche in them due to their independence of energy sources, the possibility of integrating pollutant concentrations over extended periods, and the simplicity and cost-effectiveness of sampling operations. Still, passive samplers are not without their shortcomings, the main one being the need for estimating effective sampled volumes and the uncertainty associated with these indirect estimations. For PRC-calibrated passive samplers, this uncertainty arises in part from not using isotopically labelled counterparts to each studied pollutant (an optimal but ultimately unfeasible strategy) and from the assumption of PRC dissipation rates being truly equal to uptake rates (generally true in the long run and for most studied compounds, but perhaps biased for some chemicals with slow equilibrating dynamics under specific circumstances) (Liu et al., 2013).

Despite this uncertainty, PRCs are still preferable to any other sampling estimation method like parallel active sampling measurements (Chaemfa et al., 2009a; Klánová et al., 2008; Mari et al., 2008b), experimental determinations of the extent of the linear uptake phases (Abdollahi et al., 2017; Evci et al., 2016; Heo and Lee, 2014), or directly assuming an average rate (Cheng et al., 2013; Jaward et al., 2005b; Zhang et al., 2008). The main reason for this is the ability of PRCs to reflect differences between individual samples which could be due to meteorological variation, sampler orientation, biofouling, etc. This need for a sampler-specific calibration is of foremost importance in alpine regions, as conditions may vary widely with time and between sites regardless of their closeness to each other. An example of this was recorded during the passive air sampling period PAS II. Between the end of February and the beginning of May 2018, the samplers at some sites became covered under more than two meters of snow. This

period is easily identifiable in Figure 35 at Estany de Dellui from the humidity and temperature registered by the data loggers: they remained constant at 100% and 0 °C, respectively, compared to those at Estany de Llebrete, which did not. During this period, the enclosing of the samplers prevented the renewal of air inside the housings, and thus the absorption of atmospheric pollutants. This limiting circumstance was however accounted for in the calculation of sampling rates because PRCs would not have been released from the sampler to the same extent, resulting in reduced rates.

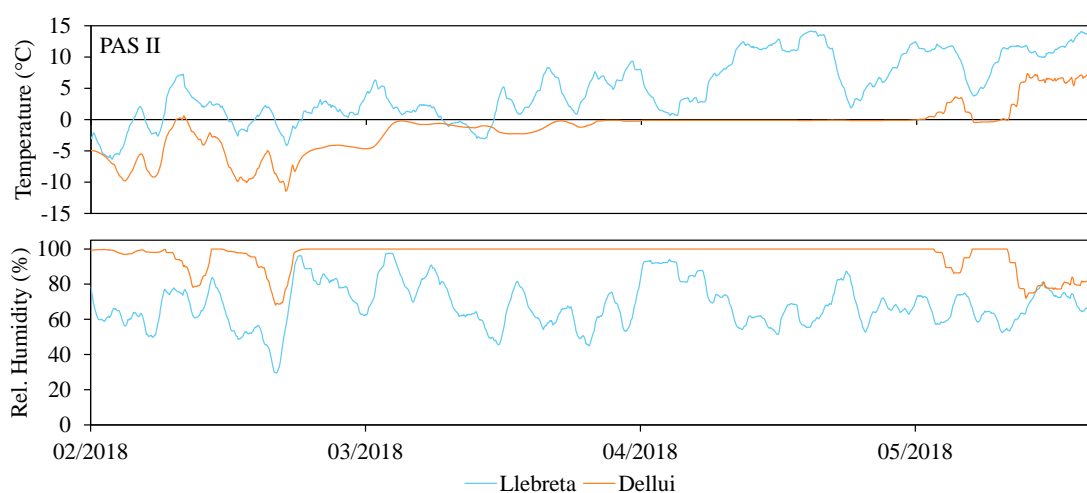


Figure 35. Moving average (48 h) of air temperature (top) and relative humidity (bottom) measured every 30 min during a portion of passive air sampling period PAS II at Estany de Llebrete and Estany de Dellui. Figure created using data collected with data loggers.

One of the main aims of the present work has been to estimate the performance of PRC-calibrated passive samplers employed in circumstances outside of their typical range of application (i.e., in a high-altitude environment with harsh meteorological conditions). This includes comparing the experimental variation of PRC-derived sampling rates between replicates to their expected theoretical uncertainties. ARTICLE 1, ARTICLE 3, and ARTICLE 4 show that the expected relative expanded uncertainties of air sampling rates were between 5.4 and 34% of the reported values. On the other hand, experimental relative standard deviations were between 1.5 and 33%, closely agreeing with the range of expected variation, which means that experimental sources of error were effectively mitigated or accounted for. This is a satisfactory result considering that intercomparison studies have shown that uncertainties in passive air sampling can be substantial (Melymuk et al., 2021). ARTICLE 1 shows that the unavoidable sources of error stem mainly from uncertainty in K_{OA} values of the PRCs (68%) and $C_{PRC,i}/C_{PRC,0}$ ratios (32%). In water, ARTICLE 5 shows that the estimated relative standard errors from the PRC calibration

were between 2.1 and 25% for LDPE samplers and between 15 and 33% for SR samplers, which is a very similar range compared to air samplers. Passive water sampling uncertainties were not compared to theoretical ones since they do not result from experimental replicates (the individual sampler sheets were pooled) and because the uncertainty in passive water sampling calibration has been well studied through the NLS adjustment of PRC retained fractions.

The concentrations of SVOCs in air determined using the PUF-PAS samplers at Estanh Redon were compared to concentrations obtained with a high-volume active air sampler (AAS) in ARTICLE 1 in order to assess the accuracy of the measurements. There was some variation in concentrations between AAS samples, probably due to the seasonal behaviour of some compounds and to the different origins of air mass trajectories at the times of sampling, as noted in Section 3.2.2. This reflects the different kind of information that passive samplers provide, an average over a sampling period instead of a picture of a specific moment, which can be useful in many contexts, but that is much more sensitive to environmental circumstances. The concentrations that both methods provided adequately correlated to each other with good figures of merit. Total PCB concentrations were the same between PAS and AAS, HCB and PeCB concentrations agreed with differences lower than 20%, as did total OPEs with differences of around 30%. AAS concentrations of total PAHs were approximately two to three times higher than those from PAS measurements, which was attributed to the marked seasonal changes that PAHs experience in rural and alpine areas due to wildfires in the summer and increased wood combustion in winter. Still, an agreement of a factor of two to three is still regarded as acceptable in similar studies (Gouin et al., 2005; He and Balasubramanian, 2010; Kalina et al., 2019). In addition to these comparisons, the effectiveness of the passive air sampler housings as wind and atmospheric particle shields was confirmed by low particle infiltration efficiencies of around 20% compared to the particle filter fractions of AAS samples, a much lower value than that of other sampler designs (Markovic et al., 2015). This means that the SVOC concentrations can confidently be considered as predominantly pertaining to the atmospheric gas-phase, which is important for the study of subsequent air–water exchange processes in ARTICLE 5, as it is only concerned with chemicals in the vapour and dissolved phases.

Regarding water samplers, no comparisons of passive sampling measurements were made with active measurements. Water pumps and instrumentation for on-site processing were unavailable, and even if they were available, the cost of transport, fuel, and operations would have been very high. Additionally, the low pollutant levels in these high-elevation lakes would have required considerably large amounts of water to be grab-sampled, transported, and processed to overcome the limits of quantification. It is in situations like these where passive water sampling makes the best use of its capabilities for accumulating pollutants over time. What was done and described in ARTICLE 5 is an assessment of reproducibility by comparison with samplers co-deployed at Estanh Redon that were independently extracted and analysed at Masaryk University's RECETOX research centre in Brno (Czech Republic). Pollutant levels determined with LDPE-PWS samplers were within a factor of four of each other with very few outliers. While the uncertainty in these results cannot be ignored, these factors are reasonable at such low concentrations compared to other more accessible and typically more polluted water bodies. The agreement between SR-PWS measurements was similar except for OPEs, which we found at concentrations up to 30 times higher than at RECETOX. Discrepancies in OPE concentrations were also observed between polymers in results from RECETOX and from our measurements, where SR samplers often yielded greater OPE levels. These disagreements with OPE concentrations could originate from the higher hydrophilicity of OPEs and a more challenging determination of their partitioning coefficients between water and polymer. As the partitioning behaviour of these compounds has been less studied than for legacy POPs and as they are not typically monitored using these passive sampler media, future research should focus on determining whether the effective assessment of OPEs can be accomplished using these sampler materials, particularly in low-concentration waters like alpine lakes.

b. NLS regression of PRC data for passive air sampling calibration

An additional consideration must be made regarding the PRC calibration of passive samplers. As seen in Section 3.1.3.1 (Figure 11) and in ARTICLE 5, the calibration of passive water samplers was performed using an NLS fit of the PRC depletion ratios after exposure of the samplers. An unweighted NLS model fits Eq. 17 to the $C_{PRC,t}/C_{PRC,0}$ ratios with B as an adjustable parameter. This method is well established and widely used

in passive water sampling studies as recommended by Booij and Smedes (2010). The main advantages of an NLS fit are the inclusion of the information contained in all PRC retained fractions into the calculation, thus producing potentially less biased sampling rates and a more robust way of determining the uncertainty in the results by calculating the curve fit error. However, this calibration strategy is generally not used in passive air sampling. As seen in Section 3.1.3.1 (Figure 10) and applied in ARTICLE 1 to ARTICLE 4, PRCs that are retained either too much or not enough are discarded for the calculation of sampling rates. While this still produces adequate rates and concentrations that are accurate enough as discussed above, one could ask why the NLS approach cannot be applied to passive air sampling as it may mitigate the possible underestimation of the uncertainty that often results from the current PRC selection approach.

Thus, it is argued that using an NLS calibration strategy for passive air sampling could be of benefit. More exhaustive studies would be required for assessing the performance of applying this method to PUF samplers or to determine a more adequate number of PRCs to be used. Still, the adjustment of a curve to $C_{PRC,t}/C_{PRC,0}$ ratios is straightforward. Eq. 12 for passive air sampling is adjusted to adopt a shape analogous to that of Eq. 17 for passive water sampling:

$$\frac{C_{PRC,t}}{C_{PRC,0}} = \exp\left(-\frac{k_A t}{K'_{PUF-A} D_{film}}\right) \quad \text{Eq. 32}$$

K'_{PUF-A} values are calculated for each PRC at the average air temperature of the sampling period, and k_A is set as the adjustable parameter of the regression. This was tested with an example PUF replicate sample (Estany de Dellui, PAS I) as shown in Figure 36 compared to the calibration of a passive water sample (Estany de Llebreta, PWS I). These regressions were performed using the *minpack.lm* package for R 4.2.1 (R Core Team, 2022) instead of the calculation template¹⁵ used in ARTICLE 5, but the results were exactly the same. For reference, the calibration of this specific water sample in the R software yielded an R_S of 21.0 L d⁻¹ and an error (sR_S) of 0.53 L d⁻¹ (2.5%), just as reported in ARTICLE 5. When applied to the passive air sample, the regression yielded an adjusted value of k_A of 93.5 m d⁻¹, resulting in an R_S of 3.45 m³ d⁻¹ and an sR_S of 0.17 m³ d⁻¹ (4.8%). The average sampling rate of the same sample replicate obtained from the

¹⁵ www.passivesampling.net/rs/rs_v3a.xls (Accessed July 2022)

non-discarded PRCs (^{13}C -PCBs 9, 15, and 32) was $3.37 \text{ m}^3 \text{ d}^{-1}$ with a standard deviation of $0.07 \text{ m}^3 \text{ d}^{-1}$ (2.2%). The difference in resulting R_S in this case was small (less than $0.1 \text{ m}^3 \text{ d}^{-1}$), but it should be noted that this was possibly a best-case scenario where all PRC retained fractions adjusted well to the curve. Other calibrations with less ideal behaviour of PRC retained fractions may produce varied results, although they would still benefit of accounting for all the information stored in PRC data. Moreover, the error estimated from the NLS adjustment is arguably more representative of the true uncertainty in the determination of sampling rates as it arises from the deviations from the ideal behaviour of all PRC retained fractions, not just a few selected ones. In fact, the bottom-right chart in Figure 36 shows that the discarded PRCs (from left to right, the first, fifth, and sixth data points) presented the largest deviations from the calculated fit, leading to an underestimation of uncertainty. In conclusion, this brief test of NLS regressions applied to passive air samplers suggests an effective and pragmatic approach to their PRC calibration that could limit systematic error and provide a better account of uncertainties. Thus, we suggest a more thorough exploration of the performance of NLS regressions in future studies with the aim of harmonizing the methodologies employed in passive air and water sampling.

c. Polymer–water partition coefficients and limitations of passive samplers

PUF samplers are a useful tool for the reliable assessment of atmospheric gas-phase concentrations of relatively nonpolar pollutants that reach high-altitude alpine areas. However, some SVOCs susceptible to long-range atmospheric transport may present physical-chemical properties at the limit of the optimal range for this sampler material. This range is defined in terms of sampler–air partition coefficients, K_{PUF-A} . For the more volatile compounds ($K_{OA} < 7$, e.g., PeCB and the lightest PAHs like Fle and Ace), K_{PUF-A} is a critical term as they tend to reach equilibrium between air and PUF very quickly, and thus the calculation of their concentrations relies mostly on the value of the partitioning coefficient. As a result, small variations in the determination of in-sampler amounts of these compounds can lead to augmented error in their calculated concentrations. For the less volatile chemicals ($K_{OA} > 7$), having an accurate estimation of K_{PUF-A} is less important as they will likely remain in the linear uptake phase which is R_S -controlled. In our experience, unrealistically high or anomalous concentrations started

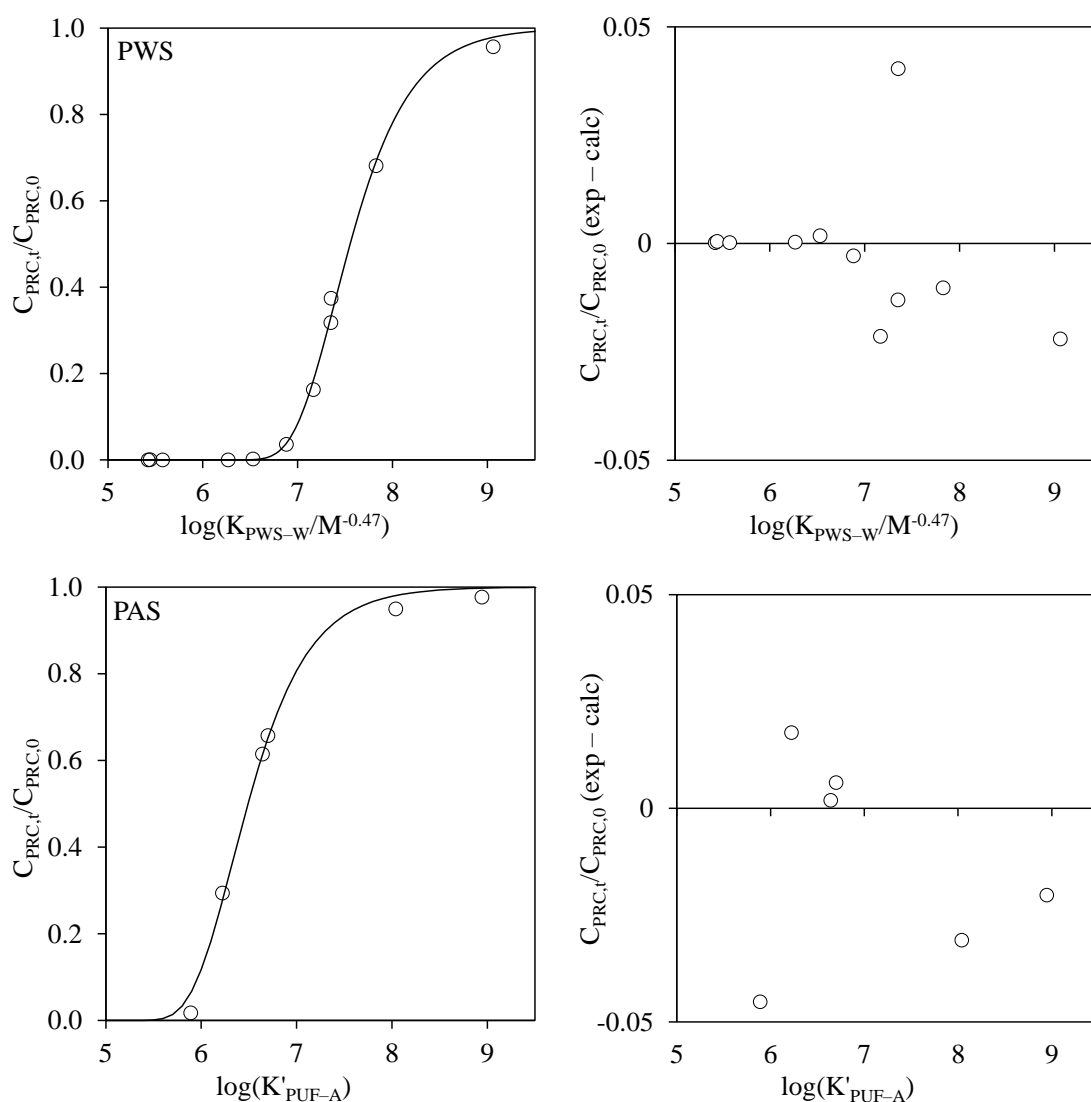


Figure 36. Example NLS regressions of PRC retained fractions in passive water sampling (PWS, top) and passive air sampling (PAS, bottom). The difference between experimental and calculated retained fractions is shown in the charts to the right.

to appear for compounds with $\log K'_{PUF-A}$ (25 °C) lower than 5, or $\log K_{OA}$ below 6. For this reason, we did not report concentrations of some compounds like naphthalene and acenaphthylene despite having detected them in some samples. OPEs like triethyl phosphate and tripropyl phosphate also suffered from these errors although their $\log K'_{PUF-A}$ are between 5 and 6. On the other hand, compounds with $\log K'_{PUF-A}$ (25 °C) greater than 8 or $\log K_{OA}$ greater than 10 are often found predominantly in the particle phase, which should be kept in mind when reporting strictly gas-phase concentrations of such compounds since a fraction of the atmospheric particulate phase may have also been sequestered by and extracted with the PUFs.

The reliability of K_{PUF-A} values is thus an important factor in passive air sampling. Here, they were derived for all compounds using Eq. 13, the regression between $\log K_{PUF-A}$ and $\log K_{OA}$ proposed by Shoeib and Harner (2002). This relationship is also used in most PUF-PAS studies (Harner, 2021) and was recently confirmed to be accurate through direct measurements in laboratory conditions (Francisco et al., 2017). However, as noted in ARTICLE 3, a case could be made against its use for relatively more polar compounds like OPEs. This was the reasoning behind the proposal for a new relationship for OPEs derived from experimental measurements in an attempt to obtain accurate K_{PUF-A} values instead of relying on a general K_{OA} regression (Saini et al., 2019). The regression resulted in K_{PUF-A} values one log unit higher than predicted by Shoeib and Harner, which could be a result of additional interactions between the relatively polar and hydrophilic OPEs and the PUF as has sometimes been observed in their particle partitioning behaviour (Möller et al., 2012; Okeme et al., 2018; Salamova et al., 2014). These higher K_{PUF-A} values would yield lower degrees of equilibrium (by up to around 30% lower based on results from ARTICLE 3). However, the proposed regression was only based on three OPEs, all of them with substituents composed exclusively of carbon and hydrogen atoms. Moreover, some studies have suggested lower particle partitioning ratios than initially suggested by K_{OA} models (Sühling et al., 2016). For these reasons, it was not used in the present work to estimate OPE K_{PUF-A} values. But, anticipating an increase in popularity of passive samplers for monitoring emerging OPEs, a more detailed study of their partitioning behaviour in PUF samplers would be beneficial.

The passive water samplers used in this work also perform best for a range of compounds with an optimal set of physical-chemical properties. Compounds with $\log K_{PWS-W}$ or $\log K_{OA}$ below 5 equilibrate quickly between water and polymer, and they are also more susceptible to uncertainties in their values. Additionally, these compounds tend to be the most volatile ones, so their occurrence in the dissolved phase of water is not to be expected at significant levels. Therefore, even small amounts detected in the sampler extracts tend to yield high concentrations that may not represent their true occurrence in water. We did not report concentrations of some low molecular weight and highly volatile chemicals with $\log K_{PWS-W}$ below 3.5 like HCHs and the lightest studied PAHs, but we did report concentrations of some OPEs with low $\log K_{PWS-W}$ because they are relatively more hydrophilic. On the other hand, compounds with $\log K_{PWS-W}$ or $\log K_{OW}$

above 6 or 7 have a higher tendency to partition towards particles, but unlike PUF-PAS samplers, polymer sheets do not directly sample the aquatic particulate phase.

Experimentally determined $\log K_{PWS-W}$ values are recommended over estimated ones for converting passive water sampling data to concentrations in the freely dissolved phase of water (Sobotka et al., 2022), which are what we used in ARTICLE 5. However, the obtention of reliable $\log K_{PWS-W}$ for OPEs can be more problematic. Their higher hydrophilicity may induce some error in the determination of K_{PWS-W} for some polymers like SR (Smedes, 2018), and no experimentally determined coefficients are available for LDPE, to the best of our knowledge. Thus, $\log K_{LDPE-W}$ for OPEs had to be estimated, so the reported concentrations of OPEs in water inevitably bear additional uncertainty. Standardized guidelines for the determination of polymer–water partition coefficients (Booij et al., 2017) suggest estimations using polymer-specific $\log K_{OW}$ correlations available for materials like LDPE (Sacks and Lohmann, 2011) and SR (Difilippo and Eganhouse, 2010). However, these guidelines also regard poly-parameter linear free energy relationships (pp-LFERs) as more adequate tools for the prediction of partition coefficients for both nonpolar and polar compounds. Pp-LFERs are linear combinations of modelled molecular variables like excess molar refraction (E), dipolarity/polarizability (S), hydrogen bond acidity (A_H), hydrogen bond basicity (B_H), and molar volume divided by 100 ($V_{/100}$). These descriptor variables are available in open databases elsewhere (Ulrich et al., 2017).¹⁶ Pp-LFER models for the estimation of K_{PWS-W} are available for different materials (Endo et al., 2011):

$$\log K_{LDPE-W} = 0.09 + 0.67E - 1.62S - 3.59A_H - 4.87B_H + 4.43V_{/100} \quad \text{Eq. 33}$$

$$\log K_{SR-W} = 0.27 + 0.60E - 1.42S - 2.52A_H - 4.11B_H + 3.64V_{/100} \quad \text{Eq. 34}$$

The performance of the pp-LFERs listed above was assessed for the prediction of K_{LDPE-W} and K_{SR-W} values for many compounds with known partition coefficients (Smedes, 2019, 2018; Smedes et al., 2009). An adequate correlation was observed between predicted and experimental coefficients for both polymers (Figure 37b, c). However, as seen in Figure 37b, predicted K_{SR-W} coefficients of OPEs did not adjust well to their experimentally determined values. This could be because of overestimated experi-

¹⁶ www.ufz.de/lserd (Accessed July 2022)

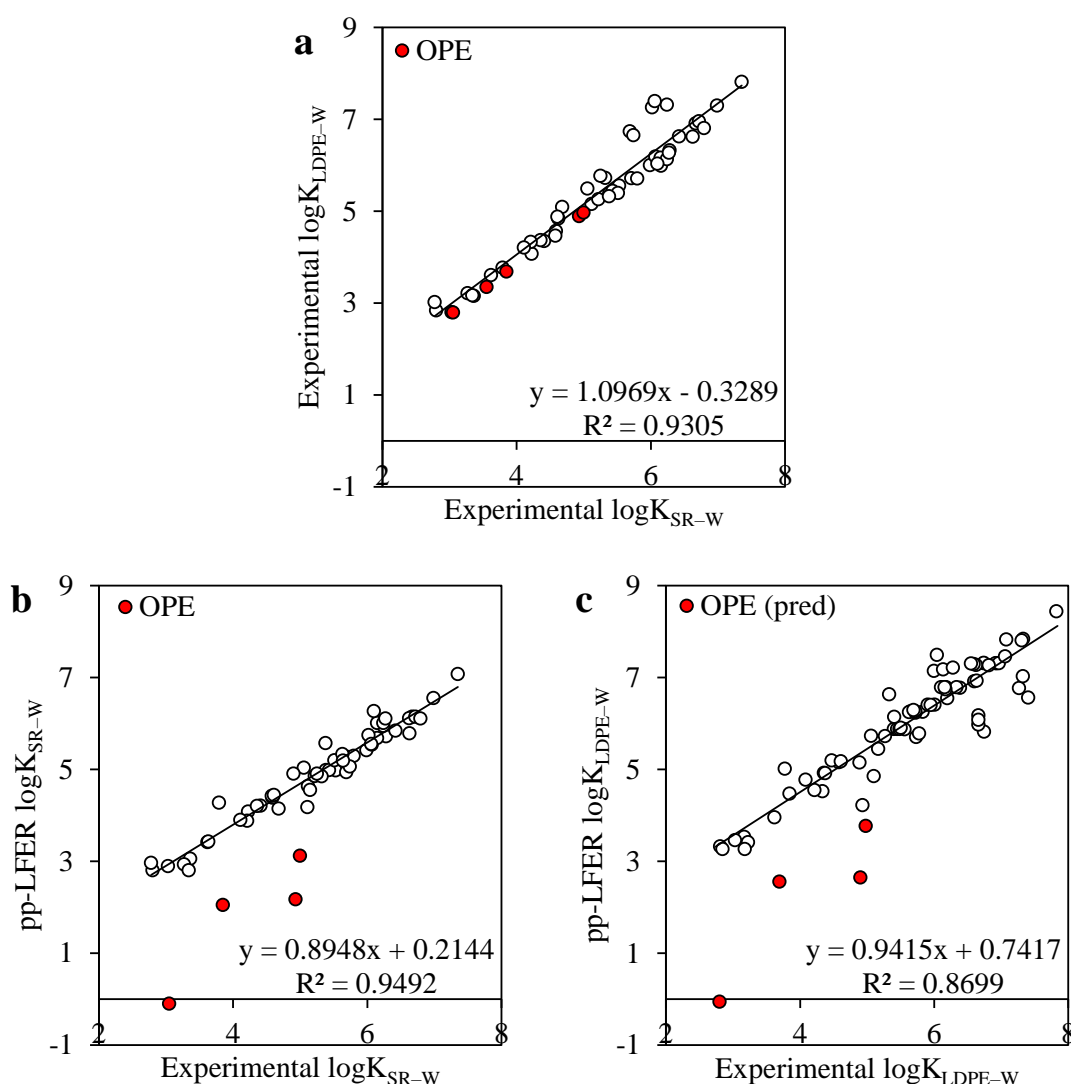


Figure 37. Prediction of OPE K_{PWS-W} using correlations between a) experimental LDPE and SR coefficients and pp-LFER models for b) SR and c) LDPE polymers. Figure created using experimental K_{LDPE-W} and K_{SR-W} values from Smedes (2019, 2018) and Smedes et al. (2009).

mental determinations or due to an inadequate pp-LFER prediction of the molecular interactions of OPEs with the polymeric matrix of the samplers. Because of this, and because molecular predictors are not available for all OPEs (e.g., TCIPP), in ARTICLE 5 we instead extrapolated OPE K_{LDPE-W} values from a linear regression of known coefficients for SR and LDPE polymers (Figure 37a). Since these coefficients were predicted from SR ones, they also deviate from pp-LFER predictions (Figure 37c). This approach assumes a similar interaction of OPEs with both polymer matrices, which is the case for all other considered compounds although it may not necessarily apply to OPEs as well. Still, it yields more predictable results based on experimental behaviour instead of purely modelled data. Other studies dealing with the absence of experimental

determinations of OPE K_{LDPE-W} values have based their estimations on water solubilities and vapour pressures (Ma et al., 2021; McDonough et al., 2018). However, the assumption of an OPE uptake in LDPE samplers similar to that of other pollutants still remains. All in all, an experimental determination of K_{LDPE-W} values would be preferable.

Even with the potential uncertainties in OPE concentrations, the majority of results in ARTICLE 5 showed acceptable agreement between LDPE and SR, except for a few more noticeable disagreements. We argue that these concentrations can be generally regarded as correct, or in the close range of true concentrations, although a detailed assessment of altitudinal and short-term temporal trends may not always be feasible. Thus, LDPE-derived concentrations of OPEs were used for the calculation of air–water diffusive exchange fluxes in ARTICLE 5, yielding reasonable estimations close to equilibrium that provide additional confidence in the results. Nevertheless, other passive sampler designs such as POCIS, which targets compounds with $\log K_{ow} < 4$ (Alvarez et al., 2004), might be an interesting alternative for monitoring OPEs that is worth studying further.

3.4.2 Urban and alpine levels of atmospheric pollutants and perspectives for their reduction

The passive air samplers deployed in Barcelona between the end of 2019 and mid-2020 were initially only intended for establishing a baseline of pollutant levels in air of a densely populated urban area, and to compare them to the expectedly lower concentrations found at the mountain sites. However, the exceptional consequences that followed the lockdown measures imposed at the beginning of the COVID-19 pandemic allowed for a more in-depth analysis of pollutant trends close to their sources. Although ARTICLE 2 contains a brief comparison of urban and preliminary alpine pollutant concentrations, better context is provided here using the more definitive atmospheric SVOC levels over the Pyrenees reported in ARTICLE 3 and ARTICLE 4. Additionally, the reductions observed in Barcelona during lockdown are further discussed.

ARTICLE 2 reports average concentrations of several SVOCs in Barcelona during three months before lockdown measures took effect. The lowest concentrations were those of PCBs, with individual congeners ranging from 5.8 to 15 pg m^{-3} and $\Sigma_7\text{PCB}$ of 58

pg m⁻³. They were followed by other organochlorine compounds like HCB (26 pg m⁻³), PeCB (8.5 pg m⁻³), and α - and γ -HCH (3.5 and 12.9 pg m⁻³, respectively). OPEs and PAHs presented up to an order of magnitude higher concentrations, between 0.1 and 4.7 ng m⁻³ (Σ_5 OPE 5.7 ng m⁻³) and between 0.1 and 18 ng m⁻³ (Σ_7 PAH 36 ng m⁻³), respectively. In general, the levels of PCBs and other organochlorine compounds were similar to those in other urban areas or lower than in industrialized areas in countries with less strict regulatory conditions (e.g., Chakraborty et al., 2010; Cui et al., 2017; Nøst et al., 2015; Zhang et al., 2010). PAH and OPE concentrations were comparable to those in other urban areas around the world, being higher or lower probably depending on differences in the amount and type of sources (e.g., Morville et al., 2011; Pratt et al., 2018; Zhou et al., 2017). Variations in the magnitude of the difference between our results and these latter studies probably reflect the amount of and distance from primary sources in the vicinity since they are actively emitted atmospheric pollutants.

Figure 38 shows these urban SVOC concentrations compared to their levels in the Pyrenees from ARTICLE 3 and ARTICLE 4. Individual sampling period average OPE concentrations in ARTICLE 3 were between 0.9 and 38 pg m⁻³ excluding outliers, with Σ_5 OPE between 16 and 53 pg m⁻³. This represents OPE concentrations in the background atmosphere of the Pyrenees 100 to almost 400 times lower than in the air of Barcelona. Individual sampling period average PAH concentrations in ARTICLE 4 ranged from 0.3 to 400 pg m⁻³, with Σ_7 PAH between 409 and 764 pg m⁻³, about 50 to 100 times lower than in Barcelona. PCB congener levels in the mountains were between 0.3 and 4.3 pg m⁻³ and Σ_7 PCB between 10 and 18 pg m⁻³, three to six times lower than the urban ones. All these differences clearly illustrate the scale of anthropogenic pollution around dense centres of population and industrial areas, especially pronounced for SVOCs with ongoing active emissions, but still significant for persistent chemicals that were regulated many decades ago. On the other hand, HCB and PeCB presented concentrations between 38 and 60 pg m⁻³ and 19 and 29 pg m⁻³, respectively. Contrary to all other studied SVOCs, these levels are somewhat higher than observed in Barcelona by factors of around two to three times. At first glance, this was somewhat surprising as legacy POPs still have their main remaining sources in industrial and urban areas. However, we have established that mountains may act as POP repositories with the ability to re-release them into the environment. ARTICLE 4 presents statistically significant evidence that points to the

re-emission of PeCB from surfaces like soils and other compartments in these mountains, which could explain the increased atmospheric PeCB levels. This was not the case for HCB, although a slight temperature dependence of its concentrations was still observed, possibly pointing at weak re-emission. However, HCB consistently presented volatilization (water to air) fluxes that were significantly different from equilibrium in most studied lakes in ARTICLE 5, meaning that water bodies might be a greater source of HCB to the atmosphere in this region of the Pyrenees rather than other compartments like soils.

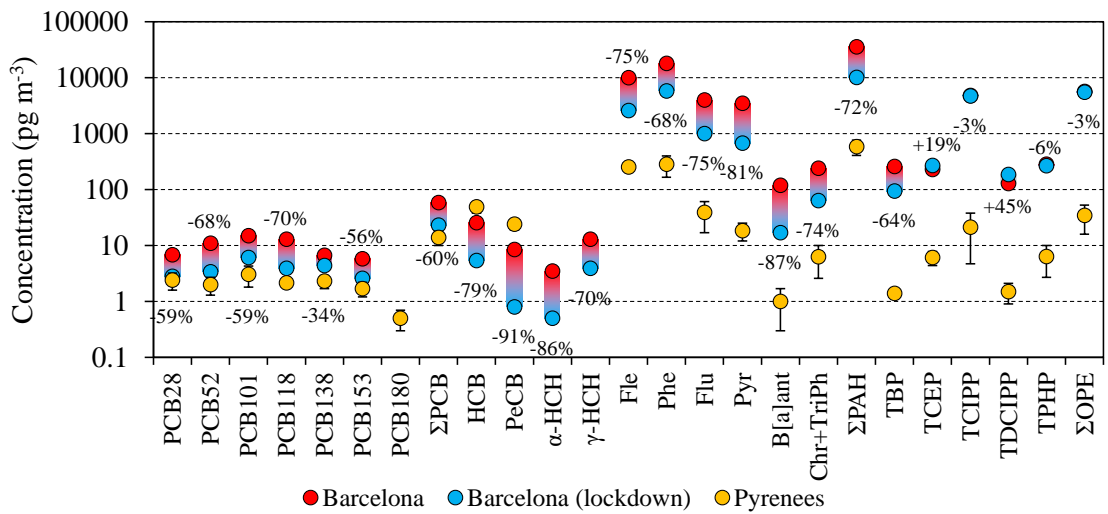


Figure 38. Pollutant concentrations in the air of Barcelona before and during lockdown compared to median levels detected in the Pyrenees (the whiskers show maximum and minimum period average concentrations).

Background–urban gradients of POP and SVOC concentrations are frequent in the literature, usually encompassing from rural areas to major cities passing through agricultural sites and industrialized areas, but sometimes also stretching to mountains and other remote sites. In general, the prevailing trend confirms higher concentrations of most pollutants close to urban areas, except for some pesticides that are higher near agricultural lands and sometimes PAHs that present varying levels depending on the season. An urban–rural gradient showed PCB concentrations that were 5 to 10 times higher near Toronto (Canada) than in the surrounding rural area, with other organochlorine compounds and pesticides including DDTs showing the same trend (Harner et al., 2004). PCBs in the same urban area were 2 to 3 times higher in the city, and PAHs presented a strong gradient with maximum urban concentrations during summer (Motelay-Massei et al., 2005). PCB and PAH concentrations were also distributed forming a clear urban–industrial–rural gradient in Chile, with 2 to 5-times higher PCB levels and 4 to 8-times

higher PAH levels at the industrial sites compared to the rural ones (Pozo et al., 2012). DDTs were 10 times higher and PCBs 6 times higher near centres of population in Italy than in the surrounding rural region (Estellano et al., 2017). PAHs were up to 4 times more abundant in rural sites in the Pyrenees compared to Barcelona (van Drooge and Grimalt, 2015). A mountain–rural–urban transect in India presented somewhat higher PAH concentrations near the city (Devi et al., 2014). Considering studies that included more remote locations, PCBs were around 10 times higher and organochlorine pesticides 10 to 20 times higher near cities in Chile (Pozo et al., 2004). PCBs were 10 times higher and DDTs and HCHs 5 times higher closer to semi-urban and urban regions in Australia (X. Wang et al., 2015). Finally, PCBs, PBDEs, and organochlorine pesticides were up to an order of magnitude higher at urban and agricultural sites across the world compared to concentrations in background locations (Pozo et al., 2006).

Figure 38 also shows the SVOC concentrations in Barcelona after lockdown measures were imposed during the start of the COVID-19 global pandemic. Very few studies have been published focusing on pollution changes due to lockdown measures outside of the typical air quality indicator gasses and particles (e.g., NO, NO₂, CO, O₃, PM₁₀) that are usually automatically monitored. A few exceptions focused on persistent organic pollutants in water (Rex and Chakraborty, 2022), volatile organic compounds and microplastics in water (Cecchi, 2021), and some PAHs in air (Li et al., 2022 and references within), but to the best of our knowledge, no other studies of changes in several atmospheric POPs during the COVID-19 lockdown are available to date. In general, ARTICLE 2 shows reductions in concentrations between -34 and -91% for all PCBs, organochlorine compounds, and PAHs, demonstrating the effects of marked reductions in road, maritime, and airborne traffic, waste disposal and incineration operations, and overall industrial and anthropogenic activity. This was possible for all studied SVOCs with emission sources directly linked to permanent human activity. Contrarily, OPEs did not experience the same reductions. Only TBP levels decreased by -64%, while the rest of OPEs remained approximately at the same concentrations (TCIPP, TPHP) or showed an increase in concentrations (TCEP +19%, TDCIPP +45%). This is due to OPEs passively volatilizing or leaching from human-made objects over time since they are not chemically bonded to the materials they are added to (Chokwe et al., 2020). A clear example of this are the elevated OPE levels found whenever buildings or enclosed spaces

are filled with new insulation or plastic materials (Olivero-Verbel et al., 2021; Vojta et al., 2017). Another example of their continuous and unaided release into the environment was found when analysing OPEs in the atmospheric gas phase of the Pyrenees, where the presence of a foam-insulated research cabin at Estanh Redon caused significant TPHP contamination in all passive air samplers used (see ARTICLE 3 for further information). In addition to SVOCs, other classical air quality indicators also suffered significant reductions in concentrations during lockdown in Barcelona (CO -28%, PM₁₀ -37%, NO -76%, NO₂ -52%), except for O₃, the concentrations of which increased (+45%) likely due to the lack of NO with which to react.

Overall, the lockdown period was extremely effective in reducing not only the concentration of contaminant gasses in the city of Barcelona but also the levels of several SVOCs in air. Some compounds like PCBs even reached levels similar to those in remote locations like Pyrenean high mountains (Figure 38). These observations provide a previously unthinkable point of reference for what can be expected in pollution abatement from future regulations on contaminant emissions. Obviously, the sudden cessation of most anthropogenic and urban activity seen in cities like Barcelona caused by the restrictive lockdown measures was, after all, a utopian scenario for the long term. Legislation and international agreements on pollutant emission thresholds cannot be expected to have an effect with comparable promptness and magnitude to what was observed in the first half of 2020. Still, the evidence presented here provides an unprecedented perspective on achievable goals that must be considered by legislating organisms and regulatory authorities given the implications it could have for the health of humans and ecosystems.

3.4.3 The lingering threat of persistent organic pollutants

The observations reported in ARTICLE 2 show that ceasing anthropogenic activities during lockdown in Barcelona led to an immediate drop in the detected concentrations of several chemicals like PCBs and other long-banned organochlorine compounds, which is a clear indication of the prevalence of current emissions of POPs from residual active sources, not just from secondary volatilization. The European Environmental Agency (EEA) estimates, based on data reported by European Union member states, that these PCB emissions are usually mostly due to industrial processes

and the use of PCB-containing products (67%), followed by energy production and distribution operations (17%) and other less predominant sources like waste treatment (6%) and commercial, institutional, and residential buildings (6%) (EEA, 2021). HCB emissions are currently mostly attributed to agriculture (38%), followed by commercial, institutional, and residential buildings (22%), industrial processes and use of HCB-containing products (19%), and energy production and distribution operations (13%) (EEA, 2021). Regulations imposed over the years, especially the implementation of the Stockholm Convention, are making a difference: reductions of -73% of PCB emissions and -97% of HCB emissions have been reported in Europe between 1990 and 2019 (EEA, 2021). But judging by the magnitude of the decrease in PCB and HCB levels reached as a result of the lockdown in Barcelona, there is still room for improvement.

The presence of PCBs and relatively volatile organochlorine compounds like HCB in high mountains and other remote environments has long been established. They are predominantly transported from their sources through the atmospheric gas phase as opposed to bound to the particulate phase (Yeo et al., 2003), which was also observed in the active air sampling particle filter measurements in ARTICLE 1. Once they reach the cold high mountains, their resistance to degradation becomes apparent as they persist unaltered for decades. Their estimated environmental half-lives are shown in Table 2. They are lower for HCHs (from a few hours to a few days in air, to almost a year in water and soil) and PeCB (a few days in water and soil, up to a year in air). DDT has half-lives in air of a few days, up to a year in water, and more than a decade in soils, and its degradation products have notable persistence in water. HCB and PCBs are remarkably persistent in all compartments, with half-lives from a few years to several decades. Agreeing with this extraordinary persistence, the analysis performed in ARTICLE 4 and ARTICLE 5 on variations in air and water concentrations compared to previous studies in Estanh Redon shows that most organochlorine levels in the Pyrenees remained fairly stable during the last twenty years despite being banned for several decades. On average, atmospheric concentrations of Σ PCBs and HCB only decreased by -15 and -22%, respectively (van Drooge et al., 2005, 2004a). Similarly, HCB levels decreased by -11% in water, although Σ PCBs and 4,4'-DDE concentrations seemed to decrease by -83 to -93% and -96%, respectively (Fernández et al., 2005; Vilanova et al., 2001b, 2001a). These greater reductions in freely dissolved water concentrations seem a bit too large

given the extraordinary persistence of these compounds in water and the observed stability of air concentrations. Possible causes could be increased levels in the measurements performed over twenty years ago due to the seasonal behaviour of input sources (e.g., snowmelt), as observed in other instances in the same area (Arellano et al., 2015), and the analysis of compounds bound to colloidal organic matter that is retained by active sampling methodologies used in those studies (Gomez-Belinchon et al., 1988). These fluctuations would increase the apparent reduction of concentrations when compared to the year-long integrative passive sampling measurements that we report. Aside from these latter disagreements, it is evident that these long-banned, persistent POPs that linger in the environment are still a reason of concern and a threat to the health of remote ecosystems.

Table 2. Environmental half-lives of most SVOCs considered in the present work. All values from Howard et al. (1991), except for PCBs from Sinkkonen and Paasivirta (2000) and OPEs from Liagkouridis et al. (2015). Units in hours (h), days (d), and years (y).

	Air	Water	Soil
HCB	156 d–4 y	3–6 y	3–6 y
PeCB	45 d–1 y	13–23 d	13–23 d
α -HCH	9 h–4 d	14–135 d	14–135 d
γ -HCH	9 h–4 d	14–240 d	14–240 d
DDTs	18 h–7 d	7 d–1 y	2–16 y
DDDs	18 h–7 d	2–16 y	2–16 y
DDEs	18 h–7 d	15 h–6 d	2–16 y
PCB28	3 d	60 d	3 y
PCB52	63 d	3 y	10 y
PCB101	125 d	7 y	10 y
PCB118	125 d	7 y	7 y
PCB153	250 d	14 y	19 y
PCB138	250 d	14 y	19 y
PCB180	1 y	27 y	38 y
Ace	1–9 h	3 h–13 d	12–102 d
Fle	7 h–3 d	32–60 d	32–60 d
Phe	2–20 h	3–25 h	16–200 d
Flu	2–20 h	21 h–3 d	140 d–1 y
Pyr	1–2 h	1–2 h	210 d–5 y
B[a]ant	1–3 h	1–3 h	102 d–2 y
Chr+TriPh	1–8 h	4–13 h	1–3 y
B[b]flu	1–14 h	9 h–30 d	1–2 y
B[k]flu	1–11 h	4 h–21 d	2–6 y
B[a]pyr	<1–1 h	<1–1 h	57 d–1 y
Ind[123cd]pyr	1–6 h	125–250 d	2 y
Db[ah]ant	<1–4 h	6 h–33 d	1–3 y
B[ghi]peryl	<1–3 h	2 y	2 y
TBP	3 h	9 d	17 d
TCEP	12 h	60 d	120 d
TCIPP	6 h	60 d	120 d
TDCIPP	14 h	180 d	360 d
TPHP	1 d	38 d	75 d

In contrast, PAHs are not considered to be POPs. They have the potential for spreading in the environment and for accumulating in different matrices, but they are not as resistant to degradation. Their accumulation happens instead because their continued emissions overcome their degradation rates. For the gas-phase PAHs studied in this work (Ace to Chr+TriPh), environmental half-lives are between 1 h and 20 h in air, between 1 h and 60 days in water, and between 12 days and 5 years in soil (Table 2). Heavier PAHs have similar or slightly higher half-lives in air but they may resist degradation to a larger degree since they are preferentially absorbed in the particulate phase (Lammel et al., 2009), as has been found and described in ARTICLE 1. Still, under these circumstances, PAHs are expected to degrade much faster than other POPs. This was also deduced from the atmospheric photodegradation estimates produced in ARTICLE 5, where PAH degradation fluxes in the air were two to three orders of magnitude higher than those of PCBs and HCB. Furthermore, as seen in ARTICLE 4, the reduction in atmospheric Σ PAH concentrations at Estanh Redon compared to over two decades ago was around -47 to -56% (Fernández et al., 2002; van Drooge et al., 2010), while the reduction in freely-dissolved Σ PAH concentrations in water was around -55 to -82% (ARTICLE 5) (Fernández et al., 2005; Vilanova et al., 2001c). The actual reduction of PAH concentrations in water is probably more towards the lower side of this range due to a different number of compounds being reported in the sum of PAHs. The decrease in atmospheric and aquatic PAH levels thus agrees well with the drop in PAH emissions over Europe of -53% between 1990 and 2019 (EEA, 2021). Their occurrence in the environment is indeed expected to follow emission patterns in the long run due to the higher degradation rates. Nowadays, PAH emissions in the European Union are attributed mainly to commercial, institutional, and household sources (81%), followed by industrial processes (9%), and a few other minor categories including road transport, agriculture, and energy production (EEA, 2021).

3.4.4 The growing issue of emerging organic pollutants

Like PAHs, OPEs are technically not POPs either. They can be transported long distances through the atmosphere and partition towards other environmental compartments, but their degradation rates are not as low as traditional POPs like PCBs. Estimated environmental half-lives of the OPEs studied in the present work are around a

few hours in air, several days or months in surface waters, and up to a year in soil, with the chlorinated OPEs typically showing higher values than TBP and TPHP (Table 2). These are comparable to or slightly higher than those of PAHs. Accordingly, estimated atmospheric photodegradation fluxes of OPEs were observed to be high enough to compete with other atmospheric removal processes in ARTICLE 5. However, although this higher degradation predicts reduced long-range transport potential of OPEs, their oxidation due to OH radicals in the particle phase has been observed to be limited (Liu et al., 2014), giving rise to a higher persistence in the atmosphere than anticipated since they generally exist mainly bound to particles (ARTICLE 1) that protect them from degradation. In light of their POP-like ability for spreading through the environment, their established occurrence in remote locations, and their lower-than-expected degradation, OPEs have sometimes been considered “persistent and mobile organic compounds” (PMOCs) (Rodgers et al., 2018). This behaviour is a problem because it means that the main issues with PBDEs that led to their substitution for OPEs as flame retardants have all turned out to be unsolved, including the potential toxicity and the ability to disperse and persist in the environment.

OPEs are currently often found at higher levels than PBDEs at their peak, making them even more regrettable substitutes (Blum et al., 2019). Since the focus of environmental research has only recently begun to shift towards OPEs, no previous measurements of OPE concentrations are available in the studied area like they are for organochlorine compounds and PAHs. Actually, very few assessments of OPE levels in high mountains are available, which makes ARTICLE 3 and ARTICLE 5 valuable contributions to the pool of knowledge on OPE reach. Unfortunately, no atmospheric gas-phase or freely-dissolved aquatic concentrations of PBDEs are available for comparison in the studied area either. The only available data on PBDE levels are for atmospheric deposition samples (Arellano et al., 2014a; Fernández et al., 2021), snow (Arellano et al., 2014b), and fish and other biota from Pyrenean high-altitude lakes (Bartrons et al., 2011; Blais et al., 2006; Gallego et al., 2007; Vives et al., 2004b). In other mountain and background sites, $\Sigma_{13}\text{PBDE}$ in air from the Tibetan Plateau were below 0.1 pg m^{-3} in 2010–2011 (Zhu et al., 2014) and $\Sigma_8\text{PBDE}$ in air around a perialpine lake in Italy was 77 pg m^{-3} in 2005 (Vives et al., 2007). In the Arctic Ocean, $\Sigma_{10}\text{PBDE}$ in air were below 2 pg m^{-3} (Möller et al., 2011b) while $\Sigma_8\text{OPE}$ were $110\text{--}1400 \text{ pg m}^{-3}$ (Möller et al., 2011a).

Finally, Σ_{15} PBDE in air from an urban–rural transect in Canada were uniform between 10 and 30 pg m^{-3} (Harner et al., 2006c). All of these PBDE concentrations were below those reported for Σ_5 OPEs in ARTICLE 3, except for those in the Italian lake, which were higher than period averages in the Pyrenees but lower than some individual samples. In water, Σ_7 PBDE concentrations in high-elevation lakes in the Himalayas were around 200 pg L^{-1} on average (dissolved and particle phases) in 2007 (Guzzella et al., 2011), total Σ_{14} PBDE were between 60 and 151 pg L^{-1} in 2011–2012 in freshwater lakes in Antarctica (Vecchiato et al., 2015), and Σ_{14} PBDE were between 0.2 and 10 pg L^{-1} (dissolved phase) in Lake Michigan in 2004 (Streets et al., 2006). Like with most atmospheric concentrations, all of these are lower than Σ_5 OPE concentrations reported in ARTICLE 5. This agrees with the observations of OPE concentrations in the environment being higher than PBDE ones during their emission peak (Blum et al., 2019), which is expected from their higher vapour pressures. Although potential toxic responses in exposed organisms are not necessarily the same for OPEs and PBDEs at equal concentrations, seeing higher amounts of chemicals being distributed through the environment and reaching remote ecosystems (when regulations were supposed to avoid it) is concerning in itself.

Future regulations relating to OPEs will have to rely not only on environmental occurrence and toxicological data but also on emission sources and amounts. ARTICLE 2 shows that OPE emissions are important and not necessarily dependent on the type of day-to-day anthropogenic activity that ceased during lockdown. The unexpected presence of OPEs in the insulating foam from the research cabin at Estanh Redon caused the contamination of passive air samples simply by diffusive release from a material that has been there for four decades. This also shows that the OPEs contained in the insulating foams analysed in ARTICLE 1 were already in use decades before they became popular in the 2000s. But keeping track of potential OPE emissions is a difficult task because there is limited information on global production and consumption of OPEs, and because of how quickly the OPE industry evolves and outdates previous manufacturing information. The specific mixtures of compounds used in products are generally kept as proprietary information by the industries and controlling OPE emissions would require a compound-by-compound analysis of their applications. Moreover, many products containing and emitting OPEs at any specific location are often imported from other countries, thus losing information on OPE composition. Still, OPE emissions are expected to correlate

directly to their global production, and there have been some estimates over the years that show an uninterrupted increase in OPE usage with time over the last decades. The global consumption of OPEs was 102,000 tons in 1995 (Du et al., 2019) and 186,000 tons in 2001, increasing from 58,000 to 83,000 in Europe between 1998 and 2001 (Marklund et al., 2005). In 2004 the global use was estimated between 210,000 and 300,000 tons (Mäkinen et al., 2009; Möller et al., 2012), and around 90,000 tons in Europe in 2006 (Reemtsma et al., 2008). Worldwide consumption of OPEs kept rising from 500,000 tons in 2011 to 680,000 tons in 2015 (Q. Wang et al., 2015), and potentially over 1 million tons in 2018 (Chokwe et al., 2020).

All in all, OPEs are yet another example of virtually unregulated compounds with increasing levels of production but, at the same time, with accumulating evidence showing adverse effects on life and ecosystems. The diffuse nature of their sources is an added obstacle to the regulation of their emissions, so regulatory action and surveillance should especially concern their production and application to products. With regards to environmental monitoring, passive air samplers have proved to be useful and reliable tools for the assessment of OPE concentrations, even in the harsh conditions of a high-mountain region (ARTICLE 1, ARTICLE 3, and ARTICLE 4). Passive water samplers can also be an asset in OPE monitoring in such remote regions. Their levels in the lakes reported in ARTICLE 5 are suitable estimates of their true concentration, but the choice of material may still leave room for limiting uncertainty and improving the determination of spatial and temporal trends. Thus, further assessment of OPE passive uptake by these and other materials should be carried out considering the physical-chemical properties of OPEs for the benefit of future monitoring programmes.

3.4.5 High mountains, sinks and secondary emitters of anthropogenic pollutants

Fluctuations of SVOC concentrations in the environment can occur in a variety of places and circumstances. Sometimes, these variations are linked to changes in primary emissions of pollutants, to the occurrence of meteorological phenomena, or to cycles in degradation and deposition processes, to name a few reasons. Occasionally, the fluctuations of atmospheric concentrations of SVOCs correlate with changes in ambient temperature. This was the case for many individual gas-phase organochlorine compounds, PAHs, and OPEs, as described in ARTICLE 3 and ARTICLE 4. When this

happens, the natural logarithm of the gas-phase concentrations regressed against the reciprocal of the absolute temperature yields a linear relationship. Wania et al. (1998) proposed that the slopes of these regressions reflect the relative importance of advection of air masses and diffusive exchange of pollutants between air and environmental surfaces. That is, the relative magnitude of these two pollutant input sources into the atmosphere can be assessed from the existence (or lack) of temperature dependence of gas-phase concentrations.

The simple model proposed by Wania et al. (1998), which is a reformulation of a previous approach (Pankow, 1993), assumes chemical equilibrium between the atmosphere and all environmental surfaces (e.g., soil, vegetation, atmospheric particles, water, snow) and that the concentration of a certain pollutant in all combined surfaces is large enough to remain essentially unchanged by volatilization processes driven by temperature. This is obviously not always the case and thus the approach is a simplistic approximation, but useful information can still be derived from it. The assumption of equilibrium is reflected by the air–surfaces partition coefficient (K_{AS}):

$$\ln K_{AS} = \ln C_A / C_S = \ln C_A - \ln C_S \quad \text{Eq. 35}$$

where C_A is the concentration of a pollutant in the gas phase of air and C_S is its concentration in all combined surfaces. The temperature dependence of any equilibrium partition coefficient conforms to the following partial derivative:

$$\frac{\partial \ln K_{AS}}{\partial T} = -\frac{\Delta U_{AS}}{RT^2} \quad \text{Eq. 36}$$

where ΔU_{AS} is the internal energy of phase change (between air and surfaces). Solving for a reference temperature (T_{ref}) at which K_{AS} is known, we obtain:

$$\ln K_{AS(T)} = \ln K_{AS(T_{ref})} - \frac{\Delta U_{AS}}{R} \left(\frac{1}{T} - \frac{1}{T_{ref}} \right) = \ln K_{AS(T_{ref})} - \frac{\Delta U_{AS}}{RT} + \frac{\Delta U_{AS}}{RT_{ref}} \quad \text{Eq. 37}$$

and inserting the solution into Eq. 35:

$$\ln C_A = \ln K_{AS} + \ln C_S = \left(\ln K_{AS(T_{ref})} + \frac{\Delta U_{AS}}{RT_{ref}} + \ln C_S \right) - \frac{\Delta U_{AS}}{R} \frac{1}{T} = b + \frac{m}{T} \quad \text{Eq. 38}$$

which takes the shape of a line with slope m and intercept b . Thus, temperature regressions of atmospheric concentrations are useful for determining thermodynamic parameters of diffusive exchange processes. Working with atmospheric concentrations on a mass per volume basis (e.g., pg m^{-3}) yields ΔU_{AS} , but enthalpies of phase change (ΔH_{AS}) are more useful for comparing with experimental data. They could be directly obtained from the equations above by working with partial pressures in air instead of concentrations, or by converting ΔU_{AS} following (Atkinson and Curthoys, 1978):

$$\Delta H = \Delta U - RT \quad \text{Eq. 39}$$

The hypothesis put forward by Wania et al. (1998) stated that pronounced slopes indicate a large contribution of evaporation of pollutants from surfaces in the vicinity of the sampling site to the concentrations observed in the gas phase, while shallow slopes indicate a larger contribution of pollutants transported by advection of air masses. The assessment of how pronounced or shallow these slopes are in the present work was performed relative to ΔH_{AS} determined in laboratory conditions. The reasoning behind it is that laboratory determinations of ΔH_{AS} reflect the ideal temperature-driven volatilization conditions for each compound in equilibrium. Therefore, any deviations from this purely evaporative behaviour (causing lower temperature regression slopes and thus lower values of ΔH_{AS}) would indicate an increased contribution of air advection as a source of atmospheric SVOCs. In ARTICLE 3, all OPEs with statistically significant temperature regressions showed ΔH_{AS} undistinguishable from their reference values (Figure 39). This indicates a predominance of diffusive exchange processes between air and environmental surfaces that controls the fluctuations of their atmospheric concentrations, which is expected for OPEs as they have a high tendency to partition with the particle phase (ARTICLE 1) and other similar compartments. The OPEs that did not present significant correlations were TBP and TDCIPP, which were found at lower and perhaps more uncertain atmospheric concentrations. Thus, at least for TCEP, TCIPP, and TPHP, these high mountains seem to be acting as important accumulators of OPEs at low temperatures and secondary emission sources at higher ones. Two such secondary sources that could be predominant at certain seasons of the year are snow (Gustavsson et al., 2019) and soils that become uncovered after snowmelt (see the detected OPEs in the supplementary soil samples in Figure S1.4), which could explain some of the observed trends based on the snow accumulation patterns at the sampling sites (ARTICLE 1).

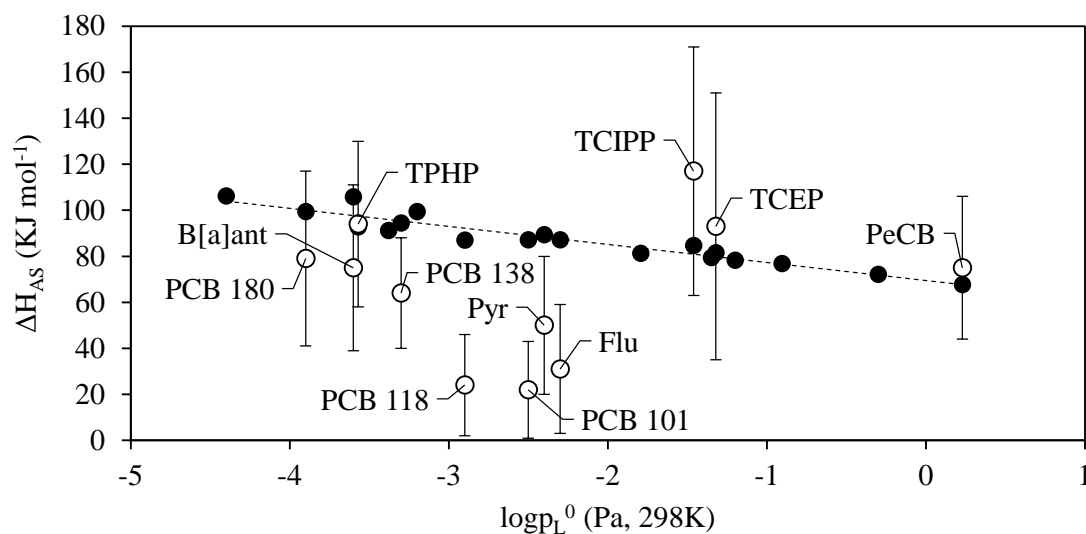


Figure 39. Air–surface phase change enthalpies measured in laboratory conditions (black) and estimated from statistically significant temperature regressions of gas-phase concentrations in the Pyrenees (white), regressed against subcooled liquid vapour pressures ($\log p_L^0$). Figure created using $\log p_L^0$ values from Allen et al. (1999), Brommer et al. (2014), Delle Site (1997), and Falconer and Bidleman (1994), and laboratory ΔH_{AS} from Nakajoh et al. (2006), Okeme et al. (2020), Panneerselvam et al. (2007), Roux et al. (2008), and Spieksma et al. (1994).

In ARTICLE 4, a greater variety of situations was observed. HCB, low molecular weight PAHs, and PCBs with a low degree of chlorination did not present statistically significant correlations with temperature because of their high volatility and limited partitioning towards soils and other surfaces. On the other hand, the concentrations of PAHs and PCBs of higher molecular weight usually increased significantly in atmospheric concentration at higher temperatures. Thus, the ΔH_{AS} derived from their regression slopes were closer to their reference values for the heaviest and less volatile compounds (Figure 39). This is likely an indication of their expected behaviour and environmental fate: re-volatilization from secondary sources can be a prominent atmospheric input of compounds that are more likely to partition towards environmental surfaces (i.e., the less volatile PCBs and PAHs). The only organochlorine compound that did not behave as expected was PeCB, which presented a steep slope and ΔH_{AS} close to the reference value (Figure 39). However, PeCB is one of the most volatile SVOCs analysed here so a higher advective influence would be expected, as observed for HCB. This abnormal behaviour would need to be investigated further to identify PeCB sources and the cause of its temperature trends.

The previous evidence, in the absence of local primary emissions of pollutants (as is expected in remote high-elevation mountains), suggests that the re-volatilization of

several SVOCs may occur during warm seasons and that these mountain sites can act as secondary emitters of accumulated chemicals. This re-emission can also be interpreted from the regression of the sum of all compounds (Figure 40, ΣOPEs $p < 2 \times 10^{-6}$ and ΣPCBs $p < 0.02$), although this assessment is much more qualitative because the calculation of a pseudo-enthalpy from the regression slope would not have thermodynamic meaning. Note that the slope for ΣPCBs is shallower than for ΣOPEs due to the range of behaviours exhibited by congeners with differing degrees of chlorination. Predominant surfaces responsible for this re-emission are likely to be soils, snow, water bodies, and vegetation. For reference, evidence of these processes that lead to mountain cold-trapping and secondary emission of SVOCs has been found in mountain slopes for soil (Qu et al., 2015; Riaz et al., 2021b; Wang et al., 2012), vegetation (Belis et al., 2009; Jaward et al., 2005a), snow (Finizio et al., 2006; Sharma et al., 2015), and alpine lakes (Meijer et al., 2006; Wilkinson et al., 2005).

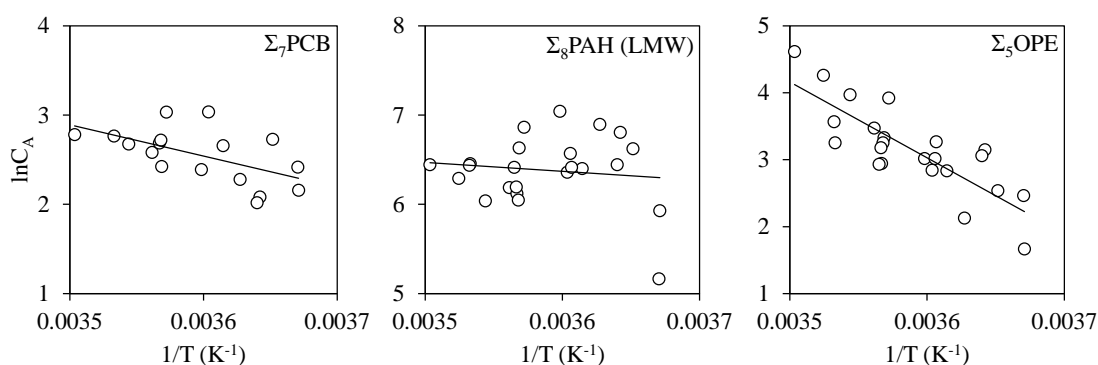


Figure 40. Sum of PCB, PAH (only gas-phase, low molecular weight –LMW– compounds except for Ret), and OPE (excluding contaminated outliers) atmospheric gas-phase concentrations regressed against the reciprocal of the absolute temperature.

Nevertheless, caution should be exercised when interpreting some SVOC trends with temperature in alpine regions, particularly in the case of PAHs. On one hand, PAHs bear a non-negligible diffuse component to their emissions that undoubtedly contributes to their environmental fate. This is reflected in the temperature trends in ARTICLE 4, possibly pointing at a cycle of absorption in environmental surfaces during cold seasons and re-volatilization during warmer seasons, which was observed for some of the heavy molecular weight PAHs as a result of their lower volatility and higher tendency for partitioning towards surfaces. Most low molecular weight PAHs did not exhibit this behaviour, which could be because of a reduced tendency for partitioning towards surfaces as a result of their higher volatility. On the other hand, PAHs also have active

sources in rural and alpine areas that typically increase their emissions in winter (van Drooge, 2013). However, no such increase is apparent when Σ PAH is regressed against temperature (Figure 40). The lack of a trend naturally follows the behaviour of the much more abundant low molecular weight PAHs that did not correlate with temperature. The reason behind the apparent absence of an increase in atmospheric PAH concentrations at lower temperatures could be twofold. Firstly, the increase in PAH emissions during colder months can sometimes be more noticeable for particle-associated PAHs (i.e., high molecular weight PAHs) than for those in the gas-phase (Fernández et al., 2002), and our measurements were strictly of the gas-phase. Secondly, the data points in Figure 40 represent different sites, so the varying temperatures do not only respond to seasonality but also to altitude and geographical location. This likely influences the temperature trends, as the coldest temperatures also occur at the highest sites, those most distant from regional sources. Unfortunately, there are not enough data points at each site for a conclusive assessment of site-specific trends over time.

The influence of regional sources of PAHs and the geographical location of the sampling sites is probably more noticeable from the levels of PAHs in water. Figure 41 shows the regressions of the sum of concentrations of each main group of SVOCs in the freely dissolved phase of water. While Σ OPEs and Σ PCBs did not present any significant temperature trends, significant correlations were seen for both low molecular weight (LMW) and high molecular weight (HMW) PAHs (both $p < 0.01$). These relationships indicate higher concentrations in water at higher temperatures, which is opposite to what is typically expected in high-elevation lakes. But again, these data points represent different sampling sites (where the warmer sites were located at lower altitudes). Since the passive water samples encompassed periods of one whole year, the differences in temperature mostly reflect variations in altitude and not seasonality. Therefore, Figure 41 may reflect the influence of regional emissions of pollutants.

Decreasing PAH concentrations with increasing altitude in mountain regions are not infrequent: they were observed for PAHs in soils, lichen, and vegetation in the Tibetan Plateau (Yang et al., 2013), soils in the Himalayas (Guzzella et al., 2011), and in Western Canadian mountains (Hussain et al., 2019). In most cases, these were hypothesized to reflect the distance from active PAH emission sources. In high-altitude mountains in eastern China, PAH concentrations in soils at mountaintops were lower than those down-

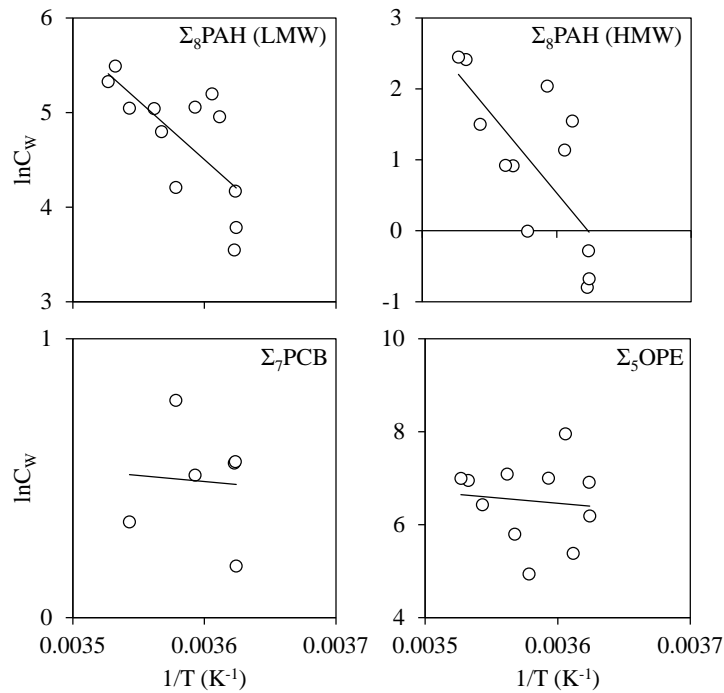


Figure 41. Sum of PCB, PAH (excluding Ret), and OPE atmospheric gas-phase concentrations regressed against the reciprocal of the absolute temperature. Low molecular weight (LMW, Fle to Chr+TriPh) and high molecular weight (HMW, B[b]Flu to B[ghi]peryl) PAHs are separated for comparison with atmospheric PAHs in the gas phase.

slope, where a forest filter effect was hypothesized to have been the cause (Wang et al., 2019). PAHs in snow from the Tyrolean Alps showed a slightly decreasing trend with altitude, a trend that was statistically significant for the sum of Phe, Flu, and Pyr, and which was attributed to snow–particle partitioning (Arellano et al., 2014b). Finally, other studies have shown no clear trends in PAH concentrations in sediments from mountain lakes at different altitudes (van Drooge et al., 2011). Aside from distance from potential regional sources, these studies indicate that there may be additional factors contributing to the observed trends depending on the area of study. Another possible determinant derived from the differences in elevation is that PAHs could be confined to the lowest altitudes during some critical periods due to temperature inversions. In winter, air masses transporting PAHs from rural sources prominently reach alpine areas during anticyclonic conditions by slowly penetrating mountain valleys instead of being transported by high altitude winds. Temperature inversions in the atmosphere are frequent under these calm conditions because the air close to the ground is relatively cold and a higher layer of warmer air traps pollution from active sources (i.e., PAHs) at lower altitudes (Daly and Wania, 2005). In fact, it is common that high-mountain sites present characteristically

tropospheric mountain peaks that remain isolated from pollutant sources at their base due to temperature inversions (Ribes et al., 2003; van Drooge et al., 2002). Temperature inversions were also identified as potential causes of increased PAH deposition and accumulation in Himalayan valleys (Hussain et al., 2016). Thus, low-elevation lakes with larger catchment areas (see Figure 13) could perhaps see an increased PAH input from catchment runoff and percolation. This would also explain the higher slope observed for HMW PAHs in Figure 41 compared to LMW ones, as the former have a higher tendency for accumulating in soils. Nevertheless, further research should be conducted to establish the existence of such effects and their influence over PAH concentrations at the highest altitudes.

With regards to future studies, a laborious but interesting objective moving forward would be to establish a more complete environmental fate and distribution model in this area of the Pyrenees. A first step towards this was achieved through the analysis of SVOC concentrations in water from the Pyrenean lakes in ARTICLE 5, which allowed for a more in-depth study of one of the main pollutant exchange processes in the area: air–water diffusive exchange at the surface of the lakes. These fluxes were determined using the concentrations in the freely dissolved phase of water determined in ARTICLE 5 and the atmospheric gas phase concentrations determined in ARTICLE 3 and ARTICLE 4. There are other atmospheric removal processes and pollutant input pathways into alpine lakes that may be relevant depending on the site and season (e.g., wet and dry deposition, snowmelt and runoff) (Fernández et al., 2021). However, diffusive exchange at the surface of the lakes is also considered a dominating transport mechanism for POPs (Bidleman and McConnell, 1995; Meijer et al., 2006). Moreover, diffusive exchange processes of POPs are often studied in lakes near pollutant sources but are infrequently reported in high-altitude lakes, hence why their determination in the present work is particularly valuable.

PAHs presented the highest fluxes, with averages up to $-70 \text{ ng m}^{-2} \text{ d}^{-1}$ denoting net deposition (except for retene at the lowest lakes due to their diagenetic formation in sediments), as expected from their predominant atmospheric emissions. Still, these PAH fluxes were several orders of magnitude lower than typical reports in lakes around the world (Qin et al., 2013; Ruge et al., 2018; Tuca et al., 2020), probably due to the remoteness of the studied lakes. ARTICLE 5 also shows that the imbalance between

atmospheric and aquatic PAHs that led to this air-to-water direction of the calculated fluxes exists despite having observed atmospheric photodegradation competing with diffusive exchange as a removal pathway of PAHs from the atmosphere. The organochlorine compounds, including most PCBs and PeCB, presented lower deposition fluxes (up to $-4.1 \text{ ng m}^{-2} \text{ d}^{-1}$) as a result of their lower concentrations and lack of current primary sources. Atmospheric degradation was shown to not influence their environmental fate. However, the estimated flux uncertainties were similar in magnitude to the fluxes themselves, so the diffusive exchange of some compounds (e.g., the two lightest PCBs, PeCB, and HCB at the two highest lakes) could sometimes not be confidently differentiated from equilibrium conditions. Note that near-equilibrium fluxes could also easily experience seasonal variations in the direction of their exchange that do not come through in the year-round averages reported in ARTICLE 5. This has been observed for PCB in Lake Superior, where volatilization dominates in late summer while deposition is most prominent during spring (Hornbuckle et al., 1994). PCBs and other organochlorine compounds have shown low but opposite fluxes in other lakes (Liu et al., 2016; Luarte et al., 2022). However, we only observed net volatilization of HCB among all organochlorine compounds ($+6.2 \text{ ng m}^{-2} \text{ d}^{-1}$). Finally, OPEs presented fluxes denoting either deposition (up to $-7.8 \text{ ng m}^{-2} \text{ d}^{-1}$) or equilibrium state. Recent reports in the Great lakes have shown much higher deposition fluxes, explained by the closeness to emission sources, and have recognized air–water exchange as a more important input mechanism than other pathways like dry deposition (Ma et al., 2021). The atmospheric photooxidation rates of the studied OPEs were similar or higher in magnitude to the diffusive exchange ones, meaning that, for some OPEs with fluxes close to equilibrium, atmospheric degradation could be acting as a competing pollutant removal process. Still, this was an assessment of gas-phase SVOCs, so the increased persistence of OPEs in the particulate phase in which they tend to predominantly exist should be accounted for in future studies of OPE input sources to these and other lakes. Given the relative novelty of OPEs and their condition of emerging pollutants, air–water exchange studies in lakes are scarce or even non-existent in alpine regions, giving special value to the present work.

Overall, it seems that the distribution dynamics of pollutants in this area are complex, although they follow some general trends. About half of the studied compounds in the atmospheric gas phase showed some indication of secondary volatilization from

surfaces, most probably soils and snow. The apparent magnitude of this re-emission behaviour generally agreed with the tendency of most of these SVOCs for partitioning with other environmental compartments. However, lake waters probably did not contribute significantly to this re-volatilization since diffusive exchange fluxes indicated predominant deposition from the atmospheric gas phase to the freely dissolved phase of water or near-equilibrium conditions. Only HCB presented consistent volatilization fluxes at most lakes. Seasonal fluctuations likely exist (Meijer et al., 2009), especially for compounds in equilibrium, both due to temperature changes and to seasonal inputs like snowmelt and increased regional emissions and transport. However, they could not be resolved from the sampling design of the present study as they are yearly averages. This contributes to the uncertainty in the reported fluxes, along with other factors that are further discussed in Section 3.4.6. But, in general, the overall scenario portrayed by the observed exchange processes in this region of the Pyrenees seems to be one of gradual accumulation of pollutants transported through the atmosphere, both legacy and emerging ones, and subsequent equilibration between matrices that, in some cases, results in re-emission that fluctuates with temperature.

3.4.6 Uncertainty in air–water exchange flux calculations

Unlike wet and dry deposition, diffusive exchange fluxes cannot be experimentally measured, so the values reported in the present work rely on a complex combination of variables, experimental parametrizations, and physical-chemical models, the individual uncertainties of which quickly add up. Since flux estimations are used to determine the direction of transport of pollutants, no absolute air-to-water or water-to-air flux value may be confidently differentiated from equilibrium conditions without an estimation of uncertainty. To complement the reported results, a few considerations on the uncertainty of flux calculations and its sources are provided next.

The theoretical error of the air–water exchange flux was calculated for each individual compound at each sampling site and period from the propagation of the error of the non-constant variables in the combination of Eq. 19 and Eq. 20:

$$F_{iAW} = k_{iAW} \left(C_{iW} - \frac{C_{iA}RT}{H_i(T)} \right) \quad \text{Eq. 40}$$

The error propagation formula for Eq. 40 is a function of five variables that are assumed to be independent (ignoring covariances between variables) and to follow a normal distribution with a standard deviation δ . Thus, δF_{iAW} is equal to the square root of the sum of squares of the partial derivatives of F_{iAW} with respect to each variable “ x ” ($\partial F_{iAW}/\partial x$), multiplied in turn by the square of their respective errors:

$$\delta F_{iAW} = \sqrt{\left(\frac{\partial F_{iAW}}{\partial k_{iAW}}\right)^2 \delta_{k_{iAW}}^2 + \left(\frac{\partial F_{iAW}}{\partial H_i}\right)^2 \delta_{H_i}^2 + \left(\frac{\partial F_{iAW}}{\partial T}\right)^2 \delta_T^2 + \left(\frac{\partial F_{iAW}}{\partial C_{iA}}\right)^2 \delta_{C_{iA}}^2 + \left(\frac{\partial F_{iAW}}{\partial C_{iW}}\right)^2 \delta_{C_{iW}}^2} \quad \text{Eq. 41}$$

The absolute value of each partial derivative from Eq. 41 is then divided by F_{iAW} to determine relative errors:

$$\left|\frac{\partial F_{iAW}}{\partial k_{iAW}}\right| = \left(C_{iW} + \frac{C_{iA}RT}{H_i}\right) \partial k_{iAW}; \quad \frac{|\partial F_{iAW}/\partial k_{iAW}|}{F_{iAW}} = \frac{1}{k_{iAW}} \quad \text{Eq. 42}$$

$$\left|\frac{\partial F_{iAW}}{\partial H_i}\right| = k_{iAW} C_{iA} RT \partial(1/H_i); \quad \frac{|\partial F_{iAW}/\partial H_i|}{F_{iAW}} = \frac{k_{iAW} C_{iA} RT}{F_{iAW} H_i^2} \quad \text{Eq. 43}$$

$$\left|\frac{\partial F_{iAW}}{\partial T}\right| = \frac{k_{iAW} C_{iA} R}{H_i} \partial T; \quad \frac{|\partial F_{iAW}/\partial T|}{F_{iAW}} = \frac{k_{iAW} C_{iA} R}{F_{iAW} H_i} \quad \text{Eq. 44}$$

$$\left|\frac{\partial F_{iAW}}{\partial C_{iA}}\right| = \frac{k_{iAW} RT}{H_i} \partial C_{iA}; \quad \frac{|\partial F_{iAW}/\partial C_{iA}|}{F_{iAW}} = \frac{k_{iAW} RT}{F_{iAW} H_i} \quad \text{Eq. 45}$$

$$\left|\frac{\partial F_{iAW}}{\partial C_{iW}}\right| = k_{iAW} \partial C_{iW}; \quad \frac{|\partial F_{iAW}/\partial C_{iW}|}{F_{iAW}} = \frac{k_{iAW}}{F_{iAW}} \quad \text{Eq. 46}$$

With some rearrangement, the equation for the relative error of the flux ($\delta F_{iAW}/F_{iAW}$) takes the following shape:

$$\frac{\delta F_{iAW}}{F_{iAW}} = \sqrt{\left(\frac{\delta_{k_{iAW}}}{k_{iAW}}\right)^2 + \left(\frac{k_{iAW} C_{iA} RT}{F_{iAW} H_i} \frac{\delta_{H_i}}{H_i}\right)^2 + \left(\frac{k_{iAW} C_{iA} R}{F_{iAW} H_i} \delta T\right)^2 + \left(\frac{k_{iAW} RT}{F_{iAW} H_i} \delta_{C_{iA}}\right)^2 + \left(\frac{k_{iAW}}{F_{iAW}} \delta_{C_{iW}}\right)^2} \quad \text{Eq. 47}$$

The estimation of the absolute errors of k_{iAW} and H_i presents the highest difficulty since they depend on the methods used for their calculation and the variables involved. However, Eq. 47 includes them both in their relative form, $\delta k_{iAW}/k_{iAW}$ and $\delta H_i/H_i$. Therefore, their approximation becomes much more practical. As recommended by Rowe

and Perlinger (2012), a relative error of 0.5 (50%) based on other studies (Blanchard et al., 2008) was used for H_i and a relative error of 0.3 (30%) based on the error analysis of Hoff (1994) was used for k_{iAW} , a value which was also later confirmed by (Liu et al., 2016). The errors of T and C_{iA} were determined as standard deviations of the temperatures measured in the area and the atmospheric concentrations analysed in the considered periods, respectively. Since only one water sampling period was considered for the calculation of F_{iAW} , the experimental error of C_{iW} could not be determined from standard deviations, so a relative error of 0.2 (20%) was used as recommended for cases with less than three samples (Rowe and Perlinger, 2012). All in all, experimental errors are undoubtedly preferable to assumed ones, but the assumptions made here are accommodating enough to account for most possible deviations in the data and variables used in the calculations. All other errors on the variables used in the calculation of exchange fluxes are indirectly accounted for in the approximation of the relative uncertainty of k_{iAW} . That includes errors from the empirical parametrizations of k_{CO_2W} and $k_{H_2O A}$.

Although contained within the aforementioned approximation of uncertainty, the existence of differing methods for the calculation of some variables or parameters can affect the results. Moreover, the practicality of sampling operations often requires some compromises to be made. Several possible sources of error were identified in this regard:

a. Diffusive exchange during winter

Diffusive exchange occurs at the interface between air and water. Therefore, pollutant transport through this mechanism does not take place during periods of the year when the surface of the lakes is covered in ice. However, the low concentrations expected in the studied environmental matrices required longer sampler exposures, meaning that the results presented here are year-round averages that do not exclude freezing periods. This inevitably resulted in fluxes that also represent the yearly average net transfer of pollutants at the provided concentrations, but it must be noted that higher time resolutions would show variation in fluxes over the different seasons, increasing in the summer when the higher temperatures facilitate compound diffusion and decreasing or stopping in winter as the lakes become covered with ice.

b. Temperature of water

The recorded temperatures in the flux calculations are used irrespective of their application to air, water, or both as the only data available in this study were air temperatures obtained on-site using data loggers and meteorological stations. But Eq. 26 uses the kinematic viscosity of water (ν_w) and its value affects all other water-side calculations. As seen in Figure 32, ν_w changes with temperature, so it must be corrected to the average water temperature of the studied period, but water temperatures at each lake had to be approximated from air temperatures. This constitutes another source of error in the calculation of the fluxes. The temperature of water in alpine lakes measured a few meters below the surface closely resembles air temperatures during ice-free periods (Catalan, 1988), so since the samplers were deployed no deeper than four meters below the water surface, air temperatures may be an acceptable approximation for ice-free periods considering that fluxes are estimated at the exchange interface between air and water.

On the other hand, freezing periods add their own set of complications. Water temperatures during ice coverage typically remain homogeneously between 0 and 4 °C, regardless of variation in air temperatures. All studied lakes freeze during winter, which may induce differences between average measured air temperatures and actual water temperatures that were not accounted for in the calculations. This could lead to fluxes with directions that would mostly remain the same based on the disequilibrium of concentrations between air and water, but with varying magnitudes compared to those reported. However, we argue that the differences would not be of concern and would still fall within the expected uncertainty range. To illustrate this, the fluxes were recalculated at 10 °C higher average water temperatures, an arbitrary but substantial increase that surpasses the expected change that would occur by establishing a water temperature baseline of 0 to 4 °C during freezing periods. Changing only the calculations directly affected by the temperature of water (ν_w) resulted in flux variations lower than 5% on average. An increase of 10 °C for all temperature values in the calculations regardless of their relevance to air, water, or both results in average flux variations between 3 and 25%, which is not that severe either.

c. Temperature correction of Henry's Law constants

Several methods can be used for obtaining H_i of a particular compound at a given temperature. Experimental temperature correlations specific to individual compounds have been published for PCBs and PAHs (e.g., Bamford et al., 1999; Cetin et al., 2006; Paasivirta et al., 1999; Parnis et al., 2015). A benefit of using temperature correlations experimentally determined specifically for each chemical is that the rate of variation of H_i with T is not assumed to be equal for all compounds. However, comprehensive studies that include data for an extensive selection of compounds are scarce. This leads to the need for obtaining correlations from different sources, which may compromise the consistency of physical-chemical variables involved in the model by introducing systematic errors in the calculations. A comparison of the effect of using different H_i determination methods is shown for some example compounds in Figure 42. H_i values for a specific compound at a given temperature can vary by a log unit between methods, and specific correlations are not always available for all studied compounds and compound groups.

Thus, a single temperature correction relationship was chosen for all studied pollutants regardless of the group (Hulscher et al., 1992). This temperature correction method uses the reference value of H_i at 25 °C (298.15 K). $H_{i,298}$ values can be obtained from several sources. A comprehensive database of references reporting H_i values for organic compounds is available (Sander, 2015). However, values from different studies are often reported at different temperatures and resulting from different determination methods ranging from experimental measurements to computational modelling and often vary by up to several orders of magnitude. For instance, most H values reported for hexachlorobenzene span a range of at least 2 orders of magnitude, between 10^{-1} and 10^{-3} mol m⁻³ Pa⁻¹ excluding outliers (Sander, 2015). Therefore, $H_{i,298}$ values from a single curated source, EPA's CompTox Chemistry Dashboard (Williams et al., 2017), were chosen in order to limit systematic variability between compounds and groups of compounds. A relative error of 50% has been proposed for H_i (Blanchard et al., 2008) as an estimate of the average uncertainty in H_i values, which was used in the present work for the calculation of uncertainties.

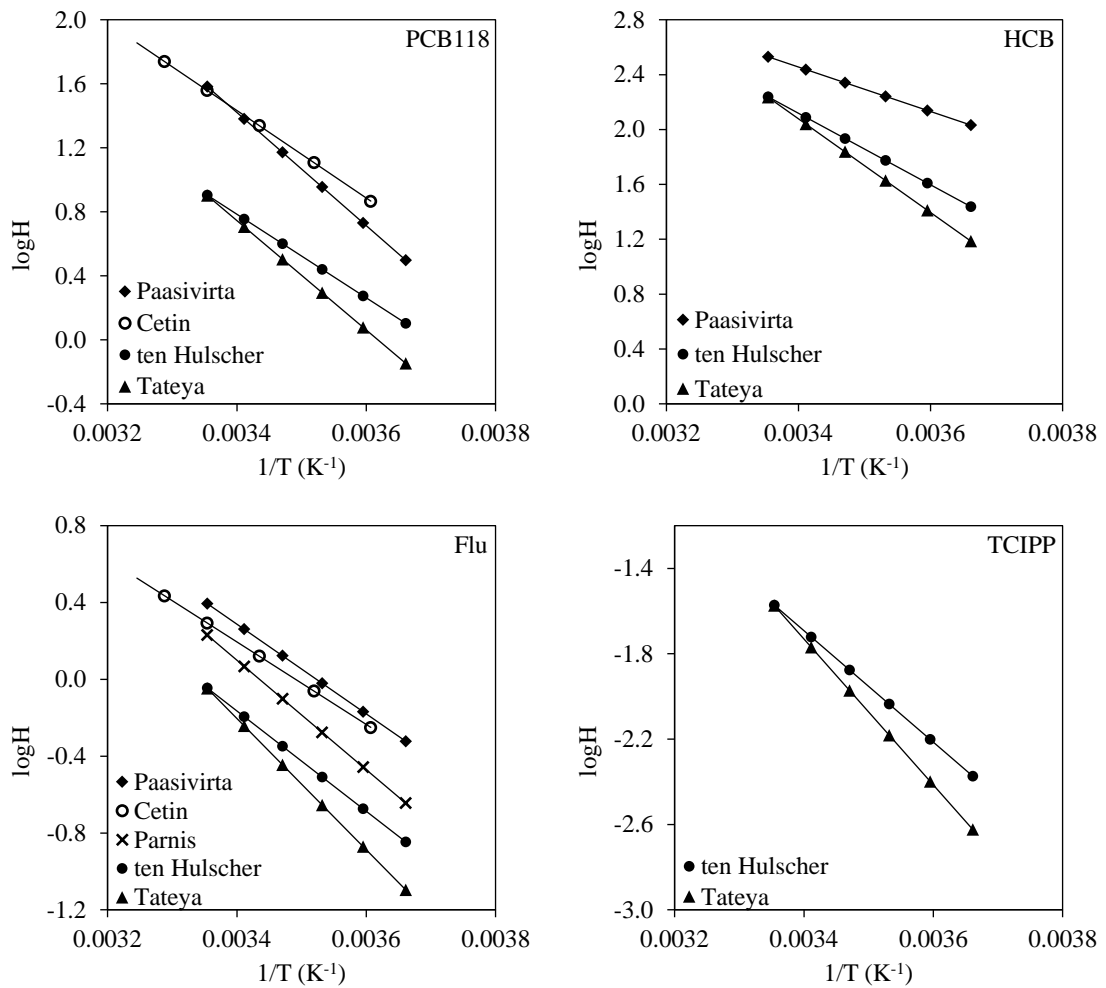


Figure 42. Temperature correction methods for Henry's Law constants ($\log H$) of PCB118, HCB, Flu, and TCIPP. Figures created using $\log H$ values and temperature correction relationships from Bamford et al. (1999), Cetin et al. (2006), Hulscher et al. (1992), Paasivirta et al. (1999), Parnis et al. (2015), and Tateya et al. (1988).

d. Reference mass transfer coefficients of H_2O and CO_2

The mass transfer coefficients of H_2O in air ($k_{H_2O A}$) and CO_2 in water ($k_{CO_2 W}$) are used as a reference value for the relative estimation of exchange velocities of other compounds. Their calculation generally relies on experimental regressions both from laboratory and field measurements, which tend to differ significantly depending on the conditions of the experiment and its location.

In air, Eq. 29 for $k_{H_2O A}$ proposed by Schwarzenbach et al. (2016) was used as a suitable approximation of data produced in other studies. A previous approximation of the same form based on laboratory studies (e.g., Liss, 1973; Mackay and Yeun, 1983;

Münnich et al., 1978) yielded different regression coefficients ($k_{H_2O A} \approx 0.2 u_{10} + 0.3$) (Schwarzenbach et al., 2005), and was used for a long time by general consensus in exchange flux calculations across the literature. Although it was a compromise between differing experimentally derived correlations between $k_{H_2O A}$ and wind speed, this approach showed good performance when applied to the calculation of evaporative loss rates of water Schwarzenbach et al. (2016). But the current understanding is that laboratory results typically overestimate the magnitude of such coefficients in the environment (Schwarzenbach et al., 2016), so the newer approximation of empirical parametrizations of $k_{H_2O A}$ was used instead. Still, the models do not differ significantly at wind speeds below 10 m s^{-1} .

In water, no such generally accepted approximation has been produced for $k_{CO_2 w}$, and experimentally derived relationships with wind speed seem to vary greatly depending on the considered water body and its size (e.g., for oceans and open sea as in González-Gaya et al., 2016; Nightingale et al., 2000; Wanninkhof and Bliven, 1991, or for lakes as in Klaus and Vachon, 2020; Vachon and Prairie, 2013). The effect of a selection of available models on $k_{CO_2 w}$ as a function of wind speed is shown in Figure 43. A recent

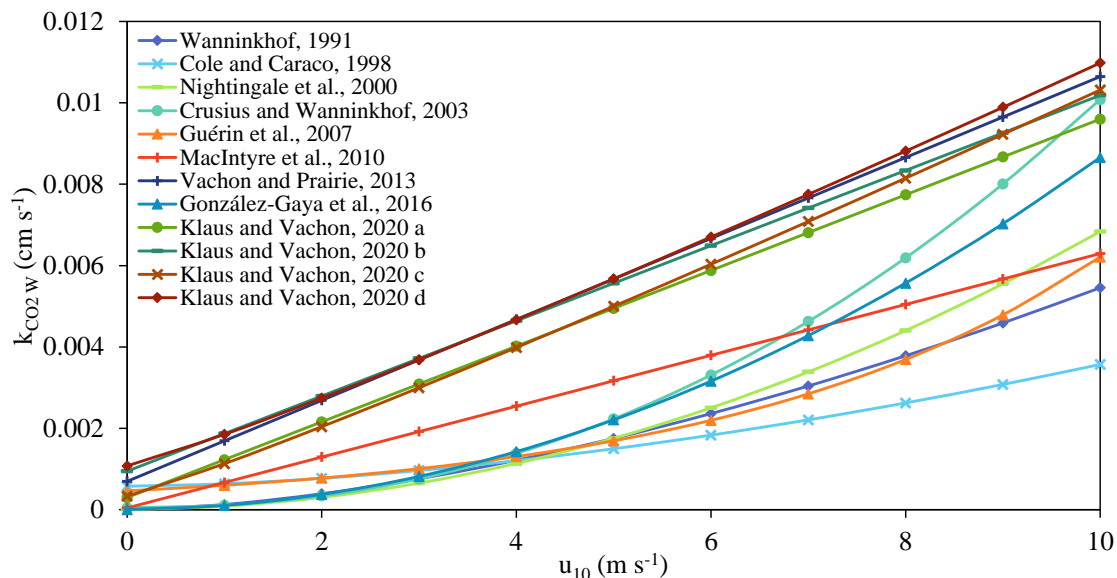


Figure 43. A selection of calculation methods reported in the last three decades for mass transfer coefficients in water of CO_2 ($k_{CO_2 w}$) depending on wind speed (u_{10}). Figure created using relationships from Cole and Caraco (1998), Crusius and Wanninkhof (2003), González-Gaya et al. (2016), Guérin et al. (2007), Klaus and Vachon (2020), MacIntyre et al. (2010), Nightingale et al. (2000), Vachon and Prairie (2013), and Wanninkhof and Bliven (1991). Klaus and Vachon's (2020) models labelled *a* to *d* are, respectively: linear regression with input variables Lake Area (LA) and space integration (SIN), linear LA, power regression with LA SIN, and power LA.

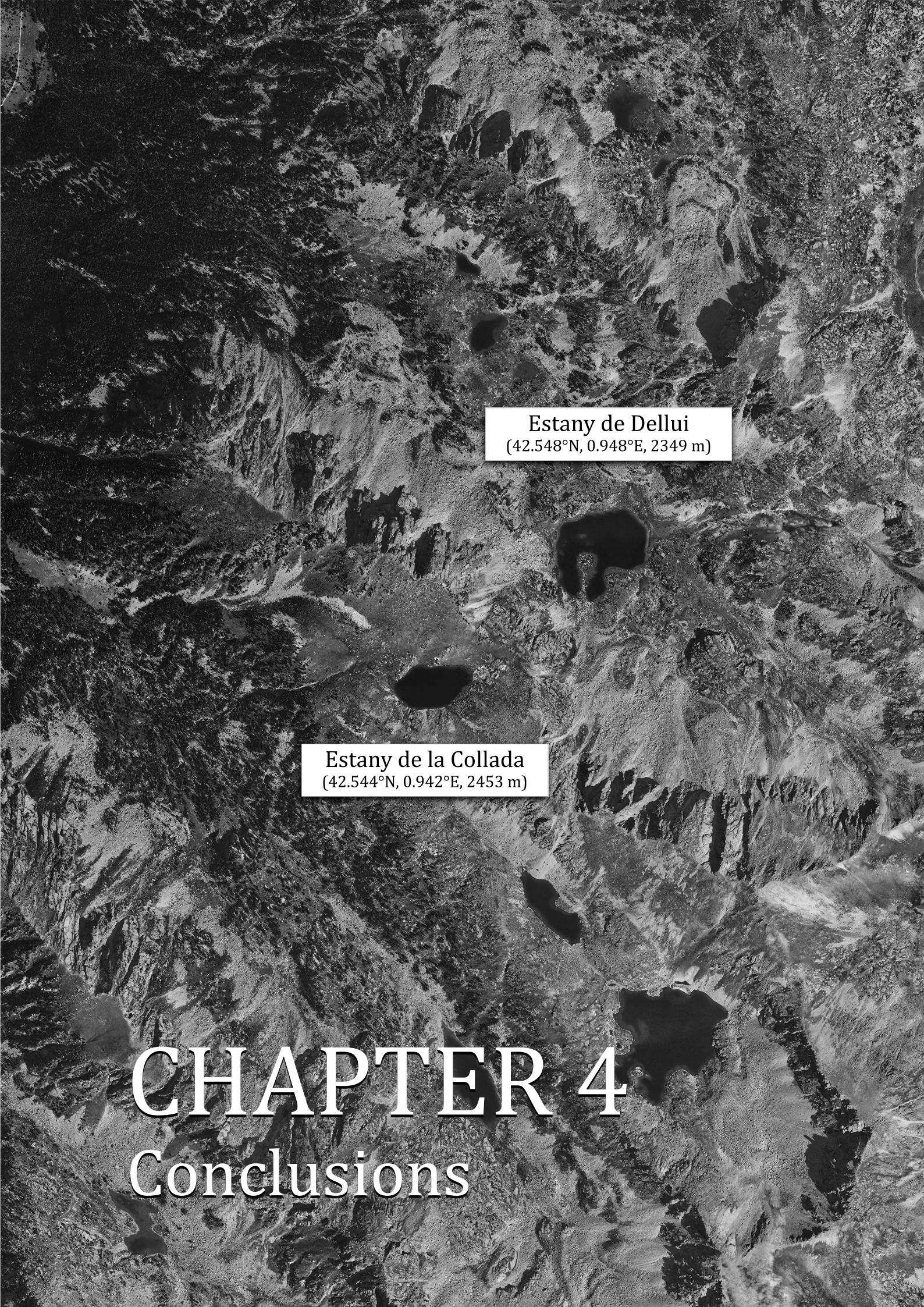
model proposed as a parametrization of literature data optimized for lake waters was used in the present work (Klaus and Vachon, 2020) as it focuses on lacustrine environmental systems by compiling data from multiple experimental studies.

e. Molar volume

Molar volumes used in Eq. 25 and Eq. 28 can be estimated in different ways with varying results, thus generating uncertainty in molecular diffusivities. One way is by dividing a compound's molar mass (M_i) by its mass density (ρ_i). A different and widespread method consists in the addition of atomic volume increments for each of the atoms and aromatic or heterocyclic rings present in the compound's molecule, as proposed by Fuller et al. (1966):

$$V_i = 16.5 C + 1.98 H + 5.48 O + 19.5 Cl + 17.0 S - 20.2 Rings \quad \text{Eq. 48}$$

However, this method is limited in the array of atoms that it considers and now falls short in front of readily available chemical calculators that base their estimations on molecular geometries and atom interactions, such as SPARC's physicochemical calculator. As an example of the uncertainty introduced by the variety of available methods, the molar volume of hexachlorobenzene, V_{HCB} , is $195.8 \text{ cm}^3 \text{ mol}^{-1}$ using Fuller's method, $161.2 \text{ cm}^3 \text{ mol}^{-1}$ from SPARC's calculation, $160.9 \text{ cm}^3 \text{ mol}^{-1}$ using SPARC's estimated density, and $139.3 \text{ cm}^3 \text{ mol}^{-1}$ using a density value from the literature (Haynes et al., 2016). This results in a relative standard deviation of V_{HCB} of almost 15%, which adds up to other errors in the determination of molecular diffusivities. In the present work, molar volumes were calculated using the SPARC calculator.



Estany de Dellui
(42.548°N, 0.948°E, 2349 m)

Estany de la Collada
(42.544°N, 0.942°E, 2453 m)

CHAPTER 4

Conclusions

The following paragraphs contain the main conclusions that were drawn from the work presented in this dissertation:

a. Applicability of passive samplers and uncertainty of the results

- The passive samplers used in the present work were a useful tool for monitoring atmospheric and aquatic pollutants in high-altitude areas of the Pyrenees. They are lightweight materials that are easily transportable to high-elevation sampling sites and that require minimal additional equipment for their deployment and retrieval, compared to traditional sampling strategies. This made possible the inexpensive monitoring of several sites at different elevations, which in turn enabled the study of pollutant distribution depending on environmental variables.
- The calibration of passive samplers using PRCs is a complex step in the determination of pollutant concentrations, but it becomes indispensable in remote sites subject to extreme meteorological conditions. In this study, PRC-derived sampling rates have allowed to account for differences in sampler exposure conditions between sample replicates and between sampling periods caused by differences in temperature, wind speed, precipitation, water currents, biofouling, and unforeseen events like the temporary entrapment of some passive air sampler housings under a few meters of snow.
- The uncertainty of the sampling rates resulting from the PRC calibration was assessed directly from the use of air and water samplers in alpine sites. For PUF air samplers, experimental errors calculated as standard deviations of replicates at each site were below 33%, agreeing with the expected errors calculated as theoretical expanded uncertainties (below 34%). For LDPE and SR water samplers, sampling rate uncertainties derived from the fit of an NLS curve to PRC data were below 25 and 33%, respectively. These values are the upper limit of uncertainties (i.e., the most uncertain measurements), so the average errors were low and within theoretical expectations.
- Atmospheric pollutant concentrations derived from passive air samplers closely agreed with active air sampling measurements in the gas phase, with only PAHs presenting some higher variability probably due to the seasonal behaviour of their regional emissions. The PUF housings acted as effective wind and particle shields and reduced the particle infiltration to around 20% compared to the active

sampler, which is low enough to consider the results as truly gas-phase concentrations.

- Aquatic pollutant concentrations derived from passive water samplers were not compared to active sampling measurements due to logistic difficulties involved with the collection and treatment of enough water volumes to overcome limits of detection. However, they were compared to independent measurements of co-deployed samplers performed elsewhere. The agreement was acceptable, generally within a factor of 2 to 4. OPEs were the main outliers in measurements performed using SR samplers, which could be due to a sub-optimal uptake by the sampler material and to uncertainty in the K_{PWS-W} values, both possibly attributed to the relatively higher hydrophilicity of OPEs.
- Overall, the passive sampling measurements in the present work were accurate enough, within the typically accepted limits in the field, and adequate for the intended purpose. The study of sampler performance and uncertainties provided a framework of confidence in the results for most studied pollutants, even in the harsh circumstances from a high-elevation alpine area, upon which the rest of the study of occurrence and distribution of pollutants was built.

b. Pollutant levels and their changes over time

- The atmospheric concentrations of SVOCs in the city of Barcelona before lockdown measures were imposed during the COVID-19 global pandemic were 3 to 6 times higher than in the Pyrenees for PCBs, 50 to 100 times higher for PAHs, and 100 to 400 times higher for OPEs. Contrarily, the concentrations of HCB and PeCB were 2 to 3 times higher in the Pyrenees, which could be due to their accumulation and re-emission as seen from atmospheric concentration trends with temperature and from air–water exchange fluxes.
- The implementation of lockdown restrictions resulted in reductions of levels of atmospheric particles PM_{10} (-37%), and gasses like CO (-28%), NO (-76%), and NO_2 (-52%), but not O_3 (+45%) because of the lower reactivity with the reduced amounts of NO. The concentrations of gas-phase SVOCs also suffered reductions: $\Sigma PAHs$ by -72%, $\Sigma PCBs$ by -60%, and HCB, PeCB, and other organochlorine compounds by -70 to -91%. This evidences the influence of their active sources in urban environments and how an immediate cease in certain anthropogenic

activities can lead to a noticeable decrease in urban pollution. On the other hand, Σ OPEs remained stable (-3%) because they passively release and volatilize from materials to which they are applied, so their levels do not directly depend as much on the day-to-day activities that were halted during lockdown.

- The atmospheric gas-phase and aquatic freely dissolved concentrations of most studied pollutants at the Pyrenean sites were in the range of or on the lower side of levels reported in other high-mountain areas and protected remote sites. However, literature and studies performed in these remote sites are often scarce given the difficulties associated with sampling operations. This gives significant value to the work presented here, particularly in the case of novel and emerging pollutants like OPEs, which are quickly becoming ubiquitous and a threat to the health of organisms and ecosystems.
- Pollutant concentrations determined in the present work were generally lower than those reported more than two decades ago in the same area. PAHs in air and water decreased by -47 to -56% and by -55 to -82%, respectively, agreeing with reductions in PAH emissions in Europe over the last decades (-53%). The atmospheric concentrations of PCBs and organochlorine compounds like HCB only decreased by -15 and -22%, respectively, despite having experienced reductions in emissions of -73 and -97% over a similar time frame. This was attributed to their remarkable persistence. In water, PCBs and other organochlorine compounds like 4,4'-DDE seemed to experience larger reductions than anticipated based on their resistance to degradation (-83 to -93% and -96%, respectively). A possible explanation could be due to comparing the year-long averages from the present work to single measurements from the literature that were sometimes performed during summer months, perhaps seeing the effect of additional input of some compounds after snowmelt or interference from POPs bound to colloidal matter.

c. Distribution of organic pollutants in high-altitude lacustrine ecosystems

- In the absence of local pollutant sources, temperature trends of gas-phase concentrations of SVOCs reflect the relative predominance of re-volatilization of chemicals accumulated in environmental compartments (e.g., soils, snow, vegetation, and water) as an input source of pollutants, in opposition to advection

of air masses. Here, the atmospheric levels of half of the studied SVOCs presented statistically significant correlations with temperature, indicating at least some influence of re-emission from secondary sources on air concentrations.

- The gas-phase concentrations of the most abundant OPEs presented significant correlations with temperature. Volatilization pseudo-enthalpies calculated from the slopes of the regressions were very similar to laboratory reference enthalpies, which point to a high influence of OPE accumulation on surfaces and subsequent evaporation at higher temperatures. This agrees with the high tendency of OPEs for partitioning towards environmental phases other than air. Moreover, snowmelt was identified as a possible main factor affecting gas-phase concentrations of OPEs because of its pollutant accumulating potential, the relative hydrophilicity of these compounds, and the observed seasonal freezing and thawing trends that coincided with variations in atmospheric OPE levels.
- The concentrations of HCB and most low molecular weight PCBs and PAHs in the atmospheric gas phase did not increase significantly with temperature. This was expected from these more volatile SVOCs, meaning that their levels in air are mainly influenced by pollutant transport through advection of air masses. In contrast, most heavier PCBs and PAHs presented significant trends with temperature. Experimental volatilization pseudo-enthalpies were confidently different from their reference values for lighter PAHs and PCBs, but they became increasingly close to laboratory-determined enthalpies as the volatility of these compounds decreased. This is thermodynamically consistent with their increasing tendency for partitioning towards environmental surfaces.
- Water concentrations of OPEs, PCBs, and most organochlorine compounds did not present significant variation between sites. Some of these, particularly OPE levels, could have been somewhat impacted by uncertainty in the measurements due to the aforementioned complications with the determination of their sampling rates. PAH concentrations in water showed higher concentrations at lower altitudes, a trend that seems contrary to mountain cold-trapping principles but that is likely related to the influence of regional sources of PAHs and the effect of geography on pollutants that reach these sites mostly entering through the valleys.

- Diffusive exchange fluxes between air and water were calculated for most studied pollutants. A general deposition (air to water) trend was observed for many compounds, especially for PAHs (as expected from their active and continued input into the atmosphere) and some PCBs. Most OPEs, some low molecular weight PCBs at a few sites, and PeCB were in equilibrium between phases. HCB presented volatilization (water to air) fluxes, as did retene at the three lowest lakes due to an imbalance in concentrations between air and water caused by diagenetic formation in lake sediments.
- The assessment of diffusive exchange is a complex subject. The calculations are intricate, and the error quickly adds up. Keeping track of this error is essential for determining the difference between the net deposition or volatilization of a flux and equilibrium conditions. Here, the uncertainty of the fluxes was accounted for by expanding the errors in the variables used in their calculation. Additionally, several sources of error were identified and studied. While the magnitude of the resulting uncertainties was sometimes high, many fluxes could be confidently distinguished from equilibrium.

d. Outlook

- Passive samplers have proved to be an invaluable tool for a relatively cheap and comprehensive study of diffuse pollution in high-altitude mountains. With a proper calibration method, not only the assessment of pollutant levels can be accomplished, but also that of temporal and environmental trends. Moving forward, the number and variety of studied compounds could be expanded, always considering the adequacy of sampler materials. Other materials could be tested for pollutants that lie at the limit of capability of those used in this study (e.g., OPEs). Moreover, the collection of additional samples from environmental compartments such as soil and snow at the sampling sites could help to identify the sources of re-emitted pollutants and their fluctuation with the seasons, as well as provide broader data for a possible multi-compartment environmental fate and exchange model.



REFERENCES

- Abdel-Shafy, H.I., Mansour, M.S.M., 2016. A review on polycyclic aromatic hydrocarbons: Source, environmental impact, effect on human health and remediation. *Egypt. J. Pet.* 25, 107–123. <https://doi.org/10.1016/J.EJPE.2015.03.011>
- Abdollahi, A., Eng, A., Jantunen, L.M., Ahrens, L., Shoeib, M., Parnis, J.M., Harner, T., 2017. Characterization of polyurethane foam (PUF) and sorbent impregnated PUF (SIP) disk passive air samplers for measuring organophosphate flame retardants. *Chemosphere* 167, 212–219. <https://doi.org/10.1016/j.chemosphere.2016.09.111>
- Abramowitz, R., Yalkowsky, S.H., 1990. Estimation of aqueous solubility and melting point of PCB congeners. *Chemosphere* 21, 1221–1229. [https://doi.org/10.1016/0045-6535\(90\)90142-G](https://doi.org/10.1016/0045-6535(90)90142-G)
- Aceves, M., Grimalt, J.O., 1993. Seasonally Dependent Size Distributions of Aliphatic and Polycyclic Aromatic Hydrocarbons in Urban Aerosols from Densely Populated Areas. *Environ. Sci. Technol.* 27, 2896–2908. <https://doi.org/10.1021/es00049a033>
- Achten, C., Andersson, J.T., 2015. Overview of Polycyclic Aromatic Compounds (PAC). *Polycycl. Aromat. Compd.* 35, 177–186. <https://doi.org/10.1080/10406638.2014.994071>
- Adams, R.G., Lohmann, R., Fernandez, L.A., MacFarlane, J.K., Gschwend, P.M., 2007. Polyethylene devices: Passive samplers for measuring dissolved hydrophobic organic compounds in aquatic environments. *Environ. Sci. Technol.* 41, 1317–1323. <https://doi.org/10.1021/es0621593>
- Agapkina, G.I., Brodskii, E.S., Shelepchikov, A.A., 2018. The Benzo(a)pyrene Total Toxicity Equivalent of Polycyclic Aromatic Hydrocarbons in Soils of Moscow and Assessment of Carcinogenic Risk to Human Beings. *Moscow Univ. Soil Sci. Bull.* 73, 186–194. <https://doi.org/10.3103/s0147687418050022>
- Allen, J.O., Sarofim, A.F., Smith, K.A., 1999. Thermodynamic properties of polycyclic aromatic hydrocarbons in the subcooled liquid state. *Polycycl. Aromat. Compd.* 13, 261–283. <https://doi.org/10.1080/10406639908020550>
- Alvarez, D.A., Petty, J.D., Huckins, J.N., Jones-Lepp, T.L., Getting, D.T., Goddard, J.P., Manahan, S.E., 2004. Development of a passive, in situ, integrative sampler for hydrophilic organic contaminants in aquatic environments. *Environ. Toxicol. Chem.* 23, 1640–1648. <https://doi.org/10.1897/03-603>
- Alzualde, A., Behl, M., Sipes, N.S., Hsieh, J.H., Alday, A., Tice, R.R., Paules, R.S., Muriana, A., Quevedo, C., 2018. Toxicity profiling of flame retardants in zebrafish embryos using a battery of assays for developmental toxicity, neurotoxicity, cardiotoxicity and hepatotoxicity toward human relevance. *Neurotoxicol. Teratol.* 70, 40–50. <https://doi.org/10.1016/j.ntt.2018.10.002>
- Andersson, J.T., Achten, C., 2015. Time to Say Goodbye to the 16 EPA PAHs? Toward an Up-to-Date Use of PACs for Environmental Purposes. *Polycycl. Aromat. Compd.* 35, 330–354. <https://doi.org/10.1080/10406638.2014.991042>
- Andresen, J.A., Grundmann, A., Bester, K., 2004. Organophosphorus flame retardants and plasticisers in surface waters. *Sci. Total Environ.* 332, 155–166. <https://doi.org/10.1016/j.scitotenv.2004.04.021>
- Arellano, L., Fernández, P., Fonts, R., Rose, N.L., Nickus, U., Thies, H., Stuchlík, E., Camarero, L., Catalan, J., Grimalt, J.O., 2015. Increasing and decreasing trends of the atmospheric deposition of organochlorine compounds in European remote areas during the last decade. *Atmos. Chem. Phys.* 15, 6069–6085. <https://doi.org/10.5194/acpd-15-3415-2015>
- Arellano, L., Fernández, P., López, J.F., Rose, N.L., Nickus, U., Thies, H., Stuchlik, E., Camarero, L., Catalan, J., Grimalt, J.O., 2014a. Atmospheric deposition of polybromodiphenyl ethers in remote mountain regions of Europe. *Atmos. Chem. Phys.* 14, 4441–4457. <https://doi.org/10.5194/acp-14-4441-2014>
- Arellano, L., Fernández, P., Tatosova, J., Stuchlik, E., Grimalt, J.O., 2011. Long-Range Transported Atmospheric Pollutants in Snowpacks Accumulated at Different Altitudes in the Tatra Mountains (Slovakia). *Environ. Sci. Technol.* 45, 9268–9275. <https://doi.org/10.1021/es202111n>
- Arellano, L., Grimalt, J.O., Fernández, P., Lopez, J.F., Nickus, U., Thies, H., 2014b. Persistent organic pollutant accumulation in seasonal snow along an altitudinal gradient in the Tyrolean Alps. *Environ. Sci. Pollut. Res.* 21, 12638–12650. <https://doi.org/10.1007/s11356-014-3196-x>

- Arellano, L., van Drooge, B.L., Rose, N.L., Nickus, U., Thies, H., Stuchlík, E., Camarero, L., Catalan, J., Grimalt, J.O., 2018. Drivers of atmospheric deposition of polycyclic aromatic hydrocarbons at European high-altitude sites. *Atmos. Chem. Phys.* 18, 16081–16097. <https://doi.org/10.5194/acp-18-16081-2018>
- Armitage, J.M., Gobas, F.A.P.C., 2007. A terrestrial food-chain bioaccumulation model for POPs. *Environ. Sci. Technol.* 41, 4019–4025. <https://doi.org/10.1021/es0700597>
- Armstrong, B., Hutchinson, E., Unwin, J., Fletcher, T., 2004. Lung cancer risk after exposure to polycyclic aromatic hydrocarbons: A review and meta-analysis. *Environ. Health Perspect.* 112, 970–978. <https://doi.org/10.1289/ehp.6895>
- Atkinson, D., Curthoys, G., 1978. The determination of heats of adsorption by gas-solid chromatography. *J. Chem. Educ.* 55, 564–566. <https://doi.org/10.1021/ed055p564>
- Bailey, R.E., van Wijk, D., Thomas, P.C., 2009. Sources and prevalence of pentachlorobenzene in the environment. *Chemosphere* 75, 555–564. <https://doi.org/10.1016/j.chemosphere.2009.01.038>
- Baker, J.E., Eisenreich, S.J., 1990. Concentrations and Fluxes of Polycyclic Aromatic Hydrocarbons and Polychlorinated Biphenyls across the Air-Water Interface of Lake Superior. *Environ. Sci. Technol.* 24, 342–352. <https://doi.org/10.1021/es00073a009>
- Baldasano, J.M., 2020. COVID-19 lockdown effects on air quality by NO₂ in the cities of Barcelona and Madrid (Spain). *Sci. Total Environ.* 741, 140353. <https://doi.org/10.1016/j.scitotenv.2020.140353>
- Bamford, H.A., Poster, D.L., Baker, J.E., 1999. Temperature dependence of Henry's law constants of thirteen polycyclic aromatic hydrocarbons between 4°C and 31°C. *Environ. Toxicol. Chem.* 18, 1905–1912. <https://doi.org/10.1002/etc.5620180906>
- Bartkow, M.E., Hawker, D.W., Kennedy, K.E., Müller, J.F., 2004. Characterizing Uptake Kinetics of PAHs from the Air Using Polyethylene-Based Passive Air Samplers of Multiple Surface Area-to-Volume Ratios. *Environ. Sci. Technol.* 38, 2701–2706. <https://doi.org/10.1021/es0348849>
- Bartkow, M.E., Jones, K.C., Kennedy, K.E., Holling, N., Hawker, D.W., Müller, J.F., 2006. Evaluation of performance reference compounds in polyethylene-based passive air samplers. *Environ. Pollut.* 144, 365–370. <https://doi.org/10.1016/j.envpol.2005.12.043>
- Bartrons, M., Grimalt, J.O., Catalan, J., 2011. Altitudinal distributions of BDE-209 and other polybromodiphenyl ethers in high mountain lakes. *Environ. Pollut.* 159, 1816–1822. <https://doi.org/10.1016/J.ENVPOL.2011.03.027>
- Beck, Jø., Hansen, K.E., 1974. The degradation of quintozene, pentachlorobenzene, hexachlorobenzene and pentachloroaniline in soil. *Pestic. Sci.* 5, 41–48. <https://doi.org/10.1002/ps.2780050108>
- Belis, C.A., Offenthaler, I., Uhl, M., Nurmi-Legat, J., Bassan, R., Jakobi, G., Kirchner, M., Knoth, W., Kräuchi, N., Levy, W., Magnani, T., Moche, W., Schramm, K.-W., Simončič, P., Weiss, P., 2009. A comparison of Alpine emissions to forest soil and spruce needle loads for persistent organic pollutants (POPs). *Environ. Pollut.* 157, 3185–3191. <https://doi.org/10.1016/j.envpol.2009.05.035>
- Bidleman, T.F., McConnell, L.L., 1995. A review of field experiments to determine air-water gas exchange of persistent organic pollutants. *Sci. Total Environ.* 159, 101–117. [https://doi.org/10.1016/0048-9697\(95\)04255-Y](https://doi.org/10.1016/0048-9697(95)04255-Y)
- Bidleman, T.F., Olney, C.E., 1974a. High-volume collection of atmospheric polychlorinated biphenyls. *Bull. Environ. Contam. Toxicol.* 11, 442–450. <https://doi.org/10.1007/BF01685302>
- Bidleman, T.F., Olney, C.E., 1974b. Chlorinated Hydrocarbons in the Sargasso Sea Atmosphere and Surface Water. *Science* 183, 516–518. <https://doi.org/10.1126/science.183.4124.516>
- Billo, E.J., 2001. Non-linear regression using the solver, in: *Excel for Chemists: A Comprehensive Guide*. John Wiley & Sons, Inc., pp. 223–238.
- Bizzotto, E.C., Villa, S., Vaj, C., Vighi, M., 2009a. Comparison of glacial and non-glacial-fed streams to evaluate the loading of persistent organic pollutants through seasonal snow/ice melt. *Chemosphere* 74, 924–930. <https://doi.org/10.1016/j.chemosphere.2008.10.013>
- Bizzotto, E.C., Villa, S., Vighi, M., 2009b. POP bioaccumulation in macroinvertebrates of alpine freshwater

- systems. *Environ. Pollut.* 157, 3192–3198. <https://doi.org/10.1016/j.envpol.2009.06.001>
- Blais, J.M., Charpentié, S., Pick, F., Kimpe, L.E., Amand, A.S., Regnault-Roger, C., 2006. Mercury, polybrominated diphenyl ether, organochlorine pesticide, and polychlorinated biphenyl concentrations in fish from lakes along an elevation transect in the French Pyrénées. *Ecotoxicol. Environ. Saf.* 63, 91–99. <https://doi.org/10.1016/j.ecoenv.2005.08.008>
- Blais, J.M., Schindler, D.W., Muir, D.C.G., Kimpe, L.E., Donald, D.B., Rosenberg, B., 1998. Accumulation of persistent organochlorine compounds in mountains of western Canada. *Nature* 395, 585–588. <https://doi.org/10.1038/26944>
- Blais, J.M., Schindler, D.W., Muir, D.C.G., Sharp, M., Donald, D., Lafrenière, M., Braekevelt, E., Strachan, W.M.J., 2001a. Melting Glaciers: A Major Source of Persistent Organochlorines to Subalpine Bow Lake in Banff National Park, Canada. *Ambio* 30, 410–415. <https://doi.org/10.1579/0044-7447-30.7.410>
- Blais, J.M., Schindler, D.W., Sharp, M., Braekevelt, E., Lafrenière, M., McDonald, K., Muir, D.C.G., Strachan, W.M.J., 2001b. Fluxes of semivolatile organochlorine compounds in Bow Lake, a high-altitude, glacier-fed, subalpine lake in the Canadian Rocky Mountains. *Limnol. Oceanogr.* 46, 2019–2031. <https://doi.org/10.4319/lo.2001.46.8.2019>
- Blanchard, P., Hulting, M.L., Brice, K.A., Backus, S.M., Dryfhout-Clark, H., Hites, R.A., 2008. Atmospheric deposition of toxic substances to the Great Lakes: IADN results through 2005, EPA-905-R-08-001. US EPA and Environment Canada.
- Blum, A., Behl, M., Birnbaum, L.S., Diamond, M.L., Phillips, A., Singla, V., Sipes, N.S., Stapleton, H.M., Venier, M., 2019. Organophosphate Ester Flame Retardants: Are They a Regrettable Substitution for Polybrominated Diphenyl Ethers? *Environ. Sci. Technol. Lett.* 6, 638–649. <https://doi.org/10.1021/acs.estlett.9b00582>
- Bogdal, C., Scheringer, M., Abad, E., Abalos, M., Van Bavel, B., Hagberg, J., Fiedler, H., 2013. Worldwide distribution of persistent organic pollutants in air, including results of air monitoring by passive air sampling in five continents. *TrAC - Trends Anal. Chem.* 46, 150–161. <https://doi.org/10.1016/j.trac.2012.05.011>
- Bonde, J.P., Toft, G., 2011. DDT and Reproductive Health, in: *Encyclopedia of Environmental Health*. Elsevier, pp. 1–5. <https://doi.org/10.1016/B978-0-444-52272-6.00404-9>
- Booij, K., Hofmans, H.E., Fischer, C. V., Van Weerlee, E.M., 2003. Temperature-dependent uptake rates of nonpolar organic compounds by semipermeable membrane devices and low-density polyethylene membranes. *Environ. Sci. Technol.* 37, 361–366. <https://doi.org/10.1021/es025739i>
- Booij, K., Sleiderink, H.M., Smedes, F., 1998. Calibrating the uptake kinetics of semipermeable membrane devices using exposure standards. *Environ. Toxicol. Chem.* 17, 1236–1245. <https://doi.org/10.1002/etc.5620170707>
- Booij, K., Smedes, F., 2010. An improved method for estimating in situ sampling rates of nonpolar passive samplers. *Environ. Sci. Technol.* 44, 6789–6794. <https://doi.org/10.1021/es101321v>
- Booij, K., Smedes, F., Allan, I.J., 2017. Guidelines for determining polymer-water and polymer-polymer partition coefficients of organic compounds. *ICES Tech. Mar. Environ. Sci.* <https://doi.org/http://dx.doi.org/10.17895/ices.pub.3285>
- Booij, K., Smedes, F., Van Weerlee, E.M., 2002. Spiking of performance reference compounds in low density polyethylene and silicone passive water samplers. *Chemosphere* 46, 1157–1161. [https://doi.org/10.1016/S0045-6535\(01\)00200-4](https://doi.org/10.1016/S0045-6535(01)00200-4)
- Boström, C.E., Gerde, P., Hanberg, A., Jernström, B., Johansson, C., Kyrklund, T., Rannug, A., Törnqvist, M., Victorin, K., Westerholm, R., 2002. Cancer risk assessment, indicators, and guidelines for polycyclic aromatic hydrocarbons in the ambient air. *Environ. Health Perspect.* 110, 451–488. <https://doi.org/10.1289/ehp.110-1241197>
- Breivik, K., Pacyna, J.M., Münch, J., 1999. Use of α -, β - and γ -hexachlorocyclohexane in Europe, 1970–1996. *Sci. Total Environ.* 239, 151–163. [https://doi.org/10.1016/S0048-9697\(99\)00291-0](https://doi.org/10.1016/S0048-9697(99)00291-0)
- Briz-Redón, Á., Belenguer-Sapiña, C., Serrano-Aroca, Á., 2021. Changes in air pollution during COVID-

- 19 lockdown in Spain: A multi-city study. *J. Environ. Sci.* 101, 16–26. <https://doi.org/10.1016/j.jes.2020.07.029>
- Brodsky, J., Ballschmiter, K., 1988. Reversed phase liquid chromatography of PCBs as a basis for the calculation of water solubility and log Kow for polychlorobiphenyls. *Fresenius' Zeitschrift für Anal. Chemie* 331, 295–301. <https://doi.org/10.1007/BF00481899>
- Brommer, S., Jantunen, L.M., Bidleman, T.F., Harrad, S., Diamond, M.L., 2014. Determination of vapor pressures for organophosphate esters. *J. Chem. Eng. Data* 59, 1441–1447. <https://doi.org/10.1021/je401026a>
- Brubaker, W.W., Hites, R.A., 1998. OH reaction kinetics of gas-phase α - and γ -hexachlorocyclohexane and hexachlorobenzene. *Environ. Sci. Technol.* 32, 766–769. <https://doi.org/10.1021/es970650b>
- Burchiel, S.W., Luster, M.I., 2001. Signaling by environmental polycyclic aromatic hydrocarbons in human lymphocytes. *Clin. Immunol.* 98, 2–10. <https://doi.org/10.1006/clim.2000.4934>
- Bytnerowicz, A., Badea, O., Barbu, I., Fleischer, P., Fraczek, W., Gancz, V., Godzik, B., Grodzińska, K., Grodzki, W., Karnosky, D., Koren, M., Krywult, M., Krzan, Z., Longauer, R., Mankovska, B., Manning, W.J., McManus, M., Musselman, R.C., Novotny, J., Popescu, F., Postelnicu, D., Prus-Głowacki, W., Skawiński, P., Skiba, S., Szaro, R., Tamas, S., Vasile, C., 2003. New international long-term ecological research on air pollution effects on the Carpathian Mountain forests, Central Europe. *Environ. Int.* 29, 367–376. [https://doi.org/10.1016/S0160-4120\(02\)00172-1](https://doi.org/10.1016/S0160-4120(02)00172-1)
- Cabrerizo, A., Dachs, J., Moeckel, C., Ojeda, M.J., Caballero, G., Barceló, D., Jones, K.C., 2011. Ubiquitous net volatilization of polycyclic aromatic hydrocarbons from soils and parameters influencing their soil?air partitioning. *Environ. Sci. Technol.* 45, 4740–4747. <https://doi.org/10.1021/es104131f>
- Calamari, D., Bacci, E., Focardi, S., Gaggi, C., Morosini, M., Vighi, M., 1991. Role of Plant Biomass in the Global Environmental Partitioning of Chlorinated Hydrocarbons. *Environ. Sci. Technol.* 25, 1489–1495. <https://doi.org/10.1021/es00020a020>
- Camarero, L., Catalan, J., 1996. Variability in the chemistry of precipitation in the Pyrenees (northeastern Spain): Dominance of storm origin and lack of altitude influence. *J. Geophys. Res. Atmos.* 101, 29491–29498. <https://doi.org/10.1029/96jd01816>
- Carrera, G., Fernández, P., Grimalt, J.O., Ventura, M., Camarero, L., Catalan, J., Nickus, U., Thies, H., Psenner, R., Guillem Carrera, Pilar Fernández, and, Grimalt*, J.O., Marc Ventura, Lluís Camarero, and, Catalan, J., Nickus, U., and, H.T., Psenner, R., 2002. Atmospheric deposition of organochlorine compounds to remote high mountain lakes of Europe. *Environ. Sci. Technol.* 36, 2581–2588. <https://doi.org/10.1021/es0102585>
- Carrera, G., Fernández, P., Vilanova, R.M., Grimalt, J.O., 2001. Persistent organic pollutants in snow from European high mountain areas. *Atmos. Environ.* 35, 245–254. [https://doi.org/10.1016/S1352-2310\(00\)00201-6](https://doi.org/10.1016/S1352-2310(00)00201-6)
- Casal, P., Casas, G., Vila-Costa, M., Cabrerizo, A., Pizarro, M., Jiménez, B., Dachs, J., 2019. Snow amplification of persistent organic pollutants at coastal antarctica. *Environ. Sci. Technol.* 53, 8872–8882. <https://doi.org/10.1021/acs.est.9b03006>
- Catalan, J., 1988. Physical properties of the environment relevant to the pelagic ecosystem of a deep high-mountain lake (Estany Redó, Central Pyrenees). *Oecologia Aquat.* 9, 89–123.
- Catalan, J., Ballesteros, E., Camarero, L., Felip, M., Gacia, E., 1992. Limnology in the Pyrenean Lakes. *Limnetica* 8, 27–38.
- Catalan, J., Bartrons, M., Camarero, L., Grimalt, J.O., 2013. Mountain waters as witnesses of global pollution, in: *Living with Water: Targeting Quality in a Dynamic World*. Springer New York, New York, NY, pp. 31–67. https://doi.org/10.1007/978-1-4614-3752-9_2
- Catalan, J., Camarero, L., Felip, M., Pla, S., Ventura, M., Buchaca, T., Bartumeus, F., De Mendoza, G., Miró, A., Casamayor, E.O., Medina-Sánchez, J.M., Bacardit, M., Altuna, M., Bartrons, M., De Quijano, D.D., 2006. High mountain lakes: Extreme habitats and witnesses of environmental changes. *Limnetica* 25, 551–584. <https://doi.org/10.23818/limn.25.38>

- Catalan, J., Ventura, M., Vives, I., Grimalt, J.O., 2004. The roles of food and water in the bioaccumulation of organochlorine compounds in high mountain lake fish. *Environ. Sci. Technol.* 38, 4269–4275. <https://doi.org/10.1021/es040035p>
- Cecchi, T., 2021. Analysis of volatiles organic compounds in Venice lagoon water reveals COVID 19 lockdown impact on microplastics and mass tourism related pollutants. *Sci. Total Environ.* 783, 146951. <https://doi.org/10.1016/j.scitotenv.2021.146951>
- Cetin, B., Ozer, S., Sofuoglu, A., Odabasi, M., 2006. Determination of Henry's law constants of organochlorine pesticides in deionized and saline water as a function of temperature. *Atmos. Environ.* 40, 4538–4546. <https://doi.org/10.1016/j.atmosenv.2006.04.009>
- Chaemfa, C., Barber, J.L., Kim, K.-S., Harner, T., Jones, K.C., 2009a. Further studies on the uptake of persistent organic pollutants (POPs) by polyurethane foam disk passive air samplers. *Atmos. Environ.* 43, 3843–3849. <https://doi.org/10.1016/j.atmosenv.2009.05.020>
- Chaemfa, C., Wild, E., Davison, B., Barber, J.L., Jones, K.C., 2009b. A study of aerosol entrapment and the influence of wind speed, chamber design and foam density on polyurethane foam passive air samplers used for persistent organic pollutants. *J. Environ. Monit.* 11, 1135–1139. <https://doi.org/10.1039/b823016a>
- Chakraborty, P., Zhang, G., Li, J., Xu, Y., Liu, X., Tanabe, S., Jones, K.C., 2010. Selected organochlorine pesticides in the atmosphere of major Indian Cities: Levels, regional versus local variations, and sources. *Environ. Sci. Technol.* 44, 8038–8043. <https://doi.org/10.1021/es102029t>
- Chen, D., Liu, W., Liu, X., Westgate, J.N., Wania, F., 2008. Cold-Trapping of Persistent Organic Pollutants in the Mountain Soils of Western Sichuan, China. *Environ. Sci. Technol.* 42, 9086–9091. <https://doi.org/10.1021/es8018572>
- Chen, Y., Cai, X., Jiang, L., Li, Y., 2016. Prediction of octanol-air partition coefficients for polychlorinated biphenyls (PCBs) using 3D-QSAR models. *Ecotoxicol. Environ. Saf.* 124, 202–212. <https://doi.org/10.1016/j.ecoenv.2015.10.024>
- Cheng, H., Deng, Z., Chakraborty, P., Liu, D., Zhang, R., Xu, Y., Luo, C., Zhang, G., Li, J., 2013. A comparison study of atmospheric polycyclic aromatic hydrocarbons in three Indian cities using PUF disk passive air samplers. *Atmos. Environ.* 73, 16–21. <https://doi.org/10.1016/j.atmosenv.2013.03.001>
- Chevrier, J., Eskenazi, B., Holland, N., Bradman, A., Barr, D.B., 2008. Effects of exposure to polychlorinated biphenyls and organochlorine pesticides on thyroid function during pregnancy. *Am. J. Epidemiol.* 168, 298–310. <https://doi.org/10.1093/aje/kwn136>
- Chokwe, T.B., Abafe, O.A., Mbelu, S.P., Okonkwo, J.O., Sibali, L.L., 2020. A review of sources, fate, levels, toxicity, exposure and transformations of organophosphorus flame-retardants and plasticizers in the environment. *Emerg. Contam.* 6, 345–366. <https://doi.org/10.1016/j.emcon.2020.08.004>
- Chuang, J.C., Wilson, N.K., Hannan, S.W., 1987. Field Comparison of Polyurethane Foam and XAD-2 Resin for Air Sampling for Polynuclear Aromatic Hydrocarbons. *Environ. Sci. Technol.* 21, 798–804. <https://doi.org/10.1021/es00162a011>
- Cole, J.J., Caraco, N.F., 1998. Atmospheric exchange of carbon dioxide in a low-wind oligotrophic lake measured by the addition of SF₆. *Limnol. Oceanogr.* 43, 647–656. <https://doi.org/10.4319/lo.1998.43.4.0647>
- Courtney, K.D., 1979. Hexachlorobenzene (HCB): A review. *Environ. Res.* 20, 225–266. [https://doi.org/10.1016/0013-9351\(79\)90001-X](https://doi.org/10.1016/0013-9351(79)90001-X)
- Crusius, J., Wanninkhof, R., 2003. Gas transfer velocities measured at low wind speed over a lake. *Limnol. Oceanogr.* 48, 1010–1017. <https://doi.org/10.4319/lo.2003.48.3.1010>
- Cui, S., Fu, Q., Li, Y.-F., Li, T., Liu, D., Dong, W., Wang, M., Li, K., 2017. Spatial–temporal variations, possible sources and soil–air exchange of polychlorinated biphenyls in urban environments in China. *RSC Adv.* 7, 14797–14804. <https://doi.org/10.1039/C6RA26864A>
- Dachs, J., Eisenreich, S.J., Hoff, R.M., 2000. Influence of Eutrophication on Air–Water Exchange, Vertical Fluxes, and Phytoplankton Concentrations of Persistent Organic Pollutants. *Environ. Sci. Technol.*

- 34, 1095–1102. <https://doi.org/10.1021/es990759e>
- Daly, G.L., Lei, Y.D., Teixeira, C., Muir, D.C.G., Castillo, L.E., Wania, F., 2007. Accumulation of current-use pesticides in neotropical montane forests. *Environ. Sci. Technol.* 41, 1118–1123. <https://doi.org/10.1021/es0622709>
- Daly, G.L., Wania, F., 2005. Organic contaminants in mountains. *Environ. Sci. Technol.* 39, 385–398. <https://doi.org/10.1021/es048859u>
- Daly, G.L., Wania, F., 2004. Simulating the Influence of Snow on the Fate of Organic Compounds. *Environ. Sci. Technol.* 38, 4176–4186. <https://doi.org/10.1021/es035105r>
- Danckwerts, P. V., 1951. Significance of Liquid-Film Coefficients in Gas Absorption. *Ind. Eng. Chem.* 43, 1460–1467. <https://doi.org/10.1021/ie50498a055>
- Datta, S., Mcconnell, L.L., Baker, J.E., Lenoir, J., Seiber, J.N., 1998. Evidence for Atmospheric Transport and Deposition of Polychlorinated Biphenyls to the Lake Tahoe Basin, California–Nevada. *Environ. Sci. Technol.* 32, 1378–1385. <https://doi.org/10.1021/ES970657T>
- Davidson, D.A., Wilkinson, A.C., Blais, J.M., Kimpe, L.E., McDonald, K.M., Schindler, D.W., 2003. Orographic cold-trapping of persistent organic pollutants by vegetation in mountains of Western Canada. *Environ. Sci. Technol.* 37, 209–215. <https://doi.org/10.1021/es020605q>
- Deacon, E.L., 1977. Gas transfer to and across an air-water interface. *Tellus* 29, 363–374. <https://doi.org/10.3402/tellusa.v29i4.11368>
- Delle Site, A., 1997. The Vapor Pressure of Environmentally Significant Organic Chemicals: A Review of Methods and Data at Ambient Temperature. *J. Phys. Chem. Ref. Data* 26, 157–193. <https://doi.org/10.1063/1.556006>
- den Besten, C., Vet, J.J.R.M., Besselink, H.T., Kiel, G.S., van Berkel, B.J.M., Beems, R., van Bladeren, P.J., 1991. The liver, kidney, and thyroid toxicity of chlorinated benzenes. *Toxicol. Appl. Pharmacol.* 111, 69–81. [https://doi.org/10.1016/0041-008X\(91\)90135-2](https://doi.org/10.1016/0041-008X(91)90135-2)
- Devi, N.L., Shihua, Q., Yadav, I.C., 2014. Atmospheric Polycyclic Aromatic Hydrocarbons (PAH) in Manipur of the Northeast India: Monitoring on Urban, Rural, and Mountain Sites. *Polycycl. Aromat. Compd.* 34, 12–34. <https://doi.org/10.1080/10406638.2013.839455>
- Difilippo, E.L., Eganhouse, R.P., 2010. Assessment of PDMS-water partition coefficients: Implications for passive environmental sampling of hydrophobic organic compounds. *Environ. Sci. Technol.* 44, 6917–6925. <https://doi.org/10.1021/es101103x>
- Dobson, R., Scheyer, A., Rizet, A.L., Mirabel, P., Millet, M., 2006. Comparison of the efficiencies of different types of adsorbents at trapping currently used pesticides in the gaseous phase using the technique of high-volume sampling. *Anal. Bioanal. Chem.* 386, 1781–1789. <https://doi.org/10.1007/s00216-006-0737-2>
- Donald, D.B., Stern, G.A., Muir, D.C.G., Fowler, B.R., Miskimmin, B.M., Bailey, R., 1998. Chlorobornanes in water, sediment, and fish from toxaphene treated and untreated lakes in western Canada. *Environ. Sci. Technol.* 32, 1391–1397. <https://doi.org/10.1021/es9709051>
- Du, J., Li, H., Xu, S., Zhou, Q., Jin, M., Tang, J., 2019. A review of organophosphorus flame retardants (OPFRs): occurrence, bioaccumulation, toxicity, and organism exposure. *Environ. Sci. Pollut. Res.* 26, 22126–22136. <https://doi.org/10.1007/s11356-019-05669-y>
- Dunnivant, F.M., Coates, J.T., Elzerman, A.W., 1988. Experimentally determined Henry's law constants for 17 polychlorobiphenyl congeners. *Environ. Sci. Technol.* 22, 448–453. <https://doi.org/10.1021/es00169a013>
- EEA, 2021. European Union emission inventory report 1990-2019 under the UNECE Convention on Long-range Transboundary Air Pollution (Air Convention). <https://doi.org/https://doi.org/10.2800/701303>
- Endo, S., Hale, S.E., Goss, K.U., Arp, H.P.H., 2011. Equilibrium partition coefficients of diverse polar and nonpolar organic compounds to polyoxymethylene (POM) passive sampling devices. *Environ. Sci. Technol.* 45, 10124–10132. <https://doi.org/10.1021/es202894k>
- Erickson, M.D., Kaley, R.G., 2011. Applications of polychlorinated biphenyls. *Environ. Sci. Pollut. Res.*

- 18, 135–151. <https://doi.org/10.1007/s11356-010-0392-1>
- Estellano, V.H., Pozo, K., Harner, T., Franken, M., Zaballa, M., 2008. Altitudinal and seasonal variations of persistent organic pollutants in the Bolivian Andes mountains. *Environ. Sci. Technol.* 42, 2528–2534. <https://doi.org/10.1021/es702754m>
- Estellano, V.H., Pozo, K., Příbylová, P., Klánová, J., Audy, O., Focardi, S., 2017. Assessment of seasonal variations in persistent organic pollutants across the region of Tuscany using passive air samplers. *Environ. Pollut.* 222, 609–616. <https://doi.org/10.1016/j.envpol.2016.08.092>
- European Commission, 2008. Regulation (EC) No 1272/2008 - classification, labelling and packaging of substances and mixtures (CLP) | Safety and health at work EU-OSHA.
- Evcı, Y.M., Esen, F., Taşdemir, Y., 2016. Monitoring of Long-Term Outdoor Concentrations of PAHs with Passive Air Samplers and Comparison with Meteorological Data. *Arch. Environ. Contam. Toxicol.* 71, 246–256. <https://doi.org/10.1007/s00244-016-0292-6>
- Fairall, C.W., Bradley, E.F., Hare, J.E., Grachev, A.A., Edson, J.B., 2003. Bulk Parameterization of Air–Sea Fluxes: Updates and Verification for the COARE Algorithm. *J. Clim.* 16, 571–591. [https://doi.org/10.1175/1520-0442\(2003\)016<0571:BPOASF>2.0.CO;2](https://doi.org/10.1175/1520-0442(2003)016<0571:BPOASF>2.0.CO;2)
- Fairall, C.W., Bradley, E.F., Rogers, D.P., Edson, J.B., Young, G.S., 1996. Bulk parameterization of air-sea fluxes for Tropical Ocean-Global Atmosphere Coupled-Ocean Atmosphere Response Experiment. *J. Geophys. Res. Ocean.* 101, 3747–3764. <https://doi.org/10.1029/95JC03205>
- Fairall, C.W., Yang, M., Bariteau, L., Edson, J.B., Helmig, D., McGillis, W., Pezoa, S., Hare, J.E., Huebert, B., Blomquist, B., 2011. Implementation of the Coupled Ocean-Atmosphere Response Experiment flux algorithm with CO₂, dimethyl sulfide, and O₃. *J. Geophys. Res. Ocean.* 116, 0–09. <https://doi.org/10.1029/2010JC006884>
- Falconer, R.L., Bidleman, T.F., 1994. Vapor pressures and predicted particle/gas distributions of polychlorinated biphenyl congeners as functions of temperature and ortho-chlorine substitution. *Atmos. Environ.* 28, 547–554. [https://doi.org/10.1016/1352-2310\(94\)90130-9](https://doi.org/10.1016/1352-2310(94)90130-9)
- Fasnacht, M.P., Blough, N. V., 2002. Aqueous photodegradation of polycyclic aromatic hydrocarbons. *Environ. Sci. Technol.* 36, 4364–4369. <https://doi.org/10.1021/es025603k>
- Fernández, P., Carrera, G., Grimalt, J.O., 2005. Persistent organic pollutants in remote freshwater ecosystems. *Aquat. Sci.* 67, 263–273. <https://doi.org/10.1007/s00027-005-0747-8>
- Fernández, P., Carrera, G., Grimalt, J.O., Ventura, M., Camarero, L., Catalan, J., Nickus, U., Thies, H., Psenner, R., 2003. Factors governing the atmospheric deposition of polycyclic aromatic hydrocarbons to remote areas. *Environ. Sci. Technol.* 37, 3261–3267. <https://doi.org/10.1021/es020137k>
- Fernández, P., Grimalt, J.O., Vilanova, R.M., Fernández, P., Grimalt, J.O., Vilanova, R.M., 2002. Atmospheric gas-particle partitioning of polycyclic aromatic hydrocarbons in high mountain regions of Europe. *Environ. Sci. Technol.* 36, 1162–1168. <https://doi.org/10.1021/es010190t>
- Fernández, P., van Drooge, B.L., Arellano, L., Grimalt, J.O., 2021. Atmospheric deposition of semivolatile organic pollutants in European high mountains: Sources, settling and chemical degradation. *Sci. Total Environ.* 784, 147099. <https://doi.org/10.1016/j.scitotenv.2021.147099>
- Fernández, P., Vilanova, R.M., Grimalt, J.O., 1999. Sediment Fluxes of Polycyclic Aromatic Hydrocarbons in European High Altitude Mountain Lakes. *Environ. Sci. Technol.* 33, 3716–3722. <https://doi.org/10.1021/ES9904639>
- Ferrario, C., Finizio, A., Villa, S., 2017. Legacy and emerging contaminants in meltwater of three Alpine glaciers. *Sci. Total Environ.* 574, 350–357. <https://doi.org/10.1016/J.SCITOTENV.2016.09.067>
- Fick, A., 1855. Ueber Diffusion. *Ann. Phys.* 170, 59–86. <https://doi.org/10.1002/andp.18551700105>
- Finizio, A., Villa, S., Raffaele, F., Vighi, M., 2006. Variation of POP concentrations in fresh-fallen snow and air on an Alpine glacier (Monte Rosa). *Ecotoxicol. Environ. Saf.* 63, 25–32. <https://doi.org/10.1016/j.ecoenv.2005.05.004>
- Fowler, D., Cape, J.N., Leith, I.D., Choularton, T.W., Gay, M.J., Jones, A., 1988. The influence of altitude on rainfall composition at great dun fell. *Atmos. Environ.* 22, 1355–1362.

[https://doi.org/10.1016/0004-6981\(88\)90160-6](https://doi.org/10.1016/0004-6981(88)90160-6)

- Francisco, A.P., Harner, T., Eng, A., 2017. Measurement of polyurethane foam – air partition coefficients for semivolatile organic compounds as a function of temperature: Application to passive air sampler monitoring. *Chemosphere* 174, 638–642. <https://doi.org/10.1016/j.chemosphere.2017.01.135>
- Fu, F., Purvis-Roberts, K.L., Williams, B., 2020. Impact of the covid-19 pandemic lockdown on air pollution in 20 major cities around the world. *Atmosphere (Basel)*. 11, 1189. <https://doi.org/10.3390/atmos11111189>
- Fuller, E.N., Schettler, P.D., Giddings, J.C., 1966. A new method for prediction of binary gas-phase diffusion coefficients. *Ind. Eng. Chem.* 58, 18–27. <https://doi.org/10.1021/ie50677a007>
- Galassi, S., Valsecchi, S., Tartari, G.A., 1997. The Distribution of PCB's and Chlorinated Pesticides in Two Connected Himalayan Lakes. *Water, Air, Soil Pollut.* 99, 717–725. <https://doi.org/https://doi.org/10.1023/A:1018301220077>
- Gallego, E., Grimalt, J.O., Bartrons, M., Lopez, J.F., Camarero, L., Catalan, J., Stuchlik, E., Battarbee, R., 2007. Altitudinal gradients of PBDEs and PCBs in fish from European high mountain lakes. *Environ. Sci. Technol.* 41, 2196–2202. <https://doi.org/10.1021/es062197m>
- García-Solorio, L., Muro, C., De La Rosa, I., Amador-Muñoz, O., Ponce-Vélez, G., 2022. Organochlorine pesticides and polychlorinated biphenyls in high mountain lakes, Mexico. *Environ. Sci. Pollut. Res.* 1, 1–18. <https://doi.org/10.1007/s11356-022-19177-z>
- Genualdi, S.A., Hageman, K.J., Ackerman, L.K., Usenko, S., Massey Simonich, S.L., 2011. Sources and fate of chiral organochlorine pesticides in western U.S. National Park ecosystems. *Environ. Toxicol. Chem.* 30, 1533–1538. <https://doi.org/10.1002/etc.538>
- Gomez-Belinchon, J.I., Grimalt, J.O., Albaiges, J., 1988. Intercomparison study of liquid-liquid extraction and adsorption on polyurethane and Amberlite XAD-2 for the analysis of hydrocarbons, polychlorobiphenyls, and fatty acids dissolved in seawater. *Environ. Sci. Technol.* 22, 677–685. <https://doi.org/10.1021/es00171a010>
- Gong, P., Wang, X., 2022. Critical roles of secondary sources in global cycling of persistent organic pollutants under climate change. *J. Hazard. Mater. Adv.* 6, 100064. <https://doi.org/10.1016/j.hazadv.2022.100064>
- Gong, P., Wang, X., Pokhrel, B., Wang, H., Liu, X.X., Liu, X.X., Wania, F., 2019. Trans-Himalayan Transport of Organochlorine Compounds: Three-Year Observations and Model-Based Flux Estimation. *Environ. Sci. Technol.* 53, 6773–6783. <https://doi.org/10.1021/acs.est.9b01223>
- González-Gaya, B., Fernández-Pinos, M.C., Morales, L., Méjanelle, L., Abad, E., Piña, B., Duarte, C.M., Jiménez, B., Dachs, J., 2016. High atmosphere-ocean exchange of semivolatile aromatic hydrocarbons. *Nat. Geosci.* 9, 438–442. <https://doi.org/10.1038/ngeo2714>
- Górecki, T., Namieśnik, J., 2002. Passive sampling. *TrAC - Trends Anal. Chem.* 21, 276–291. [https://doi.org/10.1016/S0165-9936\(02\)00407-7](https://doi.org/10.1016/S0165-9936(02)00407-7)
- Gossett, R.W., Brown, D.A., Young, D.R., 1983. Predicting the bioaccumulation of organic compounds in marine organisms using octanol/water partition coefficients. *Mar. Pollut. Bull.* 14, 387–392. [https://doi.org/10.1016/0025-326X\(83\)90604-5](https://doi.org/10.1016/0025-326X(83)90604-5)
- Gouin, T., Harner, T., Blanchard, P., Mackay, D., 2005. Passive and active air samplers as complementary methods for investigating persistent organic pollutants in the Great Lakes Basin. *Environ. Sci. Technol.* 39, 9115–9122. <https://doi.org/10.1021/es051397f>
- Gouin, T., MacKay, D., Jones, K.C., Harner, T., Meijer, S.N., 2004. Evidence for the “grasshopper” effect and fractionation during long-range atmospheric transport of organic contaminants. *Environ. Pollut.* 128, 139–148. <https://doi.org/10.1016/j.envpol.2003.08.025>
- Grandjean, P., Landrigan, P.J., 2014. Neurobehavioural effects of developmental toxicity. *Lancet Neurol.* 13, 330–338. [https://doi.org/10.1016/S1474-4422\(13\)70278-3](https://doi.org/10.1016/S1474-4422(13)70278-3)
- Greenwood, R., Mills, G., Vrana, B., 2007. *Passive Sampling Techniques in Environmental Monitoring*. Elsevier.

- Grimalt, J.O., Borghini, F., Sanchez-Hernandez, J.C., Barra, R., Torres García, C.J., Focardi, S., 2004a. Temperature dependence of the distribution of organochlorine compounds in the mosses of the Andean mountains. *Environ. Sci. Technol.* 38, 5386–5392. <https://doi.org/10.1021/es040051m>
- Grimalt, J.O., Fernandez, P., Berdie, L., Vilanova, R.M., Catalan, J., Psenner, R., Hofer, R., Appleby, P.G., Rosseland, B.O., Lien, L., Massabuau, J.C., Battarbee, R.W., 2001. Selective trapping of organochlorine compounds in mountain lakes of temperate areas. *Environ. Sci. Technol.* 35, 2690–2697. <https://doi.org/10.1021/es000278r>
- Grimalt, J.O., Fernández, P., Quiroz, R., 2009. Input of organochlorine compounds by snow to European high mountain lakes. *Freshw. Biol.* 54, 2533–2542. <https://doi.org/10.1111/j.1365-2427.2009.02302.x>
- Grimalt, J.O., Sunyer, J., Moreno, V., Amaral, O.C., Sala, M., Rosell, A., Anto, J.M., Albaiges, J., 1994. Risk excess of soft-tissue sarcoma and thyroid cancer in a community exposed to airborne organochlorinated compound mixtures with a high hexachlorobenzene content. *Int. J. Cancer* 56, 200–203. <https://doi.org/10.1002/ijc.2910560209>
- Grimalt, J.O., van Drooge, B.L., Ribes, A., Vilanova, R.M., Fernandez, P., Appleby, P., 2004b. Persistent organochlorine compounds in soils and sediments of European high altitude mountain lakes. *Chemosphere* 54, 1549–1561. <https://doi.org/10.1016/J.CHEMOSPHERE.2003.09.047>
- Guérin, F., Abril, G., Serça, D., Delon, C., Richard, S., Delmas, R., Tremblay, A., Varfalvy, L., 2007. Gas transfer velocities of CO₂ and CH₄ in a tropical reservoir and its river downstream. *J. Mar. Syst.* 66, 161–172. <https://doi.org/10.1016/j.jmarsys.2006.03.019>
- Gustavsson, J., Wiberg, K., Nguyen, M.A., Josefsson, S., Laudon, H., Ahrens, L., 2019. Seasonal trends of legacy and alternative flame retardants in river water in a boreal catchment. *Sci. Total Environ.* 692, 1097–1105. <https://doi.org/10.1016/j.scitotenv.2019.07.158>
- Guzzella, L., Poma, G., De Paolis, A., Roscioli, C., Viviano, G., 2011. Organic persistent toxic substances in soils, waters and sediments along an altitudinal gradient at Mt. Sagarmatha, Himalayas, Nepal. *Environ. Pollut.* 159, 2552–2564. <https://doi.org/10.1016/J.ENVPOL.2011.06.015>
- Harner, T., 2021. 2021 v10 Template for calculating PUF and SIP disk sample air volumes. <https://doi.org/https://doi.org/10.13140/RG.2.1.3998.8884>
- Harner, T., Bartkow, M., Holoubek, I., Klanova, J., Wania, F., Gioia, R., Moeckel, C., Sweetman, A.J., Jones, K.C., 2006a. Passive air sampling for persistent organic pollutants: Introductory remarks to the special issue. *Environ. Pollut.* 144, 361–364. <https://doi.org/10.1016/j.envpol.2005.12.044>
- Harner, T., Bidleman, T.F., 1998. Measurement of octanol-air partition coefficients for polycyclic aromatic hydrocarbons and polychlorinated naphthalenes. *J. Chem. Eng. Data* 43, 40–46. <https://doi.org/10.1021/je970175x>
- Harner, T., Farrar, N.J., Shoeib, M., Jones, K.C., Gobas, F.A.P.C., 2003. Characterization of Polymer-Coated Glass as a Passive Air Sampler for Persistent Organic Pollutants. *Environ. Sci. Technol.* 37, 2486–2493. <https://doi.org/10.1021/es0209215>
- Harner, T., Mackay, D., 1995. Measurement of Octanol-Air Partition Coefficients for Chlorobenzenes, PCBs, and DDT. *Environ. Sci. Technol.* 29, 1599–1606. <https://doi.org/10.1021/es00006a025>
- Harner, T., Pozo, K., Gouin, T., Macdonald, A.M., Hung, H., Caine, J., Peters, A., 2006b. Global pilot study for persistent organic pollutants (POPs) using PUF disk passive air samplers. *Environ. Pollut.* 144, 445–452. <https://doi.org/10.1016/j.envpol.2005.12.053>
- Harner, T., Shoeib, M., Diamond, M., Ikonou, M., Stern, G., 2006c. Passive sampler derived air concentrations of PBDEs along an urban-rural transect: Spatial and temporal trends. *Chemosphere* 64, 262–267. <https://doi.org/10.1016/j.chemosphere.2005.12.018>
- Harner, T., Shoeib, M., Diamond, M., Stern, G., Rosenberg, B., 2004. Using passive air samplers to assess urban-rural trends for persistent organic pollutants. 1. Polychlorinated biphenyls and organochlorine pesticides. *Environ. Sci. Technol.* 38, 4474–4483. <https://doi.org/10.1021/es040302r>
- Hayduk, W., Laudie, H., 1974. Prediction of diffusion coefficients for nonelectrolytes in dilute aqueous solutions. *AIChE J.* 20, 611–615. <https://doi.org/10.1002/aic.690200329>

- Haynes, W.M., Lide, D.R., Bruno, T.J. (Eds.), 2016. CRC Handbook of Chemistry and Physics (97th ed.). CRC Press. <https://doi.org/10.1201/9781315380476>
- He, J., Balasubramanian, R., 2010. A comparative evaluation of passive and active samplers for measurements of gaseous semi-volatile organic compounds in the tropical atmosphere. *Atmos. Environ.* 44, 884–891. <https://doi.org/10.1016/j.atmosenv.2009.12.009>
- Heindel, J.J., Blumberg, B., Cave, M., Machtinger, R., Mantovani, A., Mendez, M.A., Nadal, A., Palanza, P., Panzica, G., Sargis, R., Vandenberg, L.N., vom Saal, F., 2017. Metabolism disrupting chemicals and metabolic disorders. *Reprod. Toxicol.* 68, 3–33. <https://doi.org/10.1016/j.reprotox.2016.10.001>
- Heo, J., Lee, G., 2014. Field-measured uptake rates of PCDDs/Fs and dl-PCBs using PUF-disk passive air samplers in Gyeonggi-do, South Korea. *Sci. Total Environ.* 491–492, 42–50. <https://doi.org/10.1016/j.scitotenv.2014.03.073>
- Herbert, B.M.J., Villa, S., Halsall, C.J., 2006. Chemical interactions with snow: Understanding the behavior and fate of semi-volatile organic compounds in snow. *Ecotoxicol. Environ. Saf.* 63, 3–16. <https://doi.org/10.1016/J.ECOENV.2005.05.012>
- Higbie, R., 1935. The Rate of Absorption of a Pure Gas into a Still Liquid during Short Periods of Exposure. *Trans. Am. Inst. Chem. Eng.* 35, 365–389.
- Hoff, R.M., 1994. An Error Budget for the Determination of the Atmospheric Mass Loading of Toxic Chemicals in the Great Lakes. *J. Great Lakes Res.* 20, 229–239. [https://doi.org/10.1016/S0380-1330\(94\)71143-6](https://doi.org/10.1016/S0380-1330(94)71143-6)
- Holt, E., Bohlin-Nizzetto, P., Borůvková, J., Harner, T., Kalina, J., Melymuk, L., Klánová, J., 2017. Using long-term air monitoring of semi-volatile organic compounds to evaluate the uncertainty in polyurethane-disk passive sampler-derived air concentrations. *Environ. Pollut.* 220, 1100–1111. <https://doi.org/10.1016/j.envpol.2016.11.030>
- Hornbuckle, K.C., Jeremiason, J.D., Sweet, C.W., Eisenreich, S.J., 1994. Seasonal Variations in Air-Water Exchange of Polychlorinated Biphenyls in Lake Superior. *Environ. Sci. Technol.* 28, 1491–1501. <https://doi.org/10.1021/es00057a018>
- Hough, A.M., 1987. A computer modelling study of the chemistry occurring during cloud formation over hills. *Atmos. Environ.* 21, 1073–1095. [https://doi.org/10.1016/0004-6981\(87\)90235-6](https://doi.org/10.1016/0004-6981(87)90235-6)
- Howard, P.H., Boethling, R.S., Jarvis, W.F., Meylan, W.M., Michalenko, E.M., 1991. Handbook of Environmental Degradation Rates. CRC Press. <https://doi.org/10.1201/9780203719329>
- Huckins, J.N., Manuweera, G.K., Petty, J.D., Mackay, D., Lebo, J.A., 1993. Lipid-Containing Semipermeable Membrane Devices for Monitoring Organic Contaminants in Water. *Environ. Sci. Technol.* 27, 2489–2496. <https://doi.org/10.1021/es00048a028>
- Huckins, J.N., Petty, J.D., Booij, K., 2006. Monitors of organic chemicals in the environment: Semipermeable membrane devices. Springer US. <https://doi.org/10.1007/0-387-35414-X>
- Huckins, J.N., Petty, J.D., Lebo, J.A., Almeida, F. V., Booij, K., Alvarez, D.A., Cranor, W.L., Clark, R.C., Mogensen, B.B., 2002. Development of the permeability/performance reference compound approach for in situ calibration of semipermeable membrane devices. *Environ. Sci. Technol.* 36, 85–91. <https://doi.org/10.1021/es010991w>
- Huckins, J.N., Tubergen, M.W., Manuweera, G.K., 1990. Semipermeable membrane devices containing model lipid: A new approach to monitoring the bioavailability of lipophilic contaminants and estimating their bioconcentration potential. *Chemosphere* 20, 533–552. [https://doi.org/10.1016/0045-6535\(90\)90110-F](https://doi.org/10.1016/0045-6535(90)90110-F)
- Hulscher, T.E.M. Ten, van Der Velde, L.E., Bruggeman, W.A., 1992. Temperature dependence of Henry's law constants for selected chlorobenzenes, polychlorinated biphenyls and polycyclic aromatic hydrocarbons. *Environ. Toxicol. Chem.* 11, 1595–1603. <https://doi.org/10.1002/etc.5620111109>
- Hussain, B.A., Westgate, J.N., Hayward, S.J., Shunthirasingham, C., Brown, T.N., Hung, H., Lei, Y.D., Wania, F., 2019. Polycyclic aromatic hydrocarbons and polychlorinated biphenyls in soils and atmosphere of Western Canadian mountains: The role of source proximity, precipitation, forest cover and mountain cold-trapping. *Atmos. Environ.* X 1, 100004.

- <https://doi.org/10.1016/j.aeaoa.2018.100004>
- Hussain, K., Rahman, M., Prakash, A., Sarma, K.P., Hoque, R.R., 2016. Atmospheric bulk deposition of PAHs over Brahmaputra valley: Characteristics and influence of meteorology. *Aerosol Air Qual. Res.* 16, 1675–1689. <https://doi.org/10.4209/aaqr.2016.02.0060>
- Iwata, H., Tanabe, S., Sakai, N., Tatsukawa, R., 1993. Distribution of persistent organochlorines in the oceanic air and surface seawater and the role of ocean on their global transport and fate. *Environ. Sci. Technol.* 27, 1080–1098. <https://doi.org/10.1021/es00043a007>
- Jähne, B., Münnich, K.O., Böisinger, R., Dutzi, A., Huber, W., Libner, P., 1987. On the parameters influencing air-water gas exchange. *J. Geophys. Res. Ocean.* 92, 1937–1949. <https://doi.org/10.1029/JC092iC02p01937>
- Jarque, S., Bosch, C., Casado, M., Grimalt, J.O., Raldúa, D., Piña, B., 2014. Analysis of hepatic deiodinase 2 mRNA levels in natural fish lake populations exposed to different levels of putative thyroid disrupters. *Environ. Pollut.* 187, 210–213. <https://doi.org/10.1016/j.envpol.2014.01.010>
- Jarque, S., Gallego, E., Bartrons, M., Catalan, J., Grimalt, J.O., Piña, B., 2010. Altitudinal and thermal gradients of hepatic Cyp1A gene expression in natural populations of *Salmo trutta* from high mountain lakes and their correlation with organohalogen loads. *Environ. Pollut.* 158, 1392–1398. <https://doi.org/10.1016/j.envpol.2010.01.003>
- Jarque, S., Quirós, L., Grimalt, J.O., Gallego, E., Catalan, J., Lackner, R., Piña, B., 2015. Background fish feminization effects in European remote sites. *Sci. Rep.* 5, 11292. <https://doi.org/10.1038/srep11292>
- Jaward, F.M., Di Guardo, A., Nizzetto, L., Cassani, C., Raffaele, F., Ferretti, R., Jones, K.C., 2005a. PCBs and selected organochlorine compounds in Italian mountain air: The influence of altitude and forest ecosystem type. *Environ. Sci. Technol.* 39, 3455–3463. <https://doi.org/10.1021/es048160o>
- Jaward, F.M., Farrar, N.J., Harner, T., Sweetman, A.J., Jones, K.C., 2004a. Passive air sampling of polycyclic aromatic hydrocarbons and polychlorinated naphthalenes across Europe. *Environ. Toxicol. Chem.* 23, 1355–1364. <https://doi.org/10.1897/03-420>
- Jaward, F.M., Farrar, N.J., Harner, T., Sweetman, A.J., Jones, K.C., 2004b. Passive Air Sampling of PCBs, PBDEs, and Organochlorine Pesticides Across Europe. *Environ. Sci. Technol.* 38, 34–41. <https://doi.org/10.1021/es034705n>
- Jaward, F.M., Zhang, G., Nam, J.J., Sweetman, A.J., Obbard, J.P., Kobara, Y., Jones, K.C., 2005b. Passive air sampling of polychlorinated biphenyls, organochlorine compounds, and polybrominated diphenyl ethers across Asia. *Environ. Sci. Technol.* 39, 8638–8645. <https://doi.org/10.1021/es051382h>
- Jevtic, M., Matkovic, V., Van Den Hazel, P., Bouland, C., 2021. Environment-lockdown, air pollution and related diseases: Could we learn something and make it last? *Eur. J. Public Health* 31, IV36–IV39. <https://doi.org/10.1093/eurpub/ckab157>
- Johnson, M.T., 2010. A numerical scheme to calculate temperature and salinity dependent air-water transfer velocities for any gas. *Ocean Sci.* 6, 913–932. <https://doi.org/10.5194/os-6-913-2010>
- Kalina, J., White, K.B., Scheringer, M., Příbylová, P., Kukučka, P., Audy, O., Klánová, J., 2019. Comparability of long-term temporal trends of POPs from co-located active and passive air monitoring networks in Europe. *Environ. Sci. Process. Impacts* 21, 1132–1142. <https://doi.org/10.1039/c9em00136k>
- Kallenborn, R., 2006. Persistent organic pollutants (POPs) as environmental risk factors in remote high-altitude ecosystems. *Ecotoxicol. Environ. Saf.* 63, 100–107. <https://doi.org/10.1016/J.ECOENV.2005.02.016>
- Keith, L.H., 2015. The Source of U.S. EPA's Sixteen PAH Priority Pollutants. *Polycycl. Aromat. Compd.* 35, 147–160. <https://doi.org/10.1080/10406638.2014.892886>
- Kelce, W.R., Stone, C.R., Laws, S.C., Gray, L.E., Kemppainen, J.A., Wilson, E.M., 1995. Persistent DDT metabolite p,p'-DDE is a potent androgen receptor antagonist. *Nature* 375, 581–585. <https://doi.org/10.1038/375581a0>
- Kemmlin, S., Hahn, O., Jann, O., 2003. Emissions of organophosphate and brominated flame retardants

- from selected consumer products and building materials. *Atmos. Environ.* 37, 5485–5493. <https://doi.org/10.1016/j.atmosenv.2003.09.025>
- Keyte, I.J., Harrison, R.M., Lammel, G., 2013. Chemical reactivity and long-range transport potential of polycyclic aromatic hydrocarbons—a review. *Chem. Soc. Rev.* 42, 9333–9391. <https://doi.org/10.1039/c3cs60147a>
- Kim, D., Young, T.M., Anastasio, C., 2013. Phototransformation rate constants of PAHs associated with soot particles. *Sci. Total Environ.* 443, 896–903. <https://doi.org/10.1016/j.scitotenv.2012.11.055>
- Kingston, J.K., Greenwood, R., Mills, G.A., Morrison, G.M., Persson, L.B., 2000. Development of a novel passive sampling system for the time-averaged measurement of a range of organic pollutants in aquatic environments. *J. Environ. Monit.* 2, 487–495. <https://doi.org/10.1039/B003532G>
- Kirchner, M., Faus-Kessler, T., Jakobi, G., Levy, W., Henkelmann, B., Bernhöft, S., Kotalik, J., Zsolnay, A., Bassan, R., Belis, C., Kräuchi, N., Moche, W., Simončič, P., Uhl, M., Weiss, P., Schramm, K.-W., 2009. Vertical distribution of organochlorine pesticides in humus along Alpine altitudinal profiles in relation to ambient parameters. *Environ. Pollut.* 157, 3238–3247. <https://doi.org/10.1016/j.envpol.2009.06.011>
- Klánová, J., Èupr, P., Kohoutek, J., Harner, T., 2008. Assessing the Influence of Meteorological Parameters on the Performance of Polyurethane Foam-Based Passive Air Samplers. *Environ. Sci. Technol.* 42, 550–555. <https://doi.org/10.1021/es072098o>
- Klaus, M., Vachon, D., 2020. Challenges of predicting gas transfer velocity from wind measurements over global lakes. *Aquat. Sci.* 82, 53. <https://doi.org/10.1007/s00027-020-00729-9>
- Kosek, K., Ruman, M., 2021. Arctic freshwater environment altered by the accumulation of commonly determined and potentially new pops. *Water* 13, 1739. <https://doi.org/10.3390/w13131739>
- Kume, A., Numata, S., Watanabe, K., Honoki, H., Nakajima, H., Ishida, M., 2009. Influence of air pollution on the mountain forests along the Tateyama-Kurobe Alpine route. *Ecol. Res.* 24, 821–830. <https://doi.org/10.1007/s11284-008-0557-2>
- Kutz, F.W., Wood, P.H., Bottimore, D.P., 1991. Organochlorine pesticides and polychlorinated biphenyls in human adipose tissue. *Rev. Environ. Contam. Toxicol.* 120, 1–82. https://doi.org/10.1007/978-1-4612-3080-9_1
- Kwok, E.S.C., Atkinson, R., Arey, J., 1995. Rate Constants for the Gas-Phase Reactions of the OH Radical with Dichlorobiphenyls, 1-Chlorodibenzo-p-dioxin, 1,2-Dimethoxybenzene, and Diphenyl Ether: Estimation of OH Radical Reaction Rate Constants for PCBs, PCDDs, and PCDFs. *Environ. Sci. Technol.* 29, 1591–1598. <https://doi.org/10.1021/es00006a024>
- Lammel, G., Sehili, A.M., Bond, T.C., Feichter, J., Grassl, H., 2009. Gas/particle partitioning and global distribution of polycyclic aromatic hydrocarbons - A modelling approach. *Chemosphere* 76, 98–106. <https://doi.org/10.1016/j.chemosphere.2009.02.017>
- Landers, D.H., Simonich, S.M., Jaffe, D., Geiser, L., Campbell, D.H., Schwindt, A., Schreck, C., Kent, M., Hafner, W., Taylor, H.E., Hageman, K., Usenko, S., Ackerman, L., Schrlau, J., Rose, N., Blett, T., Erway, M.M., 2010. The Western Airborne Contaminant Assessment Project (WACAP): An Interdisciplinary Evaluation of the Impacts of Airborne Contaminants in Western U.S. National Parks. *Environ. Sci. Technol.* 44, 855–859. <https://doi.org/10.1021/es901866e>
- Lei, Y.D., Wania, F., 2004. Is rain or snow a more efficient scavenger of organic chemicals? *Atmos. Environ.* 38, 3557–3571. <https://doi.org/10.1016/J.ATMOSENV.2004.03.039>
- LeNoir, J.S., McConnell, L.L., Fellers, G.M., Cahill, T.M., Seiber, J.N., 1999. Summertime transport of current-use pesticides from California's Central Valley to the Sierra Nevada Mountain Range, USA. *Environ. Toxicol. Chem.* 18, 2715–2722. <https://doi.org/10.1002/ETC.5620181210>
- Li, J., He, J., Li, Y., Liu, Y., Li, W., Wu, N., Zhang, L., Zhang, Y., Niu, Z., 2019. Assessing the threats of organophosphate esters (flame retardants and plasticizers) to drinking water safety based on USEPA oral reference dose (RfD) and oral cancer slope factor (SFO). *Water Res.* 154, 84–93. <https://doi.org/10.1016/j.watres.2019.01.035>
- Li, Q., Vilela, P., Tariq, S., Nam, K., Yoo, C., 2022. Multiple land-use fugacity model to assess the transport

- and fate of polycyclic aromatic hydrocarbons in urban and suburban areas. *Urban Clim.* 45, 101263. <https://doi.org/10.1016/j.uclim.2022.101263>
- Li, Y., Wania, F., 2021. Partitioning between polyurethane foam and the gas phase: Data compilation, uncertainty estimation and implications for air sampling. *Environ. Sci. Process. Impacts* 23, 723–734. <https://doi.org/10.1039/d1em00036e>
- Liagkouridis, I., Cousins, A.P., Cousins, I.T., 2015. Physical-chemical properties and evaluative fate modelling of “emerging” and “novel” brominated and organophosphorus flame retardants in the indoor and outdoor environment. *Sci. Total Environ.* 524–525, 416–426. <https://doi.org/10.1016/j.scitotenv.2015.02.106>
- Liss, P.S., 1973. Processes of gas exchange across an air-water interface. *Deep. Res. Oceanogr. Abstr.* 20, 221–238. [https://doi.org/10.1016/0011-7471\(73\)90013-2](https://doi.org/10.1016/0011-7471(73)90013-2)
- Liss, P.S., Merlivat, L., 1986. Air-Sea Gas Exchange Rates: Introduction and Synthesis, in: Buat-Ménard, P. (Ed.), *The Role of Air-Sea Exchange in Geochemical Cycling*. Springer, Dordrecht, pp. 113–127. https://doi.org/10.1007/978-94-009-4738-2_5
- Liu, H.H., Wong, C.S., Zeng, E.Y., 2013. Recognizing the limitations of performance reference compound (PRC)-calibration technique in passive water sampling. *Environ. Sci. Technol.* 47, 10104–10105. <https://doi.org/10.1021/es403353d>
- Liu, Y., Liggio, J., Harner, T., Jantunen, L., Shoeib, M., Li, S.M., 2014. Heterogeneous OH initiated oxidation: A possible explanation for the persistence of organophosphate flame retardants in air. *Environ. Sci. Technol.* 48, 1041–1048. <https://doi.org/10.1021/es404515k>
- Liu, Y., Wang, S., McDonough, C.A., Khairy, M., Muir, D., Lohmann, R., 2016. Estimation of Uncertainty in Air-Water Exchange Flux and Gross Volatilization Loss of PCBs: A Case Study Based on Passive Sampling in the Lower Great Lakes. *Environ. Sci. Technol.* 50, 10894–10902. <https://doi.org/10.1021/acs.est.6b02891>
- Llop, S., Murcia, M., Alvarez-Pedrerol, M., Grimalt, J.O., Santa-Marina, L., Julvez, J., Goñi-Irigoyen, F., Espada, M., Ballester, F., Rebagliato, M., Lopez-Espinosa, M.J., 2017. Association between exposure to organochlorine compounds and maternal thyroid status: Role of the iodothyronine deiodinase 1 gene. *Environ. Int.* 104, 83–90. <https://doi.org/10.1016/j.envint.2016.12.013>
- Lohmann, R., 2012. Critical review of low-density polyethylene’s partitioning and diffusion coefficients for trace organic contaminants and implications for its use as a passive sampler. *Environ. Sci. Technol.* 46, 606–618. <https://doi.org/10.1021/es202702y>
- Lohmann, R., Breivik, K., Dachs, J., Muir, D., 2007. Global fate of POPs: Current and future research directions. *Environ. Pollut.* 150, 150–165. <https://doi.org/10.1016/j.envpol.2007.06.051>
- Lohmann, R., Gioia, R., Jones, K.C., Nizzetto, L., Temme, C., Xie, Z., Schulz-Bull, D., Hand, I., Morgan, E., Jantunen, L., 2009. Organochlorine pesticides and PAHs in the surface water and atmosphere of the North Atlantic and Arctic Ocean. *Environ. Sci. Technol.* 43, 5633–5639. <https://doi.org/10.1021/es901229k>
- Lohmann, R., Muir, D., 2010. Global aquatic passive sampling (AQUA-GAPS): Using passive samplers to monitor POPs in the waters of the world. *Environ. Sci. Technol.* 44, 860–864. <https://doi.org/10.1021/es902379g>
- Lohmann, R., Muir, D., Zeng, E.Y., Bao, L.-J.J., Allan, I.J., Arinaitwe, K., Booij, K., Helm, P., Kaserzon, S., Mueller, J.F., Shibata, Y., Smedes, F., Tsapakis, M., Wong, C.S., You, J., 2017. Aquatic Global Passive Sampling (AQUA-GAPS) Revisited: First Steps toward a Network of Networks for Monitoring Organic Contaminants in the Aquatic Environment. *Environ. Sci. Technol.* 51, 1060–1067. <https://doi.org/10.1021/acs.est.6b05159>
- Lopez-Espinosa, M.-J., Murcia, M., Iñiguez, C., Vizcaino, E., Costa, O., Fernández-Somoano, A., Basterrechea, M., Lertxundi, A., Guxens, M., Gascon, M., Goñi-Irigoyen, F., Grimalt, J.O., Tardón, A., Ballester, F., 2016. Organochlorine Compounds and Ultrasound Measurements of Fetal Growth in the INMA Cohort (Spain). *Environ. Health Perspect.* 124, 157–163. <https://doi.org/10.1289/ehp.1408907>

- Luarte, T., Tucca, F., Nimptsch, J., Woelfl, S., Casas, G., Dachs, J., Chiang, G., Pozo, K., Barra, R., Galbán-Malagón, C., 2022. Occurrence and air-water diffusive exchange legacy persistent organic pollutants in an oligotrophic north Patagonian lake. *Environ. Res.* 204, 112042. <https://doi.org/10.1016/J.ENVRES.2021.112042>
- Luch, A., 2005. *The Carcinogenic Effects of Polycyclic Aromatic Hydrocarbons, The Carcinogenic Effects of Polycyclic Aromatic Hydrocarbons*. Imperial College Press. <https://doi.org/10.1142/p306>
- Ma, J., Hung, H., Tian, C., Kallenborn, R., 2011. Revolatilization of persistent organic pollutants in the Arctic induced by climate change. *Nat. Clim. Chang.* 1, 255–260. <https://doi.org/10.1038/nclimate1167>
- Ma, Y., Adelman, D.A., Bauerfeind, E., Cabrerizo, A., McDonough, C.A., Muir, D., Soltwedel, T., Sun, C., Wagner, C.C., Sunderland, E.M., Lohmann, R., 2018. Concentrations and Water Mass Transport of Legacy POPs in the Arctic Ocean. *Geophys. Res. Lett.* 45, 12,972–12,981. <https://doi.org/10.1029/2018GL078759>
- Ma, Y., Vojta, S., Becanova, J., Habtemichael, A.Z., Adelman, D.A., Muir, D., Lohmann, R., 2021. Spatial distribution and air–water exchange of organophosphate esters in the lower Great Lakes. *Environ. Pollut.* 286, 117349. <https://doi.org/10.1016/j.envpol.2021.117349>
- MacIntyre, S., Jonsson, A., Jansson, M., Aberg, J., Turney, D.E., Miller, S.D., 2010. Buoyancy flux, turbulence, and the gas transfer coefficient in a stratified lake. *Geophys. Res. Lett.* 37, 24604. <https://doi.org/10.1029/2010GL044164>
- Mackay, D., Wania, F., 1995. Transport of contaminants to the Arctic: partitioning, processes and models. *Sci. Total Environ.* 160–161, 25–38. [https://doi.org/10.1016/0048-9697\(95\)04342-X](https://doi.org/10.1016/0048-9697(95)04342-X)
- Mackay, D., Yeun, A.T.K., 1983. Mass Transfer Coefficient Correlations for Volatilization of Organic Solutes from Water. *Environ. Sci. Technol.* 17, 211–217. <https://doi.org/10.1021/es00110a006>
- Mäkinen, M.S.E., Mäkinen, M.R.A., Koistinen, J.T.B., Pasanen, A.-L., Pasanen, P.O., Kalliokoski, P.J., Korpi, A.M., 2009. Respiratory and Dermal Exposure to Organophosphorus Flame Retardants and Tetrabromobisphenol A at Five Work Environments. *Environ. Sci. Technol.* 43, 941–947. <https://doi.org/10.1021/es802593t>
- Mari, M., Nadal, M., Schuhmacher, M., Domingo, J.L., 2008a. Monitoring PCDD/Fs, PCBs and metals in the ambient air of an industrial area of Catalonia, Spain. *Chemosphere* 73, 990–998. <https://doi.org/10.1016/j.chemosphere.2008.06.025>
- Mari, M., Schuhmacher, M., Feliubadaló, J., Domingo, J.L., 2008b. Air concentrations of PCDD/Fs, PCBs and PCNs using active and passive air samplers. *Chemosphere* 70, 1637–1643. <https://doi.org/10.1016/j.chemosphere.2007.07.076>
- Marklund, A., Andersson, B., Haglund, P., 2005. Organophosphorus flame retardants and plasticizers in air from various indoor environments. *J. Environ. Monit.* 7, 814–819. <https://doi.org/10.1039/b505587c>
- Markovic, M.Z., Prokop, S., Staebler, R.M., Liggio, J., Harner, T., 2015. Evaluation of the particle infiltration efficiency of three passive samplers and the PS-1 active air sampler. *Atmos. Environ.* 112, 289–293. <https://doi.org/10.1016/j.atmosenv.2015.04.051>
- Marquès, M., Mari, M., Sierra, J., Nadal, M., Domingo, J.L., 2017. Solar radiation as a swift pathway for PAH photodegradation: A field study. *Sci. Total Environ.* 581–582, 530–540. <https://doi.org/10.1016/j.scitotenv.2016.12.161>
- Martin, H., Patterson, B.M., Davis, G.B., Grathwohl, P., 2003. Field trial of contaminant groundwater monitoring: Comparing time-integrating ceramic dosimeters and conventional water sampling. *Environ. Sci. Technol.* 37, 1360–1364. <https://doi.org/10.1021/es026067z>
- Mastral, A.M., Callén, M.S., 2000. A review on polycyclic aromatic hydrocarbon (PAH): Emissions from energy generation. *Environ. Sci. Technol.* 34, 3051–3057. <https://doi.org/10.1021/es001028d>
- McDonough, C.A., De Silva, A.O., Sun, C., Cabrerizo, A., Adelman, D., Soltwedel, T., Bauerfeind, E., Muir, D.C.G., Lohmann, R., 2018. Dissolved Organophosphate Esters and Polybrominated Diphenyl Ethers in Remote Marine Environments: Arctic Surface Water Distributions and Net Transport through Fram Strait. *Environ. Sci. Technol.* 52, 6208–6216. <https://doi.org/10.1021/acs.est.8b01127>

- McFarland, V.A., Clarke, J.U., 1989. Environmental occurrence, abundance, and potential toxicity of polychlorinated biphenyl congeners: Considerations for a congener-specific analysis. *Environ. Health Perspect.* 81, 225–239. <https://doi.org/10.1289/ehp.8981225>
- Meeker, J.D., Stapleton, H.M., 2010. House Dust Concentrations of Organophosphate Flame Retardants in Relation to Hormone Levels and Semen Quality Parameters. *Environ. Health Perspect.* 118, 318–323. <https://doi.org/10.1289/ehp.0901332>
- Meijer, S.N., Dachs, J., Fernandez, P., Camarero, L., Catalan, J., Del Vento, S., van Drooge, B., Jurado, E., Grimalt, J.O., 2006. Modelling the dynamic air-water-sediment coupled fluxes and occurrence of polychlorinated biphenyls in a high altitude lake. *Environ. Pollut.* 140, 546–560. <https://doi.org/10.1016/j.envpol.2005.06.015>
- Meijer, S.N., Grimalt, J.O., Fernandez, P., Dachs, J., 2009. Seasonal fluxes and temperature-dependent accumulation of persistent organic pollutants in lakes: The role of internal biogeochemical cycling. *Environ. Pollut.* 157, 1815–1822. <https://doi.org/10.1016/J.ENVPOL.2009.01.024>
- Meijer, S.N., Steinnes, E., Ockenden, W.A., Jones, K.C., 2002. Influence of Environmental Variables on the Spatial Distribution of PCBs in Norwegian and U.K. Soils: Implications for Global Cycling. *Environ. Sci. Technol.* 36, 2146–2153. <https://doi.org/10.1021/es010322i>
- Melymuk, L., Nizzetto, P.B., Harner, T., White, K.B., Wang, X., Tominaga, M.Y., He, J., Li, J., Ma, J., Ma, W.-L.L., Aristizábal, B.H., Dreyer, A., Jiménez, B., Muñoz-Arnanz, J., Odabasi, M., Dumanoglu, Y., Yaman, B., Graf, C., Sweetman, A., Klánová, J., Dryer, A., Jiménez, B., Muñoz-Arnanz, J., Odabasi, M., Dumanoglu, Y., Yaman, B., Graf, C., Sweetman, A., Klánová, J., 2021. Global intercomparison of polyurethane foam passive air samplers evaluating sources of variability in SVOC measurements. *Environ. Sci. Policy* 125, 1–9. <https://doi.org/10.1016/j.envsci.2021.08.003>
- Mesquita, S.R., van Drooge, B., Barata, C., Vieira, N., Guimarães, L., Piña, B., 2014a. Toxicity of atmospheric particle-bound PAHs: an environmental perspective. *Environ. Sci. Pollut. Res.* 21, 11623–11633. <https://doi.org/10.1007/s11356-014-2628-y>
- Mesquita, S.R., van Drooge, B.L., Reche, C., Guimarães, L., Grimalt, J.O., Barata, C., Piña, B., 2014b. Toxic assessment of urban atmospheric particle-bound PAHs: Relevance of composition and particle size in Barcelona (Spain). *Environ. Pollut.* 184, 555–562. <https://doi.org/10.1016/j.envpol.2013.09.034>
- Meyer, T., Wania, F., 2008. Organic contaminant amplification during snowmelt. *Water Res.* 42, 1847–1865. <https://doi.org/10.1016/j.watres.2007.12.016>
- Meylan, W.M., Howard, P.H., Boethling, R.S., 1996. Improved method for estimating water solubility from octanol/water partition coefficient. *Environ. Toxicol. Chem.* 15, 100–106. <https://doi.org/10.1002/etc.5620150205>
- Miller, M.M., Wasik, S.P., Huang, G.L., Shlu, W.Y., Mackay, D., 1985. Relationships between Octanol-Water Partition Coefficient and Aqueous Solubility. *Environ. Sci. Technol.* 19, 522–529. <https://doi.org/10.1021/es00136a007>
- Moeckel, C., Harner, T., Nizzetto, L., Strandberg, B., Lindroth, A., Jones, K.C., 2009. Use of Depuration Compounds in Passive Air Samplers: Results from Active Sampling-Supported Field Deployment, Potential Uses, and Recommendations. *Environ. Sci. Technol.* 43, 3227–3232. <https://doi.org/10.1021/es802897x>
- Möller, A., Sturm, R., Xie, Z., Cai, M., He, J., Ebinghaus, R., 2012. Organophosphorus flame retardants and plasticizers in airborne particles over the Northern Pacific and Indian Ocean toward the polar regions: Evidence for global occurrence. *Environ. Sci. Technol.* 46, 3127–3134. <https://doi.org/10.1021/es204272v>
- Möller, A., Xie, Z., Caba, A., Sturm, R., Ebinghaus, R., 2011a. Organophosphorus flame retardants and plasticizers in the atmosphere of the North Sea. *Environ. Pollut.* 159, 3660–3665. <https://doi.org/10.1016/j.envpol.2011.07.022>
- Möller, A., Xie, Z., Sturm, R., Ebinghaus, R., 2011b. Polybrominated diphenyl ethers (PBDEs) and alternative brominated flame retardants in air and seawater of the European Arctic. *Environ. Pollut.* 159, 1577–1583. <https://doi.org/10.1016/j.envpol.2011.02.054>

- Morselli, M., Semplice, M., Villa, S., Di Guardo, A., 2014. Evaluating the temporal variability of concentrations of POPs in a glacier-fed stream food chain using a combined modeling approach. *Sci. Total Environ.* 493, 571–579. <https://doi.org/10.1016/j.scitotenv.2014.05.150>
- Morville, S., Delhomme, O., Millet, M., 2011. Seasonal and diurnal variations of atmospheric PAH concentrations between rural, suburban and urban areas. *Atmos. Pollut. Res.* 2, 366–373. <https://doi.org/10.5094/APR.2011.041>
- Moser, K.A., Baron, J.S., Brahney, J., Oleksy, I.A., Saros, J.E., Hundey, E.J., Sadro, S.A., Kopáček, J., Sommaruga, R., Kainz, M.J., Strecker, A.L., Chandra, S., Walters, D.M., Preston, D.L., Michelutti, N., Lepori, F., Spaulding, S.A., Christianson, K.R., Melack, J.M., Smol, J.P., 2019. Mountain lakes: Eyes on global environmental change. *Glob. Planet. Change* 178, 77–95. <https://doi.org/10.1016/j.gloplacha.2019.04.001>
- Motelay-Massei, A., Harner, T., Shoeib, M., Diamond, M., Stern, G., Rosenberg, B., 2005. Using passive air samplers to assess urban-rural trends for persistent organic pollutants and polycyclic aromatic hydrocarbons. 2. Seasonal trends for PAHs, PCBs, and organochlorine pesticides. *Environ. Sci. Technol.* 39, 5763–5773. <https://doi.org/10.1021/es0504183>
- Muir, D.C.G., Grift, N.P., Lockhart, W.L., Wilkinson, P., Billeck, B.N., Brunskill, G.J., 1995. Spatial trends and historical profiles of organochlorine pesticides in Arctic lake sediments. *Sci. Total Environ.* 160–161, 447–457. [https://doi.org/10.1016/0048-9697\(95\)04378-E](https://doi.org/10.1016/0048-9697(95)04378-E)
- Muir, D.C.G., Howard, P.H., 2006. Are there other persistent organic pollutants? A challenge for environmental chemists. *Environ. Sci. Technol.* 40, 7157–7166. <https://doi.org/10.1021/es061677a>
- Müller, J.F., Manomanii, K., Mortimer, M.R., McLachlan, M.S., 2001. Partitioning of polycyclic aromatic hydrocarbons in the polyethylene/water system. *Anal. Bioanal. Chem.* 371, 816–822. <https://doi.org/10.1007/s002160101025>
- Münnich, K.O., Clarke, W.B., Fischer, K.H., Flothmann, D., Kromer, B., Roether, W., Siegenthaler, U., Top, Z., Weiss, W., 1978. Gas Exchange and Evaporation Studies in a Circular Wind Tunnel, Continuous Radon-222 Measurements at Sea, and Tritium/Helium-3 Measurements in a Lake, in: *Turbulent Fluxes Through the Sea Surface, Wave Dynamics, and Prediction*. Springer US, Boston, MA, pp. 151–166. https://doi.org/10.1007/978-1-4612-9806-9_11
- Muñoz-Armanz, J., Roscales, J.L., Vicente, A., Ros, M., Barrios, L., Morales, L., Abad, E., Jiménez, B., 2018. Assessment of POPs in air from Spain using passive sampling from 2008 to 2015. Part II: Spatial and temporal observations of PCDD/Fs and dl-PCBs. *Sci. Total Environ.* 634, 1669–1679. <https://doi.org/10.1016/j.scitotenv.2018.04.164>
- Nakajoh, K., Shibata, E., Todoroki, T., Ohara, A., Nishizawa, K., Nakamura, T., 2006. Measurement of temperature dependence for the vapor pressures of twenty-six polychlorinated biphenyl congeners in commercial Kanechlor mixtures by the knudsen effusion method. *Environ. Toxicol. Chem.* 25, 327–336. <https://doi.org/10.1897/05-215R.1>
- Namieśnik, J., Zabiegała, B., Kot-Wasik, A., Partyka, M., Wasik, A., 2005. Passive sampling and/or extraction techniques in environmental analysis: A review. *Anal. Bioanal. Chem.* 381, 279–301. <https://doi.org/10.1007/s00216-004-2830-8>
- Nayyar, N., Sangwan, N., Kohli, P., Verma, H., Kumar, R., Negi, V., Oldach, P., Mahato, N.K., Gupta, V., Lal, R., 2014. Hexachlorocyclohexane: Persistence, toxicity and decontamination. *Rev. Environ. Health* 29, 49–52. <https://doi.org/10.1515/reveh-2014-0015>
- Nellier, Y.M., Perga, M.E., Cottin, N., Fanget, P., Malet, E., Naffrechoux, E., 2015a. Mass budget in two high altitude lakes reveals their role as atmospheric PCB sinks. *Sci. Total Environ.* 511, 203–213. <https://doi.org/10.1016/J.SCITOTENV.2014.12.052>
- Nellier, Y.M., Perga, M.E., Cottin, N., Fanget, P., Naffrechoux, E., 2015b. Particle-Dissolved Phase Partition of Polychlorinated Biphenyls in High Altitude Alpine Lakes. *Environ. Sci. Technol.* 49, 9620–9628. <https://doi.org/10.1021/acs.est.5b01274>
- Nightingale, P.D., Liss, P.S., Schlosser, P., 2000. Measurements of air-sea gas transfer during an open ocean algal bloom. *Geophys. Res. Lett.* 27, 2117–2120. <https://doi.org/10.1029/2000GL011541>

- Nøst, T.H., Halse, A.K., Randall, S., Borgen, A.R., Schlabach, M., Paul, A., Rahman, A., Breivik, K., 2015. High Concentrations of Organic Contaminants in Air from Ship Breaking Activities in Chittagong, Bangladesh. *Environ. Sci. Technol.* 49, 11372–11380. <https://doi.org/10.1021/acs.est.5b03073>
- Ockenden, W.A., Corrigan, B.P., Howsam, M., Jones, K.C., 2001. Further developments in the use of semipermeable membrane devices as passive air samplers: Application to PCBs. *Environ. Sci. Technol.* 35, 4536–4543. <https://doi.org/10.1021/es0101126>
- Ockenden, W.A., Prest, H.F., Thomas, G.O., Sweetman, A., Jones, K.C., 1998. Passive air sampling of PCBs: Field calculation of atmospheric sampling rates by triolein-containing semipermeable membrane devices. *Environ. Sci. Technol.* 32, 1538–1543. <https://doi.org/10.1021/es971020c>
- Okeme, J.O., Rodgers, T.F.M., Parnis, J.M., Diamond, M.L., Bidleman, T.F., Jantunen, L.M., 2020. Gas Chromatographic Estimation of Vapor Pressures and Octanol-Air Partition Coefficients of Semivolatile Organic Compounds of Emerging Concern. *J. Chem. Eng. Data* 65, 2467–2475. <https://doi.org/10.1021/acs.jced.9b01126>
- Okeme, J.O.O., Rodgers, T.F.M.M., Jantunen, L.M., Diamond, M.L., 2018. Examining the Gas-Particle Partitioning of Organophosphate Esters: How Reliable Are Air Measurements? *Environ. Sci. Technol.* 52, 13834–13844. <https://doi.org/10.1021/acs.est.8b04588>
- Oliveri, A.N., Bailey, J.M., Levin, E.D., 2015. Developmental exposure to organophosphate flame retardants causes behavioral effects in larval and adult zebrafish. *Neurotoxicol. Teratol.* 52, 220–227. <https://doi.org/10.1016/j.ntt.2015.08.008>
- Olivero-Verbel, R., Moreno, T., Fernández-Arribas, J., Reche, C., Minguillón, M.C., Martins, V., Querol, X., Johnson-Restrepo, B., Eljarrat, E., 2021. Organophosphate esters in airborne particles from subway stations. *Sci. Total Environ.* 769, 145105. <https://doi.org/10.1016/j.scitotenv.2021.145105>
- Othmer, D.F., Thakar, M.S., 1953. Correlating Diffusion Coefficient in Liquids. *Ind. Eng. Chem.* 45, 589–593. <https://doi.org/10.1021/ie50519a036>
- Ouyang, G., Chen, Y., Pawliszyn, J., 2005. Time-weighted average water sampling with a solid-phase microextraction device. *Anal. Chem.* 77, 7319–7325. <https://doi.org/10.1021/ac051035q>
- Paasivirta, J., Sinkkonen, S., Mikkelsen, P., Rantio, T., Wania, F., 1999. Estimation of vapor pressures, solubilities and Henry's law constants of selected persistent organic pollutants as functions of temperature. *Chemosphere* 39, 811–832. [https://doi.org/10.1016/S0045-6535\(99\)00016-8](https://doi.org/10.1016/S0045-6535(99)00016-8)
- Palm, A., Cousins, I., Gustafsson, Ö., Axelman, J., Grunder, K., Broman, D., Brorström-Lundén, E., 2004. Evaluation of sequentially-coupled POP fluxes estimated from simultaneous measurements in multiple compartments of an air-water-sediment system. *Environ. Pollut.* 128, 85–97. <https://doi.org/10.1016/j.envpol.2003.08.023>
- Pankow, J.F., 1993. A simple box model for the annual cycle of partitioning of semi-volatile organic compounds between the atmosphere and the earth's surface. *Atmos. Environ. Part A, Gen. Top.* 27, 1139–1152. [https://doi.org/10.1016/0960-1686\(93\)90149-S](https://doi.org/10.1016/0960-1686(93)90149-S)
- Panneerselvam, K., Antony, M.P., Srinivasan, T.G., Rao, P.R.V., 2007. Measurement of enthalpies of vaporization of trialkyl phosphates using correlation gas chromatography. *Thermochim. Acta* 466, 49–56. <https://doi.org/10.1016/j.tca.2007.10.007>
- Parnis, J.M., Mackay, D., Harner, T., 2015. Temperature dependence of Henry's law constants and K_{OA} for simple and heteroatom-substituted PAHs by COSMO-RS. *Atmos. Environ.* 110, 27–35. <https://doi.org/10.1016/j.atmosenv.2015.03.032>
- Pepin, N., Bradley, R.S., Diaz, H.F., Baraer, M., Caceres, E.B., Forsythe, N., Fowler, H., Greenwood, G., Hashmi, M.Z., Liu, X.D., Miller, J.R., Ning, L., Ohmura, A., Palazzi, E., Rangwala, I., Schöner, W., Severskiy, I., Shahgedanova, M., Wang, M.B., Williamson, S.N., Yang, D.Q., 2015. Elevation-dependent warming in mountain regions of the world. *Nat. Clim. Chang.* 5, 424–430. <https://doi.org/10.1038/nclimate2563>
- Piccardo, M.T., Stella, A., Pala, M., Balducci, D., Valerio, F., 2010. Field use of semipermeable membrane devices (SPMDs) for passive air sampling of polycyclic aromatic hydrocarbons: Opportunities and limitations. *Atmos. Environ.* 44, 1947–1951. <https://doi.org/10.1016/j.atmosenv.2010.03.003>

- Piliposian, G.T., Appleby, P.G., 2003. A model of the impact of winter ice cover on pollutant concentrations and fluxes in mountain lakes. *Water, Air, Soil Pollut.* 144, 101–115. <https://doi.org/10.1023/A:1022994812659>
- Poland, A., Knutson, J.C., 1982. 2,3,7,8-tetrachlorodibenzo-p-dioxin and related halogenated aromatic hydrocarbons: examination of the mechanism of toxicity. *Annu. Rev. Pharmacol. Toxicol.* 22, 517–554. <https://doi.org/10.1146/annurev.pa.22.040182.002505>
- Poma, G., Salerno, F., Roscioli, C., Novati, S., Guzzella, L., 2017. Persistent organic pollutants in sediments of high-altitude Alpine ponds within Stelvio National Park, Italian Alps. *Inl. Waters* 7, 34–44. <https://doi.org/10.1080/20442041.2017.1294345>
- Pozo, K., Harner, T., Lee, S.C., Wania, F., Muir, D.C.G., Jones, K.C., 2009. Seasonally resolved concentrations of persistent organic pollutants in the global atmosphere from the first year of the GAPS Study. *Environ. Sci. Technol.* 43, 796–803. <https://doi.org/10.1021/es802106a>
- Pozo, K., Harner, T., Shoeib, M., Urrutia, R., Barra, R., Parra, O., Focardi, S., 2004. Passive-sampler derived air concentrations of persistent organic pollutants on a north-south transect in Chile. *Environ. Sci. Technol.* 38, 6529–6537. <https://doi.org/10.1021/es049065i>
- Pozo, K., Harner, T., Wania, F., Muir, D.C.G., Jones, K.C., Barrie, L.A., 2006. Toward a Global Network for Persistent Organic Pollutants in Air: Results from the GAPS Study. *Environ. Sci. Technol.* 40, 4867–4873. <https://doi.org/10.1021/es060447t>
- Pozo, K.K., Harner, T., Rudolph, A., Oyola, G., Estellano, V.H., Ahumada-Rudolph, R., Garrido, M., Pozo, K.K., Mabilia, R., Focardi, S., 2012. Survey of persistent organic pollutants (POPs) and polycyclic aromatic hydrocarbons (PAHs) in the atmosphere of rural, urban and industrial areas of Concepción, Chile, using passive air samplers. *Atmos. Pollut. Res.* 3, 426–434. <https://doi.org/10.5094/APR.2012.049>
- Pratt, G.C., Herbrandson, C., Krause, M.J., Schmitt, C., Lippert, C.J., McMahon, C.R., Ellickson, K.M., 2018. Measurements of gas and particle polycyclic aromatic hydrocarbons (PAHs) in air at urban, rural and near-roadway sites. *Atmos. Environ.* 179, 268–278. <https://doi.org/10.1016/j.atmosenv.2018.02.035>
- Premnath, N., Mohanrasu, K., Guru Raj Rao, R., Dinesh, G.H., Prakash, G.S., Ananthi, V., Ponnuchamy, K., Muthusamy, G., Arun, A., 2021. A crucial review on polycyclic aromatic Hydrocarbons - Environmental occurrence and strategies for microbial degradation. *Chemosphere* 280, 130608. <https://doi.org/10.1016/j.chemosphere.2021.130608>
- Qin, N., He, W., Kong, X.Z., Liu, W.X., He, Q.S., Yang, B., Ouyang, H.L., Wang, Q.M., Xu, F.L., 2013. Atmospheric partitioning and the air–water exchange of polycyclic aromatic hydrocarbons in a large shallow Chinese lake (Lake Chaohu). *Chemosphere* 93, 1685–1693. <https://doi.org/10.1016/J.CHEMOSPHERE.2013.05.038>
- Qu, C., Doherty, A.L., Xing, X., Sun, W., Albanese, S., Lima, A., Qi, S., De Vivo, B., 2018. Polyurethane Foam-Based Passive Air Samplers in Monitoring Persistent Organic Pollutants: Theory and Application, in: *Environmental Geochemistry: Site Characterization, Data Analysis and Case Histories*. Elsevier, pp. 521–542. <https://doi.org/10.1016/B978-0-444-63763-5.00021-5>
- Qu, C., Xing, X., Albanese, S., Doherty, A., Huang, H., Lima, A., Qi, S., De Vivo, B., 2015. Spatial and seasonal variations of atmospheric organochlorine pesticides along the plain-mountain transect in central China: Regional source vs. long-range transport and air-soil exchange. *Atmos. Environ.* 122, 31–40. <https://doi.org/10.1016/j.atmosenv.2015.09.008>
- Querol, X., Massagué, J., Alastuey, A., Moreno, T., Gangoiti, G., Mantilla, E., Duéguéz, J.J., Escudero, M., Monfort, E., Pérez García-Pando, C., Petetin, H., Jorba, O., Vázquez, V., de la Rosa, J., Campos, A., Muñoz, M., Monge, S., Hervás, M., Javato, R., Cornide, M.J., 2021. Lessons from the COVID-19 air pollution decrease in Spain: Now what? *Sci. Total Environ.* 779, 146380. <https://doi.org/10.1016/j.scitotenv.2021.146380>
- R Core Team, 2022. *A Language and Environment for Statistical Computing*, R Foundation for Statistical Computing, Vienna, Austria.
- Ramos, D., 2014. Brominated and organophosphorus flame retardants in the air of Barcelona. University

of Barcelona.

- Rauert, C., Schuster, J.K., Eng, A., Harner, T., 2018. Global Atmospheric Concentrations of Brominated and Chlorinated Flame Retardants and Organophosphate Esters. *Environ. Sci. Technol.* 52, 2777–2789. <https://doi.org/10.1021/acs.est.7b06239>
- Reemtsma, T., García-López, M., Rodríguez, I., Quintana, J.B., Rodil, R., 2008. Organophosphorus flame retardants and plasticizers in water and air I. Occurrence and fate. *TrAC - Trends Anal. Chem.* 27, 727–737. <https://doi.org/10.1016/j.trac.2008.07.002>
- Ren, J., Wang, X., Xue, Y., Gong, P., Joswiak, D.R., Xu, B., Yao, T., 2014. Persistent organic pollutants in mountain air of the southeastern Tibetan Plateau: Seasonal variations and implications for regional cycling. *Environ. Pollut.* 194, 210–216. <https://doi.org/10.1016/j.envpol.2014.08.002>
- Ren, J., Wang, X.X., Wang, C., Gong, P., Wang, X.X., Yao, T., 2017. Biomagnification of persistent organic pollutants along a high-altitude aquatic food chain in the Tibetan Plateau: Processes and mechanisms. *Environ. Pollut.* 220, 636–643. <https://doi.org/10.1016/J.ENVPOL.2016.10.019>
- Rex, K.R., Chakraborty, P., 2022. Legacy and new chlorinated persistent organic pollutants in the rivers of south India: Occurrences, sources, variations before and after the outbreak of the COVID-19 pandemic. *J. Hazard. Mater.* 437, 129262. <https://doi.org/10.1016/j.jhazmat.2022.129262>
- Riaz, R., de Wit, C.A., Malik, R.N., 2021a. Persistent organic pollutants (POPs) in fish species from different lakes of the lesser Himalayan region (LHR), Pakistan: The influence of proximal sources in distribution of POPs. *Sci. Total Environ.* 760, 143351. <https://doi.org/10.1016/j.scitotenv.2020.143351>
- Riaz, R., Malik, R.N., de Wit, C.A., 2021b. Soil-air partitioning of semivolatile organic compounds in the Lesser Himalaya region: Influence of soil organic matter, atmospheric transport processes and secondary emissions. *Environ. Pollut.* 291, 118006. <https://doi.org/10.1016/j.envpol.2021.118006>
- Ribes, A., Grimalt, J.O., García, C.J.T., Cuevas, E., 2003. Polycyclic Aromatic Hydrocarbons in Mountain Soils of the Subtropical Atlantic. *J. Environ. Qual.* 32, 977–987. <https://doi.org/10.2134/jeq2003.9770>
- Rignell-Hydbom, A., Lidfeldt, J., Kiviranta, H., Rantakokko, P., Samsioe, G., Agardh, C.D., Rylander, L., 2009. Exposure to p,p'-DDE: A Risk Factor for Type 2 Diabetes. *PLoS One* 4, e7503. <https://doi.org/10.1371/JOURNAL.PONE.0007503>
- Risebrough, R.W., Rieche, P., Peakall, D.B., Herman, S.G., Kirven, M.N., 1968. Polychlorinated Biphenyls in the Global Ecosystem. *Nature* 220, 1098–1102. <https://doi.org/10.1038/2201098a0>
- Rodgers, T.F.M., Truong, J.W., Jantunen, L.M., Helm, P.A., Diamond, M.L., 2018. Organophosphate Ester Transport, Fate, and Emissions in Toronto, Canada, Estimated Using an Updated Multimedia Urban Model. *Environ. Sci. Technol.* 52, 12465–12474. <https://doi.org/10.1021/acs.est.8b02576>
- Roscales, J.L., Muñoz-Arnanz, J., Ros, M., Vicente, A., Barrios, L., Jiménez, B., 2018. Assessment of POPs in air from Spain using passive sampling from 2008 to 2015. Part I: Spatial and temporal observations of PBDEs. *Sci. Total Environ.* 634, 1657–1668. <https://doi.org/10.1016/j.scitotenv.2018.03.043>
- Roux, M.V., Temprado, M., Chickos, J.S., Nagano, Y., 2008. Critically evaluated thermochemical properties of polycyclic aromatic hydrocarbons. *J. Phys. Chem. Ref. Data* 37, 1855–1996. <https://doi.org/10.1063/1.2955570>
- Rowe, M.D., Perlinger, J.A., 2012. Micrometeorological measurement of hexachlorobenzene and polychlorinated biphenyl compound air-water gas exchange in Lake Superior and comparison to model predictions. *Atmos. Chem. Phys.* 12, 4607–4617. <https://doi.org/10.5194/acp-12-4607-2012>
- RPA Europe, 2020. Legislative Mapping: Polycyclic Aromatic Hydrocarbons. Project Ref. EEA/HSR/RO/19/001. Summary Document prepared for European Environment Agency (EPA).
- Ruge, B.Z., Muir, D., Helm, P., Lohmann, R., 2018. Concentrations, Trends, and Air-Water Exchange of PCBs and Organochlorine Pesticides Derived from Passive Samplers in Lake Superior in 2011. *Environ. Sci. Technol.* 52, 14061–14069. <https://doi.org/10.1021/acs.est.8b04036>
- Rusina, T.P., Smedes, F., Brborić, M., Vrana, B., 2019. Investigating levels of organic contaminants in

- Danube River sediments in Serbia by multi-ratio equilibrium passive sampling. *Sci. Total Environ.* 696, 1–10. <https://doi.org/10.1016/j.scitotenv.2019.133935>
- Rusina, T.P., Smedes, F., Klanova, J., Booij, K., Holoubek, I., 2007. Polymer selection for passive sampling: A comparison of critical properties. *Chemosphere* 68, 1344–1351. <https://doi.org/10.1016/j.chemosphere.2007.01.025>
- Rusina, T.P., Smedes, F., Koblizkova, M., Klanova, J., 2010. Calibration of silicone rubber passive samplers: Experimental and modeled relations between sampling rate and compound properties. *Environ. Sci. Technol.* 44, 362–367. <https://doi.org/10.1021/es900938r>
- Sacks, V.P., Lohmann, R., 2011. Development and use of polyethylene passive samplers to detect triclosans and alkylphenols in an Urban estuary. *Environ. Sci. Technol.* 45, 2270–2277. <https://doi.org/10.1021/es1040865>
- Saeedi Saravi, S.S., Dehpour, A.R., 2016. Potential role of organochlorine pesticides in the pathogenesis of neurodevelopmental, neurodegenerative, and neurobehavioral disorders: A review. *Life Sci.* 145, 255–264. <https://doi.org/10.1016/j.lfs.2015.11.006>
- Safe, S.H., 1994. Polychlorinated biphenyls (PCBs): Environmental impact, biochemical and toxic responses, and implications for risk assessment. *Crit. Rev. Toxicol.* 24, 87–149. <https://doi.org/10.3109/10408449409049308>
- Saha, L., Kumar, A., Kumar, S., Korstad, J., Srivastava, S., Baudh, K., 2022. The impact of the COVID-19 lockdown on global air quality: A review. *Environ. Sustain.* 5, 5–23. <https://doi.org/10.1007/s42398-021-00213-6>
- Saini, A., Clarke, J., Harner, T., 2019. Direct measurements of polyurethane foam (PUF) – air partitioning coefficients for chemicals of emerging concern capable of equilibrating in PUF disk samplers. *Chemosphere* 234, 925–930. <https://doi.org/10.1016/j.chemosphere.2019.06.134>
- Saini, A., Harner, T., Chinnadhurai, S., Schuster, J.K., Yates, A., Sweetman, A., Aristizabal-Zuluaga, B.H., Jiménez, B., Manzano, C.A., Gaga, E.O., Stevenson, G., Falandysz, J., Ma, J., Miglioranza, K.S.B., Kannan, K., Tominaga, M., Jariyasopit, N., Rojas, N.Y., Amador-Muñoz, O., Sinha, R., Alani, R., Suresh, R., Nishino, T., Shoeib, T., 2020. GAPS-megacities: A new global platform for investigating persistent organic pollutants and chemicals of emerging concern in urban air. *Environ. Pollut.* 267, 115416. <https://doi.org/10.1016/j.envpol.2020.115416>
- Sala, M., Sunyer, J., Herrero, C., To-Figueras, J., Grimalt, J., 2001. Association between serum concentrations of hexachlorobenzene and polychlorobiphenyls with thyroid hormone and liver enzymes in a sample of the general population. *Occup. Environ. Med.* 58, 172–177. <https://doi.org/10.1136/oem.58.3.172>
- Salamova, A., Hermanson, M.H., Hites, R.A., 2014. Organophosphate and halogenated flame retardants in atmospheric particles from a European Arctic site. *Environ. Sci. Technol.* 48, 6133–6140. <https://doi.org/10.1021/es500911d>
- Salim, F., Górecki, T., 2019. Theory and modelling approaches to passive sampling. *Environ. Sci. Process. Impacts* 21, 1618–1641. <https://doi.org/10.1039/c9em00215d>
- Sander, R., 2015. Compilation of Henry's law constants (version 4.0) for water as solvent. *Atmos. Chem. Phys.* 15, 4399–4981. <https://doi.org/10.5194/acp-15-4399-2015>
- Schmid, P., Bogdal, C., Blüthgen, N., Anselmetti, F.S., Zwyssig, A., Hungerbühler, K., 2011. The missing piece: Sediment records in remote mountain lakes confirm glaciers being secondary sources of persistent organic pollutants. *Environ. Sci. Technol.* 45, 203–208. <https://doi.org/10.1021/es1028052>
- Schuster, J.K., Harner, T., Eng, A., Rauert, C., Su, K., Hornbuckle, K.C., Johnson, C.W., 2021. Tracking POPs in Global Air from the First 10 Years of the GAPS Network (2005 to 2014). *Environ. Sci. Technol.* 55, 9479–9488. <https://doi.org/10.1021/acs.est.1c01705>
- Schwarzenbach, R.P., Gschwend, P.M., Imboden, D.M., 2016. *Environmental Organic Chemistry*, 3rd Edition. John Wiley & Sons, Ltd.
- Schwarzenbach, R.P., Gschwend, P.M., Imboden, D.M., 2005. *Environmental Organic Chemistry*, 2nd Edition. John Wiley & Sons, Ltd.

- Seethapathy, S., Górecki, T., Li, X., 2008. Passive sampling in environmental analysis. *J. Chromatogr. A* 1184, 234–253. <https://doi.org/10.1016/J.CHROMA.2007.07.070>
- Semeena, V.S., Lammel, G., 2005. The significance of the grasshopper effect on the atmospheric distribution of persistent organic substances. *Geophys. Res. Lett.* 32, 1–5. <https://doi.org/10.1029/2004GL022229>
- Sharma, B.M., Nizzetto, L., Bharat, G.K., Tayal, S., Melymuk, L., Sáňka, O., Příbylová, P., Audy, O., Larssen, T., 2015. Melting Himalayan glaciers contaminated by legacy atmospheric depositions are important sources of PCBs and high-molecular-weight PAHs for the Ganges floodplain during dry periods the authors dedicate this paper to the memory of their dear friend and coll. *Environ. Pollut.* 206, 588–596. <https://doi.org/10.1016/j.envpol.2015.08.012>
- Shoeib, M., Harner, T., 2002. Characterization and comparison of three passive air samplers for persistent organic pollutants. *Environ. Sci. Technol.* 36, 4142–4151. <https://doi.org/10.1021/es020635t>
- Shoeib, M., Harner, T., Sum, C.L., Lane, D., Zhu, J., 2008. Sorbent-impregnated polyurethane foam disk for passive air sampling of volatile fluorinated chemicals. *Anal. Chem.* 80, 675–682. <https://doi.org/10.1021/ac701830s>
- Shunthirasingham, C., Oyiliagu, C.E., Cao, X., Gouin, T., Wania, F., Lee, S.C., Pozo, K., Harner, T., Muir, D.C.G., 2010. Spatial and temporal pattern of pesticides in the global atmosphere. *J. Environ. Monit.* 12, 1650–1657. <https://doi.org/10.1039/c0em00134a>
- Shunthirasingham, C., Wania, F., Macleod, M., Lei, Y.D., Quinn, C.L., Zhang, X., Scheringer, M., Wegmann, F., Hungerbühler, K., Ivemeyer, S., Heil, F., Klocke, P., Pacepavicius, G., Alae, M., 2013. Mountain cold-trapping increases transfer of persistent organic pollutants from atmosphere to cows' milk. *Environ. Sci. Technol.* 47, 9175–9181. <https://doi.org/10.1021/es400851d>
- Sicard, P., De Marco, A., Agathokleous, E., Feng, Z., Xu, X., Paoletti, E., Rodriguez, J.J.D., Calatayud, V., 2020. Amplified ozone pollution in cities during the COVID-19 lockdown. *Sci. Total Environ.* 735, 139542. <https://doi.org/10.1016/j.scitotenv.2020.139542>
- Simonich, S.L., Hites, R.A., 1995. Global distribution of persistent organochlorine compounds. *Science* 269, 1851–1854. <https://doi.org/10.1126/science.7569923>
- Sinkkonen, S., Paasivirta, J., 2000. Degradation half-life times of PCDDs, PCDFs and PCBs for environmental fate modeling. *Chemosphere* 40, 943–949. [https://doi.org/10.1016/S0045-6535\(99\)00337-9](https://doi.org/10.1016/S0045-6535(99)00337-9)
- Smedes, F., 2019. SSP silicone–lipid– and SPMD–water partition coefficients of seventy hydrophobic organic contaminants and evaluation of the water concentration calculator for SPMD. *Chemosphere* 223, 748–757. <https://doi.org/10.1016/j.chemosphere.2019.01.164>
- Smedes, F., 2018. Silicone–water partition coefficients determined by cosolvent method for chlorinated pesticides, musks, organo phosphates, phthalates and more. *Chemosphere* 210, 662–671. <https://doi.org/10.1016/j.chemosphere.2018.07.054>
- Smedes, F., Booij, K., 2012. Guidelines for passive sampling of hydrophobic contaminants in water using silicone rubber samplers. *ICES Tech. Mar. Environ. Sci.* 52. <https://doi.org/http://dx.doi.org/10.25607/OBP-236>
- Smedes, F., Geertsma, R.W., Van Der Zande, T., Booij, K., 2009. Polymer-water partition coefficients of hydrophobic compounds for passive sampling: Application of cosolvent models for validation. *Environ. Sci. Technol.* 43, 7047–7054. <https://doi.org/10.1021/es9009376>
- Sobotka, J., Smedes, F., Vrana, B., 2022. Performance comparison of silicone and low-density polyethylene as passive samplers in a global monitoring network for aquatic organic contaminants. *Environ. Pollut.* 119050. <https://doi.org/10.1016/j.envpol.2022.119050>
- Söderström, H.S., Bergqvist, P.A., 2004. Passive air sampling using semipermeable membrane devices at different wind-speeds in situ calibrated by performance reference compounds. *Environ. Sci. Technol.* 38, 4828–4834. <https://doi.org/10.1021/es049637z>
- Spieksma, W., Luijk, R., Govers, H.A.J., 1994. Determination of the liquid vapour pressure of low-volatility compounds from the Kováts retention index. *J. Chromatogr. A* 672, 141–148.

- [https://doi.org/10.1016/0021-9673\(94\)80602-0](https://doi.org/10.1016/0021-9673(94)80602-0)
- Starek-Świechowicz, B., Budziszewska, B., Starek, A., 2017. Hexachlorobenzene as a persistent organic pollutant: Toxicity and molecular mechanism of action. *Pharmacol. Reports* 69, 1232–1239. <https://doi.org/10.1016/j.pharep.2017.06.013>
- Stein, A.F., Draxler, R.R., Rolph, G.D., Stunder, B.J.B., Cohen, M.D., Ngan, F., 2015. NOAA's HYSPLIT Atmospheric Transport and Dispersion Modeling System. *Bull. Am. Meteorol. Soc.* 96, 2059–2077. <https://doi.org/10.1175/BAMS-D-14-00110.1>
- Streets, S.S., Henderson, S.A., Stoner, A.D., Carlson, D.L., Simcik, M.F., Swackhamer, D.L., 2006. Partitioning and bioaccumulation of PBDEs and PCBs in Lake Michigan. *Environ. Sci. Technol.* 40, 7263–7269. <https://doi.org/10.1021/es061337p>
- Sührling, R., Wolschke, H., Diamond, M.L., Jantunen, L.M., Scheringer, M., 2016. Distribution of Organophosphate Esters between the Gas and Particle Phase-Model Predictions vs Measured Data. *Environ. Sci. Technol.* 50, 6644–6651. <https://doi.org/10.1021/acs.est.6b00199>
- Sum, C.L., Harner, T., Pozo, K., Shoeib, M., Wania, F., Muir, D.C.G., Barrie, L.A., Jones, K.C., 2007. Polychlorinated naphthalenes in the global atmospheric passive sampling (GAPS) study. *Environ. Sci. Technol.* 41, 2680–2687. <https://doi.org/10.1021/es062352x>
- Tateya, S., Tanabe, S., Tatsukawa, R., 1988. PCBs on the globe: possible trend and future levels in the open ocean environment, in: W. Schmidtke, N. (Ed.), *Toxic Contamination in Large Lakes*, Vol. III. Lewis Publishers, pp. 237–281.
- Tatton, J.O.G., Ruzicka, J.H.A., 1967. Organochlorine pesticides in Antarctica. *Nature* 215, 346–348. <https://doi.org/10.1038/215346a0>
- Taylor, A.C., Fones, G.R., Vrana, B., Mills, G.A., 2021. Applications for Passive Sampling of Hydrophobic Organic Contaminants in Water—A Review. *Crit. Rev. Anal. Chem.* 51, 20–54. <https://doi.org/10.1080/10408347.2019.1675043>
- Tobías, A., Carnerero, C., Reche, C., Massagué, J., Via, M., Minguillón, M.C., Alastuey, A., Querol, X., 2020. Changes in air quality during the lockdown in Barcelona (Spain) one month into the SARS-CoV-2 epidemic. *Sci. Total Environ.* 726, 138540. <https://doi.org/10.1016/j.scitotenv.2020.138540>
- Tremolada, P., Guazzoni, N., Smilovich, L., Moia, F., Comolli, R., 2012. The effect of the organic matter composition on POP accumulation in soil. *Water, Air, Soil Pollut.* 223, 4539–4556. <https://doi.org/10.1007/s11270-012-1216-3>
- Tremolada, P., Villa, S., Bazzarin, P., Bizzotto, E., Comolli, R., Vighi, M., 2008. POPs in Mountain Soils from the Alps and Andes: Suggestions for a 'Precipitation Effect' on Altitudinal Gradients. *Water, Air, Soil Pollut.* 188, 93–109. <https://doi.org/10.1007/s11270-007-9527-5>
- Tucca, F., Luarte, T., Nimptsch, J., Woelfl, S., Pozo, K., Casas, G., Dachs, J., Barra, R., Chiang, G., Galbán-Malagón, C., 2020. Sources and diffusive air–water exchange of polycyclic aromatic hydrocarbons in an oligotrophic North–Patagonian lake. *Sci. Total Environ.* 738, 139838. <https://doi.org/10.1016/j.scitotenv.2020.139838>
- Tuduri, L., Harner, T., Hung, H., 2006. Polyurethane foam (PUF) disks passive air samplers: Wind effect on sampling rates. *Environ. Pollut.* 144, 377–383. <https://doi.org/10.1016/j.envpol.2005.12.047>
- Tuduri, L., Millet, M., Briand, O., Montury, M., 2012. Passive air sampling of semi-volatile organic compounds. *TrAC - Trends Anal. Chem.* 31, 38–49. <https://doi.org/10.1016/j.trac.2011.08.007>
- Turusov, V., Rakitsky, V., Tomatis, L., 2002. Dichlorodiphenyltrichloroethane (DDT): Ubiquity, persistence, and risks. *Environ. Health Perspect.* 110, 125–128. <https://doi.org/10.1289/ehp.02110125>
- Ulbrich, B., Stahlmann, R., 2004. Developmental toxicity of polychlorinated biphenyls (PCBs): A systematic review of experimental data. *Arch. Toxicol.* 78, 252–268. <https://doi.org/10.1007/S00204-003-0519-Y>
- Ulrich, N., Endo, S., Brown, T.N., Watanabe, N., Bronner, G., Abraham, M.H., Goss, K., 2017. UFZ - LSER Database v 3.2.1, Leipzig, Germany, Helmholtz Centre for Environmental Research-UFZ.

- Usenko, S., Hageman, K.J., Schmedding, D.W., Wilson, G.R., Simonich, S.L., 2005. Trace analysis of semivolatile organic compounds in large volume samples of snow, lake water, and groundwater. *Environ. Sci. Technol.* 39, 6006–6015. <https://doi.org/10.1021/es0506511>
- Usenko, S., Landers, D.H., Appleby, P.G., Simonich, S.L., 2007. Current and historical deposition of PBDEs, pesticides, PCBs, and PAHs to Rocky Mountain National Park. *Environ. Sci. Technol.* 41, 7235–7241. <https://doi.org/10.1021/es0710003>
- Usenko, S., Simonich, S.L.M., Hageman, K.J., Schrlau, J.E., Geiser, L., Campbell, D.H., Appleby, P.G., Landers, D.H., 2010. Sources and deposition of polycyclic aromatic hydrocarbons to western U.S. national parks. *Environ. Sci. Technol.* 44, 4512–4518. <https://doi.org/10.1021/es903844n>
- Vachon, D., Prairie, Y.T., 2013. The ecosystem size and shape dependence of gas transfer velocity versus wind speed relationships in lakes. *Can. J. Fish. Aquat. Sci.* 70, 1757–1764. <https://doi.org/10.1139/cjfas-2013-0241>
- van der Veen, I., de Boer, J., 2012. Phosphorus flame retardants: Properties, production, environmental occurrence, toxicity and analysis. *Chemosphere* 88, 1119–1153. <https://doi.org/10.1016/j.chemosphere.2012.03.067>
- van Drooge, B.L., 2013. Human exposure to polycyclic aromatic hydrocarbons in urban and rural ambient air. *ACS Symp. Ser.* 1149, 59–82. <https://doi.org/10.1021/bk-2013-1149.ch004>
- van Drooge, B.L., 2006. Polychlorinated biphenyls in mountain pine (*Pinus uncinata*) needles from Central Pyrenean high mountains (Catalonia, Spain). *Ecotoxicol. Environ. Saf.* 63, 61–67. <https://doi.org/10.1016/j.ecoenv.2005.06.005>
- van Drooge, B.L., Fernández, P., Grimalt, J.O., Stuchlík, E., García, C.J.T., Cuevas, E., 2010. Atmospheric polycyclic aromatic hydrocarbons in remote European and Atlantic sites located above the boundary mixing layer. *Environ. Sci. Pollut. Res.* 17, 1207–1216. <https://doi.org/10.1007/s11356-010-0296-0>
- van Drooge, B.L., Grimalt, J.O., 2015. Particle size-resolved source apportionment of primary and secondary organic tracer compounds at urban and rural locations in Spain. *Atmos. Chem. Phys.* 15, 7735–7752. <https://doi.org/10.5194/acp-15-7735-2015>
- van Drooge, B.L., Grimalt, J.O., Booij, K., Camarero, L., Catalan, J., 2005. Passive sampling of atmospheric organochlorine compounds by SPMDs in a remote high mountain area. *Atmos. Environ.* 39, 5195–5204. <https://doi.org/10.1016/j.atmosenv.2005.05.020>
- van Drooge, B.L., Grimalt, J.O., Camarero, L., Catalan, J., Stuchlík, E., Torres García, C.J., 2004a. Atmospheric semivolatile organochlorine compounds in European high-mountain areas (Central Pyrenees and High Tatras). *Environ. Sci. Technol.* 38, 3525–3532. <https://doi.org/10.1021/es030108p>
- van Drooge, B.L., Grimalt, J.O., Torres García, C.J., Cuevas, E., 2002. Semivolatile organochlorine compounds in the free troposphere of the Northeastern Atlantic. *Environ. Sci. Technol.* 36, 1155–1161. <https://doi.org/10.1021/es010189u>
- van Drooge, B.L., López, J., Fernández, P., Grimalt, J.O., Stuchlík, E., 2011. Polycyclic aromatic hydrocarbons in lake sediments from the High Tatras. *Environ. Pollut.* 159, 1234–1240. <https://doi.org/10.1016/j.envpol.2011.01.035>
- van Drooge, B.L., Ribes, A., Fernández, P., Appleby, P., 2004b. Polycyclic aromatic hydrocarbon composition in soils and sediments of high altitude lakes. *Environ. Pollut.* 131, 13–24. <https://doi.org/10.1016/j.envpol.2004.02.024>
- Vecchiato, M., Zambon, S., Argiriadis, E., Barbante, C., Gambaro, A., Piazza, R., 2015. Polychlorinated biphenyls (PCBs) and polybrominated diphenyl ethers (PBDEs) in Antarctic ice-free areas: Influence of local sources on lakes and soils. *Microchem. J.* 120, 26–33. <https://doi.org/10.1016/J.MICROC.2014.12.008>
- Vilanova, R.M., Fernández, P., Grimalt, J.O., 2001a. Polychlorinated biphenyl partitioning in the waters of a remote mountain lake. *Sci. Total Environ.* 279, 51–62. [https://doi.org/10.1016/S0048-9697\(01\)00725-2](https://doi.org/10.1016/S0048-9697(01)00725-2)
- Vilanova, R.M., Fernández, P., Martínez, C., Grimalt, J.O., 2001b. Organochlorine Pollutants in Remote

- Mountain Lake Waters. *J. Environ. Qual.* 30, 1286–1295. <https://doi.org/10.2134/jeq2001.3041286x>
- Vilanova, R.M., Fernández, P., Martínez, C., Grimalt, J.O., 2001c. Polycyclic aromatic hydrocarbons in remote mountain lake waters. *Water Res.* 35, 3916–3926. [https://doi.org/10.1016/S0043-1354\(01\)00113-0](https://doi.org/10.1016/S0043-1354(01)00113-0)
- Vives, I., Canuti, E., Castro-Jiménez, J., Christoph, E.H., Eisenreich, S.J., Hanke, G., Huber, T., Mariani, G., Mueller, A., Skejo, H., Umlauf, G., Wollgast, J., 2007. Occurrence of polychlorinated dibenzo-p-dioxins and dibenzofurans (PCDD/Fs), polychlorinated biphenyls (PCBs) and polybrominated diphenyl ethers (PBDEs) in Lake Maggiore (Italy and Switzerland). *J. Environ. Monit.* 9, 589–598. <https://doi.org/10.1039/b700919d>
- Vives, I., Grimalt, J.O., Catalan, J., Rosseland, B.O., Battarbee, R.W., 2004a. Influence of Altitude and Age in the Accumulation of Organochlorine Compounds in Fish from High Mountain Lakes. *Environ. Sci. Technol.* 38, 690–698. <https://doi.org/10.1021/es030089j>
- Vives, I., Grimalt, J.O., Lacorte, S., Guillamón, M., Barceló, D., Rosseland, B.O., 2004b. Polybromodiphenyl Ether Flame Retardants in Fish from Lakes in European High Mountains and Greenland. *Environ. Sci. Technol.* 38, 2338–2344. <https://doi.org/10.1021/es030107x>
- Vives, I., Grimalt, J.O., Ventura, M., Catalan, J., Rosseland, B.O., 2005. Age dependence of the accumulation of organochlorine pollutants in brown trout (*Salmo trutta*) from a remote high mountain lake (Redó, Pyrenees). *Environ. Pollut.* 133, 343–350. <https://doi.org/10.1016/j.envpol.2004.05.027>
- Vojta, Š., Melymuk, L., Klánová, J., 2017. Changes in Flame Retardant and Legacy Contaminant Concentrations in Indoor Air during Building Construction, Furnishing, and Use. *Environ. Sci. Technol.* 51, 11891–11899. <https://doi.org/10.1021/acs.est.7b03245>
- Wang, Q., Lam, J.C.W., Man, Y.C., Lai, N.L.S., Kwok, K.Y., Guo, Y., yong, Lam, P.K.S., Zhou, B., 2015. Bioconcentration, metabolism and neurotoxicity of the organophorous flame retardant 1,3-dichloro 2-propyl phosphate (TDCPP) to zebrafish. *Aquat. Toxicol.* 158, 108–115. <https://doi.org/10.1016/j.aquatox.2014.11.001>
- Wang, Q., Zhao, H., Wang, Y., Xie, Q., Chen, J., Quan, X., 2017. Determination and prediction of octanol-air partition coefficients for organophosphate flame retardants. *Ecotoxicol. Environ. Saf.* 145, 283–288. <https://doi.org/10.1016/j.ecoenv.2017.07.040>
- Wang, X., Halsall, C., Codling, G., Xie, Z., Xu, B., Zhao, Z., Xue, Y., Ebinghaus, R., Jones, K.C., 2014. Accumulation of perfluoroalkyl compounds in Tibetan mountain snow: Temporal patterns from 1980 to 2010. *Environ. Sci. Technol.* 48, 173–181. <https://doi.org/10.1021/es4044775>
- Wang, X., Kennedy, K., Powell, J., Keywood, M., Gillett, R., Thai, P., Bridgen, P., Broomhall, S., Paxman, C., Wania, F., Mueller, J.F., 2015. Spatial distribution of selected persistent organic pollutants (POPs) in Australia's atmosphere. *Environ. Sci. Process. Impacts* 17, 525–532. <https://doi.org/10.1039/c4em00594e>
- Wang, X.P., Sheng, J.J., Gong, P., Xue, Y.G., Yao, T.D., Jones, K.C., 2012. Persistent organic pollutants in the Tibetan surface soil: Spatial distribution, air-soil exchange and implications for global cycling. *Environ. Pollut.* 170, 145–151. <https://doi.org/10.1016/j.envpol.2012.06.012>
- Wang, Z., Altenburger, R., Backhaus, T., Covaci, A., Diamond, M.L., Grimalt, J.O., Lohmann, R., Schäffer, A., Scheringer, M., Selin, H., Soehl, A., Suzuki, N., 2021. We need a global science-policy body on chemicals and waste. *Science* 371, 774–776. <https://doi.org/10.1126/science.abe9090>
- Wang, Z., Liu, S., Zhang, T., 2019. Characteristics of polycyclic aromatic hydrocarbons (PAHs) in soil horizon from high-altitude mountains in Northeastern China. *Chemosphere* 225, 93–103. <https://doi.org/10.1016/j.chemosphere.2019.03.001>
- Wania, F., 2003. Assessing the potential of persistent organic chemicals for long-range transport and accumulation in polar regions. *Environ. Sci. Technol.* 37, 1344–1351. <https://doi.org/10.1021/es026019e>
- Wania, F., 1999. On the origin of elevated levels of persistent chemicals in the environment. *Environ. Sci. Pollut. Res.* 6, 11–19. <https://doi.org/10.1007/BF02987114>
- Wania, F., Haugen, J.-E., Lei, Y.D., Mackay, D., 1998. Temperature Dependence of Atmospheric

- Concentrations of Semivolatile Organic Compounds. *Environ. Sci. Technol.* 32, 1013–1021. <https://doi.org/10.1021/es970856c>
- Wania, F., Mackay, D., 1995. A global distribution model for persistent organic chemicals. *Sci. Total Environ.* 160–161, 211–232. [https://doi.org/10.1016/0048-9697\(95\)04358-8](https://doi.org/10.1016/0048-9697(95)04358-8)
- Wania, F., Mackay, D., 1993. Global fractionation and cold condensation of low volatility organochlorine compounds in polar regions. *Ambio* 22, 10–18. <https://doi.org/10.2307/4314030>
- Wania, F., MacKay, D., 1996. Peer Reviewed: Tracking the Distribution of Persistent Organic Pollutants. *Environ. Sci. Technol.* 30, 390A–396A. <https://doi.org/10.1021/es962399q>
- Wania, F., Shen, L., Lei, Y.D., Teixeira, C., Muir, D.C.G., 2003. Development and Calibration of a Resin-Based Passive Sampling System for Monitoring Persistent Organic Pollutants in the Atmosphere. *Environ. Sci. Technol.* 37, 1352–1359. <https://doi.org/10.1021/es026166c>
- Wania, F., Shunthirasingham, C., 2020. Passive air sampling for semi-volatile organic chemicals. *Environ. Sci. Process. Impacts* 22, 1925–2002. <https://doi.org/10.1039/d0em00194e>
- Wania, F., Westgate, J.N., 2008. On the mechanism of mountain cold-trapping of organic chemicals. *Environ. Sci. Technol.* 42, 9092–9098. <https://doi.org/10.1021/es8013198>
- Wanninkhof, R.H., Bliven, L.F., 1991. Relationship between gas exchange, wind speed, and radar backscatter in a large wind-wave tank. *J. Geophys. Res. Ocean.* 96, 2785–2796. <https://doi.org/10.1029/90jc02368>
- Wei, G.L., Li, D.Q., Zhuo, M.N., Liao, Y.S., Xie, Z.Y., Guo, T.L., Li, J.J., Zhang, S.Y., Liang, Z.Q., 2015. Organophosphorus flame retardants and plasticizers: Sources, occurrence, toxicity and human exposure. *Environ. Pollut.* 196, 29–46. <https://doi.org/10.1016/j.envpol.2014.09.012>
- Wenger, D., Gerecke, A.C., Heeb, N. V., Hueglin, C., Seiler, C., Haag, R., Naegeli, H., Zenobi, R., 2009. Aryl hydrocarbon receptor-mediated activity of atmospheric particulate matter from an urban and a rural site in Switzerland. *Atmos. Environ.* 43, 3556–3562. <https://doi.org/10.1016/j.atmosenv.2009.04.012>
- Westgate, J.N., Wania, F., 2013. Model-based exploration of the drivers of mountain cold-trapping in soil. *Environ. Sci. Process. Impacts* 15, 2220–2232. <https://doi.org/10.1039/c3em00385j>
- Whitman, W.G., 1923. The two film theory of gas absorption. *Chem. Metall. Eng.* 29, 146–148.
- Wilkinson, A.C., Kimpe, L.E., Blais, J.M., 2005. Air–water gas exchange of chlorinated pesticides in four lakes spanning a 1,205 meter elevation range in the Canadian Rocky Mountains. *Environ. Toxicol. Chem.* 24, 61. <https://doi.org/10.1897/04-071R.1>
- Willett, K.L., Ulrich, E.M., Hites, R.A., 1998. Differential toxicity and environmental fates of hexachlorocyclohexane isomers. *Environ. Sci. Technol.* 32, 2197–2207. <https://doi.org/10.1021/es9708530>
- Williams, A.J., Grulke, C.M., Edwards, J., McEachran, A.D., Mansouri, K., Baker, N.C., Patlewicz, G., Shah, I., Wambaugh, J.F., Judson, R.S., Richard, A.M., 2017. The CompTox Chemistry Dashboard: A community data resource for environmental chemistry. *J. Cheminform.* 9, 61. <https://doi.org/10.1186/s13321-017-0247-6>
- Winneke, G., Walkowiak, J., Lilienthal, H., 2002. PCB-induced neurodevelopmental toxicity in human infants and its potential mediation by endocrine dysfunction. *Toxicology* 181–182, 161–165. [https://doi.org/10.1016/S0300-483X\(02\)00274-3](https://doi.org/10.1016/S0300-483X(02)00274-3)
- World Health Organization, 1989. Indoor air quality: Organic pollutants. *Environ. Technol. Lett.* 10, 855–858. <https://doi.org/10.1080/09593338909384805>
- Wu, X., Davie-Martin, C.L., Steinlin, C., Hageman, K.J., Cullen, N.J., Bogdal, C., 2017. Understanding and Predicting the Fate of Semivolatile Organic Pesticides in a Glacier-Fed Lake Using a Multimedia Chemical Fate Model. *Environ. Sci. Technol.* 51, 11752–11760. <https://doi.org/10.1021/acs.est.7b03483>
- Yang, J., Zhao, Y., Li, M., Du, M., Li, X., Li, Y., 2019. A Review of a Class of Emerging Contaminants: The Classification, Distribution, Intensity of Consumption, Synthesis Routes, Environmental Effects

- and Expectation of Pollution Abatement to Organophosphate Flame Retardants (OPFRs). *Int. J. Mol. Sci.* 20, 2874. <https://doi.org/10.3390/ijms20122874>
- Yang, R., Yao, T., Xu, B., Jiang, G., Xin, X., 2007. Accumulation features of organochlorine pesticides and heavy metals in fish from high mountain lakes and Lhasa River in the Tibetan Plateau. *Environ. Int.* 33, 151–156. <https://doi.org/10.1016/j.envint.2006.08.008>
- Yang, R., Zhang, S., Li, A., Jiang, G., Jing, C., 2013. Altitudinal and spatial signature of persistent organic pollutants in soil, lichen, conifer needles, and bark of the southeast tibetan plateau: Implications for sources and environmental cycling. *Environ. Sci. Technol.* 47, 12736–12743. <https://doi.org/10.1021/es403562x>
- Yeo, H.G., Choi, M., Chun, M.Y., Sunwoo, Y., 2003. Gas/particle concentrations and partitioning of PCBs in the atmosphere of Korea. *Atmos. Environ.* 37, 3561–3570. [https://doi.org/10.1016/S1352-2310\(03\)00361-3](https://doi.org/10.1016/S1352-2310(03)00361-3)
- Zhang, G., Chakraborty, P., Li, J., Sampathkumar, P., Balasubramanian, T., Kathiresan, K., Takahashi, S., Subramanian, A., Tanabe, S., Jones, K.C., 2008. Passive Atmospheric Sampling of Organochlorine Pesticides, Polychlorinated Biphenyls, and Polybrominated Diphenyl Ethers in Urban, Rural, and Wetland Sites along the Coastal Length of India. *Environ. Sci. Technol.* 42, 8218–8223. <https://doi.org/10.1021/es8016667>
- Zhang, W., Ye, Y., Hu, D., Ou, L., Wang, X., 2010. Characteristics and transport of organochlorine pesticides in urban environment: Air, dust, rain, canopy throughfall, and runoff. *J. Environ. Monit.* 12, 2153–2160. <https://doi.org/10.1039/c0em00110d>
- Zhou, L., Hiltcher, M., Gruber, D., Püttmann, W., 2017. Organophosphate flame retardants (OPFRs) in indoor and outdoor air in the Rhine/Main area, Germany: comparison of concentrations and distribution profiles in different microenvironments. *Environ. Sci. Pollut. Res.* 24, 10992–11005. <https://doi.org/10.1007/s11356-016-6902-z>
- Zhu, N., Schramm, K.W., Wang, T., Henkelmann, B., Fu, J., Gao, Y., Wang, Y., Jiang, G., 2015. Lichen, moss and soil in resolving the occurrence of semi-volatile organic compounds on the southeastern Tibetan Plateau, China. *Sci. Total Environ.* 518–519, 328–336. <https://doi.org/10.1016/j.scitotenv.2015.03.024>
- Zhu, N., Schramm, K.W., Wang, T., Henkelmann, B., Zheng, X., Fu, J., Gao, Y., Wang, Y., Jiang, G., 2014. Environmental fate and behavior of persistent organic pollutants in Shergyla Mountain, southeast of the Tibetan Plateau of China. *Environ. Pollut.* 191, 166–174. <https://doi.org/10.1016/j.envpol.2014.04.031>

An aerial, black and white photograph of a rugged, mountainous landscape. The terrain is characterized by a dense network of roads, valleys, and ridges. The lighting creates strong shadows, emphasizing the topography. The word "APPENDICES" is overlaid in large, white, serif capital letters at the bottom of the image.

APPENDICES

Appendix I: Lake catchments

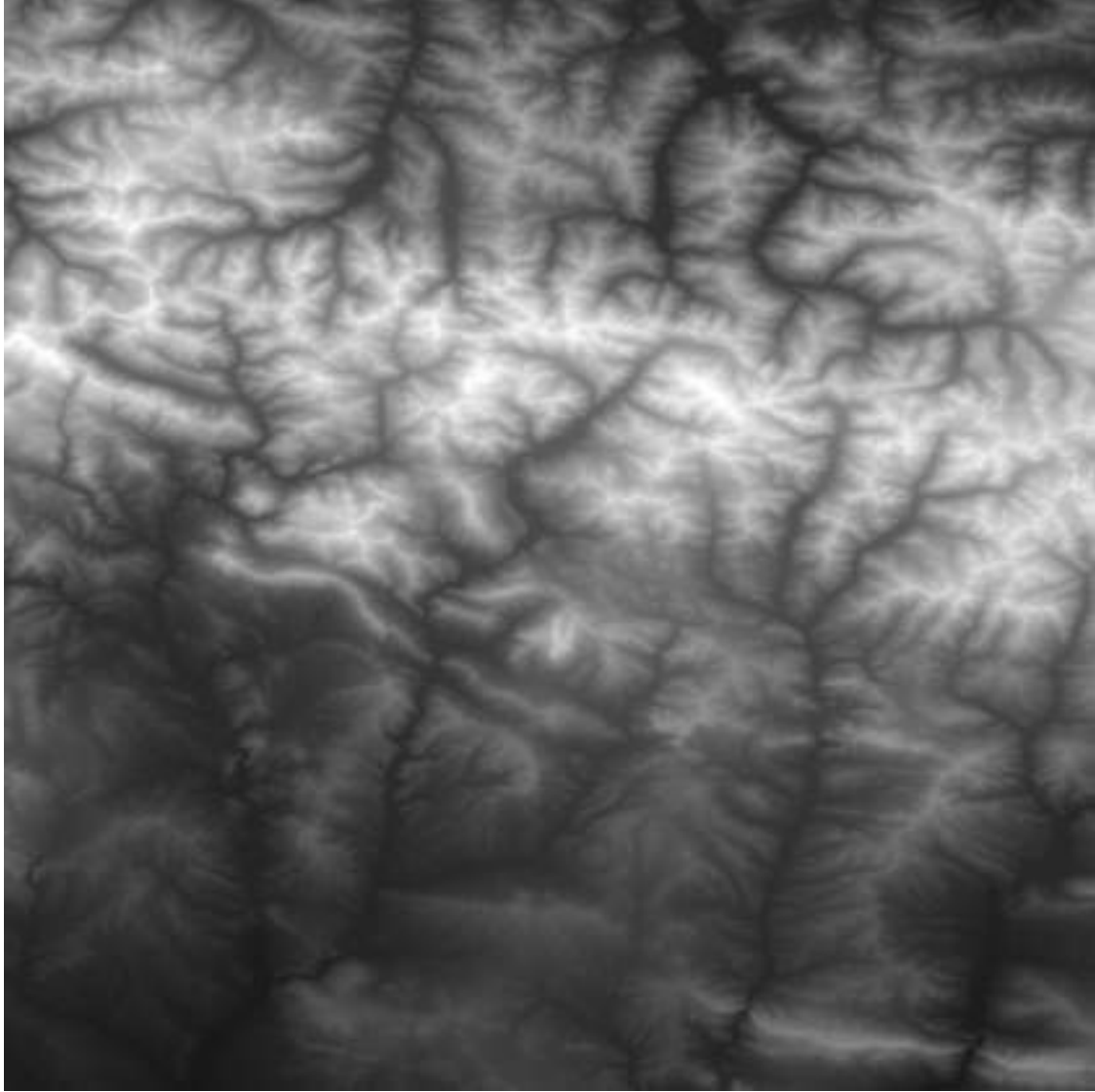


Figure 44. Digital elevation model (DEM) of the area of study (ASTGTM2-N42E000) sourced from the Advanced Spaceborne Thermal Emission and Reflection Radiometer (ASTER) global digital elevation model (GDEM) (ASTGTM v002, doi.org/10.5067/ASTER/ASTGTM.002). The image has been brightened for clarity. ASTER GDEM is a product of the Ministry of Economy, Trade, and Industry (METI) of Japan and the United States National Aeronautics and Space Administration (NASA).



Figure 45. Flow direction grid for the calculation of water drainage pathways in the area of study. Each colour represents a different slope direction. The lakes and main drainage streams have been superimposed for reference. Calculations performed and figure created using the Arc Hydro data model and toolset in ArcGIS (Esri, Redlands, CA, USA). Calculations performed using ASTER GDEM data (ASTGTM v002, doi.org/10.5067/ASTER/ASTGTM.002). ASTER GDEM is a product of the Ministry of Economy, Trade, and Industry (METI) of Japan and the United States National Aeronautics and Space Administration (NASA).

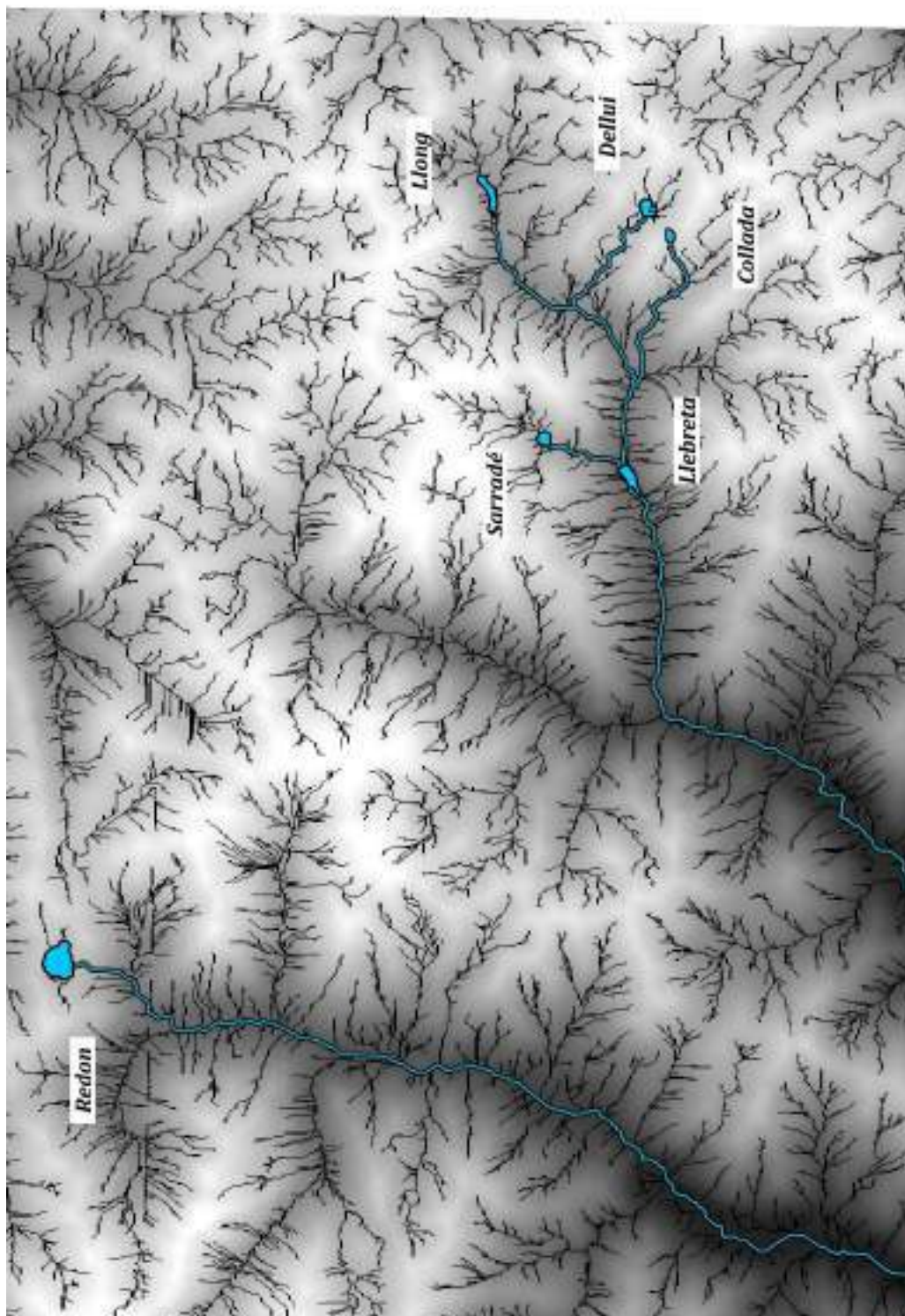


Figure 46. Water drainage pathways displayed over the DEM and used for the calculation of lake catchment areas. The lakes and main drainage streams have been superimposed for reference. Calculations performed and figure created using the Arc Hydro data model and toolset in ArcGIS (Esri, Redlands, CA, USA). Calculations performed using ASTER GDEM data (ASTGTM v002, doi.org/10.5067/ASTER/ASTGTM.002). ASTER GDEM is a product of the Ministry of Economy, Trade, and Industry (METI) of Japan and the United States National Aeronautics and Space Administration (NASA).

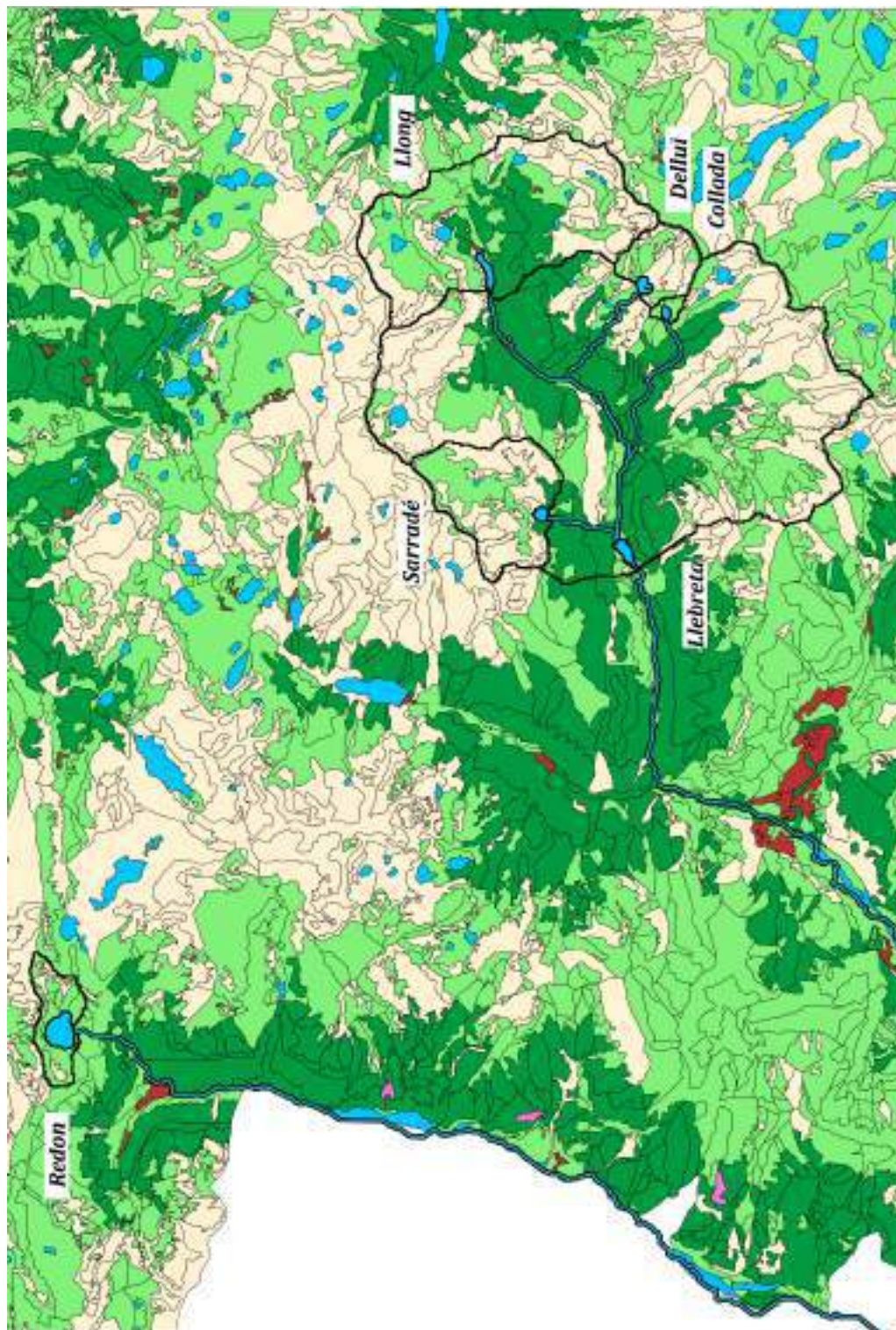


Figure 47. Lake catchment areas and soil coverage habitats: water (blue), shrubs (light green), forests (dark green), rock (beige), wetlands (brown), urban (maroon), industrial/other (pink). The lakes and main drainage streams have been superimposed for reference. Figure created using the Arc Hydro data model and toolset in ArcGIS (Esri, Redlands, CA, USA). Figure created using data from Servei de Planificació de l'Entorn Natural, Direcció General de Polítiques Ambientals i Medi Natural (Cartografia dels hàbitats d'interès comunitari a Catalunya, versió 2 (2018), last updated 30/11/2018) (Generalitat de Catalunya, Departament de Territori i Sostenibilitat).

Appendix II: Meteorology

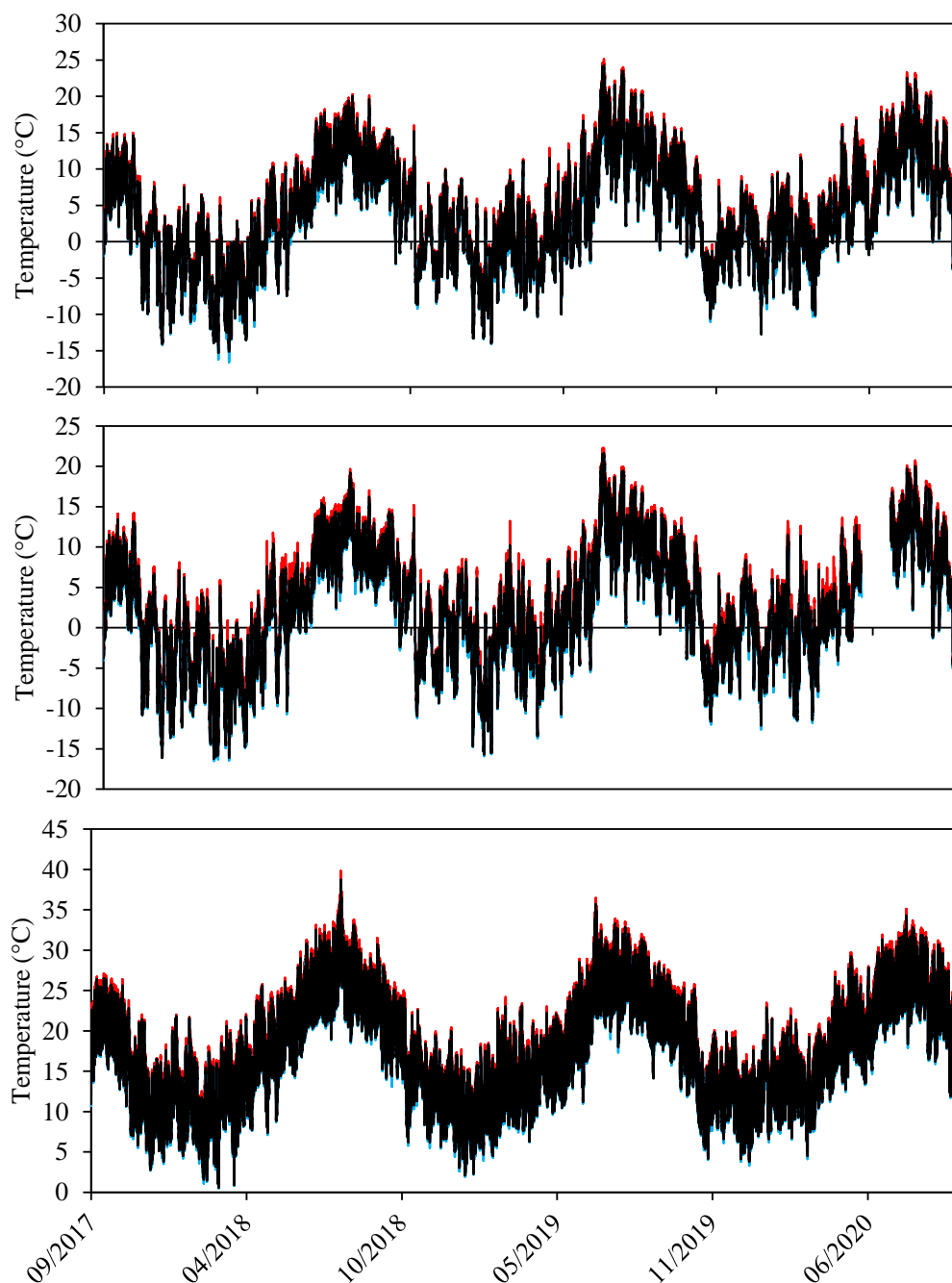


Figure 48. Average (black), maximum (red), and minimum (blue) temperature recorded every 30 min at Estanh Redon (top, 2247 m), Boí (center, 2535 m), and Barcelona (bottom, 79 m) during all sampling periods. Figure created using data from Xarxa d'Estacions Meteorològiques Automàtiques (XEMA) del Servei Meteorològic de Catalunya (METEOCAT) (Dades meteorològiques de la XEMA, last updated 06/09/2022) (Generalitat de Catalunya, Departament de Territori i Sostenibilitat).

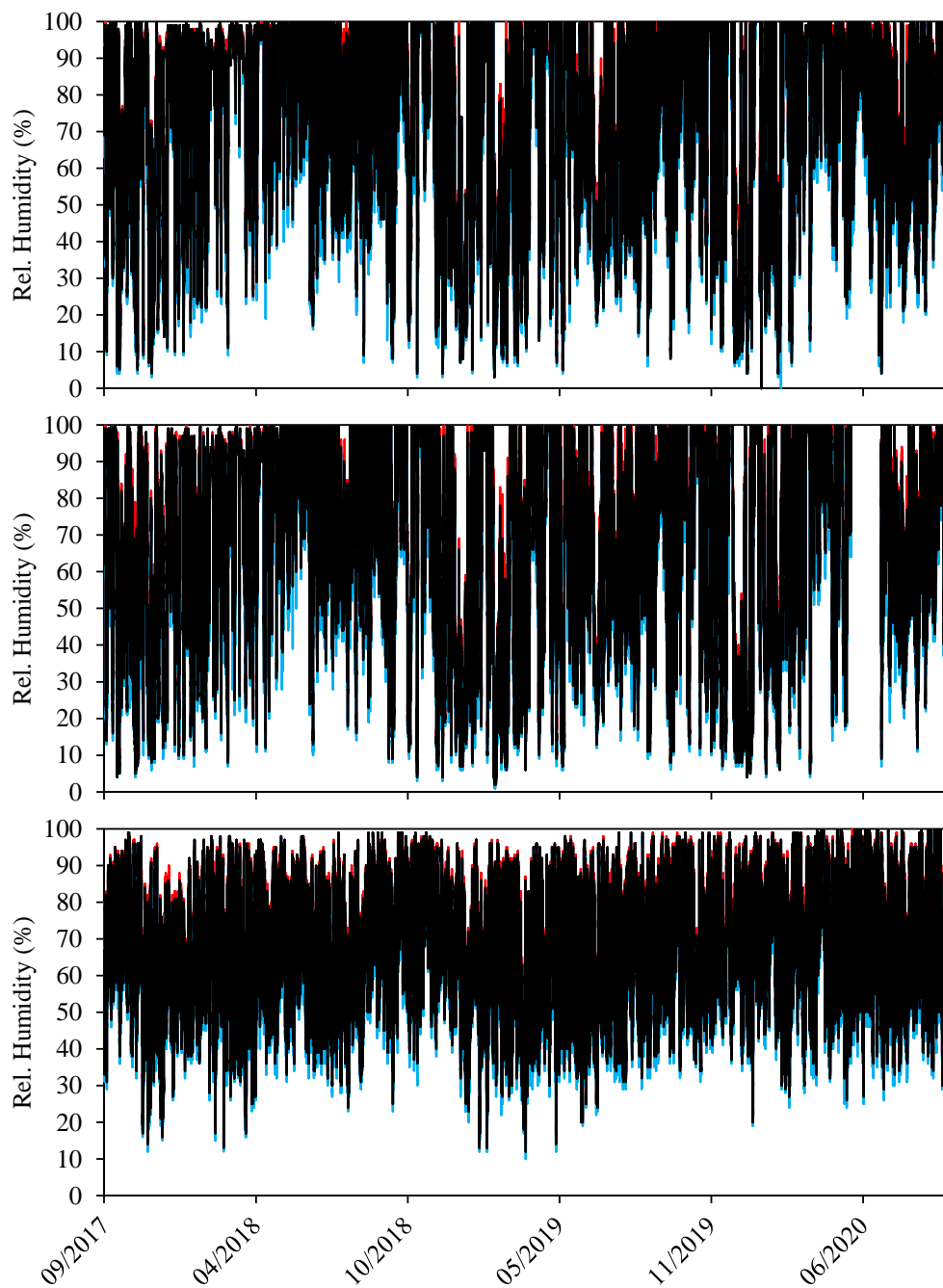


Figure 49. Average (black), maximum (red), and minimum (blue) relative humidity recorded every 30 min at Estanh Redon (top, 2247 m), Boí (center, 2535 m), and Barcelona (bottom, 79 m) during all sampling periods. Figure created using data from Xarxa d'Estacions Meteorològiques Automàtiques (XEMA) del Servei Meteorològic de Catalunya (METEOCAT) (Dades meteorològiques de la XEMA, last updated 06/09/2022) (Generalitat de Catalunya, Departament de Territori i Sostenibilitat).

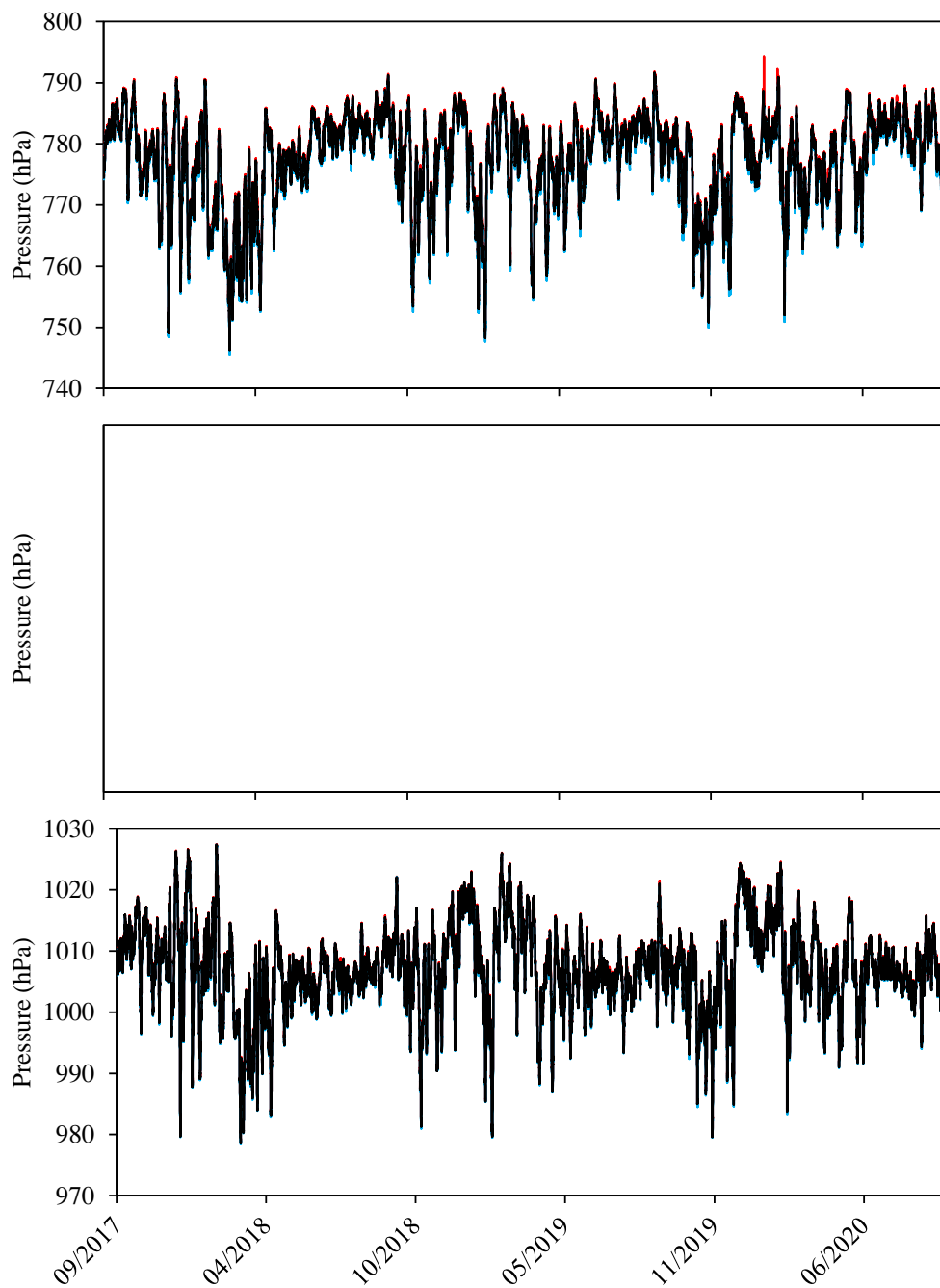


Figure 50. Average (black), maximum (red), and minimum (blue) atmospheric pressure recorded every 30 min at Estanh Redon (top, 2247 m) and Barcelona (bottom, 79 m) during all sampling periods. Data from Boí (center) not available. Figure created using data from Xarxa d'Estacions Meteorològiques Automàtiques (XEMA) del Servei Meteorològic de Catalunya (METEOCAT) (Dades meteorològiques de la XEMA, last updated 06/09/2022) (Generalitat de Catalunya, Departament de Territori i Sostenibilitat).

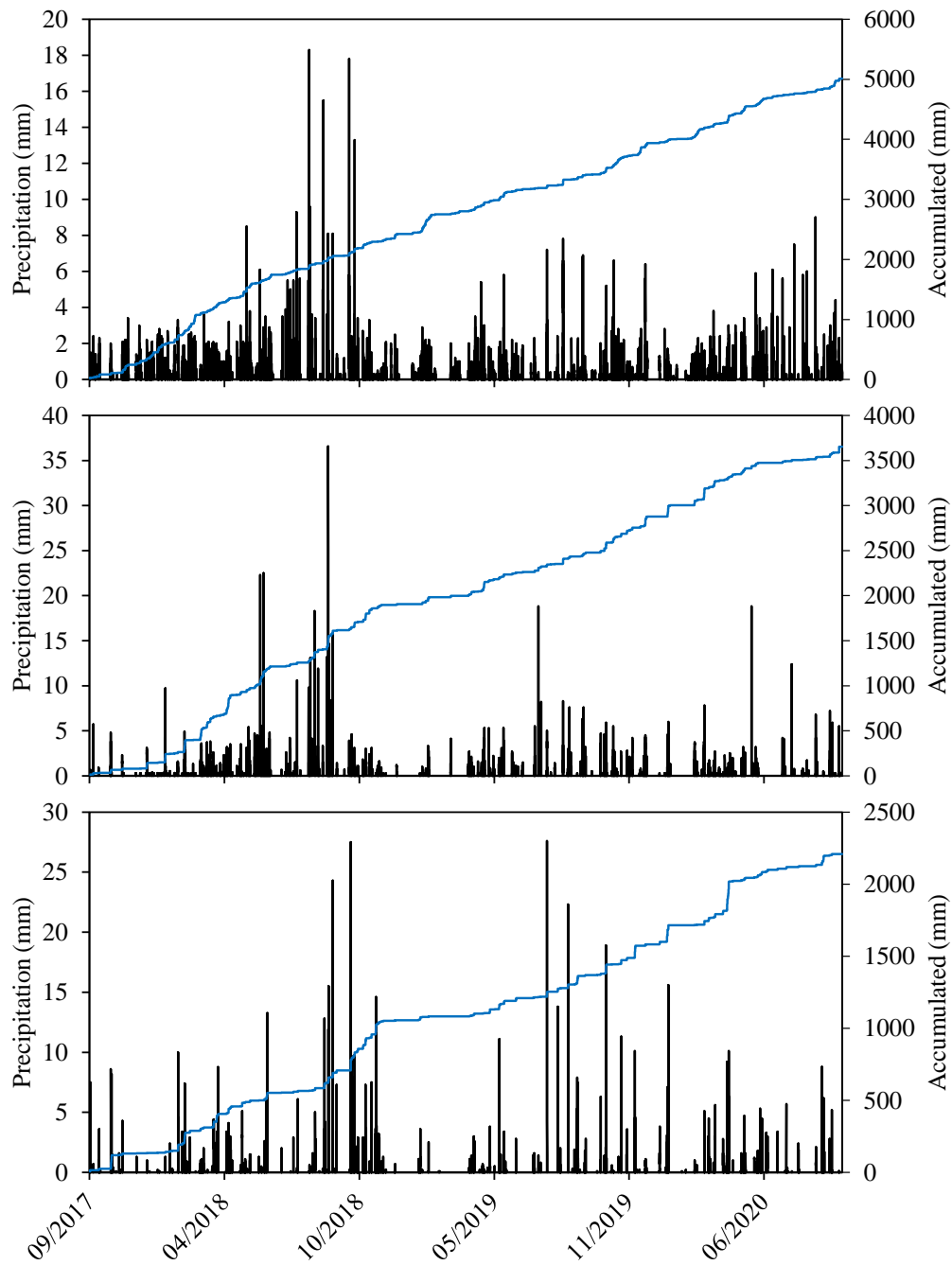


Figure 51. Precipitation recorded every 30 min (black) and accumulated precipitation (blue) at Estanh Redon (top, 2247 m), Boí (center, 2535 m), and Barcelona (bottom, 79 m) during all sampling periods. Figure created using data from Xarxa d'Estacions Meteorològiques Automàtiques (XEMA) del Servei Meteorològic de Catalunya (METEOCAT) (Dades meteorològiques de la XEMA, last updated 06/09/2022) (Generalitat de Catalunya, Departament de Territori i Sostenibilitat).

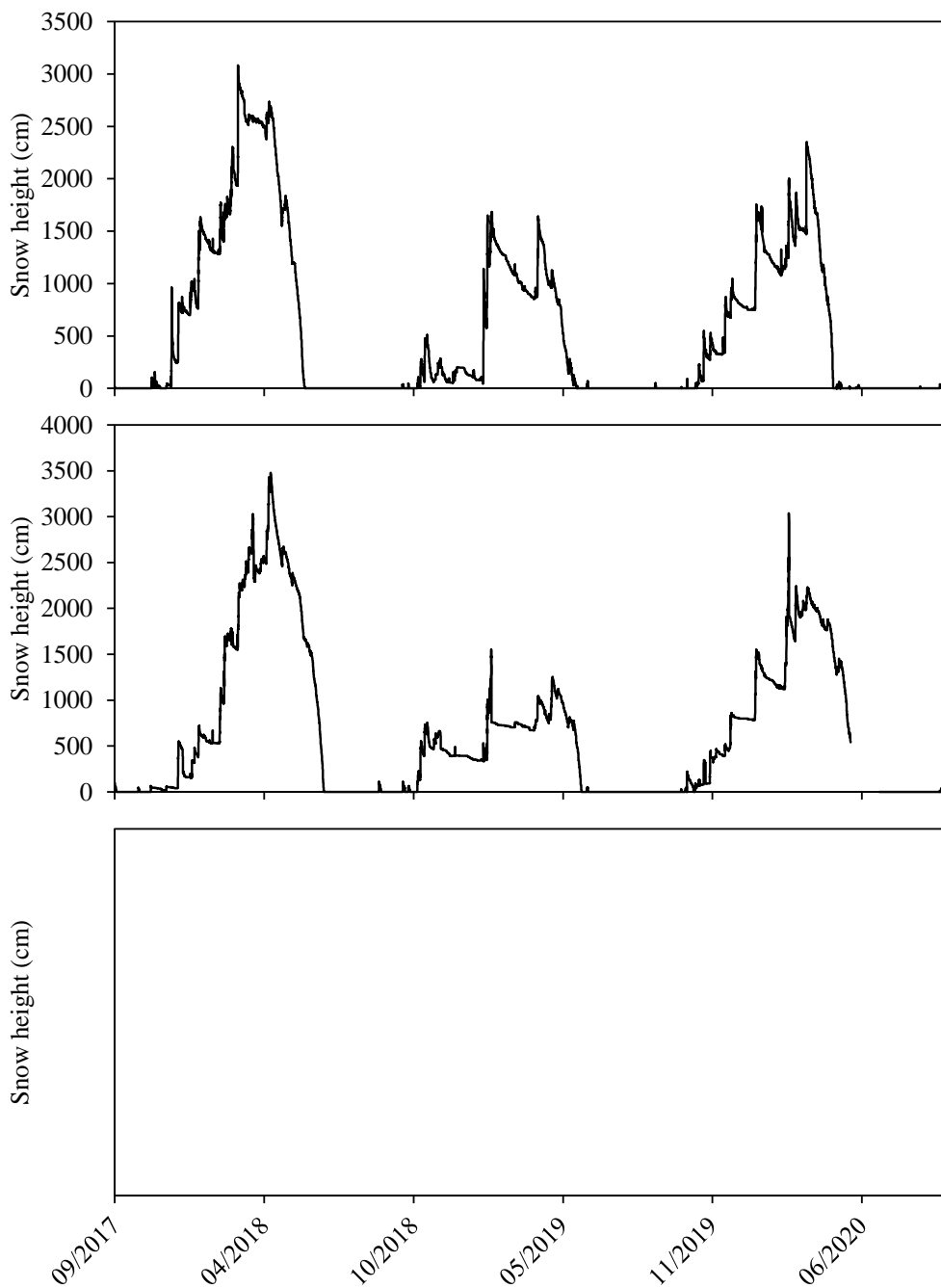


Figure 52. Snow height recorded every 30 min at Estanh Redon (top, 2247 m) and Boí (center, 2535 m) during all sampling periods. Data from Barcelona (center) not available but assumed to remain at 0 cm. Figure created using data from Xarxa d'Estacions Meteorològiques Automàtiques (XEMA) del Servei Meteorològic de Catalunya (METEOCAT) (Dades meteorològiques de la XEMA, last updated 06/09/2022) (Generalitat de Catalunya, Departament de Territori i Sostenibilitat).

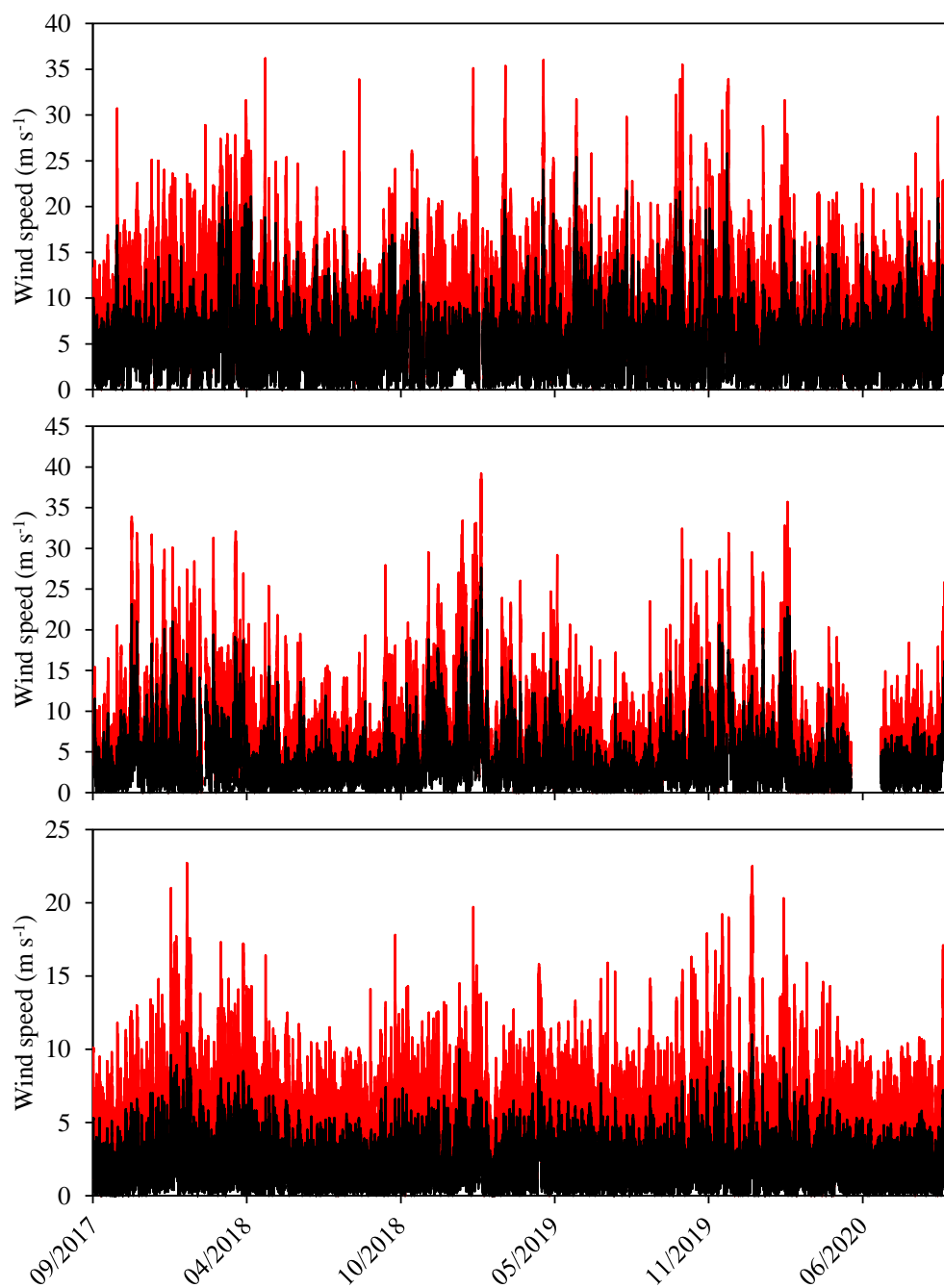


Figure 53. Average (black) and maximum (red) wind speed recorded every 30 min at Estanh Redon (top, 2247 m), Boí (center, 2535 m), and Barcelona (bottom, 79 m) during all sampling periods. Figure created using data from Xarxa d'Estacions Meteorològiques Automàtiques (XEMA) del Servei Meteorològic de Catalunya (METEOCAT) (Dades meteorològiques de la XEMA, last updated 06/09/2022) (Generalitat de Catalunya, Departament de Territori i Sostenibilitat).

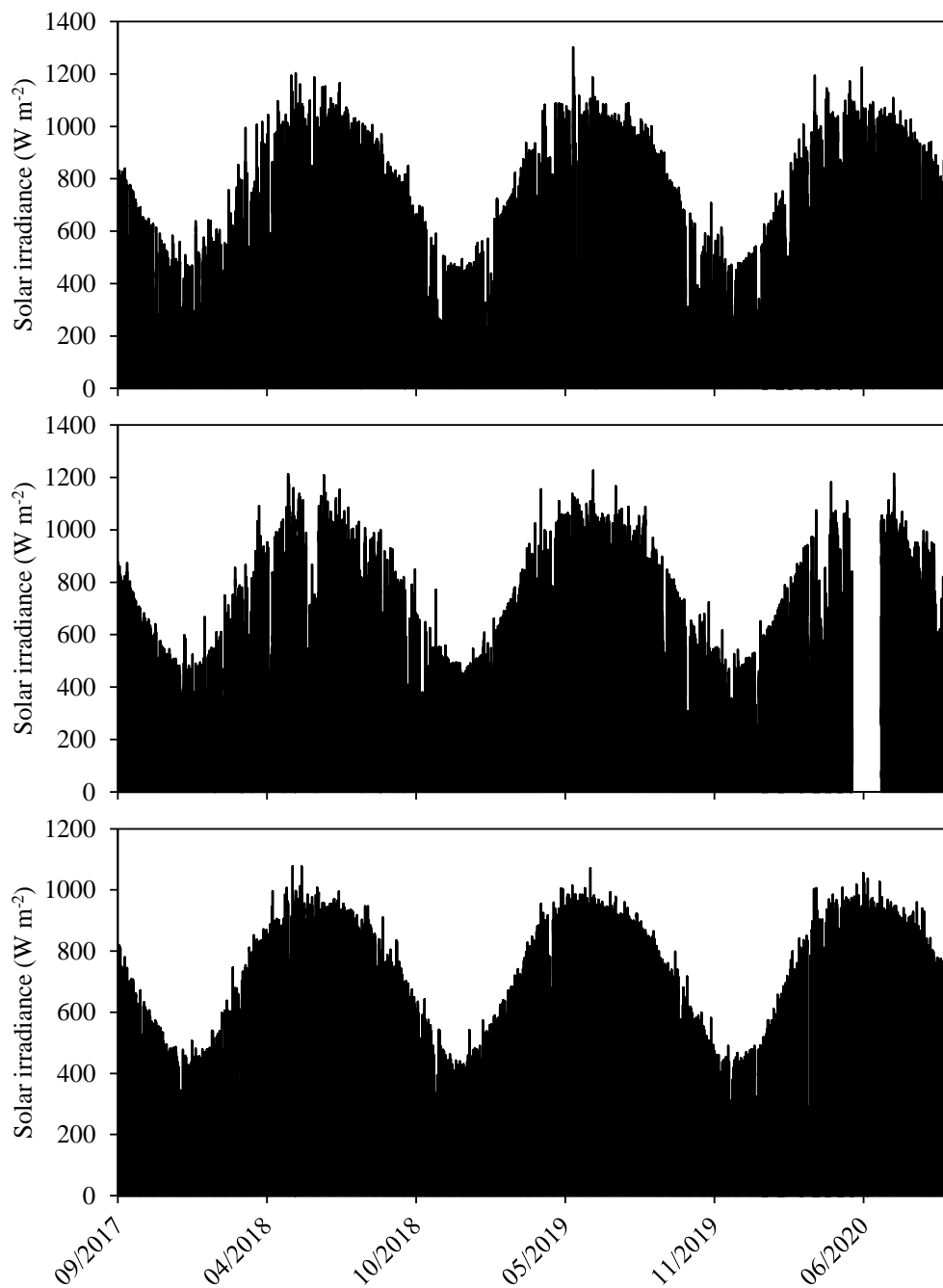


Figure 54. Average solar irradiance recorded every 30 min at Estanh Redon (top, 2247 m), Boí (center, 2535 m), and Barcelona (bottom, 79 m) during all sampling periods. Figure created using data from Xarxa d'Estacions Meteorològiques Automàtiques (XEMA) del Servei Meteorològic de Catalunya (METEOCAT) (Dades meteorològiques de la XEMA, last updated 06/09/2022) (Generalitat de Catalunya, Departament de Territori i Sostenibilitat).

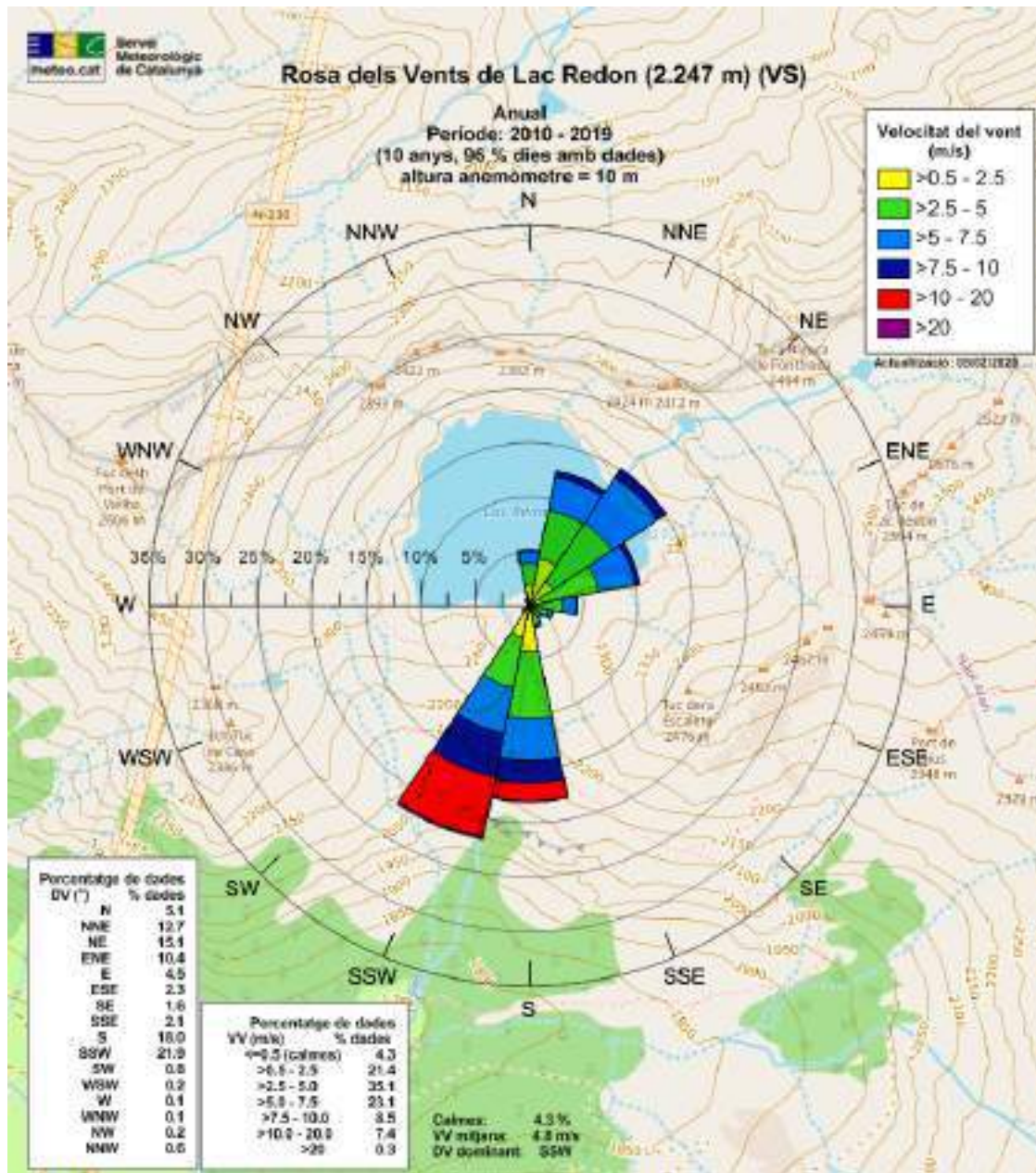


Figure 55. Wind rose representing the average distribution of wind speeds and directions over the last decade (2010–2019) at Estanh Redon (2247 m). Wind rose from Xarxa d’Estacions Meteorològiques Automàtiques (XEMA) del Servei Meteorològic de Catalunya (METEOCAT) (Dades meteorològiques de la XEMA, last updated 06/09/2022) (Generalitat de Catalunya, Departament de Territori i Sostenibilitat). Base map: Produced Work by the OpenStreetMap Foundation using OpenStreetMap data under the Open Database License, © OpenStreetMap contributors.

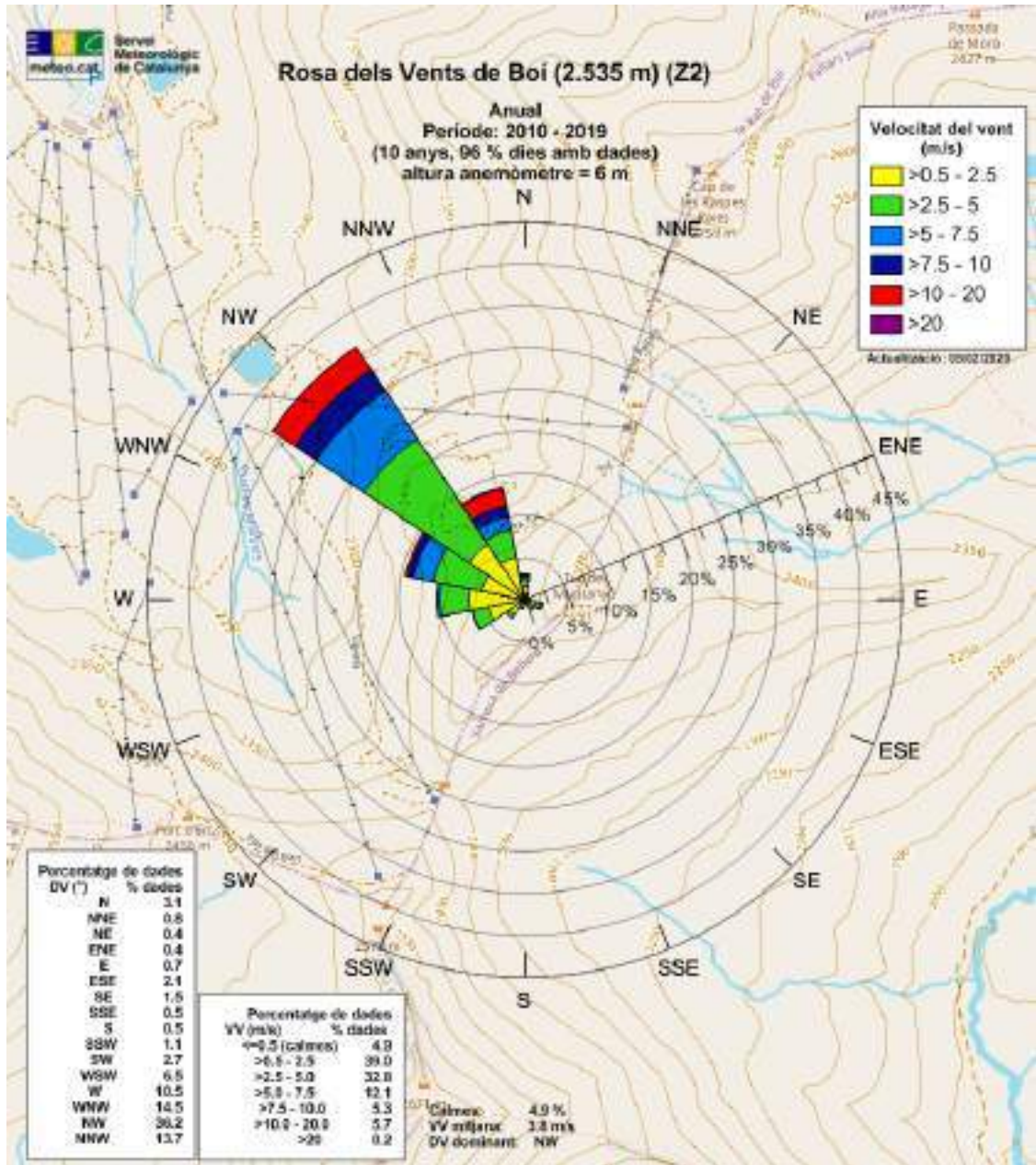


Figure 56. Wind rose representing the average distribution of wind speeds and directions over the last decade (2010–2019) at Boí (2535 m). Wind rose from Xarxa d'Estacions Meteorològiques Automàtiques (XEMA) del Servei Meteorològic de Catalunya (METEOCAT) (Dades meteorològiques de la XEMA, last updated 06/09/2022) (Generalitat de Catalunya, Departament de Territori i Sostenibilitat). Base map: Produced Work by the OpenStreetMap Foundation using OpenStreetMap data under the Open Database License, © OpenStreetMap contributors.

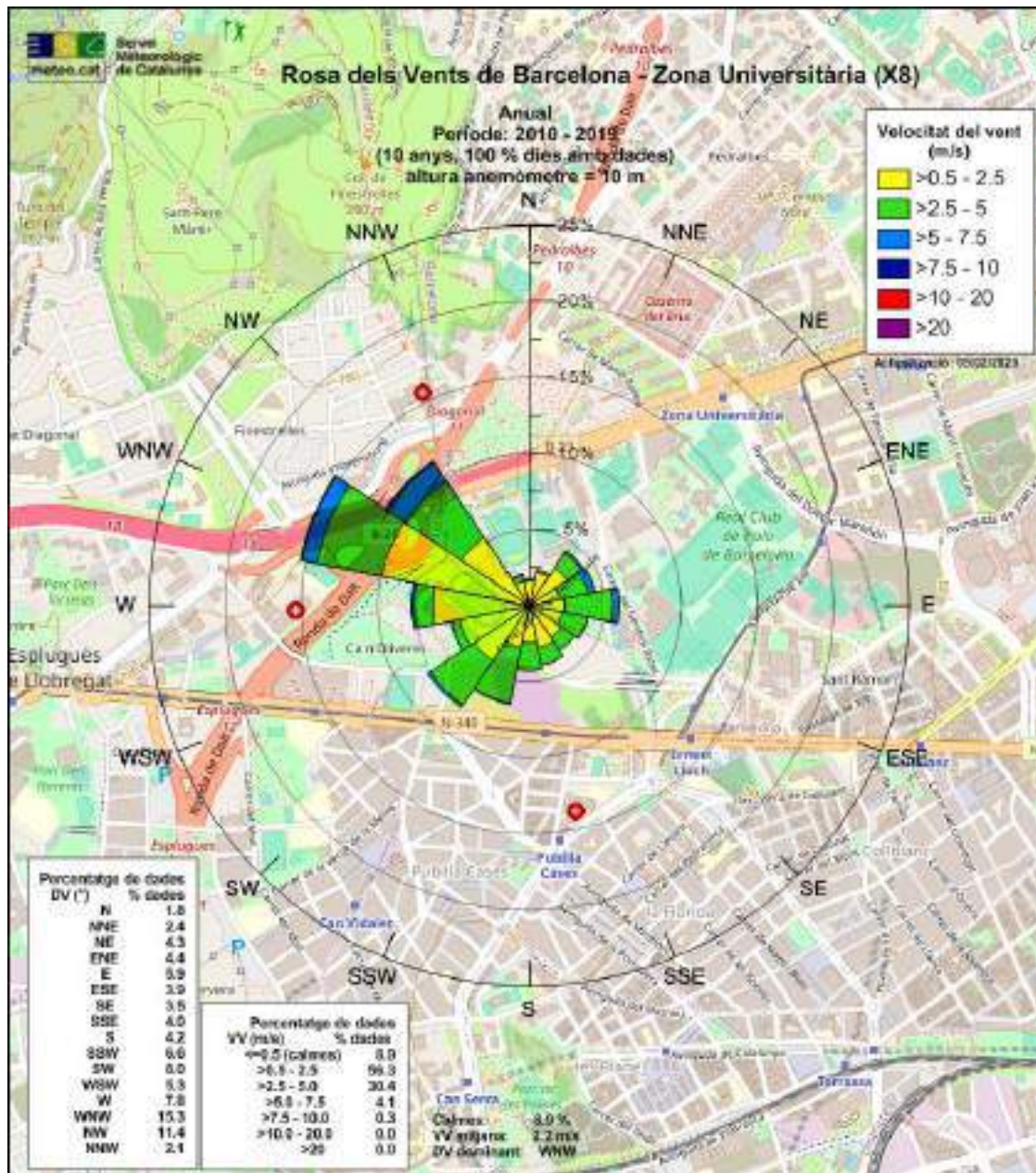


Figure 57. Wind rose representing the average distribution of wind speeds and directions over the last decade (2010–2019) at Barcelona (79 m). Wind rose from Xarxa d’Estacions Meteorològiques Automàtiques (XEMA) del Servei Meteorològic de Catalunya (METEOCAT) (Dades meteorològiques de la XEMA, last updated 06/09/2022) (Generalitat de Catalunya, Departament de Territori i Sostenibilitat). Base map: Produced Work by the OpenStreetMap Foundation using OpenStreetMap data under the Open Database License, © OpenStreetMap contributors.

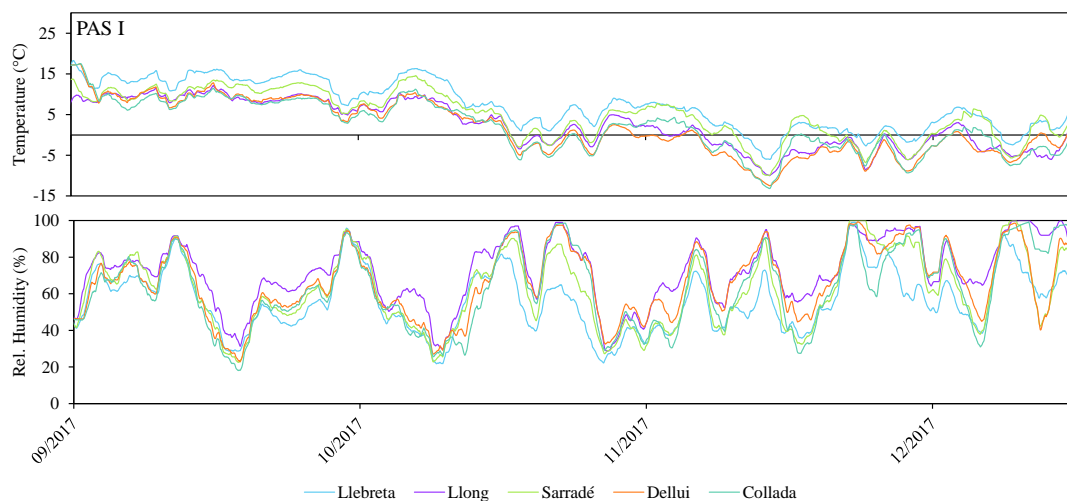


Figure 58. Moving average (48 h) of air temperature (top) and relative humidity (bottom) measured every 30 min during passive air sampling period PAS I. Figure created using data collected with data loggers co-deployed at each site with the passive samplers.

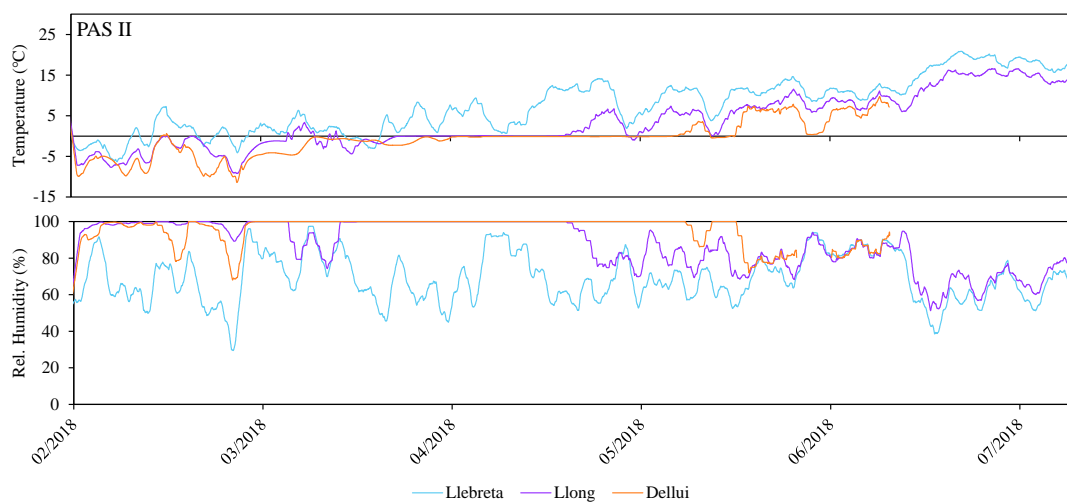


Figure 59. Moving average (48 h) of air temperature (top) and relative humidity (bottom) measured every 30 min during passive air sampling period PAS II. Figure created using data collected with data loggers co-deployed at each site with the passive samplers.

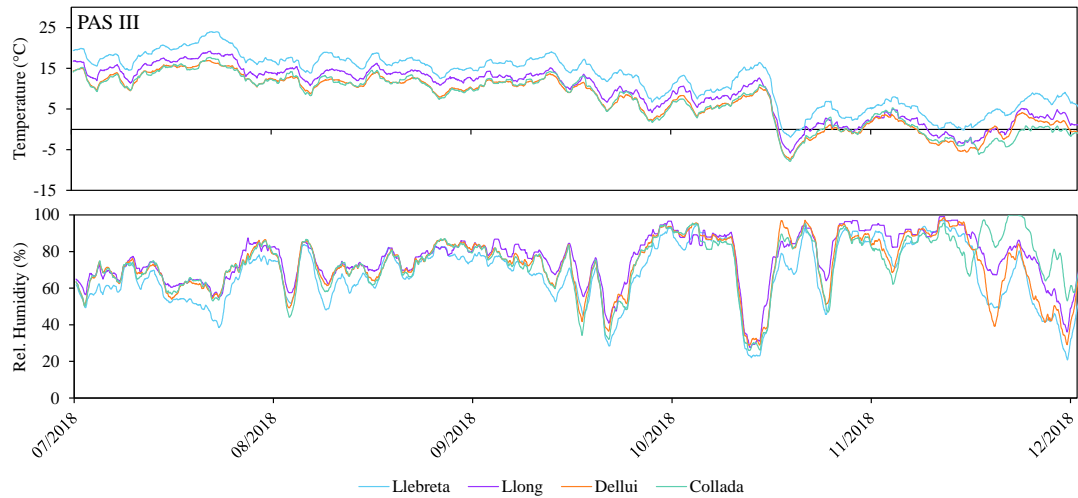


Figure 60. Moving average (48 h) of air temperature (top) and relative humidity (bottom) measured every 30 min during passive air sampling period PAS III. Figure created using data collected with data loggers co-deployed at each site with the passive samplers.



Figure 61. Moving average (48 h) of air temperature (top) and relative humidity (bottom) measured every 30 min during passive air sampling period PAS IV. Figure created using data collected with data loggers co-deployed at each site with the passive samplers.

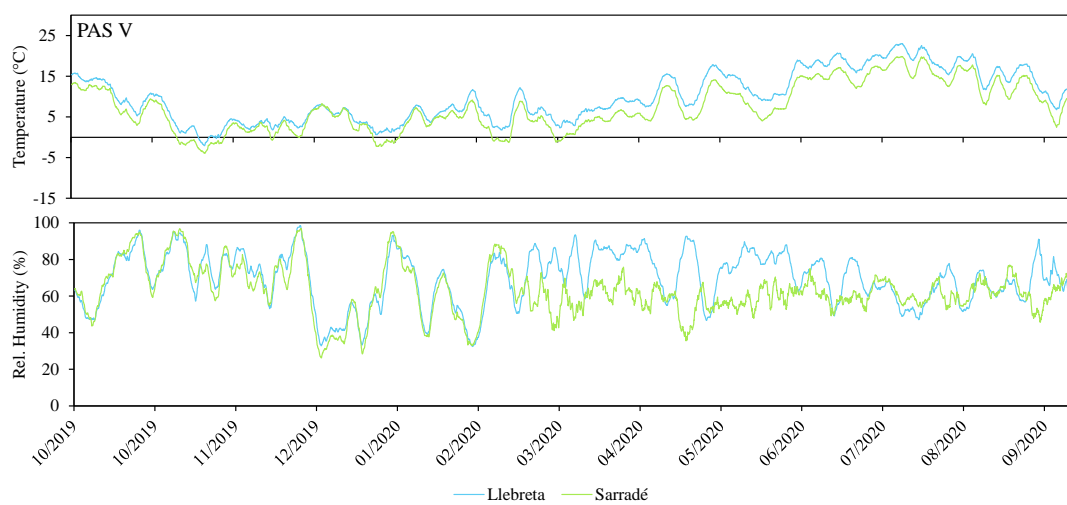


Figure 62. Moving average (48 h) of air temperature (top) and relative humidity (bottom) measured every 30 min during passive air sampling period PAS V. Figure created using data collected with data loggers co-deployed at each site with the passive samplers.

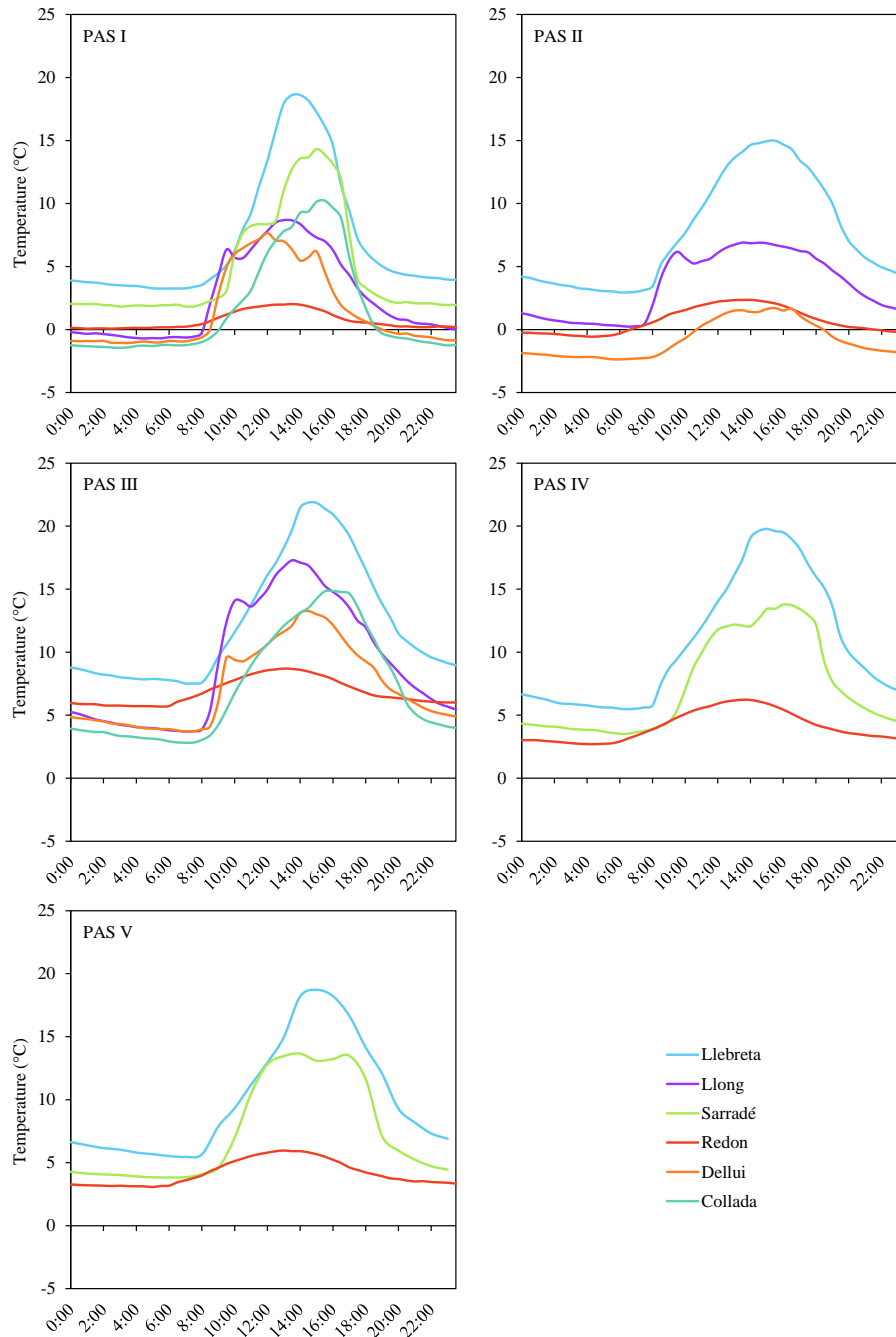


Figure 63. Daily average air temperature profiles at the studied sites over the five passive air sampling periods. Figure created using data collected with data loggers co-deployed at each site with the passive samplers and data from Xarxa d'Estacions Meteorològiques Automàtiques (XEMA) del Servei Meteorològic de Catalunya (METEOCAT) (Dades meteorològiques de la XEMA, last updated 06/09/2022) (Generalitat de Catalunya, Departament de Territori i Sostenibilitat).

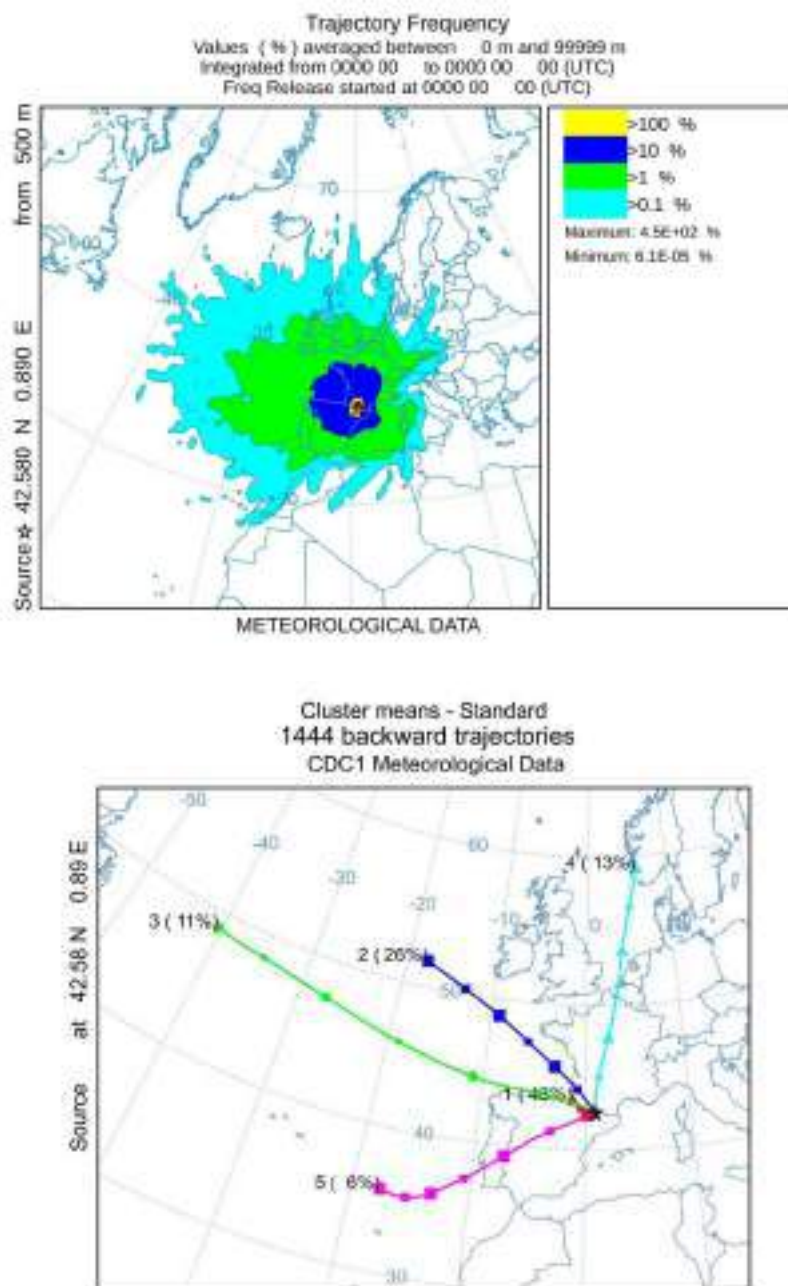


Figure 64. Trajectory frequency plot (72 h backwards, one trajectory every 6 h from 09/2017 to 08/2018) for air trajectories ending at the studied area (top) and cluster trajectory plot (bottom). Calculations performed and figures created using NOAA’s HYSPLIT transport and dispersion model (National Oceanic and Atmospheric Administration, USA).

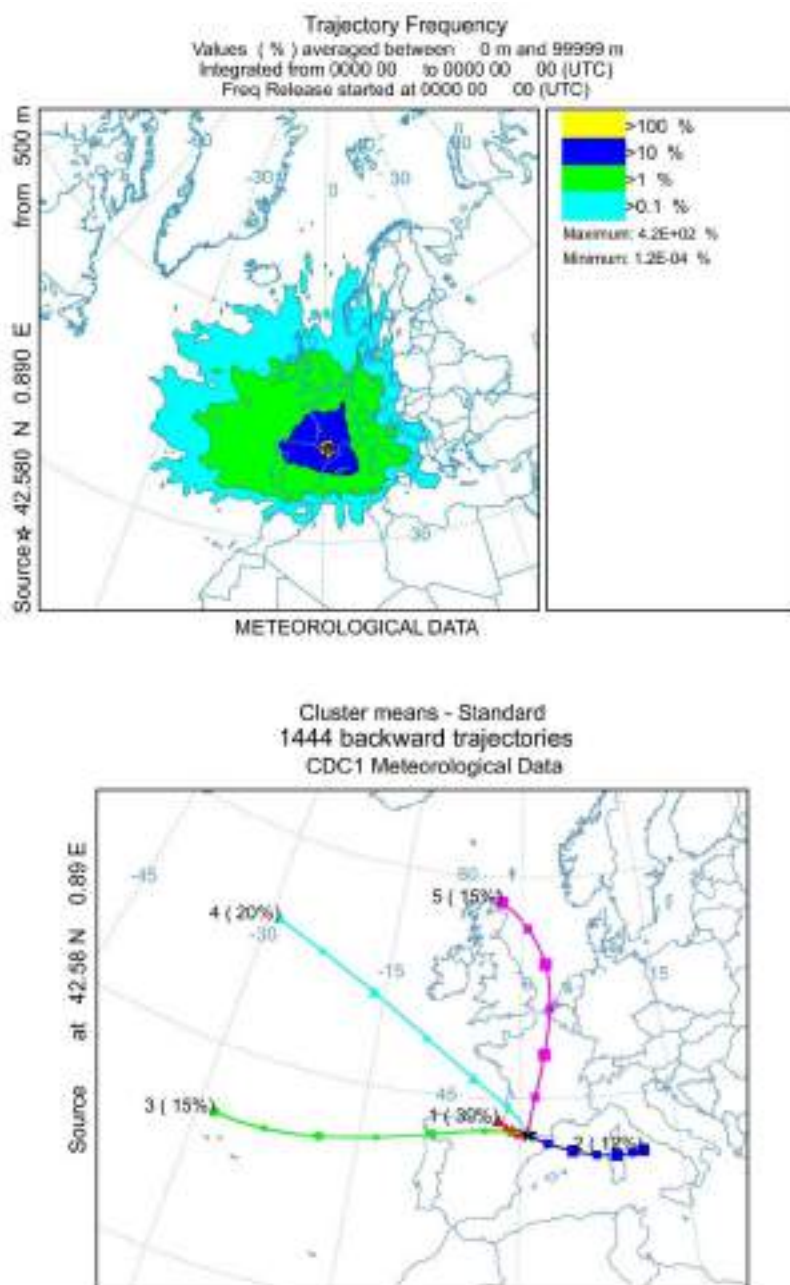


Figure 65. Trajectory frequency plot (72 h backwards, one trajectory every 6 h from 09/2018 to 08/2019) for air trajectories ending at the studied area (top) and cluster trajectory plot (bottom). Calculations performed and figures created using NOAA's HYSPLIT transport and dispersion model (National Oceanic and Atmospheric Administration, USA).

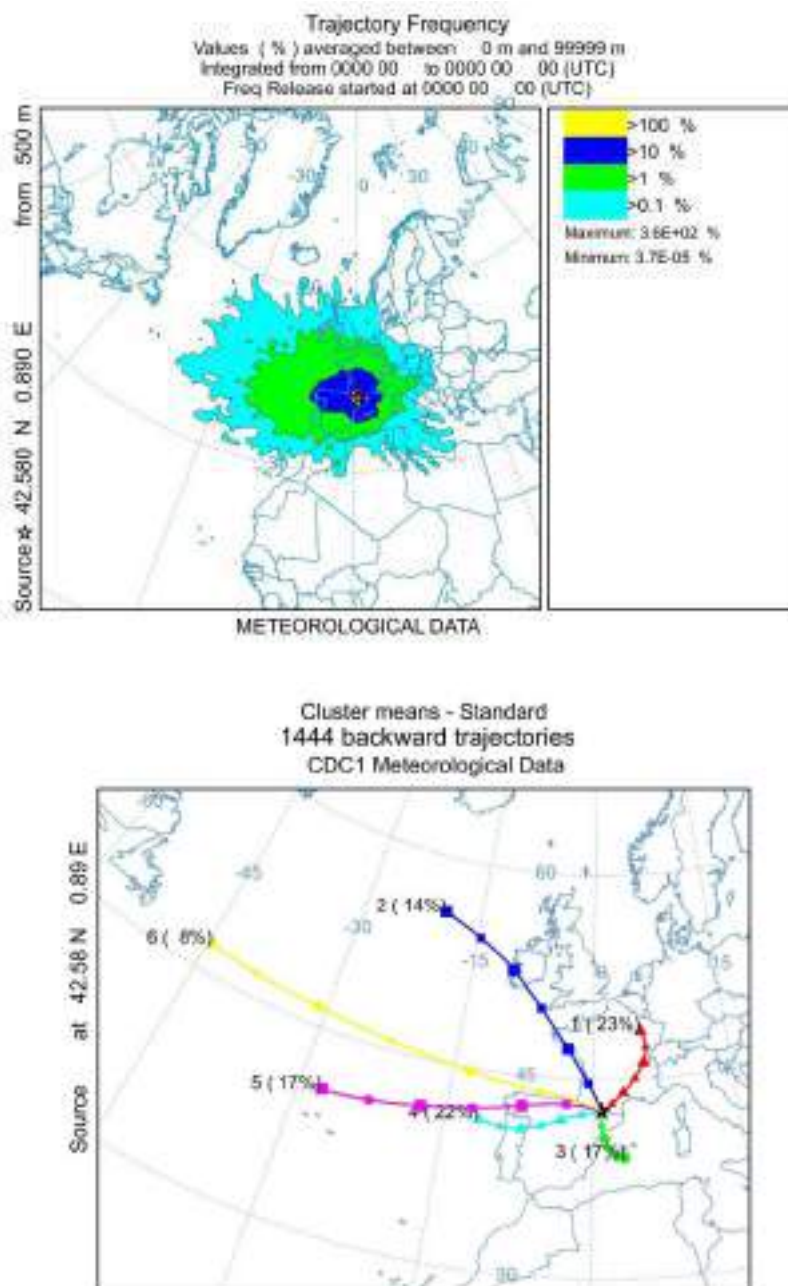


Figure 66. Trajectory frequency plot (72 h backwards, one trajectory every 6 h from 09/2019 to 08/2020) for air trajectories ending at the studied area (top) and cluster trajectory plot (bottom). Calculations performed and figures created using NOAA’s HYSPLIT transport and dispersion model (National Oceanic and Atmospheric Administration, USA).

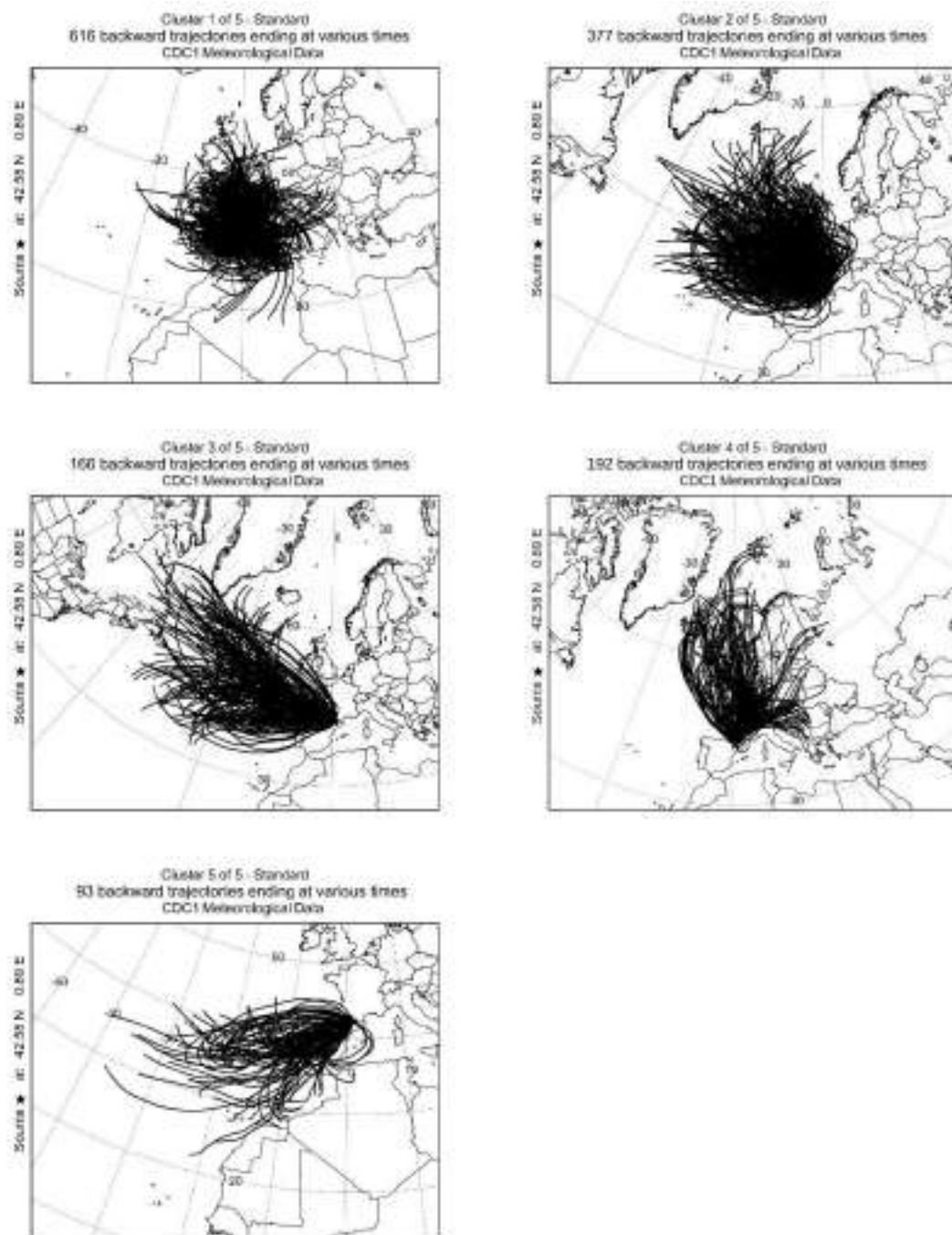


Figure 67. Backwards (72 h) air trajectories forming each cluster in the cluster trajectory plot from 09/2017 to 08/2018 for air trajectories ending at the studied area. Calculations performed and figures created using NOAA's HYSPLIT transport and dispersion model (National Oceanic and Atmospheric Administration, USA).

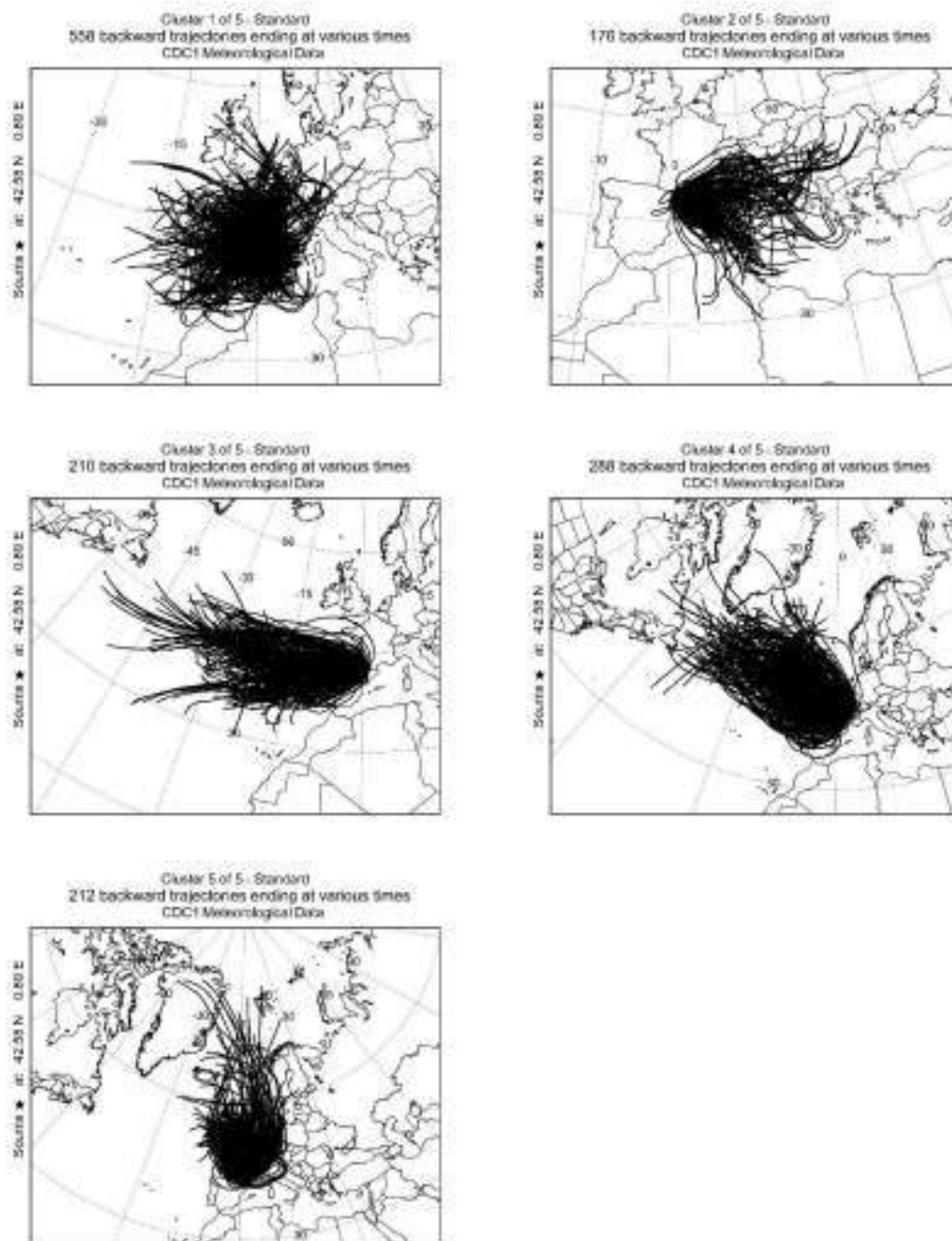


Figure 68. Backwards (72 h) air trajectories forming each cluster in the cluster trajectory plot from 09/2018 to 08/2019 for air trajectories ending at the studied area. Calculations performed and figures created using NOAA’s HYSPLIT transport and dispersion model (National Oceanic and Atmospheric Administration, USA).

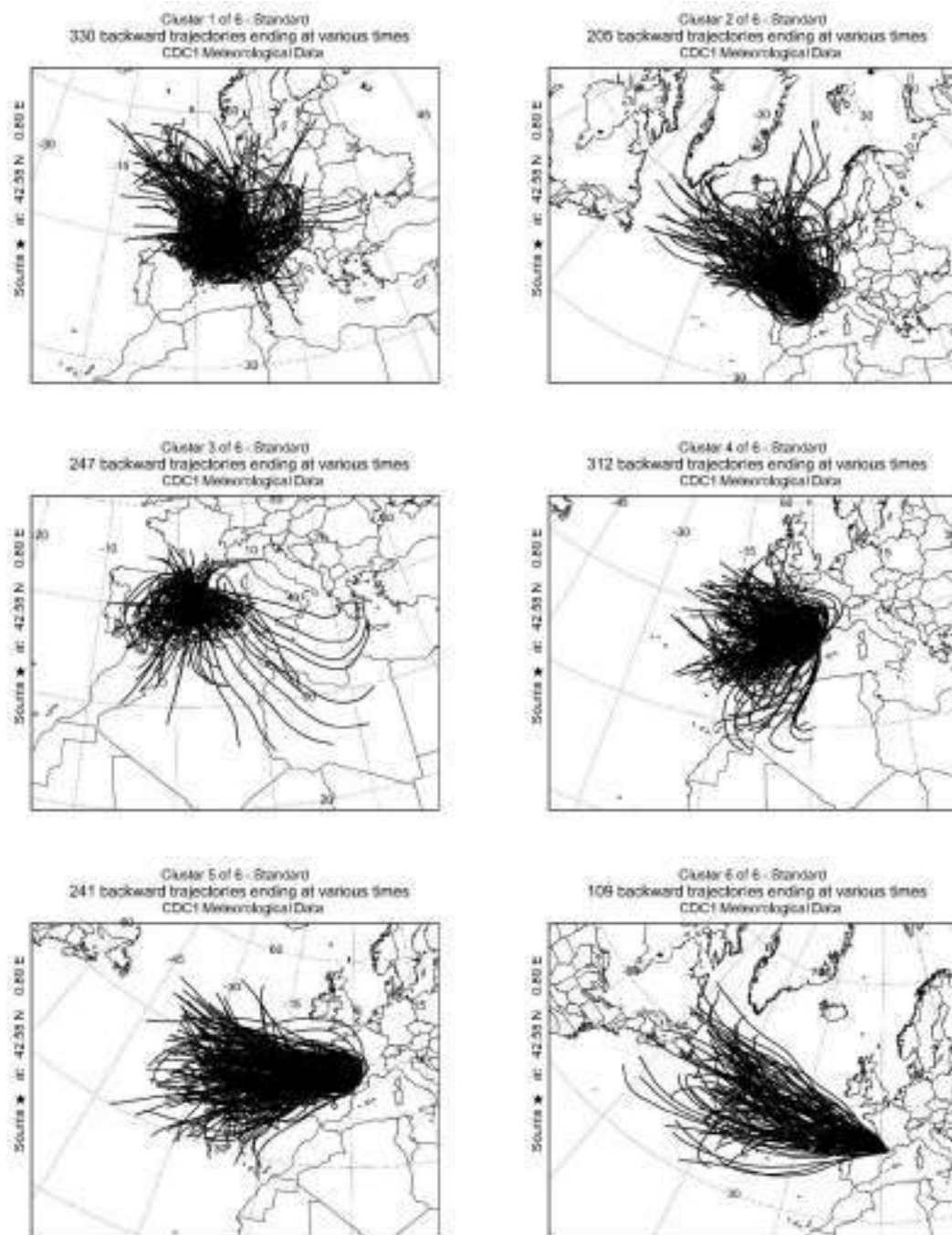


Figure 69. Backwards (72 h) air trajectories forming each cluster in the cluster trajectory plot from 09/2019 to 08/2020 for air trajectories ending at the studied area. Calculations performed and figures created using NOAA’s HYSPLIT transport and dispersion model (National Oceanic and Atmospheric Administration, USA).

